Quantum Study of the H_3 System

Thesis by

Zhengwei Peng

In partial Fulfillment of the Requirements

for the Degree

Doctor of Philosophy

California Institute of Technology

Pasadena, California

1991

(submitted October 5, 1990)

To my parents

ACKNOWLEDGMENTS

It is a great pleasure to take this opportunity to thank all of those who have made a contribution to my graduate studies at Caltech, and also to thank those who have made my life in Pasadena interesting.

Special thanks go to my advisor, Prof. Aron Kuppermann, who has patiently given me much encouragement and expert advice throughout my years here. My fellow group mates Paul Hipes, Steve Cuccaro, Mark Wu, Isaac Xavier, Mary Rodgers, Garth Parker, Maria Giorgi, Dr. Bruno Lepetit, Dr. Joseph Wong and visiting scholar Qiu Jin, gave me a lot of support and interesting discussions.

My short visit to Ottawa in April 1989 turned out to be a wonderful experience for me. Prof. Jim Wright, Dr. Pablo Bruna, Dr. Victoria Barckley and Mr. Steve Hernadi gave me a lot of help with the electronic structure calculation, which I knew little about at the time.

I also would like to thank those in the machine shop and in the electronic shop: Tony, Ray, Guy, Delmar, and Tom. Qui and I had many cheerful hours with them.

I would also like to thank all of my friends in the Caltech Men's Glee Club, the Caltech C and the Hong Kong Soccer Team for their friendship, stimulating conversation and happy hours.

Abstract

In this thesis, an *ab initio* quantum study of both electronic and nuclear motions of the H_3 system is presented. Results of the *ab initio* calculations for the lowest four electronic potential energy surfaces of the H_3 system are given, as well as for the electric dipole transition moments between them. The calculated Rydberg spectra compare well with previous calculations and with known experimental results. The ground state and the third excited state surfaces have been fitted using the rotated Morse cubic spline (RMCS) method. The ro-vibrational eigenstates of H_3 on the upper sheet of the Double Many Body Expansion (DMBE) surface were calculated using a variational method and a new hyperspherical coordinate propagation method. The full P_3 nuclear permutation symmetry and the molecular Aharonov-Bohm (MAB) (or geometric phase) effect were included in the hyperspherical coordinate propagation method. The MAB effect has a profound influence on the bound ro-vibrational states of the H_3 system. The ro-vibrational bound states of H_3 in the third excited $2p_z\ ^2A_2''$ electronic state were also studied. The Rydberg nature of this electronic state leads to ro-vibrational nuclear motion similar to that of the H_3^+ ion. The comparison between the calculated values of the ro-vibrational constants and the corresponding experimental results suggests that the $2p_z\ ^2A_2''$ RMCS surface still needs some improvement.

Table of Contents

Chapter 1

Background

1.1. Introduction

Shortly after quantum mechanics was developed in the first part of this century, it was used in an attempt to understand the rich structures and the complex dynamical processes of molecular systems. Although the Schrödinger equation, which fully describes the motion of any molecular system, has been known for a long time, the number of electrons and nuclei in many chemically interesting molecules poses numerous difficulties. In most cases this difficulty has prevented, until recent year, accurate solution of the Schrödinger equation from being obtained, even though such solutions are of great importance for the ultimate understanding of these systems from first principles.

With only three electrons and three protons, the H_3 system is the simplest triatomic molecular neutral species. Because of its simplicity, it is an ideal system for *ab initio* quantum studies, and has been and is being investigated extensively via the most up-to-date techniques available, both experimentally and theoretically. These studies have been very fruitful and have offered many surprises even for such a simple system. The advance of both the theoretical and experimental investigations and a comparison of the results obtained with each other have greatly enhanced our understanding of several fundamentals in chemistry and our ability to predict chemical structure and dynamics from first principles.

The potential energy surface of the non-bound ground state of H_3 has been calculated since the beginning of quantum chemistry[1-14]. The surface is genuinely repulsive except for a very shallow van der Waals well of 20

cm^{-1} at the nuclear configuration where the H atom is about 3.5 Å from the center of mass of the H_2 diatomic molecule in the collinear configuration[15-16]. The large scale quantum *ab initio* electronic calculation of Liu[6] and Siegbahn and Liu[7] are estimated to be of chemical accuracy, about 1 Kcal/mol (or 43 meV) above the non-relativistic Born-Oppenheimer limit. It is still the most accurate study available today. The fitted potential energy surfaces of the Liu-Siegbahn-Trular-Horowitz (hereafter LSTH)[13] and the recent double-many-body-expansion (hereafter DMBE) of Varandas and co-workers[14] offer a solid starting point for the quantum scattering calculation of the H + H_2 reaction, which is the prototypical gas phase atom-diatomic molecule reaction. This is the simplest example of one of the most important chemical processes which involves the breaking of a chemical bond and the formation of a new one:

$$A + BC \rightarrow AB + C \tag{1}$$

Those scattering calculations[17-35] have demonstrated that from first principles we have reached the understanding of quantum dynamics of chemical reactions.

Interest in the electronic excited states of H_3 arose from the early experimental reports of long-lived H_3 species[36-42], especially from the work of Devienne and co-workers[36]. But those studies were not conclusive enough to demonstrate beyond doubt the existence of bound H_3 species in its excited electronic states. In 1979, in an attempt to study the infrared spectra of the H_3^+ ion, Herzberg accidentally observed the visible emission spectra of H_3 between the quasi-bound excited Rydberg electronic states in a hollow hydrogen gas discharge tube[43]. His experiment unambiguously identified the existence of the metastable H_3 species in its Rydberg electronic states, which inspired many experimental[44-63] and theoretical[64-75] studies. Reviews on the Rydberg states

of H_3 have been given in the recent publications of Herzberg[76], Watson[77], and Gellene and Porter[78].

Both experimental and theoretical studies show clearly that the H_3 system in these Rydberg states behaves like a hydrogen atom, with a tight H_3^+ equilateral triangle ion core plus an electron in a diffuse Rybderg state. The rotation and vibration constants of the metastable H_3 molecule are close to the corresponding values for the H_3^+ ion[44-47]. At the same time, the experiments also show the intricate interaction between the H_3^+ ion core and the Rydberg electron, which offers a great challenge to theoretical understanding of such seemingly simple systems[53-56].

Potential energy surfaces, transition moments and coupling elements

The electronic energy levels and correlation diagram of H_3 in an equilateral triangle nuclear configuration with an internuclear distance of 1.64 bohr (from the study of King and Morokuma[66]) is depicted in Fig. 1. Since the molecular point group for an equilateral triangle is D_{3h}, all electronic states are labeled according to the symmetry representation of this point group, along with the labels of the united-atom (UA) limits. For example, the ground electronic state and the first excited state are spin doublets. They are degenerate, and together form an E' representation of D_{3h}. Since in the united-atom limit the H_3 system becomes a Li atom, these two E' wave functions will correspond to the $2p_x$, $2p_y$ atomic orbitals of the Li atom (with the z axis perpendicular to the plane of the H_3 triangle). We label them as $2p_{x,y}\ ^2E'$. Applying the same scheme to other excited Rydberg states, the second excited state is labeled as $2s\ ^2A_1'$, the third one as $2p_z\ ^2A_2''$, and so on. Studies show that except for the ground electronic state, potential energy

surfaces of all Rydberg excited electronic states have global energy minima, and therefore might be able to support bound ro-vibrational nuclear states.

So far, all theoretical studies of these excited H_3 Rydberg states were more or less aimed at explaining the most obvious features of the experimental Rydberg spectroscopic results. The restricted nuclear geometries in these studies for which *ab initio* calculations have been done prevented the construction of full potential energy surfaces. In this sense, the theoretical study of the accurate rotational and vibrational structures of the H_3 Rydberg states is not possible because of the lack of potential energy surfaces, even though there is a great deal of experimental data available on this subject[44-47,53-63,76-78].

Since the ground electronic state of H_3 is repulsive, and does not support any bound ro-vibrational states of nuclear motion, any H_3 species in the excited Rydberg electronic states which decays into this ground electronic state will dissociate. This decay can occur via two mechanisms: radiation and predissociation. The radiation lifetime is related to the transition moments between the initial and final states[79-80]. The predissociation process comes from the electronically non-adiabatic couplings between the excited Rydberg electronic state and the repulsive ground electronic state[79-80]. There are quite a few experimental studies of the lifetime of the H_3 Rydberg states[44-53]. Since it is hard to separate experimentally the contributions from the radiation and predissociation processes, theoretical investigations are in a better position to address the lifetime issue.

The $2p_z\ ^2A_2''$ low-lying Rydberg electronic state is a very special one among the H_3 Rydberg species. From symmetry arguments, Herzberg has analyzed the decay processes of this state to be the ro-vibronic predissociation into the ground state and the electric-dipole radiational one into the lower $2s\ ^2A_1'$ Rydberg

state[43-44]. When the H_3 species in this $2p_z\ ^2A_2''$ state is rotationless, the ro-vibronic coupling becomes zero and the only decay channel left is the slow radiation process to the lower $2s\ ^2A_1'$ Rydberg state (which has been estimated to be about 90 μsec[48]) and to the ground state due to deviations from the Frank-Condon approximation or via higher order transition moments. Many experiments have taken advantage of the fact that some μseconds after the generation of the excited H_3 species, all H_3 molecules in excited electronic states have decayed away, except those in the rotationless $2p_z\ ^2A_2''$ Rydberg state. This greatly reduces and simplifies the observed spectrum since the initial state has been naturally prepared to be in this specific Rydberg state.

As discussed earlier, the radiation and predissociation decay processes involve at least two electronic states. A full understanding of these processes is possible only after the potential energy surfaces, the nuclear ro-vibrational structure and dynamics on these potential energy surfaces, and the electric dipole transition moment and the non-adiabatic coupling element between the two electronic states involved are known. This has been the major motivation for the present work.

In recent years, a chemical dynamical method named Transition State Spectroscopy (TTS), which involves two or more potential energy surfaces, attracted a lot of attention[81-89]. For the H_3 system, the continuum radiation absorption spectrum between the ground electronic state and the third excited electronic state (in the D_{3h} nuclear geometry, they correspond to one of the $2p_{x,y}\ ^2E'$ states and the $2p_z\ ^2A_2''$ state) has been studied theoretically and the results have shown many phenomena that reveal the rich and complex dynamics between these two potential energy surfaces[81-89]. In these studies, the potential energy surface of the excited state and the electric dipole transition moment

between these two states were obtained not from an accurate *ab initio* calculation but from a less accurate DIM (diatom-in-molecule) method[84], while the LSTH surface was used for the ground state. Any improvement in the calculation of the excited potential energy surface and the electric dipole transition moment will make the theoretical studies closer to reality and improve the comparison between the theoretical and experimental results.

The potential energy surface of the first excited state of H_3 has also been obtained by Varandas and co-workers[14] using the functional extrapolation scheme of the DMBE method, since this state is degenerate with the ground state and together their potential energy surfaces form a conical intersection in the equilateral triangle nuclear configuration. The dominant non-adiabatic coupling elements between these two states are also obtained. Because the DMBE functional extrapolation is valid only in the close vicinity of the conical intersection, the potential energy surface in regions far away from the conical intersection might not be accurate[14]. So far, the quantum scattering calculations[64-75] of the H + H_2 system have been carried out on the single ground electronic potential energy surface, even though the geometric phase[90] induced by the conical intersection between the ground and first excited states has been demonstrated to have a profound effect on the ro-vibrational level structure of the upper state (in the absence of coupling to the ground state) and may be important for the reaction scattering on the ground state at energy above 2.2 eV[91-99]. When the total energy of H + H_2 scattering system approaches 2.75 eV, which is the lowest value of the first excited potential energy surface, it is necessary to study the H_3 scattering process with both electronic potential energy surfaces included, because the Born-Oppenheimer separation of these two surfaces is not valid anymore.

In summary, a consistent and coherent study of the lowest four electronic potential energy surfaces is necessary in the understanding of:

- the ro-vibrational structure of the metastable H_3 $2p_z$ $^2A_2''$ Rydberg species, and
- the lifetime associated with both the radiation and predissociation processes for those ro-vibrational bound nuclear states;
- the transition state spectroscopy of H_3 between the ground state and the third excited state;
- the quantum scattering dynamics at high total energy ($\geq$ 2.75 eV).

Bound ro-vibrational bound states

The calculation of the bound ro-vibrational nuclear states on a single potential energy surface that supports bound nuclear motion is also of great importance, as it offers the second part of the quantum study of a molecular system (the first one being the study of the electronic motion). There are two reasons for making such studies for H_3. The first is the theoretical understanding of the ro-vibrational structure of H_3 in the metastable Rydberg electronic states. Comparison between the calculated energy levels and the experimental ones serves as the ultimate test for the accuracy of the potential energy surface obtained from the electronic structure calculation. The second motivation is that bound ro-vibrational nuclear wave functions are needed in the accurate calculation of both the radiation lifetime and the predissociation lifetime, and also of other chemically interesting dynamical processes such as the transition state spectroscopy.

Overview

As the first step toward calculating the lifetimes of the $2p_z\ ^2A_2''$ state of H_3, we have initiated a quantum study of its electronic and nuclear ro-vibrational motions. In chapter 2 of this thesis, we present the Schrödinger equation for molecular systems, and discuss the Born-Oppenheimer approximation to its solution. The bound molecular ro-vibrational structure and the chemical dynamics involving single or double potential energy surfaces are also discussed, along with the effect of the electronically non-adiabatic coupling elements. In chapter 3, the *ab initio* calculation of the lowest four electronic state potential energy surfaces of H_3 is presented. The results for the ground state and the third excited state have been fitted by an easy-to-use mathematical form. In chapter 4, a variational study of bound ro-vibrational states on the DMBE first excited potential energy surface is presented. The non-adiabatic coupling between the ground and the first excited electronic states of H_3 has been neglected in this model calculation. The same study using a hyperspherical propagation method is presented in chapter 5, with the full identical permutation symmetry embedded into the calculation as well as the geometric phase[97]. In chapter 6, the bound ro-vibrational levels on the third excited potential energy surface (that for the $2p_z\ ^2A_2''$ state) are obtained, using a variational method. The ro-vibrational level spacings are compared with the corresponding experimental values. A summary is presented in chapter 7.

1.2. References

1. J.O. Hirschfelder, H. Eyring and N. Rosen, *J. Chem. Phys.* **4**, 121 (1936).
2. R.N. Poter and M. Karplus, *J. Chem. Phys.* **40**, 1105 (1964).
3. H. Conroy and B.L. Brunner, *J. Chem. Phys.* **42**, 4047 (1965).
4. I. Shavitt, R.M. Stevens, F.L. Minn and M. Karplus, *J. Chem. Phys.* **48**, 2700 (1968).
5. R.N. Porter, R.M. Stevens and M. Karplus, *J. Chem. Phys.* **49**, 5163 (1968).
6. B. Liu, *J. Chem. Phys.* **58**, 1925 (1973).
7. P. Siegnahn and B. Liu, *J. Chem. Phys.* **68**, 2457 (1978).
8. A.J.C. Varandas and J. Tennyson, *Chem. Phys. Lett.* **77**, 181 (1981).
9. A.A. Wu, *Mol. Phys.*, **38**, 843 (1979).
10. A.A. Wu, *Mol. Phys.*, **42**, 379 (1981).
11. C.W. Eaker and L.R. Allard, *J. Chem. Phys.* **74**, 1821 (1981).
12. M.R.A. Blomberg and B. Liu, *J. Chem. Phys.* **82**, 1050 (1985).
13. D.G. Truhlar and C.J. Horowitz, *J. Chem. Phys.* **68**, 2466 (1978).
14. A.J.C. Varandas, F.B. Brown, C.A. Mead, D.G. Truhlar and N.C. Blais, *J. Chem. Phys.* **86**, 6258 (1987).
15. G.D. Carney and R.N. Porter, *J. Chem. Phys.* **60**, 4251 (1974).
16. R. Gengenbach, Ch. Hahn, J.P. Toennies, *J. Chem. Phys.* **62**, 3620 (1975).
17. G.C. Schatz and A. Kuppermann, *J. Chem. Phys.* **65**, 4668 (1976).
18. R.T. Ling and A. Kuppermann, in *Electronic and Atomic Collisions, Abstract of the 9th International Conference on the Physics of Electronic and Atomic Collisions*, Seattle, Washington, 24–30 July 1975, Vol. 1, eds. J.S. Risley, R. Geballe (Univ. Washington Press, Seattle, 1975) pp. 353-354.
19. A. Kuppermann and P.G. Hipes, *J. Chem. Phys.* **84**, 5962 (1986).
20. P.G. Hipes and A. Kuppermann, *Chem. Phys. Lett.* **133**, 1 (1987).

21. S.A. Cuccaro, P.G. Hipes and A. Kuppermann, *Chem. Phys. Lett.* **154**, 155 (1989).

22. S.A. Cuccaro, P.G. Hipes and A. Kuppermann, *Chem. Phys. Lett.* **157**, 440 (1989).

23. G.A. Parker, R.T. Pack, B.J. Archer, and R.B. Walker, *Chem. Phys. Lett.* **137**, 564 (1987).

24. R.T. Pack and G.A. Parker, *J. Chem. Phys.* **87**, 3888 (1987).

25. J. Linderberg, S. Padkjaer, Y Öhrn, and B. Vessal, *J. Chem. Phys.* **90**, 6254 (1989).

26. B. Lepetit, J.M. Launay and M. Le Dourneuf, *Chem. Phys.* **106**, 103 (1986).

27. J.M. Launay and M. Le Dourneuf, *Chem. Phys. Lett.* **163**, 178 (1989).

28. J.Z.H. Zhang and W.H. Miller, *Chem. Phys. Lett.* **140**, 329 (1987).

29. J.Z.H. Zhang and W.H. Miller, *Chem. Phys. Lett.* **159**, 130 (1989).

30. G.C. Schatz, *Chem. Phys. Lett.* **150**, 92 (1988).

31. J.Z.H. Zhang, D.J. Kouri, K. Haug, D.W. Schwenke, Y. Shima, and D.G. truhlar, *J. Chem. Phys.* **88**, 2492 (1988).

32. M. Mladenovic, M. Zhao, D.G. Truhlar, D.W. Schwenke, Y. Sun, and D.J. Kouri, *Chem. Phys. Lett.* **146**, 358 (1988).

33. C.H. Yu, D.J. Kouri, M. Zhao, and D.G. Truhlar, *Chem. Phys. Lett.* **157**, 491 (1989).

34. D.E. Manopoulos and R.E. Waytt, *Chem. Phys. Lett.* **159**, 123 (1989).

35. F. Webster and J.C. Light, *J. Chem. Phys.* **90**, 300 (1989).

36. F.M. Devienne, J.C. Rousteau, *Acad. Sci. Paris*, **263B**, 1389 (1966); **267B**, 1279 (1968); **268B**, 1303 (1969).

37. T. Nagasaki, H. Doi, K. Wada, K. Higashi, and F. Fukuzawa, *Phys. Lett.*, **A 38**, 381 (1972).

38. N.V. Castro de Faria, M.J. Gaillard, J.C. Poizat, and J. Remillieuz, *Ann. Isr. Phys. Soc.*, **4**, 134 (1981)

39. C. Cisneros, I. Alverez, G.R. Garcia, C.F. Burnett, J.A. Ray, and A. Russek, *Phys. Rev.*, **A 19**, 631 (1979).

40. M. Vogler, *Phys. Rev.* **A 19**, 1 (1979).

41. J.K.G. Watson, *Phys. Rev.* **A 22**, 2279 (1980).

42. P.M. Curtis, B.W. Williams, and R.F. Porter, *Chem. Phys. Lett.* **65**, 296 (1979).

43. H. Herzberg, *J. Chem. Phys.* **70**, 4806 (1979).

44. I. Dabrowski and G. Herzberg, *Can. J. Phys.*, **58**, 1238 (1980).

45. G. Herzberg and J.G.K. Watson, *Can. J. Phys.*, **58**, 1250 (1980).

46. G. Herzberg, H. Lew, J.J. Sloan, and J.K.G. Watson, *Can. J. Phys.*, **59**, 428 (1981).

47. G. Herzberg, J.T. Hougen, and J.K.G. Watson, *Can. J. Phys.*, **60**, 1261 (1982).

48. G.I. Gellene and R.F. Porter, *J. Chem. Phys.* **79**, 5975 (1983).

49. J.F. Garvey and A. Kuppermann, *Chem. Phys. Lett.* **107**, 491 (1984).

50. J.F. Garvey and A. Kuppermann, *J. Chem. Phys.* **86**, 6766 (1987).

51. J.F. Garvey and A. Kuppermann, *J. Chem. Phys.* **88**, 5985 (1988).

52. S.J. Jeon, A.B. Raksit, G.I. Gellen, and R.F. Porter, *J. Chem. Phys.* **82**, 4916 (1985).

53. Hanspeter Helm, *Phy. Rev. Lett.*, **56**, 42 (1986).

54. Hanspeter Helm, *Phy. Rev. A*, **38**, 3425 (1988).

55. Hanspeter Helm, *Phy. Rev. Lett.*, **61**, 298 (1988).

56. H. Helm, L.J. Lembo, P.C. Cosby and D.L. Huestis, "Fundamentals of Laser Interactions."edited by Ehlotzky, p. 264-289 (Springer-Verlag, 1989).

57. A. Dodhy, W. Ketterle, H.P. Messmer and H. Walther, *Chem. Phys. Lett.* **151**, 133 (1988).

58. S.F. Selgren and G.I. Gellene, *Chem. Phys. Lett.* **146**, 485 (1988).

59. H. Figger, M.N. Dixit, R. Maier, W. Schrepp, and H. Walther, and I.R. Peterkin and J.G.K. Watson, *Phys. Rev. Lett.*, **52**, 906 (1984).

60. H. Figger, Y. Fukuda, W. Ketterle, and H. Walther, *Can. J. Phys.*, **62**, 1274 (1984).

61. A.B. Raksit, R.F. Porter, W.P. Garver, and J.J. Leventhal, *Phys. Rev. Lett.*, **55**, 378 (1985).

62. W. Ketterle, H.P. Messmer and H. Walther, *Europhys. Lett.*, **8**, 333 (1989).

63. Wolfgang Ketterle, *Chem. Phys. Lett.* **160**, 139 (1989).

64. E. Frenkel, *Z. Natureforsch. Teil*, **A 25**, 1265 (1970).

65. J.N. Murrell and A.J.C. Varandas, *Mol. Phys.*. **81**, 1129 (1976).

66. H.F. King and K. Morokuma, *J. Chem. Phys.* **71**, 3213 (1979).

67. M. Jungen, *J. Chem. Phys.* **71**, 3540 (1979).

68. R.L. Martin, *J. Chem. Phys.* **71**, 3541 (1979).

69. K.C. Kulander and M.F. Guest, *J. Phys.* **B 12**, L501 (1979).

70. A.V. Zaitsevskii, A.V. Nemukhin and N.F. Stepanov, *Mol. Phys.*, **41**, 377 (1980).

71. Ch. Nager and M. Jungen, *Chem. Phys.* **70**, 189 (1982).

72. S. Raynor and D.R. Herschbach, *J. Phys. Chem.* **86**, 3592 (1982).

73. A.C. Roach and P.J. Kuntz, *J. Chem. Phys.* **84**, 822 (1986).

74. I. Petsalakis, J. Theodorakopoulos and J.S. Wright, *J. Chem. Phys.* **89**, 6850 (1988).

75. G.H.F. Diercksen, W. Duch and J. Karwowski, *Chem. Phys. Lett.* **168**, 69 (1990).

76. G. Herzberg, *Ann. Rev. Phys. Chem.* **38**, 27 (1987).

77. J.K.G. Watson, in press.

78. G.I. Gellene and R.F. Porter, *Acc. Chem. Res.*, **23**, 141 (1990).

79. G. Herzberg, in: *Spectra of Diatomic Molecules*, Van Nostrand, Princeton, 2nd. edition, 1950.

80. G. Herzberg, in: *Electronic Spectra and Electronic Structure of Polyatomic Molecules*, Van Nostrand, Princeton, 2nd. edition, 1950.

81. H.J. Foth, H.R. Mayne, R.A. Poirier, J.C. Polanyi and H.H. Teller, *Laser Chem.*, **2**, 229 (1983).

82. H.R. Mayne, R.A. Poirier and J.C. Polanyi, *J. Chem. Phys.* **80**, 4025 (1984).

83. V. Engel, Z. Bacic, R. Schinke and M. Shapiro, *J. Chem. Phys.* **82**, 4844 (1984).

84. H.R. Mayne, J.C. Polanyi, N. Sathyamurthy and S. Raynor, *J. Chem. Phys.* **88**, 4064 (1984).

85. V. Engel and R. Schinke, *Chem. Phys. Lett.* **122**, 103 (1985).

86. P.M. Agrawal, V. Mohan, and N. Sathyamurthy, *Chem. Phys. Lett.* **114**, 343 (1985).

87. B.A. Collings, J.C. Polanyi, M.A. Stolow, and J.W. Tarr, *Phys. Rev. Lett.*, **59**, 2551 (1987).

88. T. Seidenman and M. Shapiro, *J. Chem. Phys.* **88**, 5525 (1988).

89. J.L. Krause and M. Shapiro, *J. Chem. Phys.* **90**, 6401 (1989).

90. M.V. Berry, *Proc. Roy. Soc.* **A 392**, 45 (1984).

91. C.A. Mead and D.G. Truhlar, *J. Chem. Phys.* **49**, 23 (1979).

92. C.A. Mead, *Chem. Phys.* **49**, 23 (1980).

93. H.C. Longguet-Higgins, U. Opik, M.H.L. Pryce and R.A. Sack, *Proc. Roy. Soc.* **A 244**, 1 (1958).

94. G. Herzberg and H.C. Longguet-Higgins, *Disc. Far. Soc.* **35**, 77 (1963).

95. H.C. Longguet-Higgins, *Advan. Spectry.* **2** 429 (1961).

96. C. Alen Mead, *Chem. Phys.* **49**, 23 (1980).

97. B. Lepetit, Z. Peng and A. Kuppermann, *Chem. Phys. Lett.* **166**, 572 (1990).

98. C. Alen Mead, *J. Chem. Phys.* **72**, 3839 (1980).

99. B. Lepetit and A. Kuppermann, *J. Chem. Phys.* **166**, 581 (1990).

1.3. Figure and caption

Fig. 1. Energy level and correlation diagram for H_3. The energy spacing of the H_3 energy levels was obtained theoretically for an equilateral triangle configuration[66] and referred to the energy of dissociated products by the results of a separated calculation[69].

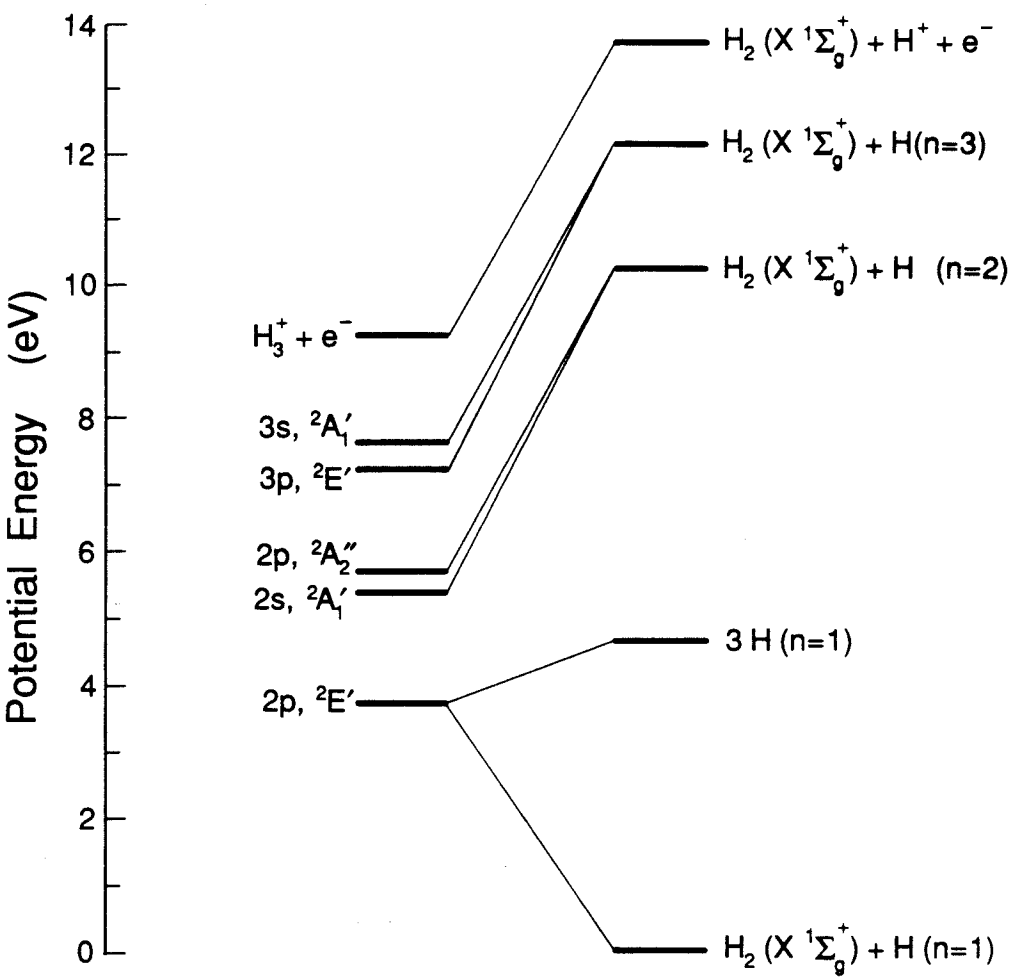
Potential Energy (eV)
14
12
10
8
6
4
2
0
$H_2 (X\ ^1\Sigma_g^+) + H^+ + e^-$
$H_2 (X\ ^1\Sigma_g^+) + H(n=3)$
$H_2 (X\ ^1\Sigma_g^+) + H\ (n=2)$
$H_3^+ + e^-$
3s, $^2A_1'$
3p, $^2E'$
2p, $^2A_2''$
2s, $^2A_1'$
2p, $^2E'$
3 H (n=1)
$H_2 (X\ ^1\Sigma_g^+) + H\ (n=1)$

Fig. 1

Chapter 2

Formulation of the Quantum Study of the H_3 System

In this chapter, a brief overview of the quantum mechanics of polyatomic molecules is presented. Several important concepts like the Born-Oppenheimer separation of the electronic and nuclear motions, potential energy surfaces, and electronically non-adiabatic coupling elements are discussed. Several dynamical processes in a molecular system are discussed briefly. It will serve as a starting point for our present electronic and nuclear calculation. At the end, the exact forms of the non-adiabatic coupling terms are presented in a molecular body-fixed coordinate system.

2.1. Born-Oppenheimer expansion

For an isolated molecular system with N_e electrons and N_n nuclei, the Hamiltonian of the system can be expressed in the form[1-2]

$$\hat{H}_t = \hat{T}_N + \hat{T}_e + V_{Ne} \tag{1}$$

$\hat{T}_N$ and $\hat{T}_e$ are the kinetic energy operators of the nuclei and the electrons respectively. V_{Ne} is the Coulomb interaction energy between all charged particles. They can be expressed as

$$\hat{T}_N = \sum_{A=1}^{N_n} -\frac{\hbar^2}{2M_A}\nabla_A^2 \tag{2}$$

$$\hat{T}_e = \sum_{i=1}^{N_e} -\frac{\hbar^2}{2m}\nabla_i^2 \tag{3}$$

$$V_{Ne} = \sum_{A>B=1}^{N_n} \frac{Q_A Q_B}{|\,\mathbf{R}_A - \mathbf{R}_B\,|} - \sum_{A=1,i=1}^{N_n,N_e} \frac{Q_A e}{|\,\mathbf{R}_A - \mathbf{r}_i\,|} + \sum_{i>j=1}^{N_e} \frac{e^2}{|\,\mathbf{r}_i - \mathbf{r}_j\,|} \tag{4}$$

i j and A B are indexes for the electrons and nuclei respectively. The Q_A and M_A are the charge and mass of the A'th nucleus. $\mathbf{R}_A$ and $\mathbf{r}_i$ are the coordinate vectors of A'th nucleus and i'th electron with respect to a laboratory reference frame. The Coulomb interaction only depends on the relative positions of all charged particles and hence is invariant under any rigid translation and rotation of the whole molecule. In Eq. (1) we have neglected all spin containing and relativistic terms. For molecules formed by light atoms, these terms are small, and their effects can be accurately included *a posteriori* by low order perturbation methods.

The Schrödinger equation for the molecular system is:

$$\hat{H}_t \Psi(\mathbf{r},\ \mathbf{R}) = E\Psi(\mathbf{r},\ \mathbf{R}) \tag{5}$$

This equation is extremely difficult to solve directly because it is a second order partial differential equation in a $3(N_n + N_e)$-dimensional space. To simplify its treatment, use is made of the large difference in mass of the electrons and nuclei. To that effect we define an electronic Hamiltonian $\hat{H}_e$ as

$$\hat{H}_e = \hat{T}_e + V_{Ne} \tag{6}$$

For each set of fixed nuclear coordinate variables $\{\mathbf{R}\}$, there is a set of adiabatic solutions $\{\mid \phi_k(\mathbf{r};\ \mathbf{R})\rangle\}$ that satisfy

$$\hat{H}_e \mid \phi_k(\mathbf{r};\ \mathbf{R})\rangle = E_k(\mathbf{R}) \mid \phi_k(\mathbf{r};\ \mathbf{R})\rangle \tag{7}$$

Here $\mathbf{r}$ and $\mathbf{R}$ represent all electronic and nuclear coordinate variables respectively. Notice that the wave functions $\mid \phi_k(\mathbf{r};\ \mathbf{R})\rangle$ and the eigenvalues $E_k(\mathbf{R})$ depend on the nuclear coordinates. The index k represents the set of all quantum numbers needed to specify the eigenfunctions $\mid \phi_k(\mathbf{r};\ \mathbf{R})\rangle$. In general the spectrum E_k of this set of solutions can include a discrete as well

as a continuous part (for example, in an ionization process). Usually only the discrete electronic spectrum is considered. This set of functions then forms a discrete orthonormal electronic basis set that satisfies

$$\langle \phi_k(\mathbf{r};\ \mathbf{R}) \mid \phi_{k'}(\mathbf{r};\ \mathbf{R}) \rangle = \delta_{k,k'} \tag{8}$$

The integral in Eq. (8) is over all electronic coordinate variables, and Eq. (8) is valid for all nuclear configurations $\{\mathbf{R}\}$.

We now expand the total wave function in this electronic basis set of functions

$$\Psi(\mathbf{r},\ \mathbf{R}) = \sum_k \chi_k(\mathbf{R}) \mid \phi_k(\mathbf{r};\ \mathbf{R}) \rangle \tag{9}$$

The coefficients $\chi_k(\mathbf{R})$ in this expansion are functions of the nuclear coordinates and are called the nuclear wave functions. Using Eqs. (5) to (9), the set of coupled equations that the $\chi_k(\mathbf{R})$ must satisfy are easily found to be

$$\{\hat{T}_N + E_k(\mathbf{R})\}\chi_k(\mathbf{R}) + \sum_{k'} F_{k,k'}(\mathbf{R})\chi_{k'}(\mathbf{R}) + \sum_{k'} G_{k,k'}(\mathbf{R})\chi_{k'}(\mathbf{R}) = E\chi_k(\mathbf{R}) \tag{10}$$

where

$$F_{k,k'}(\mathbf{R}) = \sum_{A=1}^{N_n} \langle \phi_k \mid -\frac{\hbar^2}{M_A}\nabla_A \mid \phi_{k'} \rangle \cdot \nabla_A \tag{11}$$

$$G_{k,k'}(\mathbf{R}) = \sum_{A=1}^{N_n} \langle \phi_k \mid -\frac{\hbar^2}{2M_A}\nabla_A^2 \mid \phi_{k'} \rangle \tag{12}$$

where the integration is over all electronic coordinates. The coupling terms $F_{k,k'}(\mathbf{R})$ and $G_{k,k'}(\mathbf{R})$ are named electronically non-adiabatic coupling terms.

If these electronically non-adiabatic terms are neglected, Eq. (10) gives the usual Born-Oppenheimer approximation[3]

$$\{\hat{T}_N + E_k(\mathbf{R})\}\chi_{k,\nu}(\mathbf{R}) = E\chi_{k,\nu}(\mathbf{R}) \tag{13}$$

and the total wave function expansion in Eq. (9) reduces to a single term which is the product of the electronic wave function and the nuclear wave function

$$\Psi_{k,\nu}(\mathbf{r},\ \mathbf{R}) = \chi_{k,\nu}(\mathbf{R}) \mid \phi_k(\mathbf{r};\ \mathbf{R})\rangle \tag{14}$$

where ν is the set of quantum numbers which describes the nuclear wave function. It can be discrete (for bound rotational and vibrational molecular motions) or continuous (for processes of scattering and chemical reactions). The $E_k(\mathbf{R})$ is named the potential energy surface of the $\mid \phi_k(\mathbf{r};\ \mathbf{R})\rangle$ electronic state. It acts as an effective interaction potential between nuclei.

The Born-Oppenheimer approximation enables us to decompose the total molecular motion into the electronic part and the nuclear part, which are solutions of two different equations (Eq. (7) and Eq. (13)). It greatly reduces the difficulties in solving Eq. (5), and is the fundamental building block of molecular physics.

2.2. Chemical dynamics on a single potential energy surface or on several non-interacting surfaces

The possible physical and chemical processes of a molecular system involving just a single potential energy surface (that is, in a single electronic state) are many. The equilibrium structure of the molecule can be obtained by locating the global and local minima of the potential energy surface. The surface might support bound nuclear ro-vibrational states with discrete energy levels. In some situations, rotational and vibrational transitions can be observed between those energy levels. If the surface is purely repulsive, or the total energy is high enough to be in the continuous region of the spectrum of the nuclear motion, the scattering process can be studied to give information on the dynamics of molecular collision and the breaking and forming of chemical bonds[4-23].

A radiation field can couple two molecular states on two different non-interacting potential energy surfaces. In the limit of a weak radiation field, the perturbation coupling strength can be obtained from the famous Fermi Golden Rule as[24]

$$\langle \chi_{k.\nu}\phi_k \mid \hat{O}_r \mid \phi_{k'}\chi_{k',\nu'} \rangle \tag{15}$$

where $\mid \chi_{k.\nu}\phi_k \rangle$ and $\mid \phi_{k'}\chi_{k',\nu'} \rangle$ are the initial and final total wave functions and $\hat{O}_r$ is the coupling operator between the molecule and the radiation field. The electric dipole interaction usually is the dominant term in $\hat{O}_r$. Again the nuclear wave functions can be discrete or continuous. The bound-to-bound transition is what is observed in ordinary spectroscopic experiments, with discrete lines of the spectrum. The bound-to-continuous transitions provide continuous spectra with the possibility of some fine structures embedded in the continuous background, as observed in Transition State Spectroscopy experiments[25-33]. So far, the continuum-to-continuum transition has not received much attention. Although spectra of this kind are relatively featureless, and experiments are hard to do, it offers an exciting research field of laser-assisted chemical reactions that might have great possibilities in the future[34-38].

2.3. Chemical dynamics involving two interacting potential energy surfaces

When the electronically non-adiabatic coupling terms neglected in the Born-Oppenheimer approximation are important, we must go back to the coupled equations (Eq. (10)) for the correct solution. In most cases, the coupling terms are very small, which means that a perturbative treatment can be used. Furthermore when couplings between only two of the electronic states are important, as is usually the case when the Born-Oppenheimer approximation

breaks down, we can employ the two-state approximation and limit our attention to those two interacting electronic states.

In the case where only discrete total wave functions are involved, the electronically non-adiabatic terms will shift the positions of the eigen-energies of those discrete states. Those shifts caused by the electronically non-adiabatic couplings have been observed in spectroscopic experiments as they introduce irregularities in the spectral lines[39-41]. For the case of continuum-to-continuum interactions, the electronically non-adiabatic terms can introduce new chemical reaction channels, and this topic itself is an interesting subject in quantum scattering studies[42-47].

The case of a discrete bound state interacting with a continuous state deserves special attention because the coupling will give the bound state a finite probability to decay into the continuous one and become a quasi-bound metastable state. This process is named predissociation. We will consider a simple treatment in order to understand its essence.

Fano's theory of predissociation[48-49]

In the simplest case, there are two quantum states of a system associated with the Hamiltonian $\hat{H}$. One is a discrete and bound state denoted as $\mid \phi_n\rangle$ and the other one continuous and unbound, denoted as $\mid E\rangle$. They are not exact eigenstates of $\hat{H}$ and satisfy only the following conditions:

$$\langle \phi_n \mid \phi_n \rangle = 1 \tag{16}$$

$$\langle \phi_n \mid E \rangle = 0 \tag{17}$$

$$\langle E \mid E' \rangle = \delta(E - E') \tag{18}$$

$$\langle \phi_n \mid \hat{H} \mid \phi_n \rangle = E_n \tag{19}$$

$$\langle E \mid \hat{H} \mid E' \rangle = E\delta(E - E') \tag{20}$$

$$\langle \phi_n \mid \hat{H} \mid E \rangle = V_n(E) \tag{21}$$

where n designates the set of quantum numbers that label the bound state, and E is the energy for the unbound state. $V_n(E)$ is the coupling between the bound and unbound states and is usually very small. We expand the true eigenstate of $\hat{H}$ as

$$\mid \Psi_n(E) \rangle = A_n(E) \mid \phi_n \rangle + \int B_n(E', E) \mid E' \rangle dE' \tag{22}$$

where

$$\hat{H} \mid \Psi_n(E) \rangle = E \mid \Psi_n(E) \rangle \tag{23}$$

It satisfies the normalization condition

$$\langle \Psi_n(E) \mid \Psi_n(E') \rangle = \delta(E - E') \tag{24}$$

After replacing Eq. (22) into Eq. (23) and using Eqs. (14) to (21) and Eq. (24), the result is

$$\mid A_n(E) \mid^2 = \frac{\mid V_n(E_n) \mid^2}{(E - E_n - \Delta_n)^2 + \pi^2 \mid V_n(E_n) \mid^4} \tag{25}$$

$$\Delta_n = \mathrm{P} \int \frac{\mid V_n(E') \mid^2}{E - E'} dE' \tag{26}$$

where P means principal part.

We now switch from the time-independent description to the time-dependent one in order to analyze the decay process. Let us prepare the system in state $\mid \phi_n \rangle$ at $t = 0$. The system then evolves with time as

$$\mid \Psi(t) \rangle = \int \langle \Psi_n(E) \mid \phi_n \rangle \mid \Psi_n(E) e^{-iEt/\hbar} dE \tag{27}$$

After a simple and straightforward integral over the energy variables, we find that the probability $P_n(t)$ of finding the system still in the bound $\mid \phi_n \rangle$ state at time t is

$$P_n(t) = \exp(-t/\tau_n) \tag{28}$$

where

$$\tau_n = \frac{\hbar}{2\pi \mid V_n(E_n) \mid^2} \tag{29}$$

The above discussion can be generalized to where one bound state is coupled with many unbound states $\mid E, m\rangle$, as happens when the final predissociated system can be characterized by the set of quantum numbers m describing the internal states of the fragments. The result is

$$\tau_n = \frac{\hbar}{2\pi \sum_m \mid V_n^m(E_n) \mid^2} \tag{30}$$

with the coupling between the bound state $\mid \phi_n\rangle$ and the mth unbound state $\mid E, m\rangle$ as

$$V_n^m(E) = \langle \phi_n \mid \hat{H} \mid E, m\rangle \tag{31}$$

The non-adiabatic terms in the coordinate system used are relatively simple as expressed in Eqs. (11) and (12). There is one drawback in this formulation, however, namely that these non-adiabatic coupling terms $F_{k,k'}$ and $G_{k,k'}$ are obtained in a coordinate system that does not take advantage of the simple motion of the center of mass of the molecule, and of the rigid rotation of the molecule. Furthermore, the electronic wave functions are usually obtained in the body-fixed coordinate system of the nuclei. For this reason, body-fixed coordinates are used to describe the electronic and internal nuclear motions of the molecular system. The form of the Hamiltonian operators for the electronic motion, nuclear motion, and of the non-adiabatic coupling terms for the H_3 system will be present explicitly.

2.4. The triatomic system H_3

First we introduce Jacobi coordinates to separate the motion of the center of mass from the internal motion[50-51]. These coordinates are depicted in Fig. 1. In this new coordinate system, the total Hamiltonian of the internal motion could be expressed as:

$$\hat{H}_t = -\frac{\hbar^2}{2M}\nabla^2_{\mathbf{R}_{cm}} - \frac{\hbar^2}{2\mu_{\mathbf{R}}}\nabla^2_{\mathbf{R}} - \frac{\hbar^2}{2\mu_{\mathbf{r}}}\nabla^2_{\mathbf{r}} + \sum_{i=1}^{3} -\frac{\hbar^2}{2\mu_i}\nabla^2_{\mathbf{r}_i} + V \tag{32}$$

M is the mass and $\mathbf{R}_{cm}$ the position vector of the center of mass of the whole system, $\mu_{\mathbf{R}}$ and $\mu_{\mathbf{r}}$ are the reduced masses for $\mathbf{R}$ and $\mathbf{r}$ respectively. The μ_i are the reduced masses of $\mathbf{r}_i$.

$$M = M_A + M_B + M_C + 3m \tag{33}$$

$$\mu_{\mathbf{r}} = \frac{M_A M_B}{M_A + M_B} \tag{34}$$

$$\mu_{\mathbf{R}} = \frac{M_C(M_A + M_B)}{M_A + M_B + M_C} \tag{35}$$

$$\mu_1 = \frac{m(M_A + M_B + M_C)}{M_A + M_B + M_C + m} \tag{36}$$

$$\mu_2 = \frac{m(M_A + M_B + M_C + m)}{M_A + M_B + M_C + 2m} \tag{37}$$

$$\mu_3 = \frac{m(M_A + M_B + M_C + 2m)}{M_A + M_B + M_C + 3m} \tag{38}$$

If we remove the term related to the motion of the center of mass of the system, and express the kinetic energy operators in terms of their radial and angular components, we get:

$$\hat{H} = -\frac{\hbar^2}{2\mu_{\mathbf{R}}}\frac{1}{R}\frac{\partial^2}{\partial R^2}R - \frac{\hbar^2}{2\mu_{\mathbf{r}}}\frac{1}{r}\frac{\partial^2}{\partial r^2}r + \frac{\mathbf{l}^2}{2\mu_{\mathbf{R}}R^2} + \frac{\mathbf{j}^2}{2\mu_{\mathbf{r}}r^2} + \sum_{i=1}^{3} -\frac{\hbar^2}{2\mu_i}\frac{1}{r_i}\frac{\partial^2}{\partial r_i^2}r_i + \sum_{i=1}^{3}\frac{\mathbf{j}_i^2}{2\mu_i r_i^2} + V \tag{39}$$

Here l, j, and $\mathbf{j}_i$ are the angular momenta associated with **R**, **r**, and $\mathbf{r}_i$ respectively. In space-fixed coordinates, angular momenta are expressed in terms of the angular variables for the system $(\phi_{\mathbf{R}}, \theta_{\mathbf{R}}, \phi_{\mathbf{r}}, \theta_{\mathbf{r}}, \phi_{\mathbf{r}_i}, \theta_{\mathbf{r}_i})$.

2.4.1. Body-fixed coordinates

Since the system is isolated, the square J^2 of the total angular momentum **J** and its projection J_Z onto the space-fixed Z axis commute with the Hamiltonian $\hat{H}$ and hence could have good quantum numbers. We now define two body-fixed coordinate systems[52]. The body-fixed 1 system is defined by rotating the space-fixed axis, moved to the center of mass of the molecule, by Euler angles $(\phi_{\mathbf{R}}, \theta_{\mathbf{R}}, 0)$, where $(\phi_{\mathbf{R}}, \theta_{\mathbf{R}})$ are the polar angles of **R** in that space-fixed system. The z_1 axis of the body-fixed 1 system is orientated along **R**. The body-fixed 2 system is then obtained by rotating the body-fixed 1 system by Euler angles $(0, 0, \psi_{\mathbf{r}})$ where $\psi_{\mathbf{r}}$ is the angle between the **RZ** and **R**, **r** half-planes measured counter clockwise as viewed from the positive **R** axis. The z_2 axis coincides with the z_1 axis (*i.e.*, lies along **R**) and the x_2 axis lies in the **R**, **r** plane such that the $x_{\mathbf{r}}$ component of **r** is positive. The body-fixed 2 system can be obtained directly from the space-fixed one by rotation through Euler angles $(\phi_{\mathbf{R}}, \theta_{\mathbf{R}}, \psi_{\mathbf{r}})$.

In the body-fixed 2 system, the vector **R** needs only one coordinate R to be uniquely specified; the vector **r** needs two variables, r and the angle $\gamma_{\mathbf{r}}$ between **r** and **R** (or z_2). The position vectors of the electrons in this body-fixed 2 system require three polar coordinates each to be specified which we label r_i, $\xi_{\mathbf{r}_i}$, and $\gamma_{\mathbf{r}_i}$. The angular variables we will use to specify the angular momenta appearing in Eq. (39) are therefore $\phi_{\mathbf{R}}$, $\theta_{\mathbf{R}}$, $\psi_{\mathbf{r}}$, $\gamma_{\mathbf{r}}$, $\xi_{\mathbf{r}_1}$, $\gamma_{\mathbf{r}_1}$, $\xi_{\mathbf{r}_2}$, $\gamma_{\mathbf{r}_2}$, $\xi_{\mathbf{r}_3}$, $\gamma_{\mathbf{r}_3}$ It is easy to see that if we change the first three of these angles and keep the rest of them unchanged, the whole system undergoes a rigid-body rotation and the relative positions between the particles remain unchanged. These first three angles can

be considered as the Euler angles of the system which describe rigid rotations of the system. In what follows, we will drop the $\mathbf{R}$ subscript in $\phi_{\mathbf{R}}$, $\theta_{\mathbf{R}}$ and the $\mathbf{r}$ subscript in $\psi_{\mathbf{r}}$, $\gamma_{\mathbf{r}}$.

The total wave function of the system which is a simultaneous eigenfunctios of $\hat{H}$, J^2 and J_Z will be labeled Ψ^{JM}. It can be written in the form

$$\Psi^{J,M}(\mathbf{r}_i,\mathbf{R},\mathbf{r}) = \sum_{\Omega} D^J_{M,\Omega}(\phi,\theta,\psi)\Phi^{J,\Omega}(\gamma,\xi_{\mathbf{r}_i},\gamma_{\mathbf{r}_i},R,r,r_i) \tag{40}$$

$D^J_{M,\Omega}(\phi,\theta,\psi)$ is the Wigner function[53] and satisfies the following equations:

$$\mathbf{J}^2 D^J_{M,\Omega}(\phi,\theta,\psi) = J(J+1)\hbar^2 D^J_{M,\Omega}(\phi,\theta,\psi) \tag{41}$$

$$J_Z D^J_{M,\Omega}(\phi,\theta,\psi) = M\hbar D^J_{M,\Omega}(\phi,\theta,\psi) \tag{42}$$

$$J_{z_2} D^J_{M,\Omega}(\phi,\theta,\psi) = \Omega\hbar D^J_{M,\Omega}(\phi,\theta,\psi) \tag{43}$$

The equations that the $\Phi^{J,\Omega}(\gamma,\xi_{\mathbf{r}_i},\gamma_{\mathbf{r}_i},R,r,r_i)$ satisfy can be obtained from the equations above[52] and are

$$\hat{H}^J_{\Omega,\Omega-1}\Psi^J_{\Omega-1} + \hat{H}^J_{\Omega,\Omega}\Psi^J_{\Omega} + \hat{H}^J_{\Omega,\Omega+1}\Psi^J_{\Omega+1} = E\Psi^J_{\Omega} \tag{44}$$

The definition of the operators appearing in Eq. (44) are

$$\hat{H}^J_{\Omega,\Omega\pm1} = \frac{\xi_{\pm}(J,\Omega)}{2\mu_{\mathbf{R}}R^2}\{\hbar^2[(\Omega\pm1)\cot\gamma \pm \frac{\partial}{\partial\gamma}] - \hbar[\cot\gamma L_{z2} + L^{bf2}_{\pm}]\} \tag{45}$$

$$\begin{aligned}\xi_{\pm}(J,\Omega) &= [(J\pm\Omega+1)(J\mp\Omega)]^{\frac{1}{2}} \\ &= [J(J+1)-\Omega(\Omega\pm1)]^{\frac{1}{2}}\end{aligned} \tag{46}$$

In order to specify the expressions for the operators $\hat{H}^J_{\Omega,\Omega\pm1}$ and $\hat{H}^J_{\Omega,\Omega}$, we introduce the total electronic angular momentum $\mathbf{L}$ of the system:

$$\mathbf{L} = \sum_{i=1}^{3}\mathbf{j}_{\mathbf{r}_i} \tag{47}$$

In terms of it, the system's total angular momentum is given by

$$\mathbf{J} = \mathbf{l} + \mathbf{j} + \mathbf{L} \tag{48}$$

$\hat{H}^J_{\Omega,\Omega}$ can be written as

$$\begin{aligned}
\hat{H}^J_{\Omega,\Omega} = & -\frac{\hbar^2}{2\mu_{\mathbf{R}}}\frac{1}{R}\frac{\partial^2}{\partial R^2}R - \frac{\hbar^2}{2\mu_{\mathbf{r}}}\frac{1}{r}\frac{\partial^2}{\partial r^2}r \\
& + \frac{\hbar^2}{2\mu_{\mathbf{R}}R^2}\{[J(J+1) - 2\Omega^2] - (\frac{\partial^2}{\partial\gamma^2} + \cot\gamma\frac{\partial}{\partial\gamma} - \frac{\Omega^2}{\sin^2\gamma})\} \\
& + \frac{\hbar^2}{2\mu_{\mathbf{r}}r^2}\{-(\frac{\partial^2}{\partial\gamma^2} + \cot\gamma\frac{\partial}{\partial\gamma} - \frac{\Omega^2}{\sin^2\gamma})\} \\
& + \frac{1}{2\mu_{\mathbf{R}}R^2}\Big\{L^2_{bf2} + (\cot^2\gamma - 1)L^2_{z2} - \cot\gamma L_{z2}(L^{bf2}_+ + L^{bf2}_-) \\
& - 2\hbar\Omega\cot^2\gamma L_{z2}\Big\} \\
& + \frac{1}{2\mu_{\mathbf{R}}R^2}\{-\hbar\Omega\cot\gamma(L^{bf2}_+ + L^{bf2}_-) - \hbar(\cot\gamma + \frac{\partial}{\partial\gamma})(L^{bf2}_+ - L^{bf2}_-)\} \\
& + \frac{1}{2\mu_{\mathbf{r}}r^2}\frac{1}{\sin^2\gamma}\{L^2_{z2} - 2\hbar\Omega L_{z2}\} \\
& + \sum_{i=1}^{3} -\frac{\hbar^2}{2\mu_i}\frac{1}{r_i}\frac{\partial^2}{\partial r_i^2}r_i + \sum_{i=1}^{3}\frac{\mathbf{j}_i^2}{2\mu_i r_i^2} + V
\end{aligned} \tag{49}$$

with Ω having $(2J+1)$ values from $-J$ to J.

2.4.2. Born-Oppenheimer expansion

Following tradition, we define an electronic Hamiltonian in the **Body-fixed 2** coordinate system

$$\hat{H}_e = \sum_{i=1}^{3} -\frac{\hbar^2}{2\mu_i}\frac{1}{r_i}\frac{\partial^2}{\partial r_i^2}r_i + \sum_{i=1}^{3}\frac{\mathbf{j}_i^2}{2\mu_i r_i^2} \tag{50}$$

and use this $\hat{H}_e$ operator to define an electronic basis set $\{|\phi_n(\mathbf{r}_i; R, r, \gamma)\rangle\}$ which depends on the nuclear coordinates (R, r, γ) only parametrically and does

not depend on the Euler angles (ϕ, θ, ψ) of the total system. These electronic functions satisfy

$$\hat{H}_e|\phi_n(\mathbf{r}_i; R, r, \gamma)\rangle = E_n(R, r, \gamma)|\phi_n(\mathbf{r}_i; R, r, \gamma)\rangle \tag{51}$$

where n is the set of quantum numbers which specifies the electronic eigenstate. This basis set is orthonormal and Ω-independent:

$$\langle\phi_n(\mathbf{r}_i; R, r, \gamma)|\phi_{n'}(\mathbf{r}_i; R, r, \gamma)\rangle = \delta_{n,n'} \tag{52}$$

We are not interested in the continuous spectrum of the electronic wavefunction as we will only consider states in which all electrons are bound. It should be kept in mind that the masses for electrons are not m but μ_1, μ_2 and μ_3, although the difference is really small.

Let us expand the total wavefunction of the system in products of the Wigner rotation function, the electronic basis function, and the nuclear wavefunction:

$$|\Psi^{J,M}(\mathbf{r}_i, \mathbf{R}, \mathbf{r})\rangle = \sum_n \sum_\Omega D^J_{M,\Omega}(\phi, \theta, \psi)|\phi_n(\mathbf{r}_i; R, r, \gamma)\rangle|\chi^{J,\Omega}_n(R, r, \gamma)\rangle \tag{53}$$

Let's put Eq. (53) into the Schrödinger equation Eq. (44) of the total system, and multiply the result with $\langle\phi_n(\mathbf{r}_i; R, r, \gamma)|$, then integrate over all electronic variables. Using the orthonormality property in Eq. (52), we get the equations which the nuclear wavefunctions $|\chi^{J,\Omega}_n(R, r, \gamma)\rangle$ have to satisfy.

$$\sum_n \{\langle\phi_m|H^J_{\Omega,\Omega-1}|\phi_n\chi^{J,\Omega-1}_n\rangle + \langle\phi_m|H^J_{\Omega,\Omega+1}|\phi_n\chi^{J,\Omega+1}_n\rangle$$
$$+\langle\phi_m|H^J_{\Omega,\Omega}|\phi_n\chi^{J,\Omega}_n\rangle\} = E|\chi^{J,\Omega}_m\rangle \tag{54}$$

The expanded form of Eq. (54) is complicated:

$$
\begin{aligned}
&\frac{\xi_-(J,\Omega)}{2\mu_{\mathbf{R}}R^2}\{\hbar^2[(\Omega-1)\cot\gamma+\frac{\partial}{\partial\gamma}]\}|\chi_m^{J,\Omega-1}\rangle \\
&-\frac{\xi_-(J,\Omega)}{2\mu_{\mathbf{R}}R^2}\hbar\sum_n\langle\phi_m|-\hbar\frac{\partial}{\partial\gamma}+\cot\gamma L_{z_2}+L_-^{bf2}|\phi_n\rangle|\chi_n^{J,\Omega-1}\rangle \\
&\frac{\xi_+(J,\Omega)}{2\mu_{\mathbf{R}}R^2}\{\hbar^2[(\Omega+1)\cot\gamma-\frac{\partial}{\partial\gamma}]\}|\chi_m^{J,\Omega+1}\rangle \\
&-\frac{\xi_+(J,\Omega)}{2\mu_{\mathbf{R}}R^2}\hbar\sum_n\langle\phi_m|\hbar\frac{\partial}{\partial\gamma}+\cot\gamma L_{z_2}+L_+^{bf2}|\phi_n\rangle|\chi_n^{J,\Omega+1}\rangle \\
&\{-\frac{\hbar^2}{2\mu_{\mathbf{R}}}\frac{1}{R}\frac{\partial^2}{\partial R^2}R-\frac{\hbar^2}{2\mu_{\mathbf{r}}}\frac{1}{r}\frac{\partial^2}{\partial r^2}r+\frac{\hbar^2}{2\mu_{\mathbf{R}}R^2}[J(J+1)-2\Omega^2] \\
&-(\frac{\hbar^2}{2\mu_{\mathbf{R}}R^2}+\frac{\hbar^2}{2\mu_{\mathbf{r}}r^2})(\frac{\partial^2}{\partial\gamma^2}+\cot\gamma\frac{\partial}{\partial\gamma}-\frac{\Omega^2}{\sin^2\gamma})\}|\chi_m^{J,\Omega}\rangle \\
&+\sum_n\Big\{\langle\phi_m|-\frac{\hbar^2}{\mu_{\mathbf{R}}}\frac{\partial}{\partial R}|\phi_n\rangle\frac{\partial}{\partial R}+\langle\phi_m|-\frac{\hbar^2}{\mu_{\mathbf{r}}}\frac{\partial}{\partial r}|\phi_n\rangle\frac{\partial}{\partial r} \\
&+\langle\phi_m|-(\frac{\hbar^2}{\mu_{\mathbf{R}}R^2}+\frac{\hbar^2}{\mu_{\mathbf{r}}r^2})\frac{\partial}{\partial\gamma}-\frac{\hbar}{2\mu_{\mathbf{R}}R^2}(L_+^{bf2}-L_-^{bf2})|\phi_n\rangle\frac{\partial}{\partial\gamma}\Big\}|\chi_n^{J,\Omega}\rangle \\
&+\sum_n\Big\{\langle\phi_m|-\frac{\hbar^2}{2\mu_{\mathbf{R}}}\frac{1}{R}\frac{\partial^2}{\partial R^2}R|\phi_n\rangle+\langle\phi_m|-\frac{\hbar^2}{2\mu_{\mathbf{r}}}\frac{1}{r}\frac{\partial^2}{\partial r^2}r|\phi_n\rangle \\
&-(\frac{\hbar^2}{2\mu_{\mathbf{R}}R^2}+\frac{\hbar^2}{2\mu_{\mathbf{r}}r^2})\langle\phi_m|\frac{\partial^2}{\partial\gamma^2}+\cot\gamma\frac{\partial}{\partial\gamma}|\phi_n\rangle \\
&+\frac{1}{2\mu_{\mathbf{R}}R^2}\langle\phi_m|L_{bf2}^2+(\cot^2\gamma-1)L_{z_2}^2-\cot\gamma L_{z_2}(L_+^{bf2}+L_-^{bf2})-2\hbar\Omega\cot^2\gamma L_{z_2} \\
&-\hbar\Omega\cot\gamma(L_+^{bf2}+L_-^{bf2})-\hbar(\cot\gamma+\frac{\partial}{\partial\gamma})(L_+^{bf2}+L_-^{bf2})|\phi_n\rangle \\
&+\frac{1}{2\mu_{\mathbf{r}}r^2}\frac{1}{\sin^2\gamma}\langle\phi_m|L_{z_2}^2-2\hbar\Omega L_{z_2}|\phi_n\rangle\Big\}|\chi_n\rangle \\
&=\{E-E_m(R,r,\gamma)\}|\chi_m^{J,\Omega}\rangle
\end{aligned}
\tag{55}
$$

Here $L_\pm^{bf2}$ are the usual step-up and step-down operators in the body-fixed 2 system associated with the total electronic angular momentum $\mathbf{L}$. The integrals are respect to all electronic coordinate variables in the body-fixed 2 system. Although the equation is messy, we can still identify that there are three kinds

of electronically non-adiabatic coupling elements. The first is associated with the change of the nuclear shape. It contains the operators $\frac{\partial}{\partial R}$, $\frac{\partial}{\partial r}$, $\frac{\partial}{\partial \gamma}$, and also second derivatives in these variables. Elements of the second kind contain L_{z_2}, $L_{\pm}^{bf2}$ and L_{bf2}^{2} which involve derivatives with respect to the electronic angular coordinates only. The third kind has terms like $L_{\pm}^{bf2}\frac{\partial}{\partial \gamma}$ involving derivatives with respect to both electronic angular coordinates and γ. The definition of $\mathbf{L}^{bf2}$ clearly shows that all terms containing L^{bf2} are related to the relative rotation of all electrons with respect the fixed nuclei.

The exact treatment is also available for diatomic molecules[54-56]. Our treatment actually can be generalized easily for all triatomic systems. Of course, even though Eq. (55) offers the exact equation of the H_3 system, so far, its complexity has prevented any attempt to obtain an exact solution. The most important of these electronically non-adiabatic coupling elements are likely to be those involving derivatives with respect to R, r, and γ, in analogy to the case of diatomic molecules.

2.5. References

1. A.C. Hurley, *Introduction to the Electron Theory of Small Molecules*, (Academic Press, 1976), Ch. 1.
2. E.E. Nikitin and L. Zülicke, *Theory of Elementary Processes*, Lecture Notes in Chemistry, (Springer-Verlag,1978).
3. M. Born and J.R. Oppenheimer, *Ann. Phys.*, **84**, 458 (1927).
4. D.C. Clary (editor), *The Theory of Chemical Reaction Dynamics*, (D. Reidel, 1985).
5. G.C. Schatz and A. Kuppermann, *J. Chem. Phys.* **65**, 4668 (1976).
6. R.T. Ling and A. Kuppermann, in *Electronic and Atomic Collisions, Abstract of the 9th International Conference on the Physics of Electronic and Atomic Collisions*, Seattle, Washington, 24–30 July 1975, Vol. 1, eds. J.S. Risley, R. Geballe (Univ. Washington Press, Seattle, 1975) pp. 353-354.
7. A. Kuppermann and P.G. Hipes, *J. Chem. Phys.* **84**, 5962 (1986).
8. P.G. Hipes and A. Kuppermann, *Chem. Phys. Lett.* **133**, 1 (1987).
9. S.A. Cuccaro, P.G. Hipes and A. Kuppermann, *Chem. Phys. Lett.* **154**, 155 (1989).
10. S.A. Cuccaro, P.G. Hipes and A. Kuppermann, *Chem. Phys. Lett.* **157**, 440 (1989).
11. G.A. Parker, R.T. Pack, B.J. Archer, and R.B. Walker, *Chem. Phys. Lett.* **137**, 564 (1987).
12. R.T. Pack and G.A. Parker, *J. Chem. Phys.* **87**, 3888 (1987).
13. J. Linderberg, S. Padkjaer, Y Öhrn, and B. Vessal, *J. Chem. Phys.* **90**, 6254 (1989).
14. B. Lepetit, J.M. Launay and M. Le Dourneuf, *Chem. Phys.* **106**, 103 (1986).
15. J.M. Launay and M. Le Dourneuf, *Chem. Phys. Lett.* **163**, 178 (1989).

16. G.C. Schatz, *Chem. Phys. Lett.* **150**, 92 (1988).

17. J.Z.H. Zhang and W.H. Miller, *Chem. Phys. Lett.* **140**, 329 (1987).

18. J.Z.H. Zhang and W.H. Miller, *Chem. Phys. Lett.* **159**, 130 (1989).

19. J.Z.H. Zhang, D.J. Kouri, K. Haug, D.W. Schwenke, Y. Shima, and D.G. truhlar, *J. Chem. Phys.* **88**, 2492 (1988).

20. M. Mladenovic, M. Zhao, D.G. Truhlar, D.W. Schwenke, Y. Sun, and D.J. Kouri, *Chem. Phys. Lett.* **146**, 358 (1988).

21. C.H. Yu, D.J. Kouri, M. Zhao, and D.G. Truhlar, *Chem. Phys. Lett.* **157**, 491 (1989).

22. D.E. Manopoulos and R.E. Waytt, *Chem. Phys. Lett.* **159**, 123 (1989).

23. F. Webster and J.C. Light, *J. Chem. Phys.* **90**, 300 (1989).

24. M. Weissbluth, *Atoms and Molecules*, (Academic Press, 1978), p. 299-301.

25. H.J. Foth, H.R. Mayne, R.A. Poirier, J.C. Polanyi and H.H. Teller, *Laser Chem.*, **2**, 229 (1983).

26. H.R. Mayne, R.A. Poirier and J.C. Polanyi, *J. Chem. Phys.* **80**, 4025 (1984).

27. V. Engel, Z. Bacic, R. Schinke and M. Shapiro, *J. Chem. Phys.* **82**, 4844 (1984).

28. H.R. Mayne, J.C. Polanyi, N. Sathyamurthy and S. Raynor, *J. Chem. Phys.* **88**, 4064 (1984).

29. V. Engel and R. Schinke, *Chem. Phys. Lett.* **122**, 103 (1985).

30. P.M. Agrawal, V. Mohan, and N. Sathyamurthy, *Chem. Phys. Lett.* **114**, 343 (1985).

31. B.A. Collings, J.C. Polanyi, M.A. Stolow, and J.W. Tarr, *Phys. Rev. Lett.*, **59**, 2551 (1987).

32. T. Seidenman and M. Shapiro, *J. Chem. Phys.* **88**, 5525 (1988).

33. J.L. Krause and M. Shapiro, *J. Chem. Phys.* **90**, 6401 (1989).

34. M. Shapiro and P. Brumer, *J. Chem. Phys.* **84**, 4103 (1986).

35. P. Brumer and M. Shapiro, *Chem. Phys. Lett.* **126**, 1986 ().

36. P. Brumer and M. Shapiro, *Faraday. Dis.*, **82**, 177 (1986).

37. C. Asaro, P. Brumer and M. Shapiro, *Phys. Rev. Lett.*, **60**, 1634 (1988).

38. M. Shapiro and Y. Zeiri, *J. Chem. Phys.* **85**, 6449 (1986).

39. Hélène Lefebvre-Brion and R.W. Field, *Perturbations in the Spectra of Diatomic Molecules*, (Academic press, 1986).

40. G. Herzberg, in: *Spectra of Diatomic Molecules*, Van Nostrand, Princeton, 2nd. edition, 1950.

41. G. Herzberg, in: *Electronic Spectra and Electronic Structure of Polyatomic Molecules*, Van Nostrand, Princeton, 2nd. edition, 1950.

42. B.C. Garrett and D.G. Truhlar, in: *Theoretical Chemistry: Theory of Scattering: Papers in Honor of Henry Eying*, edited by D. Henderson, Vol **6A**, (Academic Press, 1981), p. 216-289.

43. F. Rebentrost, in: *Theoretical Chemistry: Theory of Scattering: Papers in Honor of Henry Eying*, edited by D. Henderson, **Vol 6B**, (Academic Press, 1981), p. 3-77.

44. M. Baer, in: *Theory of Chemical Reaction Dynamics*, edited by M. Baer, **Vol II**, (CRC Press, 1985), p. 219-280.

45. J.C. Tully and R.K. Preston, *J. Chem. Phys.* **55**, 562 (1971).

46. J.P. Braga, H. Guo, J.N. Murrell and L.J. Dunne, *Mol. Phys.*, **65**, 909 (1988).

47. B. Lepetit, J.M. Launay, and M. Le Dourneuf, *Chem. Phys.*, **117**, 17 (1987).

48. U. Fano, *Phy. Rev.*, **124**, 1866 (1961).

49. S.H. Lin (editor), *Radiationless Transitions*, (Academic Press, 1980).

50. L.M. Delves, *Nucl. Phys.*, **9**, 391 (1959).

51. L.M. Delves, *Nucl. Phys.*, **20**, 275 (1960).

52. A. Kuppermann, unpublished notes on *Considerations about Angular Momentum Operators and Derivation of Body-fixed Scattering Equations for N-particle Systems*, July, 1984.

53. A.S. Davydov, *Quantum Mechanics*, 2nd ed., (Pergamon Press, 1976), p. 151-161.

54. P.R. Bunker, *J. Mole. Spectr.*, **28**, 422 (1968).

55. R.L. Kronig, *Band Spectra and Molecular Structure*, (Cambridge Univ. Press, New York), p. 6-16 and p.40-44.

56. W.R. Thorson, *J. Chem. Phys.* **34**, 1744 (1961).

2.6. Figure and caption

Fig. 1. Jacobi coordinates of H_3. A, B, C and e_1, e_2, e_3 are the protons and electrons of the H_3 system respectively. **R** is defined as the vector from the center of mass of $\underline{AB}$ to C. $\mathbf{r}_1$ is defined as the vector from the center of mass of $\underline{ABC}$ to e_1, $\mathbf{r}_2$ from the center of mass of $\underline{ABCe_1}$ to e_2, and $\mathbf{r}_3$ from the center of mass of $\underline{ABCe_1e_2}$ to e_3. The position vector of the center of mass of the whole system with respect to a laboratory-fixed frame is not depicted. OXYZ is the coordinate system of the laboratory reference frame.

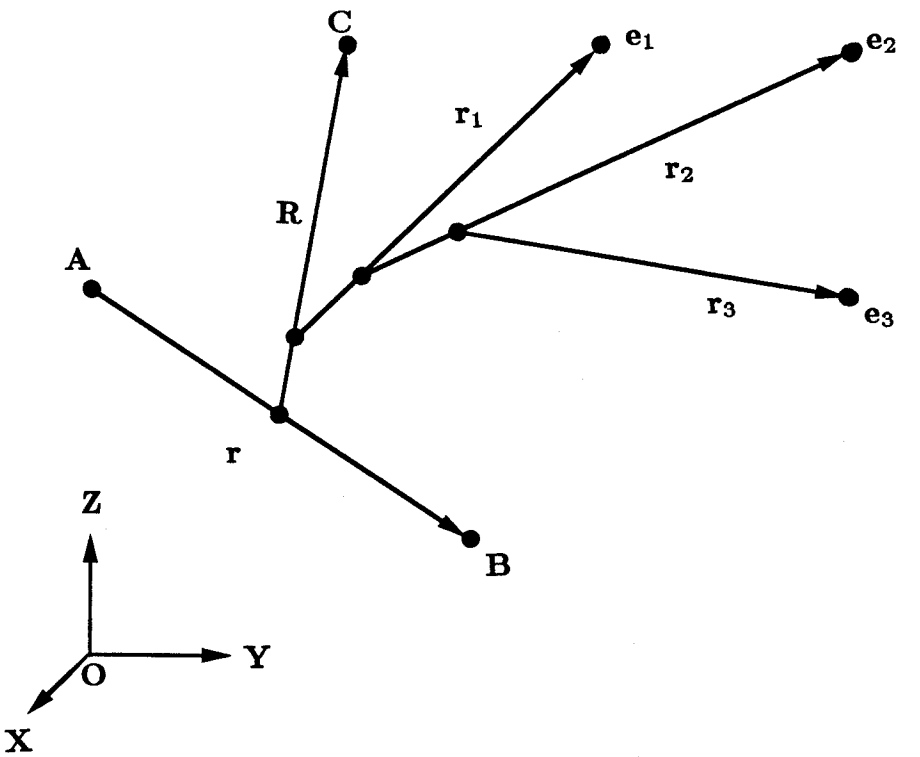

Fig. 1

Chapter 3

Ab Initio Calculation of the Lowest Four Electronic States of H_3

3.1. Introduction

The first step toward understanding not only the structure but also the dynamics of a molecular system, as mentioned in chapter 2, is to generate the potential energy surfaces of its electronic states. Furthermore, if physical or chemical processes involving multi-electronic states are of interest, the electronically non-adiabatic coupling matrix elements and (or) the radiation assisted coupling elements (such as the electric dipole transition moment) between two electronic states are also needed.

Some good global surfaces have been obtained for the $H + H_2$ reaction. The high quality ground electronic state potential energies calculated by Liu[1] and by Siegbahn and Liu[2] (hereafter LS) were fitted by Truhlar and Horowitz[3] to give the LSTH surface, which incorporated some scaling to produce accurate diatomic limits, and for several years provided a standard of accuracy for the field. The more recent double many-body expansion (DMBE) surface of Varandas and co-workers[4] provides another fit to LS's energy data. Although it has a larger rms error than that of the LSTH surface, the DMBE surface is believed to be more accurate at higher energies.

For excited states of the $H + H_2$ system, the number of available *ab initio* calculations is sparse and of small scale, although they are of considerable current interest. Important early work on the excited states of H_3 includes the theoretical study of Rydberg spectra of H_3 by King and Morokuma[5], Jungen[6], Martin[7], Kulander and Guest[8], Nager and Jungen[9], and Raynor and Herschbach[10], and

the series on transition state spectroscopy by Polanyi and co-workers[11-13]. A thorough study of excited electronic potential energy surfaces of H_3 was done by Roach and Kuntz[14] using the semiempirical DIM method. Some recent work on H_3 was done by Petsalakis, Theodorakopoulos and Wright[15] (hereafter PTW) and also by Diercksen and co-workers[16]. In general, most of the studies mentioned above were done in some limited range of nuclear geometric configurations, which were not sufficient to generate the full potential energy surfaces.

The major terms of the electronically non-adiabatic coupling elements near the equilateral triangle configuration of H_3 between the upper and lower sheets of the DMBE surface have been obtained through a functional analysis[4,17]. So far there have not been any direct calculations of the non-adiabatic coupling terms for any other pair of H_3 surfaces.

Reviews of the Rydberg spectra of H_3 have been given by Herzberg[18], Watson[19], and Gellene and Porter[20]. Fig. 1 shows the Rybderg electronic states of H_3 and the correlation diagram to its dissociated products. The $2p_z\ ^2A_2''$ electronic state has drawn a lot of attention in experimental work because it has been found experimentally to have a lifetime longer than 40 μsec.[22] (the theoretical estimation is about 90 μsec.[21]). The decay mechanisms of the H_3 species in this electronic state have been identified first by Herzberg and co-workers[23-27] as the electric dipole allowed transition to the $2s\ ^2A_1'$ state, and the predissociation to the unbound ground $2p_{xy}\ ^2E'$ electronic states. In order to understand these decay processes, and other dynamical processes involving the four low-lying electronic states of H_3 [11-13,21-22], we have calculated the electronic energy of these states using an *ab initio* quantum chemical method, along with the electric transition dipole moments between each pair of states. It

is obvious that the potential energy surface of the $2p_z\ ^2A_2''$ electronic state had the highest priority in our current study.

In the following sections, the general approach to calculating electronic states in molecular systems by the method we used - Multi reference single and double excitation configuration interaction (MRD-CI) - is outlined. The choice of atomic orbital (AO) basis set functions is then examined, the results obtained are discussed and compared with those of previous studies. Finally, the rotated Morse cubic spline (RMCS) fits to the potential energy surfaces for the ground and the third excited electronic states of H_3 are obtained.

3.2. Methodology

3.2.1 General considerations

In the clamped-nucleus Born-Oppenheimer approximation, with neglect of spin and other relativistic effects, the electronic Hamiltonian operator in atomic units for a molecule having n electrons and N nuclei in the absence of external fields, takes the form[28-29] (also see chapter 2)

$$\hat{H} = -\frac{1}{2}\sum_{i=1}^{n}\nabla_i^2 - \sum_{A=1}^{N}\sum_{i=1}^{n} Z_A r_{Ai}^{-1} + \sum_{i>j=1}^{n} r_{ij}^{-1} + \sum_{A>B=1}^{N} Z_A Z_B R_{AB}^{-1} \qquad (1)$$

Indexes i and j are used to label the electrons. Indexes A and B denote nuclei with charges Z_A and Z_B. r_{Ai} is the electron-nucleon distance, r_{ij} the electron-electron distance, and R_{AB} the nuclear-nuclear one. The terms in Eq. (1) comprise the electron kinetic energy, the nuclear–electron attraction, the electron repulsion, and the nuclear repulsion, respectively. This Hamiltonian commutes with all symmetry operations of the molecular point group. The goal is to obtain solutions to the time–independent electronic Schrödinger wave equation

$$\hat{H}\Psi = E\Psi \qquad (2)$$

This is a partial differential equation in $3n$ mathematical dimensions. The eigen-energy E is the potential energy surface, a function of all internal nuclear coordinate variables. Although some limited progress has been made in approaching Eq. (2) by analytical methods[30], this is a very difficult procedure that is not yet suited to the production of accurate results. Instead, most methods make (implicit or explicit) use of basis set expansion techniques and variational approaches. The unknown eigen-functions of Eq. (2) are expressed in terms of a set of n-particle basis functions $\{\Phi\}$. While it is possible to consider

rather exotic functional forms for the Φ, by far the most common approach is to construct each Φ using a product of molecular orbitals (MOs, one–electron functions) $\{\psi\}$:

$$\Phi_K = \hat{P} \prod_{i=1}^{n} \psi_i \tag{3}$$

Here a given function Φ_K involves an n–fold product of MOs, to which is applied the permutation operator $\hat{P}$ which ensures that the function Φ_K is anti–symmetric with respect to exchanges of any two electrons as required by Pauli principle. The Φ obtained in this way are generally referred to as configuration state functions (CSFs).

The molecular orbitals (MOs) are usually obtained as linear combinations of a one–particle basis

$$\psi_i = \sum_{\mu} C_{i\mu} \chi_\mu \tag{4}$$

The one-particle basis functions $\{\chi\}$ are often referred to as atomic orbitals (AOs). As a result, this scheme is also referred to as the linear-combination-of-atomic-orbital molecular-orbital method (LCAO-MO). The MO coefficients C are obtained by solving an electronic structure problem simpler than that of Eq. (2), such as the independent particle (Hartree-Fock self-consistent-field) approximation. It has the advantage that these approximations generally provide a rather good estimate of the solutions of Eq. (2) — perhaps 99% of the total energy or more — thus suggesting that an analysis of the many-electron problem and (possible) computational schemes for attacking it can be formulated around them. Since the Hartree–Fock method is an independent particle model, with the correlation of electrons neglected, the terms "correlation energy" and "correlation problem" have been coined by Löwdin[31] to denote respectively the difference

between the exact energy obtained from Eq. (2) and the Hartree–Fock energy, and the problem of computing this energy difference.

The most obvious use of the n–particle basis $\{\Phi\}$ in solving Eq. (2) is the linear configuration interaction (CI) expansion

$$\Psi = \sum_K c_K \Phi_K \tag{5}$$

If the one–particle basis is complete, the use of all possible Φ (complete CI) in Eq. (5) will yield the exact eigenvalues and eigenfunctions of Eq. (2). The coefficients c_K are determined by making the energy stationary with respect to variations in them, subject to normalization of Ψ; any guess at the c_K will yield an upper bound to the true energy.

In practice, a complete one-particle function space is infinite, which means that the complete CI problem is also infinite in dimension. If we choose a finite, truncated one–particle space, but approximate Ψ as in Eq. (5) using all the possible n–particle basis functions, we have a full CI wave function (FCI). It can be regarded as the exact solution to the Schrödinger equation projected onto the finite subspace generated by the truncated one–particle basis. The number of all the possible n–particle basis functions has a factorial dependence on the number of electrons correlated and the number of MOs. This can create insuperable computational difficulties for most problems of chemical interest. For example, in order to obtain the dissociation energy of the N_2 molecules to within 5 kcal/mole (about 0.22 eV) of the correct one, one requires about 10^{14} CSFs[29]. There are only a few FCI bench-mark calculations available that follow the advances of the supercomputer industry[32–37]. In real applications, especially in calculations

aimed at obtaining the potential energy surface of a molecular system, the n-particle space needs to be truncated as well for the practical reason of limited computer memory and speed.

A simple way to implement n–particle space truncation is to use the uncorrelated wave function (which as noted above is a very substantial fraction of the exact wave function) to classify terms in the n–particle space. If we consider the Hartree–Fock MOs, all CSFs in the full n–particle space can be constructed by successively exciting one, two, ... electrons from the occupied Hartree–Fock MOs to unoccupied ones. For cases in which several CSFs are present in the zeroth–order wave functions, the same formal classification can be applied to each reference CSF. It is possible however that the n–th excitation with respect to one reference CSF is the n'–th excitation ($n' > n$) with respect to another reference CSF. Since only singly and doubly excited CSFs can interact with the zeroth–order wave function via the Hamiltonian in Eq. (1), it is natural to truncate the n–particle expansion at this level, at least as a first approximation. We thus obtain single and double excitations from Hartree–Fock (denoted SDCI) or its multi–configurational reference analog, multi–reference CI (denoted MR–SDCI). The accuracy of this scheme of single and double excitation has been confirmed as good by recent full CI (FCI) bench–mark calculations[29].

Some properties of the truncated CI method are worth mentioning. It is variational in nature and therefore yields approximate energies which are upper bounds of the true ones. It can be readily formulated to handle the case in which the zeroth-order wave function is multi-configurational in character. It is one of the most widely used schemes in electronic state calculations nowadays.

3.2.2 MRD-CI method of Buenker

In some cases, even the use of a severely truncated CSF space can give rise to an MR-SDCI expansion that is too long for practical calculations. There are several ways to further reduce the dimension of the CSF space[38-44]. Here we outline the one developed by Buenker and co-workers[40-44], which we have used in our H_3 application. It is based on the individual configuration selection and energy extrapolation technique.

Since in most cases only several low-lying electronic states are of interest, the resulting eigenfunctions of those states usually are dominated by a very small number of CSFs with a very small contributions from the rest of the CSFs. It is conceivable that the removal of those CSFs with small contributions has a negligible effect on the final wave functions and their eigen-energies for those electronic states of interest. This suggests that this set of dominant CSFs can be used as a set of reference configurations and the full single and double excited CSFs (generated with respect to this set) can be tested individually to see if they are important or not. Let us assume that there are N_{ref} dominant reference configurations. First a small CI calculation with this limited set of N_{ref} reference configurations is performed and M eigenvalues of interest are obtained. Since this set of reference CSFs is made out of the dominant CSFs for those M eigenstates, we expect those M eigenvalues to be quite close to those obtained from the full MR–SDCI calculation. Then one by one, each generated single and double excited CSF with respect to the set of reference configurations is tested by being added to the reference configurations and another small scale CI calculation of $N_{ref} + 1$ CSFs is performed. The variational nature of CI ensures that each eigenvalue obtained by using $N_{ref} + 1$ CSFs is lower than the corresponding

eigenvalue from the CI calculation with N_{ref} reference CSFs. Only those CSFs that are able to lower the energy of any one of these M states by an amount bigger than a threshold energy (to be chosen at the beginning of the selection process) are included in the final CI calculation. Obviously, if the threshold is chosen to be very big, all generated single and double CSFs will fail the test and be rejected, while if the threshold is zero, all generated CSFs will pass the test and we return to the situation of a full MR–SDCI calculation. In order to ensure the convergence of the final CI calculation, the set of reference configurations has to be chosen to be big enough to include all possible dominant CSFs so that the final eigenfunction of each state of interest has at least 90% of its contribution from the set of reference configurations. This is a very effective way of drastically reducing the size of the final CI space without missing important contributions from any part of the full single and double excitation CI space.

As mentioned above, the resulting eigenvalues decrease with a decrease of the chosen threshold energy monotonically. Since the dominant CSFs are included in the set of reference configurations, the difference between the eigenvalues obtained using a big threshold and the eigenvalues obtained with the threshold being zero (full MR-SDCI limit) would be small. As Buenker and co-workers have pointed out, the eigen–value dependence on the threshold when the threshold is approaching zero is essentially linear[40–44]. It is possible that by using the results of two or more CI calculations with different but small enough thresholds, the eigen–values of zero threshold (MR–SDCI limit) can be obtained through extrapolation. This gives the eigen-energies at zero threshold without using in the actual CI calculation a possibly very large CSF space.

These two features of the MRD-CI (multi–reference single and double excitation configuration interaction) method of Buenker and co-workers have

been very successful in many applications[40-44]. The configuration selection procedure is equally applicable to all types of electronic states in any nuclear geometry, and the results of the associated CI calculations are seen to be essentially equivalent to a complete treatment in which all single and double excitation CSFs with respect to a set of dominant configurations (in those given states of interest) are included[40-44].

The Cray version of the MRD-CI codes we used was supplied directly by Buenker's group[40-44]. These codes do not have the capacity of calculating the electronically non-adiabatic coupling matrix elements between two electronic states, and will have to be modified in the future to permit such calculations. As pointed out in chapter 1, these elements are needed in treatment of multi-surface physical and chemical processes such as predissociation and collision-induced electronic transitions. The electric dipole transition moment between two electronic states can be handled by this MRD-CI package, with only a small fraction of the CPU time used, compared with the CPU time used in the CI energy calculation.

Without going into detail, the flowchart of this package is presented in Fig. 2 with some explanation about the functions. Conceptually, the following steps are taken in our H_3 application:

1. First, Gaussian-Type atomic orbitals (GTO) are used[45]. We will discuss the choice of AOs in detail in the next section.

2. In the second step, the Hartree–Fock Self–Consistent–Field (SCF) calculation with the AO set is conducted in an iterative manner. The molecular orbitals (MO) obtained from the SCF serve as the starting point for the CI calculation.

3. In the third step, an appropriate set of reference configurations for a given number of electronic states and a threshold energy are chosen. This might require several iterations to achieve that good. Then all single and double excitation CSFs with respect to the reference configurations are generated and selected.

4. The fourth step is the diagonalization of the electronic Hamiltonian, including all of the configurations selected.

5. Another iteration of Step 3 and Step 4, with the same set of reference configurations but a new threshold twice as large as the one used before is carried out. The extrapolation to zero threshold is performed based on the CI results with two different thresholds and finally the eigen-energies of the full single and double excitation (over the set of reference configurations) CI are obtained.

6. With the resulting electronic wave functions (from the CI calculation with the first threshold), the electric dipole transition moment between any two known electronic states is then calculated.

3.3. Atomic orbital basis set

In papers by Huzinaga[45], Wilson[46] and Davidson and Feller[47], there are good reviews in–depth on the basis set selection for molecular calculations. In this section, the general considerations for selecting a basis set for an *ab initio* calculation will be discussed, and several useful concepts introduced. We will then discuss the criteria of basis selection for our specific H_3 application and the basis set used in our work.

3.3.1 General considerations

All CI methods for electronic state calculations are based on the variational approach. Although in principle one complete set of basis functions is equivalent to any other complete set, in reality only finite size basis sets are practical. Since the computational effort goes up very quickly with the size of the basis set, the basis set of choice should be flexible enough to produce **good** results over the range of molecular geometries of interest on one hand, and still small enough to leave the problem computationally tractable and economically within reason on the other hand.

In the early days of quantum chemistry, the basis sets used were usually of the atom-centered Slater-type orbital form[48]. Slater-type orbitals (STO) are defined as:

$$\mathrm{X}_{nlm}(r,\theta,\phi) = \mathrm{R}_{nl}(r)\mathrm{Y}_{lm}(\theta,\phi) \tag{6}$$

$$\mathrm{R}_{nl}(r) = (2\xi)^{n+1/2}[(2n)!]^{-1/2} r^{n-1} e^{-\xi r}. \tag{7}$$

where l and m are angular momentum quantum numbers while Y_{lm} is the usual spherical harmonics. ξ_{nl} is the orbital exponent. The coordinate variables (r,θ,ϕ) describe the position of an electron with respect to the position of

the nucleus. The main advantages of STO are their short- and long-range behavior (the form of the exact radial wave functions of H atom is very close to that of STO-type functions). The major disadvantage is the difficulty of the numerical integrations required in molecular calculations involving this kind of basis functions.

In order to overcome this bottle-neck of numerical integrations in the process of constructing the Hamiltonian matrix, Gaussian-type orbitals (GTO) have been introduced by Boys[49]. They are defined as:

$$\mathrm{X}_{nlm}(r,\theta,\phi;\alpha) = \mathrm{R}_{nl}(r)\mathrm{Y}_{lm}(\theta,\phi) \tag{8}$$

$$\mathrm{R}_{nl}(r) = \mathrm{N}(n,\alpha)r^{n-1}e^{-\alpha r^2}. \tag{9}$$

$$\mathrm{N}(n,\alpha) = 2^{n+1}[(2n-1)!!]^{-1/2}(2\pi)^{-1/4}\alpha^{(2n+1)/2}, \tag{10}$$

$$n = l+1,\ l+3,\ l+5,....$$

where the !! sign indicates the product $(2n-1)(2n-3)(2n-5)\ldots$, α is a conventionally chosen range parameter and $N(n,\alpha)$ the normalization coefficient. In molecular calculations, the Cartesian coordinate system has been commonly used and the normalized, primitive GTOs in these coordinates are defined as[50–52]:

$$\mathrm{X}_{kmn}(x,y,z;\alpha) = \mathrm{N}(k,m,n;\alpha)x^k y^m z^n e^{-\alpha r^2} \tag{11}$$

$$\mathrm{N}(k,m,n;\alpha) = (2/\pi)^{3/4}[(2k-1)!!(2m-1)!!(2n-1)!!]^{-1/2}$$

$$\alpha^{[k+m+n+3/4)]/2} \tag{12}$$

Note that (k,m,n) in Eq. (11) are completely different from (n,l,m) in Eq. (8). Explicitly, the GTOs are of the following types:

$$\mathrm{s-type}: k+m+n=0$$

$$\mathrm{X} \propto e^{-\alpha r^2} \tag{13}$$

$$\mathrm{p-type}: k+m+n=1$$

$$\mathrm{X} \propto (x,y,z)e^{-\alpha r^2} \tag{14}$$

$$\mathrm{d-type}: k+m+n=2$$

$$\mathrm{X} \propto (x^2,y^2,z^2,xy,xz,yz)e^{-\alpha r^2} \tag{15}$$

The choice of the Cartesian primitive GTOs has been made for the practical reason of easy coding. However, this choice generates two important consequences that must be kept in mind. The first is a self-imposed restriction on the power of r in Eq. (9) for atomic calculation. The power is restricted to the lowest for each symmetry, $n = l + 1$. Only 1s-type GTOs are used to expand all s-type atomic orbitals, only 1p-type GTOs are used to expand all p-type atomic orbitals, and so on. Fortunately the combination of many 1s-type (or 1p-type) functions with different exponents αs provides enough flexibility to compensate for this restriction. The second consequence of the choice of the Cartesian primitive GTOs is the redundancy in the d- and higher symmetries. The d-orbitals can be viewed as a proper five-membered d-type orbital set plus one isotropic 3s-type orbital

$$(3z^2-r^2, x^2-y^2, xy, xz, yz)e^{-\alpha r^2} \tag{16}$$

$$(x^2+y^2+z^2)e^{-\alpha r^2} = r^2 e^{-\alpha r^2} \tag{17}$$

Similarly, the 10-membered f-type orbitals contains three redundant 4p-type orbitals

$$(x,y,x)r^2 e^{-\alpha r^2} \tag{18}$$

in addition to the proper seven-membered f-orbitals.

The exponents α and the number of GTO functions are parameters which need to be tuned to suit a given molecular system under investigation. Although more tunable parameters result in flexibility, too many can make the problem untractable, especially if there are too many exponents α which could only be optimized by a much time-consuming non-linear optimization process. Integrals involving GTOs cab be completed analytically which is a major reason for their choice. However because an individual Gaussian-type function has the wrong behavior both near the nucleus and far away from the nucleus, it is clear that more GTOs would be required to describe an atomic wave function than if STOs were used. On the other hand, integrals involving STOs at best are expensive and, at worse are intractable for molecules.

To some extent the disadvantage associated with the large number of GTOs (which means many parameters in the basis set need to be determined and optimized) compared to STOs is reduced by the introduction of **contracted** Gaussians[50-52]. In this scheme, the basis function for molecules becomes not individual Gaussian-type functions, but rather fixed linear combinations like

$$\mathrm{X}_{contr}(k,m,n) = \sum_i C_i \mathrm{X}_{kmn}(\alpha_i). \tag{19}$$

with the coefficients C_i chosen to give a good description of the atomic wave functions. It is easy to see that this scheme has the advantage of easy integration of primitive Gaussian-type functions, and at the same time gives a much better behavior to the basis functions. It also made the final basis set more compact. It has become a method of choice.

The first task in obtaining contracted basis functions is to choose a good set of primitive Gaussian-type functions. It is generally assumed that molecules can be viewed as a collection of slightly distorted atoms. It is therefore natural to

require that the primitive basis set provide an accurate description of the atoms. Most Gaussian primitive sets are constructed by optimization of the Hartree–Fock–Self–Consistent–Filed (SCF) energy of the atoms. This is definitely the case for the H atom since there is only one electron involved. The first optimized Gaussian primitive set for atomic SCF energies was published by Huzinaga[53]. After that, several improvements have been made[54−55]. Their results can be used directly for the choice of Gaussian primitives for any new calculation.

Inspection of the optimal exponents of a set of Gaussian primitives reveals that the ratio between successive exponents of the Gaussian primitives in the valence region is nearly constant. This fact suggests that an **even–tempered** or geometric sequence (that is, $\alpha_i = a * \beta^i$, where a and β are two parameters) of exponents would represent a good approximation to the independently optimized exponent set[56−57]. This offers a big reduction of the number of parameters needing to be optimized and makes the construction of the basis set much easier. Comparison between results from independent optimized exponent sets and even-tempered ones shows good agreements[58−59]. This scheme has also become the method of choice.

There are several ways to obtain the contraction coefficients. Since Slater-type functions provide better descriptions of atoms, several Gaussian-type functions are linearly combined together to mimic the behavior of a single Slater-type function (referred to in the literature as STO-nG scheme)[53]. The orbital exponents for STOs are chosen as the average best exponents from molecular calculations. The results of the STO-nG expansion will give the exponents and the the contraction coefficients needed. This method actually produces rather poor atomic energies. The second way is to obtain contraction coefficients through a direct optimization of atomic SCF calculations, treating

those coefficients as independent variables to be optimized. The last approach is the simultaneous optimization of the Gaussian exponents and contraction coefficients based on atomic SCF energies. It is quite clear that the first method is the easiest one (giving rather poor results) while the third one is the most accurate but the most time consuming one because of the non-linear optimization procedure.

3.3.2 Selection criteria and the basis set

Our goal is to achieve good descriptions for the lowest four electronic states of the H_3 system. Results from a previous empirical diatom-in-molecule (DIM) calculation[14] show that the lowest five states in the asymptotic region of H_2 + H correlate with the states

$$H_2(X\ ^1\Sigma_g^+) + H(1s)$$

$$H_2(X\ ^1\Sigma_g^+) + H(2s, 2p_x, 2p_y, 2p_z)$$

and

$$H_2(b\ ^3\Sigma_u^+) + H(1s) \rightarrow 3H(1s).$$

It is clear that our basis set of choice should be able to describe the atomic states of H(n=1) and H(n=2), and the lowest two diatomic states $H_2(X\ ^1\Sigma_g^+)$, and $H_2(b\ ^3\Sigma_u^+)$. In our study, the choice of an appropriate basis set for our H_3 application was determined by the necessity of obtaining the following:

1 . Accurate atomic excitation energies for $1s \rightarrow 2s$ and $1s \rightarrow 2p$ transitions.

2 . Accurate values for the H_2 energy in its ground electronic state $X\ ^1\Sigma_g^+$ and excited state $b\ ^3\Sigma_u^+$.

3 . A ground-state surface for H_3 of accuracy comparable to that of the LSTH surface.

4 . A reasonably good agreement with the known Rydberg spectrum of H_3 and the results of recent calculations of PTW[15] and Diercksen[16].

Since there are quite a few studies on the H_3^+ and the H_3 systems, both in their ground electronic states[1-2,60-62] and their Rydberg excited electronic states[5-16,63], the choice of basis sets used in those calculations has guided us in the selection of our basis functions.

After some experimentation, the basis sets used by Liu and Sieghban[2] for the ground state of H_3 and by Talbi and Saxon[63] for the Rydberg spectrum of H_3^+ were adapted for the present purpose. Those two sets of basis functions have been proven to provide good descriptions of the electronic valance bond and the Rydberg $n = 2$ states of H. The valence $(9s/4s)$ (four s-type contracted GTO basis functions obtained from nine s-type primitive GTO functions) basis was taken from LS, and has an outer exponent of 0.06618. Three more Rydberg s—functions were added, with an approximately even-tempered ratio of 2.4, giving exponents 0.02758, 0.01149 and 0.00420. The polarization/Rydberg p—basis was taken from Talbi and Saxon[63], with exponents 1.6, 0.4, 0.09 and 0.025. Finally, the 6-component d—function with exponent 1.0 was taken from LS[1,2]. The full basis set, denoted $(12s4p1d/7s4p1d)$ has therefore 25 contracted AOs, of which three s—functions and two p—functions are essentially Rydberg in nature. The parameters of the $(12s4p1d/7s4p1d)$ basis set are listed in Table 1.

In order to allow for proper dissociation, it was found necessary to place the full AO set on each nuclear center, for a total basis set size of 75 AOs. This is because we are interested in mapping out the potential energy surface over a wide range of nuclear geometric configuration, unlike previous work on the Rydberg states of H_3 with an equilateral triangle configuration (for example, in the study

of PTW[15], a set of diffuse Rydberg AOs were placed at the center of the H_3 equilateral triangle).

This diffuse overlapping basis of size 75 could lead to linear dependence problems[63]. To minimize the chance of this occurring, we used the HONDO routine[64] for evaluating the necessary integrals. The high accuracy of that routine led to no linear dependence when this basis set was used in our calculations.

As described in the following sections, the results from basis set calibrations show that this basis set satisfies all requirements we have set for all four lowest electronic states over the nuclear geometric configurations of present interest.

3.4. RMCS surface fitting method

The internal coordinate system of describing the shape of a triatomic molecule has three variables only such as the three internuclear distances R_1, R_2, and R_3. The energy results of the *ab initio* quantum calculations at many nuclear geometric configurations have to be fitted into some easy-to-use form $V(R_1, R_2, R_3)$ in order to be utilized in the studies of the dynamics of the molecular system. The need for this fitting arises because the *ab initio* calculations are sufficiently time consuming and expensive that explicit calculation of energies (and energy gradients) at every nuclear configurations needed in the dynamical studies is rarely feasible. In addition, *ab initio* energy data are not usually accurate enough to be used directly without at least some adjustment, and surface fitting procedures facilitate this adjustment. Furthermore, the analytical representation of the potential energy surfaces is proved to be essential for the visualization of the surface features and of the surface topological characters that may not be evident from a coarse-grained *ab initio* study (especially in the case of high dimensionality).

The surface fitting methods have been reviewed by many authors[65-70], and recently by Schatz[71]. In general, it would be desirable to ask that:

1: the fitting procedure be simple;

2: the resulting surface be in good agreement with the *ab initio* energy data inside the region of nuclear geometric configuration of interest;

3: the fitting functions have the right kind of functional form built into them such that it only takes a small number of *ab initio* points to obtain the surface with correct surface features and topology, since the *ab initio* calculations are expensive and time-consuming.

This can go the other way. After a brief exploration of a potential energy surface and an understanding of its main features and topology, a surface fitting method can be selected. Then the selection the nuclear geometric configuration points at which additional *ab initio* calculations need to be performed will be **guided carefully** by this fitting method. This will greatly reduce the number of points at which expensive *ab initio* calculations need to be performed, while ensuring the high accuracy of the fitting[72,73].

In our present application to the H_3 system, the rotated Morse cubic spline (RMCS)[74-76] method is used. It has been shown to satisfy most criteria of surface fittings[76], with many successful applications[72-73,77-79].

We use the two internuclear distances R_1 and R_2 and the bond angle γ between them in the description of the shape of the triatomic system, depicted in Fig. 3. For a fixed γ, we define a swing point $P_s(R_1^s, R_2^s)$ in the orthogonal Cartesian coordinate system formed by (R_1, R_2) and depicted in Fig. 4. In our application $R_1^s = R_2^s = 10.0$ bohr, well into the dissociation region of H_3[76,79]. For a point P in (R_1, R_2) coordinates, we define the distance l and the swing angle θ with respect to the swing point P_s as the internal coordinates instead of using R_1 and R_2 (see Fig. 4). In this coordinate system, $\theta = 0°$ corresponds to the ray at $R_2 = 10$ bohr, with R_1 variable. It also corresponds to the asymptotic region of separated H + H_2. For $\theta = 45°$, we get symmetric $R_1 = R_2$ configurations. Rays of constant θ were chosen at 0°, 20°, 30°, 35°, 40°, 41°, 42°, 43°, 44° and 45° for the *ab initio* calculations. Because of the symmetry of the identical particles in the H_3 system, $V(R_1, R_2, \gamma) = V(R_2, R_1, \gamma)$, which also leads to $V(l, \theta, \gamma) = V(l, \frac{\pi}{2} - \theta, \gamma)$. This symmetric property reduces the number of *ab initio* points needed by a factor of 2.

It is important to note that along a ray of constant θ (and for a given bond angle γ), most potential energy surfaces for low-lying electronic states have the shape of a Morse function, with the parameters of the Morse function depending on γ and θ. In order to achieve better fitting accuracy, a generalized Morse function with five parameters (GMF5) defined by

$$V = D_e\{(1 - e^{\beta x})^2 - 1\} \tag{20}$$

$$\beta = \beta_e(1 + \lambda_1 x + \lambda_2 x^2) \tag{21}$$

$$x = l - l_e \tag{22}$$

is used to represent the potential energy along such constant γ and θ cuts[80-81]. The variables are D_e (well depth relative to the swing point, in eV), l_e (distance in bohr from the minimum of the GMF5 function to the swing point), β_0 (curvature parameter in bohr^{-1}), λ_1 (linear correction to β_e in bohr^{-1}), and λ_2 (quadratic correction to β_0 in bohr^{-2}). Eq. (21) clearly requires that the magnitude of λ_1 and λ_2 should be small for the GMF5 function in Eq. (20) to behave like a Morse function. Those parameters for a given bond angle and swing angle $D_e(\gamma,\theta)$, $l_e(\gamma,\theta)$, $\beta_e(\gamma,\theta)$, $\lambda_1(\gamma,\theta)$, and $\lambda_2(\gamma,\theta)$ are obtained by fitting the *ab initio* data along the rays of constant (γ, θ) cut using the functional form in Eq. (20) and a non-linear least-square fitting technique[72].

Data points along the swing ray were taken at increments of 0.2 bohr in R_1 in the range of 1.0 bohr to 3.0 bohr where the bottoms of the GMF5 curves of the lowest four electronic states of present interest are located. Typically 7 to 9 data points were calculated per ray (giving the energies of the lowest four electronic states and the electric dipole transition moments for each point), with more points added when necessary. A similar treatment was used by Mayne *et al.*[12], who interpolated DIM data using a rotated Morse curve approach.

The Morse parameter data were reflected about $\theta = 45°$ to generate data at 19 θ-rays, and then the five Morse parameters were interconnected using cubic splines with a fixed γ. The reason for the reflection is that the correct first derivatives of the Morse parameters at $\theta = 45°$ are zero. Only by using data over 0° to 90° can cubic spline fits give first derivatives at $\theta = 45°$ equal to zero. The fit provided a set of five θ-dependent parameters ($D_e(\theta)$, etc.), which map out the (R_1, R_2) space for a given γ. Finally, the spline fits were examined for smoothness and any nonphysical oscillations were removed. Our results showed that only $\lambda_1(\theta)$ and $\lambda_2(\theta)$, the first order and second order corrections to $\beta_e(\theta)$, displayed roughness and needed to be smoothed.

Again, because of the P_3 permutation symmetry of the identical particles, the choice of the nuclei used to define R_1, R_2 and γ is arbitrary and the potential energy should be the same for all three possible choices of γ for a given configuration. This angle is always in the range of [0°, 180°]. If we always choose the largest bond angle γ_{max} and the corresponding two bond distances as the internal coordinate variables for the description of the triangle, the range of γ can be reduced by a factor of $\frac{3}{2}$ since the γ_{max} is in this case bigger than (or equal to) 60° and less than (or equal to) 180°. For this reason, the γ cuts of our *ab initio* calculation have been chosen to be at 60°, 90°, 120°, 150°, and 180°. Since we only perform *ab initio* calculations in the range of θ from 0° to 45° out of the full range from 0° to 90°, the number of *ab initio* points needed is reduced by a factor of 2. The choice of γ gives a reduction factor of $\frac{3}{2}$. So the total reduction factor we have achieved is $2 \times \frac{3}{2} = 3$. If the full P_3 symmetry is implemented, the total reduction factor would be 6. The remaining ambiguity in our present choice of γ and θ occurs for $60° < \gamma_{max} < 120°$. In this region,

there is a possibility that the second largest bond angle might be bigger than or equal to 60°

Ab initio calculations were made for the two-dimensional mesh of θ = 0°, 20°, 30°, 35°, 40°, 41°, 42°, 43°, 44°, 45°, and γ = 60°, 90°, 120°, 150°, 180° and 7 to 9 values along each γ = constant, θ = constant ray. The potential is assumed to have GMF5 form. For a given γ value, the GMF5 parameters for θ in the range of 45° to 90° are obtained by reflecting the GMF5 parameters in the range of 0° to 45° with respect to line of θ = 45°. After all values of the GMF5 parameters are known at all points of the (γ, θ) mesh, a full potential energy surface can be obtained by two-dimensional cubic spline fit method in the domain with $\gamma \in [60°, 180°]$. and $\theta \in [0°, 90°]$. For any given nuclear geometry R_1, R_2, and R_3, the corresponding variables $(l, \gamma = \gamma_{max}, \theta)$ can be obtained by a simple transformation. The Morse parameters of GMF5 at (γ_{max}, θ) can be computed by a two-dimensional cubic spline methods using the known values on the nodes of the γ and θ mesh. The resulting GMF5 parameters are then used in Eqs. (20) to (22) to compute the potential energy at this nuclear geometric configuration.

It is not difficult to see that the choice of γ_{max} and the two bond distances that form γ_{max} is unique, and is invariant under any P_3 identical particle permutation. For this reason, the RMCS potential energy surface has the correct P_3 symmetry built in.

3.5. Results and discussion

The results of the *ab initio* calculations for 560 individual nuclear geometries are given in an extensive series of tables included as Appendix 1 to this thesis.

Before discussing these results, we present some of the details of our application of the MRD-CI method to H_3. The molecule was placed in the xy plane (see Fig. 3), and all calculations were carried out using the point group C_s, even though at some special nuclear geometries the symmetry of the molecular point group could be higher (C_{2v}, D_{3h}, $C_{\infty v}$, $C_{\infty h}$). The reason for that choice is that we wanted the calculated energies to vary smoothly over the full range of nuclear geometries. In C_s point symmetry, the symmetry type A' is symmetric with respect to the xy plane whereas A'' is antisymmetric.

The SCF-MOs were constructed using the occupation $(1a')^2(1a'')^1$, which is the most dominant MO configuration for the $2p_z\ ^2A_2''$ electronic state when the molecule is in an equilateral triangle configuration, as is the case for its equilibrium configuration. Since our first priority is to obtain high quality results for this state, this choice of occupation configuration will lead to MOs which are able to offer a good description of this $2p_z\ ^2A_2''$ state. At the same time, this choice of occupation configuration will also lead to a more even-handed description for the two degenerate $2p_{xy}\ ^2E'$ (the ground and first excited) electronic states for equilateral triangle configurations. Such configurations may be important for transitions from bound ro-vibrational states of $2p_z\ ^2A_2''$.

Since we have chosen 75 AOs, the SCF step gives 75 MOs as well, as linear combination of these AOs. If it were necessary to reduce the size of CI space or to remove possible linear dependencies in the AO basis set, some of the MOs

could be deleted before the CI step. In our H_3 application, we did not find it necessary to do this and all 75 MOs were kept in the final CI step.

The CI space of A' symmetry was constructed using 45 to 49 reference configurations, depending on the nuclear geometry. The selection threshold energy used was 2 μhartree, and the lowest three eigenvalues of this symmetry were obtained. This resulted in the generation of 50,000 to 60,000 configuration functions out of which 5,000 to 6,000 were selected for the final CI calculation. For the lowest eigenvalue A'' calculations, 19 to 32 reference configurations were employed. Use of a threshold energy of 0.5 μhartree resulted in 800 to 3,000 selected configurations out of 20,000 to 40,000 generated.

There are four states of interest, which we label E_1, E_2, E_3 and E_4, where the first three are the states of A' symmetry and E_4 is the A'' one. Using the symmetry notation appropriate for the equilateral triangular (D_{3h}) geometry, E_1 corresponds to the ground state $^2E'$ ($1a'^2 1e'$), E_2 to the state degenerate with the ground one in the equilateral triangle geometry, E_3 to the $^2A_1'$ ($1a'^2 2s$) state and E_4 to the $^2A_2''$ ($1a'^2 2p_z$) state. Although E_1 and E_2 are degenerate in that geometry, the degeneracy is lifted as the triangle is distorted, and this is what generates the conical intersection between E_1 and E_2.

Electric dipole transition moments between all electronic states were calculated at most nuclear geometric configurations. We label the moment between states E_i and E_j as $\mathbf{T}_{ij}$. The C_s symmetry ensures that the electric dipole transition moments between the antisymmetric E_4 state and the symmetric E_1, E_2, and E_3 states have only z components, and that the ones between these symmetric states have no z components. Since the electronic wave functions have been determined by the variational calculation up to a phase factor

(real electronic wave functions can have a phase factors of ± 1 only), all electric dipole transition moments are subject to a possible sign change.

The major portion of the calculation has been done on the CRAY Y-MP machines of the NSF-San Diego Supercomputing Center and of the NAS program of the NASA-Ames Research Center, and on the CRAY X-MP machine of the Jet Propulsion Laboratory. The CPU time on the CRAY Y-MP machines for a complete calculation at a single nuclear geometry took about 4 to 10 minutes. The intermediate files generated during a calculation can be as large as 38 Mwords.

3.5.1. Basis set calibration

The first question to be addressed is the quality of the AO basis set we have chosen. Results for atomic and molecular hydrogen are given in Table 2. With the basis set of $(12s4p1d/7s4p1d)$, the $1s \rightarrow 2s$ transition energy is very accurate (10.2045 eV, which is within 0.0001 eV of the exact value), whereas the $1s \rightarrow 2p$ transition energy is less accurate (10.2118 eV, giving an error of 0.0074 eV) due to the smaller Rydberg $p-$basis, but still reasonably good.

The energy of ground-state $H_2(X\ ^1\Sigma_g^+)$ is close to that of Liu[1] and better than that of LS[2]. The computed D_e at 1.40 bohr is 4.7255 eV whereas the exact value is 4.7477 eV[82], an error of 0.02 eV. The excited state $b\ ^3\Sigma_u^+$, which has configuration $\sigma_g\sigma_u$, is calculated to lie 10.605 eV above the ground state, compared to the 10.623 eV value of Kolos and Wolniewicz[82], so this important valence-shell transition is also accurate to within 0.02 eV.

Tables 3, 4 and 5 show the MRD-CI energy of the four electronic states of H_3, for equilateral triangular, symmetric collinear and non-symmetric collinear configurations respectively. In the appropriate point group notation, the dominant configurations are the following:

D_{3h}: E_1: $1a_1'^2\ 1e'$, E_2: $1a_1'^2\ 1e'$, E_3: $1a_1'^2\ 2p_x$, E_4: $1a_1'^2\ 2p_z$;

$D_{\infty h}$: E_1: $1\sigma_g^2\ 1\sigma_u$, E_2: $1\sigma_g^2\ 2s$, E_3: mixed, E_4: $1\sigma_g^2\ 2p_z$;

$C_{\infty v}$: E_1: $1\sigma^2\ 2\sigma$, E_2: $1\sigma^2\ 2s$, E_3: mixed, E_4: $1\sigma^2\ 2p_z$.

In fact, assigning single dominant configurations to E_2 and E_3 in $D_{\infty h}$ and $C_{\infty v}$ symmetries is oversimplified, since an avoided crossing was found for $D_{\infty h}$ near $R_1 = 1.85$ bohr and for $C_{\infty v}$ near $R_1 = 1.4$ bohr and $R_2 = 10.0$ bohr (see also ref. 14).

The lowest-energy conical intersection for the E_1 surface occurs at $R_1 = R_2 = R_3 = 1.973$ bohr, and at an energy of -1.572084 hartree. This result was obtained by GMF5 fit to the *ab initio* data in the equilateral triangle configuration. The reference energy at the swing point P_s (Fig. 4) was chosen to be -1.499994 hartree (or three times the SCF value for an isolated H($1s$) atom with our present $12s/7s, 4p, 1d$ basis set. See Table 2). The reason for choosing this value instead of the theoretical value of -1.500000 hartree is for self-consistency. When fitting the E_3 surface, the reference energy at the swing point was chosen to be the SCF value of -1.124988 hartree instead of the theoretical value of -1.125000 hartree for the separated H($2s$) + 2H($1s$) configuration. For E_4, the reference value at the swing point was chosen to be -1.124718 hartree for the separated H($2p_z$) + 2H($1s$) configuration.

The minimum of E_1 energy with $\gamma = 180°$ and $R_2 = 10$ bohr occurs at $R_1 = 1.403$ bohr, and at an energy of -1.673019 hartree (GMF5 fit). This gives a lowest conical intersection energy with respect to the separated H + H_2 of 0.100935 hartree or 2.747 eV. For comparison, the corresponding energy for the LSTH surface[3] is 2.756 eV and occurs at $R_1 = R_2 = R_3 = 1.981$ bohr. For the DMBE surface[4] the corresponding values are 2.749 eV and 1.973 bohr. These results are listed in Table 6.

The saddle point in the collinear nuclear configuration for the E_1 surface occurs at $R_1 = R_2 = \frac{1}{2}R_3 = 1.758$ bohr, and at an energy of 0.440 eV (or 10.1 kcal/mole) (GMF5 fit) with respect to the energy of the separated H + H_2 configuration (at $R_1 = 1.403$ bohr, $R_2 = 10$ bohr and $R_3 = R_1 + R_2 = 11.403$ bohr, or the GMF5 fitted minimum point of E_1 along the cut with $\gamma = 180°$ and $\theta = 0°$). We use this energy difference as the collinear barrier height of the H + H_2 reaction[2-4]. For comparison, the corresponding values for the LSTH surface[3] are 0.425 eV (or 9.80 kcal/mole) and 1.757 bohr, and for the DMBE surface[4], 0.418 eV (or 9.65 kcal/mole) and 1.755 bohr. These results are listed in Table 7. As a result, the lowest conical intersection energy and the corresponding geometry are in good agreement with accurate published values. For the saddle point in the collinear configuration, our calculated barrier height and its location also agree well with the corresponding values of LSTH and DMBE surfaces.

The $E_1 \rightarrow E_2$ transition energy for symmetric collinear configurations, corresponding to $\sigma_u \rightarrow 2s$, can be obtained from the analytically-continued DMBE function[4], giving 5.728 eV, and from the DIM calculation of Roach and Kuntz[14], who obtained 6.292 eV at $R_1 = 2.0$ bohr. The present data from Table 4 show a value of 5.555 eV. At $R_1 = 1.76$ bohr the three calculations are in better agreement, giving 6.379 eV (DMBE), 6.466 eV (ref. 14) and our value of 6.529 eV.

The $E_1 \rightarrow E_4$ transition energy for equilateral triangle configurations, corresponding to $e' \rightarrow 2p_z$, has been computed by Diercksen *et al.*[16] as well as by PTW[15]. Using $R_1 = 1.633$ bohr and CI spaces of 15290, 22570 and 47060 CSFs, Diercksen *et al.* obtained transition energies of 2.17, 2.21 and 2.11 eV, respectively. Our data at $R_1 = 1.633$ bohr give 2.23 eV and PTW obtained 2.24 eV. From the experimental spectrum[19], we estimate that the vertical transition

at $R_1 = 1.633$ bohr should occur at about 2.15 eV, so that our present E_4 energy appears to be too high by about 0.08 eV. Possibly another more diffuse p–function in the basis set would help to correct this error. However, in general our criteria for accurate multiple surface energetics have been met.

The squares $| \mathbf{T}_{ij} |^2$ of the electric dipole transition moments between states E_i and E_j ($ij = 21, 31, 32, 43$) for equilateral triangle geometry (D_{3h}) are given in Table 8. Allowed transitions in D_{3h} occur for $e' \rightarrow 2s$ ($\mathbf{T}_{31}$ and $\mathbf{T}_{32}$) and $2s \rightarrow 2p_z$ ($\mathbf{T}_{43}$). It can be seen that the $E_1 \rightarrow E_2$ electric dipole transition moment between two degenerate states is not zero since the calculation is carried out in C_s symmetry and the description of the two states is not quite equivalent (see also Table 3, where the C_s energies are not perfectly degenerate), but this transition moment is nevertheless very small. $| \mathbf{T}_{43} |^2$ increases with R_1, as expected (since it should become 9.00 a.u.^{2} in the limit of $R_1 \rightarrow \infty$). Its value of 7.24 a.u.^{2} compares well with the PTW one of 7.23 a.u.^{2} at 1.64 bohr. If the same method of estimation is used as in PTW[15], both results from PTW and the present work lead to the same lifetime of about 70 μs for the $2p_z \rightarrow 2s$ electric dipole radiation process. In Table 8, $| \mathbf{T}_{31} |^2$ and $| \mathbf{T}_{32} |^2$ are almost identical. They would be exactly identical if D_{3h} symmetry instead of C_s symmetry had been used in the wavefunction calculations. Their sum at 1.64 bohr is 5.12 a.u.^{2} while PTW obtained 4.89 a.u.^{2}. One reason for the difference is that the present calculation employed a larger basis set than that of PTW. Another is that in the current treatment we located Rydberg AOs on each nucleus, whereas PTW used a single set located at the center of the triangle.

In conclusion, the basis set we have used does satisfy all the selection criteria set previously and gives good results for our present study of the low-lying electronic states of H_3.

3.5.2 General features of the potential energy surfaces and of the electric dipole transition moments

In this section, the features of these four potential energy surfaces and of the electric dipole transition moments are discussed in details in some specific nuclear configurations.

3.5.2.1 Equilateral triangle configurations (D_{3h})

More detailed studies of the *ab initio* results reveals some interesting points in the equilateral triangle nuclear configuration. In Table 3, the energies of the lowest four electronic states are listed. These results are plotted in Fig. 5. In Table 9, we list all non-vanishing and some vanishing components of the electric dipole transition moments between these four electronic states for this geometry.

Although C_s is the only symmetry embedded into the calculation, when three nuclei form an equilateral triangle, the full molecular symmetry group D_{3h} associated with this geometry will manifest itself in the results of the electronic calculations via the following features:

1. The $2p_{xy}\ ^2E'$ (E_1 and E_2) states are degenerate, but this degeneracy will not be exact due to the intrinsic inaccuracies in the calculation.
2. The electric dipole transition moments $\mathbf{T}_{41}$, $\mathbf{T}_{42}$ from the $2p_z\ ^2A_2''$ state to the $2p_{xy}\ ^2E'$ states vanish due to symmetry reasons, and should be close to zero in the actual calculations.
3. Because of the degeneracy of the $2p_{xy}\ ^2E'$ states (under the symmetry of an equilateral triangle), they can always be written as:

$$| 2p_x\ ^2E' \rangle = \cos\varphi \mid \phi_1 \rangle + \sin\varphi \mid \phi_2 \rangle \tag{23}$$

$$| 2p_y\ ^2E' \rangle = -\sin\varphi \mid \phi_1 \rangle + \cos\varphi \mid \phi_2 \rangle \tag{24}$$

$| \phi_1\rangle$, $| \phi_2\rangle$ are solutions of the electronic wave equation with the same energy, which form another E' representation of the D_{3h} group. The phase angle φ is not determined by the variational method alone, and can have an arbitrary value. For two calculations with different inter-nuclear distances, the relative phases of these two electronic calculations is random, which in turn causes the x and y components of the electric dipole transition moments ($\mathbf{T}_{31}$, $\mathbf{T}_{32}$, and $\mathbf{T}_{21}$) to vary greatly (see Table 9). Even so, the D_{3h} symmetry ensures that:

- The magnitudes of $\mathbf{T}_{31}$, $\mathbf{T}_{32}$, and $\mathbf{T}_{21}$ do not depend on the phase φ and thus should change smoothly with the inter-nuclear distance.
- $|\ \mathbf{T}_{31}\ | = |\ \mathbf{T}_{32}\ |$, $|\ T_{31}(x)\ | = |\ T_{32}(y)\ |$, and $|\ T_{31}(y)\ | = |\ T_{32}(x)\ |$. Due to the approximations involved, these relations will not be fulfilled exactly.

All of these features are confirmed numerically by the results in Tables 9 and by Figs. 6 and 7. Since the molecular properties are more sensitive to the quality of the molecular wavefunctions than are the energy eigenvalues, the results of the electric dipole transition moment calculations offer another strong indication that the wavefunctions obtained are of good quality.

The results of the GMF5 fit shows that the E_1 and E_2 states have a potential well of 1.962 eV at $R_1 = R_2 = R_3 = 1.973$ bohr. The corresponding values for the E_3 state are 9.721 eV and 1.604 bohr, and for the E_4 state, 9.558 eV and 1.642 bohr. The E_3 and the E_4 states have much deeper wells in comparison with that of the E_1 and the E_2 states. At the equilateral triangular geometry with an inter-nuclear distance $R_1 = R_2 = R_3 = 1.64$ bohr (corresponding approximately to the equilibrium geometry of the metastable ($2p_z\ ^2A_2''$) state), the *ab initio* energy

spacing between states $2s\ ^2A_1'$ and $2p\ ^2A_2''$ is 1299 cm^{-1} while the best value previously calculated by PTW[15] is 1422 cm^{-1} and the experimentally estimated value for the energy difference between the minima of those two states[15,19] is 1256 cm^{-1}. Because $R = 1.64$ bohr is not the location of the real minimum of the E_3 curve, the estimations of energy differences between the $2s\ ^2A_1'$ state and the $2p_z\ ^2A_2''$ state at 1.64 bohr is not appropriate to be compared directly with the experimental value of 1256 cm^{-1}. The bottom of the E_3 equilateral triangle curve is located at 1.604 bohr and that of the corresponding E_4 curve at 1.642 bohr (GMF5 fit). These two values agree with the experimental values of 1.606 bohr and 1.640 bohr very well. The corresponding energy difference is 1374 cm^{-1}, which is still a better result than that of PTW. One more p-type Rydberg function in the AO basis set might give a better agreement.

3.5.2.2 Collinear configurations ($C_{\infty v}$)

The energies of E_1, E_2, E_3, and E_4 in symmetric collinear geometries ($R_1 = R_2 = \frac{1}{2}R_3$) are listed in Table 4. Figs. 8a and 8b show the good agreement between our present *ab initio* results and that of the lower sheet of the DMBE surface[4]. The bottoms of the curves for the DMBE surface and for our E_1 GMF5 fit are located at $R_1 = R_2 = \frac{1}{2}R_3 = 1.755$ bohr and 1.758 bohr respectively, an almost perfect agreement. Even in this collinear symmetric stretch mode, the E_4 state still has a deep well of 7.62 eV for $R_1 = R_2 = \frac{1}{2}R_3 = 1.519$ bohr (GMF5 fit). Following the $C_{\infty h}$ symmetry argument, the electric dipole transition moment between the E_1 and E_4 states is supposed to be zero, with which our $\mathbf{T}_{41}$ results agree. Since the upper sheet of DMBE surface did not include the effect of avoided crossings of that state with other states, its behavior is quite different from our *ab initio* results (see Fig. 9). The behavior of our results are in good agreement with those obtained by PTW[15]. As can be seen from the *ab initio*

results in Fig. 9, an avoided crossing occurs around $R_1 = R_2 = 1.8$ bohr. This is also demonstrated by the sudden decrease of the electric dipole transition moment $\mathbf{T}_{42}(z)$ as R increases form 1.7 bohr to 1.9 bohr (see Table 10). An even more abrupt change occurs in $\mathbf{T}_{43}(z)$ around the some location, although the energy behavior does not show any obvious changes (see Fig. 10).

In the non-symmetric collinear configuration with $R_2 = 10.0$ bohr and R_1 variable ($\gamma = 180°$, $\theta = 0°$), which corresponds to the asymptotic H + H_2 situation, the potential curves of the E_1 and E_4 states are parallel to each other (see Table 5), with almost the identical GMF5 Morse parameters. Both curves give well depths of 4.707 eV around $R_1 = 1.403$ bohr. The corresponding accurate value for isolated $H_2(X\ ^1\Sigma_g^+)$ from Kolos and Wolniewicz[82] is 4.7477 eV at a bond distance of 1.401 bohr. Our basis set calibration full CI results for $H_2(X\ ^1\Sigma_g^+)$ gives 4.7255 eV at a bond distance of 1.40 bohr. These three sets of data agree with each other reasonably well. The electric dipole transition moment $\mathbf{T}_{41}$ between these two states varies little with the diatomic bond distance and has a value between 0.74 a.u. and 0.75 a.u. (as can be seen from Table 11). For comparison, the electric dipole transition moment of an isolated H atom, from $1s \rightarrow 2p_z$ is 0.745 a.u.. This excellent agreement confirms that our calculated E_1 and E_4 states are very close to the theoretical predictions of separated $H(1s, 2p_z)$ + $H_2(X\ ^1\Sigma_g^+)$ states.

In the DIM study of Roach and Kuntz[14], using only information obtained from diatomic energies, they have shown that for a separated H + H_2 system, the repulsive potential energy curve for $H(1s)$ + $H_2(b\ ^3\Sigma_u^+)$ intersects those potential curves for $H(2s, 2p_x, 2p_y, 2p_z)$ + $H_2(X\ ^1\Sigma_g^+)$ around a diatomic bond distance of 1.45 bohr. They have also shown that the potential energy curves for $H(2s, 2p_x, 2p_y, 2p_z)$ + $H_2(X\ ^1\Sigma_g^+)$ intersect the curve for $H(1s)$ + $H_2(B\ ^1\Sigma_u^+)$

around a diatomic bond distance of 2.2 bohr, and the curve for $H(1s) + H_2(c\,^3\Pi_u)$ around 2.4 bohr.

In the presence of the full interactions of the triatomic H_3, many crossings are avoided among the electronic states mentioned above. From our *ab initio* data along the ray of $\gamma = 180°$ and $\theta = 0°$ (see Table 5 and Fig. 11), the change in the nature of the E_2 state with diatomic bond distance across the region of the avoided crossing around 1.4 bohr can be seen clearly. Its potential energy curve has a sharp downward turn with increasing R_1. The electric dipole transition moment $\mathbf{T}_{42}$ between the E_4 and E_2 states also has a sudden change in the same region (see Table 11). The calculated value of $|\ \mathbf{T}_{42}(z)\ |$ is around 2.5 a.u. before the crossing and drops below 0.002 a.u. after that, while the corresponding value for the $H(2s) \rightarrow H(2p_z)$ transition is 3.00 a.u., and the values for the $H(2p_{x,y}) \rightarrow H(2p_z)$ transitions vanish according to symmetry argument.

The potential energy curve for the E_3 state is relatively smooth, although there are some very sudden changes in $|\ \mathbf{T}_{43}(z)\ |$ for $R_1 > 1.2$ bohr which are due to the properties of this state. The most probable reason is associated with the fact that there are several states nearly degenerate with the E_3 state in the separated $H + H_2$ nuclear configuration. This near degeneracy could extend down to 1.2 bohr, in which case there could be avoided crossings between the E_3 state and these other states. This is expected to cause large changes in the E_3 wavefunction but not in its energy. As shown below, these wavefunction changes result in rapid fluctuations in the electric dipole transition moment for this state.

By studying the dominant coefficients of the MOs for the E_2 and E_3 CI wavefunctions in the R_1 range from 1.0 bohr to 2.1 bohr, we found five kinds of CI wavefunctions with unique patterns of dominant MO coefficients. Here we label them as S_1, S_2, S_3, S_4 and S_5. S_1 can be associted with the asymptotic

$H(2s) + H_2(X\ ^1\Sigma_g^+)$ state, S_2 with the $H(2p_{xy}) + H_2(X\ ^1\Sigma_g^+)$ state, and S_4 with the $H(1s) + H_2(b\ ^3\Sigma_u^+)$ state. The S_3 and S_5 states have different characteristics, but we were not able to assign them to the known asymptotic states of the H_3 system. The investigation of the E_1 and E_4 states also confirmed that the E_1 state correspondes to the asymptotic $H(1s) + H_2(X\ ^1\Sigma_g^+)$ state, and the E_4 state correspondes to the asymptotic $H(2p_z) + H_2(X\ ^1\Sigma_g^+)$ state at $\gamma = 180°$ and $\theta = 0°$. The electric dipole transition moments between the S_1, S_2, S_3, S_4 and S_5 states and the E_4 state vary relatively slow as functions of R_1.

For R_1 values of 1.0, 1.1 and 1.2 bohr, E_2 is of the S_1 kind and E_3 is of the S_2 kind. This explains the smooth variations in the values of $|\ \mathbf{T}_{42}(z)\ |$ and $|\ \mathbf{T}_{43}(z)\ |$ in this region of R_1.

At $R_1 = 1.3$ bohr, E_2 becomes the S_2 kind and E_3 the S_3 kind. This gives $|\ \mathbf{T}_{42}(z)\ |$ a value of 0.756×10^{-8} a.u. and $|\ \mathbf{T}_{43}(z)\ |$ a value of 0.942 a.u..

At $R_1 = 1.4$ bohr, E_2 becomes the S_3 kind and E_3 the S_2 kind. This crossing can been seen in the values of these two electric dipole transition moments.

At $R_1 = 1.5$ bohr, E_2 becomes the S_4 kind and E_3 remains in the S_2 kind. This gives $|\ \mathbf{T}_{42}(z)\ |$ a sudden drop from 1.52 a.u. to 0.152×10^{-2} a.u..

At $R_1 = 1.6$ bohr, E_2 is still of the S_4 kind and E_3 changes into the S_3 kind once again. This gives $|\ \mathbf{T}_{43}(z)\ |$ an increase from near zero to 1.31 a.u..

For R_1 in the range from 1.5 bohr to 2.1 bohr, E_2 does not change character, which explains the smooth variation of $|\ \mathbf{T}_{42}(z)\ |$ as a function of R_1.

For R_1 in the range from 1.6 bohr to 2.0 bohr, E_3 remains type S_3 and so the variation of $|\ \mathbf{T}_{43}(z)\ |$ is also smooth.

At $R_1 = 2.1$ bohr, E_3 changes into the S_5 kind and causes a drop in $|\ \mathbf{T}_{43}(z)\ |$.

As shown above, we have established an one-to-one correspondence between the sudden changes in $|\mathbf{T}_{42}(z)|$ and $|\mathbf{T}_{43}(z)|$ and the changes in the nature of the E_2 and E_3 states. The full association of the E_2 and E_3 states at $\gamma = 180°$ and $\theta = 0°$ with the theoretical asymptotic states such as $H(2s, 2p_x, 2p_y) + H_2(X\,^1\Sigma_g^+)$ and $H(1s) + H_2(b\,^3\Sigma_u^+)$ requires further analysis of the wavefunctions of the E_2 and E_3 states, which are in the form of linear combinations of MOs (which themselves are in turn the linear combinations of AOs).

3.5.2.3 General features of the E_2 and E_3 states

Because the number of *ab initio* calculations is large, let us limit our scope to the bond angle $\gamma = 60°$ for the discussion of general features of the E_2 and E_3 states. For γ values of 90°, 120°, 150° and 180°, the behavior is more or less the same. The potential energy curves of the E_2 state with $\gamma = 60°$ and ten different θ values are depicted in Figs. 12a to 12j. The plots of the same nature from Figs. 13a to 13j are for the curves of the E_3 state.

In the equilateral triangle geometry ($\gamma = 60°, \theta = 45°$), the E_2 state is degenerate with the ground state E_1, and has a shallow well at an internuclear distance of 1.978 bohr. When θ decreases, the well depth also decreases and disappears at $\theta = 42°$. After that, the curve becomes purely repulsive. When θ reaches 30°, one more feature appears around $R_1 = 1.5$ bohr, signaling an avoided crossing. At this $\gamma = 60°, \theta = 30°$ cut of the E_2 potential energy surface, the internuclear distances are not too large, and the interaction between the two electronic states involved in the avoided crossing is strong. For this reason, the transition from one state to another is smooth over a wide range of nuclear geometries. When θ further decreases, the nuclear configuration approaches the separated H + H_2 asymptotic situation and the interaction between the two states involved in the avoided crossing becomes weaker. As

a result, the transition from one state to another becomes more abrupt in a small region of nuclear configuration. Because the wave function of the E_4 state (which correlates asymptotically with the $H(2p_z)$ + $H(X\ ^1\Sigma_g^+)$ state) is anti-symmetric with respect to the plane of the molecule, it will not be involved in the avoided crossing since E_2 is symmetric with respect to that plane. The possible asymptotic states responsible for this avoided crossing are the $H(1s)$ + $H_2(b\ ^3\Sigma_u^+)$ repulsive state, and the $H(2s, 2p_x, 2p_y)$ + $H_2(X\ ^1\Sigma_g^+)$ states.

The behavior of the E_3 state is more complicated. In the θ range of 45° to 42°, the potential energy curve for this state has a deep well, with a Morse-function-like behavior along the R_1 bond distance. In Fig. 13d ($\theta = 42°$), the *ab initio* data for $R_1 = 1.0$ bohr and 1.2 bohr were not calculated, so were the *ab initio* data for $R_1 = 1.0$ bohr in Fig. 13e ($\theta = 41°$). At $\theta = 41°$, a new feature appears around $R_1 = 2.4$ bohr. This feature becomes more pronounced at $\theta = 40°$ and the slope of the curve for large R_1 becomes small. When θ reaches 30°, the potential curve does not have well in the range where our *ab initio* data are available. At $\theta = 20°$, again there are two features in the potential curve with a transition point at $R_1 = 1.8$ bohr. At $\theta = 0°$, the potential curve has a very nice Morse shape up to $R_1 = 2.0$ bohr. From the limited amount of *ab initio* data available, we are already able to see the significant complexity in the potential energy surface of the E_3 state. We have attempted an understanding of what asymptotic states are involved in the fine surface features, but without success. Calculations involving higher energy surfaces may be required for this purpose.

For $\gamma = 90°, 120°, 150°$, and 180°, the main features of the E_2 and E_3 states are similar to those they display for $\gamma = 60°$. Since the energies of all states have weak dependencies on γ when θ is close to 0° (approaching the separated

$H + H_2$ limit), we have restricted ourselves to display the variations of E_2 and E_3 with γ for the single value $\theta = 45°$ (see Figs 14a to 14e). Again an avoided crossing in E_2 around $R_1 = R_2 = 1.8$ bohr is seen for γ in the range of 150° and 180°.

In conclusion, more *ab initio* points are needed for a better understanding of these two surfaces, and more importantly, more electronic states need to be calculated. For our present research interest, we are content with the results obtained so far.

It is obvious that the RMCS surface fitting method is not appropriate to be applied to fit the potential energy surfaces of the E_2 and E_3 states because of their rich and complicated features resulting from several avoided crossings among several electronic states. More elaborate methods will be necessary in order to fit these two potential energy surfaces[84-85].

The only electric dipole transition moment which displays reasonably smooth behavior is $\mathbf{T}_{41}$ between the E_1 and E_4 states. Since it is a combination of both electronic states plus a electronic dipole operator, the $\mathbf{T}_{41}$ surface will have more features and variations than the potential energy surfaces of either the E_1 or E_4 states. For the rest of the electric dipole transition moments involving the E_2 and E_3 states, the situation is more complicated. Fortunately, in ordinary applications, these electric dipole transition moments are only needed in a very limited range of nuclear configuration. A localized fit to the electric dipole transition moments will suffice for most practical needs.

The potential energies of the E_1 and E_4 states on cuts of constant γ and θ display a very simple Morse-like behavior. The RMCS surface fitting method has been applied to obtain the RMCS potential energy surfaces for both states. The results are discussed in the next section.

3.5.3. RMCS surfaces for the E_1 and E_4 states

The potential energy surfaces for the lowest state of A_1' symmetry (E_1) and the lowest state of A_2'' symmetry (E_4) display simple functional properties and can be described easily using the RMCS potential energy surface fitting method. In the following, we will first discuss the GMF5 non-linear fits to the *ab initio* energies of the E_1 and E_4 states along the constant (γ, θ) cuts and the quality of the fits. Then the full three dimensional RMCS fits to the E_1 and E_4 states and the quality of the RMCS fits will be discussed. At the end, the surface features and topology displayed by the E_1 and E_4 RMCS surfaces will be presented.

3.5.3.1 GMF5 fits along the constant (γ, θ) cuts

Since the data points at which *ab initio* energies are calculated were chosen to be along the cuts of constant (γ, θ), the GMF5 non-linear fitting was straightforwardly done. The reference energies at the swing point P_s (see Fig. 3) are chosen to be -1.499994 hartree for E_1 and -1.124718 hartree for E_4 (see section 3.5.1 also). The quality of those fits was monitored in two ways. The first is the rms of the difference between the *ab initio* data and the values of the fitting function. The second is the maximum deviation of the values of the fitting function from the *ab initio* data. If some *ab initio* points were too far away from the fitting function, then they were removed and a new GMF5 fit was done. The resulting maximum rms deviation was less than 2.3 meV and the maximum deviation was less than 3.5 meV in the fitting of the E_4 energies for all constant (γ, θ) cuts. For the E_1 state, the rms deviation was less than 2.4 meV and the maximum deviation was less that 4.6 meV.

The Morse parameters $D_e(\gamma,\theta)$, $l_e(\gamma,\theta)$, $\beta_e(\gamma,\theta)$, $\lambda_1(\gamma,\theta)$, and $\lambda_2(\gamma,\theta)$ are the results of the GMF5 fits. For a given γ value, after all 10 sets of GMF5

fits were done, the smoothness of these parameters with respect to θ was tested. If the parameters displayed excessively large fluctuations we went back to the GMF5 fit step and made some adjustments, trying to reduce these fluctuations. After one or two iterations, the resulting Morse parameters became reasonably smooth.

The GMF5 parameters obtained are depicted in Figs. 15a to 15e (for the E_1 state) and in Figs. 16a to 16e (for the E_4 state) with a fixed $\gamma = 60°$. The behaviors of these parameters are similar for $\gamma = 90°, 120°, 150°$, and $180°$. The first three parameters D_e, l_e and β_e are smooth functions of θ, but λ_1 and λ_2 display some rapid fluctuations. The results for λ_1 and λ_2 and their one-σ statistical error bars from the GMF5 fits are depicted in Figs. 15d and 15e (for E_1) and Figs. 16d and 16e (for E_4). Since they are first and second order corrections to β_e, their effect in the GMF5 function is minor. For the same reason, they are very sensitive to the locations of the *ab initio* points. This kind of non-physical fluctuation of λ_1 and λ_2 as functions of θ was minimized by choosing the smoothest curve going through almost all of the error bars. (except for a small number of points). We can see that the smoothed λ_1 and λ_2 curves as functions of θ usually do not pass through the centers of the error bars. Our results show that the smoothed GMF5 fits are still in good agreement with the *ab initio* data in the region of the nuclear geometry configurations for which they were calculated. Of course this hand-smoothing did decrease the accuracy of the GMF5 fits, but since the effect of λ_1 and λ_2 is more prominent in the region far away from the bottom of the GMF5 curve (that is, high potential energies) which is of less chemical interest, this degradation of the fitting quality is not too serious for the practical applications of those surfaces.

The behavior of these five Morse parameters at $\theta = 45°$ is of importance. For the E_1 state, because of the conical intersection between the E_1 and E_2 states in the equilateral triangular configurations, the discontinuity of the first derivatives of those GMF5 parameters at $\theta = 45°$ in Figs. 15a through 15e is well justified. For the E_4 state, the first derivative of β_e (see Fig. 16c) with respect to θ is not zero. For a potential energy surface with a global minimum at $\gamma = 60°$ and $\theta = 45°$, that derivative should vanish. The reason it did not is presently unknown. It is possible that the curve representing the variation of β_e with θ for $\gamma = 60°$ in the neighborhood of $\theta = 45°$ has a sufficiently large curvature to require a θ grid finer than the one used. Additional calculations are needed to elucidate this point.

3.5.3.2 Three dimensional RMCS fits

With this set of smoothed GMF5 parameters known at all nodes of the two dimensional (γ, θ) mesh, the three dimensional RMCS potential energy surfaces for the E_1 and E_4 states were then coded into Fortran subroutines in an easy-to-use form.

For all constant $\gamma = 60°, 90°, 120°, 150°$ and $180°$, the rms deviation for RMCS E_4 surface is less that 6.6 meV, and for that of E_1 it is less that 4.4 meV. This means that even after the hand-smoothing of the λ_1 and λ_2 parameters as a function of θ, the fitting quality is still reasonably good.

It has been discussed before that there is a two-fold identical particle symmetry reduction left that has not been implemented in our calculation. In the case of two bond angles of the H_3 molecule bigger than (or equal to) 60°, there are two ways of obtaining the potential energy from the RMCS surface. The permutation symmetry of identical particles requires those two results to be equal. But the RMCS method does not have this property of the potential

surface built in and the two choices of γ and the other two internal coordinate variables might lead to different RMCS energies for lack of self-consistency.

We used the maximum bond angle as γ to resolve the ambiguity, and the resulting surface does have the full P_3 symmetry. The drawback of this scheme is that the fitting accuracy is decreased. Even though for $\gamma = 90°, 120°, 150°$, and $180°$, the RMCS energies are still in good agreement with the *ab initio* ones, for $\gamma = 60°$, the agreement decreases. For example, for a set of *ab initio* points of the E_4 state along the cut of $\gamma = 60°, \theta = 0°$, the GMF5 fit is very good, with a rms deviation of 0.6 meV and a maximum deviation of 1.6 meV. For a given nuclear geometry configuration on this cut with $R_1 = 2.0$ bohr (which corresponds to $R_1 = 2.0$ bohr, $R_2 = 10$ bohr and $R_3 = 9.27$ bohr), the three bond angles of the triangle have values of 105.6°, 60°, and 14.4°. Choosing the maximum bond angle one uses $\gamma = 105.6°$, $\theta = 5.2°$, and $l = 8.03$ bohr instead of $\gamma = 60°$, $\theta = 0°$, and $l = 8.0$ bohr to evaluate the E_4 RMCS energy. Even though both sets of values describe the same nuclear geometry configuration, the first set leads to a RMCS energy 82.7 meV away from the *ab initio* result while the second set leads to a RMCS energy less than 1.6 meV away from the *ab initio* value.

This problem can be solved in two ways. The first is to use a coordinate system which implemented the full P_3 identical particle symmetry. This will remove the two-fold redundancy and the ambiguity left in our RMCS fitting procedure. The difficulty with this procedure is that our present *ab initio* data might not be located at the best positions in the new coordinates for an easy and good fit. The second is to fine-tune the current RMCS surface fit in order to achieve the self-consistency of the surface. Since the ambiguity occurs in the range of $\gamma = 60°$ to $\gamma = 120°$, in which the Morse parameters change noticeably, it would be desirable to obtain more *ab initio* points for γ values in addition to

$\gamma = 60°$, $90°$, and $120°$. Furthermore, the two dimensional cubic spline fit used in the (γ, θ) mesh gives the fitted $X(\gamma, \theta)$ (any one of the five Morse parameters) zero second partial derivatives along the normal directions of the γ, θ boundary at $\theta = 0°$, $\theta = 90°$, $\gamma = 60°$, and $\gamma = 180°$, but not necessarily zero first partial derivatives. It is conceivable that the correct boundary conditions should be zero first derivatives for the Morse parameters along the normal directions of the (γ, θ) boundaries. It is apparent that the boundary conditions for the RMCS fit should be correctly built in with some changes in the two dimensional Morse parameter evaluation step. This will make the RMCS fit more accurate, especially, more consistent in the region of γ ranging from $60°$ to $120°$.

3.5.3.3 Quality of the RMCS fits

In order to address the quality of the three dimensional RMCS fits to the *ab initio* results of the E_1 and E_4 states, we did the direct comparison between the energies of RMCS fits and the *ab initio* ones. For the E_1 state, we also did several comparisons of the *ab initio* results and the RMCS ones with the known LSTH and DMBE surfaces. Surface features in some selected nuclear geometry configurations are also presented and compared.

For the E_1 RMCS surface, we compared its values with the *ab initio* results at 560 nuclear geometries. The results of this comparison are given in Table 12. The rms deviation is 24 meV (0.55 kcal/mole) and the maximum deviation is 0.27 eV (6.2 kcal/mole).

We also did the same kind of comparison between the *ab initio* data and the LSTH and DMBE surface, and between the E_1 RMCS surface and the LSTH and DMBE ones. The results of these comparisons are also listed in Table 12. The average difference between the *ab inito* energies and the corresponding LSTH values is 0.051 eV (1.2 kcal/mole), the corresponding rms deviation is 0.059 eV (1.4 kcal/mole) and maximum deviation 0.34 eV (7.8 kcal/mole). The closeness between the values of the average difference and that of the rms deviation means that the present *ab inito* E_1 surface is more or less parallel to but 0.05 eV above the LSTH one. The individual energy differences for all 560 individual nuclear geometries confirm this conclusion with few exceptions. The average difference between the present *ab initio* energies and the corresponding values of the DMBE surface is 0.053 eV (1.2 kcal/mole), the rms deviation is 0.057 eV (1.3 kcal/mole) and maximum deviation 0.12 eV (2.8 kcal/mole). This set of data shows that the present *ab initio* results agree better with the DMBE surface than with the LSTH one. It is worth mentioning that when the E_1 RMCS surface is compared

with the *ab initio* data, the average difference is 0.7 meV, much smaller than the two previous average values. This is expected to be the case since the RMCS surface is a fit to the set of *ab initio* data.

The comparisons between the E_1 RMCS surface (with the same set of nuclear configurations for which we did the comparison between the *ab inito* surface and the LSTH and DMBE surfaces) with the LSTH and DMBE ones show similar trends, with an increase of about 4% to 5% in the corresponding rms values.

Since the saddle point of the ground electronic potential energy surface in the collinear nuclear geometry configuration has a very important role in the study of the chemical dynamics of the H + H_2 system, we list its location, the barrier height, and the two corresponding force constants in Table 7. The complete definitions of those quantities can be found in refs. 3 and 4.

All surfaces have a very similar location for the collinear saddle point, ranging from 1.755 to 1.758 bohr. The barrier heights of the E_1 RMCS surface and the *ab initio* surface are about 22 to 25 meV higher than the corresponding DMBE value, or 5% to 6% higher. The two force constants for all surfaces agree among themselves quite well. This means that these potential energy surfaces have similar shapes in the vicinity of the saddle point. The comparison shows that the present *ab initio* results and also the E_1 RMCS surface furnish a fairly good description of the collinear saddle point.

The E_1 state is degenerate with the E_2 state for the equilateral triangle configurations. Together they form a conical intersection in the vicinity of this geometry. The behavior of the E_1 and E_2 potential energy surfaces is of importance for quantum reactive scattering calculations at high energy (> 2.75 eV), for the study of the possible ro-vibrational states on the E_2 potential energy surface, and also for the decay processes from the upper Rydberg states to these

two low-lying E_1 and E_2 states. We did the GMF5 fit and also the ordinary three-parameter Morse fit to the *ab inito* data for equilateral triangle configurations. For comparison, the same fits were conducted for the calculated energies at the same set of nuclear geometry configurations for the LSTH, DMBE, and the E_1 RMCS surfaces. The parameters obtained for these two fits are listed in Table 13.

The first three GMF5 parameters of the E_1 RMCS surface (D_e, R_e and β_e) are the same as the corresponding values of the *ab initio* surface, while the λ_1 and λ_2 parameters might be different for these two surfaces, since the values of the E_1 RMCS surface were obtained from the *ab inito* ones after smoothing. Because the latter parameters represent higher order corrections to β_e, the corresponding values for these four surfaces are all small but differ from each other. Comparatively the fitted values of parameters D_e, R_e and β_e for these four surfaces agree with each other quite well. The well depths of the E_1 RMCS surface and the *ab initio* surface are 0.03 eV smaller than that of the LSTH surface, and 0.038 eV smaller than that of the DMBE surface. For the fitted D_e, we can easily obtain the energy of the minimum point (E_e in Table 13) in the equilateral triangular configuration with respect to that of the H + H_2 configuration. It is worth mentioning that because of the slightly different choices of the energies of the H + H_2 reference configurations used (see footnote f of Table 13), the values of E_e for these four surfaces agree better with each other than they would if the same H + H_2 reference energy were used. The equilibrium distances of the E_1 RMCS surface and the *ab initio* surface are 0.003 bohr smaller than that of the LSTH surface, and 0.004 bohr larger that that of the DMBE surface. The corresponding β_e values are about 0.04 larger that those of the LSTH and DMBE surfaces.

The three-parameter Morse fits show the same trends displayed in the GMF5 fits. With only three parameters, the Morse fit is less flexible, and the fitting quality is lower than that of GMF5 fit. The three-parameters Morse fit gives a larger well depth D_e, a smaller equilibrium distance R_e and a larger exponent β_e.

For the E_4 RMCS surface, we compared the RMCS values with the *ab initio* results at 560 different nuclear configurations. The average deviation is 0.3 meV (7 cal/mole), the rms deviation is 24 meV (0.551 kcal/mole) and the maximum deviation is 0.25 eV (5.70 kcal/mole). The maximum deviation occurs at the point of nuclear configuration with $\gamma = 60°$, $\theta = 45°$ and $R_1 = 1.0$ bohr. For such a small R_1, the E_4 state has a high energy and also changes steeply with R_1. The RMCS fit is not flexible enough to fit this point well. These deviations for the E_4 RMCS surface are very close to the corresponding values for the E_1 RMCS surface (Table 12) when compared with the *ab initio* data.

The dominant feature of the E_4 surface is the deep well for equilateral triangular energy configurations. The same GMF5 parameters for the equilateral triangular configuration for the E_4 surface are listed in Table 14, together with the results of the three-parameter Morse fit.

Since this surface does support ro-vibrational bound states of the three protons, we will discuss the calculation of the corresponding low-lying energy levels in chapter 6. The comparison between these ro-vibrational energies and experimental values will serve as the ultimate test for the quality of the E_4 RMCS surface.

In conclusion, the RMCS fits of the E_1 and E_4 potential energy surfaces display the correct behavior and surface feature characteristics for the two most important regions of nuclear configuration space, namely the equilateral triangle

and collinear configuration regions. They offer a good representation of the present *ab inito* data. Since the RMCS fit is simple and very flexible, both RMCS surfaces can be modified easily when new *ab initio* data of higher quality become available.

3.5.3.4 Contour plots of the E_1 and E_4 potential energy surfaces

The equipotential plots of both RMCS surfaces in the Cartesian coordinates of the bond distances R_1 and R_2 with constant bond angle γ are shown in Figs. 17a to 17e (for the E_1 state) and Figs. 18a to 18e (for the E_4 state).

The general features of the E_1 RMCS surface agree well with those of LSTH[3] and DMBE[4] surfaces. The contours of E_1 in Fig. 17d ($\gamma = 60°$) have a sharp turn for $R_1 = R_2$ (or $\theta = 45°$) because of the conical intersection between the E_1 and E_2 states. Contour lines with high energy are not as smooth as those with low energy, because the effects of fluctuation of the λ_1 and λ_2 parameters obtained from GMF5 fits are more prominent in the high energy configuration region.

The deep global well of the E_4 RMCS potential energy surface is clearly depicted in Figs. 18a through 18i. The equipotential contour lines should be perpendicular to the line of $R_1 = R_2$ (or $\theta = 45°$) for accurate potential energy surfaces. In Fig. 18d ($\gamma = 60°$), this requirement is not exactly fulfilled. One reason for this is because of the no-vanishing first derivative of the parameter β_e as a function of θ for $\gamma = 60°$ and $\theta = 45°$ (see Fig. 16c), the second reason might be the inconsistency of the RMCS fit to the H_3 system mentioned before.

The E_1 potential curve and the corresponding DMBE one in equilateral triangle configuration are depicted in Fig. 19. The comparison shows that the E_1 RMCS curve is not as deep as the DMBE one. These two curves are

nearly parallel to each other near their energy minimum locations. The DMBE curve varies more slowly with internuclear distance when this distance is large comparatively. This is an indication that the GMF5 fitting function dose not have the correct long range behavior of a potential energy surface built into itself.

The equipotential plots of both states are also plotted in a symmetrized hyperspherical coordinates[85]. In the hypersperical coordinates, the C_{3v} symmetry of the potential energy surfaces of H_3 can be seen clearly.

We first briefly introduce this symmetrized hyperspherical coordinates. Let $A_\alpha, A_\beta, A_\gamma$ of masses $m_\alpha, m_\beta, m_\gamma$ be the three atoms of the triatomic system, and (λ, ν, κ) be any cyclic permutation of (α, β, γ). This notation satisfies the requirement that no extra attention has been paid to any given atom.

Let us define $\vec{r'}_\lambda$ as the internuclear vector between A_ν and A_κ and $\vec{R'}_\lambda$ as the vector of A_λ with respect to the center of mass of $A_\nu A_\kappa$ complex.

A mass-scaled coordinates introduced by Delves[86,87] is then defined as

$$\vec{R}_\lambda = a_\lambda \vec{R}'_\lambda \tag{25}$$

$$\vec{r}_\lambda = a_\lambda^{-1} \vec{r}'_\lambda \tag{26}$$

$$a_\lambda = \left(\frac{\mu_{\lambda,\nu\kappa}}{\mu_{\nu\kappa}}\right)^{\frac{1}{4}} = \left(\frac{\mu_{\lambda,\nu\kappa}}{\mu}\right)^{\frac{1}{2}} \tag{27}$$

$$\mu = \left(\frac{m_\lambda m_\nu m_\kappa}{m_\lambda + m_\nu + m_\kappa}\right)^{1/2} \tag{28}$$

where the effective masses are defined by

$$\mu_{\nu\kappa}{}^{-1} = m_\nu^{-1} + m_\kappa^{-1} \tag{29}$$

$$\mu_{\lambda,\nu\kappa}{}^{-1} = m_\lambda^{-1} + m_{\nu\kappa}^{-1} \tag{30}$$

The shape of the instantaneous triatomic triangle is fully specified by the internal coordinates R_λ, r_λ, and the angle γ_λ between $\vec{R}_\lambda$ and $\vec{r}_\lambda$.

The hyperspherical coordinates are defined by

$$\rho = (R_\lambda^2 + r_\lambda^2)^{\frac{1}{2}} \tag{31}$$

$$\omega_\lambda = 2 \arctan(\frac{r_\lambda}{R_\lambda}) \tag{32}$$

The coordinates (ρ, ω_λ, γ_λ) describe the shape of the triatomic system. The angles $(\omega_\lambda, \gamma_\lambda)$ are interpreted as the spherical polar angles in the abstract internal three dimensional space in which a point P has the Cartesian coordinates $(X_\lambda, Y_\lambda, Z_\lambda)$ defined by

$$X_\lambda = \rho \sin\omega_\lambda \cos\gamma_\lambda \tag{33}$$

$$Y_\lambda = \rho \sin\omega_\lambda \sin\gamma_\lambda \tag{34}$$

$$Z_\lambda = \rho \cos\omega_\lambda \tag{35}$$

Since $0 \leq \omega_\lambda \leq \pi$ and $0 \leq \gamma_\lambda \leq \pi$, these internal angles parametrize the surface of a hemisphere. Only the half-space of positive Y_λ coordinates provides a one-to-one correspondence between points in the nuclear geometry configuration space and a point in this three dimensional internal space. In order to visualize the variation of the potential energy surfaces with the internal angles $(\omega_\lambda, \gamma_\lambda)$, a mapping of the hemispherical surface onto a plane is defined. Consider the plane polar radius ϱ and plane polar angle ϖ as parameterizing the plane of the figures. These plane polar coordinates are defined from the internal angles $(\omega_\lambda, \gamma_\lambda)$ by

$$\varrho = \omega_\lambda \qquad 0 \leq \varrho \leq \frac{\pi}{2} \tag{36}$$

$$\varpi = \gamma_\lambda \qquad 0 \leq \varpi \leq 2\pi \tag{37}$$

The central point in such a plot is the intersection of the Z_λ axis with the hypersphere of radius ρ. The curve $\omega_\lambda = \frac{\pi}{2}$ is a circle in this mapping centered

on the Z_λ axis. We call this the north pole view because it is a certain projection of the spherical surface onto a plane tangent to the sphere at the Z_λ or north pole.

The south pole view is defined similarly to the north pole view, except that the projection is onto a plane tangent to the sphere at the negative Z_λ or the south pole. The mapping is defined by replacing ω_λ with $\pi - \omega_\lambda$ in Eq. (36).

We also wish to define a similar mapping of the sphere onto a plane tangent to the sphere at the Y_λ axis. This axis is the C_{3v} axis of the potential energy surface and a view from this axis shows all regions of the internal configuration space simultaneously and also shows the symmetry of the functions plotted. It is called the equatorial view.

Figs. 20 (for the E_1 state) and 21 (for the E_4 state) are equipotential plots of the potential energy surfaces on planes defined by constant Y_λ. The C_{3v} symmetry is clearly displayed. Fig. 20a shows a local maximum of the E_1 surface at the center of the plot at which the nuclei form an equilateral triangle and the E_1 and E_2 states have a conical intersection. Fig. 20b and 20c show the familiar Y-shape structures shown by LSTH and DMDE surfaces. Fig. 21a clearly shows a very deep global potential well located at $Y_\lambda = 2.16$ bohr.

Figs. 22 and 23 are the north and south pole views of the E_1 surface with $\rho = 6.0$ bohr. Together they show the three possible channels of the $H(1s) + H_2$ reaction. These surface features are very close to those displayed by LSTH and DMBE surfaces. The jaggedness displayed by the contour line of energy 4.0 eV in Figs. 22 and 23 is related to the fact that the corresponding region of internal configuration space lies outside the region for which *ab initio* calculations were performed and is reached by extrapolating those *ab initio* values.

Figs. 24 and 25 display plots of the equatorial views of the E_1 and E_4 RMCS surfaces respectively. In Fig. 24, the local maximum of the E_1 RMCS surface is located at the center of the plots and correspond to equilateral triangle configurations. The presence of three separated H($1s$) + H_2 channels is clearly demonstrated in Fig. 24c where ρ equals to 6.0 bohr. Again for the contour line of energy 4.0 eV, the jaggedness is due to the same kind of extrapolation as the one mentioned in the previous paragraph. In Figs. 25a and 25b, a local minimum of the E_4 is located at the center of the plots. In Fig. 25c where ρ equals to 6.0 bohr, the surface features are similar to that in Fig. 24c, except now they correspond to that of three separated H($2p_z$) + H_2 channels instead. The jaggedness of the high energy contours (with contour energies 12.5 eV, 13.0 eV and 13.5 eV) is once more due to extrapolation into regions of the internal configuration space outside that in which *ab initio* calculations were performed.

In conclusion, the RMCS potential energy surfaces of both the E_1 state and the E_4 state are obtained and coded into an easy-to-use form. The surface features are all reasonable, and in the case of the E_1 state, in good agreement with those from LSTH[3] and DMBE[4] surfaces. The GMF5 functional form has been satisfying in our application. Future efforts need to be directed toward the consistency of the two dimensional Morse parameter cubic spline fit in the (γ, θ) mesh with correct boundary conditions. Because a surface in the RMCS form has a high degree of flexibility, it can be shifted, scaled easily, using only a much smaller number of better *ab initio* energies, to obtain a new and improved potential energy surface.

3.6. References

1. B. Liu, *J. Chem. Phys.* **58**, 1925 (1973).
2. P. Siegbahn and B. Liu, *J. Chem. Phys.* **68**, 2457 (1978).
3. D.G. Truhlar and C.J. Horowitz, *J. Chem. Phys.* **68**, 2466 (1978); **71**, 1514(E) (1979).
4. A.J.C. Varandas, F.B. Brown, C.A. Mead, D.G. Truhlar and N.C. Blais, *J. Chem. Phys.* **86**, 6258 (1987).
5. H.F. King and K. Morokuma, *J. Chem. Phys.* **71**, 3213 (1979).
6. M. Jungen, *J. Chem. Phys.* **71**, 3540 (1979).
7. R.L. Martin, *J. Chem. Phys.* **71**, 3541 (1979).
8. K.C. Kulander and M.F. Guest, *J. Phys.* **B 12**, L501 (1979).
9. Ch. Nager and M. Jungen, *Chem. Phys.* **70**, 189 (1982).
10. S. Raynor and D.R. Herschbach, *J. Phys. Chem.* **86**, 3592 (1982).
11. H.J. Foth, H.R. Mayne, R.A. Poirier, J.C. Polanyi and H.H. Teller, *Laser Chem.*, **2**, 229 (1983).
12. H.R. Mayne, R.A. Poirier and J.C. Polanyi, *J. Chem. Phys.* **80**, 4025 (1984).
13. H.R. Mayne, J.C. Polanyi, N. Sathyamurthy and S. Raynor, *J. Chem. Phys.* **88**, 4064 (1984).
14. A.C. Roach and P.J. Kuntz, *J. Chem. Phys.* **84**, 822 (1986).
15. I. Petsalakis, J. Theodorakopoulos and J.S. Wright, *J. Chem. Phys.* **89**, 6850 (1988).
16. G.H.F. Diercksen, W. Duch and J. Karwowski, *Chem. Phys. Lett.* **168**, 69 (1990).
17. N.C. Blais, D.G. Truhlar and C. Alden Mead, *J. Chem. Phys.* **89**, 6204 (1988).
18. G. Herzberg, *Ann. Rev. Phys. Chem.* **38**, 27 (1987).

19. J.K.G. Watson, in press.

20. G.I. Gellene and R.F. Porter, *Acc. Chem. Res.*, **23**, 141 (1990).

21. G. Gellene and R. Porter, *J. Chem. Phys.* **79**, 5975 (1983).

22. J.F. Garvey and A. Kuppermann, *Chem. Phys. Lett.* **107**, 491 (1984).

23. H. Herzberg, *J. Chem. Phys.* **70**, 4806 (1979).

24. I. Dabrowski and G. Herzberg, *Can. J. Phys.*, **58**, 1238 (1980).

25. G. Herzberg and J.G.K. Watson, *Can. J. Phys.*, **58**, 1250 (1980).

26. G. Herzberg, H. Lew, J.J. Sloan, and J.K.G. Watson, *Can. J. Phys.*, **59**, 428 (1981).

27. G. Herzberg, J.T. Hougen, and J.K.G. Watson, *Can. J. Phys.*, **60**, 1261 (1982).

28. K.P. Lawley, Ed. *Adv. in Chem. Phys.: Ab Initio Methods in Quantum Chemistry*, **Vol. 67 69**, Wiley, New York, 1987.

29. C.W. Bauschlicher, Jr. and S. Langhoff, and P.R. Taylor, *Adv. in Chem. Phys.*, **xx**, 103 (1990).

30. K. McIsaac and E.N. Maslen, *Int. J. Quam. Chem.*, **31**, 361 (1987), and references therein.

31. P.O. Löwdin, *Adv. Chem. Phys.*, **2**, 207 (1959).

32. P.E.M. Siegbahn, in *Quantum Chemistry: The State of Art*, V.R. Saunders and J. Brown, Eds., Science Research Council, Didcot Oxon., 1975, p. 81.

33. P.E.M. Siegbahn, *Chem. Phys. Lett.* **109**, 417 (1984).

34. P.J. Knowles and N.C. Handy, *Chem. Phys. Lett.* **111**, 315 (1984).

35. C.W. Bauschlicher and P.R. Taylor, *J. Chem. Phys.* **85**, 2779 (1986).

36. P.J. Knowles, *Chem. Phys. Lett.* **155**, 513 (1989).

37. P.J. Knowles and N.C. Handy, *J. Chem. Phys.* **91**, 2396 (1989).

38. P.E.M. Siegbahn, *Int. J. Quam. Chem.*, **23**, 1869 (1983).

39. H.J. Werner and P.J. Knowles, *J. Chem. Phys.* **89**, 5803 (1988).

40. R.J. Buenker and S.D. Peyerimhoff, *Theoret. Chim. Acta*, **35**, 33 (1974).

41. R.J. Buenker, S.D. Peyerimhoff and W. Butscher, *Mol. Phys.*, **35**, 771 (1978).

42. R.J. Buenker, in: *Molecular Physics and Quantum Chemistry into the 80s*, Ed. P.G. Burton (Univ. of Wollongong, Wollongong, 1980).

43. R.J. Buenker, in: *Studies in Physical and Theoretical Chemistry*, **Vol. 21** (Current Aspect of Quantum Chemistry 1981), Ed. R. Carbo (Elsevier Scientific, Amsterdam, 1982), p. 17.

44. R.J. Buenker and R.A. Phillips, *J. Mol. Struct.*, THEOCHEM **123**, 291 (1985)

45. S. Huzinaga, *Comp. Phys. Report*, **2**, 279 (1985).

46. S. Wilson, in *Methods in Computational Molecular Physics*, G.H. Diercksen and S. Wilson, Eds. Dorrecht, The Netherlands, Reidel, 1983.

47. E.R. Davidson and D. Feller, *Chem. Rev.*, **86**, 681 (1986).

48. J.C. Slater, *Phys. Rev.*, **36**, 57 (1930).

49. S.F. Boys, *Proc. Roy. Soc. London*, **A 200**, 542 (1950).

50. E. Clementi, *IBM J. Res. and Dev.*, **9**, 2 (1965).

51. J.L. Whitten, *J. Chem. Phys.* **44**, 359 (1966).

52. E. Clementi and D.R. Davis, *J. Comput. Phys.*, **1**, 223 (1967).

53. S. Huzinaga, *J. Chem. Phys.* **42**, 1293 (1965).

54. E.R. Davidson, L.E. McMurchie, and S. Days, *J. Chem. Phys.* **74**, 739 (1981).

55. E.R. Davidson and D. Feller, *Chem. Phys. Lett.* **104**, 54 (1984).

56. K. Ruedenberg, R.C. Raffenetti, R.D. Bardo, in *Energy, Structure and Reactivity, Proc. of the 1972 Boulder Conference*, (Wiley, New York, 1973).

57. R.D. Bardo and K. Ruedenberg, *J. Chem. Phys.* **60**, 918 (1974).

58. D. Feller and K. Ruedenberg, *Theor. Chim. Acta*, **71**, 231 (1979).

59. M.W. Schmidt and K. Ruedenberg, *J. Chem. Phys.* **71**, 3951 (1979).

60. G.D. Carney and R.N. Porter, *J. Chem. Phys.* **65**, 3547 (1976).

61. C.E. Dykstra and W.C. Swope, *J. Chem. Phys.* **70**, 1 (1979).

62. W. Meyer, P. Botschwina, and P. Burton, *J. Chem. Phys.* **84**, 891 (1986).

63. D. Talbi and R.P. Saxon, *J. Chem. Phys.* **89**, 2235 (1988).

64. The program HONDO can be obtained from the Quantum Chemistry Program Exchange. In the MRD-CI package, it has been solely used in the integral evaluation step.

65. J.N.L. Connor, *Comp. Phys. Comm.*, **17**, 117 (1979).

66. J.N. Murrell, S. Carter, S.C. Farantos, P. Huxley and A.J.C. Varandas, *Molecular Potential Energy Functions*, (Wiley, New York, 1984).

67. D.M. Hirst, *Potential Energy Surfaces*, (Taylor and Francis, London, 1985).

68. N. Sathyamurthy, *Comp. Phys. Report*, **3**, 1 (1985).

69. P.J. Kuntz, in *Theoretical Reaction Dynamics*, edited by M. Baer, (CRC Press, Boca Raton, FL, 1985), p. 71.

70. D.G. Truhlar, R. Steckler and M.S. Gordon, *Chem. Rev.*, **87**, 217 (1987).

71. G.C. Schatz, *Rev. Mod. Phys.*, **61**, 669 (1989).

72. G.C. Schatz, in *Potential Energy Surfaces and Dynamics Calculations*, edited by D.G. Truhlar, (Plenum, New York, 1981), p.287.

73. B.C. Garrett, D.G. Truhlar, A.F. Wagner, and T.H. Dunning, Jr., *J. Chem. Phys.* **78**, 4400 (1983).

74. J.M. Bowman and A. Kuppermann, *Chem. Phys. Lett.* **34**, 523 (1975).

75. J.N.L. Connor, W. Jakubetz and J. Manz, *Mol. Phys.* **29**, 347 (1975).

76. J.S. Wright and S.K. Gray, *J. Chem. Phys.* **69**, 67 (1978).

77. J.S. Wright and E. Kruus, *J. Chem. Phys.* **85**, 7251 (1986).

78. J.S. Wright, D.J. Donaldson, and R.J. Williams, *J. Chem. Phys.* **81**, 397 (1984).

79. T. Joseph, D.G. Truhlar, and B.C. Garrett, *J. Chem. Phys.* **88**, 6982 (1988).

80. P.J. Kuntz and A.C. Roach, *J. Chem. Soc. Faraday Trans.* 2, **68** 259 (1972).

81. J.S. Wright, *J. Chem. Soc., Fara. Trans. II*, **84**, 219 (1988).

82. W. Kolos and L. Wolniewiez, *J. Chem. Phys.* **43**, 2429 (1965).

83. Sukarma Thareja and N. Sathyamurthy, *J. Chem. Soc., Faraday Trans. 2* **81**, 717 (1985)

84. S. Chapman, M. Dupuis and S. Green, *Chem. Phys.* **78**, 93 (1983).

85. A. Kuppermann, *Chem. Phys. Lett.* **32**, 374 (1975).

86. L.M. Delves, *Nucl. Phys.*, **9** 391 (1959).

87. L.M. Delves, *Nucl. Phys.*, **20** 275 (1960).

3.7. Tables

Table 1

$(12s/7s,\ 4p,\ 1d)$ Gaussian-type basis set.

orbital	i	ξ_i	C_i
1s	1	837.22	.000112
	2	123.524	.000895
	3	27.7042	.004737
	4	7.82599	.019518
	5	2.6504	.065862
	6	.938258	.178008
2s	1	.372145	1.00000
3s	1	.155838	1.00000
4s	1	.066180	1.00000
5s	1	.027580	1.00000
6s	1	.011490	1.00000
7s	1	.004200	1.00000
1p	1	1.6	1.00000
2p	1	.40	1.00000
3p	1	.09	1.00000
4p	1	.025	1.00000
1d	1	1.0	1.00000

Table 2

Selected results for the CI energy[a] for H and H_2, using the (12*s*4p1*d*/7*s*4p1*d*) basis set.

Species	R^b (bohr)	Energy (hartree)	Reference
H(1*s*)		-0.499998	This work
H(1*s*)		-0.500000	exact
H(2*s*)		-0.124992	This work
H(2*s*)		-0.125000	exact
H(2*p*)		-0.124723	This work
H(2*p*)		-0.125000	exact
H_2 ($X\ ^1\Sigma_g^+$)	1.40	-1.173652	This work
		-1.173704	Liu, ref. 1
		-1.1733	LS, ref. 2
		-1.174474	KW, ref. 82
H_2 ($b\ ^3\Sigma_u^+$)	1.40	-0.783904	This work
		-0.784150	KW, ref. 82

a. Atomic energies are SCF orbital energies; molecular energies are full single and double excitation CI energies.

b. Internuclear distance for H_2.

Table 3

Electronic potential energies (in hartree)

for equilateral triangle geometries[a].

R^b	E_1	E_2	E_3	$E_4{}^c$
1.0	-1.286448	-1.286430	-1.280663	-1.258265
1.2	-1.441703	-1.441650	-1.415028	-1.398848
1.4	-1.518046	-1.518017	-1.468988	-1.458043
1.6	-1.554349	-1.554268	-1.482113	-1.475586
1.633	-1.557748	-1.557719	-1.481972	-1.475958
1.64	-1.558556	-1.558507	-1.481895	-1.475980
1.8	-1.569022	-1.568989	-1.474258	-1.471001
2.0	-1.571945	-1.571928	-1.455205	-1.454669
2.2	-1.568548	-1.568561	-1.430550	-1.432079
2.4	-1.561349	-1.561420	-1.403023	-1.406783
2.6	-1.552813	-1.552907	-1.375206	-1.380527
2.8	-1.544312	-1.544450	-1.347990	-1.354630
3.0	-1.536907	-1.536859	-1.322044	-1.329407

a. The origin of energy is that of the three electrons and the three protons at infinite separation. The energy of three separated $H(1s)$ atoms is -1.500000 hartree with respect to this origin.

b. in bohr. $R_1 = R_2 = R_3 = R$.

c. this state is antisymmetric with respect to the xy plane.

Table 4

Electronic potential energies (in hartree)

for symmetric linear geometries[a].

R^b	E_1	E_2	E_3	$E_4{}^c$
1.0	-1.434609	-1.301948	-1.283374	-1.283540
1.1	-1.510762	-1.353007	-1.336663	-1.336849
1.2	-1.564466	-1.384957	-1.370293	-1.370514
1.3	-1.601646	-1.403383	-1.390318	-1.390402
1.4	-1.626915	-1.412905	-1.400325	-1.400933
1.5	-1.643011	-1.416094	-1.403978	-1.404503
1.6	-1.652252	-1.415210	-1.402812	-1.403312
1.7	-1.656114	-1.413906	-1.398229	-1.398664
1.73	-1.656952	-1.413952	-1.396053	-1.396637
1.75	-1.656479	-1.414190	-1.395340	-1.395903
1.78	-1.656513	-1.416482	-1.392451	-1.393023
1.8	-1.656594	-1.418199	-1.391131	-1.391509
1.9	-1.653957	-1.431787	-1.385831	-1.382534
2.0	-1.649371	-1.445225	-1.377716	-1.372591
2.2	-1.636000	-1.465544	-1.358956	-1.350585

a. The origin of energy is that of the six particles (three electrons and three protons) at infinite separation. The energy of three separated $H(1s)$ atoms is -1.500000 hartree with respect to this origin.

b. in bohr. $R_1 = R_2 = R_3 = R$.

c. this state is antisymmetric with respect to the xy plane.

Table 5

Electronic potential energies (in hartree)

for non-symmetric linear geometries[a].

R^b	E_1	E_2	E_3	$E_4{}^c$
1.0	-1.622411	-1.247049	-1.246984	-1.247192
1.1	-1.648203	-1.273168	-1.272737	-1.272967
1.2	-1.663273	-1.287824	-1.287778	-1.288010
1.3	-1.670766	-1.295267	-1.295108	-1.295499
1.4	-1.673020	-1.297438	-1.297381	-1.297734
1.5	-1.671435	-1.309302	-1.295808	-1.296085
1.6	-1.667258	-1.331377	-1.291770	-1.291910
1.7	-1.661156	-1.350706	-1.285466	-1.285818
1.8	-1.653795	-1.367858	-1.278349	-1.278448
1.9	-1.645634	-1.383097	-1.270268	-1.270237
2.0	-1.636842	-1.396687	-1.261682	-1.261512
2.1	-1.627985	-1.408843	-1.254054	-1.252511

a. The origin of energy is that of the six particles (three electrons and three protons) at infinite separation. The energy of three separated $H(1s)$ atoms is -1.500000 hartree with respect to this origin.

b. in bohr. The geometry is such that $R_1 = R$, $R_2 = 10.0$ bohr and $R_3 = R_1 + R_2 = R + 10.0$ bohr.

c. this state is antisymmetric with respect to the xy plane.

Table 6

Lowest conical intersection energy and its corresponding geometry.

	E_1	LSTH[a]	DMBE[b]
R^c	1.973	1.981	1.973
E^d	2.747	2.756	2.748

a. See ref. 3.

b. See ref. 4.

c. $R_1 = R_2 = R_3 = R$ in bohr.

d. The lowest conical intersection energy with respect to that of the separated H + H_2 configuration. For the LSTH and DMBE surfaces, the accurate H + H_2 energy is used as the reference. For the present *ab initio* surface, the energy at the nuclear configuration with $R_1 = 1.402$ bohr, $R_2 = 10$ bohr and $R_3 = R_1 + R_2 = 11.402$ bohr is used instead. The difference between the second and the first of these reference energies is 0.040 eV.

Table 7

Saddle point properties

of the E_1 potential energy surface.

	Liu[b]	LSTH[b]	DMBE[c]	RMCS[d]	*ab initio*[e]
R_{sp}(bohr)[a]	1.757	1.757	1.755	1.758	1.758
E_{sp}(eV)[a]	0.425	0.4251	0.418	0.440	0.443
k_s (eV/bohr^2)[a]	2.90	2.93	2.95	2.90	2.90
k_a (eV/bohr^2)[a]	-1.6	-1.57	-1.54	-1.46	[e]

a. The saddle point geometry is described by $R_1 = R_2 = \frac{1}{2}R_3 = R_{sp}$. E_{sp} is the barrier height of the saddle point. k_s is the force constant for the symmetric stretch mode defined by $g_s = \frac{\sqrt{3}}{2}(R_1 + R_2 - 2R_{sp})$. k_a is the one for the asymmetric stretch mode defined by $g_a = \frac{1}{2}(R_1 - R_2)$.

b. See ref. 3. The barrier height is defined as the difference between the saddle point energy and the accurate value[82] of the H(1s) + $H_2(X\ ^1\Sigma_g^+)$ energy.

c. See ref. 4. The barrier is defined in the same way as in footnote b.

d. Present results for the E_1 RMCS surface. The barrier height is defined as the difference between the saddle point energy and the energy at the nuclear configuration defined by $R_2 = 10$ bohr and $R_1 = 1.402$ bohr (at which value of R_1 for the given R_2 the present *ab initio* calculation has a minimum, so does the E_1 RMCS surface). The accurate Kolos and Wolniewiez[82] equilibrium internuclear distance is $R_1 = 1.401$ bohr, and has an energy 0.040 eV below the present one.

e. The data in the *ab initio* column are obtained from the results of the one-dimensional GMF5 fits. The definition of the barrier height is the same one defined in footnote d. The k_a value was not calculated for lack of proper fit in the asymmetric mode to the *ab initio* data.

Table 8

Square of the absolute value of the electric dipole transition transition moment $|\mathbf{T}_{ij}|^2$ (in units of a.u.^{2}) of H_3 for the equilateral triangular geometries.

R (bohr)	$\|\mathbf{T}_{21}\|^2$	$\|\mathbf{T}_{31}\|^2$	$\|\mathbf{T}_{32}\|^2$	$\|\mathbf{T}_{43}\|^2$
1.2	0.009	4.20	4.20	6.92
1.4	0.018	3.38	3.42	7.02
1.6	0.030	2.70	2.68	7.18
1.633	0.032	2.59	2.60	7.22
1.64	0.033	2.54	2.58	7.24
1.8	0.047	2.12	2.12	7.34
2.0	0.061	1.70	1.70	7.51
2.2	0.071	1.32	1.30	7.56
2.4	0.077	1.07	1.05	7.73

a. $\mathbf{T}_{ij}$ is the transition dipole vector between i and j states. The indices (1, 2, 3, 4) refer to states E_1, E_2, E_3 and E_4 respectively.

Table 9

Absolute value of the component of the electric dipole transition moment[a] (in a.u.) between the four calculated electronic states for equilateral triangle geometries.

R^b	$\lvert T_{41}(z) \rvert$	$\lvert T_{42}(z) \rvert$	$\lvert T_{43}(z) \rvert$
1.0	.432(-3)	.194(-3)	2.61
1.2	.541(-3)	.120(-3)	2.63
1.4	.483(-3)	.489(-3)	2.65
1.6	.809(-3)	.546(-3)	2.68
1.633	.557(-3)	.922(-3)	2.69
1.64	.830(-3)	.378(-3)	2.69
1.8	.647(-3)	.538(-3)	2.71
2.0	.497(-3)	.732(-3)	2.74
2.2	.140(-3)	.100(-2)	2.75
2.4	.904(-3)	.556(-3)	2.78
2.6	.152(-2)	.153(-3)	2.80
2.8	.150(-2)	.206(-3)	2.81
3.0	.710(-3)	.758(-4)	2.82

R^b	$\lvert T_{31}(x) \rvert$	$\lvert T_{31}(y) \rvert$	$\lvert T_{32}(x) \rvert$	$\lvert T_{32}(y) \rvert$	$\lvert T_{21}(x) \rvert$	$\lvert T_{21}(y) \rvert$
1.0	2.25	.944(-1)	.927(-1)	2.26	.586(-1)	.521(-1)
1.2	.199	2.04	2.04	.198	.916(-1)	.182(-1)
1.4	.161	1.83	1.84	.159	.131	.227(-1)
1.6	1.22	1.10	1.09	1.22	.202(-1)	.172
1.633	1.21	1.06	1.06	1.21	.235(-1)	.179
1.64	1.38	.801	.803	1.39	.909(-1)	.157
1.8	.362	1.41	1.41	.361	.189	.103
2.0	.372	1.25	1.25	.371	.207	.135
2.2	.424	1.07	1.06	.421	.194	.182
2.4	.474	.918	.917	.472	.161	.225
2.6	.446	.812	.814	.444	.148	.226
2.8	.443	.702	.700	.439	.111	.226
3.0	.388	.639	.632	.385	.104	.196

a. T_{ij} is the transition dipole vector between i and j states. The indices (1, 2, 3, 4) refer to states E_1, E_2, E_3 and E_4 respectively. .432(-3) means $.432\times10^{-3}$.

b. in bohr. $R_1 = R_2 = R_3 = R$.

Table 10

Absolute value of the Z component of the electric dipole transition moment[a] (in a.u.) from E_4 to E_1, E_2, and E_3 for symmetric collinear geometries.

R[b]	$\mid T_{41}(z) \mid$	$\mid T_{42}(z) \mid$	$\mid T_{43}(z) \mid$
1.0	0.130(-5)	2.68	0.656(-5)
1.1	0.227(-5)	2.69	0.505(-5)
1.2	0.853(-6)	2.68	0.361(-5)
1.3	0.675(-6)	2.69	0.464(-5)
1.4	0.278(-5)	2.68	0.160(-4)
1.5	0.517(-6)	2.65	0.175(-5)
1.6	0.202(-5)	2.57	0.548(-5)
1.7	0.151(-7)	2.22	0.199(-5)
1.8	0.558(-6)	1.24	0.142(-6)
1.9	0.195(-6)	0.513	2.68
2.0	0.137(-5)	0.260	2.66
2.2	0.111(-6)	0.879(-1)	2.49

a. T_{ij} is the transition dipole vector between i and j states.
The indices (1, 2, 3, 4) refer to states E_1, E_2, E_3 and E_4 respectively.
.432(-3) means $.432 \times 10^{-3}$.

b. in borh. $R_1 = R_2 = \frac{1}{2}R_3 = R$.

Table 11

Absolute value of the Z component of the electric dipole transition moment[a] (in a.u.) between E_4 and E_1, E_2, and E_3 for non-symmetric collinear geometries.

R^b	$\mid \mathbf{T}_{41}(z) \mid$	$\mid \mathbf{T}_{42}(z) \mid$	$\mid \mathbf{T}_{43}(z) \mid$
1.0	0.743	2.46	0.436(-6)
1.1	0.743	2.45	0.872(-6)
1.2	0.742	2.55	0.469(-7)
1.3	0.741	.756(-8)	0.942
1.4	0.741	1.52	0.186(-6)
1.5	0.747	.152(-2)	0.104(-7)
1.6	0.740	.702(-3)	1.31
1.7	0.751	.388(-3)	[c]
1.8	0.751	.282(-3)	0.208
1.9	0.749	.190(-3)	0.284
2.0	0.748	.158(-3)	0.310
2.1	0.756	.935(-3)	0.128(-2)

a. $\mathbf{T}_{ij}$ is the transition dipole vector between i and j states.
The indices (1, 2, 3, 4) refer to states E_1, E_2, E_3 and E_4 respectively.
.432(-3) means $.432 \times 10^{-3}$.

b. in bohr. $R_1 = R$, $R_2 = 10.0$ bohr, and $R_3 = R_1 + R_2$.

c. not available.

Table 12

Comparisons of the E_1 *ab initio* and RMCS surfaces with the LSTH and DMBE surfaces.

	Δ^a_{ave} (eV)	Δ^b_{rms} (eV)	$\mid \Delta \mid^c_{max}$ (eV)
ab initio – LSTH	0.51(-1)	0.59(-1)	0.34
ab initio – DMBE	0.53(-1)	0.57(-1)	0.12
ab initio – RMCS	0.70(-3)	0.24(-1)	0.27
RMCS – LSTH	0.50(-1)	0.62(-1)	0.38
RMCS – DMBE	0.52(-1)	0.59(-1)	0.20

a. Average value of the difference between the potential energy surfaces identified in the first column for the 560 nuclear configurations at which the *ab initio* surface was calculated.

b. Root mean square value of the difference defined in footnote a.

c. Maximum of the absolute value of the difference defined in footnote a.

Table 13

Fits of the $E_{1,2}$ potential energy surfaces for equilateral triangle configuration.

A. GMF5 parameters[a].

	LSTH [b]	DMBE [c]	RMCS [d]	*ab initio* [e]
D_e (eV)	1.992	2.000	1.962	1.962
E_e (eV) [f]	2.756	2.748	2.747	2.747
R_e (bohr)	1.976	1.969	1.973	1.973
β_e (bohr^{-1})	.726	.732	.772	.772
λ_1 (bohr^{-1})	.036	.027	-.045	-.045
λ_2 (bohr^{-2})	.022	.028	.046	.049

B. Morse parameters

	LSTH [b]	DMBE [c]	RMCS [d]	*ab initio* [e]
D_e (eV)	2.030	2.039	1.976	1.978
R_e (bohr)	1.932	1.924	1.935	1.932
β_e (bohr^{-1})	.825	.831	.822	.828

a. See text (Eqs. 20 to 22 of section 3.4) for the definitions of the GMF5 parameters.

b. The fit used the LSTH energies at the same set of nuclear configurations as in the GMF5 fit of the *ab initio* data. The reference energy is the theoretical value of three isolated H atoms. The values of D_e and R_e for the LSTH surface (not obtained from a Morse function) are 1.992 eV and 1.981 bohr[3].

c. See footnote b for the selection of the nuclear configurations and choice of reference energy. The values of D_e and R_e for the DMBE surface (not obtained from a Morse function) are 2.000 eV and 1.973 bohr[4].

d. See footnote b for the selection of the nuclear geometry configurations. The reference energy is chosen to be three times the value of the present SCF H($1s$) energy with the $12s4p1d/7s4p1d$ basis (see Tables 1 and 2), which is about 0.2 meV above the theoretical value.

e. The reference energy is the same defined in footnote d.

f. The energy of the minimum point with respect to that of an separated H + H_2 configuration. It is not one of the GMF5 parameters, and has been listed in Table 6. For the LSTH and DMBE surfaces, the accurate H + H_2 energy[82] is used as the reference. For the E_1 RMCS and the *ab initio* surfaces, the energy at the nuclear configuration with $R_1 = 1.402$ bohr, $R_2 = 10$ bohr and $R_3 = R_1 + R_2 = 11.402$ bohr is used instead. The difference between the second and the first of these reference energies is 0.040 eV.

Table 14

Fits of the E_4 potential energy surface for equilateral triangle configuration.

A. GMF5 parameters[a]

	RMCS [b]	*ab initio* [c]
D_e (eV)	9.558	9.558
E_e (eV) [d]	2.747	2.747
R_e (bohr)	1.642	1.642
β_e (bohr^{-1})	.575	.575
λ_1 (bohr^{-1})	.084	.084
λ_2 (bohr^{-2})	.027	.043

B. Morse parameters

	RMCS [b]	*ab initio* [c]
D_e (eV)	9.623	9.632
R_e (bohr)	1.658	1.656
β_e (bohr^{-1})	.614	.623

a. See text (Eqs. 20 to 22 of section 3.4) for the definitions of the GMF5 parameters.

b. The reference energy is chosen to be the sum of the present SCF energies of H($2p_z$) + 2H($1s$) with the $12s4p1d/7s4p1d$ basis (see Tables 1 and 2), which is about 0.2 meV above the theoretical value.

c. The reference energy is the one defined in footnote d.

d. Energy of the minimum point with respect to that of a separated H + H_2 configuration. E_e is not one of the GMF5 parameters (see Table 13). The energy of the *ab initio* E_1 surface at the nuclear configuration with $R_1 = 1.402$ bohr, $R_2 = 10$ bohr and $R_3 = R_1 + R_2 = 11.402$ bohr is used as the reference energy. This is higher than the accurate energy reference[82] by 0.040 eV.

3.8. Figures and captions

Fig. 1. Energy level and correlation diagram of H_3. The spacing of the H_3 energy levels was calculated for an equilateral triangle configuration[5] and referred to the energy of dissociated products by the results of a separated calculation[8].

Fig. 2. Flow-chart of the MRD-CI programs. The name of each individual routine is listed along with a brief description of its function.

Fig. 3. Coordinate system used in the MRD-CI program. P_i is the ith proton of H_3. The three protons are all in the **x y** plane. The bond distance R_1 between P_1 and P_3, R_2 between P_1 and P_2, and the bond angle γ between them are used as the variables describing the shape of the triangle.

Fig. 4. Internal coordinate system used in the RMCS surface fitting scheme. In the R_1, R_2 Cartesian coordinates, P_s is the swing point with $R_1 = R_1^s$ and $R_2 = R_2^s$. A point P can be described by the swing angle θ and the swing distance l with respect to the swing point P_s.

Fig. 5. Potential energy curves for equilateral H_3. R is the length of the side of the triangle. In equilateral configurations, the E_1 and E_2 states are degenerate with each other. The energy origin is that of the accurate H + H_2 value obtained by Kolos and Wolniewiez[82].

Fig. 6. Magnitude of the electric dipole transition moment $\mathbf{T}_{31}$ between the E_3 and E_1 states for equilateral H_3. R is the length of the side of the triangle.

Fig. 7. Magnitude of the electric dipole transition moment $\mathbf{T}_{21}$ between the E_2 and E_1 states for equilateral H_3. R is the length of the side of the triangle.

Fig. 8. Comparison between the DMBE ground potential energy surface (E_1^{DMBE}) and the present *ab initio* results. The molecule is in a symmetric collinear configuration with $R_1 = R_2 = \frac{1}{2}R_3$, corresponding to $\gamma = 180°$ and $\theta = 45°$. The energy origin is defined in the caption for Fig. 5. Fig. 8a displays the energies, and the differences between them are depicted in Fig. 8b. The energy origin is that of Fig. 5.

Fig. 9. Comparison between the upper sheet of the DMBE surface (E_2^{DMBE}) and the present *ab initio* results for the E_2 state. The molecule is in the same nuclear configuration as in Fig. 8. The energy origin is that of Fig. 5.

Fig. 10. Potential energy curves for the E_2 and E_3 States. The molecular geometry is the same as in Fig. 8. The energy origin is that of Fig. 5.

Fig. 11. Potential energy curves for the E_2 and E_3 states. The molecule is in a non-symmetric collinear configuration with $R_2 \equiv 10$ bohr and $R_3 = R_1 + R_2$, corresponding to $\gamma = 180°$ and $\theta = 0°$. The energy origin is that of Fig. 5.

Fig. 12. Potential energy curves for the E_2 state. The nuclear configuration is given by γ, θ, and R_1. γ is fixed at 60°. θ varies from 45° to 0° in the plots of Figs. 12a through 12j. The energy origin is that of Fig. 5.

Fig. 13. Potential energy curves for the E_3 state. The nuclear configuration is given by γ, θ, and R_1. γ is fixed at 60°. θ varies from 45° to 0° in the plots of Figs. 13a through 13j. The energy origin is that of Fig. 5.

Fig. 14. Potential energy curves for the E_2 and E_3 states. The molecular geometry is given by γ, θ, and R_1. θ is fixed at 45° which means that $R_1 \equiv R_2$. γ varies from 60° to 180° in the plots of Figs. 14a through 14e. The energy origin is that of Fig. 5.

Fig. 15. GMF5 parameters for the E_1 state as functions of θ. γ is fixed at 60°. All curves are symmetric with respect to $\theta = 45°$ because of identical particle permutation symmetry. In Figs. 15d and 15e, λ_1 and λ_2 and their one-σ statistical error bars in the GMF5 fits are given. The curves in Figs 15d and 15e are the smoothed λ_1 and λ_2 used in the E_1 RMCS surface.

Fig. 16. GMF5 parameters for the E_4 state as functions of θ. γ is fixed at 60°. See the caption for Fig. 15 for details.

Fig. 17. Two-dimensional equipotential contour plots of the E_1 RMCS potential energy surface. The molecular geometry is given by two bond distances R_1, R_2, and bond angle γ. γ values are chosen to be 15°, 30°, 45°, 60°, 75°, 90°, 120°, 150°, and 180° in plots of Figs. 17a through 17i. The contour energies are in the range [0.5 eV, 6.0 eV] with increments of 0.5 eV. All contour plots have an outermost contour with an energy of 6.0 eV and an innermost one of 0.5 eV. The energy origin is that of Fig. 5.

Fig. 18. Two-dimensional equipotential contour plots of the E_4 RMCS potential energy surface. The molecular geometry is given by two bond distances R_1, R_2, and bond angle γ. The values of γ are 15°, 30°, 45°, 60°, 75°, 90°, 120°, 150°, and 180° in the plots of Figs. 18a through 18i respectively. All contour plots have an outermost contour with an energy of 10.0 eV. The energy step used for all plots is 0.5 eV. The energy origin is that of Fig. 5.

Fig. 19. Potential energy curves for the equilateral triangular configurations of the DMBE and E_1 RMCS surfaces. R is the internuclear distance.

Fig. 20. Two-dimensional equipotential contour plots of the E_1 RMCS potential energy surface in hyperspherical coordinates[85] with constant Y_λ (see Eqs. (33) through (35) of section 3.5.3). The contour energies are in the range

[0.5 eV, 3.5 eV] with increment of 0.5 eV. The outermost contour has an energy of 3.5 eV. The values of Y_λ are 2.6 bohr, 1.0 bohr, and 0.0 bohr respectively for Figs. 20a, 20b, and 20c. The energy origin is that of Fig. 5. The small closed contour in the center of Fig. 20a has an energy of 2.0 eV.

Fig. 21. Two-dimensional equipotential contour plots of the E_4 RMCS potential energy surface in hyperspherical coordinates[85] with constant Y_λ (see Eqs. (33) through (35) of section 3.5.3). All contour plots have an outermost contour with an energy of 10.0 eV. The energy step for all plots is 0.5 eV. The energy origin is that of Fig. 5. The values of Y_λ are 2.16 bohr, 1.0 bohr, and 0.0 bohr respectively for Figs. 21a, 21b, and 21c.

Fig. 22. North pole view of the E_1 RMCS potential energy surface at $\rho = 6.0$ bohr. The mapping is defined by Eqs. (36) and (37) of section 3.5.3. The contour energies are in the range [0.5 eV, 6.0 eV] with increments of 0.5 eV. The energy origin is that of Fig. 5.

Fig. 23. South pole view of the E_1 RMCS potential energy surface at $\rho = 6.0$ bohr. See the caption for Fig. 22 and the text for other details.

Fig. 24. Equatorial view of the E_1 RMCS potential energy surface. The ρ values are 2.0 bohr, 3.27 bohr, and 6.0 bohr respectively for Figs. 24a, 24b and 24c. See the caption for Fig. 22 and text for other details. The contour energies are in the range [3.5 eV, 10.0 eV] in Fig. 24a, [1.0 eV, 6.0 eV] in Fig. 24b and [0.5 eV, 6.0 eV] in Fig. 24c, with increments of 0.5 eV. In Fig. 24a, the two innermost contours have an energy of 3.5 eV. They indicate that there is a shallow valley between them and a local maximum at the center of the plot. The same features can be seen in Figs. 24b and 24c. In Fig. 24c, the valley has been pushed to the edge of plot, and has been separated into

three local valleys. They correspond to the diatomic bonding in the H + H_2 configuration. The energy origin is that of Fig. 5.

Fig. 25. Equatorial view of the E_4 potential energy surface contours. The ρ values are 1.0 bohr, 2.16 bohr, and 6.0 bohr respectively for Figs. 25a, 25b and 25c. The contour energies are in the range [25 eV, 45 eV] with increments of 5 eV in Fig. 25a, [5.5 eV, 10.0 eV] with increments of 0.5 eV in Fig. 25b, and [10.5 eV, 13.5 eV] with increments of 0.5 eV in Fig. 25c. See the caption for Fig. 22 for other details. Fig. 25b shows a deep minimum at the center of the plot. Fig. 25c has features similar to those seen in Fig. 24c. The three local potential valleys correspond to the diatomic bonding in the H($2p_z$) + $H_2(X^1\Sigma_g^+)$ configuration. The energy origin is that of Fig. 5.

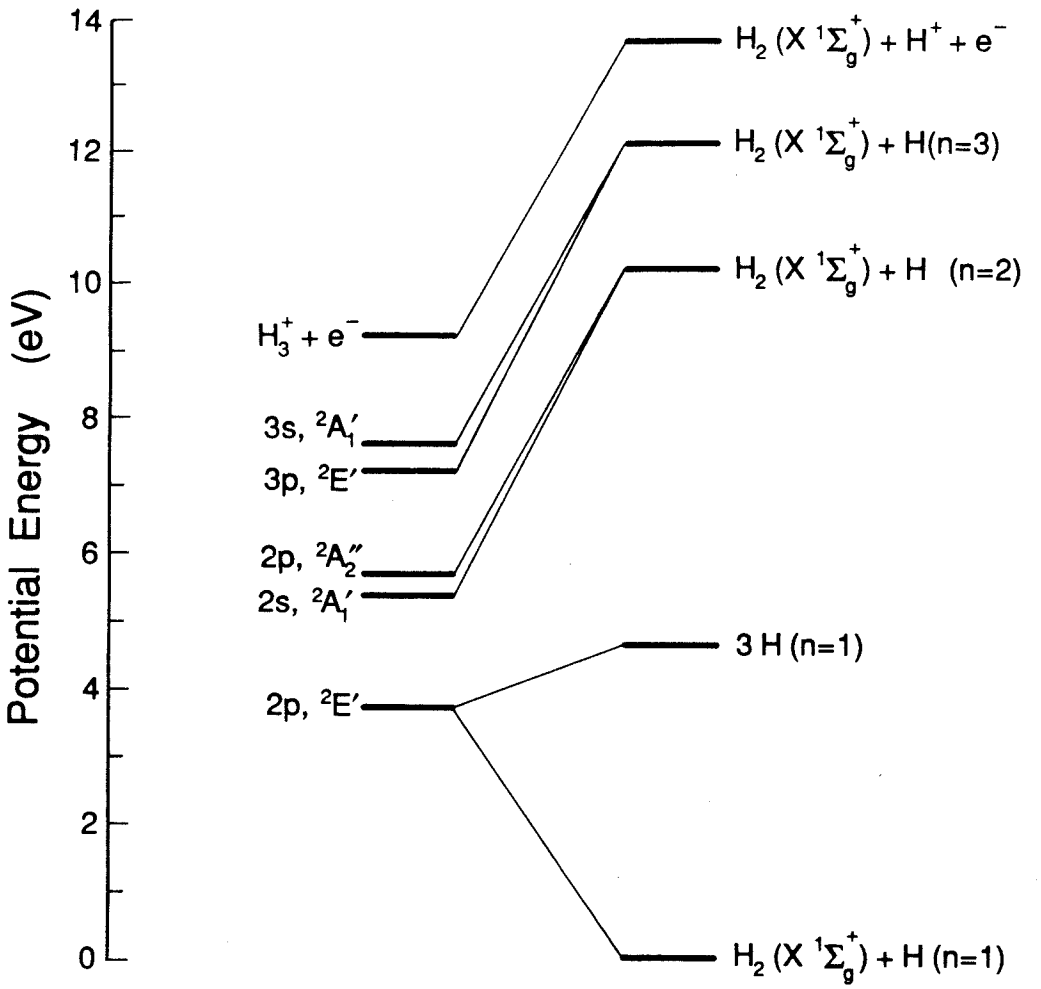
Potential Energy (eV)
14
12
10
8
6
4
2
0
$H_2 (X\ ^1\Sigma_g^+) + H^+ + e^-$
$H_2 (X\ ^1\Sigma_g^+) + H(n=3)$
$H_2 (X\ ^1\Sigma_g^+) + H\ (n=2)$
$H_3^+ + e^-$
3s, $^2A_1'$
3p, $^2E'$
2p, $^2A_2''$
2s, $^2A_1'$
2p, $^2E'$
3 H (n=1)
$H_2 (X\ ^1\Sigma_g^+) + H\ (n=1)$

Fig. 1

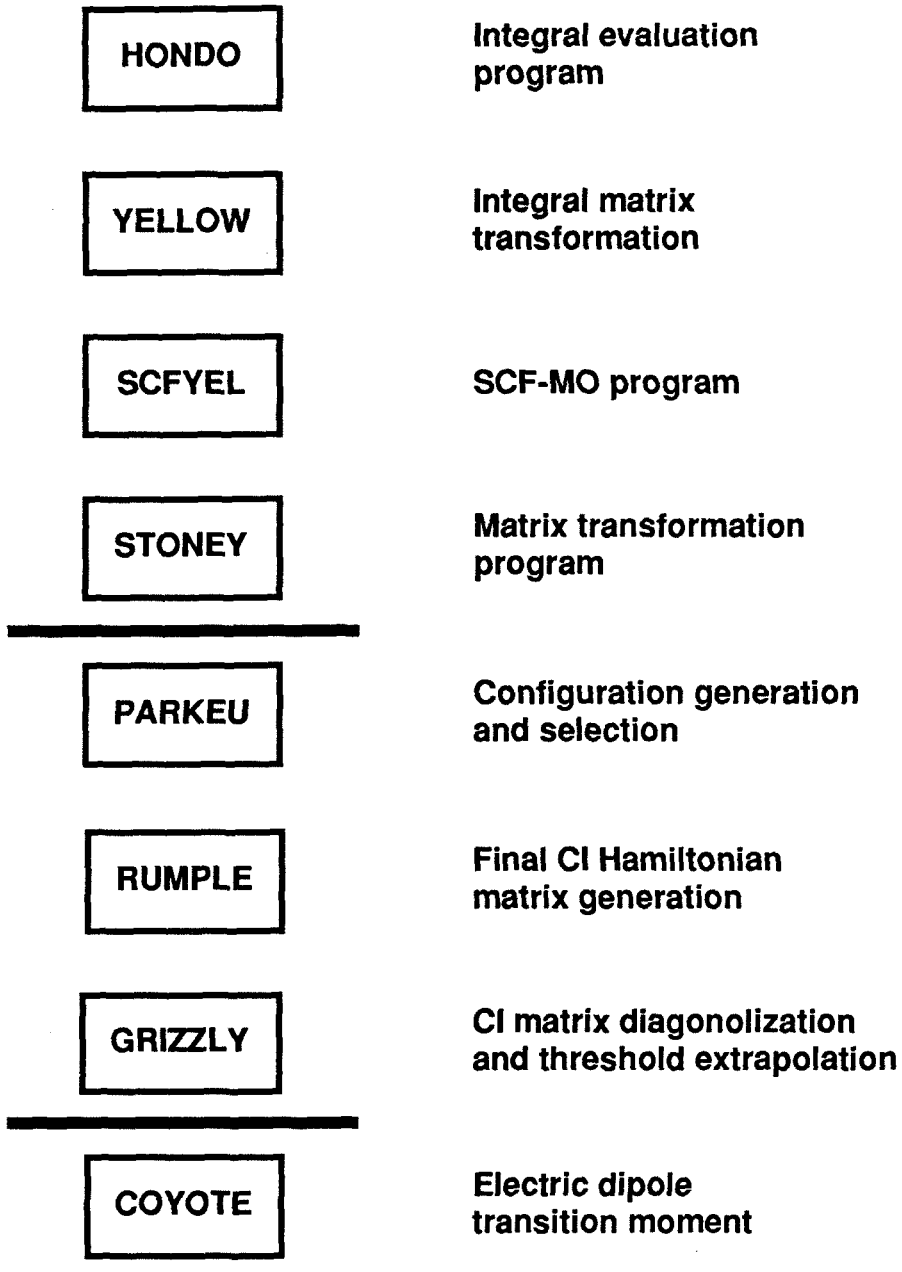
HONDO
Integral evaluation program
YELLOW
Integral matrix transformation
SCFYEL
SCF-MO program
STONEY
Matrix transformation program
PARKEU
Configuration generation and selection
RUMPLE
Final CI Hamiltonian matrix generation
GRIZZLY
CI matrix diagonolization and threshold extrapolation
COYOTE
Electric dipole transition moment

Fig. 2

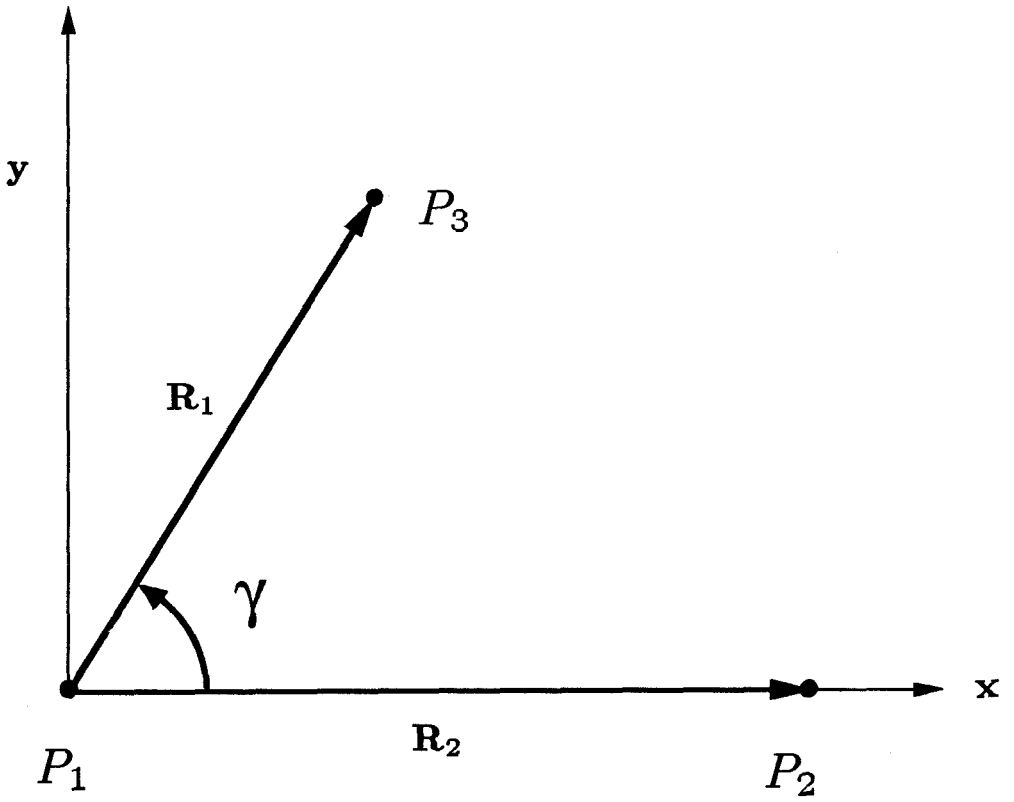

Fig. 3

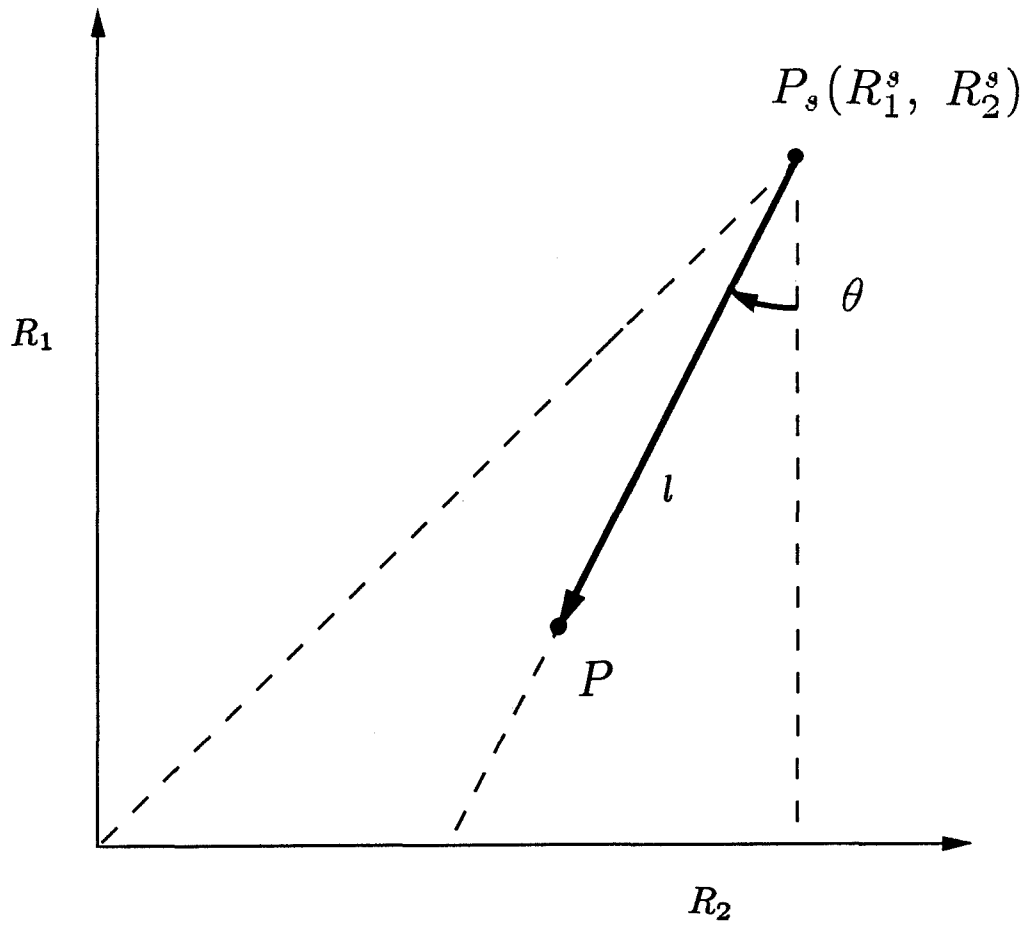

Fig. 4

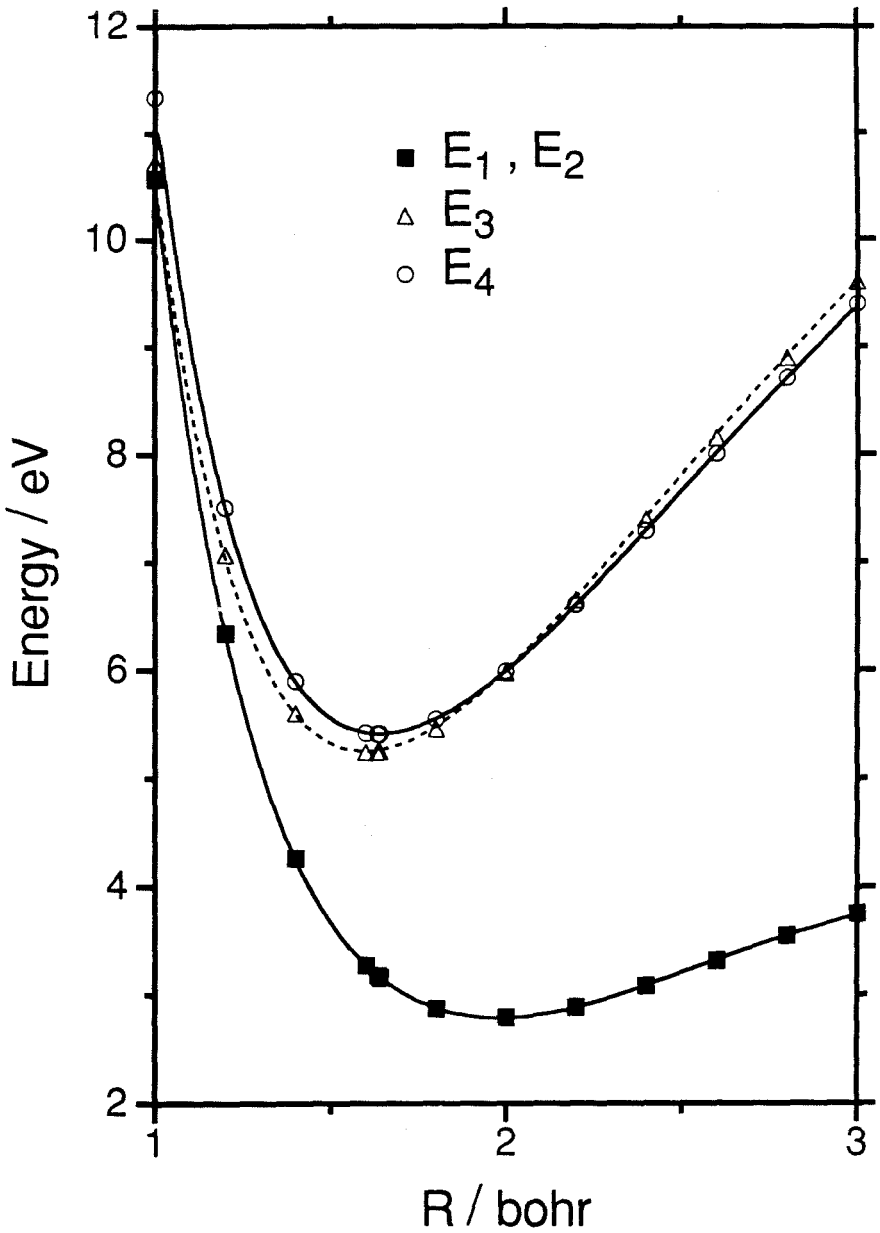

Fig. 5

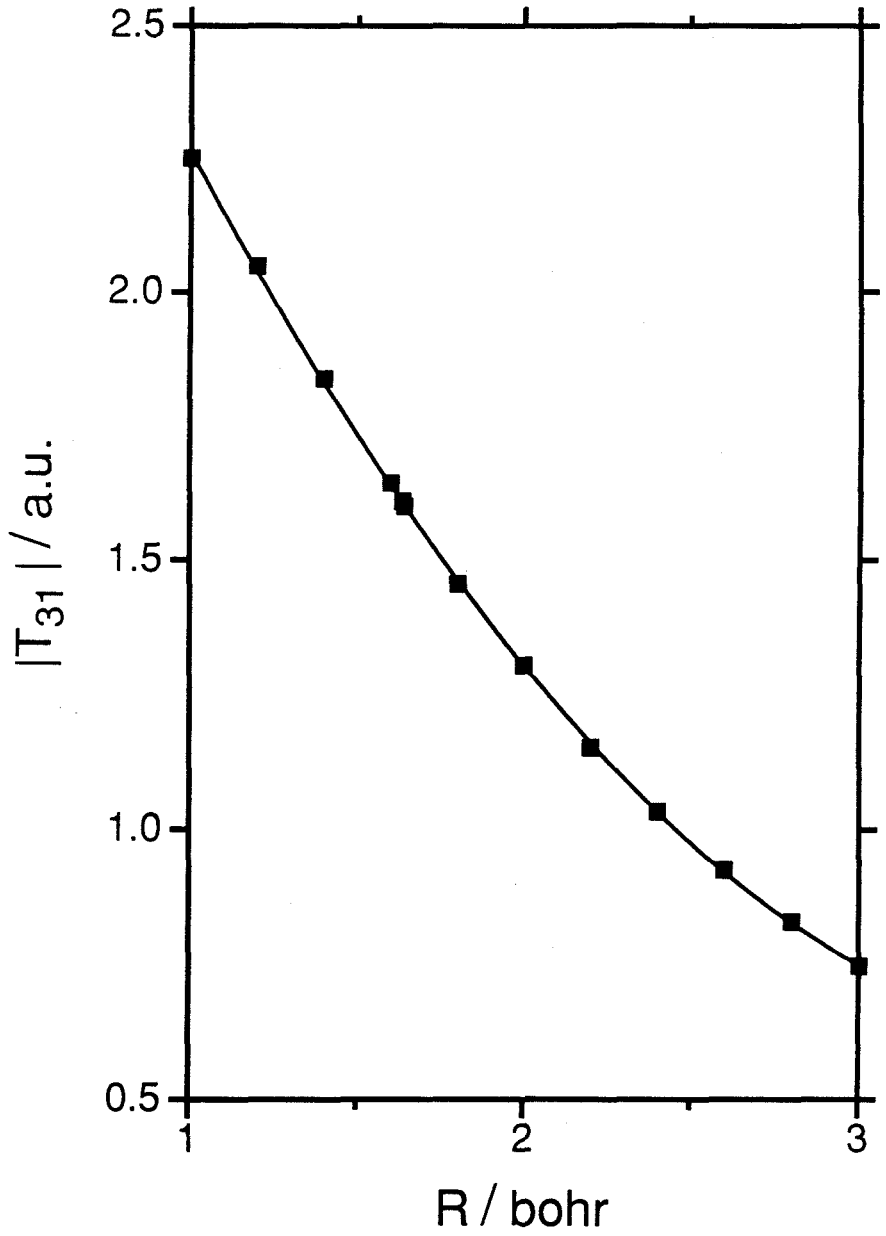

Fig. 6

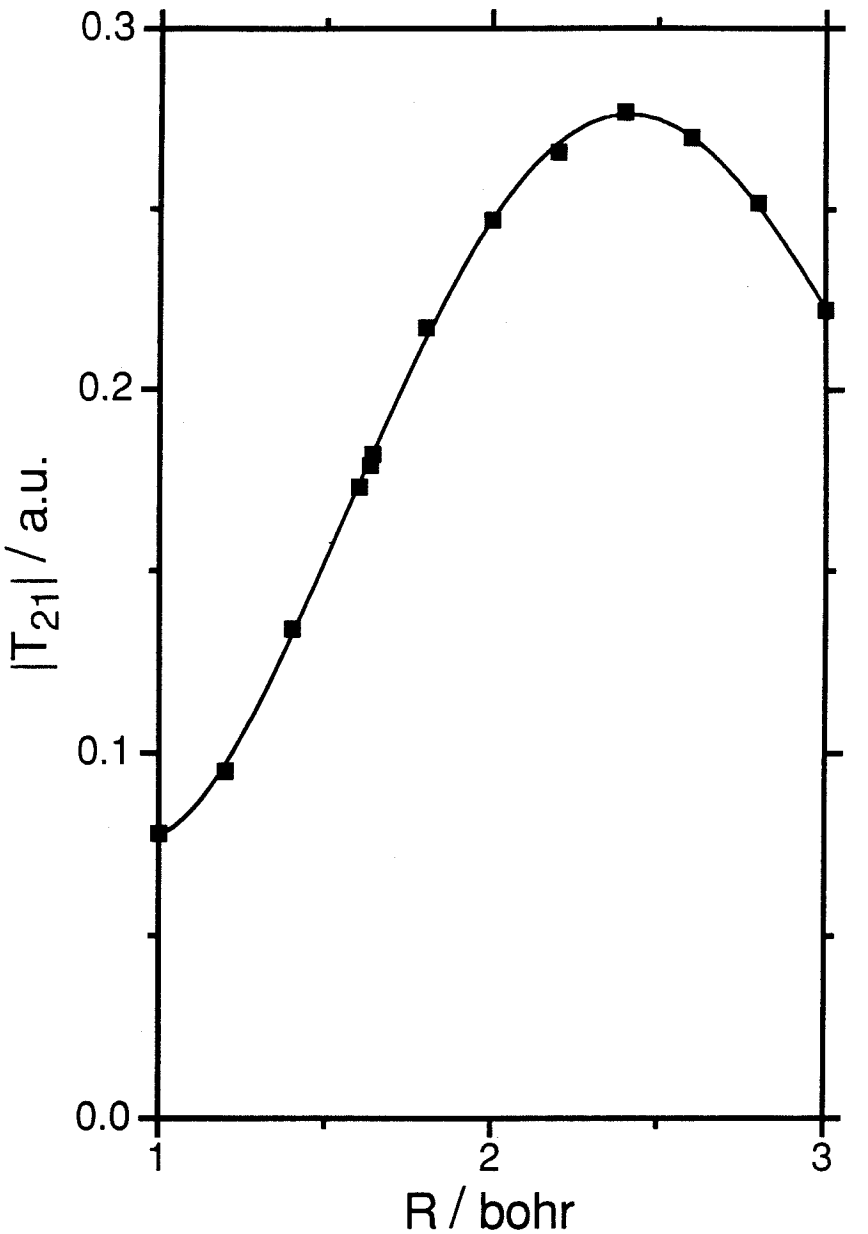

Fig. 7

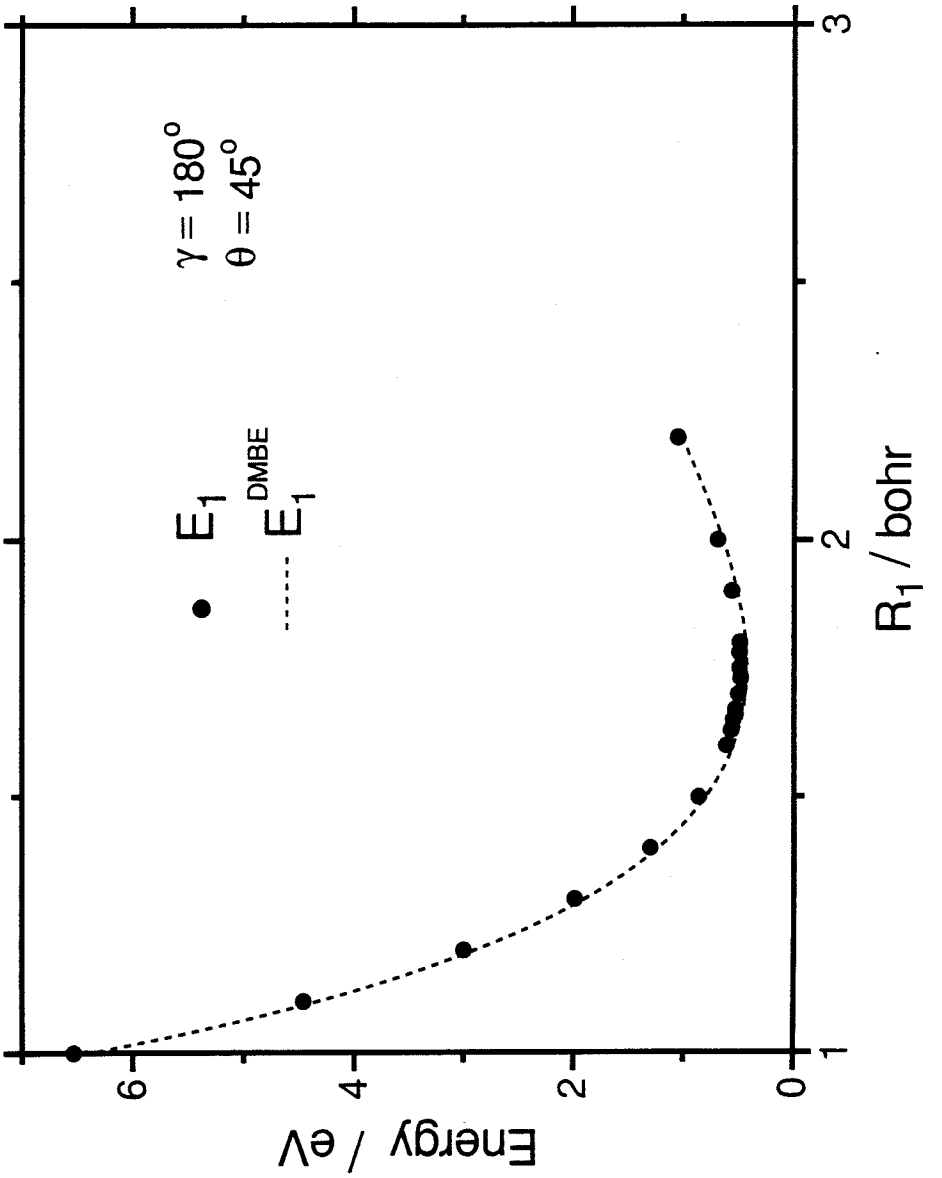

Fig. 8a

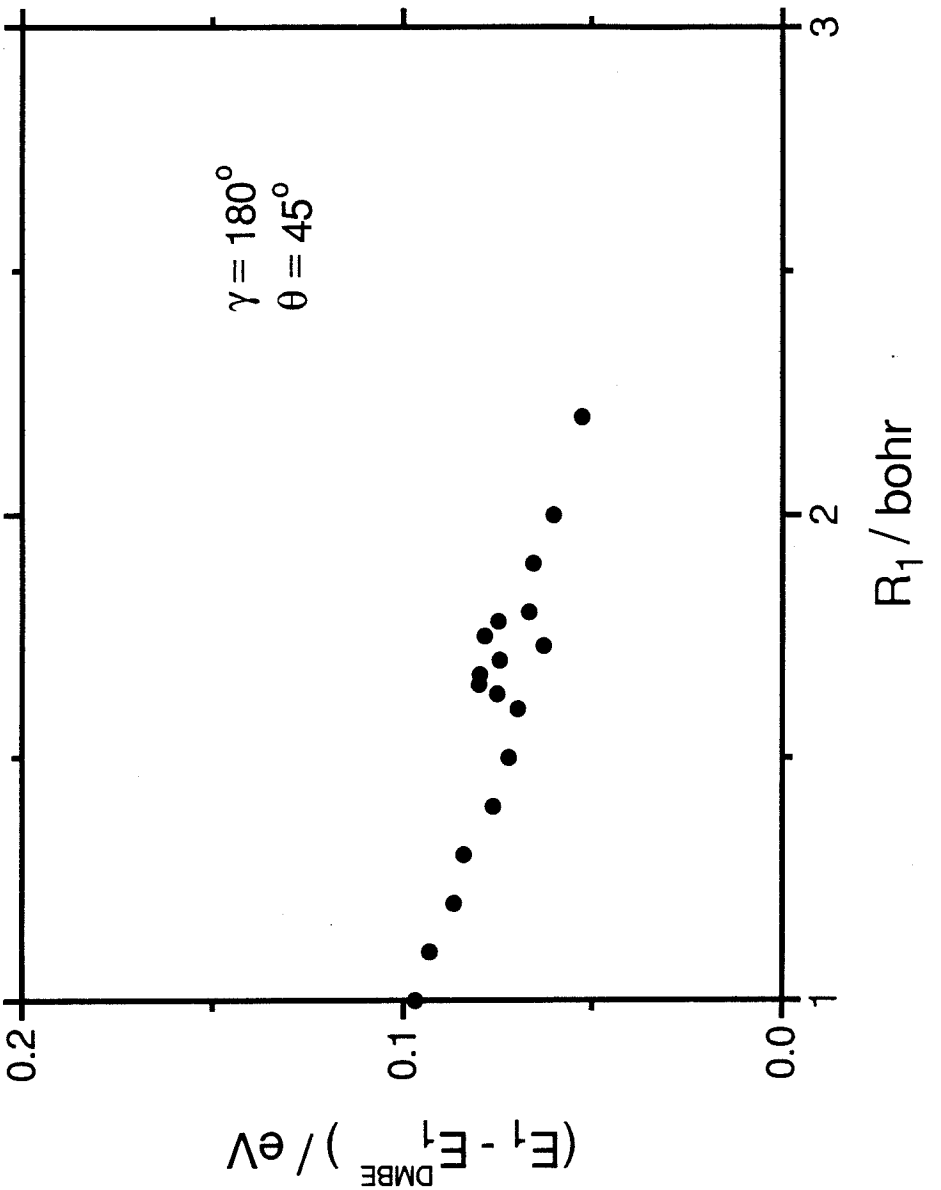

Fig. 8b

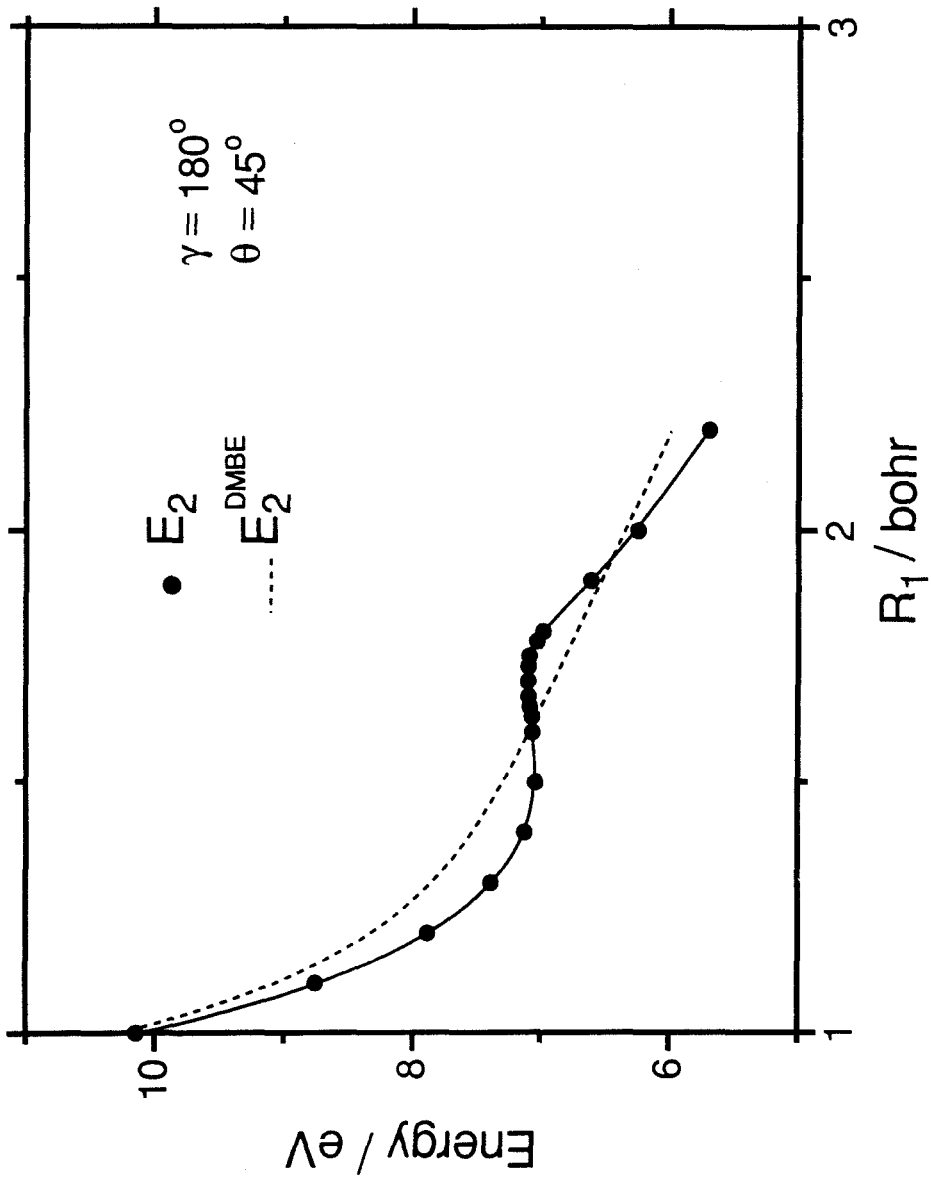

Fig. 9

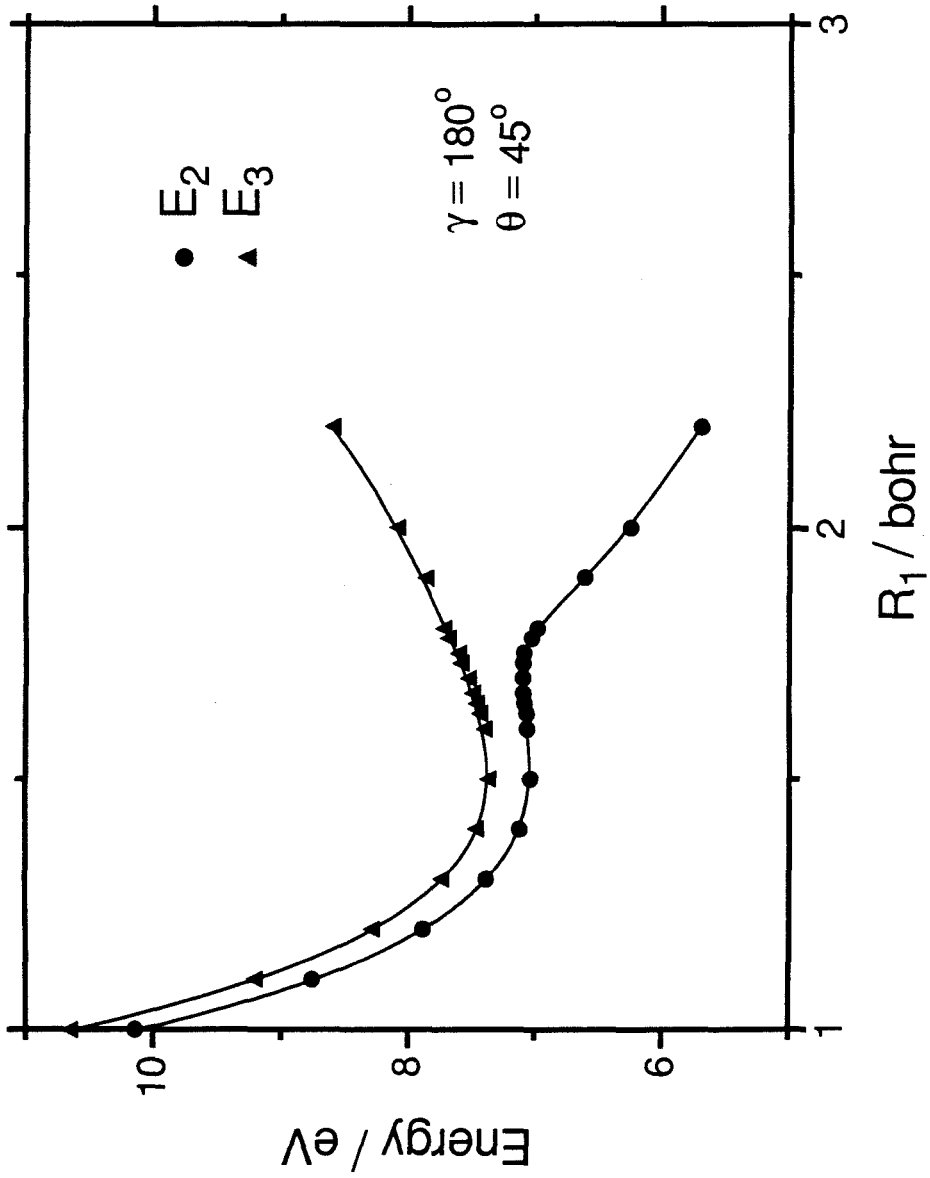

Fig. 10

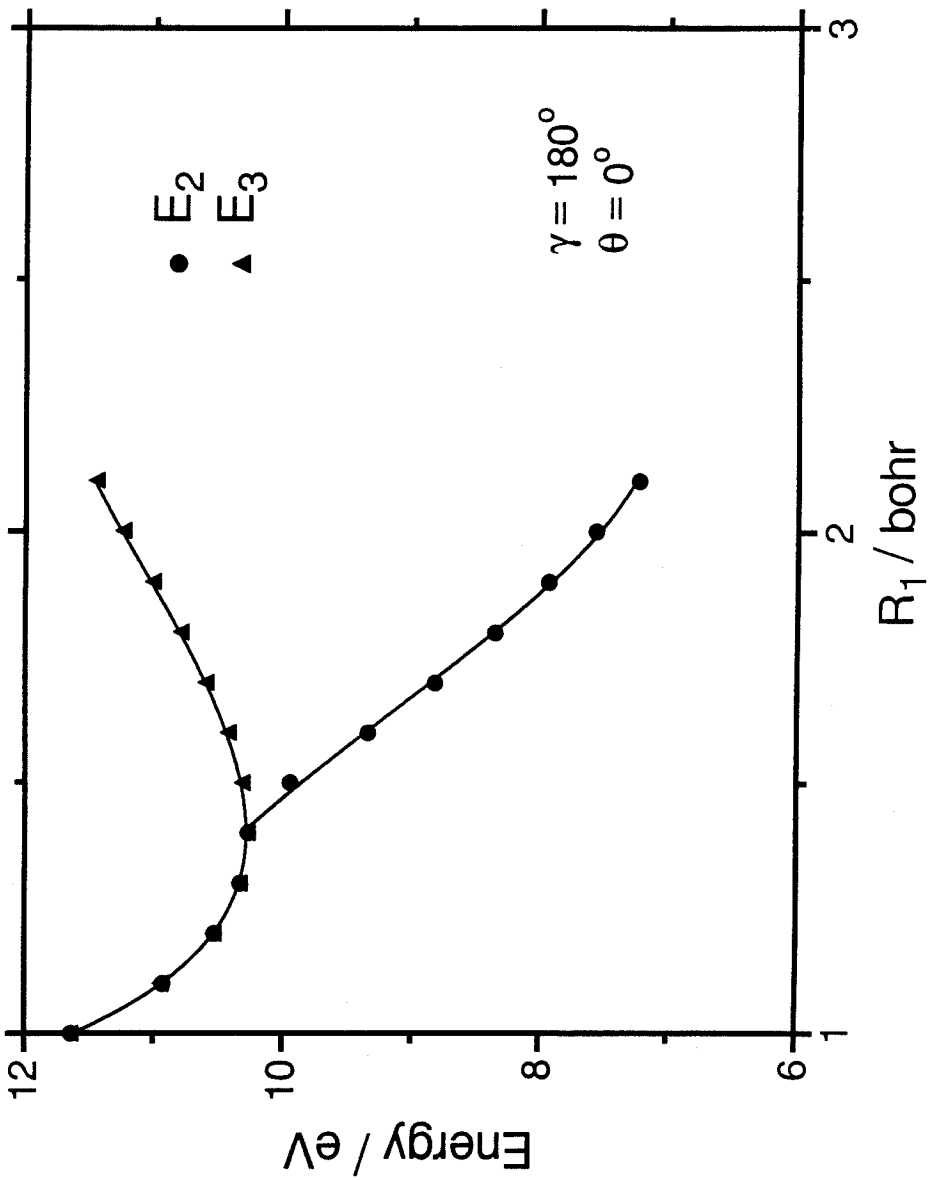

Fig. 11

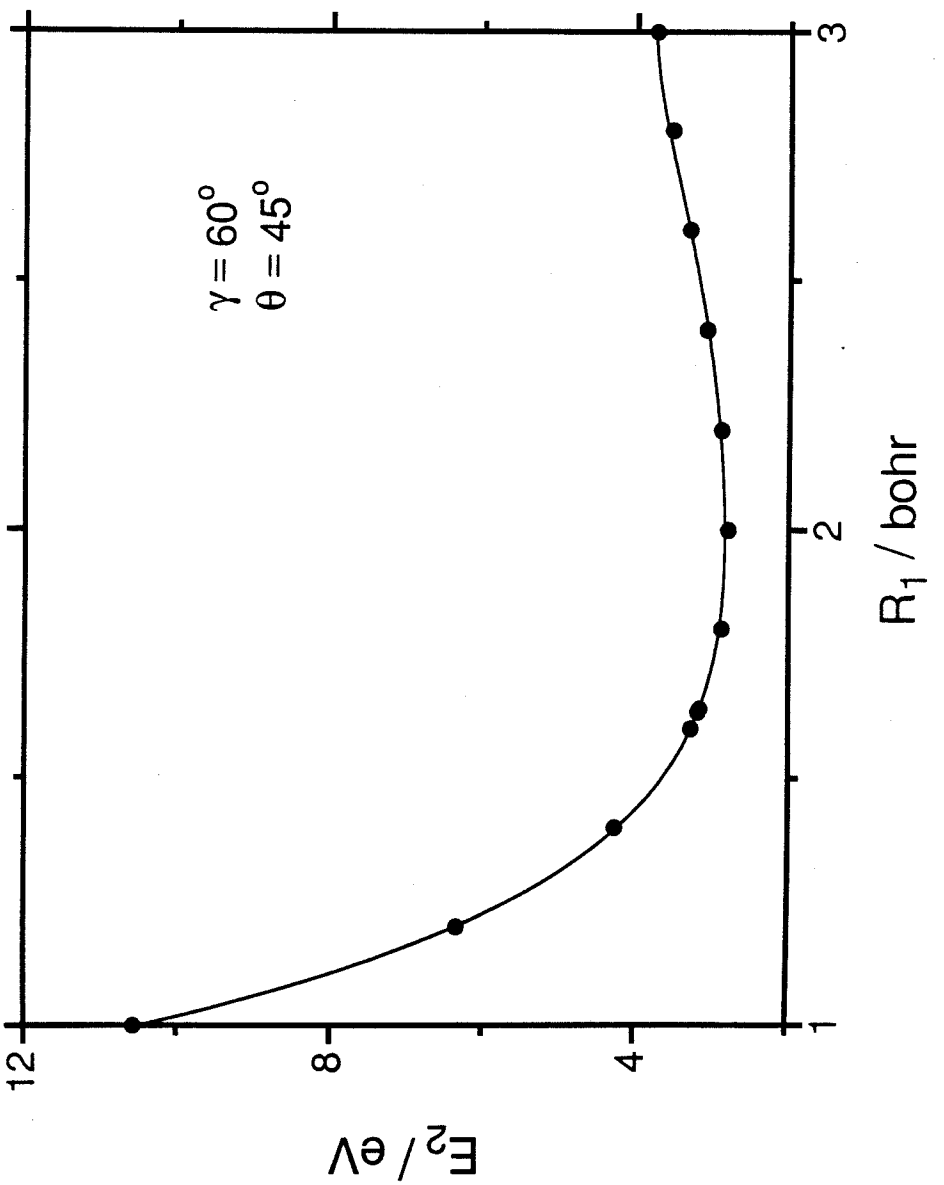

Fig. 12a

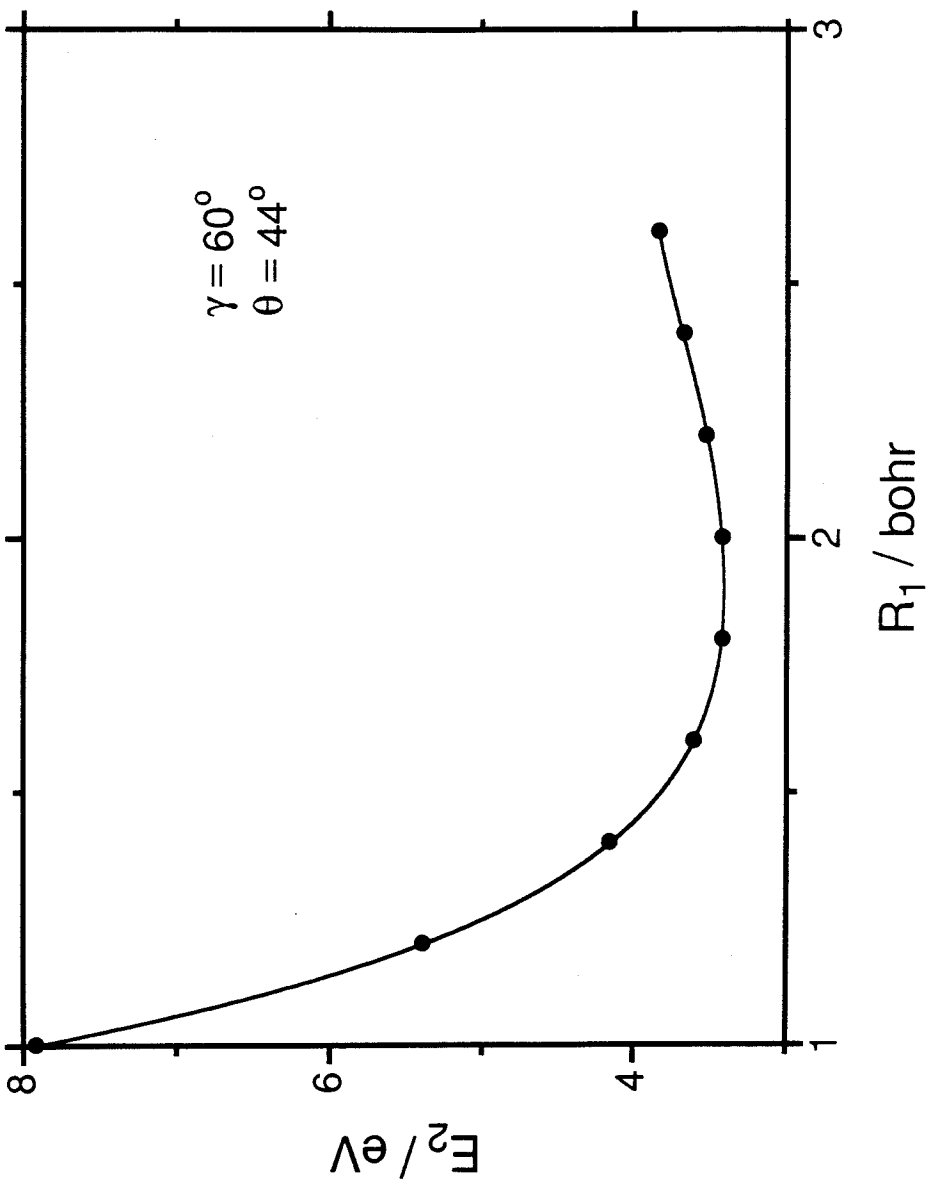

Fig. 12b

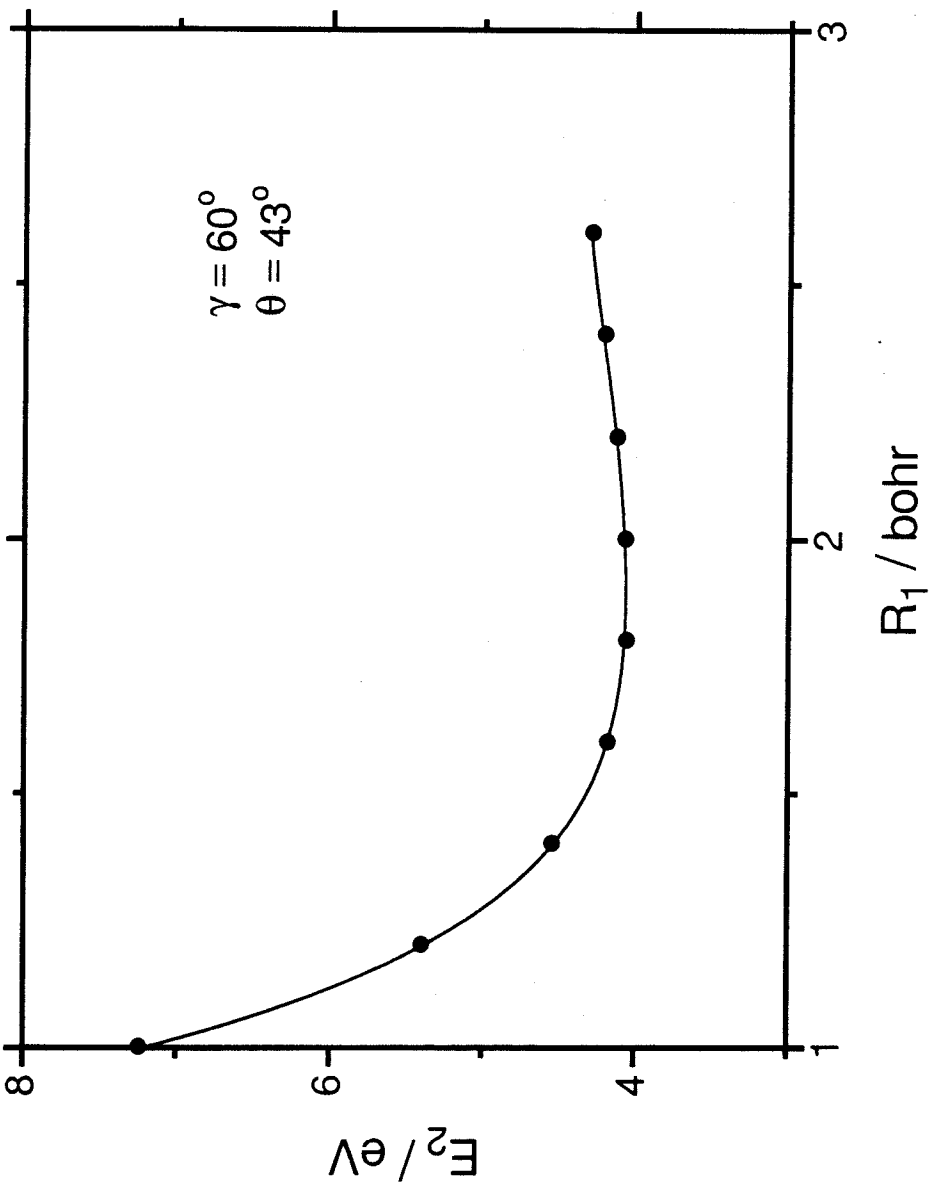

Fig. 12c

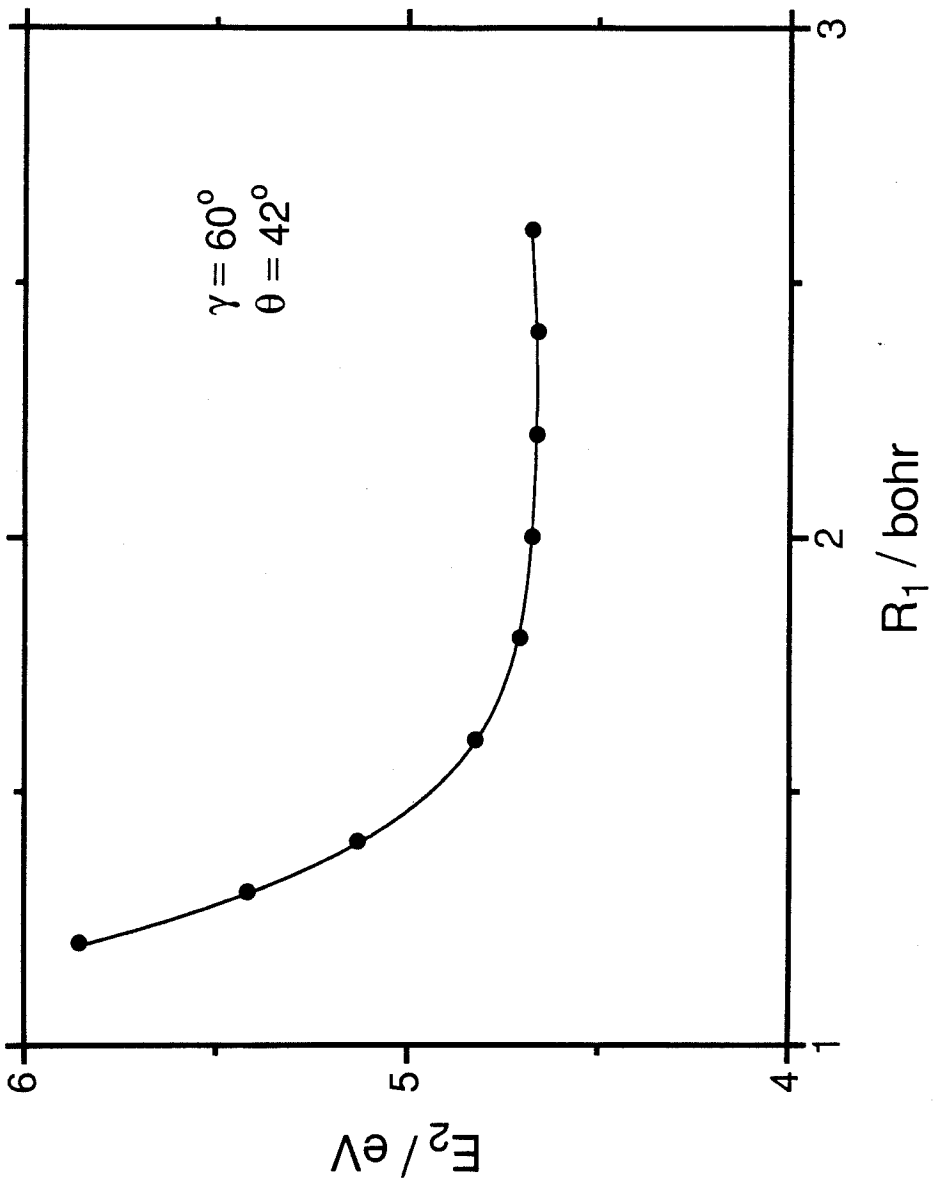

Fig. 12d

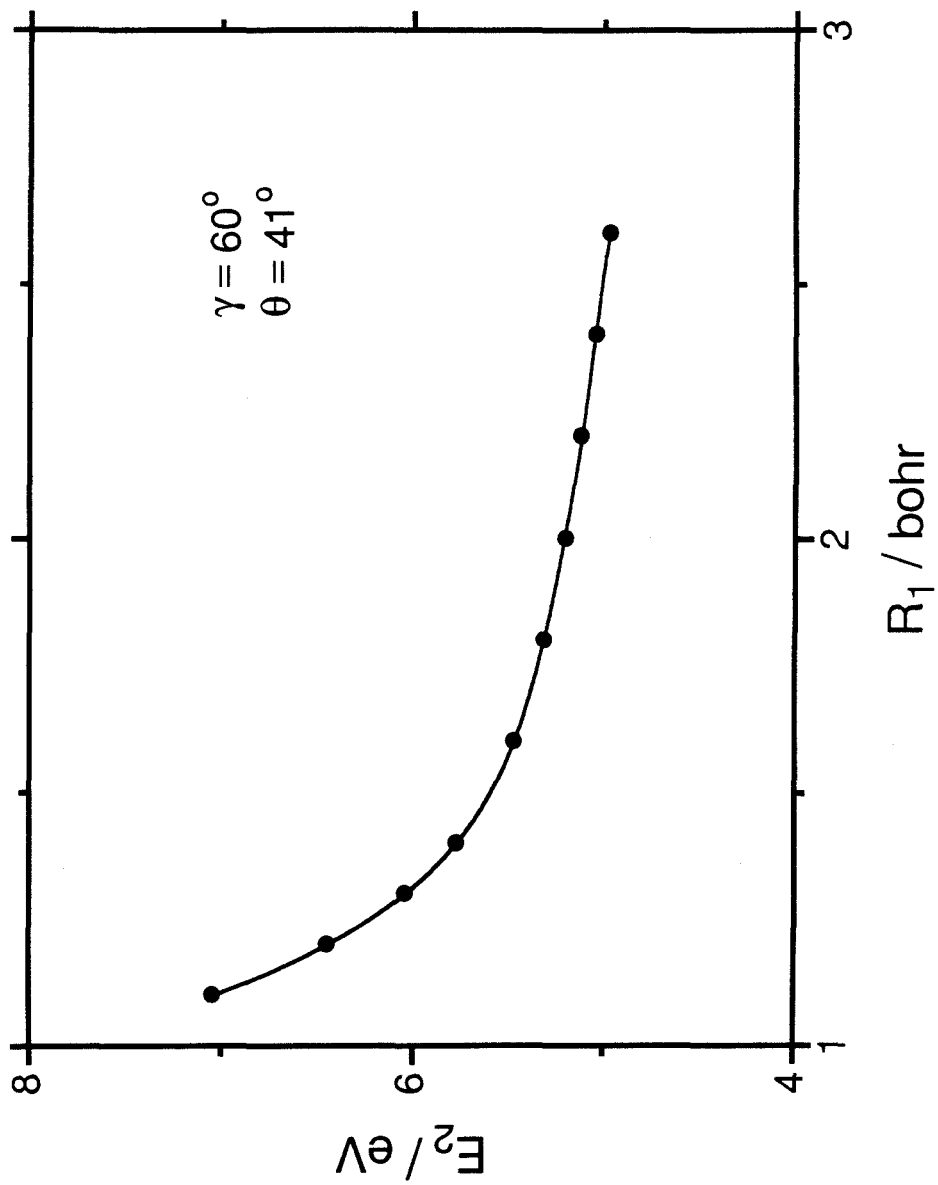

Fig. 12e

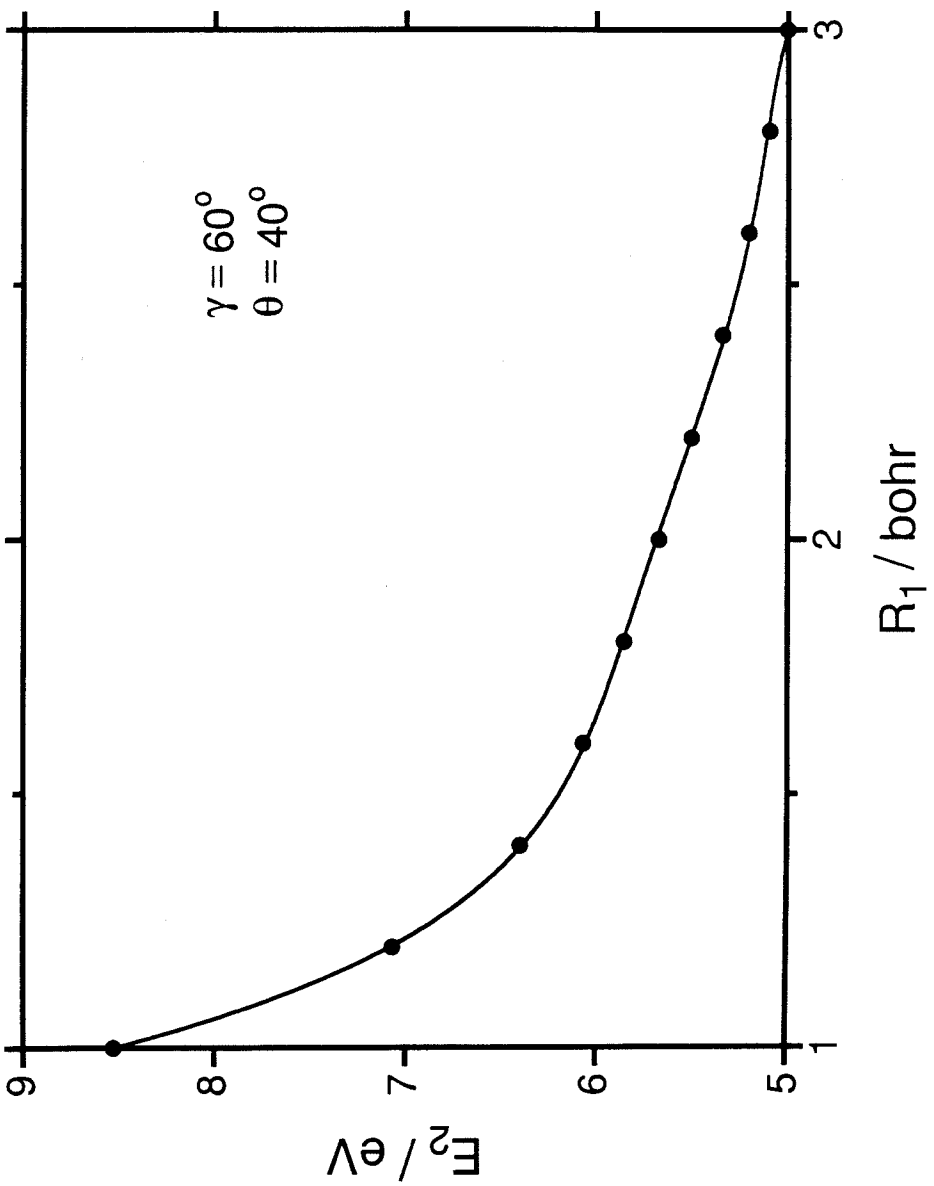

Fig. 12f

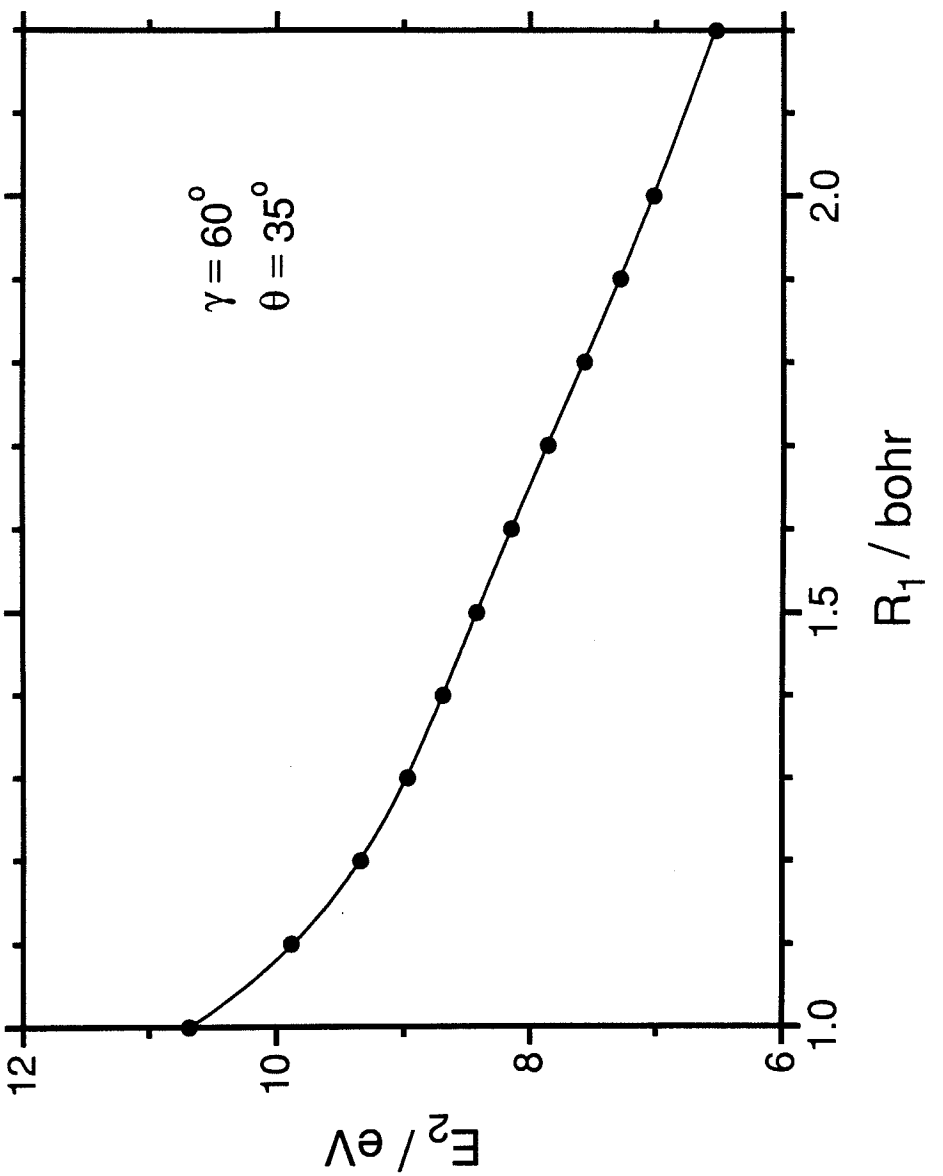

Fig. 12g

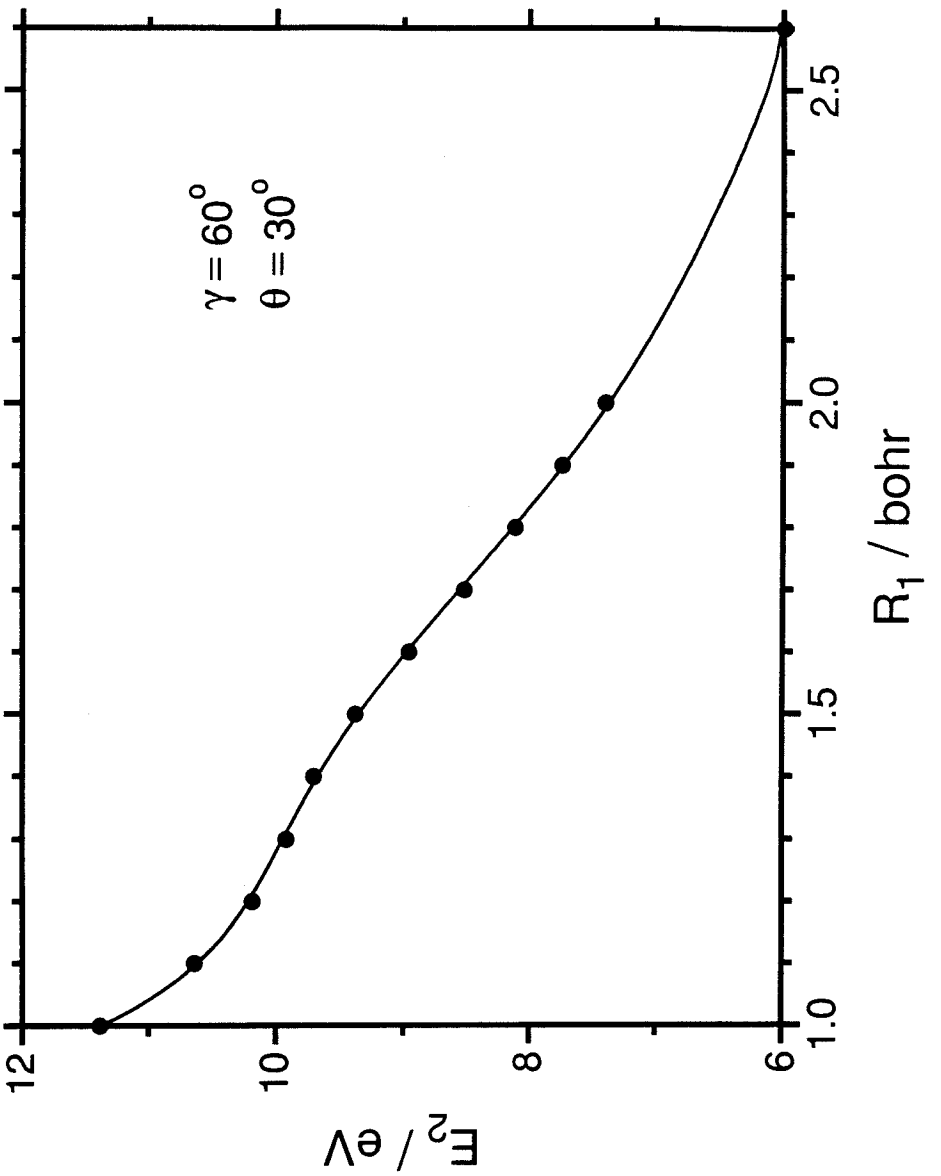

Fig. 12h

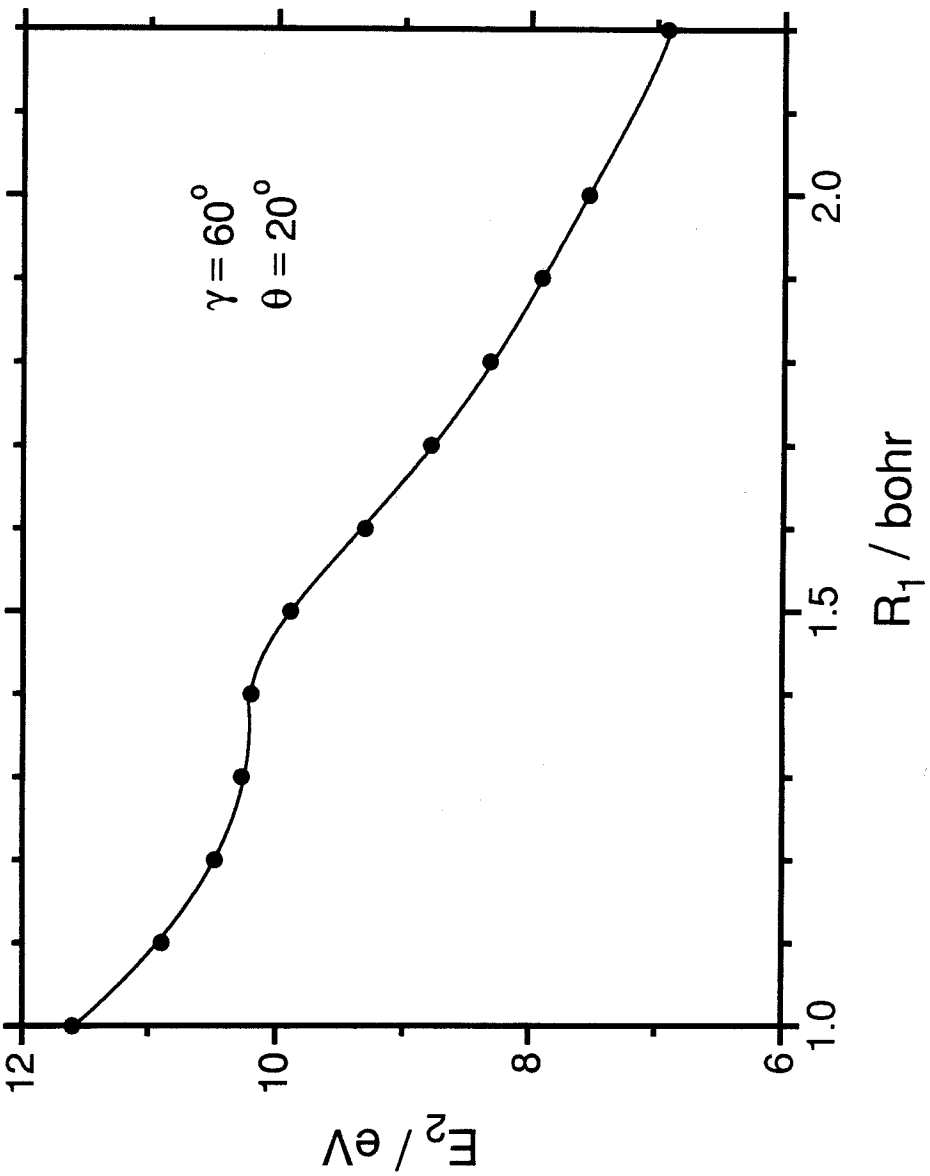

Fig. 12i

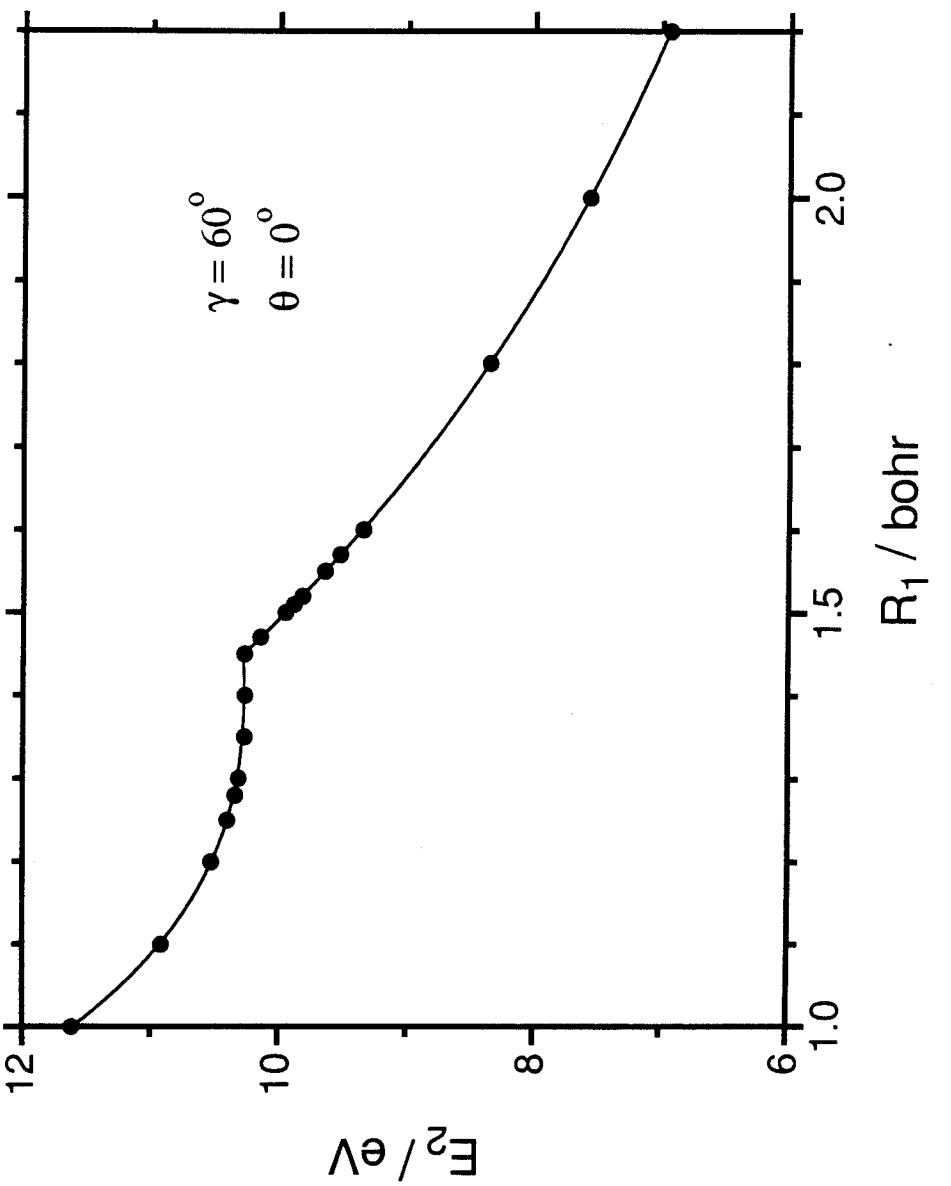

Fig. 12j

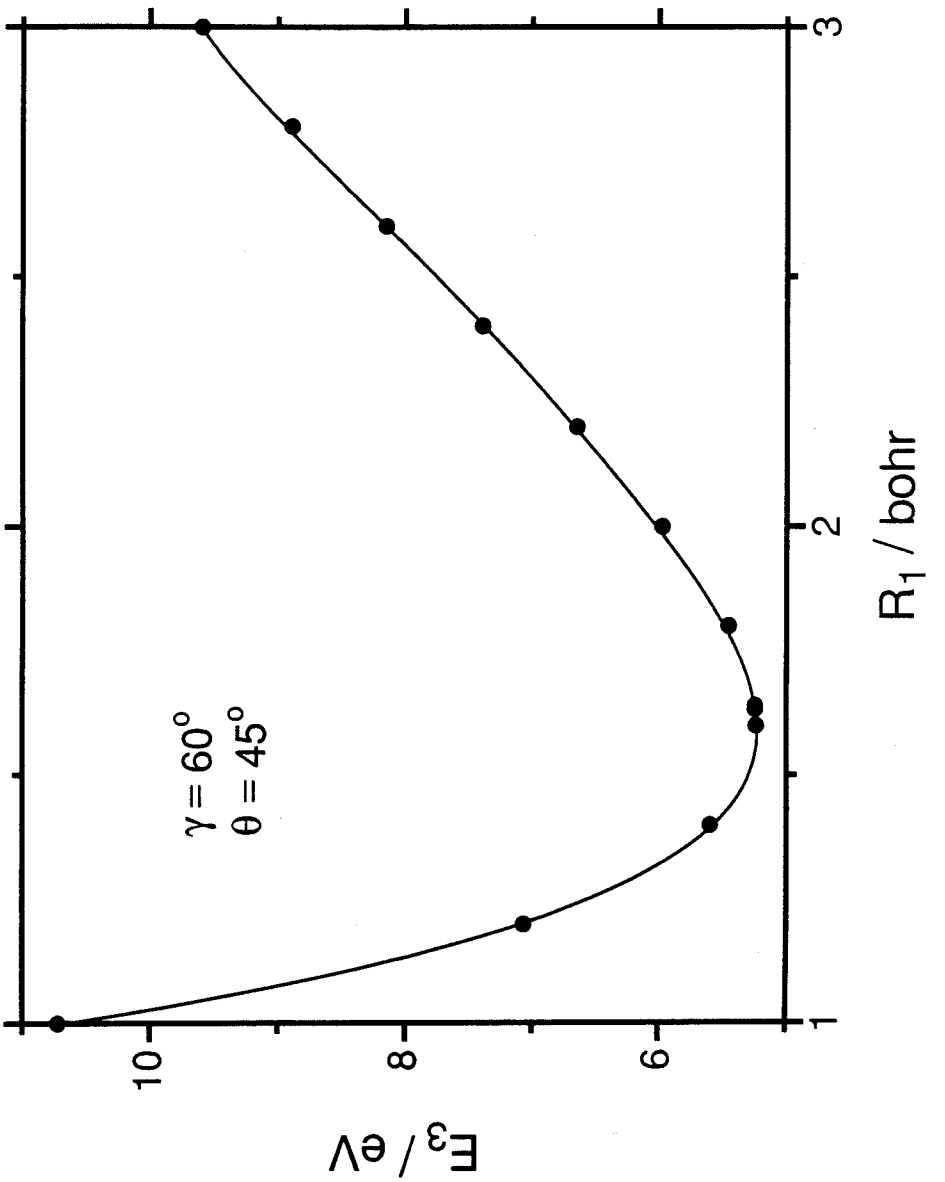

Fig. 13a

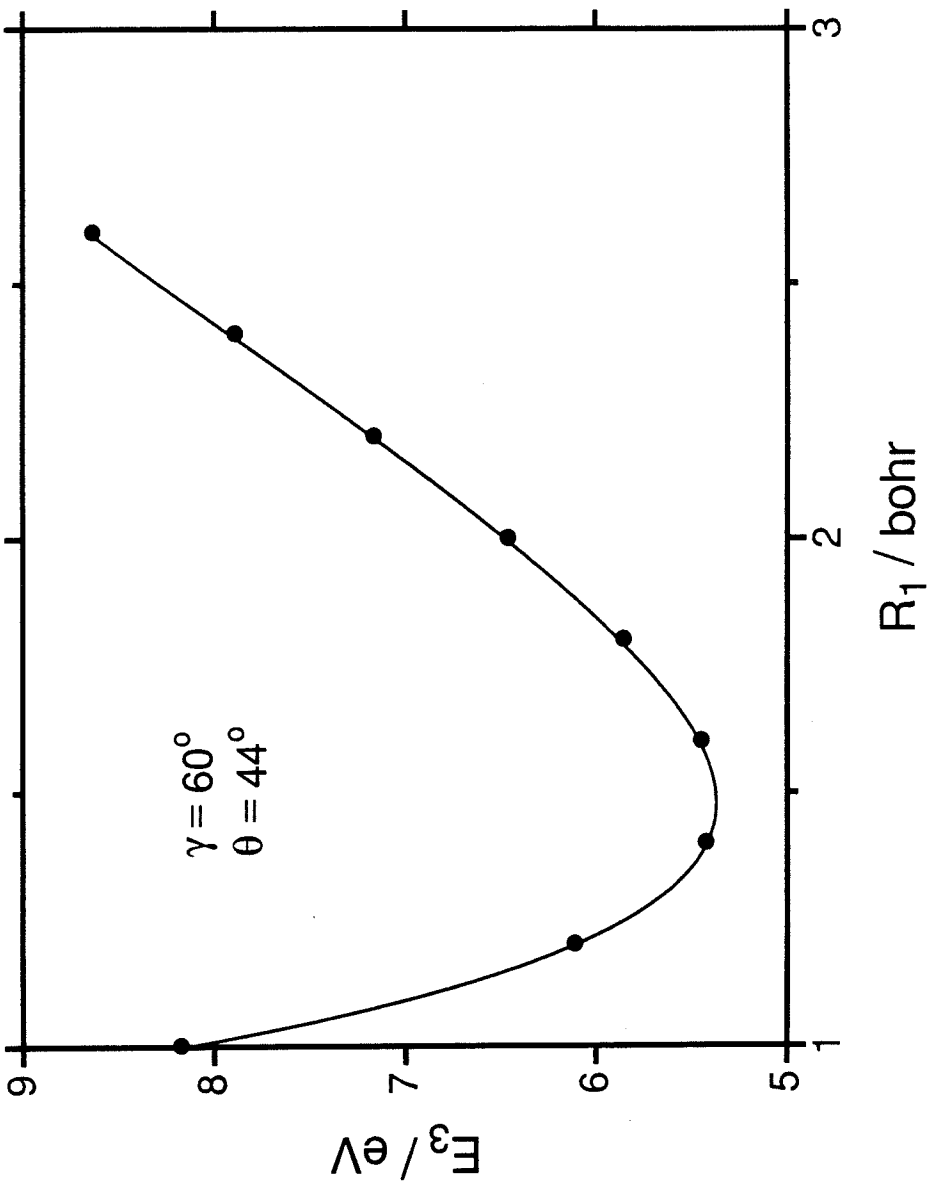

Fig. 13b

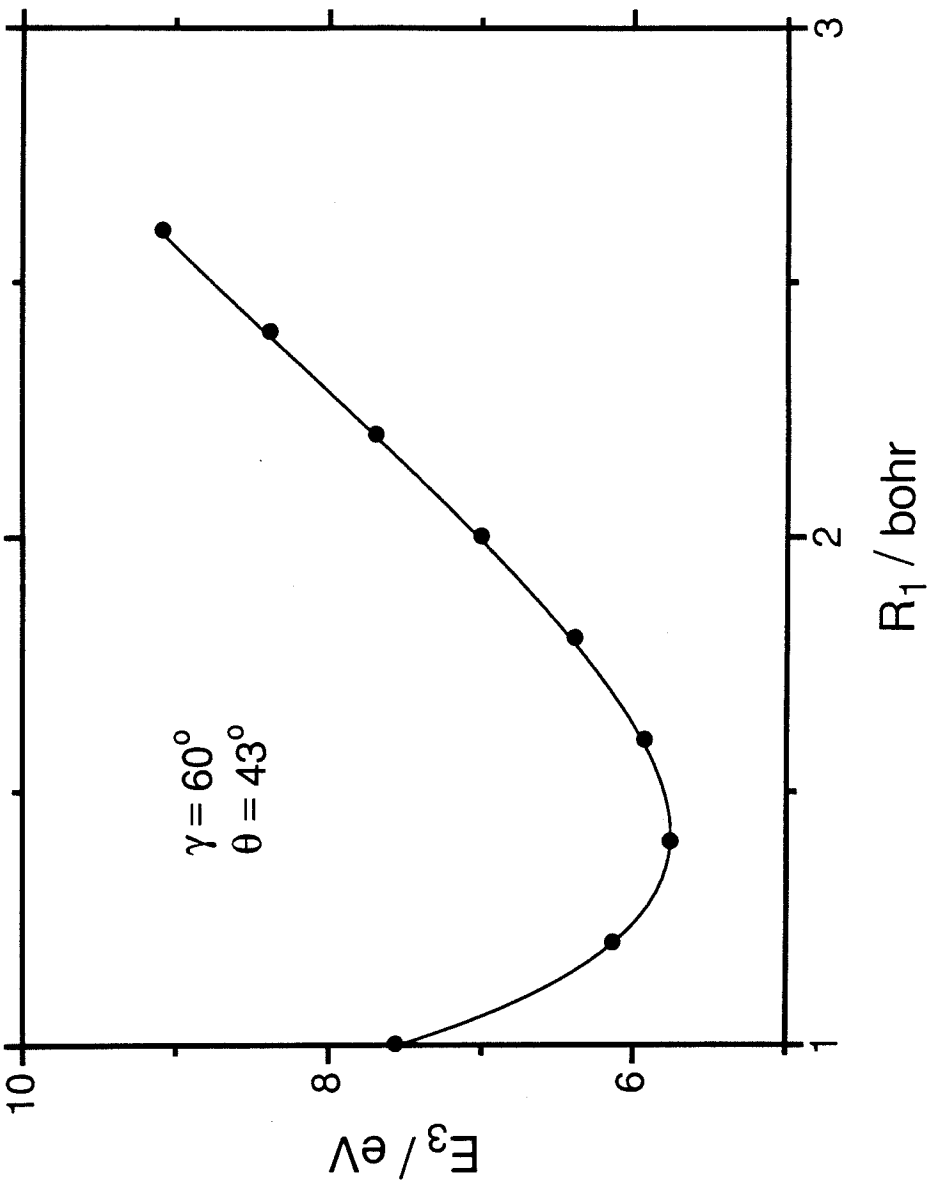

Fig. 13c

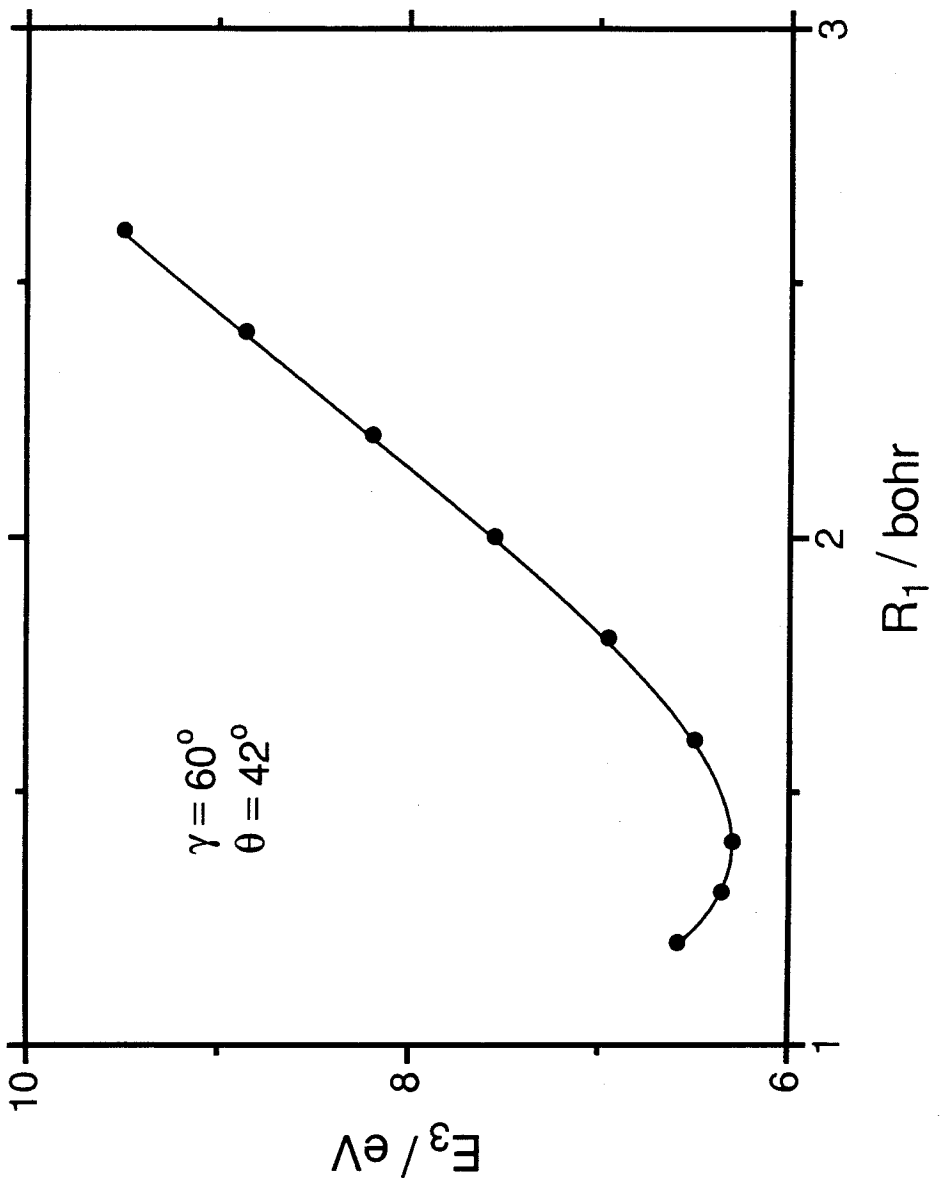

Fig. 13d

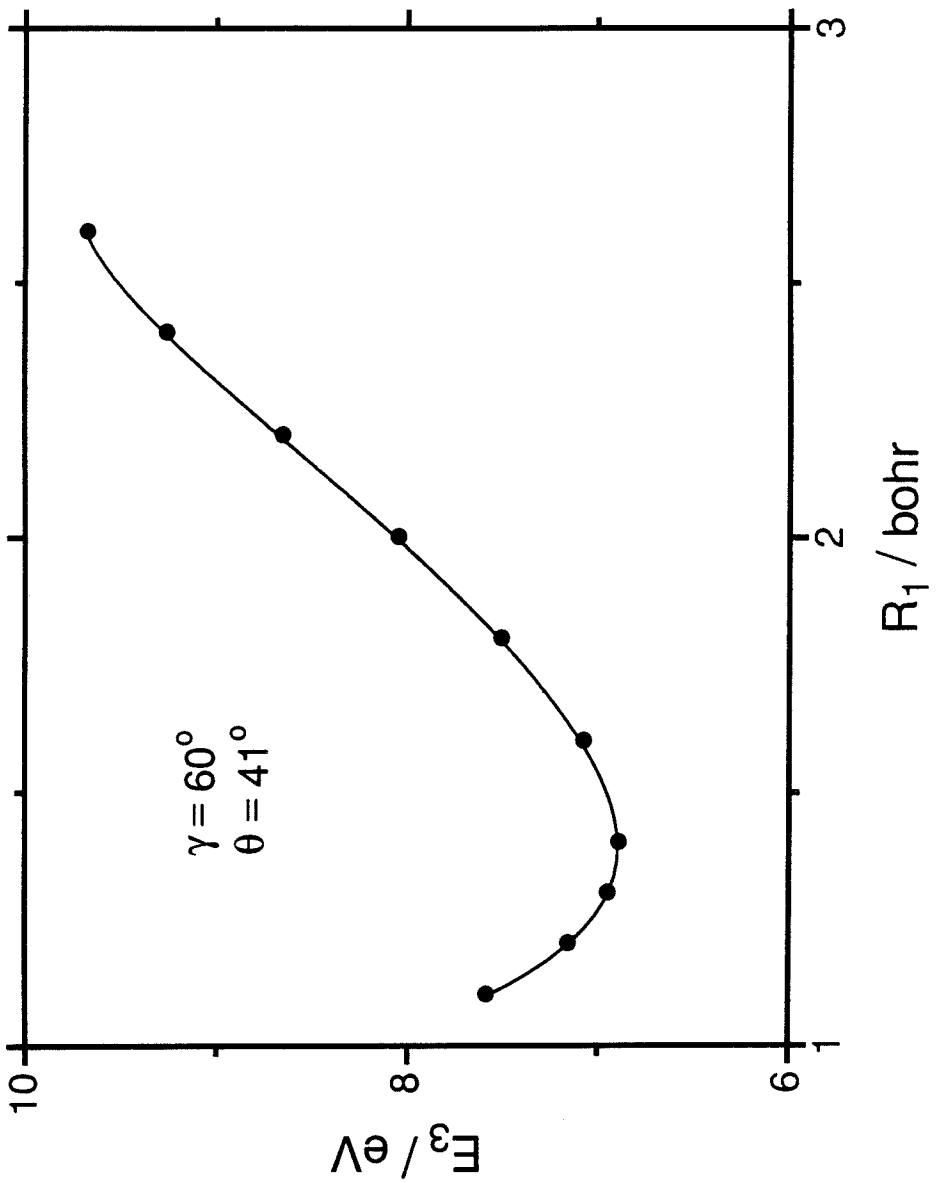

Fig. 13e

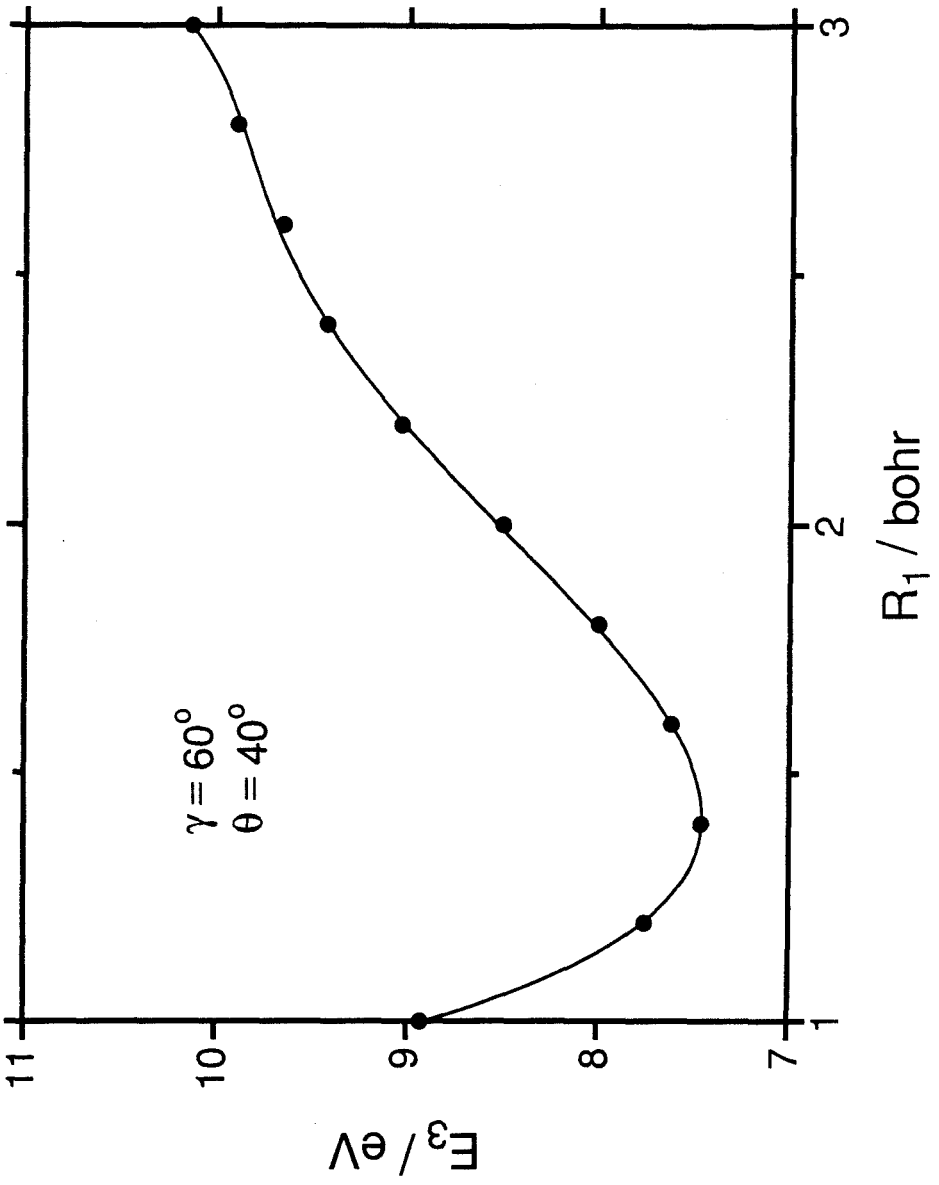

Fig. 13f

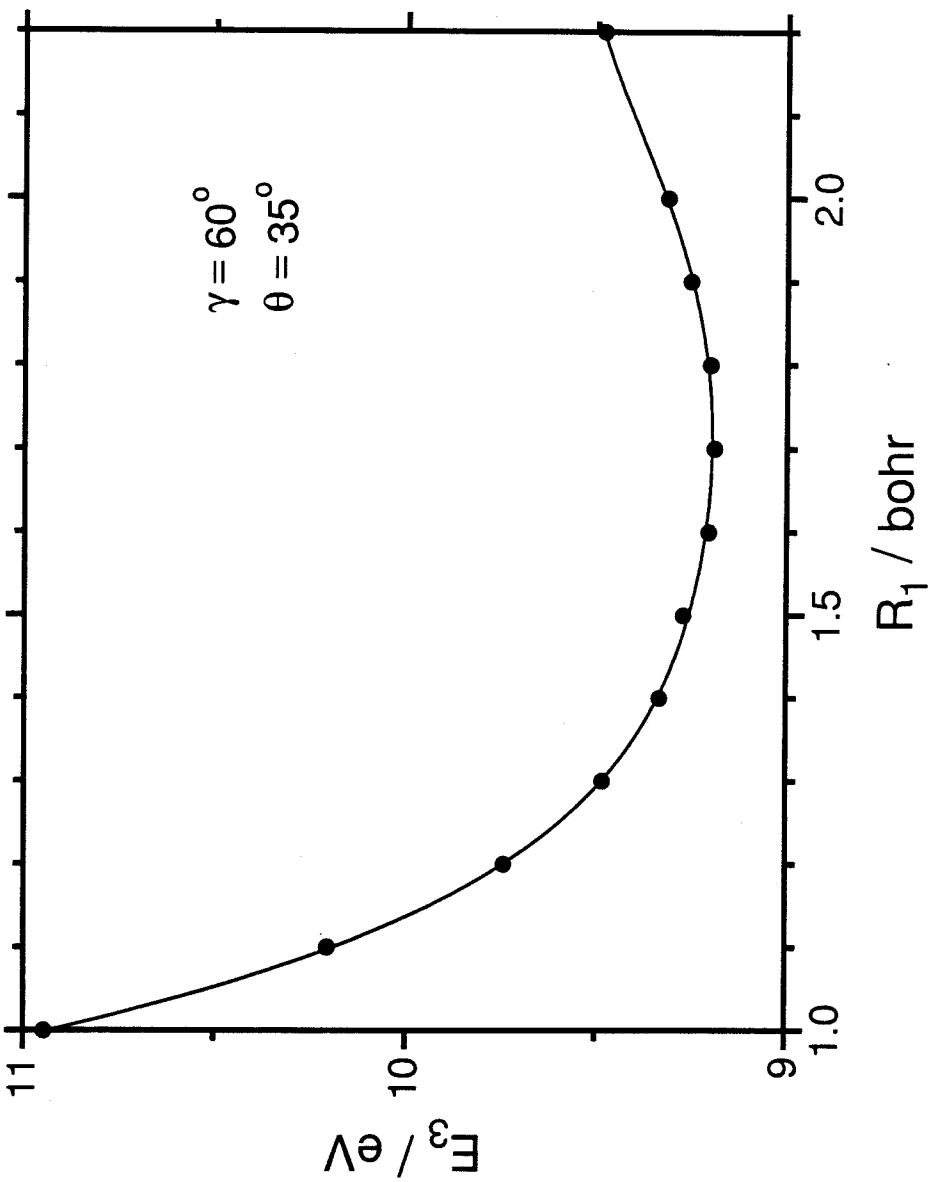

Fig. 13g

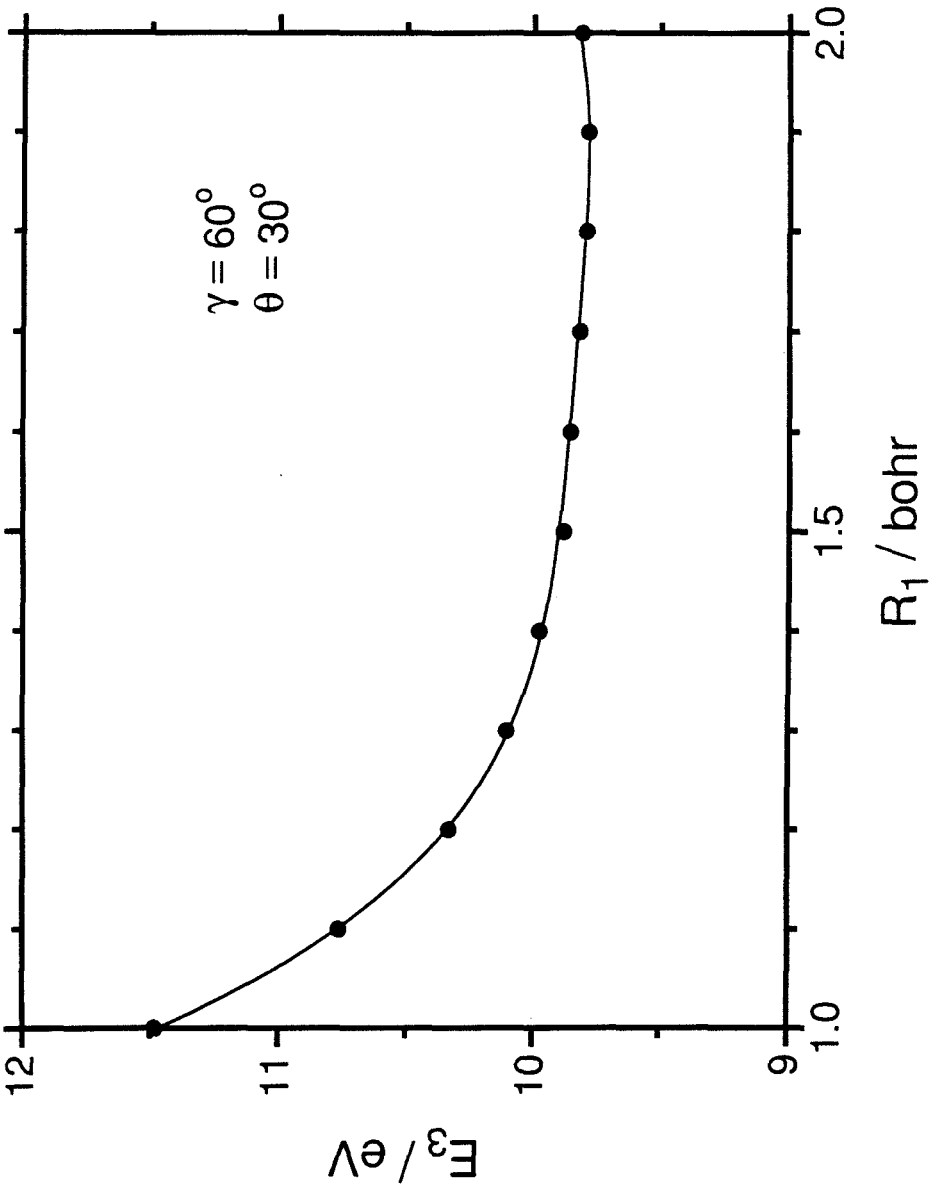

Fig. 13h

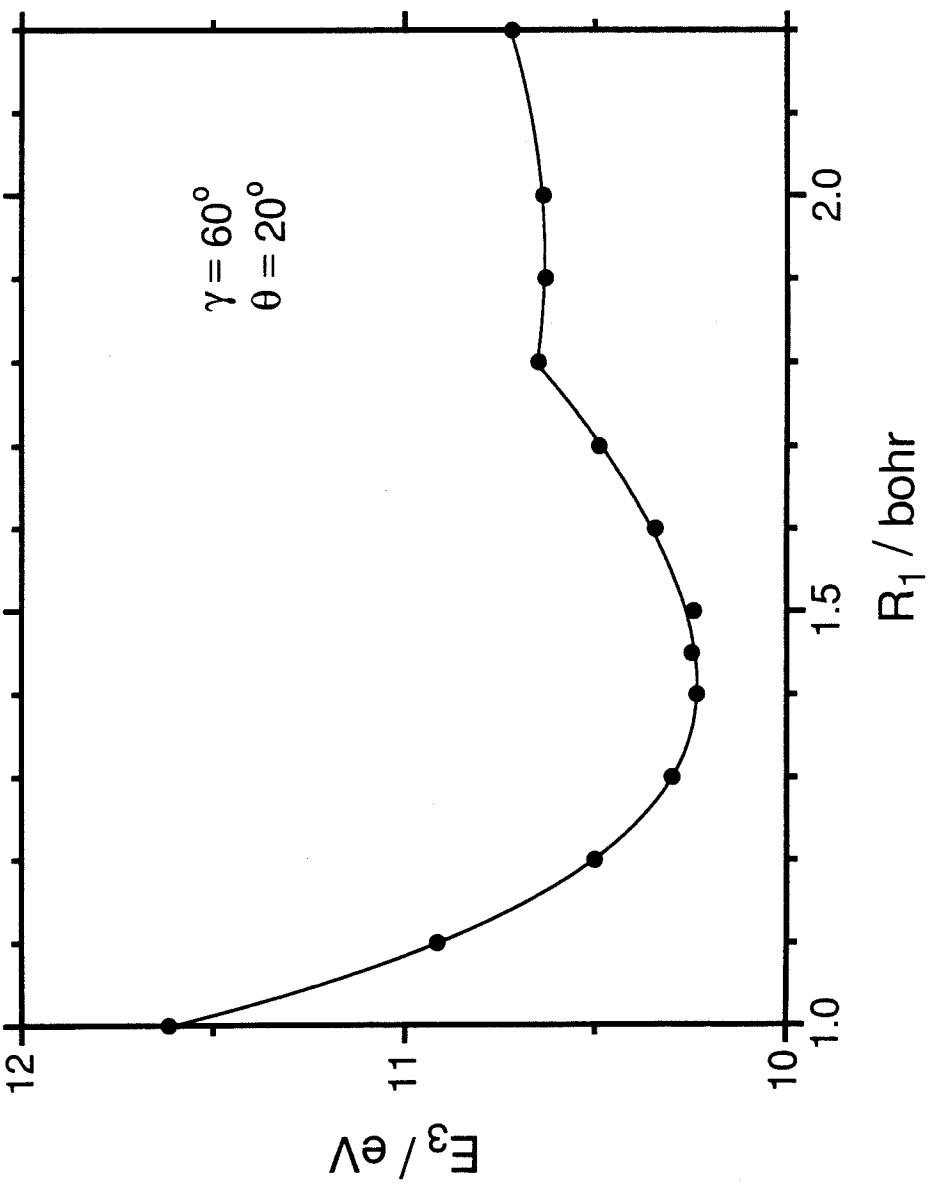

Fig. 13i

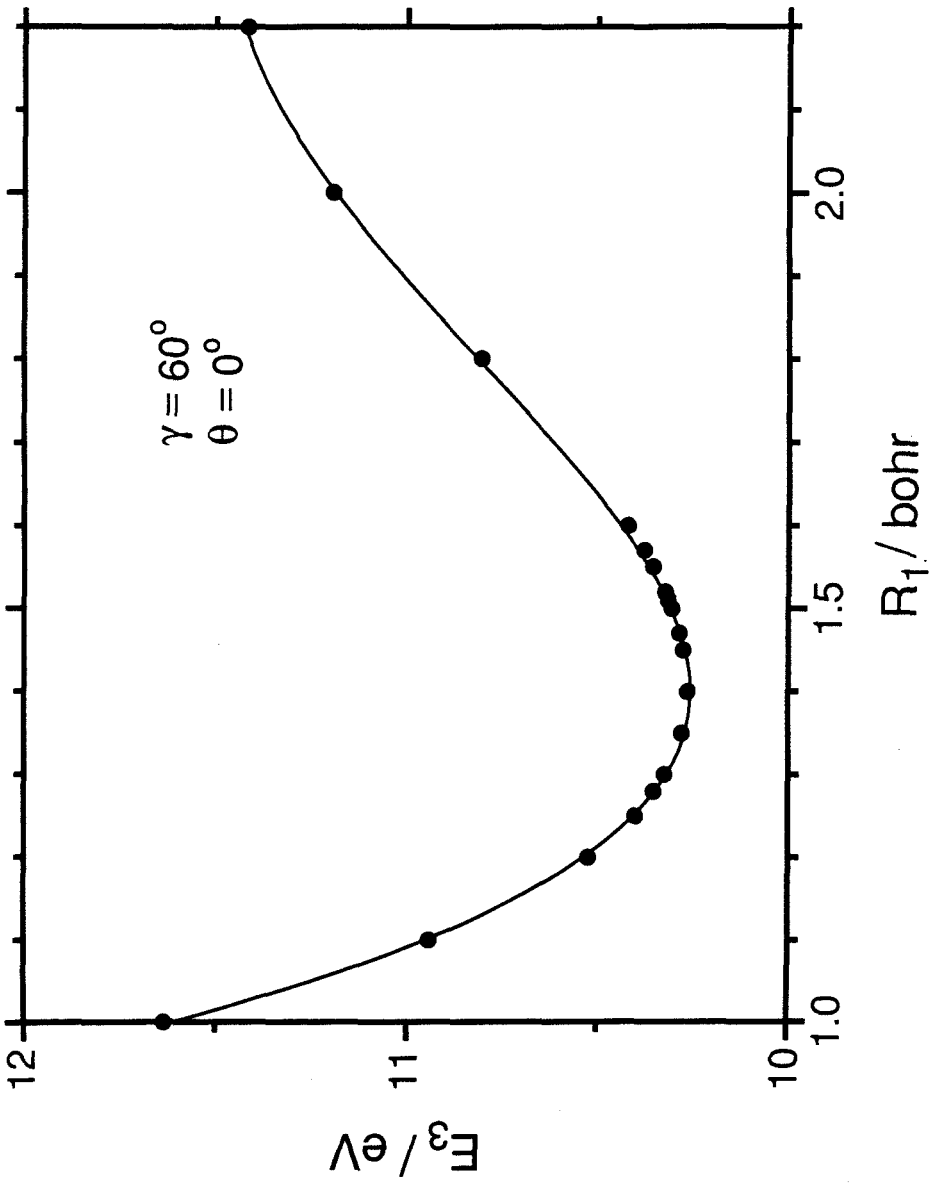

Fig. 13j

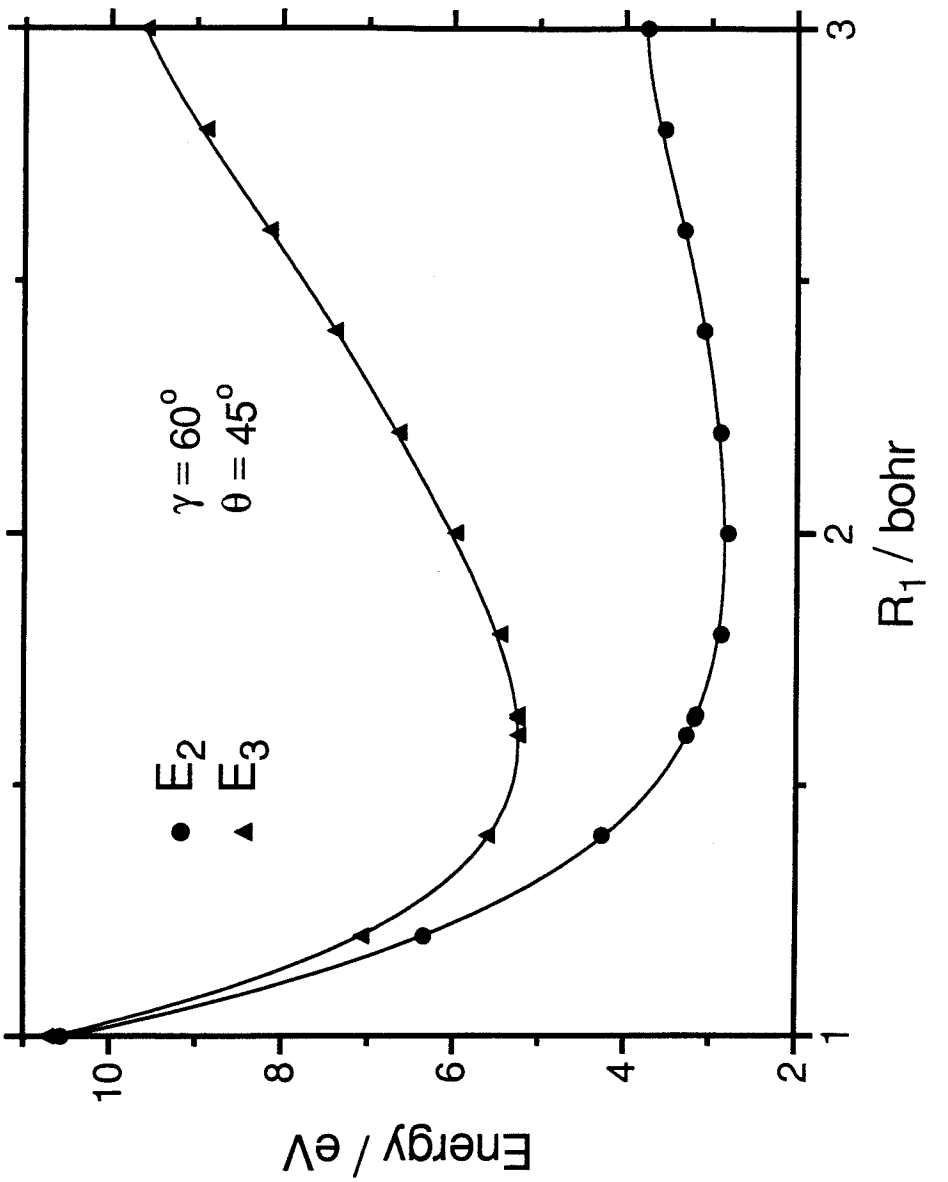

Fig. 14a

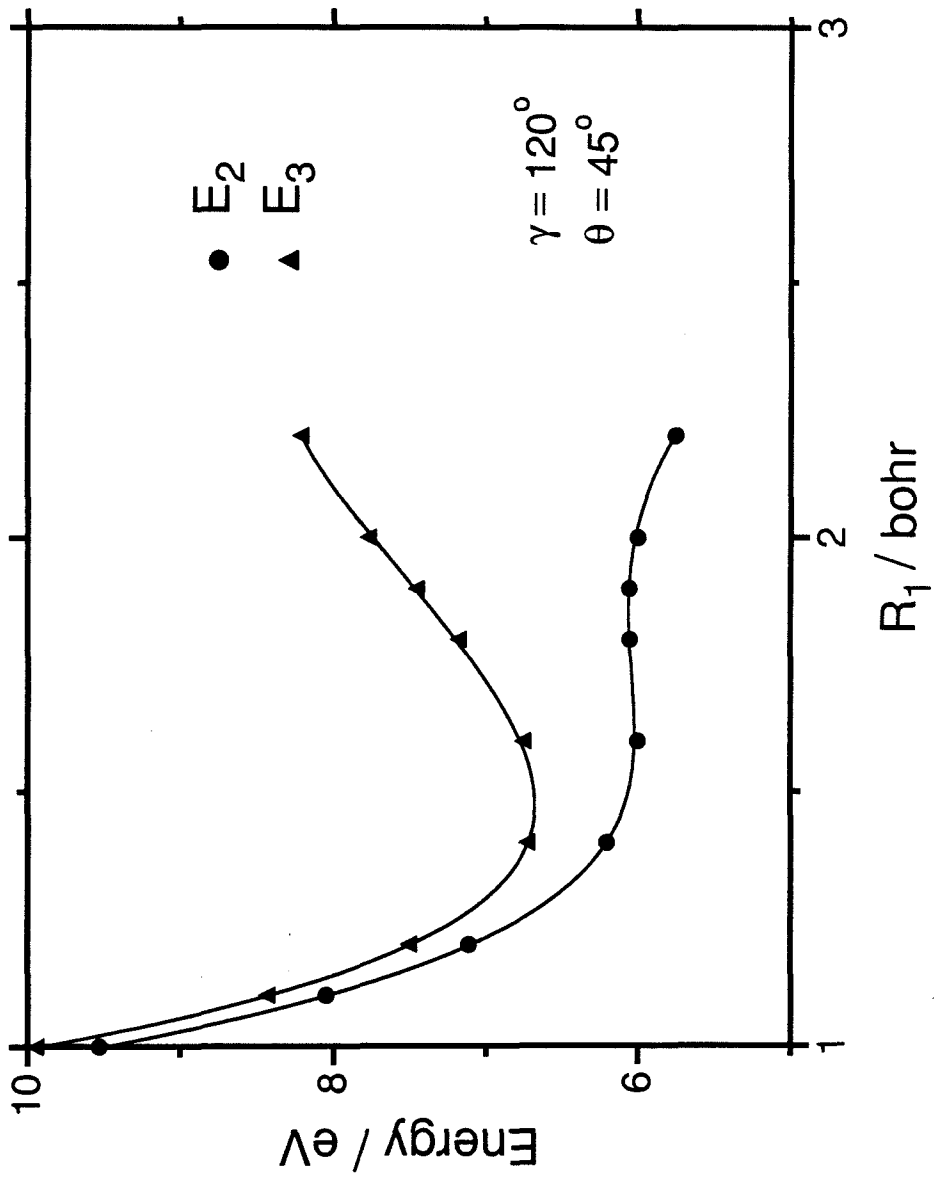

Fig. 14b

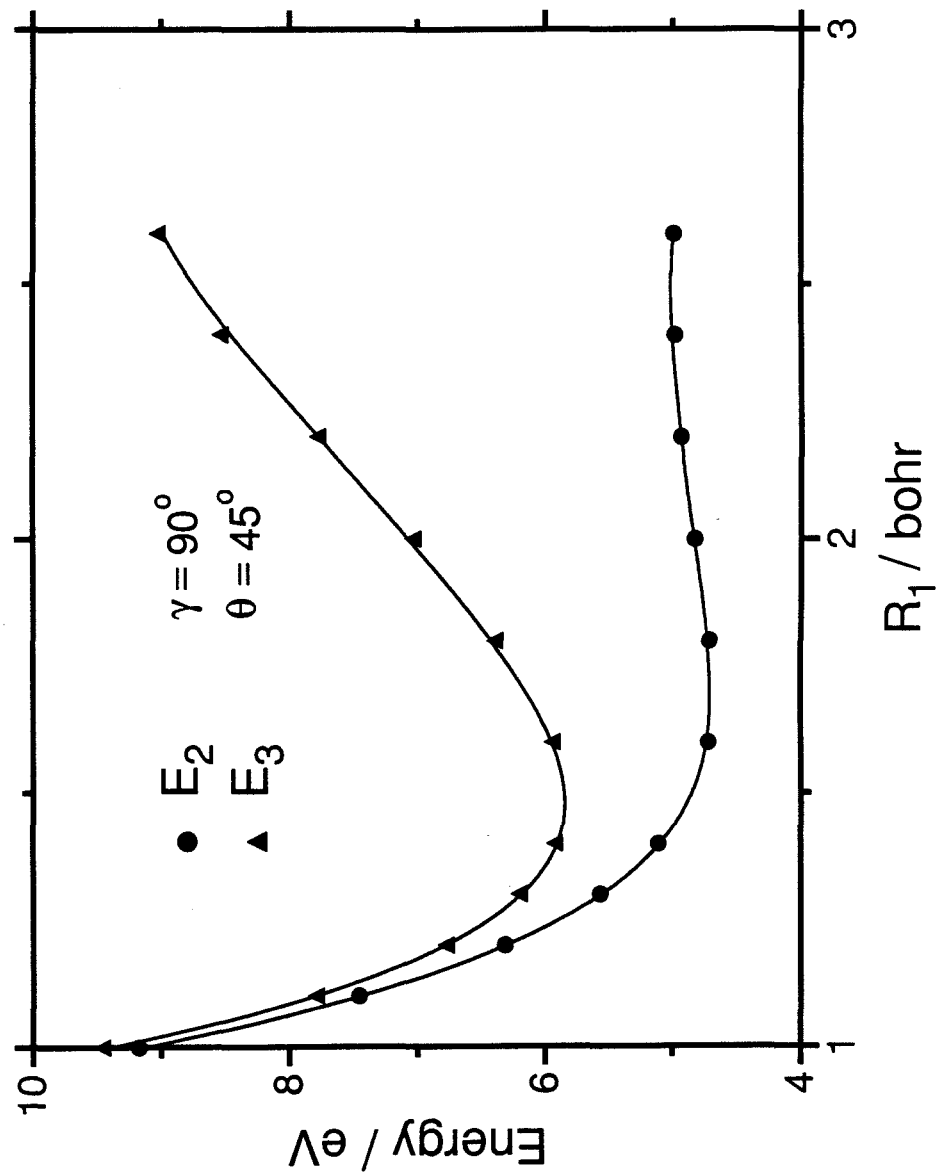

Fig. 14c

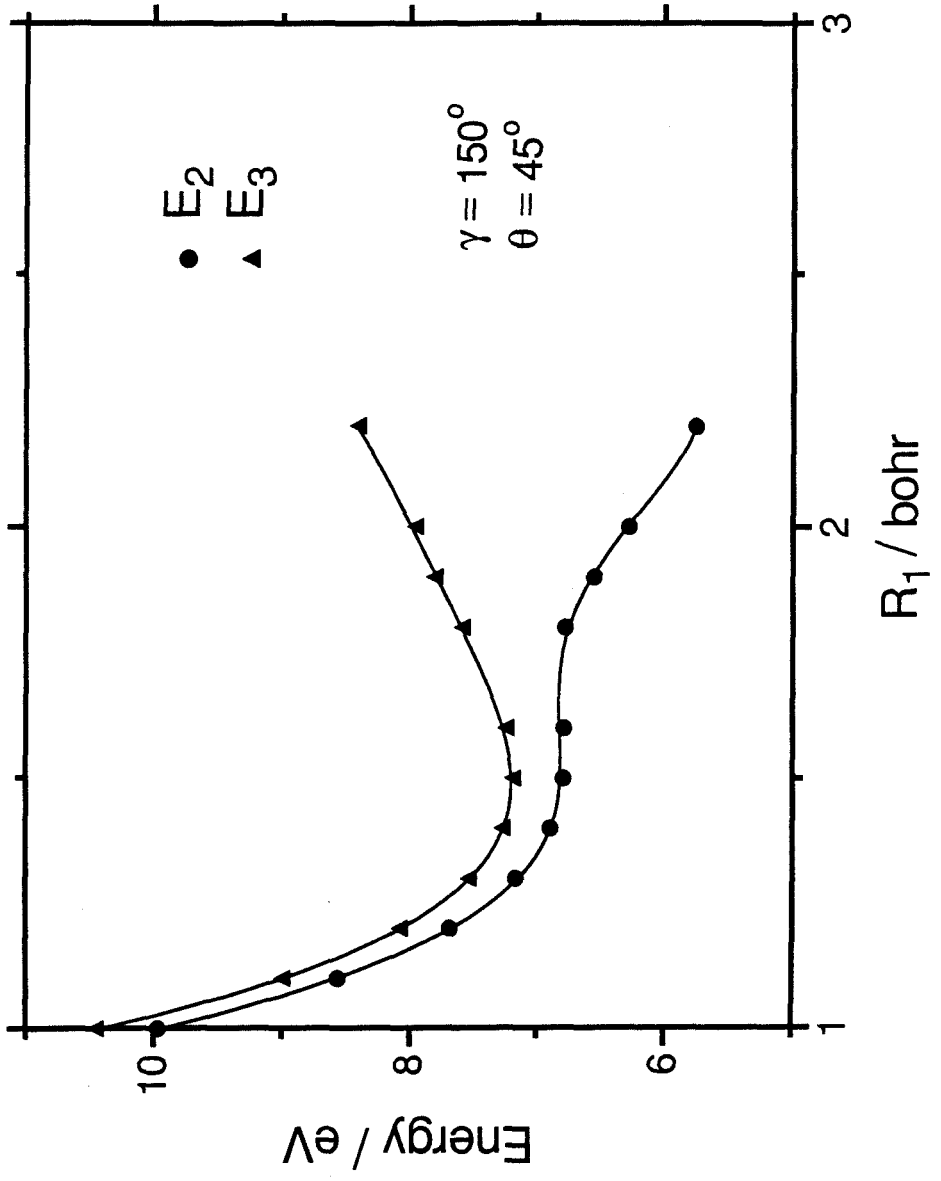

Fig. 14d

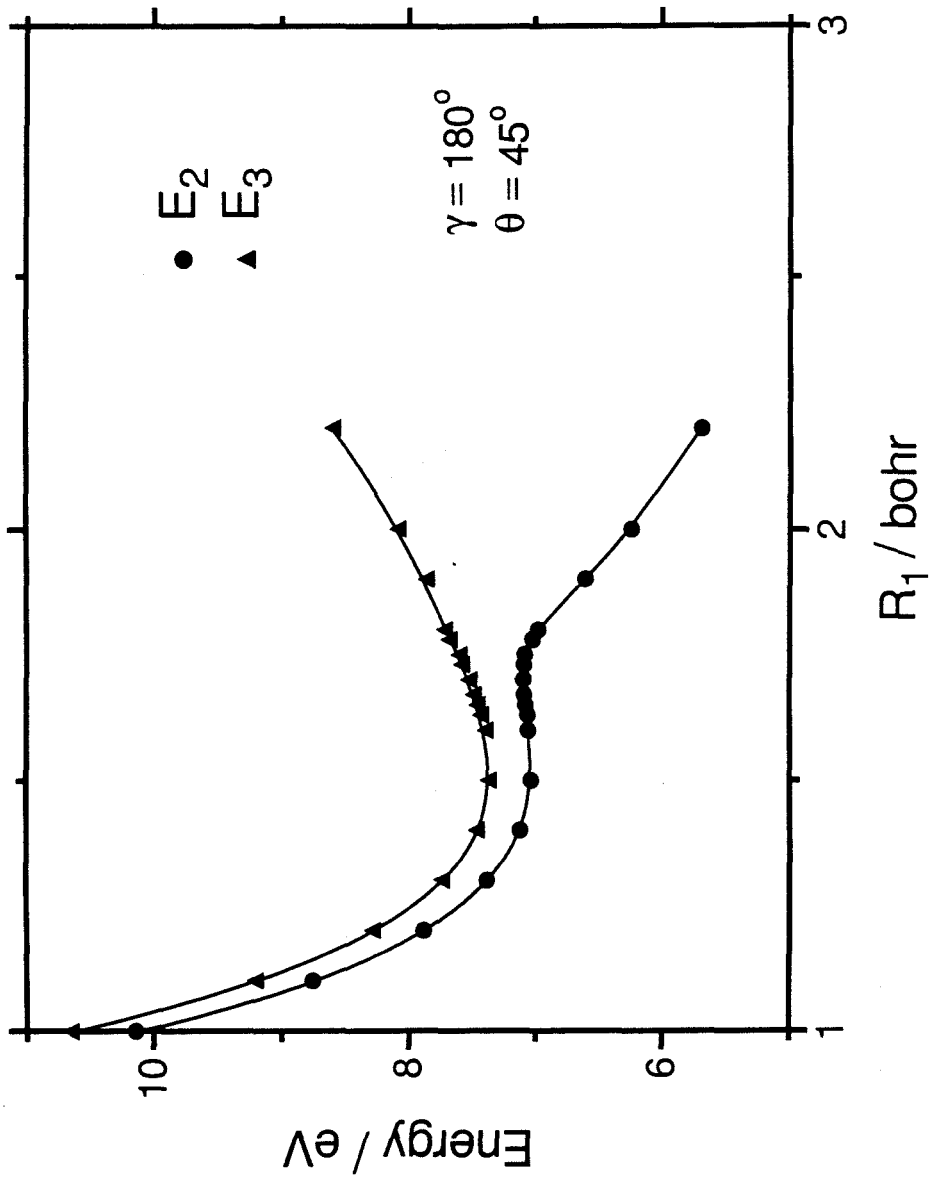

Fig. 14e

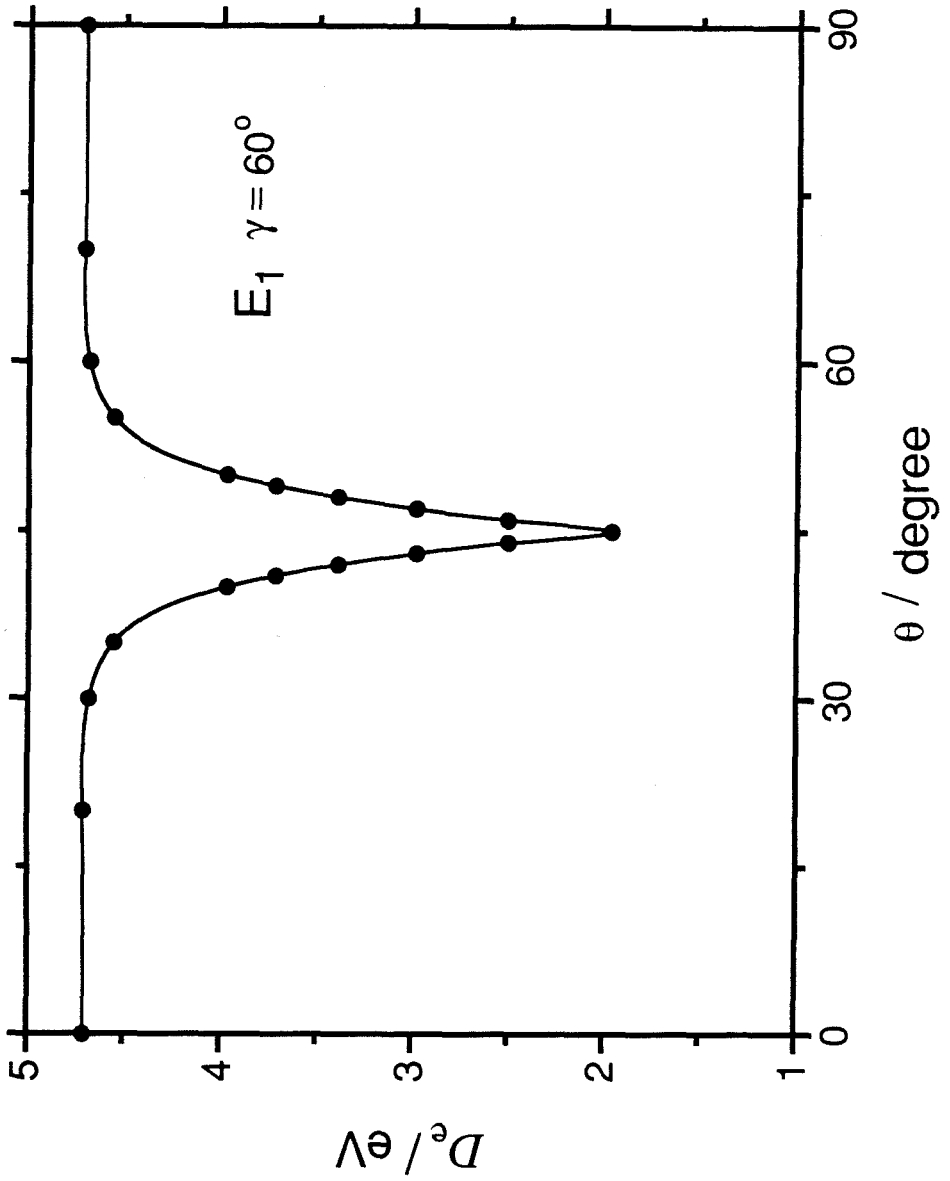

Fig. 15a

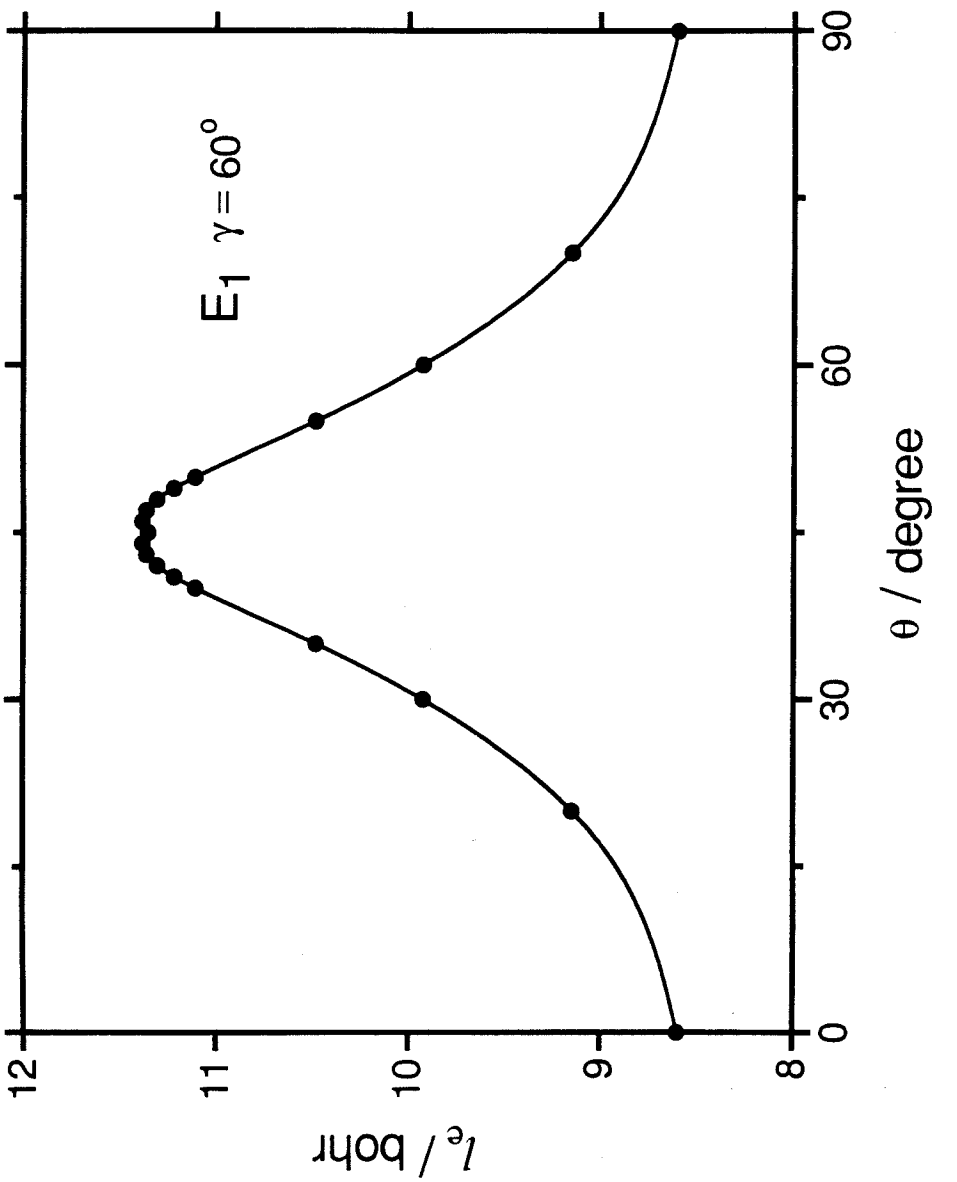

Fig. 15b

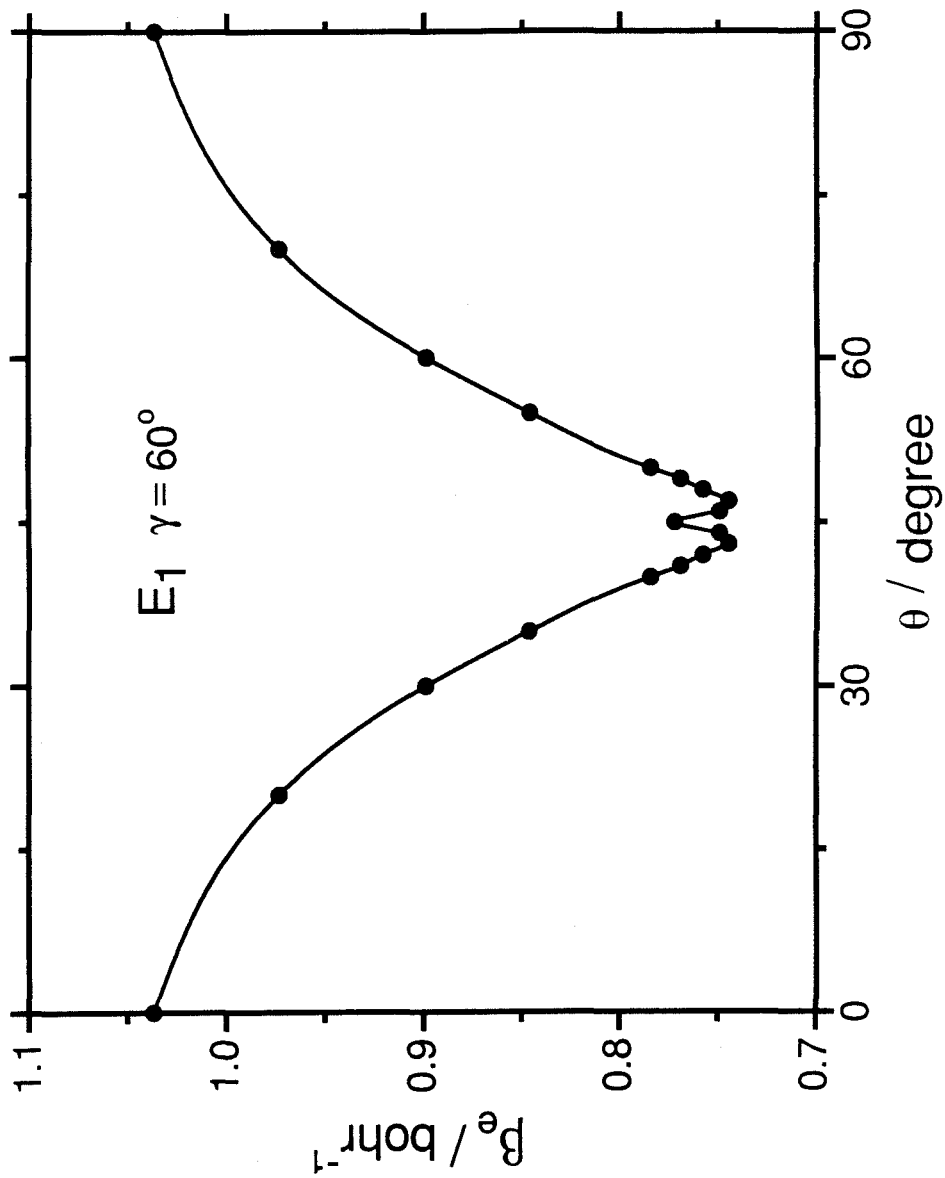

Fig. 15c

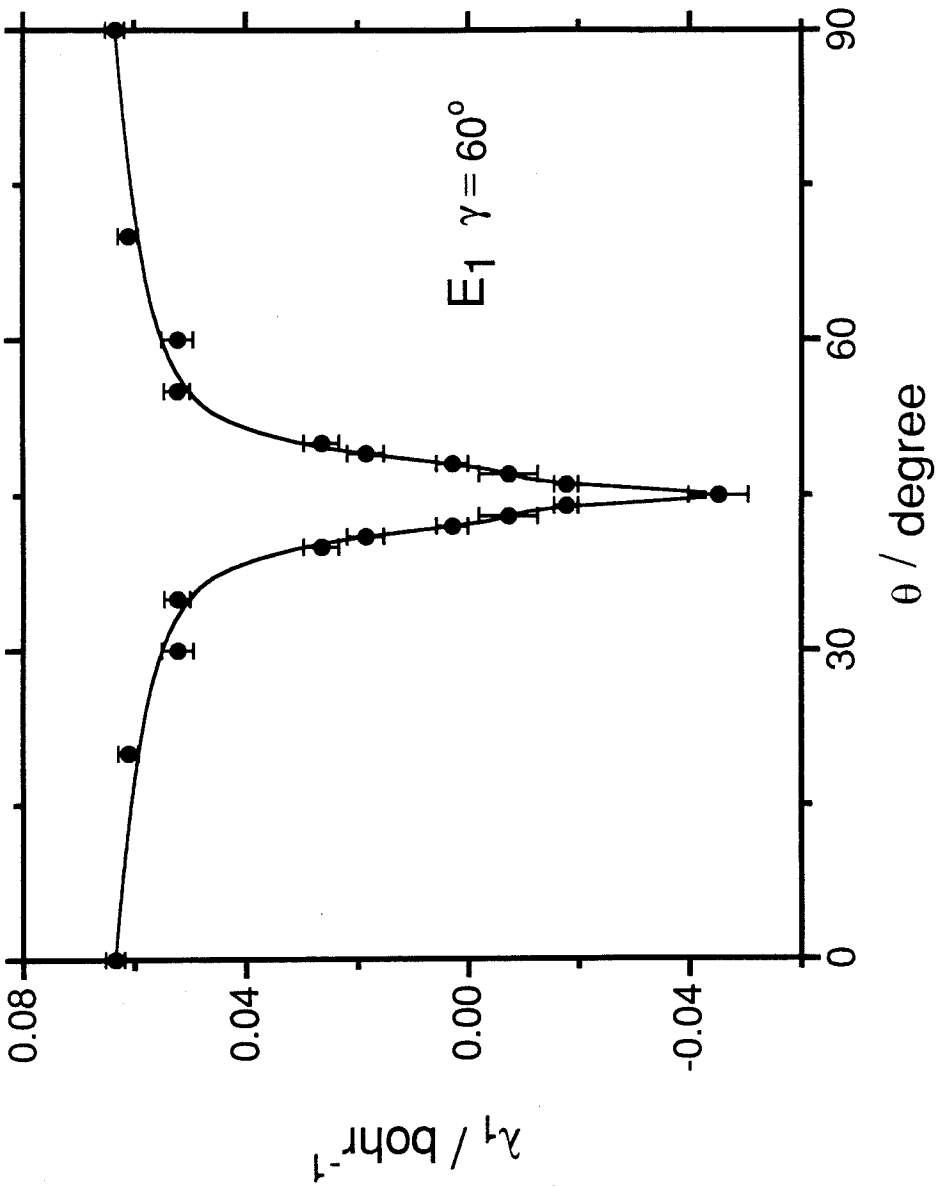
E_1 $\gamma = 60^\circ$
λ_1 / bohr^{-1}
0.08
0.04
0.00
-0.04
0
30
60
90
θ / degree

Fig. 15d

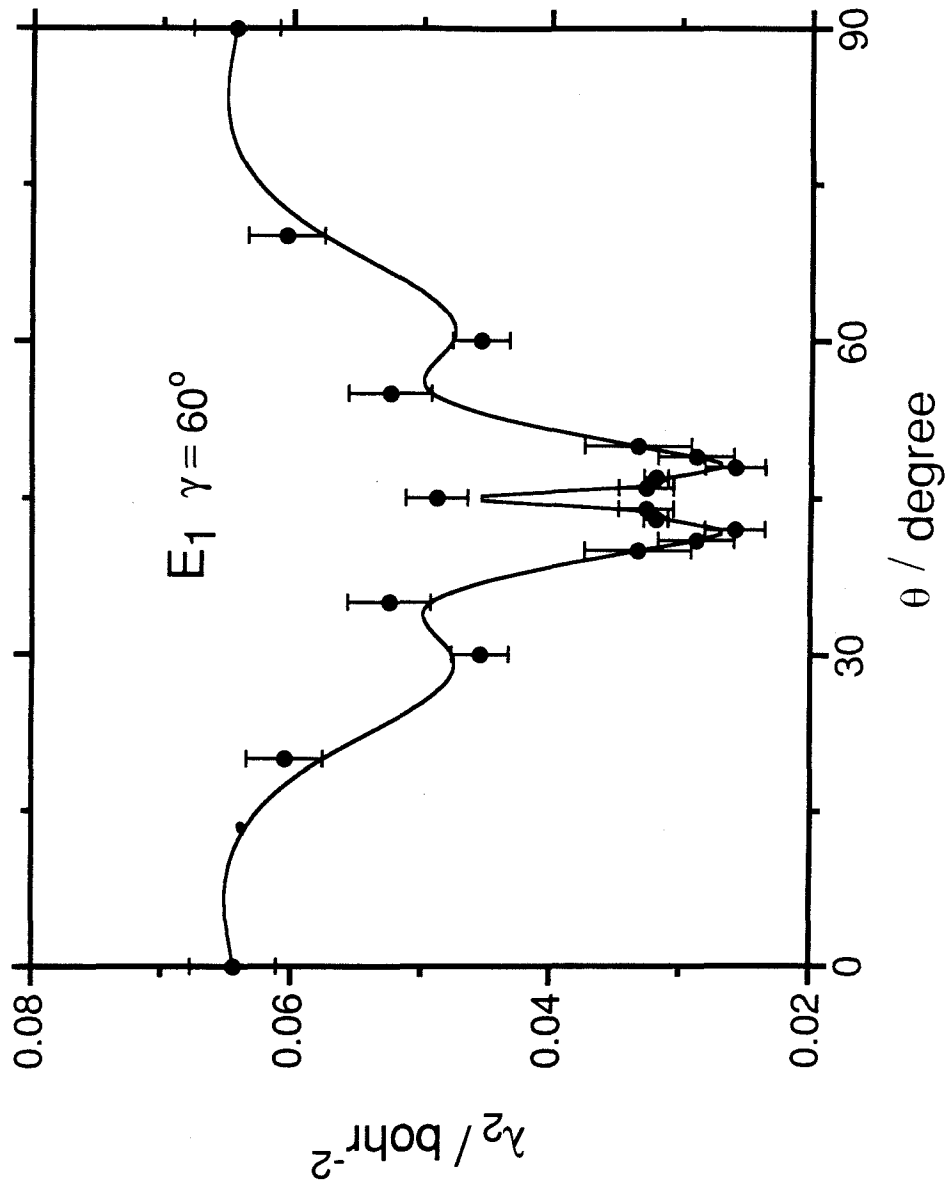
E_1 $\gamma = 60^\circ$
λ_2 / bohr^{-2}
0.08
0.06
0.04
0.02
0
30
60
90
θ / degree

Fig. 15e

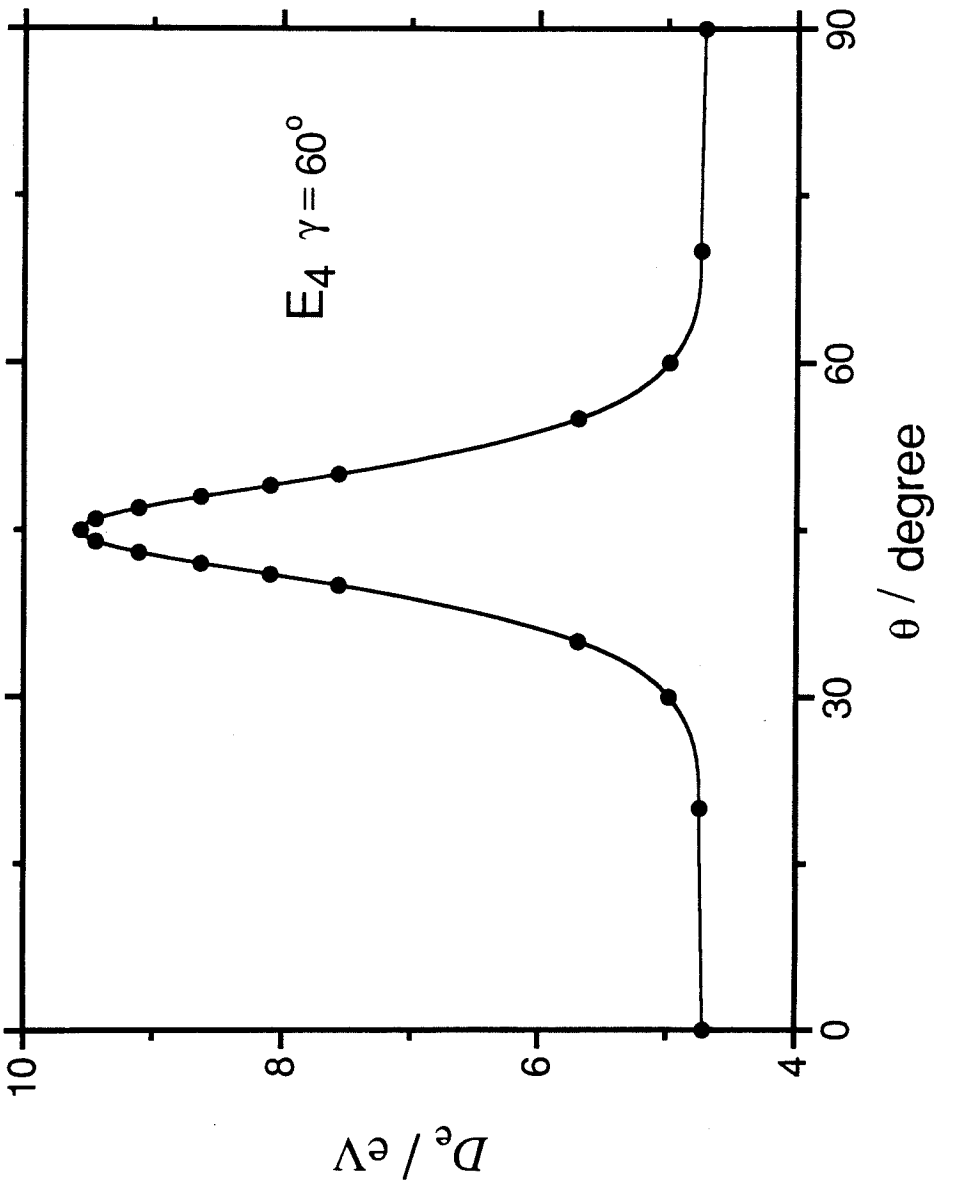

Fig. 16a

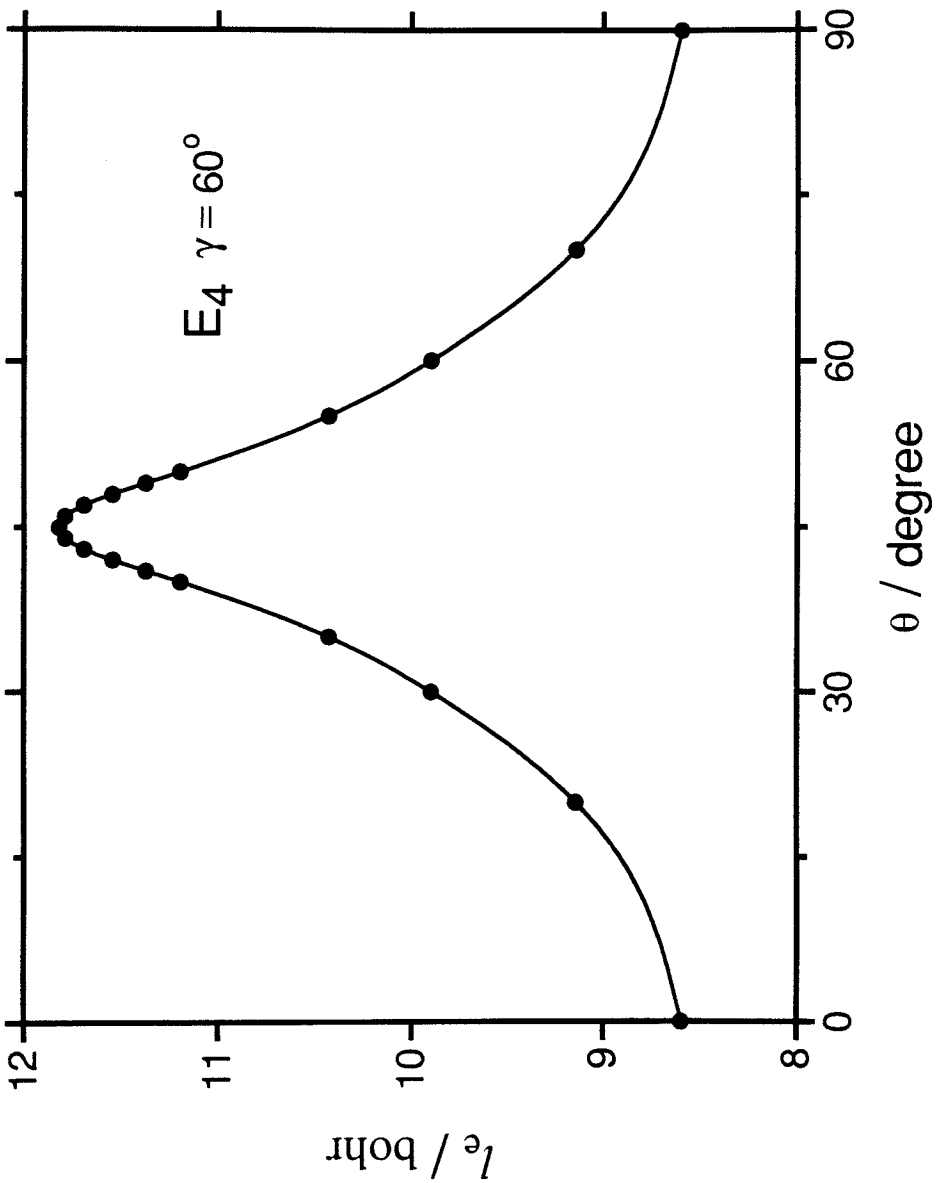

Fig. 16b

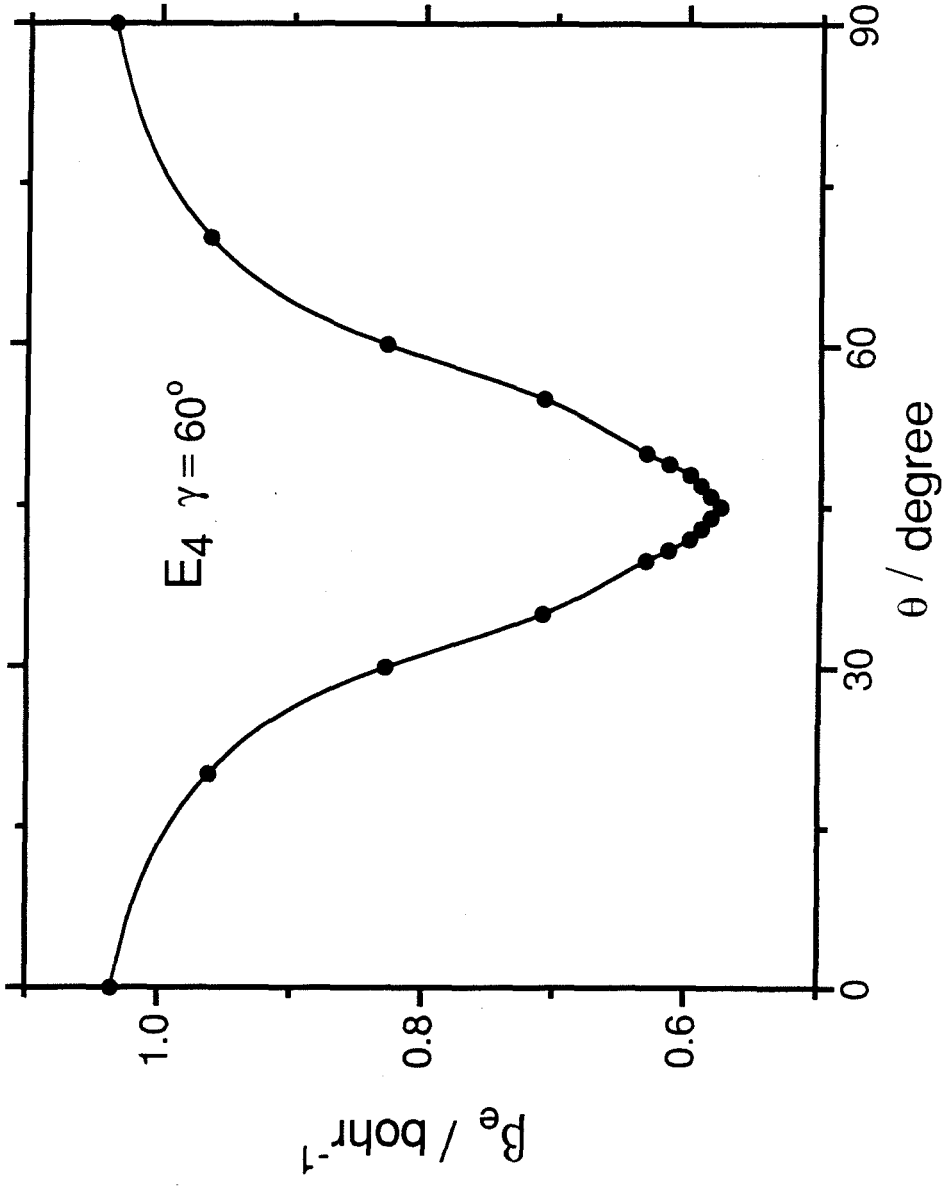

Fig. 16c

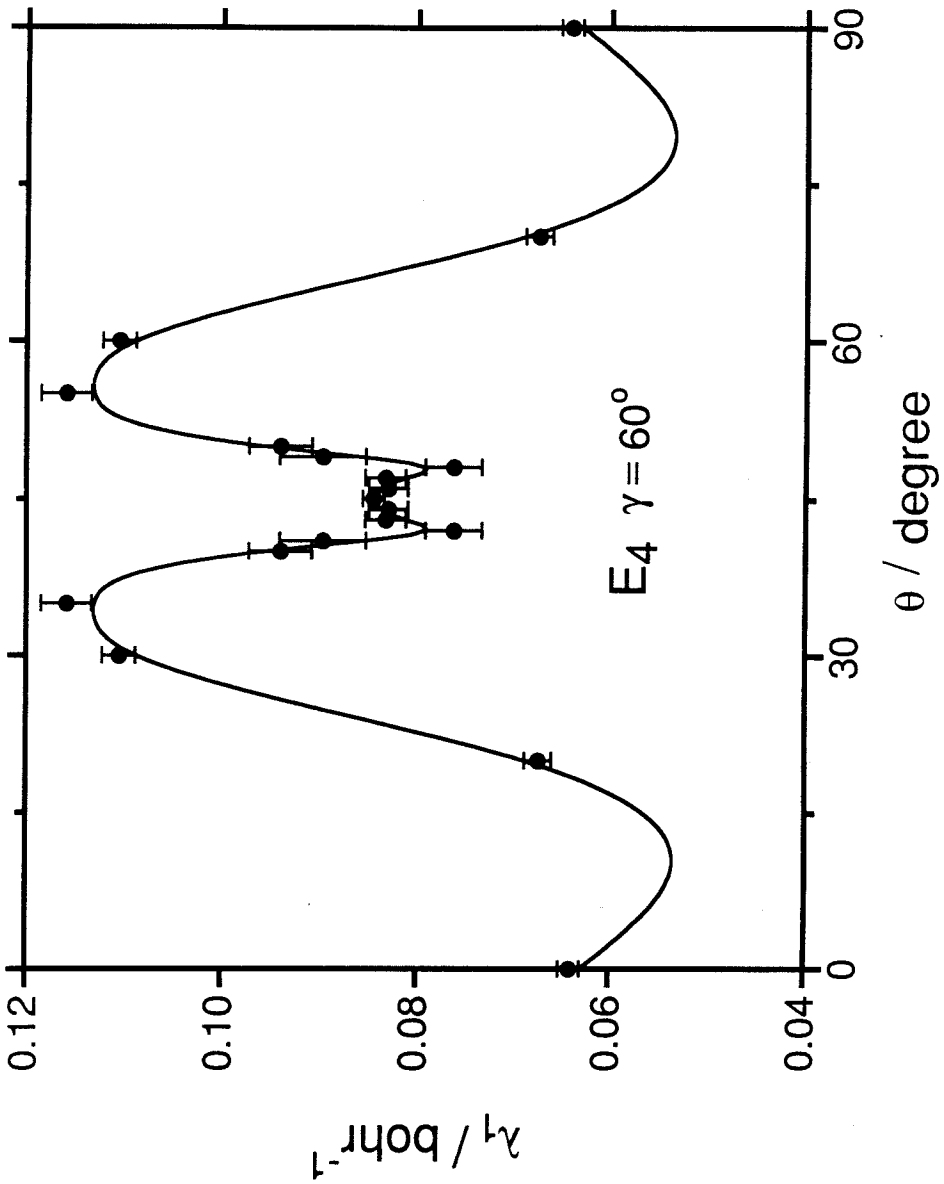

Fig. 16d

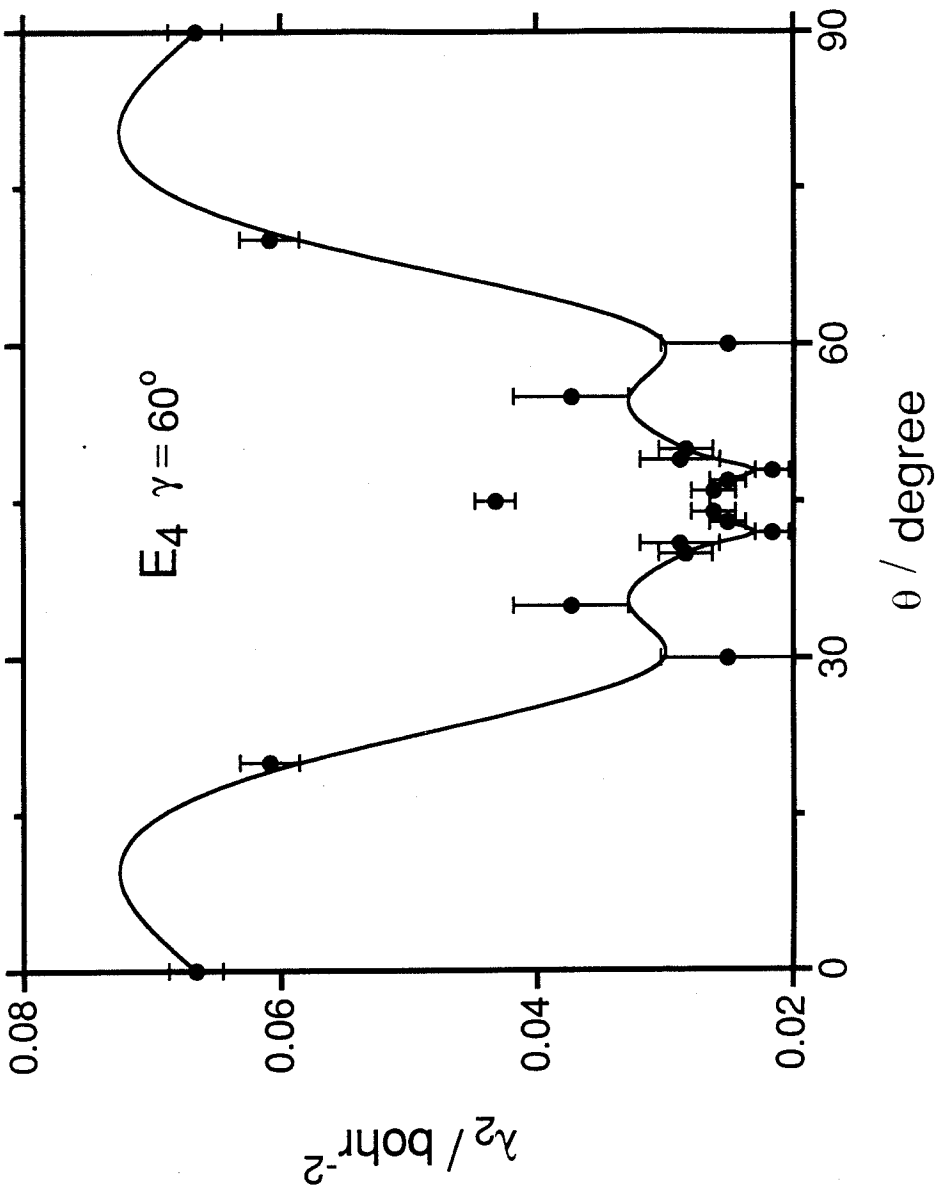
E_4 $\gamma = 60^\circ$
λ_2 / bohr^{-2}
0.08
0.06
0.04
0.02
0
30
60
90
θ / degree

Fig. 16e

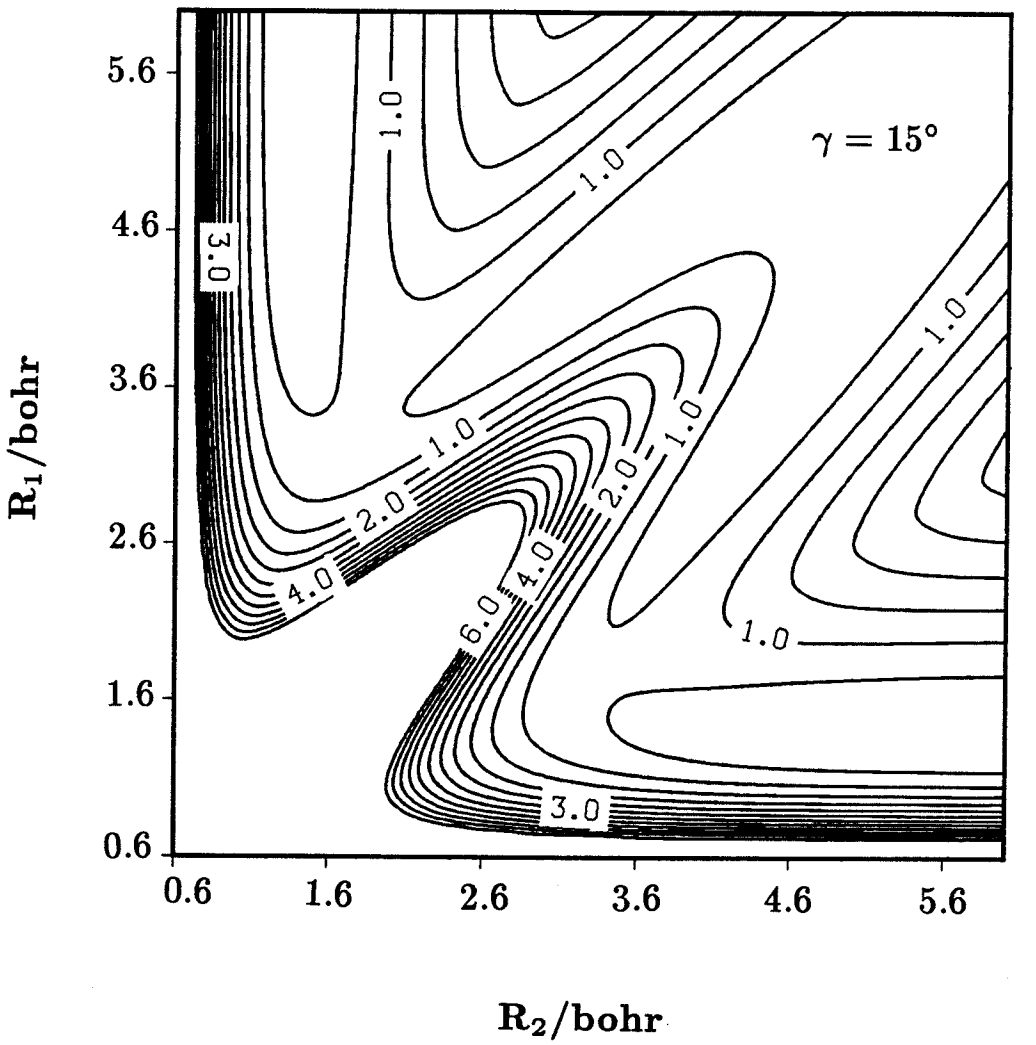

Fig. 17a

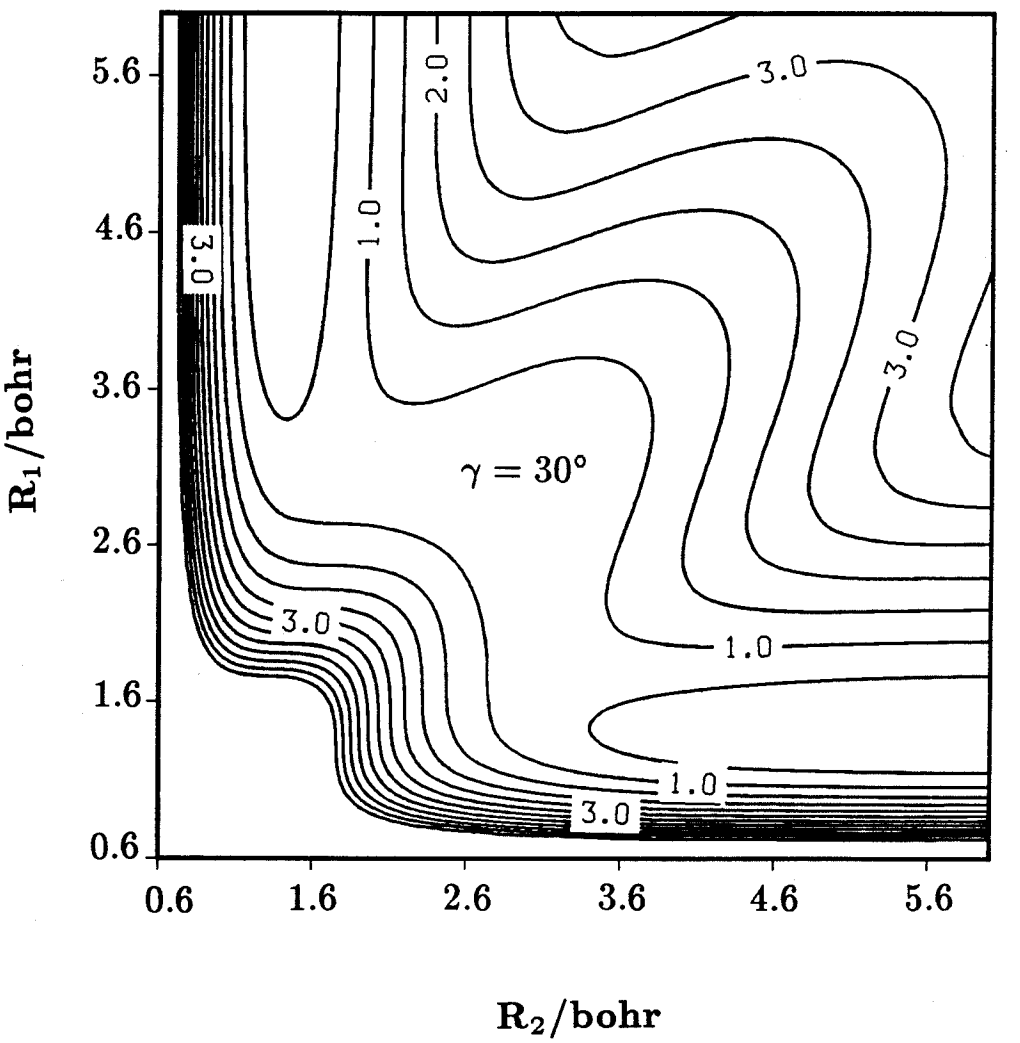
5.6
4.6
3.6
2.6
1.6
0.6
0.6
1.6
2.6
3.6
4.6
5.6
R_1/bohr
R_2/bohr
$\gamma = 30°$
3.0
2.0
1.0
3.0
3.0
3.0
1.0
1.0
3.0

Fig. 17b

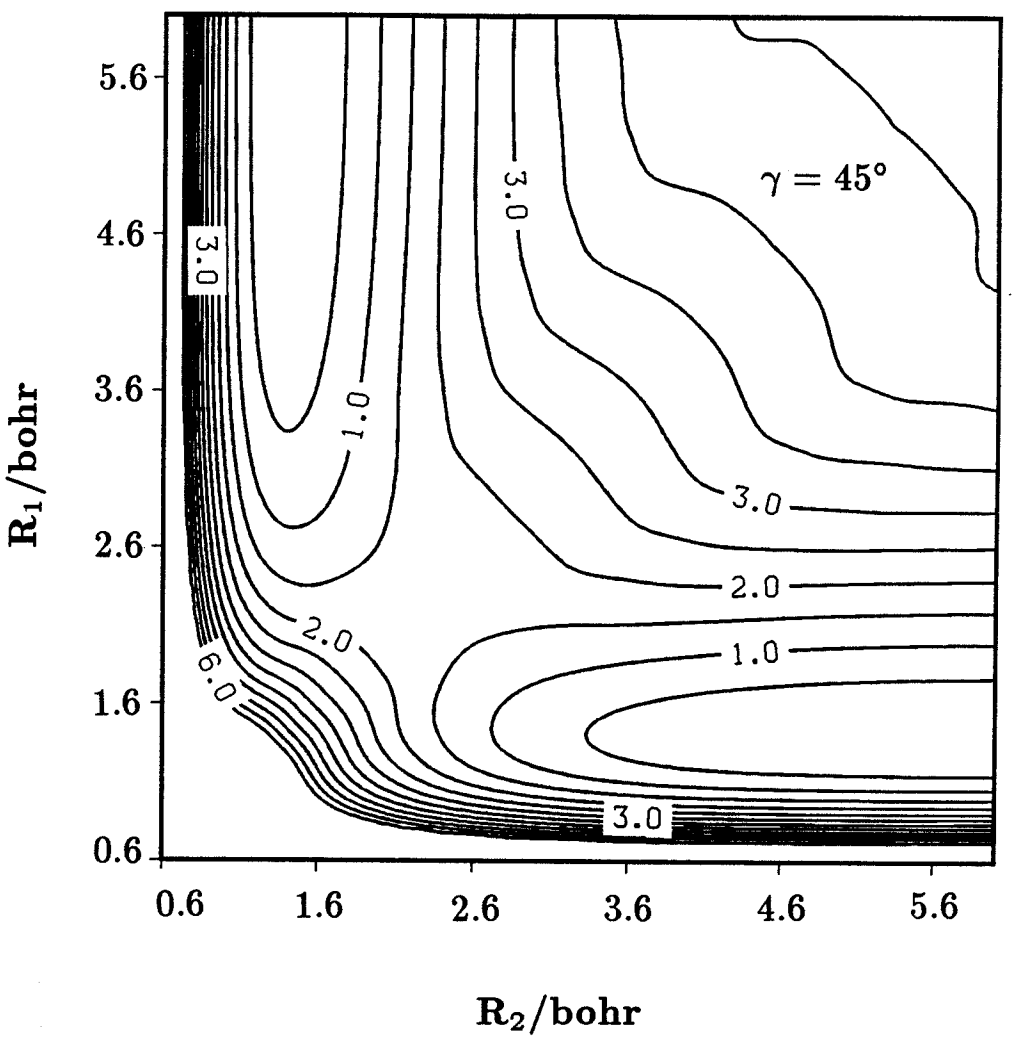
5.6
4.6
3.6
2.6
1.6
0.6
R_1/bohr
0.6
1.6
2.6
3.6
4.6
5.6
R_2/bohr
$\gamma = 45°$
3.0
1.0
3.0
3.0
2.0
2.0
1.0
6.0
3.0

Fig. 17c

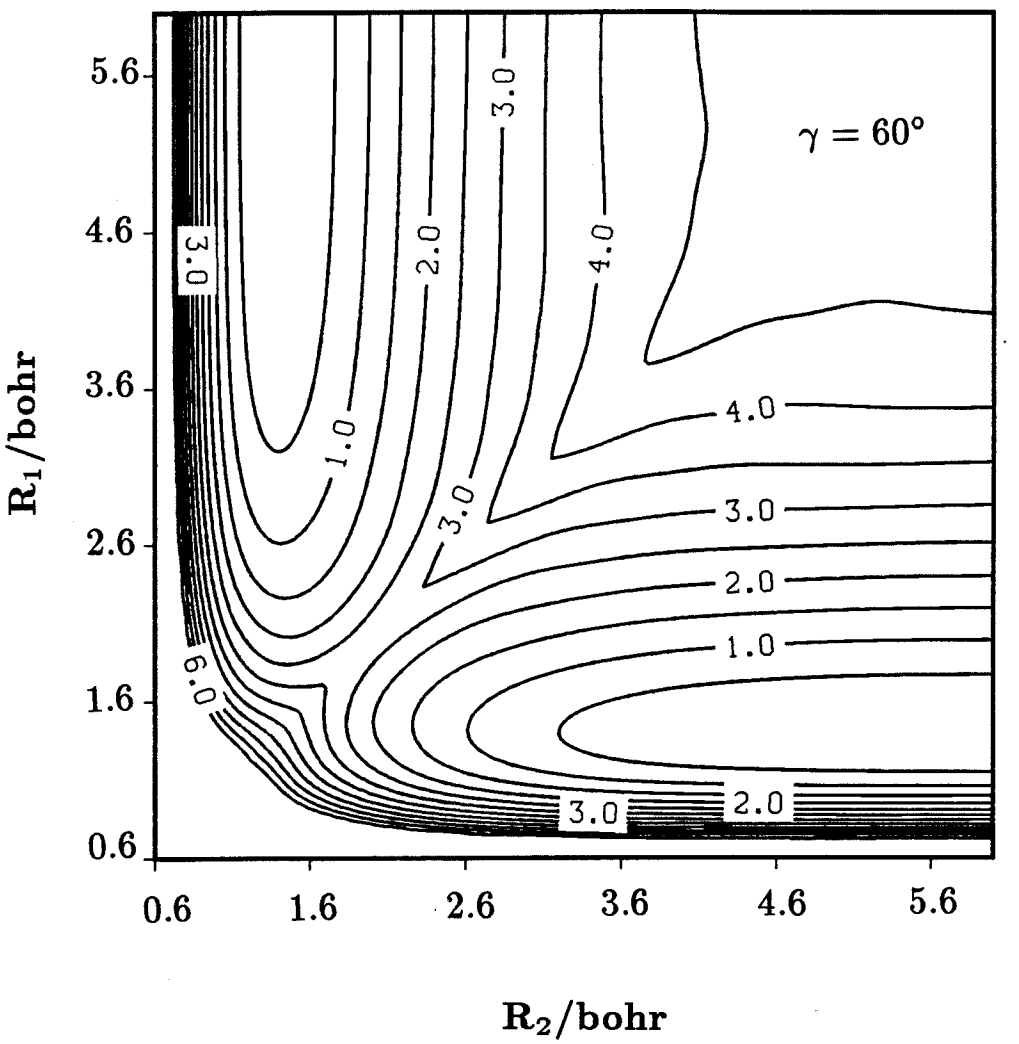

Fig. 17d

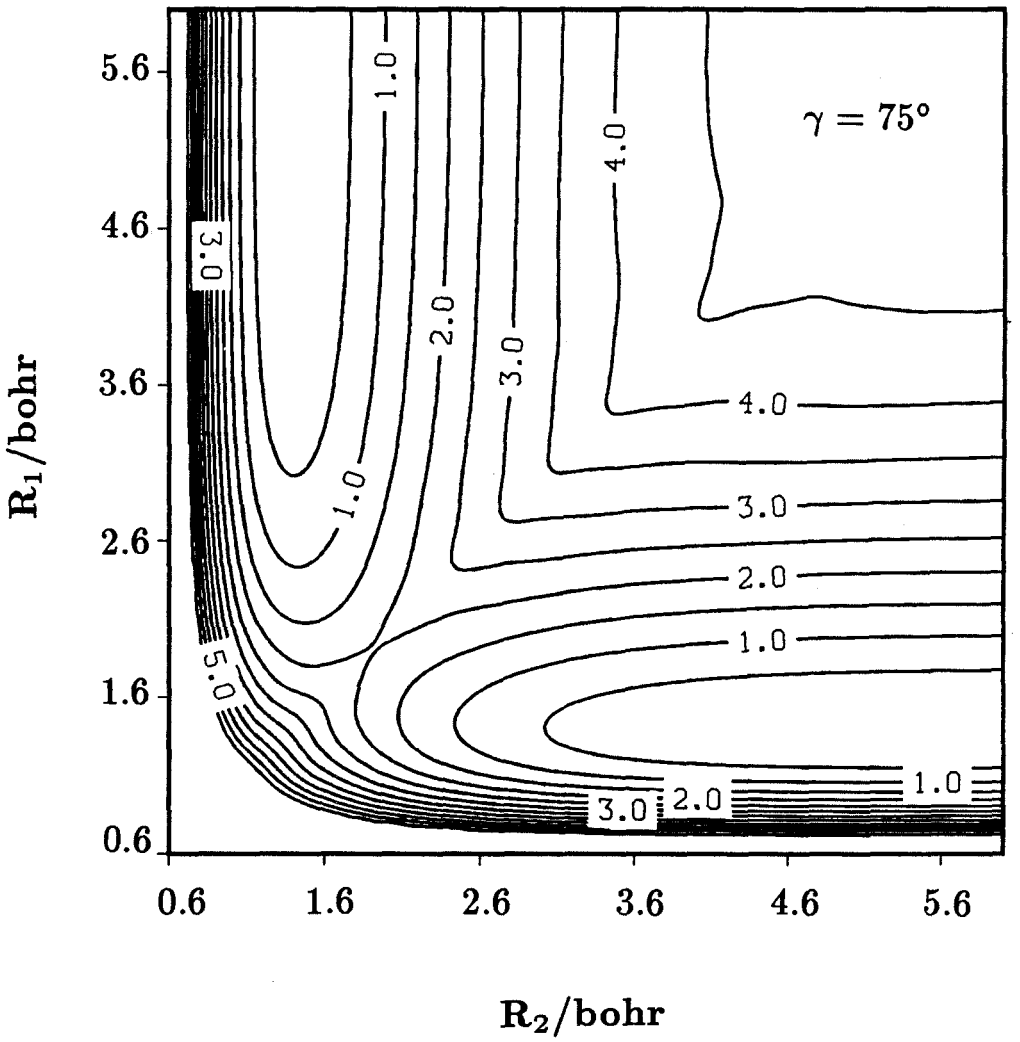

Fig. 17e

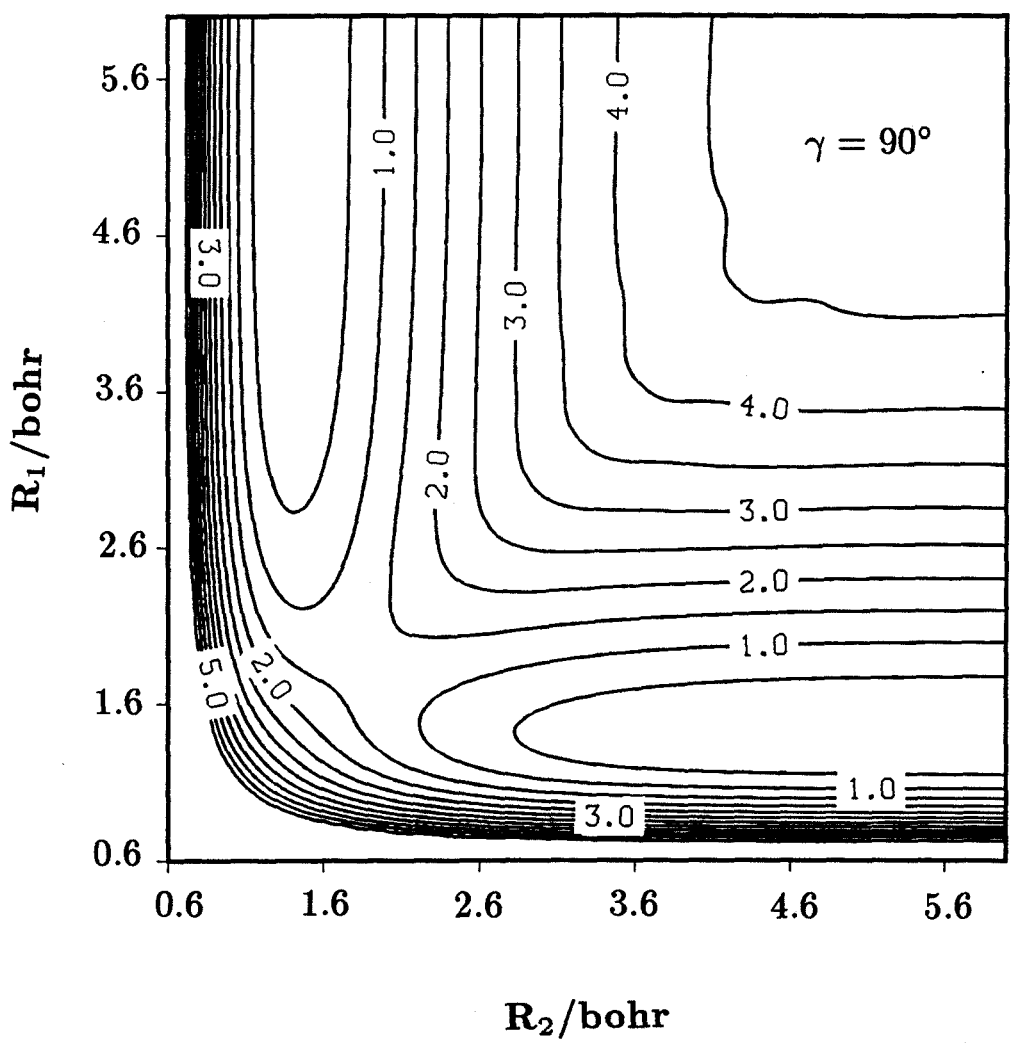
$\gamma = 90°$
5.6
4.6
3.6
2.6
1.6
0.6
0.6
1.6
2.6
3.6
4.6
5.6
R_1/bohr
R_2/bohr
1.0
2.0
3.0
4.0
5.0

Fig. 17f

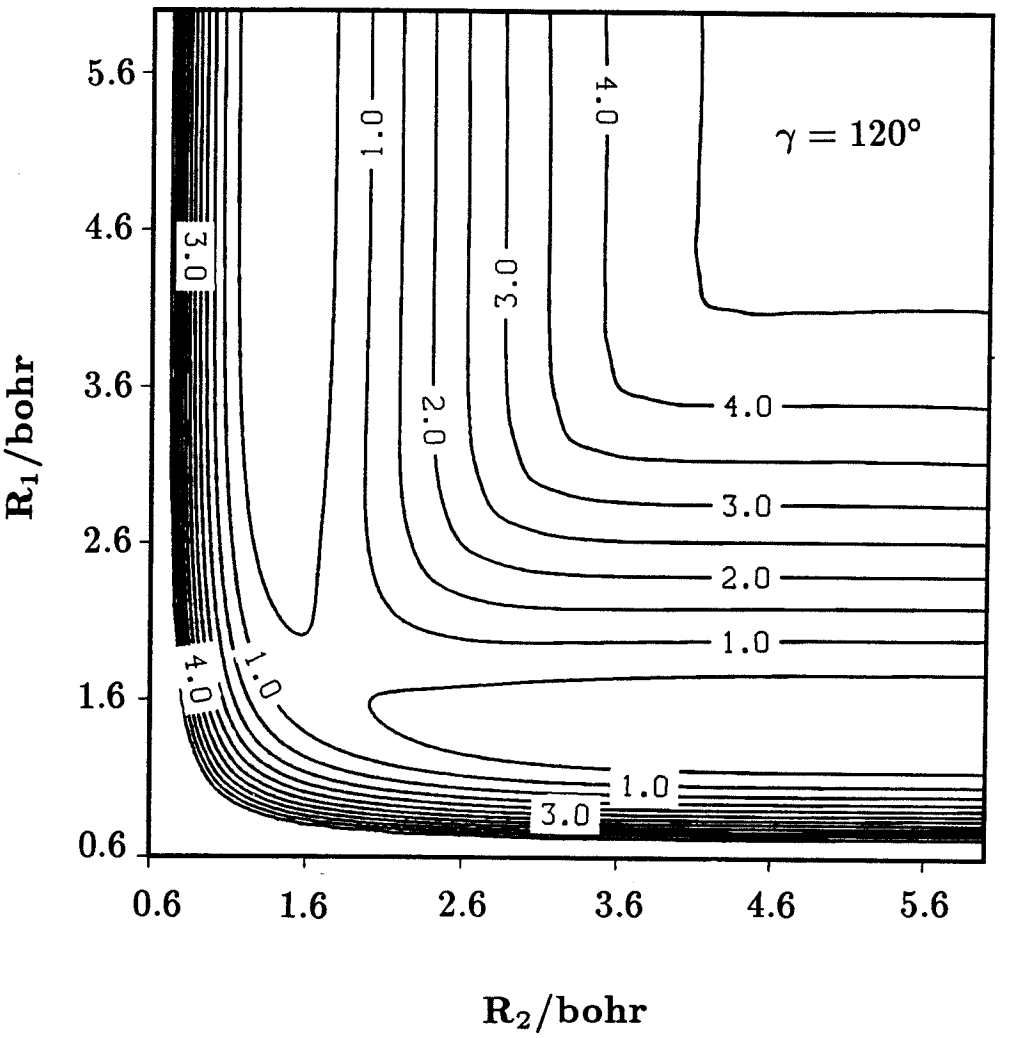
$\gamma = 120°$
5.6
4.6
3.6
2.6
1.6
0.6
0.6
1.6
2.6
3.6
4.6
5.6
R_1/bohr
R_2/bohr
1.0
2.0
3.0
4.0

Fig. 17g

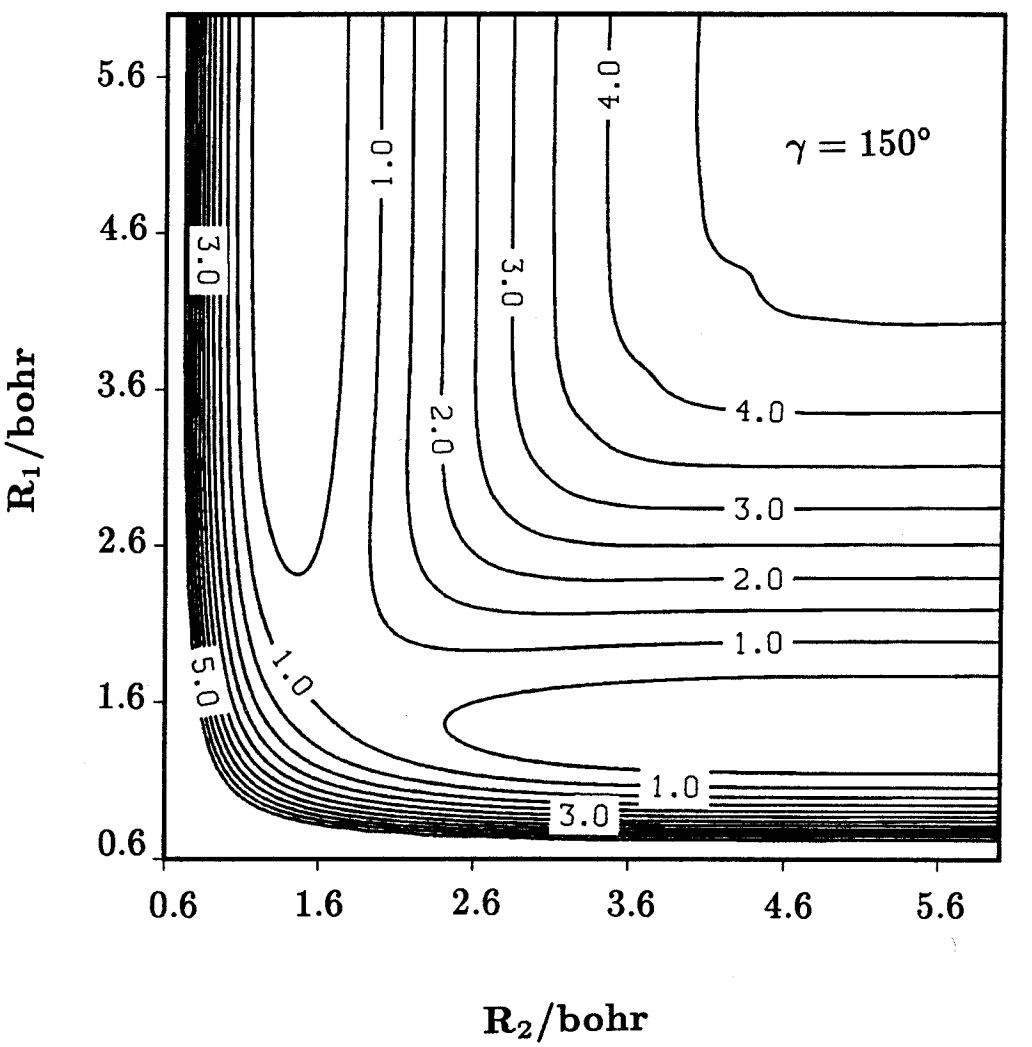
γ = 150°
4.0
1.0
3.0
2.0
3.0
4.0
3.0
2.0
1.0
5.0
1.0
1.0
3.0
5.6
4.6
3.6
2.6
1.6
0.6
0.6
1.6
2.6
3.6
4.6
5.6
R1/bohr
R2/bohr

Fig. 17h

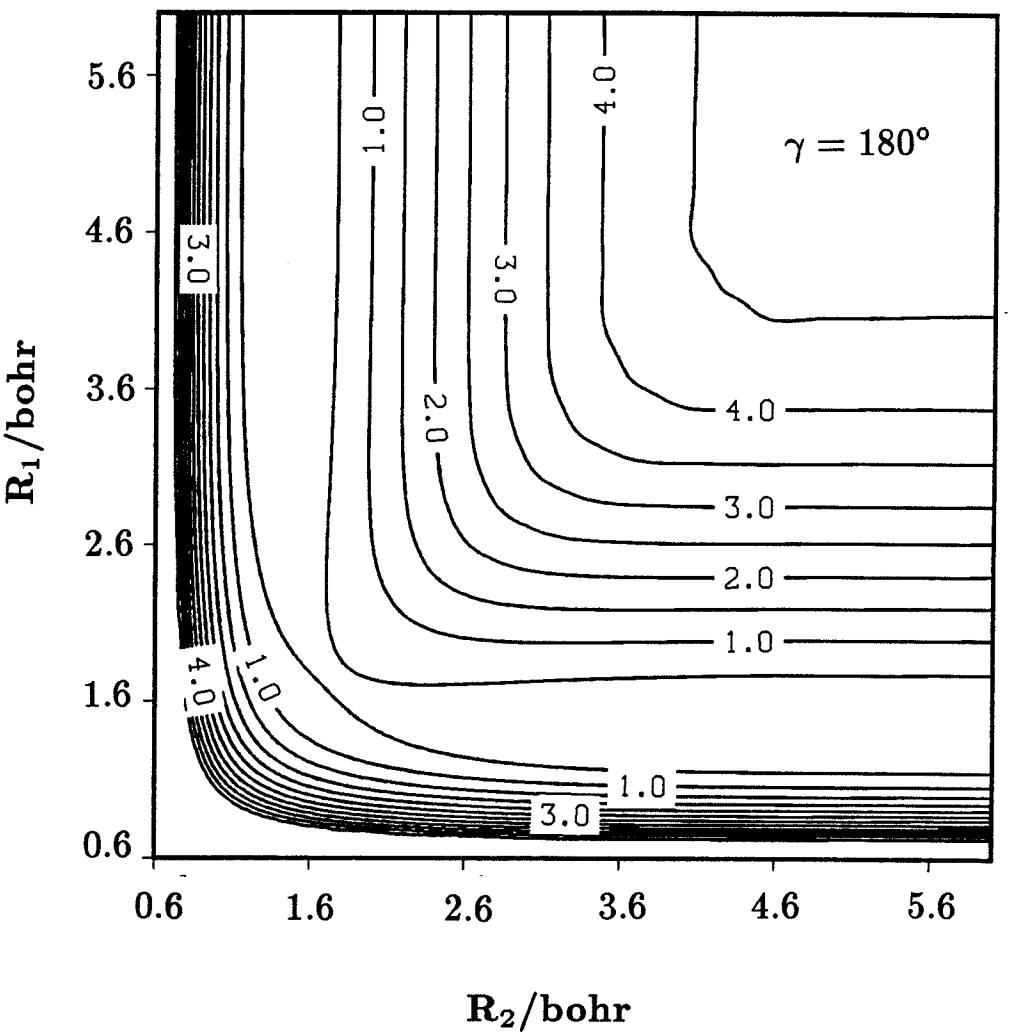
$\gamma = 180°$
5.6
4.6
3.6
2.6
1.6
0.6
R_1/bohr
0.6
1.6
2.6
3.6
4.6
5.6
R_2/bohr
1.0
2.0
3.0
4.0

Fig. 17i

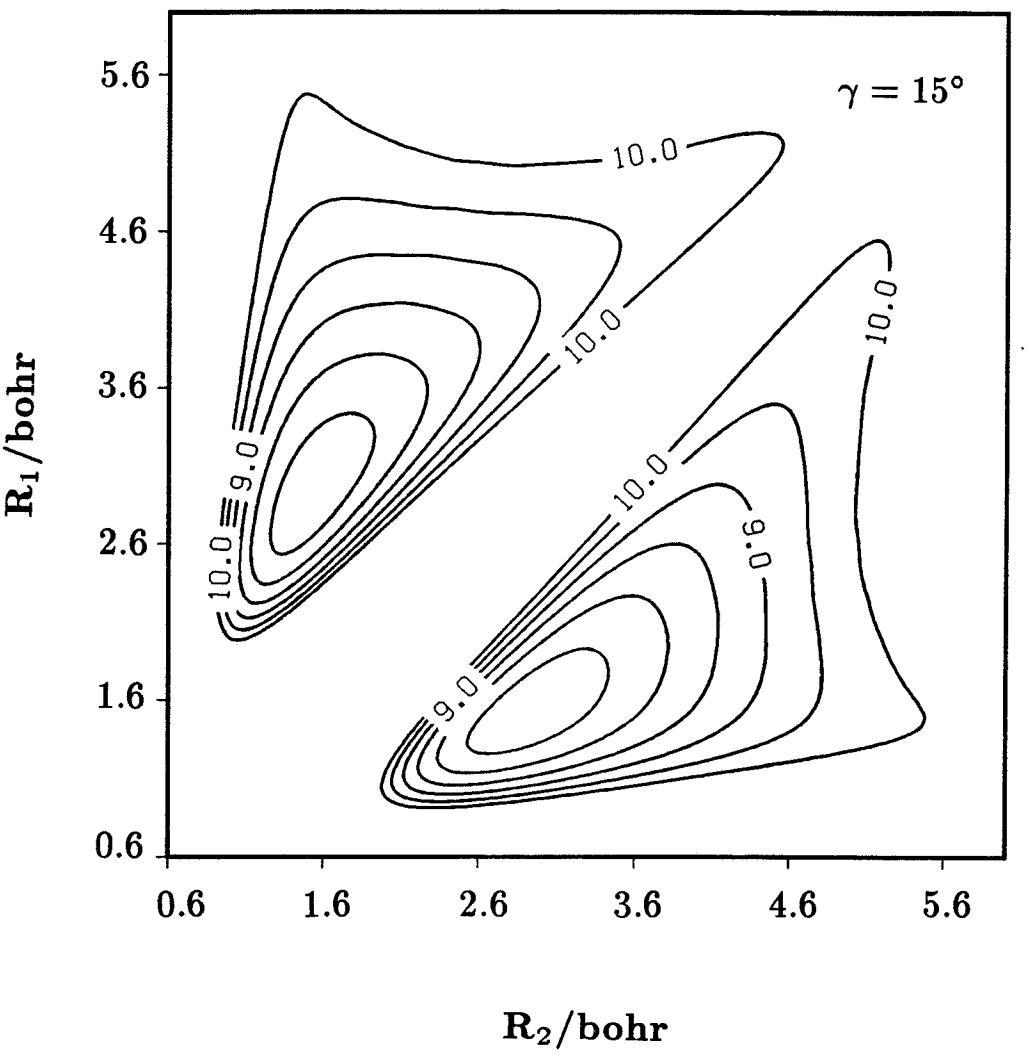
γ = 15°
10.0
10.0
10.0
9.0
10.0
10.0
9.0
9.0
5.6
4.6
3.6
2.6
1.6
0.6
0.6
1.6
2.6
3.6
4.6
5.6
R1/bohr
R2/bohr

Fig. 18a

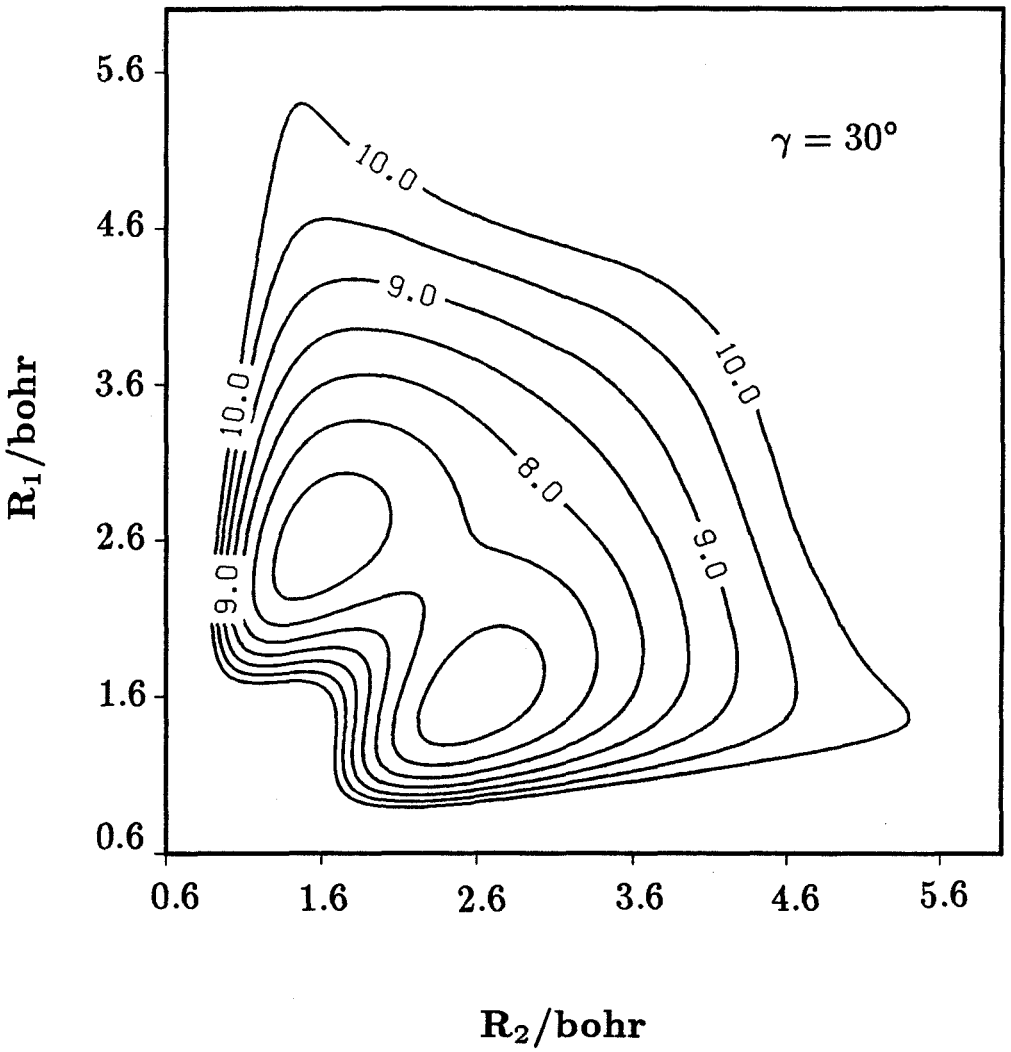
$\gamma = 30°$
10.0
9.0
8.0
10.0
9.0
10.0
9.0
5.6
4.6
3.6
2.6
1.6
0.6
0.6
1.6
2.6
3.6
4.6
5.6
R_1/bohr
R_2/bohr

Fig. 18b

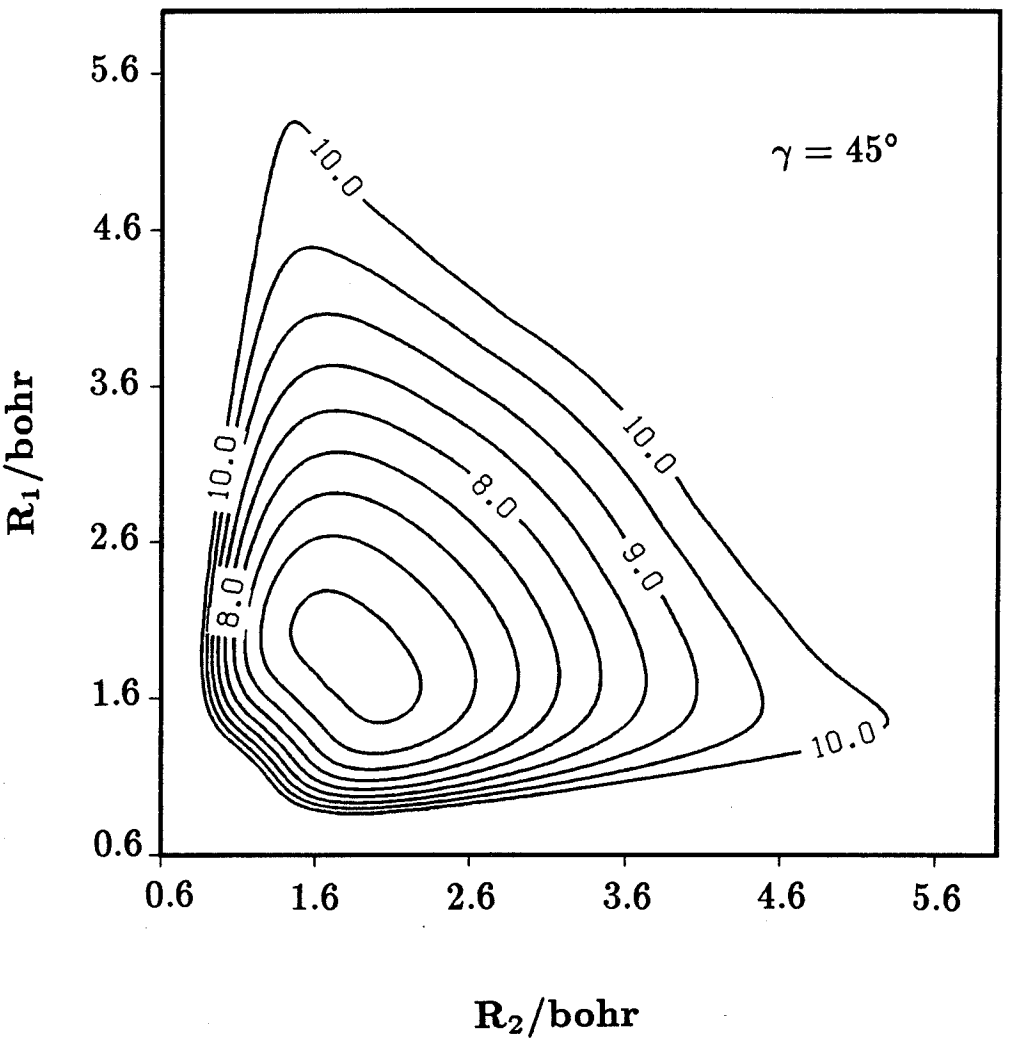
$\gamma = 45°$
10.0
10.0
10.0
8.0
8.0
9.0
5.6
4.6
3.6
2.6
1.6
0.6
R_1/bohr
0.6
1.6
2.6
3.6
4.6
5.6
R_2/bohr

Fig. 18c

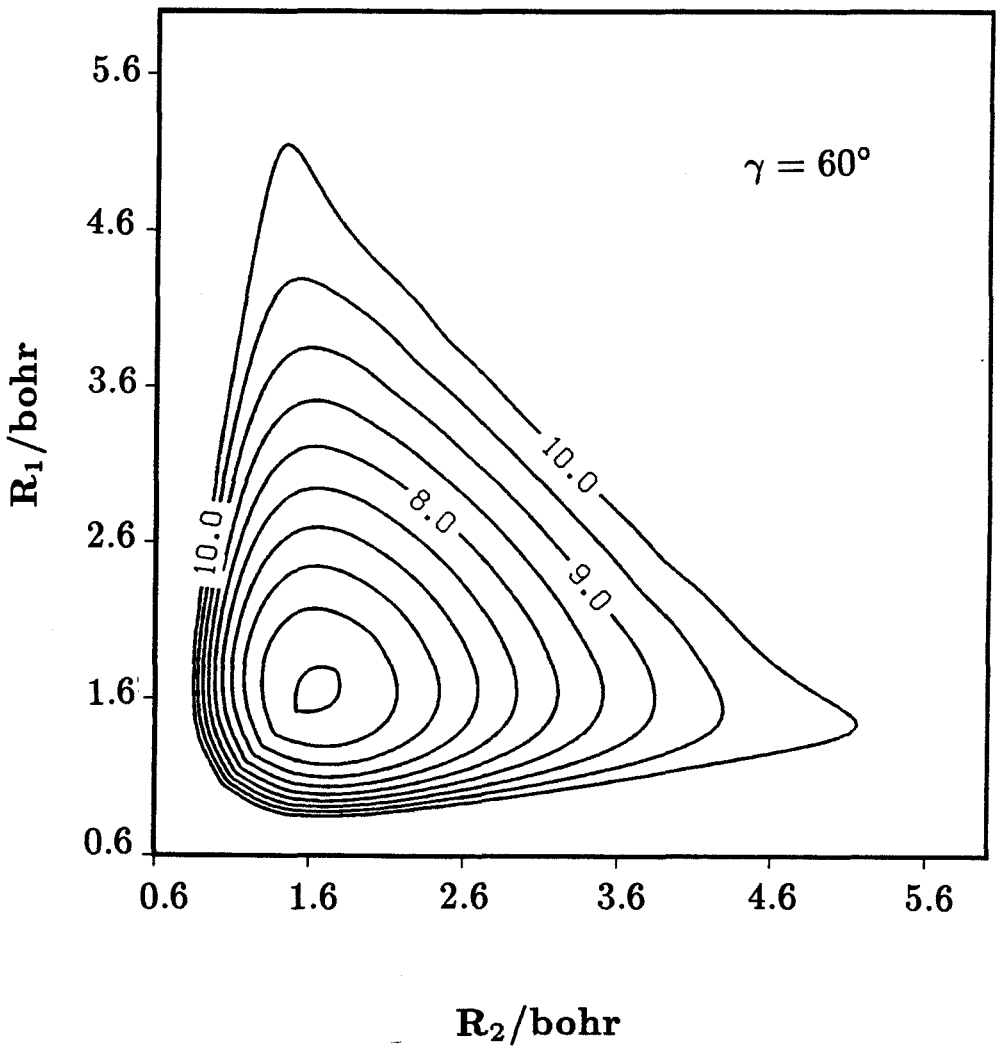
$\gamma = 60°$
10.0
8.0
9.0
10.0
5.6
4.6
3.6
2.6
1.6
0.6
0.6
1.6
2.6
3.6
4.6
5.6
R_1/bohr
R_2/bohr

Fig. 18d

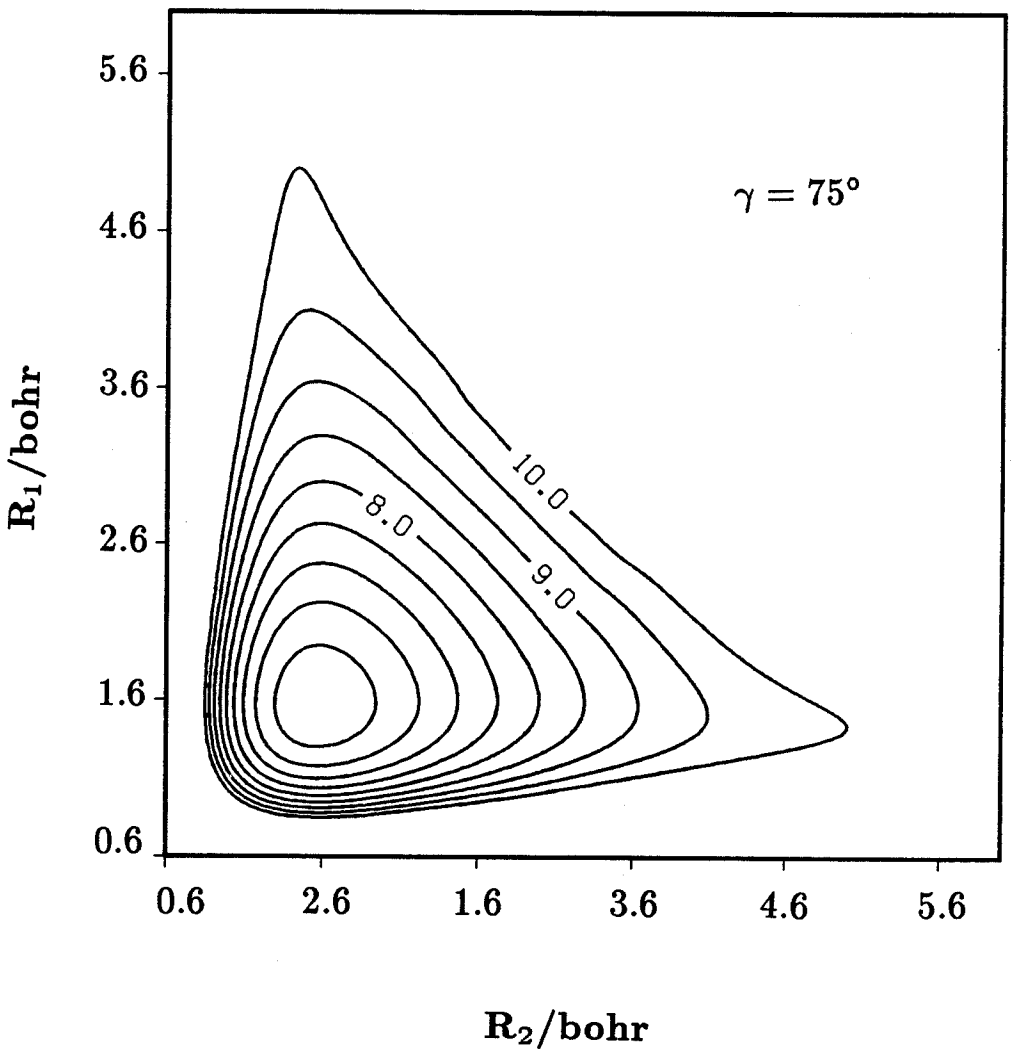
5.6
4.6
3.6
2.6
1.6
0.6
$\gamma = 75°$
10.0
8.0
9.0
0.6
2.6
1.6
3.6
4.6
5.6
R_1/bohr
R_2/bohr

Fig. 18e

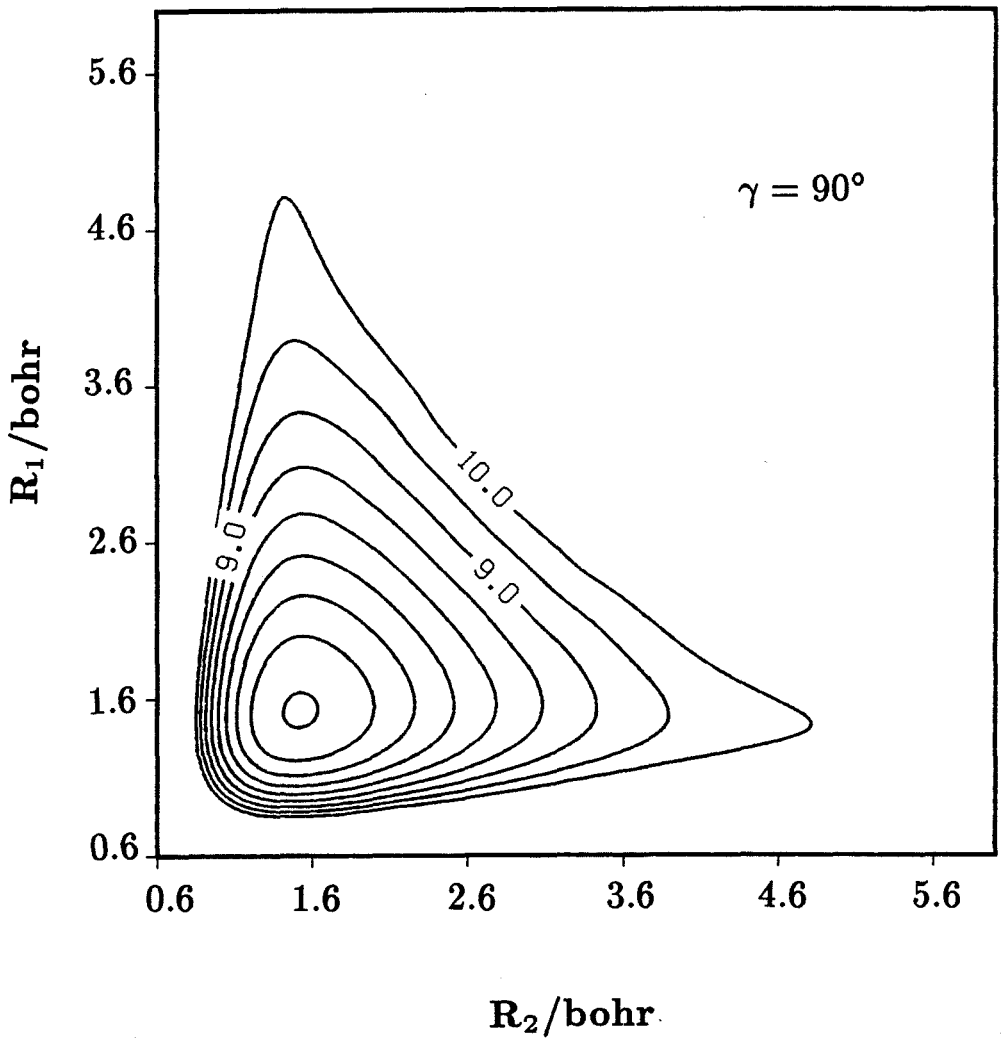
$\gamma = 90°$
10.0
9.0
9.0
5.6
4.6
3.6
2.6
1.6
0.6
0.6
1.6
2.6
3.6
4.6
5.6
R_1/bohr
R_2/bohr

Fig. 18f

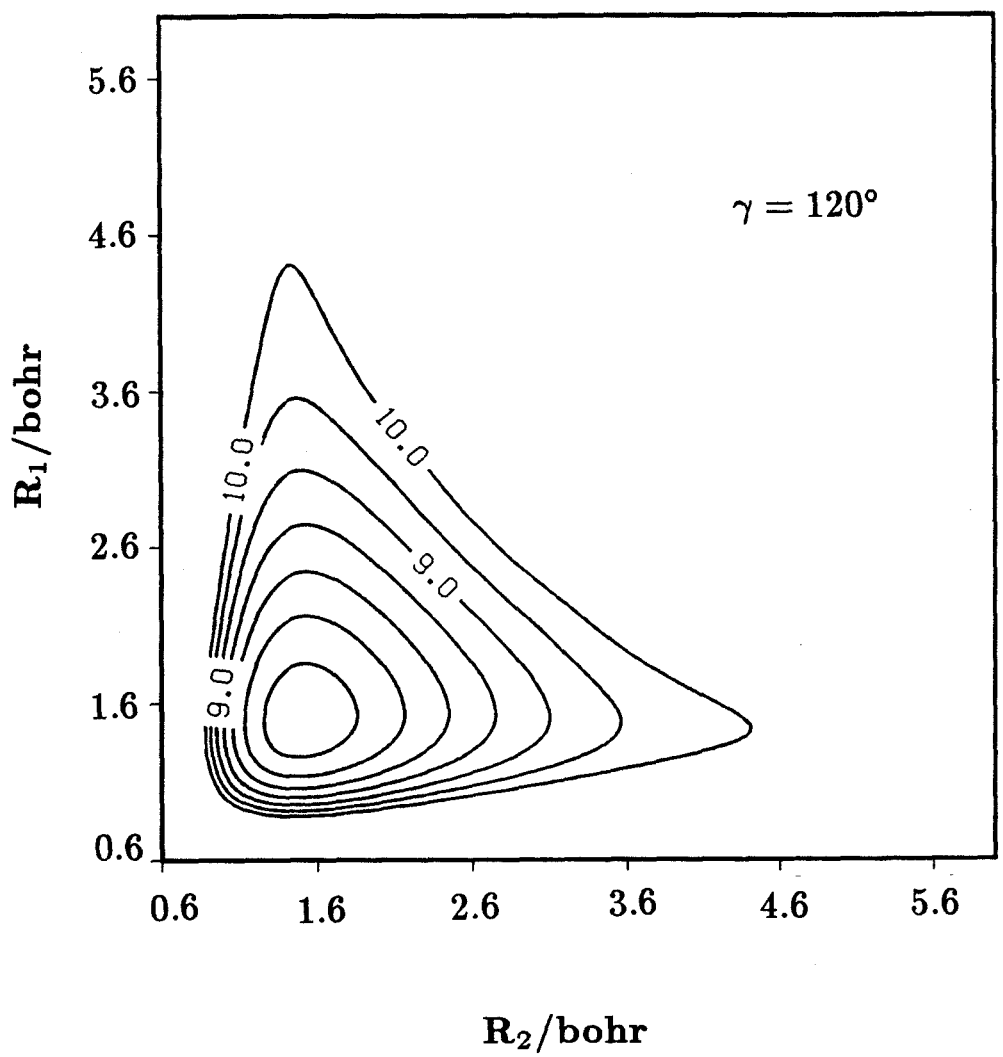
$\gamma = 120°$
10.0
10.0
9.0
9.0
5.6
4.6
3.6
2.6
1.6
0.6
0.6
1.6
2.6
3.6
4.6
5.6
R_1/bohr
R_2/bohr

Fig. 18g

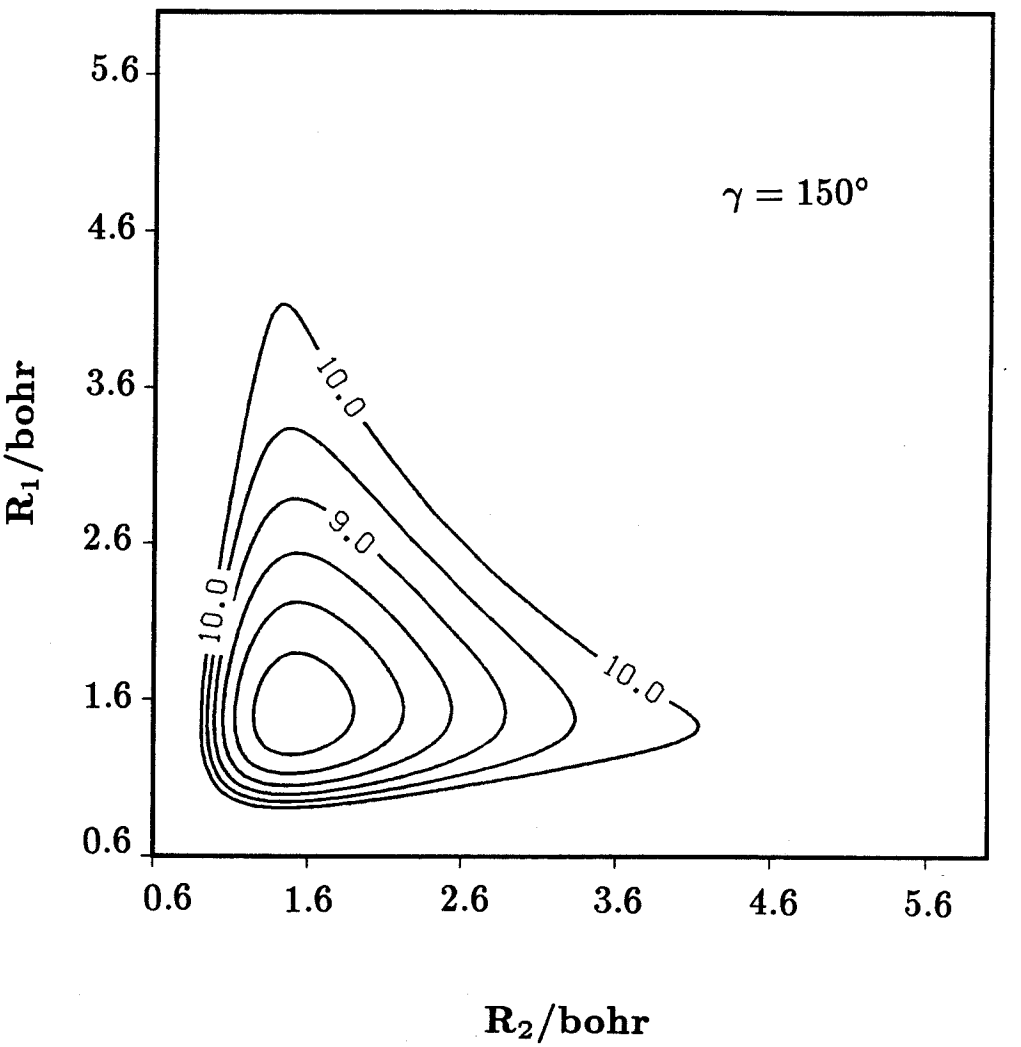
$\gamma = 150°$
10.0
9.0
10.0
10.0
5.6
4.6
3.6
2.6
1.6
0.6
0.6
1.6
2.6
3.6
4.6
5.6
R_1/bohr
R_2/bohr

Fig. 18h

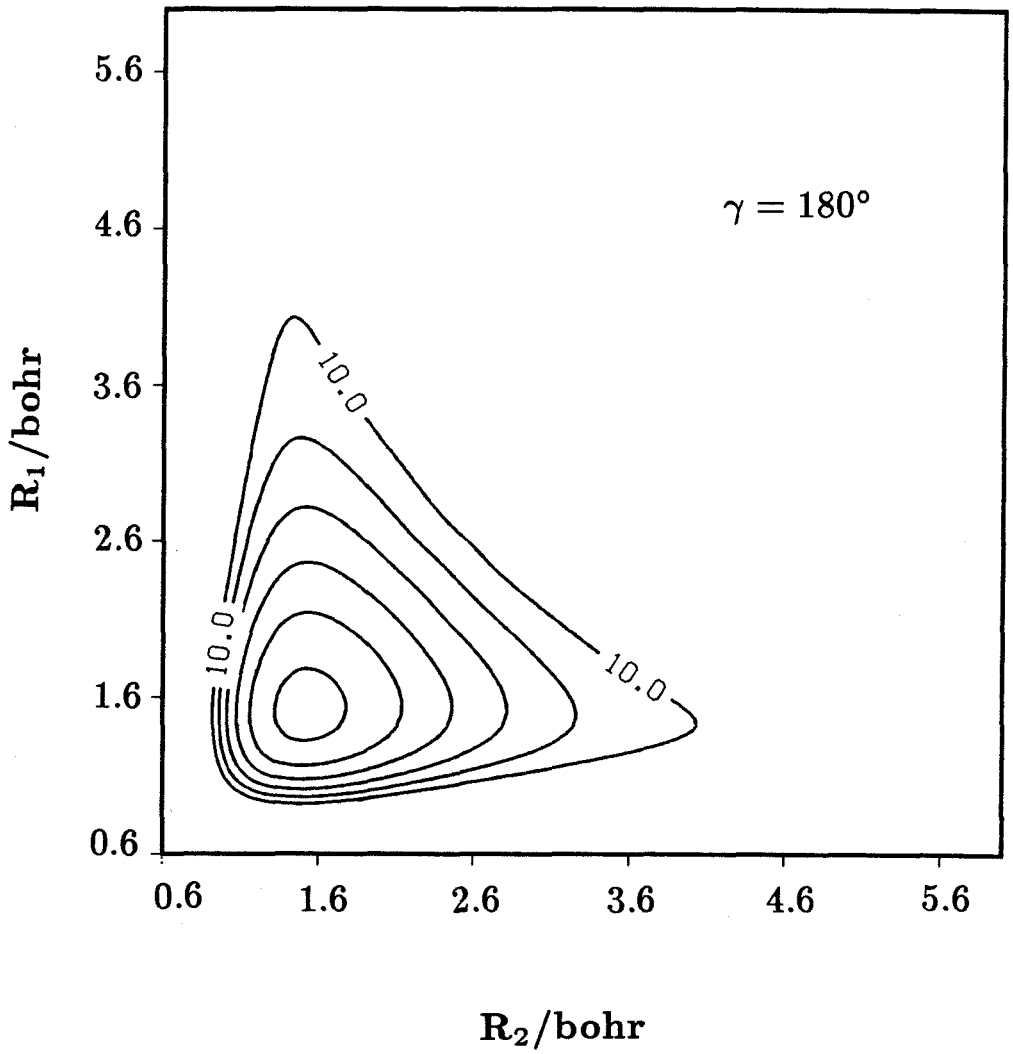
5.6
4.6
3.6
2.6
1.6
0.6
$\gamma = 180°$
10.0
10.0
10.0
R_1/bohr
0.6
1.6
2.6
3.6
4.6
5.6
R_2/bohr

Fig. 18i

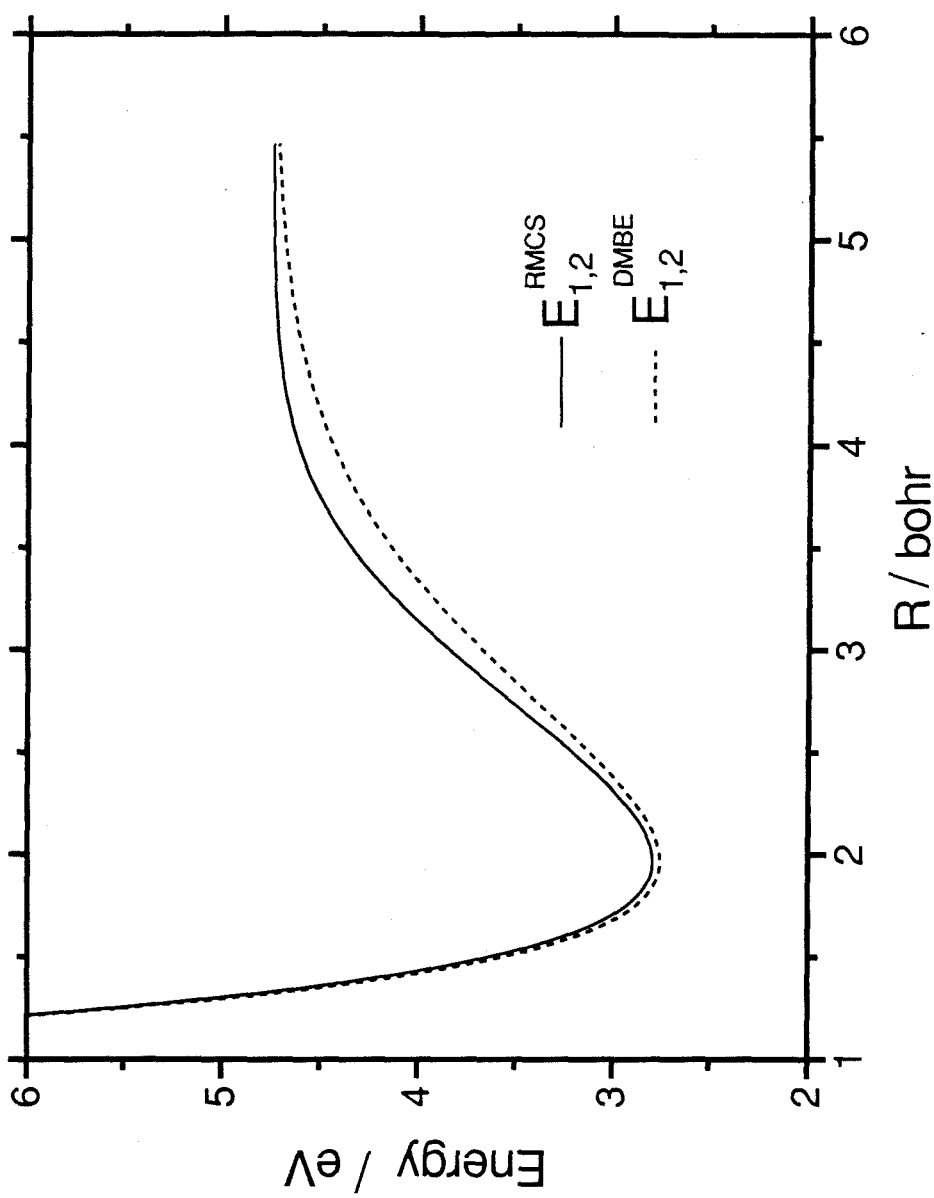

Fig. 19

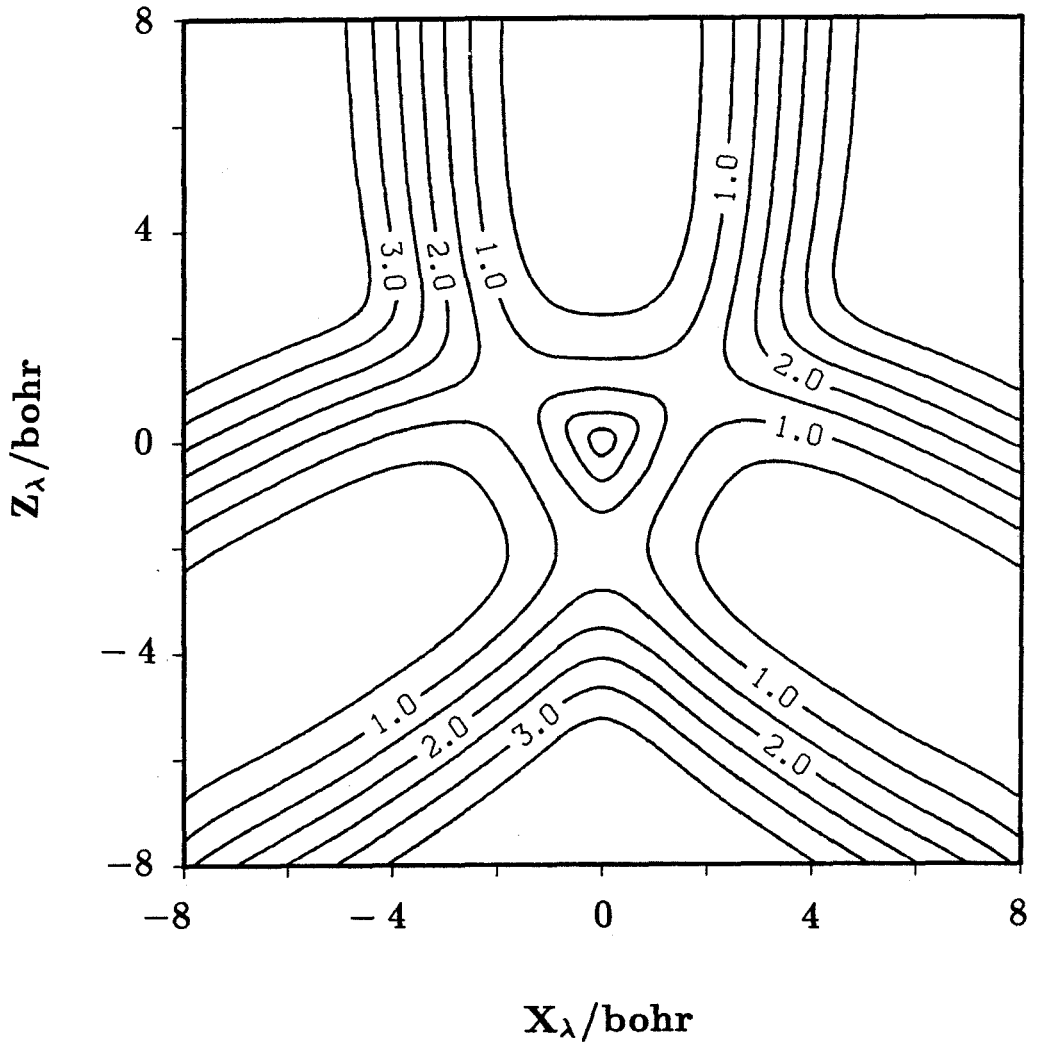
8
4
0
− 4
−8
−8
− 4
0
4
8
Z_λ/bohr
X_λ/bohr
3.0
2.0
1.0
1.0
2.0
1.0
1.0
2.0
3.0
1.0
2.0
3.0

Fig. 20a

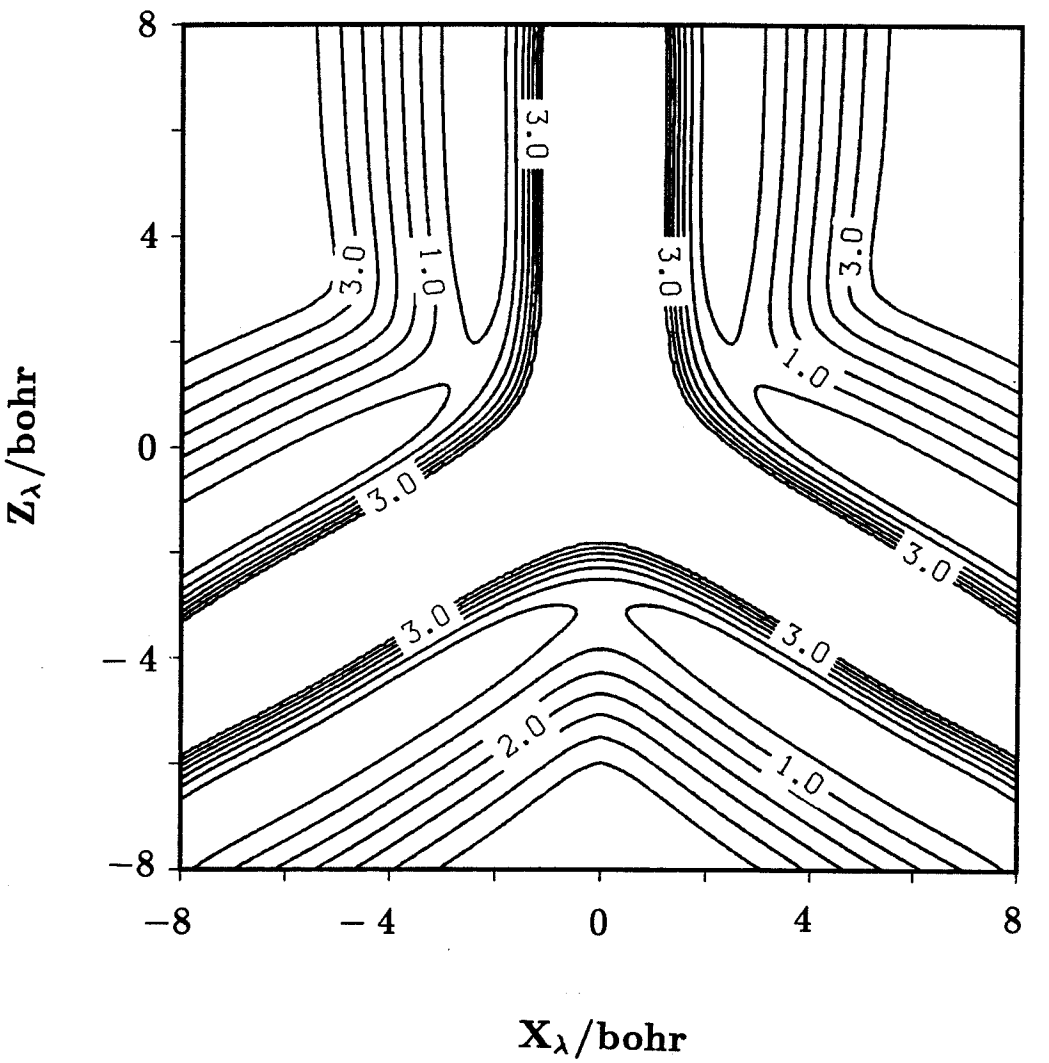

Fig. 20b

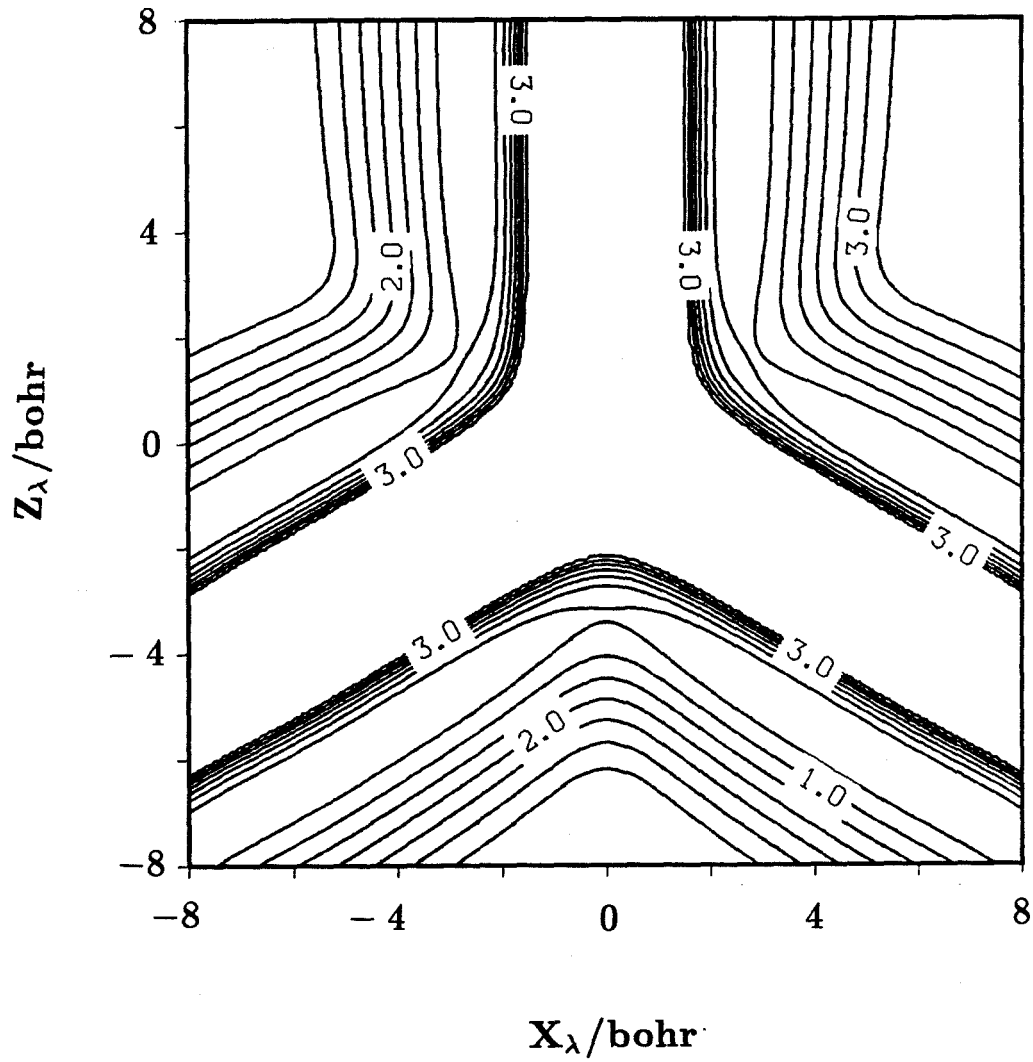

Fig. 20c

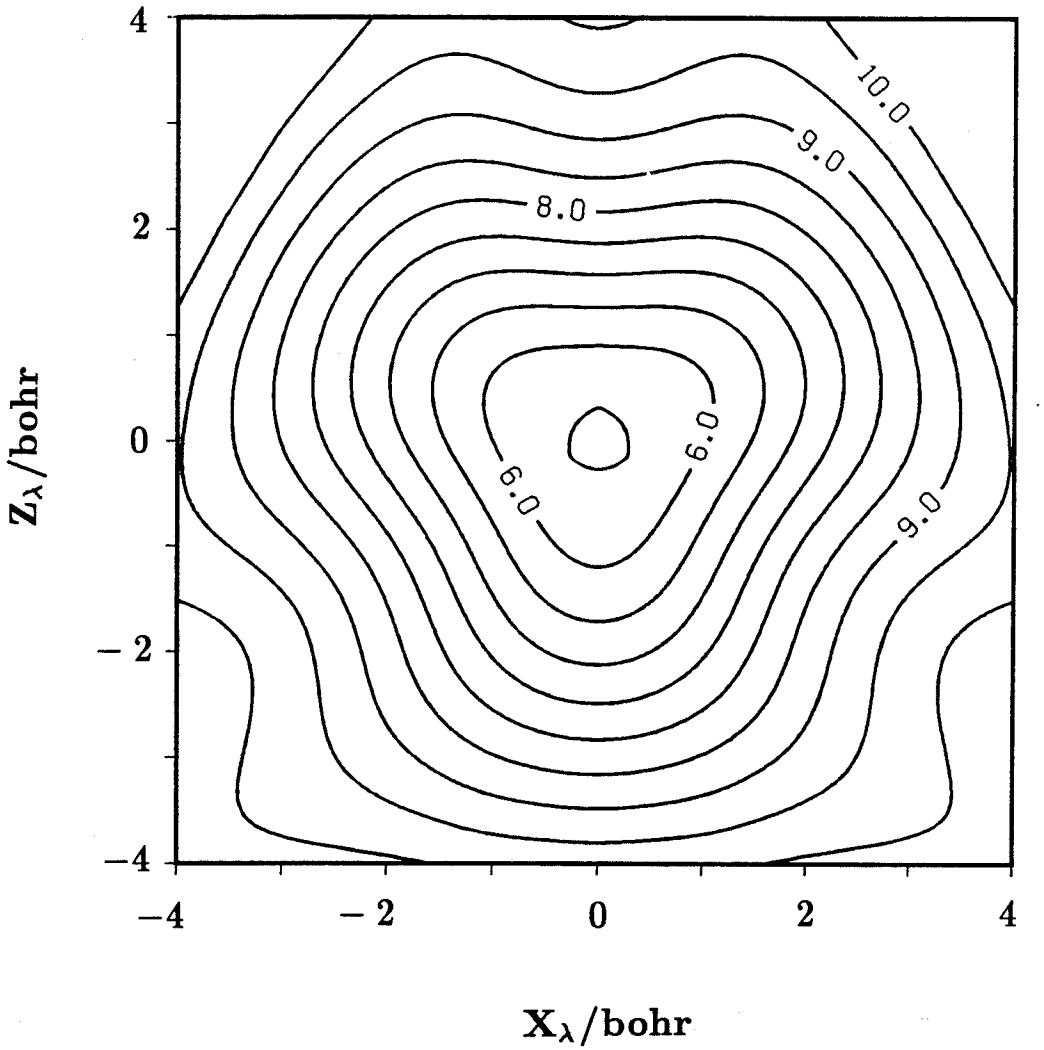

Fig. 21a

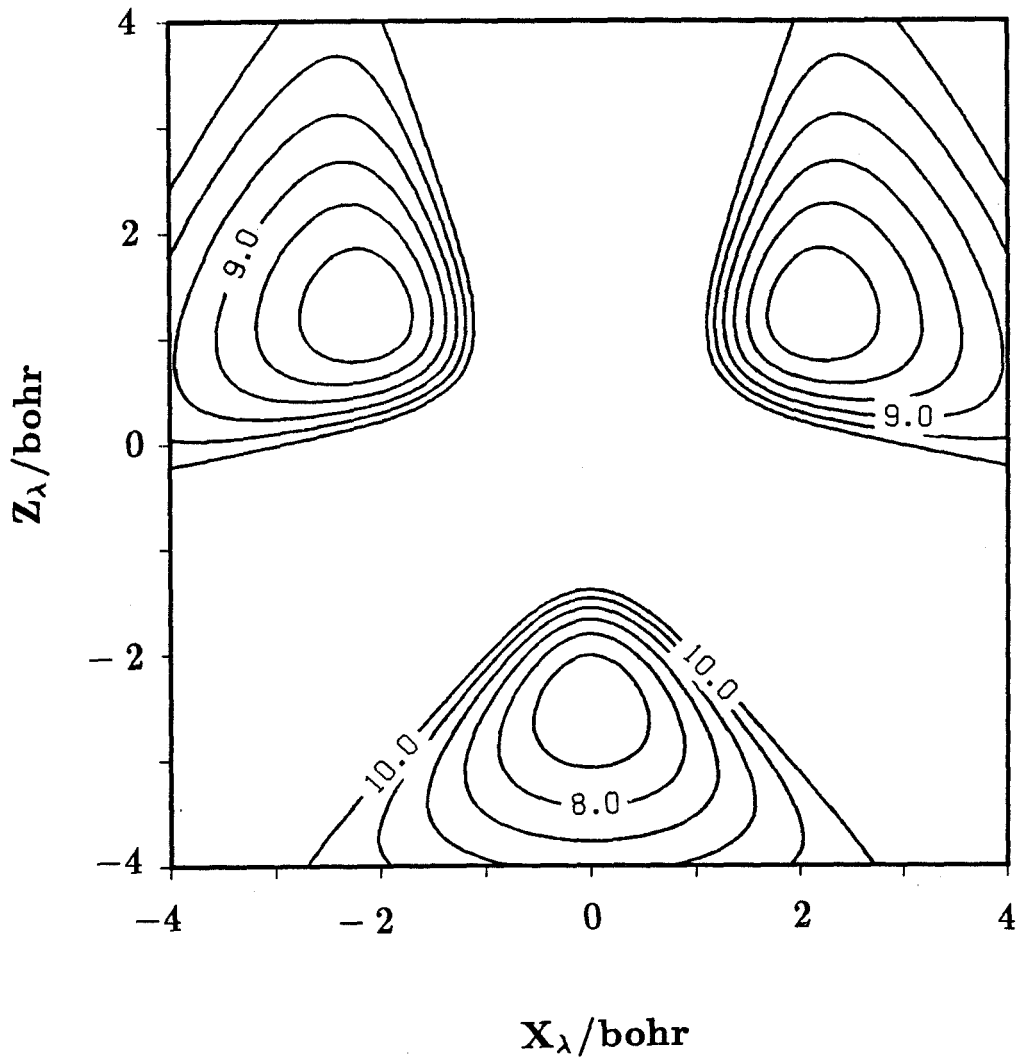

Fig. 21b

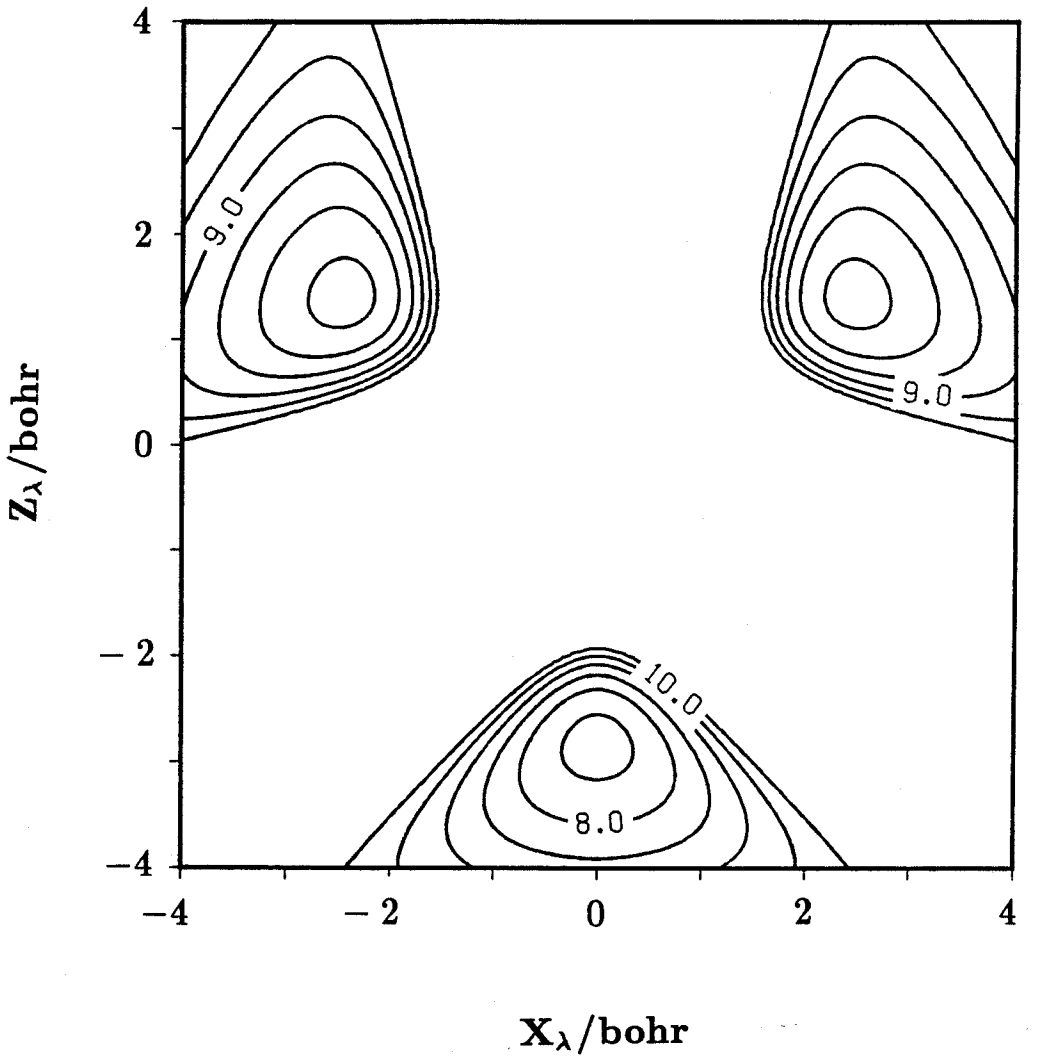

Fig. 21c

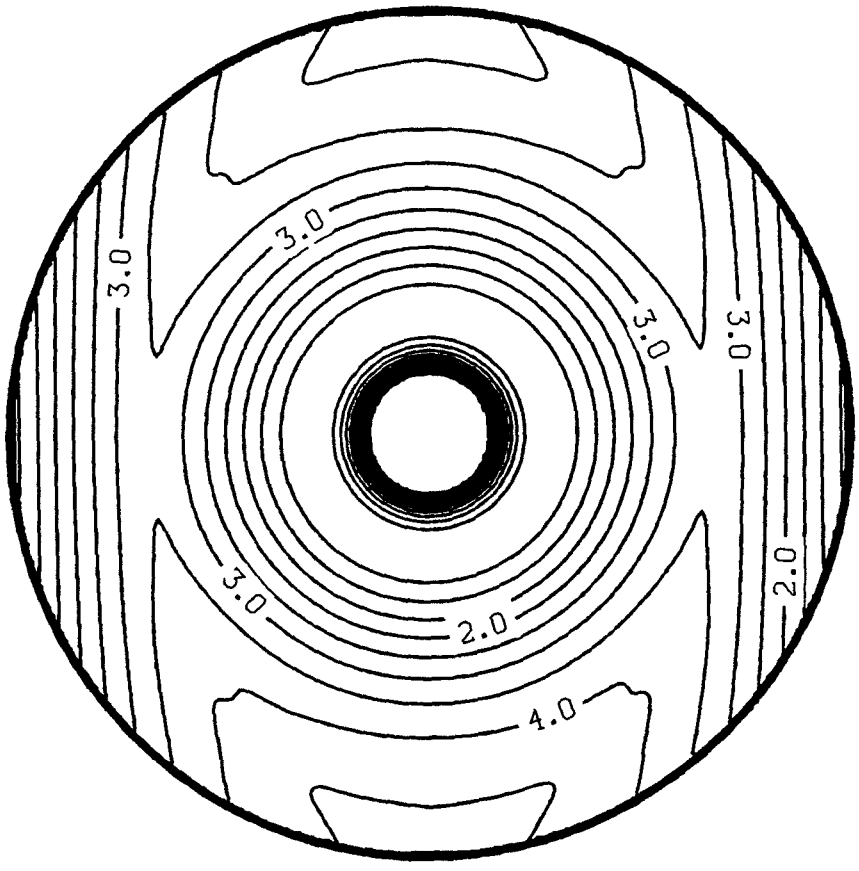

$\rho = 6.0$ **bohr**

Fig. 22

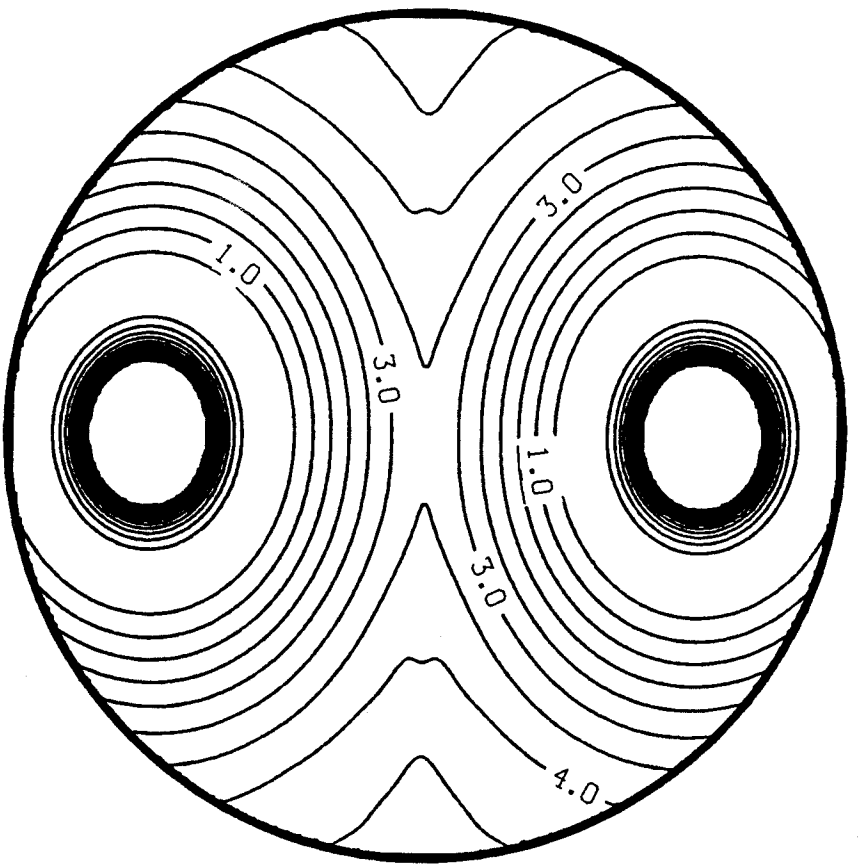

$\rho = 6.0$ **bohr**

Fig. 23

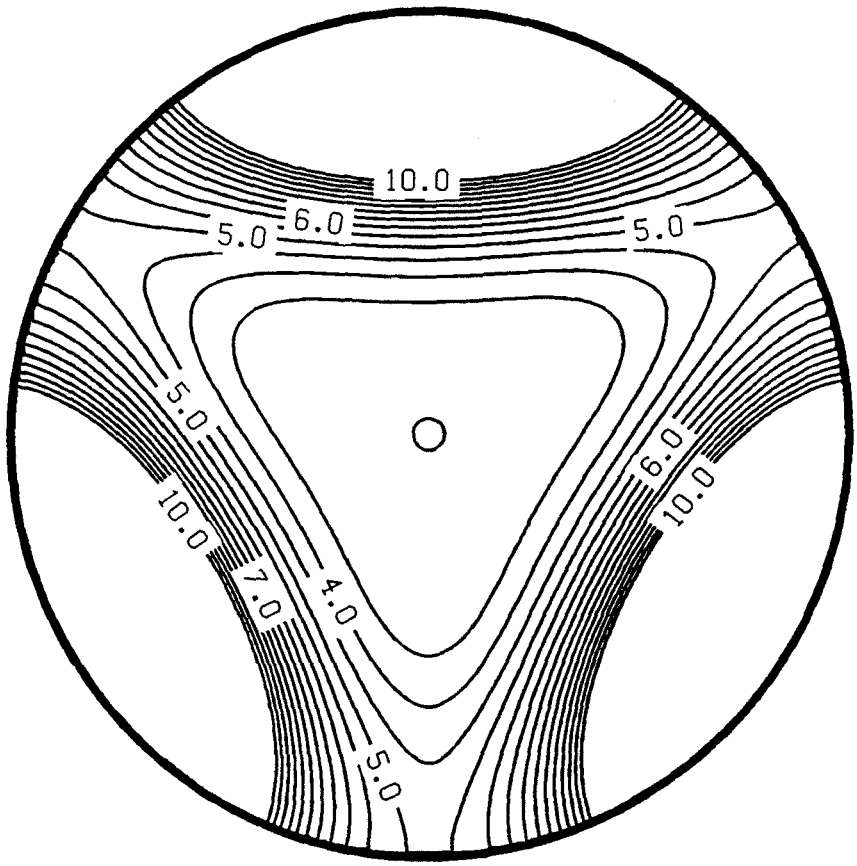

$\rho = 2.0$ **bohr**

Fig. 24a

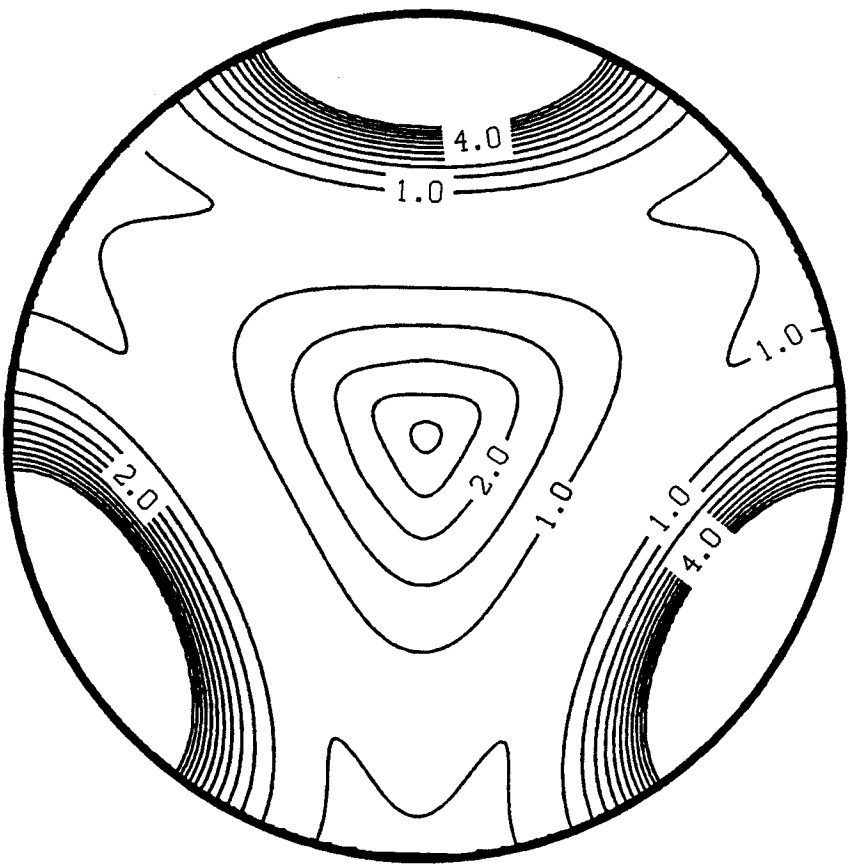

$\rho = 3.27$ **bohr**

Fig. 24b

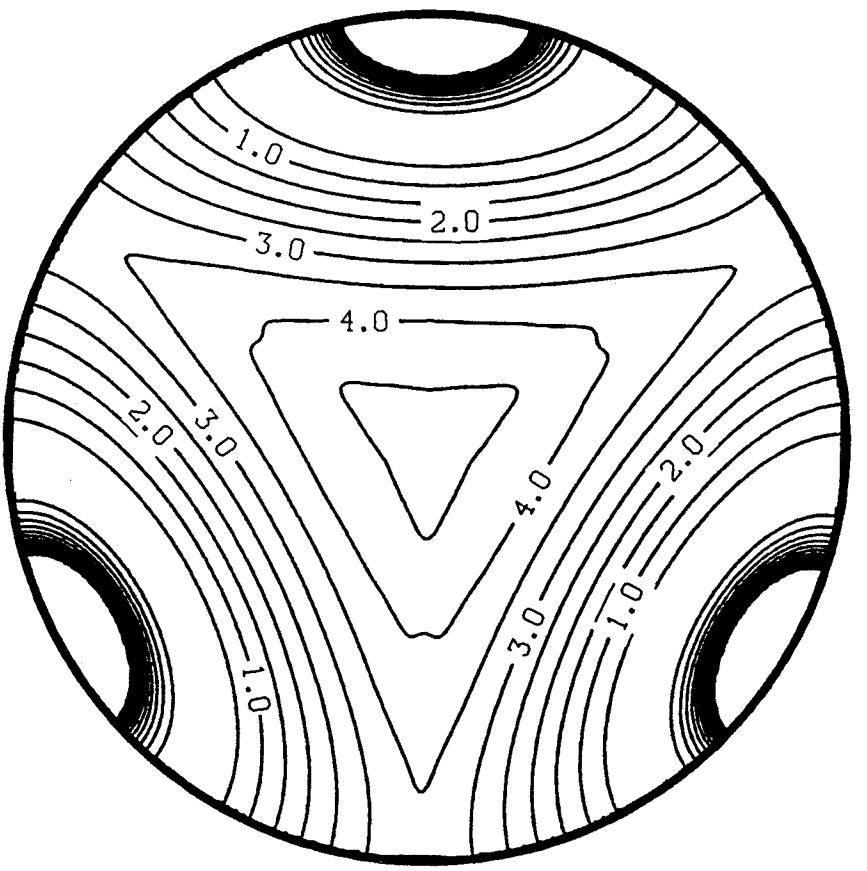

$\rho = 6.0$ **bohr**

Fig. 24c

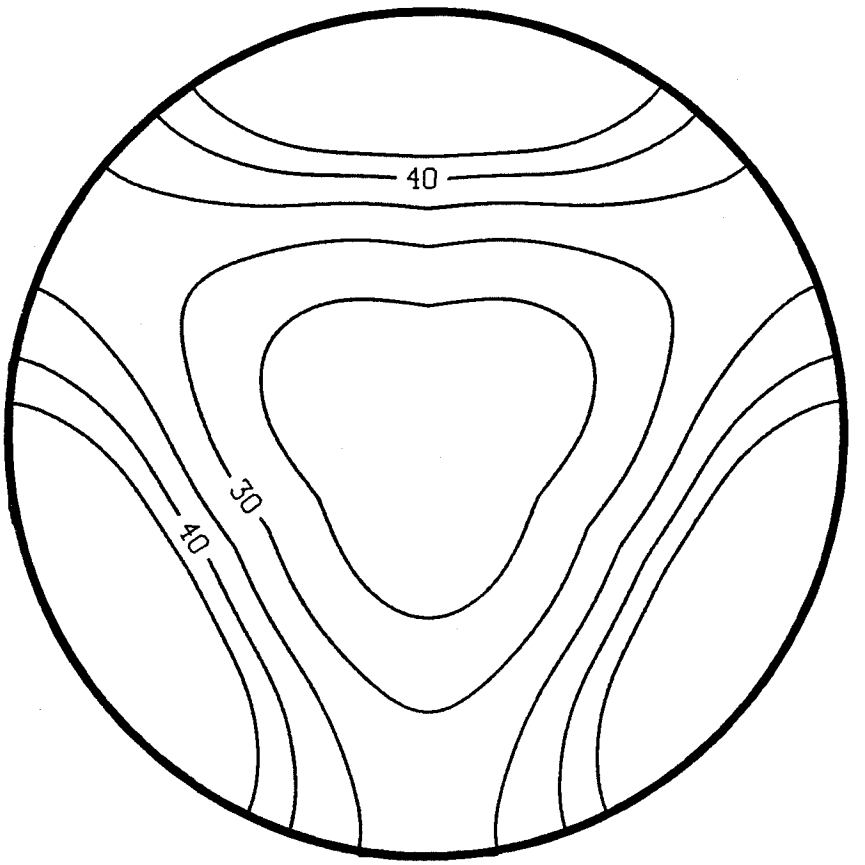

$\rho = 1.0$ **bohr**

Fig. 25a

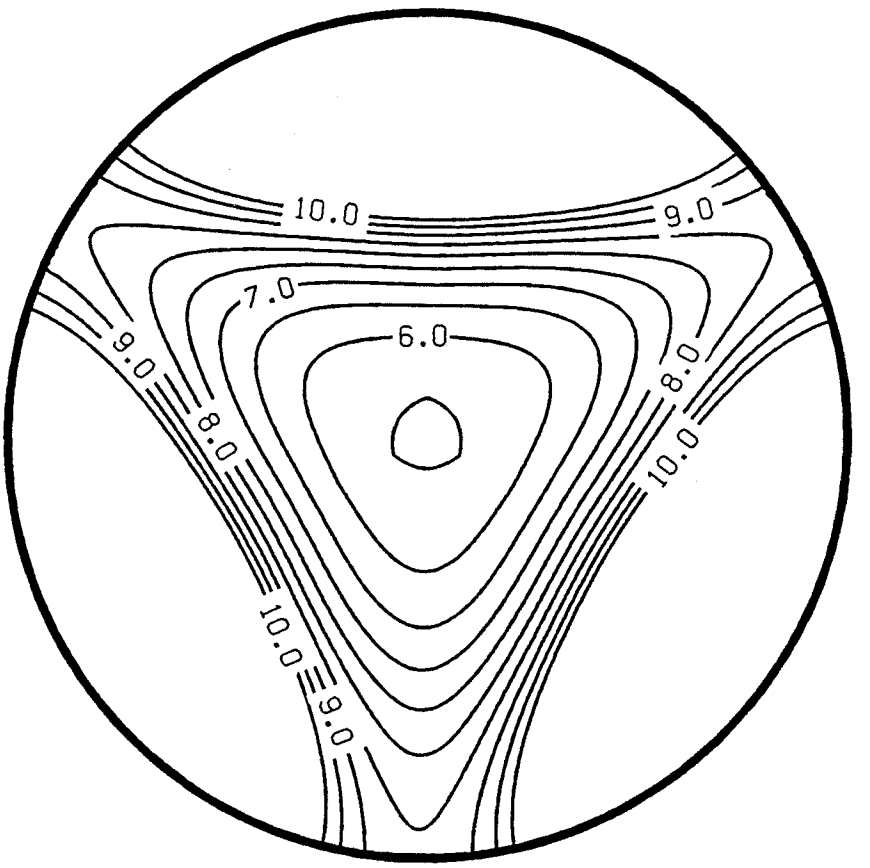

$\rho = 2.16$ **bohr**

Fig. 25b

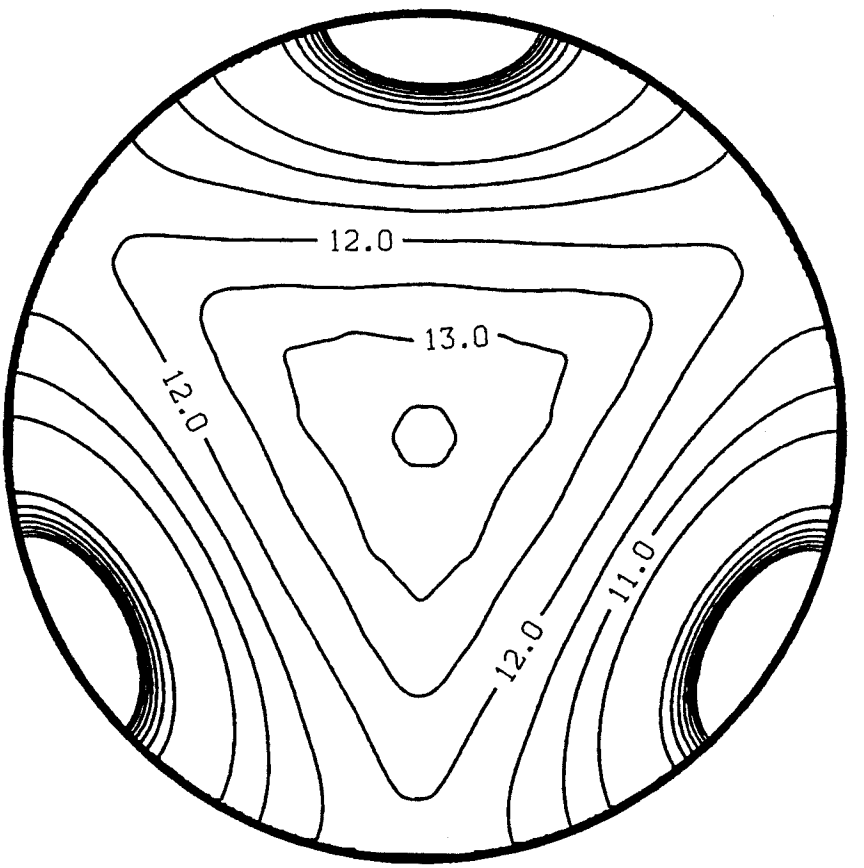

$\rho = 6.0$ **bohr**

Fig. 25c

Chapter 4

Calculation of the Ro-vibrational Bound States of H_3 in Its First Excited Electronic State

4.1. Introduction

In this chapter, the ro-vibrational bound states of H_3 in its first electronically excited state are calculated via a variational method under the assumption that its electronically non-adiabatic coupling to the electronic ground state vanishes. In the future, the effect of such coupling must be included.

First a general review of the methods that treat ro-vibrational bound states of triatomic systems is presented. Then an outline of the Tennyson and Sutcliffe method is presented in section 4.2. Section 4.3 contains the results and discussions.

It has been known for a long time that the ground electronic state potential energy surface is repulsive and therefore does not support any ro-vibrational bound states of the nuclear motion. Before the present work on excited electronic states (see chapter 2) of H_3, there were no reliable excited potential energy surfaces except the DMBE one of Varandas and co-workers[1] for the first excited electronic state. If one neglects the non-adiabatic coupling between this state and the ground state of H_3, this surface does have a potential well which supports bound ro-vibrational nuclear motion. There have been no definitive experimental observations of those bound states. The theoretical results of those bound states will be able to provide clues and guidance for the experimentalists[2,3]. Also the DMBE surface served as a test ground for ro-vibrational state calculations before we obtained the $2p_z\ ^2A_2''$ potential energy surface which is of great theoretical and experimental importance. This was our initial motivation for this study.

Later, it turned out that because of the geometric phase[4-6] related to the conical intersection[7-9] between the ground and the first excited electronic states (or the molecular Aharanov-Bohm effect), we developed a hyperspherical coordinate propagation method for the study of ro-vibrational bound states on this DMBE surface which made us realize the impact of that geometric phase, in the studies of both the bound state[10,11] and the scattering states[12,13].

The last decade has seen the recognition that the theoretical calculations are of importance for the understanding of the ro-vibrational motion of triatomic molecules[14]. The real drive behind such calculations are the impressive progress in the laser spectroscopy of small and medium sized molecules and the availability of the supercomputers. The problem to be solved may be stated very simply: given a potential energy surface, what are the ro-vibrational energy levels and their associated wavefunctions, including the high energy ones which harmonic approximations are invalid?

The concept of potential energy surface is the most fundamental one in chemistry. Potential energy surfaces are usually obtained by some kind of analytical fitting of the results of *ab initio* electronic state calculations at a finite number of nuclear configurations[15]. More and more potential energy surfaces are becoming available due to advances in quantum chemistry and in supercomputers. In order to test the analytical potential energy surfaces, one of the best ways that we know is that if they support bound states of nuclear motion, they should produce the same energy level results as those observed spectroscopically. This approach is very fruitful in studies of diatomic molecules because of the simplicity of those systems. The spectra of triatomic (or polyatomic) molecules are of higher complexity, which makes the experimental assignment of the ro-vibrational lines in those spectra much more difficult than

in the case of diatomic molecules. For this reason, results from theoretical calculations will be very helpful in order to understand the complicated results of spectroscopy. Furthermore, if analytical representations of the dipole (or higher moment) surfaces are available, tests of these representations can be made by comparison with experimental transition moments. It is possible to calculate fully coupled ro-vibrational energy levels of triatomic molecules from the first principle with an accuracy (0.1 cm^{-1}) that is competitive with experimental data from high resolution laser spectroscopy[16,17].

Most of the techniques used for the study of the ro-vibrational motion are of the variational type[14]. The Rayleigh-Ritz variational method is applied straightforwardly. Given a Hamiltonian $\hat{H}$ and some expansion basis set ψ_i, the secular equations

$$< \psi_j \mid \hat{H} - E_i \mid \sum_{k=1}^{M} C_k^i \psi_k > = 0 \qquad (1)$$

are solved for the eigenvalues E_i and the eigenvectors $\mathbf{C^i}$. If we denote the eigenvalues for M expansion functions in increasing order by E_1^M, E_2^M, ..., E_M^M, then MacDonald's theorem[18] states that

$$E_{i-1}^{M-1} < E_i^M < E_i^{M+1} \qquad (2)$$

This theorem shows the advantages and disadvantages of the variational method. The great advantage is that all the eigenvalues are upper bounds of the corresponding exact eigenvalues. The main weakness is that in order to ensure the convergence of a certain number of eigenvalues, we might need a much large number of expansion functions than the number of eigenstates wanted, which in turn makes the numerical diagonalization of the Hamiltonian matrix very demanding.

Returning to the secular equation Eq. (1), the choice of expansion functions is crucial if the dimension of the matrix is to be minimal. Before this problem can be addressed, it is necessary to chose the coordinate system which will be used for the problem. In the laboratory fixed axes system, a molecule with N atoms is described by $3N$ coordinates $\mathbf{x}$. Because the molecule is an isolated system, the motion of its center of mass is simple but not relevant to our interest and can be removed, and the square of total angular momentum and its Z component commute with the Hamiltonian $\hat{\mathrm{H}}$. As a result, it is usual practice to introduce three Eular angles α, β, γ to describe the orientation of some "molecule-fixed axes" relative to the laboratory fixed frame. The remaining $3N-6$ coordinates will describe the internal motion of the molecule. There are of course infinite ways to define the molecule-fixed axes and the internal coordinates.

Having decided on the definition of the coordinate system, it is necessary to derive the form of kinetic energy operator $\hat{\mathbf{T}}$ in terms of these coordinates, which is quite complicated. Sutcliffe was the first one who demonstrated a straightforward method to derive the kinetic operator $\hat{\mathbf{T}}$ of a triatomic molecule in any internal coordinate system[19]. His effort was followed by that of Handy which takes advantage of a computer algebra program and also treats tetra-atomic molecules as well[20].

In practice, the normal coordinate system has been used along with an expansion function set involving the direct product of three harmonic oscillator functions[21]. Difficulties occur when higher vibrational levels are required where the associated wave functions sample the anharmonic regions of the potential energy surface far away from the potential minimum, or when the triatomic molecule is linear or quasi-linear in which case the kinetic energy operator in this body-fixed coordinate system has a singularity. In order to overcome this

problem Carter and Handy introduced an internal coordinate system of two bond lengths and the bond angle between them[22]. The expansion functions are chosen to be the product of two Morse oscillator functions for the motion of two bond lengths and the associated Legendre polynomials for the motion of the bond angle. Tennyson, Sutcliffe, and co-workers introduced Jacobi coordinates (more commonly used in scattering calculations)[23]. Their expansion functions also have the form of a product of two Morse (or harmonic) oscillator functions and an associated Legendre function.

In the bond-length-bond-angle coordinates of Carter and Handy and the Jacobi coordinates of Tennyson and Sutcliffe, the Hamiltonian is sufficiently simple and all motion on the potential energy surface can be treated without approximation. Both methods are straightforward, robust and easy to use, with many applications of high quality results to triatomic systems[14,16,17].

Besides these variational approaches using products of known analytical functions, Burden and Cuno have tried SCF-type numerical basis functions in the studies of H_2O, OCS and CH_2^+ systems[24]. This approach provides a compact and flexible way to construct expansion functions and ensures the convergence with a comparatively small basis set. In the studies of van der Waals complexes, Born-Oppenheimer type separation has been commonly used to separate the radial and angular motion of the van der Waals bonding[25–27].

In recent years, the techniques for ro-vibrational motion of triatomic systems reached another level of sophistication. In the usual variational methods of Carter and Handy, and Tennyson and Sutcliffe, the expansion functions are products of known analytical functions of single center type (Harmonic or Morse oscillator functions with few tunable parameters), which are not flexible enough to treat very highly excited states with very large amplitudes of motion, which

might cover more than one minima of the potential energy surface (so-called "floppy" molecules). The convergence for the highly excited floppy states is not good enough even for very large basis sets. Several techniques have been introduced to overcome this difficulty. The Gaussian distributed basis (GDB) method developed by Hamilton and Light[28] uses many localized Gaussian basis functions. Their centers are placed all over the interesting part of a potential energy surface by following physical intuition. This method greatly extends the flexibility of the basis functions. It keeps the advantages of the usual variational method, while using localized Gaussian basis functions and acquires a certain degree of simplicity in the finite difference method. The discrete variable representation (DRV) developed by Lill, Bacic, Light and co-workers has been shown to be very effective both in scattering[29–31] calculations and bound states studies[32–36]. The combination of GDB and DVR leads to a substantial decrease in the computational effort as compared to that required for more usual basis sets such as direct products of orthogonal functions. They have proved to be very effective, especially for the studies of highly excited states of "floppy" triatomic molecules. With their collocation method, Yang and Peet demonstrated a non variational approach to the bound solutions of the Schrodinger equation[37]. This collocation method is easily implemented, and the construction of the Hamiltonian is very simple and does not require any evaluation of integrals over the basis set. Combined with the GDB method, Yang and Peet were able to treat highly excited vibrational states of the Ar-HCl system with the same accuracy achieved by the DVR-GDB method[38].

For triatomic systems having identical nuclei (like H_3^+, H_3), it is desirable to take advantage of the full P_3 nuclear permutation symmetry. Carter and Handy and Tennyson and Sutcliffe have shown that for basis functions which are

products of 1D functions, it is easy to embed the P_2 permutation symmetry of the AB_2 systems into the basis functions but very hard for the full P_3 permutation symmetry[23]. In order to implement the full P_3 symmetry into the basis set, hyperspherical coordinate systems are used in the calculation of the bound ro-vibrational states of triatomic systems[11,36,39,40]. When viewed in symmetrized hyperspherical coordinates[41], potential energy surfaces of identical triatomic systems demonstrate a C_{3v} geometrical symmetry, which allows the easy implementation of the full P_3 nuclear permutation symmetry. More details are given in the next chapter where we discuss one of the implementations of symmetrized hyperspherical coordinates for the ro-vibrational bound state calculation.

4.2. Methodology

In this section, the variational method developed by Tennyson and Sutcliffe is outlined. More detailed information is available in their original papers[23,42].

Within the Born-Oppenheimer approximation, the Hamiltonian for the nuclear motion of a triatomic system is

$$H = -\sum_{i=1}^{3} \frac{\hbar^2}{2m_i} \nabla^2_{\mathbf{x}_i} + V, \tag{3}$$

where $\nabla^2_{\mathbf{x}_i}$ is the Laplacian for the ith nucleus of mass m_i and laboratory frame position coordinate $\mathbf{x}_i$, and V is the electronic potential energy surface, that acts as the effective interaction between the nuclei and depends only on the relative (or internal) nuclear coordinates.

4.2.1. Removal of the motion of the center of mass

The first step in the construction of any ro-vibrational Hamiltonian is the removal of the overall translation of the center of mass. To do this, a new set of coordinates may be introduced

$$\mathbf{R} = \mathbf{x}_1 - \mathbf{x}_d, \tag{4}$$

$$\mathbf{r} = \mathbf{x}_3 - \mathbf{x}_2, \tag{5}$$

$$\mathbf{X} = M^{-1} \sum_{i=1}^{3} m_i \mathbf{x}_i, \tag{6}$$

where

$$m_d = m_2 + m_3, \tag{7}$$

$$M = m_1 + m_d = m_1 + m_2 + m_3 \tag{8}$$

$$\mathbf{x}_d = m_d^{-1}(m_2\mathbf{x}_2 + m_3\mathbf{x}_3). \tag{9}$$

$\mathbf{r}$ is the diatomic bond vector and $\mathbf{R}$ is the vector connecting the diatomic center of mass to the third atom. The position vector of the center of mass of the whole

complex in the laboratory frame is **X**. These coordinates are shown in Fig. 1. Using the chain rule of differentiation, we get

$$\sum_{i=1}^{3} \frac{1}{m_i} \nabla^2_{\mathbf{x}_i} = M^{-1} \nabla^2_{\mathbf{X}} + \mu^{-1} \nabla^2_{\mathbf{R}} + \mu_d^{-1} \nabla^2_{\mathbf{r}} \tag{10}$$

with effective masses

$$\mu_d = \frac{m_2 m_3}{(m_2 + m_3)} \tag{11}$$

$$\mu = \frac{m_1 (m_2 + m_3)}{(m_1 + m_2 + m_3)} \tag{12}$$

Removing the center of mass motion and expressing the Laplacian operators in polar coordinates, one obtains the space-fixed Hamiltonian

$$H = -\frac{\hbar^2}{2\mu R} \frac{\partial^2}{\partial R^2} R - \frac{\hbar^2}{2\mu_d r} \frac{\partial^2}{\partial r^2} r + \frac{\mathbf{l}^2}{2\mu R^2} + \frac{\mathbf{j}^2}{2\mu_d r^2} + V, \tag{13}$$

where **l** and **j** are the angular momentum operators associated with vectors **R** and **r** respectively. The total rotational angular momentum operator is given by their sum

$$\mathbf{J} = \mathbf{l} + \mathbf{j} \tag{14}$$

4.2.2. Body-fixed coordinates

Although the space-fixed representation has been successfully used for several ro-vibrational calculations, it is generally desirable to work with a body-fixed frame, which has the advantage that vibrational and rotational coordinates can be easily identified, along with the Coriolis terms that couple them. The resulting coupled-channel equations are usually simpler than those derived from the space-fixed Hamiltonian.

There are many ways to define a body-fixed frame. In the case of triatomic systems, we chose it to be such that the z-axis of the body-fixed frame is along

the direction of **R**, and **r** is in the x-z plane with a positive projection on the x-axis. Fig. 2 depicts these axis. Three Euler angles α, β and γ fully specify the orientation of the body-fixed frame with respect to the space-fixed frame. In this body-fixed frame

$$\hat{H} = \hat{K}_v + \hat{K}_{vr} + V(R, r, \theta), \tag{15}$$

where θ is the angle between **R** and **r**. The vibrational kinetic energy operator is

$$\begin{aligned}\hat{K}_v = &- \frac{\hbar^2}{2\mu R}\frac{\partial^2}{\partial R^2}R - \frac{\hbar^2}{2\mu_d r}\frac{\partial^2}{\partial r^2}r \\ &- \frac{\hbar^2}{2}\left(\frac{1}{\mu R^2} + \frac{1}{\mu_d r^2}\right)\frac{1}{\sin\theta}\frac{\partial}{\partial\theta}\left(\sin\theta\frac{\partial}{\partial\theta}\right),\end{aligned} \tag{16}$$

and the vibration-rotation kinetic energy operator is

$$\begin{aligned}\hat{K}_{vr} = &\frac{1}{2}\{\frac{1}{\mu R^2}(\Pi_x^2 + \Pi_y^2) + \left(\frac{\cot^2\theta}{\mu R^2} + \frac{\mathrm{cosec}^2\theta}{\mu_d r^2}\right)\Pi_z^2\} \\ &+ \frac{\cot\theta}{2\mu R^2}(\Pi_x\Pi_z + \Pi_z\Pi_x) + \frac{\hbar}{i}\frac{1}{\mu R^2}\left(\frac{\partial}{\partial\theta} + \frac{\cot\theta}{2}\right)\Pi_y,\end{aligned} \tag{17}$$

where Π_x, Π_y, Π_z are the components of the total angular momentum **J** that only acts on the Euler angles α, β, γ which rotate the space-fixed frame to the body-fixed frame. α and β are the polar angles of **R** in the space-fixed frame. γ is the angle between the $\mathbf{R}Z_{\mathrm{space-fixed}}$ and **R**, **r** half-planes measured counter clockwise as viewed from the top of the **R** vector.

4.2.3. Basis functions

After the form of the Hamiltonian has been obtained in the body-fixed coordinates, a set of basis functions is chosen. Of these six coordinates, four are angular variables: the three Euler angles α, β, γ and the angle θ between vectors **R** and **r**. The other two are the radial distances R and r.

A suitably symmetrized angular basis set for the variational calculation is chosen to be:

$$|J,M,j,k\rangle = (1+\delta_{k,0})^{-1/2}\ 2^{-1/2}\{\Theta_{j,k}(\theta)D^J_{M,k}(\alpha,\beta,\gamma) + (-1)^p\Theta_{j,-k}(\theta)D^J_{M,-k}(\alpha,\beta,\gamma)\} \tag{18}$$

where $\delta_{k,0}$ equals 1 when $k=0$ and zero otherwise. $D^J_{M,k}(\alpha,\beta,\gamma)$ is the Wigner rotation function[43] and $\Theta_{j,k}(\theta)$ is the associated Legendre function[44]. p is a quantum number which is associated with the parity of the system with respect to inversion through its center of mass; it that can assume the values 0 or 1 (see below). J is the total angular momentum quantum number, with M and k being the quantum numbers of its projections along the space-fixed z axis and the body-fixed z axis respectively. j is the quantum number of the angular momentum associated with the diatomic vector $\mathbf{r}$. $|\ JMjk\rangle$ is the simultaneous eigenfunction of the angular momentum operators J^2, j^2, j_Z, J_Z. p, J, M are good quantum numbers for the triatomic system. The allowed values of j and k are:

$$k = (0,1,\ldots,J-1,J) \tag{19}$$

$$j = (|k|,|k|+1,|k|+2,\ldots) \tag{20}$$

The quantum number p is defined by requiring that the total parity of the spatial wavefunction under inversion through the system's center of mass be $(-1)^{J+p}$.

Let us consider two special cases. When $J=0$, M and k have to be zero as well. p also has to be zero since in this case the system has even parity. j now is the only quantum number left and can assume the values 1, 2, 3, ... etc. The angular basis function in this case is very simple:

$$|\ 0,0,j,0\rangle = |\ j\rangle = \Theta_{j,0}(\theta) \tag{21}$$

which is just the ordinary Legendre polynomial $P_j(\cos\theta_\lambda)$.

If we consider the situation of $J = 1$ and even total parity, then $p = 1$. For this value of J, k can be 0 or 1. For $k = 0$ and $p = 1$, the right hand side of Eq. (18) vanishes. Therefore, the only appropriate value of k is 1 and the angular basis becomes

$$|\, j\rangle_{\text{even}} = 2^{-1/2}\{\Theta_{j,1}D^1_{M,1} - \Theta_{j,-1}D^1_{M,-1}\} \tag{22}$$

where j can assume the values 1, 2, 3, ... etc. If we consider $J = 1$ and odd total parity, we must have $p = 0$ and k can be 0 and 1. The angular basis function will be

$$|\, j,k,\rangle_{\text{odd}} = (1+\delta_{k,0})^{-1/2}\ 2^{-1/2}$$
$$\{\Theta_{j,k}D^J_{M,k} + \Theta_{j,-k}D^J_{M,-k}\} \tag{23}$$

The basis functions for the two radial variables R, r are chosen to be product of analytic Morse oscillator-like functions:

$$\Psi_{m,n}(r,\ R) = \frac{1}{rR}H_m(r)H_n(R) \tag{24}$$
$$m,n = \{0,1,2,3,4,\ldots\}$$

where

$$H_n(r) = \beta^{1/2}N_{n,\alpha}\exp(-y/2)y^{(\alpha+1)/2}L^\alpha_n(y) \tag{25}$$
$$A = \frac{4D_e}{\beta} \tag{26}$$
$$\beta = \omega_e(\frac{\mu}{2D_e})^{1/2} \tag{27}$$
$$\alpha = \text{integer part of } A \tag{28}$$
$$y = A\exp[-\beta(r - r_e)] \tag{29}$$

$N_{n,\alpha}L_n^\alpha$ is the normalized associated Laguerre polynomial[45]. An equivalent definition is valid for $H_m(R)$. The parameters μ, r_e, ω_e and D_e are the reduced mass, equilibrium separation, fundamental frequency and dissociation energy associated with the corresponding radial coordinate. In practice, r_e, ω_e, and D_e are usually treated as variational parameters and optimized accordingly.

4.2.4. Symmetry considerations

If two or all three of the nuclei are identical particles, then the wavefunctions of the triatomic system have to form representations of the nuclear permutation symmetry group (P_2 or P_3). It is desirable to embed the nuclear permutation symmetry into the basis functions. This not only ensures that the final wavefunction obtained from the variational calculation has appropriate nuclear permutation symmetry properties, but also decomposes the Hamiltonian matrix into smaller independent sub-blocks, which in turn require much smaller computational effort.

It is difficult to embed the P_3 permutation symmetry of A_3-type molecules consisting of three identical nuclei in Tennyson's method without destroying the simplicity of constructing the basis functions in the form of direct products of basis functions in angular variables and the radial variables[42].

On the other hand, the P_2 permutation symmetry of AB_2-type molecules can be easily built in (see Eq. (18)). Since the potential energy function of such a molecule is invariant under an interchange of the two identical B atoms, the Hamiltonian does not couple the angular basis functions of even j with angular basis functions of odd j, and we can treat these two cases separately[42].

Even though we treat an A_3-type system with only the P_2 symmetry embedded into the basis set functions, a fully converged result is still needed to satisfy the P_3 symmetry. This symmetry should manifest itself in the degeneracy

of the energy levels and in the shape of the eigenfunctions if plotted in a set of appropriately symmetrized coordinates. If an eigenstate obtained by using even basis functions is nondegenerate, it must belong to an A_1 irreducible representation of P_3. If an eigenstate obtained by using odd basis functions is nondegenerate, then it generates an A_2 irreducible representation of P_3. If one eigenstate of even basis functions and another of odd basis functions are degenerate with each other, together they must form an E irreducible representation of P_3.

4.2.5. Basis set selection

As for all variational methods, the basis set of choice should be flexible and large enough for the problem at hand, and also as compact as possible in order to reduce the computational effect. In the Tennyson and Sutcliffe method, the basis functions in the internal coordinates have the form of the products of three one-dimensional functions. There are three schemes to select the basis set. The first one is that any basis function with quantum numbers j, m, and n for which

$$N_{max} \geq \frac{j}{L_j} + \frac{m}{M_m} + \frac{n}{N_n} \tag{30}$$

is satisfied is selected. Here N_{max}, L_j, M_m, and N_n are selection parameters. For example, we may chose $N_{max} = 1$, $L_j =$ The rationale behind this scheme is an energy consideration, since the basis functions with larger quantum numbers tend to contribute more to the higher eigen-states. The second scheme is to select basis functions directly according to the value of the diagonal matrix element of the Hamiltonian $\langle j,m,n \mid H \mid j,m,n \rangle$. The lowest number LBASS of basis functions can be selected in this way in a manner consistent with number of eigenstates desired. The selection parameters (N_{max}, L_j, M_m, N_n, LBASS) can be tuned independently so that the final effective selection criterion can be

either the first scheme or the second, or even some kind of combination of both. Finally, basis functions can be selected manually if necessary.

After basis selection is done, the Hamiltonian matrix is constructed by both analytical and numerical means. Tennyson[46] went to special pains to optimized his code for evaluating the necessary numerical quadratures, and this is a very important features of this code. The eigenfunctions and eigenvalues are then obtained after a straightforward diagonalization of the Hamiltonian matrix.

4.3. Results and discussion

The code we used for the variational state calculation is called TRIATOM, and was obtained from the CPC Program Library of Queen's University, Belfast, Northern Ireland[46]. We initially made small test runs on Sun workstations and a micro VAX. The major part of the calculations was done on the SCS-40 mini-supercomputer of the San Diego Supercomputer Center (SDSC). The code itself was highly portable. The modifications made to suit each computer system were minimum.

4.3.1. Application to the H_3^+ ion with $J = 0$

The ro-vibrational motion of the H_3^+ ion has been extensively treated by Tennyson *et al.*[47,48]. Since this triatomic ion has some resemblance with the H_3 system in which we were interested, we repeated their calculation for total angular momentum $J = 0$ in order to gain experience in using this code. We adopted the same values of the parameters r_e, ω_{r_e}, D_{r_e}, R_e, ω_{R_e} and D_{R_e} they used[47], as listed in Table 1. The H_3^+ potential surface used in our calculation is the one included in the TRIATOM package for code testing[49], and different from (simpler and better than) the one used in previous publications[50]. As a consequence, the optimized parameters in these published calculations[47,48] would not be optimal for the test potential energy surface we used, our results should not be in perfect agreement with those calculations.

The potential energy surface of ground electronic state for H_3^+ has a deep smooth rounded well that can support many bound states of ro-vibrational nuclear motion. Figs. 3 and 4 show some cuts of this surface. Because of this property, the method of Tennyson and Sutcliffe is appropriate for this system. In our calculation, the zero of the potential energy surface was chosen to be the

energy of $2H(1s) + H^+$. There are other natural choices of zero for this potential energy surface, such as the energy of $H_2(X\,^1\sum_g^+) + H^+$ or $H_2^+(X\,^2\Sigma_g^+) + H(1s)$. Since we were only interested in the lower vibrational eigenstates, any choice of zero would be equivalent to any other one both conceptually and practically.

The convergence tests are listed in Table 2, which show that the lowest ten eigenstates with even j basis functions and the lowest five eigenstates with odd j basis functions are converged to 0.1 cm^{-1}. For the largest basis sets, the size of the basis sets are the same as those used previously by Tennyson and Sutcliffe[47,48]. The eigenenergies are listed along with the latter in Table 3. To permit a better comparison, the energy origin was taken to be the ground ro-vibrational states of each calculations. The energies of the levels clearly show the degeneracy of the results obtained by using even and odd j basis functions, which makes it possible to do symmetry assignments for those eigen-states. The difference between Tennyson's results and the present ones ranges from 5 cm^{-1} to 60 cm^{-1}. This can be attributed to the use of different potential energy surfaces and Morse parameters, that were not optimized in the present work. The quanta for the asymmetric stretch mode ν_E and the symmetric one ν_A resulting from our calculations are 2518.5 cm^{-1} and 3175.3 cm^{-1}. They agree much better with the experimental values of Oka[51] ($\nu_E = 2521.56$ cm^{-1}) and of Ketterle and co-workers[52] ($\nu_A = 3178.29$ cm^{-1}) than the corresponding ones obtained by Tennyson and Sutcliffe[47,48], namely 2494.4 cm^{-1} and 3185.32 cm^{-1}. We attribute this better agreement to the improved potential energy surface we used.

4.3.2. Application to H_3 with $J = 0, 1$

For the H_3 system, if the coupling between the ground electronic state and the first excited electronic state, (which is degenerate with the ground electronic

state in equilateral triangle nuclear configuration), is neglected, the potential energy surface of the first excited electronic states would support bound ro-vibrational states. The corresponding potential energy surface has been obtained by Varandas *et al.* using the functional extrapolation in the double-many-body-expansion (DMBE) scheme[1]. The upper manifold of DMBE surfaces is shown in Figs. 5 through 8. The striking feature of this potential energy surface, which is quite different from the ground potential energy surface of the H_3^+ ion, is the cone-shaped tip at the bottom of the well. As the function of the internuclear distance R of equilateral configuration, both surfaces display the same Morse-like smooth behavior (see Figs. 3 through 5). The cone-shape feature comes from the well-known conical intersection between the ground and the first excited electronic states of H_3[7-9] for motion in the X_λ and Z_λ directions as seen in Figs. 7 and 8. No bound ro-vibrational states on this excited potential energy surface have been observed experimentally so far. There are some indications that the quasi-bound ro-vibrational states which would exist in the absence of coupling to the ground electronic state will predissociate by ro-vibronic coupling to that state[2,3].

We used in our bound ro-vibrational state calculations those upper manifold of the DMBE surfaces. The zero of energy chosen was that of three isolated H atoms in their ground state. For the same reason as in the case of the H_3^+ ion, the choice of zero of energy is of no major importance.

The first step was to optimize those Morse parameters r_e, ω_{r_e}, D_{r_e}, R_e, ω_{R_e} and D_{R_e} used in the radial basis functions. Basis sets of small size were used for this purpose. Since it had been showed previously by Tennyson *et al.* that the optimized parameters for even j basis functions are more or less the same as those for odd j basis[42,46], and also that the Morse parameters are not sensitive

to the total parity of eigenstates, we only did the optimization in the calculation with even j basis functions, for $J = 1$ and odd total parity.

For the $J = 0$ case, the optimization was done using a basis set defined to be $N_{max} = 1$, $M_m = 8$, $N_n = 8$, $L_j = 16$ which resulted in a total number of basis functions equal to 576. The lowest five states were monitored with respect to the tuning of the Morse parameters. By varying one parameter with the others fixed, a one–dimensional optimization was conducted manually. After the optimized value was found for this Morse parameter, it was then fixed and the next Morse parameter was optimized in the same fashion. After the last parameter was optimized in this one–dimensional manual scheme, another iteration was started over again with the first Morse parameter. After two or three iterations, the variation of the eigenenergies for the lowest five state became very small and the optimization was stopped. The final optimized parameters for $J = 0$ are listed in Table 4. It is important to keep in mind that optimization in multi-dimensional space is generally difficult, not to mention how much more difficult it would be if done manually. Because the optimization process is actually done in this way, in a finite portion of the six–dimensional parameter space, with only limited guidance from physical considerations, it is quite possible that a local minimum may be accepted as the global one since there is no sure indication that the global minimum has been reached. This is a well known problem in global optimization. Fortunately, the larger the basis set, the less sensitive the results are to changes of those parameters.

For the case $J = 1$, a basis set with $N_{max} = 1$, $M_m = 6$, $N_n = 6$, $L_j = 15$ and a total of 382 functions was used in the Morse parameter optimization. For $J = 1$, the lowest twelve eigenenergies were monitored during the parameter

tuning. The same optimization scheme was used as in the case $J = 0$. The results of the optimized parameters are also listed in Table 4.

With the optimized Morse parameters, the size of the basis sets was increased in order to test the convergence of the eigen-energies. As mentioned before, the cone-shaped potential energy surface was not an ideal system for the use of Morse-type radial basis functions. The eigenenergies converged very slowly with basis set size. We analyzed the importance of each basis function for a given basis size carefully, and let the results guide us to achieve a more sensible way of increasing the size of the basis set. The convergence test results for $J = 0$ are listed in Table 5, which shows that the energy levels are not well converged as for H_3^+. The results of the convergence tests for $J = 1$ are similar to those for $J = 0$, so they are not given in tables. In general the lower states are better converged than the upper ones. Even with basis sets of size more than 1000, the eigenenergies did not appear to be converged at all. The calculation turned out to be limited by the amount of computer memory we could access at that time, which was 3 64-bit Mwords. This prevented us from further increasing the basis set size to achieve the convergence of those eigenenergies.

The final results for H_3 are listed in Tables 6 through 8, with the sizes of basis sets in the range of 1104 to 1542 and SCS-40 CPU times ranging from 10 to 30 minutes.

For $J = 0$, the degeneracy of states for even and odd j basis functions was identified with errors ranging from 0.7 cm^{-1} to 62 cm^{-1}. So the last E symmetry assignment was quite tentative. It is interesting to note that no A_2-type states were identified among the lowest ten states calculated.

The eigenfunctions are expressed as an expansion in basis set functions. It is hard to visualize these wavefunctions by examining those coefficients of

those expansions. Although the cone-shaped behavior of the potential energy surface prevented us from using the harmonic approximation in the two nuclear coordinates describing motions away from equilateral triangular shapes, we could still try to understand the nature of the A_1-type states.

Let us assume that the motion of the symmetric stretch is independent of that of the asymmetric ones and also assume that all A_1-type states are excitations in the symmetric stretch mode plus the ground state motion in the asymmetric stretch modes. Using the Morse-type function to describe the potential energy along the symmetric stretch, the spectra of the symmetric mode is described by the well known form[53] as

$$E(\nu) = \hbar\omega_e(\nu + \frac{1}{2}) - \hbar\omega_e\chi_e(\nu + \frac{1}{2})^2. \tag{31}$$
$$\nu = 0,\ 1,\ 2, \ldots.$$

Here ω_e is the oscillation frequency, and $\omega_e\chi_e$ is known as the anharmonicity constant. Let us define the first order and second order differences as

$$\delta^1(\nu) \equiv E(\nu + 1) - E(\nu) \tag{32}$$
$$= \hbar\omega_e - 2\hbar\omega_e\chi_e(\nu + 1) \tag{33}$$
$$\nu = 1,\ 2, \ldots.$$

and

$$\delta^2(\nu) \equiv \delta^1(\nu + 1) - \delta^1(\nu) \tag{34}$$
$$= -2\hbar\omega_e\chi_e \tag{35}$$
$$\nu = 2,\ 3, \ldots.$$

In Table 9, all A_1-type eigenenergies are listed along with the corresponding δ^1 and δ^2. The result for δ^1 has the right behavior of getting smaller between higher

excited states. For the lower levels, δ^2 is constant as predicted by Eq. (35). At least the lowest five states can be understood with such a simple model, with the symmetric excitation quantum ν_{A_1} being equal to 1617.15 cm^{-1} and the anti-symmetric excitation quantum ν_E equal to 4571.27 cm^{-1}.

For $J = 1$, the convergency is about the same as that for $J = 0$. When J is small, the coupling between rotation and vibration is small. If that coupling is neglected, then the eigenenergies would be the same as the ones for $J = 0$ except that each state is now triply degenerate $(2J + 1)$. If the coupling is turned on slowly, the triple degeneracy will be lifted gradually. From Tables 6 through 8, we can see that an A_1-type singlet state for $J = 0$ corresponds to three states for $J = 1$, one A_2-type with odd parity and one E-type(doublet) with even parity. An E-type doublet for $J = 0$ corresponds to six states for $J = 1$, one E-type doublet with odd parity and two E-type doublets with even parity. The grouping in Tables 6 through 8 shows this feature clearly. Using the well-known form[54]

$$F(J,K) = B_e J(J+1) - (B_e - C_e)K^2 + ... \tag{38}$$

we were able to estimate B_e to be 30.6 cm^{-1} which leads to the equilibrium bond length of the equilateral triangular H_3[54] as 1.975 bohr which agrees with the position of the bottom of the potential energy well at 1.973 bohr.

Finally, let us consider the shapes of the ro-vibrational wavefunctions to see if the final converged calculations yield wavefunctions with the right P_3 symmetry. We plotted the wavefunctions in a system of symmetrized hyperspherical coordinates[41]. Fig. 9 contains contour lines of the wavefunctions for H_3^+ with total angular momentum $J = 0$ and basis set size of 880, and Fig. 10 for H_3 with $J = 0$ and basis set size of 1363. The plots show that the variational wavefunctions do not display the exact P_3 symmetry property,

even for the highly converged states of H_3^+. The reason for this behavior is that in general, the convergence of the eigenvector with basis set size is slower than that of the eigenvalue in a numerical eigenvalue-eigenvector problem. In order to get the right symmetry with a reasonable number of basis functions, the symmetry has to be embedded into this basis set before the variational calculation is performed. It is difficult to achieve that with Tennyson's code without seriously compromise its efficiency, we developed a new method, which is described in the next chapter.

4.4. References

1. A.J.C. Varandas, F.B. Brown, C.A. Mead, D.G.Truhlar and N.C. Blais, *J. Chem. Phys.* **86**, 6258 (1987).
2. M. Vogler, *Phys. Rev.* **A 19**, 1 (1979).
3. J.K.G. Watson, *Phys. Rev.* **A 22**, 2279 (1980).
4. M.V. Berry, *Proc. Roy. Soc.* **A 392**, 45 (1984).
5. C.A. Mead and D.G. Truhlar, *J. Chem. Phys.* **49**, 23 (1979).
6. C.A. Mead, *Chem. Phys.* **49**, 23 (1980).
7. H.C. Longguet-Higgins, U. Opik, M.H.L. Pryce and R.A. Sack, *Proc. Roy. Soc.* **A 244**, 1 (1958).
8. G. Herzberg and H.C. Longguet-Higgins, *Disc. Far. Soc.* **35**, 77 (1963).
9. H.C. Longguet-Higgins, *Advan. Spectry.* **2** 429, (1961).
10. C. Alden Mead, *Chem. Phys.* **49**, 23 (1980).
11. B. Lepetit, Z. Peng and A. Kuppermann, *Chem. Phys. Lett.* **166**, 572 (1990).
12. C. Alden Mead, *J. Chem. Phys.* **72**, 3839 (1980).
13. B. Lepetit and A. Kuppermann, *J. Chem. Phys.* **166**, 581 (1990).
14. S. Carter and N.C. Handy, *Comp. Phys. Report* **5**, 115-172 (1986).
15. C.C Schatz, *Rev. Modern Phys.* **61**, 669-688 (1989).
16. S. Miller, J. Tennyson and B.T. Sutcliffe, *Mol. Phys.* **66**, 429-456 (1989).
17. S. Carter, P. Rosmus, N.C. Handy, S. Miller, and J. Tennyson, *Comp. Phys. Communication* **55**, 71-75 (1989).
18. J.K.L. MacDonald, *Phys. Rev.* **43**, 830 (1933).
19. B.T. Sutfliffe, *Mol. Phys.* **48**, 561 (1983).
20. N.C. Handy, *Mol. Phys.* **61**, 207 (1987).
21. R.J. Whitehead and N.C. Handy, *J. Mol. Spectrosc.* **55**, 356 (1975).

22. S. Carter and N.C. handy, *Mol. Phys.* **47**, 1445 (1982).

23. B.T. Sutcliffe and J. Tennyson, *Mol. Phys.* **58**, 1053 (1986).

24. F.R. Burden and A. Cuno, *Mol. Phys.* **62**, 33 (1987).

25. S.L. Holmgren, M. Waldman and W. Klemperer, *J. Chem. Phys.* **67**, 4414 (1977).

26. J.M. Hutson and B.J. Howard, *Mol. Phys.* **41**, 1123 (1980).

27. B.R. Reid and K.C. Janda, *J. Phys. Chem.* **92**, 587 (1988).

28. I.P. Hamilton and J.C. Light, *J. Chem. Phys.* **84**, 306 (1986).

29. J.V. Lill, G.A. Parker and J.C. Light, *Chem. Phys. Lett.* **89**, 483 (1982).

30. R.W. Heather and J.C. Light, *J. Chem. Phys.* **79**, 147 (1983).

31. J.C. Light, I.P. Hamilton and J.V. Lill, *J. Chem. Phys.* **82**, 1400 (1985).

32. Z. Bacic and J.C. Light, *J. Chem. Phys.* **85**, 4594 (1986).

33. Z. Bacic and J.C. Light, *J. Chem. Phys.* **86**, 3065 (1987).

34. J.C. Light and Z. Bacic, *J. Chem. Phys.* **87**, 4008 (1987).

35. Z. Bacic, D. Watt and J.C. Light, *J. Chem. Phys.* **89**, 947 (1988).

36. R.M. Whitnell and J.C. Light, *J. Chem. Phys.* **90**, 1774 (1989).

37. W.T. Yany and A.C. Peet, *Chem. Phys. Lett.* **153**, 98 (1988).

38. A.C. Peet and W.T. Yang, *J. Chem. Phys.* **90**, 1746 (1989).

39. J.G. Frey and B.J. Brain, *Chem. Phys.* **99**, 415 (1985).

40. J.M. Hutson and S. Jain, *J. Chem. Phys.* **91**, 4197 (1989).

41. Aron Kuppermann, *Chem. Phys. Lett.* **32**, 374 (1975).

42. J. Tennyson, *Comp. Phys. Communication* **42**, 257 (1986).

43. D.M. Brink and G.R. Satchler, *Angular Momentum*, 2nd ed. (Clarendon Press, Oxford, 1968).

44. E.U. Condon and G.H. Shortley, *The Theory of Atomic Spectra* (Cambridge Univ. Press, Oxford, 1968).

45. I.S. Gradshteyn and I.H. Ryzhik, *Tables of Integrals, Series and Products* (Academic Press, New York, 1980).

46. J. Tennyson, *Comp. Phys. Report* **4**, 1 (1986).

47. J. Tennyson and B.T. Sutcliffe, *Mol. Phys.* **51**, 887 (1984).

48. J. Tennyson and B.T. Sutcliffe, *J. Chem. Soc., Faraday Trans. 2* **82**, 1151 (1986).

49. B. Martire and P.G. Burton, *Chem. Phys. Lett.* **121**, 475 (1985).

50. R. Schinke, M. Dupuis and W.A. Lester, Jr., *J. Chem. Phys.* **72**, 374 (1980).

51. T. Oka, *Phys. Rev. Lett.*, **45**, 531 (1980).

52. W. Ketterle, H.P. Messmer and H. Walther, *Europhys. Lett.*, **8**, 333 (1989).

53. M. Weissbluth, *Atoms and Molecules*, student edition, p609, (Academic Press, New York, 1978).

54. I. Dabroski and G. Herzberg, *Can. J. Phys.*, **58**, 1238 (1980).

4.5. Tables

Table 1

Parameters of the Morse–like functions

in R and r for H_3^+ and $J = 0$.

Coordinate	$D_e(a.u.)$	$\omega_e(a.u.)$	$r_e(a.u.)$
R	0.230	0.0085	1.71
r	0.205	0.0118	2.10

Table 2

Convergence tests[a] for H_3^+ and $J = 0$.

Even j basis functions		
M_m=9, N_n=7, L_j=14 N_{basis} = 340	M_m=10,N_n=8, L_j=14 N_{basis} = 616	M_m=11,N_n=8, L_j=18 N_{basis} = 880
-7.067955	-7.067967	-7.067967
-6.816079	-6.816119	-6.816119
-6.750378	-6.750437	-6.750437
-6.590602	-6.590784	-6.590786
-6.567921	-6.568055	-6.568060
-6.512097	-6.512965	-6.512967
-6.441278	-6.441708	-6.441708
-6.367264	-6.367514	-6.367530
-6.338421	-6.338839	-6.338893
-6.290215	-6.290872	-6.290870

Odd j basis functions		
M_m=10, N_n=10, L_j=15 N_{basis} = 381	M_m=10,N_n=8, L_j=15 N_{basis} = 616	M_m=11,N_n=8, L_j=19 N_{basis} = 880
-6.816137	-6.816141	-6.816141
-6.568061	-6.568066	-6.568067
-6.513084	-6.513112	-6.513113
-6.367650	-6.367662	-6.367664
-6.317290	-6.317270	-6.317277

a. The numbers given are the lowest eigenenergies in 10^4 cm^{-1}. The origin of energy is that of the $2H(1s) + H^+$ configuration.

Table 3

H_3^+ $J = 0$ bound state energies[a].

Even j basis			Odd j basis	
Tennyson's results	present results	Symmetry	Tennyson's results	present results
0.00000	0.00000	A_1		
0.24944	0.25185	E	0.24943	0.25183
0.31911	0.31753	A_1		
0.47250	0.47718	A_1		
0.49583	0.49991	E	0.49580	0.49990
0.55453	0.55500	E	0.55449	0.55485
0.62768	0.62627	A_1		
0.69444	0.70044	E	0.69433	0.70030
0.72350	0.72907	A_1		
		A_2	0.74513	0.75069
0.77403	0.77710	A_1		

a. The energy is in 10^4 cm^{-1} and its origin is the ground ro-vibrational state energy.

Table 4

Optimized parameters for the Morse–like functions in R and r for H_3 with $J = 0$ and $J = 1$.

Coordinate	$D_e(a.u.)$	$\omega_e(a.u.)$	$r_e(a.u.)$
R	0.230 0.262	0.0130 0.0100	1.96 2.01
r	0.262 0.232	0.0122 0.0102	2.09 2.32

Table 5

Convergence tests[a] for H_3, $J = 0$ and j even

M_m=15, N_n=13, L_j=16 N_{basis} = 757	M_m=16, N_n=13, L_j=18 N_{basis} = 1067	M_m=19, N_n=19, L_j=26 N_{basis} = 1368
-0.824614	-0.826261	-0.827333
-0.662336	-0.664153	-0.665618
-0.512776	-0.514696	-0.516372
-0.376072	-0.377987	-0.379855
-0.369457	-0.369877	-0.370206
	-0.253486	-0.256018
	-0.236860	-0.237305
	-0.134838	-0.140441
	-0.119736	-0.120358
	-0.049332	-0.053411

a. The numbers given are the lowest eigenenergies in 10^4 cm^{-1}.

The origin of energy is that of 3H(1s).

Table 6

Bound state energies[a] of H_3 for $J = 0$.

State assignment (ν_{A_1}, ν_E, l)	even j^b Origin I[d]	even j^b Origin II[e]		odd j^c Origin I[d]	odd j^c Origin II[e]
0,0,0	-8.27333	0.00000	A_1		
1,0,0	-6.65618	1.61715	A_1		
2,0,0	-5.16372	3.10961	A_1		
3,0,0	-3.79855	4.47478	A_1		
0,1,1	-3.70206	4.57127	E	-3.70130	4.57203
4,0,0	-2.56018	5.71315	A_1		
1,1,1	-2.37305	5.90028	E	-2.36592	5.90741
	-1.40441	6.86892	A_1		
	-1.20357	7.06976	E	-1.14159	7.13174
	-0.53410	7.73923	A_1		

a. In 10^3 cm^{-1}.

b. $N_{max} = 1, M_m = 19, N_N = 19, L_j = 28$ and $N_{basis} = 1368$.

c. $N_{max} = 1, M_m = 12, N_N = 12, L_j = 23$ and $N_{basis} = 1104$.

d. The origin of energy is that of 3H($1s$).

e. The origin of energy is the calculated ground ro-vibrational state energy.

Table 7

Bound state energies[a] of H_3 for $J = 1$ and even total parity.

even j M_m=12, N_n=12, L_J=22 N_{basis} = 1112	symmetry	odd j M_m=16, N_n=16, L_J=21 N_{basis} = 1413
	A2	-8.21206
	A2	-6.59660
	A2	-5.10612
	A2	-3.73977
-3.64495	E	-3.64513
	A2	-2.49187
-2.32024	E	-2.32090
	A2	-1.34863
-1.15258	E	-1.15155
	A2	-0.46950
	A2	-0.23097
	A2	-0.10195

a. In 10^3 cm^{-1}. The origin of energy is that of 3H(1s).

Table 8

Bound state energies[a] of H_3 for $J = 1$ and odd total parity.

even j M_m=14, N_n=14, L_J=20 N_{basis} = 1542	symmetry	odd j M_m=15, N_n=15, L_J=21 N_{basis} = 1497
-8.22467	E	-8.22659
-6.60765	E	-6.60940
-5.11495	E	-5.11718
-3.74344	E	-3.74620
-3.68313	E	-3.68423
-3.62973	E	-3.63233
-2.47708	E	-2.48225
-2.35299	E	-2.35378
-2.30491	E	-2.30696
-1.25477	E	-1.27558
-1.16935	E	-1.16786
-1.12307	E	-1.11498
-0.47488	E	-0.48178
-0.08479	E	-0.09701

a. In 10^3 cm^{-1}. The origin of energy is that of 3H($1s$).

Table 9

Analysis of the A_1-type eigenenergies of H_3 for $J = 0$.

energy	δ^1	δ^2
-8.27333		
-6.65618	1.61715	
-5.16372	1.49246	-0.12469
-3.79855	1.36517	-0.12729
-2.56018	1.23837	-0.12680
-1.40441	1.15577	-0.08250
-0.53410	0.87031	-0.28546

a. In 10^3 cm^{-1}.

4.6. Figures and captions

Fig. 1. Laboratory-fixed coordinates $\mathbf{x}_1$, $\mathbf{x}_2$ and $\mathbf{x}_3$, Jacobi coordinates $\mathbf{r}$ and $\mathbf{R}$, and position vector $\mathbf{X}$ of the center of mass G.

Fig. 2. Coordinates in the body-fixed frame. The $\mathbf{Z}$ axis is along the $\mathbf{R}$ vector and the $\mathbf{X}$ axis is chosen in such a way that vector $\mathbf{r}$ is in the $\mathbf{XZ}$ plane and has a positive projection along the $\mathbf{X}$ axis.

Fig. 3. Potential energy curve for the H_3^+ ion in its ground electronic state[49]. R is the internuclear distance for an equilateral triangle configuration. The minimum of the curve is located at $R = 1.65$ bohr. The origin of energy is that of $H^+ + 2H(1s)$. The potential energy surface has been cutoff near $R = 4.0$ bohr.

Fig. 4. Equipotential contours of the ground electronic state potential energy surface for H_3^+[49]. The symmetrized hyperspherical coordinates used are defined in ref. 41. The two-dimensional contour plot corresponds to $Y_\lambda = 2.17$ bohr. The origin of energy is the same as that of Fig. 3. The equipotentials are equally spaced by 0.5 eV in the range [-9.0 eV, -6.5 eV].

Fig. 5. DMBE potential energy curve of H_3 in its first excited electronic state for equilateral triangle configurations. R is the internuclear distance and for these configurations, is proportional to the coordinate Y_λ defined in ref. 41. The minimum of the curve is located at $R = 1.973$ bohr. The origin of energy is that of $H(1s) + H_2(X\ ^1\Sigma_g^+, r_e)$.

Fig. 6. Equipotential contours of the DMBE potential energy surface for the first excited state of H_3 for $Y_\lambda = 2.60$ bohr. See ref. 41 for the coordinates used. The origin of energy is the one defined in the caption for Fig. 5. The

contours are in the range [3.0 eV, 6.0 eV] equally spaced by 0.5 eV, with the innermost one having an energy of 3.0 eV.

Fig. 7. DMBE potential energies for $Y_\lambda = 2.6$ bohr and $Z_\lambda = 0.0$ bohr in the symmetrized hyperspherical coordinates[41]. $E_1^{\rm DMBE}$ is the DMBE potential energy for the ground state of H_3 and $E_2^{\rm DMBE}$ is that for the first excited state. The origin of energy is the one defined in the caption for Fig. 5. The conical intersection between $E_1^{\rm DMBE}$ and $E_2^{\rm DMBE}$ can be clearly seen at $X_\lambda = 0$.

Fig. 8. DMBE potential energy for $Y_\lambda = 2.6$ bohr and $X_\lambda = 0.0$ bohr. See caption for Fig. 7 for other details.

Fig. 9. Contour plot of the wave function Ψ for the lowest $J = 0$, A_1-type H_3^+ ro-vibrational state, in symmetrized hyperspherical coordinates[41]. Depicted is a cut at $Y_\lambda = 2.17$ bohr, for which the ground electronic state potential energy function of H_3^+ has a global minimum (at $X_\lambda = Z_\lambda = 0$). The maximum of the wave function was set equal to 1.0, and contours for $\Psi = 0.9$ to 0.1 in steps of 0.1 are displayed.

Fig. 10. Contour plot of the wave function Ψ for the lowest $J = 0$, A_1-type H_3 ro-vibrational state, in symmetrized hyperspherical coordinates[41]. Depicted is a cut at $Y_\lambda = 2.588$ bohr, near which the first excited electronic state potential energy function of H_3 has a global minimum (at $Y_\lambda = 2.60$ bohr, and $X_\lambda = Z_\lambda = 0$). The maximum of the wave function was set equal to 1.0, and contours for $\Psi = 0.9$ to 0.1 in steps of 0.1 are displayed.

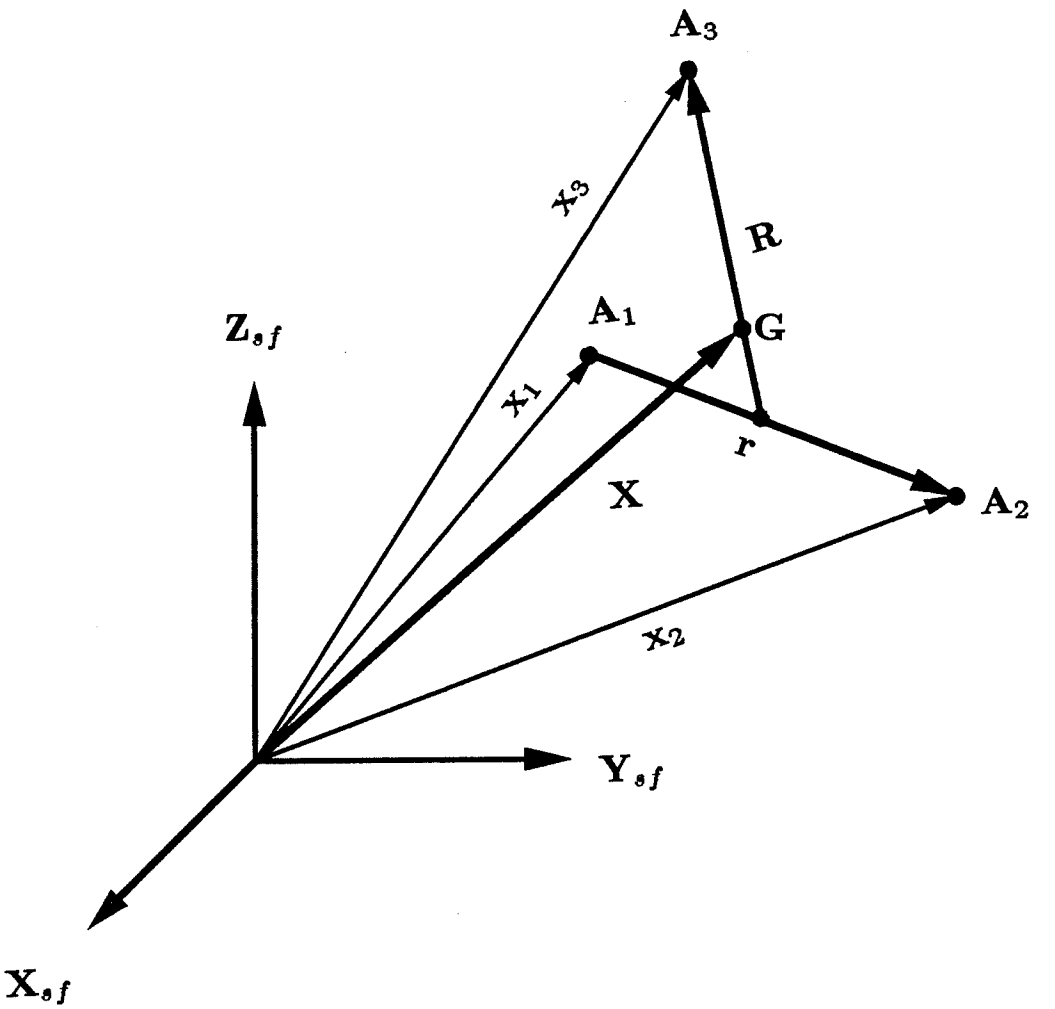

Fig. 1

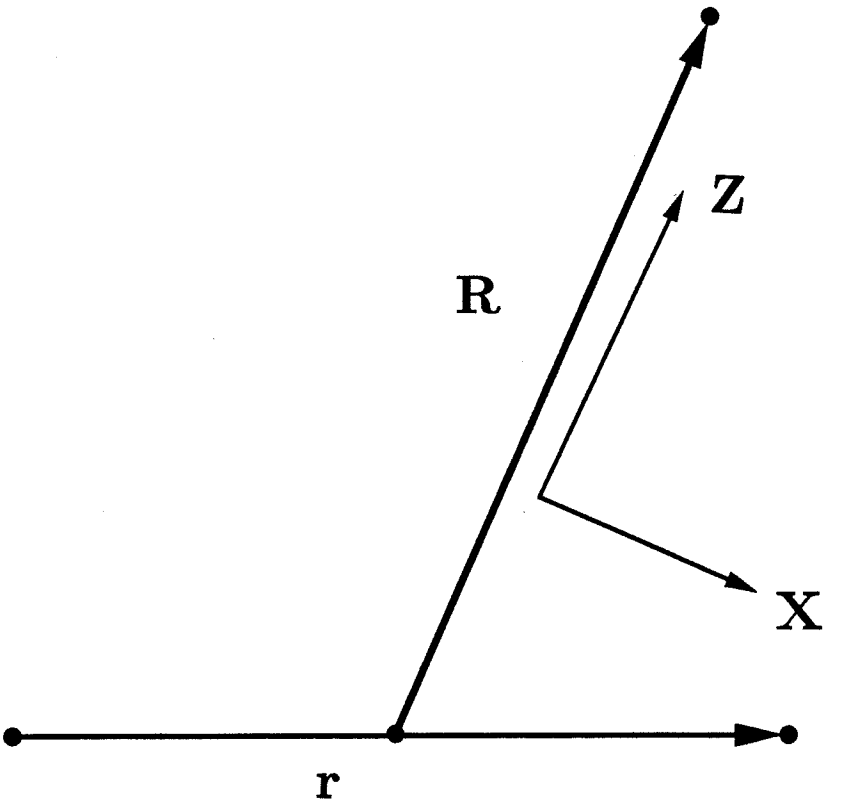

Fig. 2

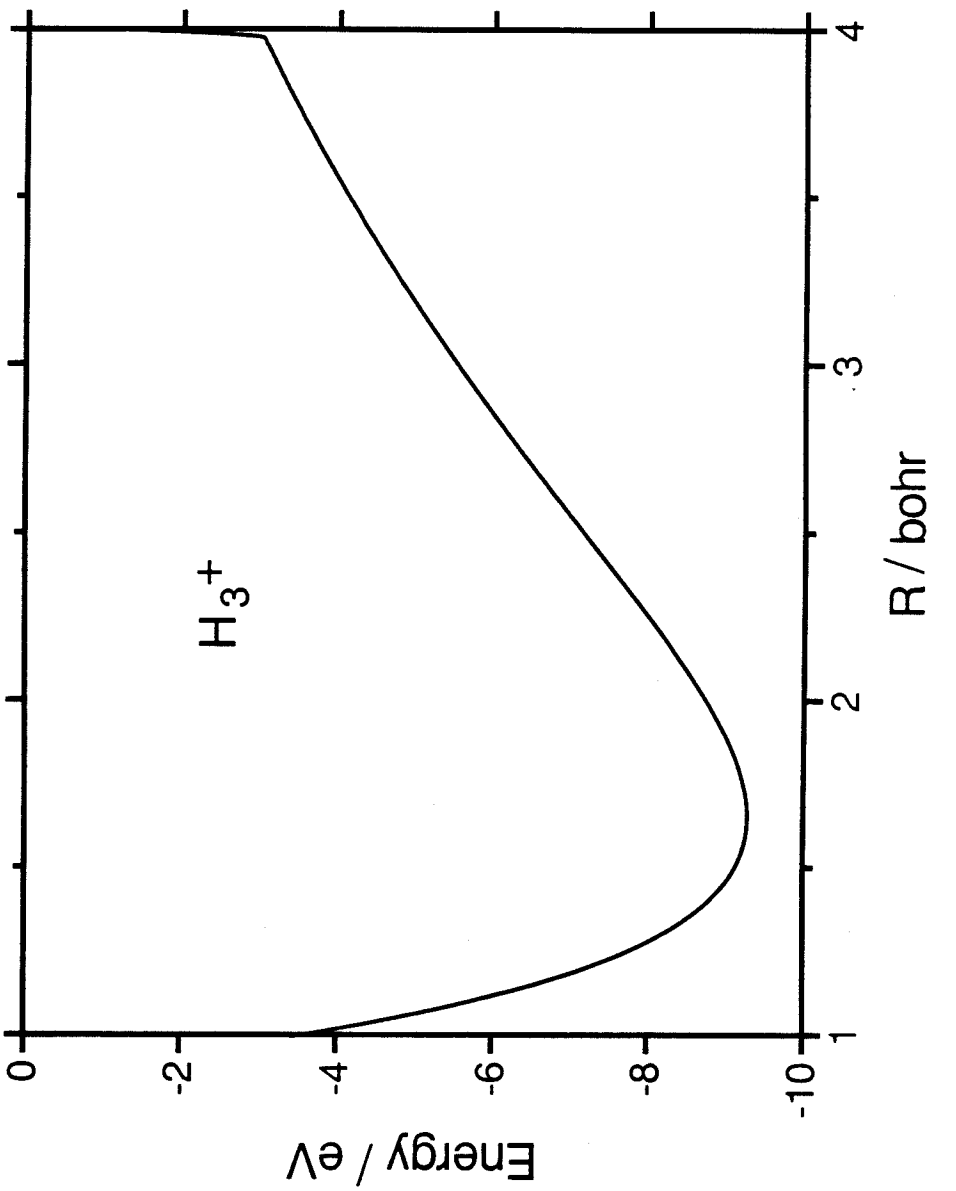

Fig. 3

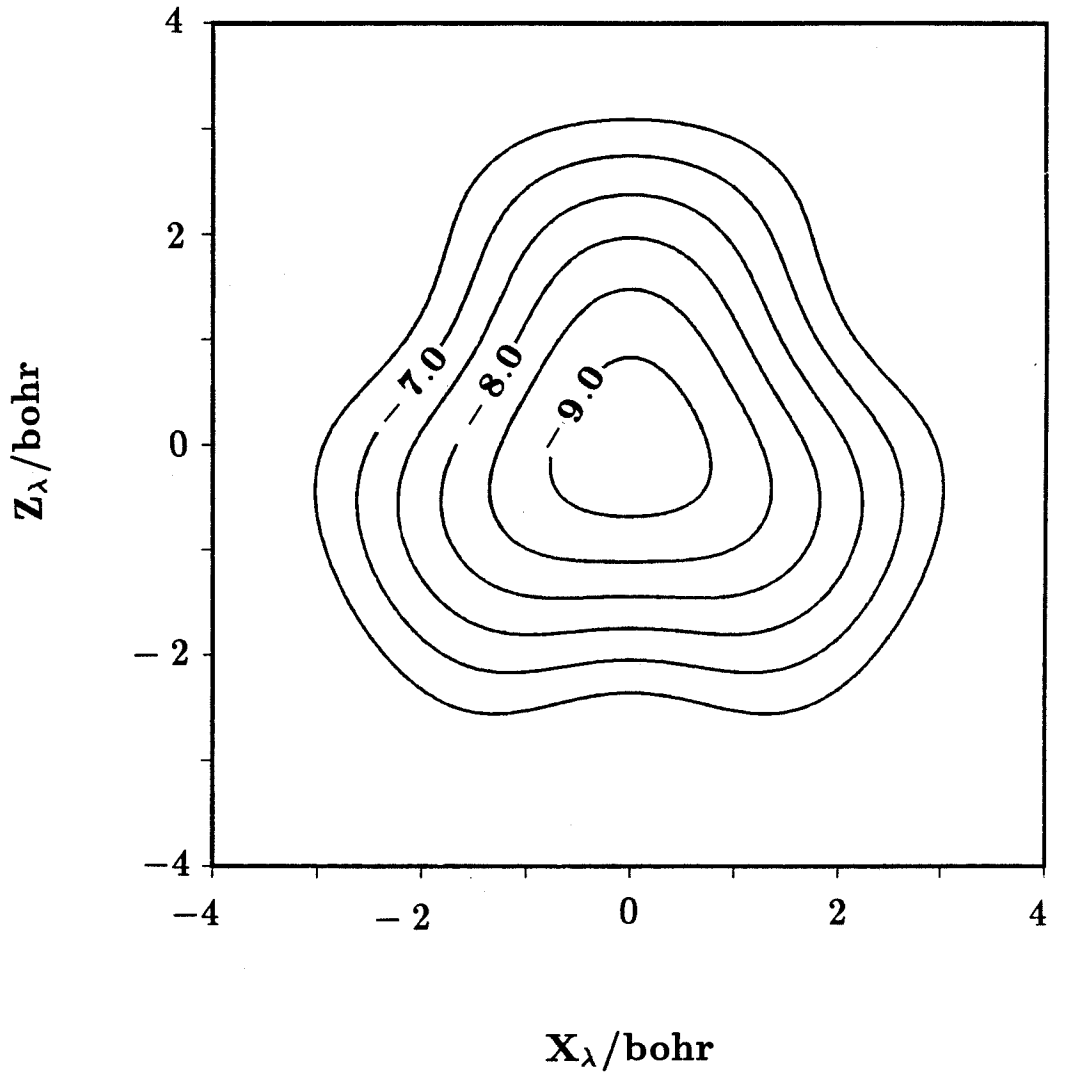

Fig. 4

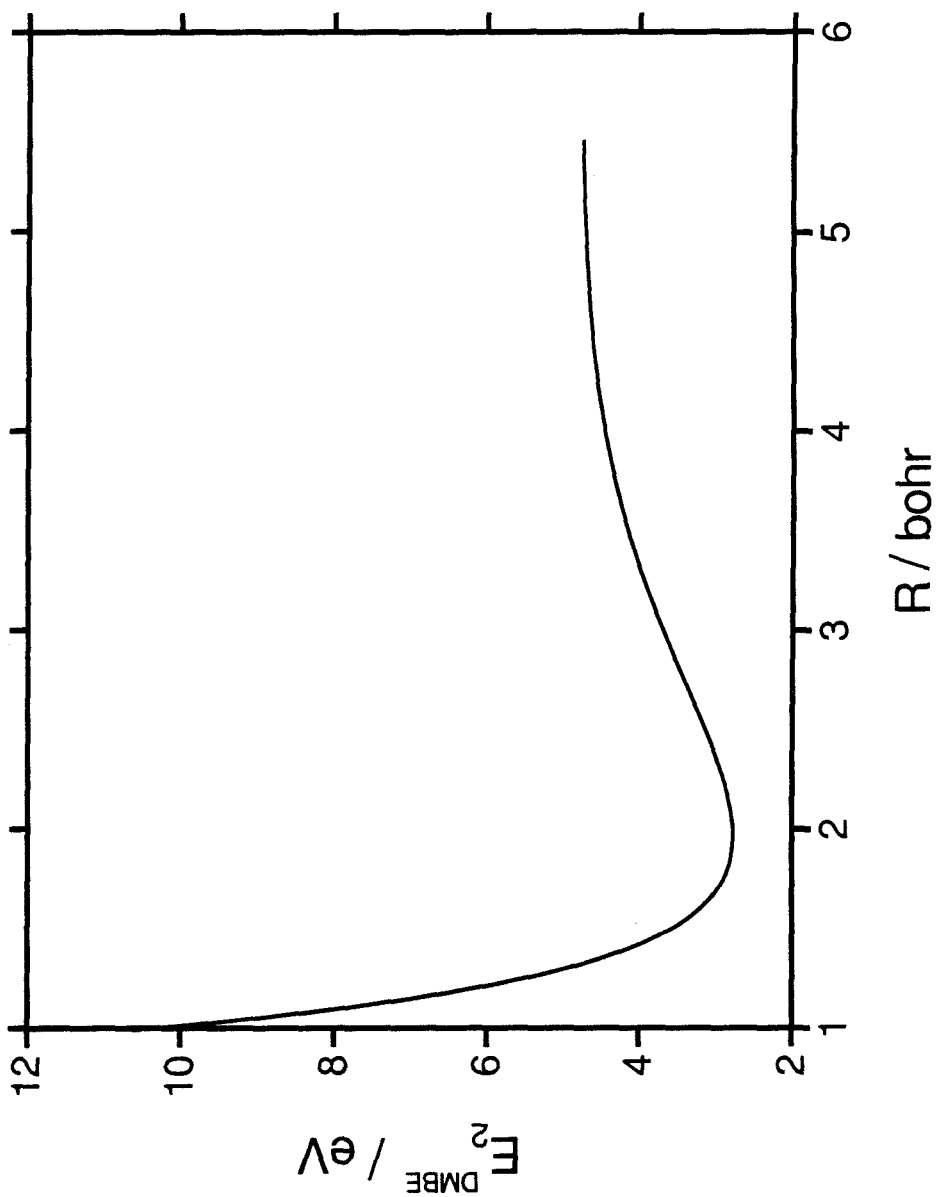

Fig. 5

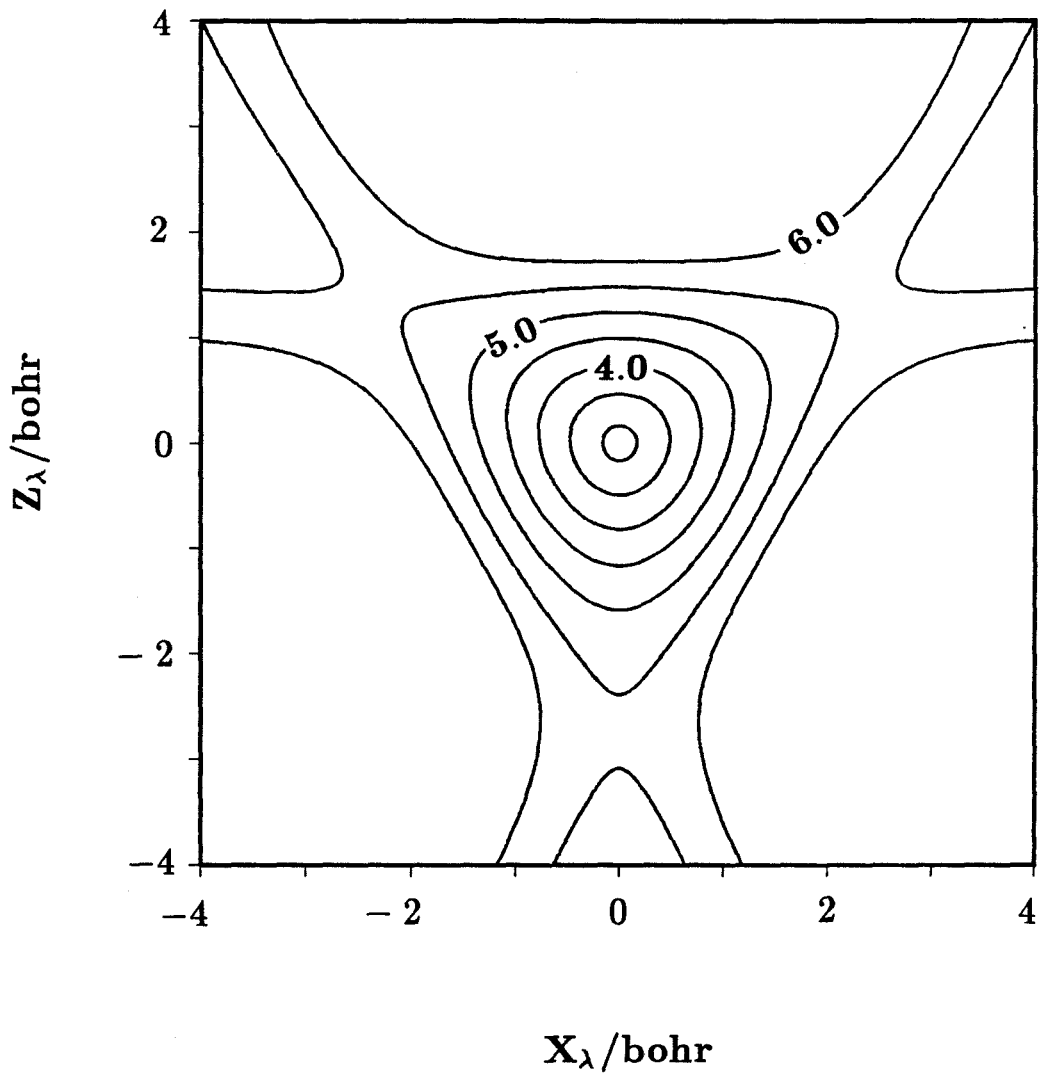

Fig. 6

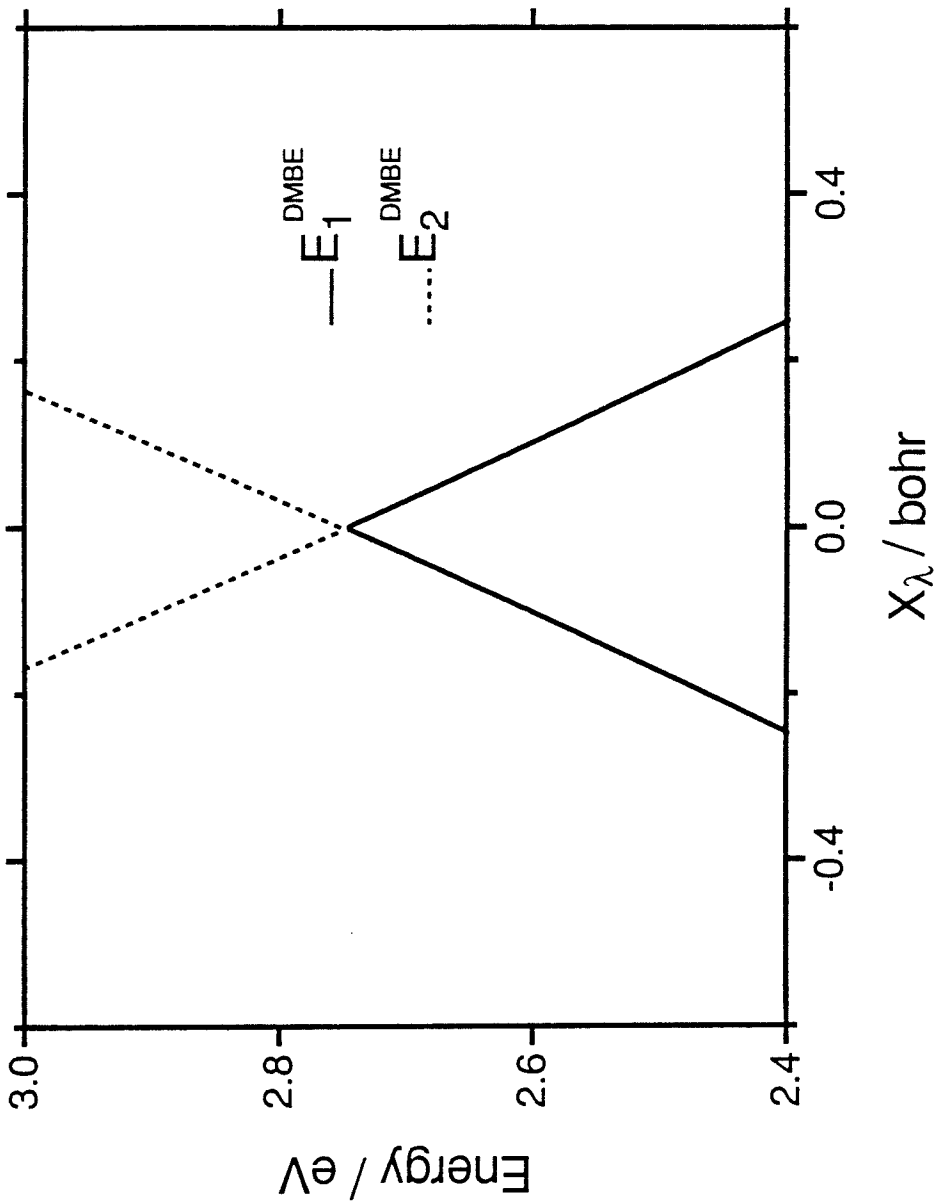

Fig. 7

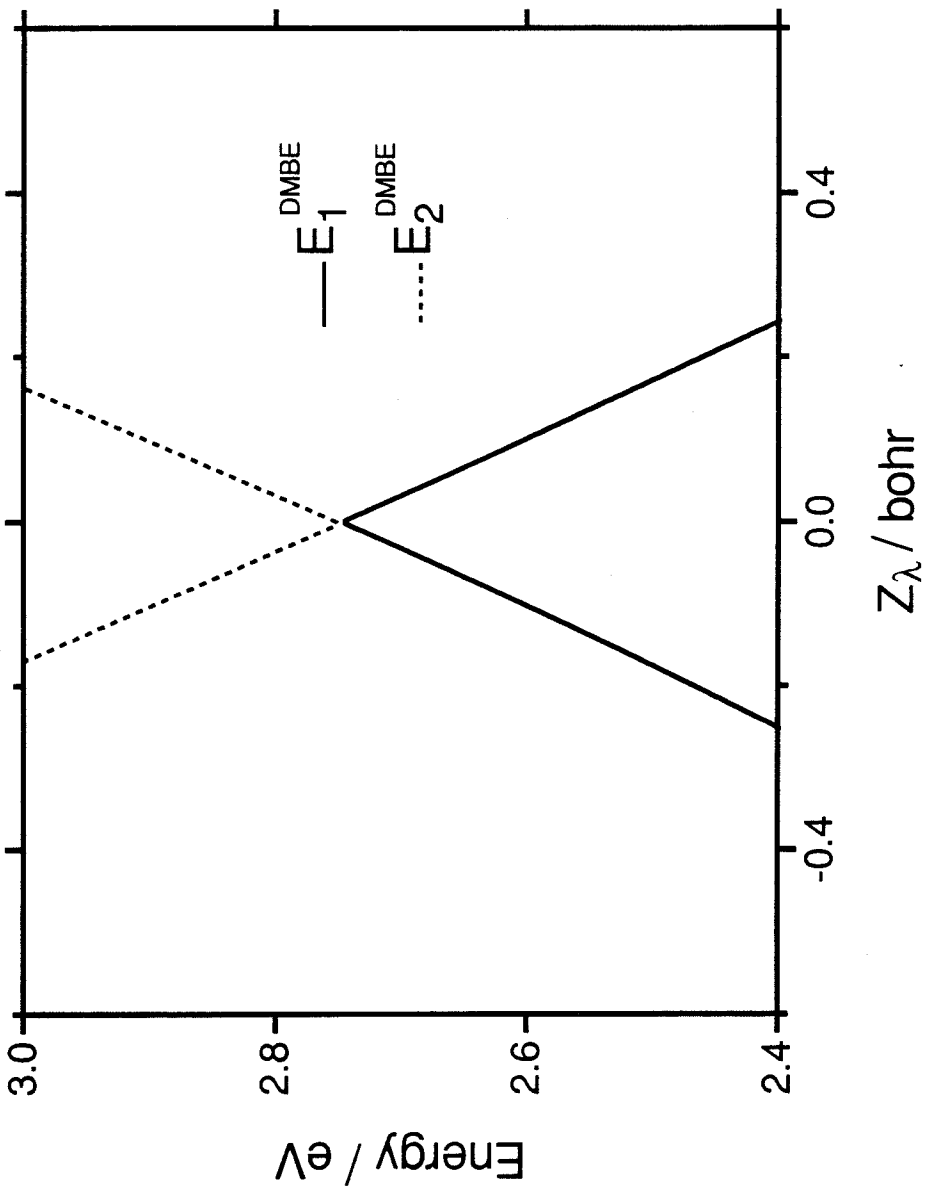

Fig. 8

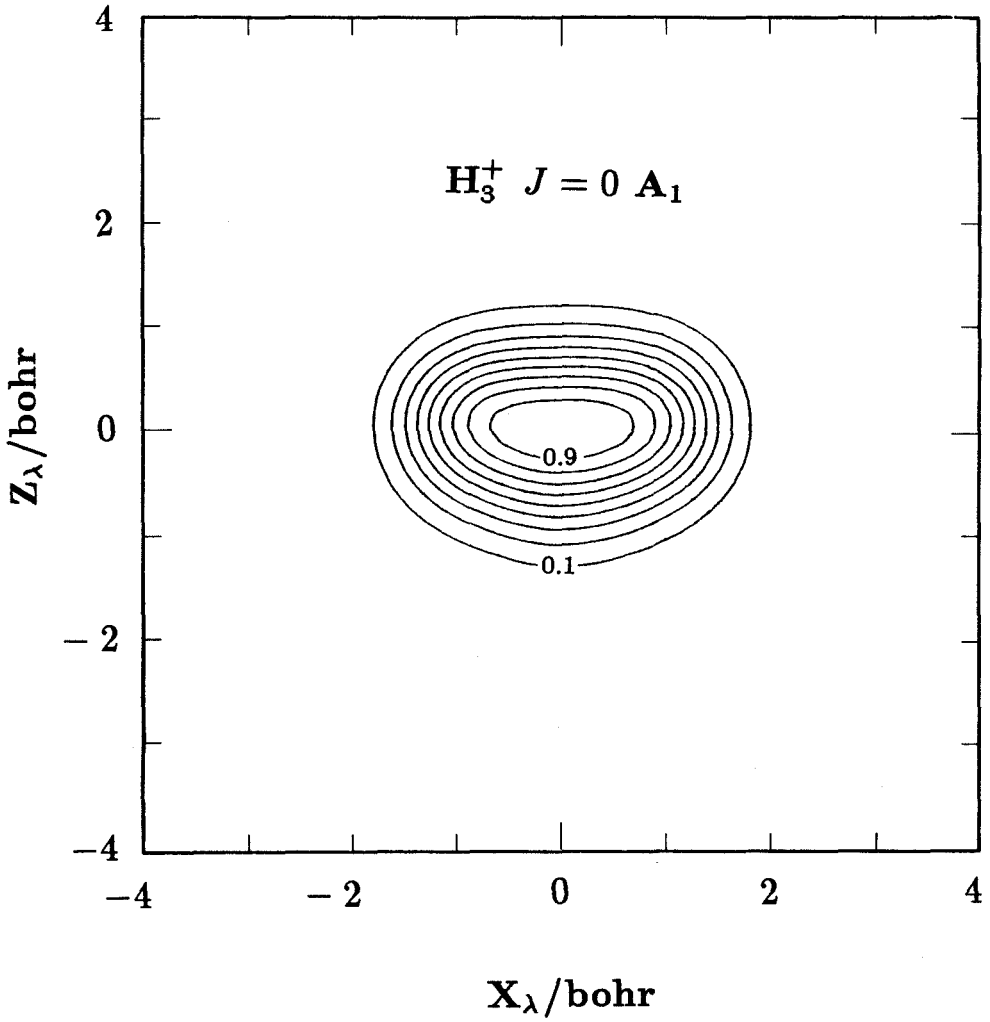

Fig. 9

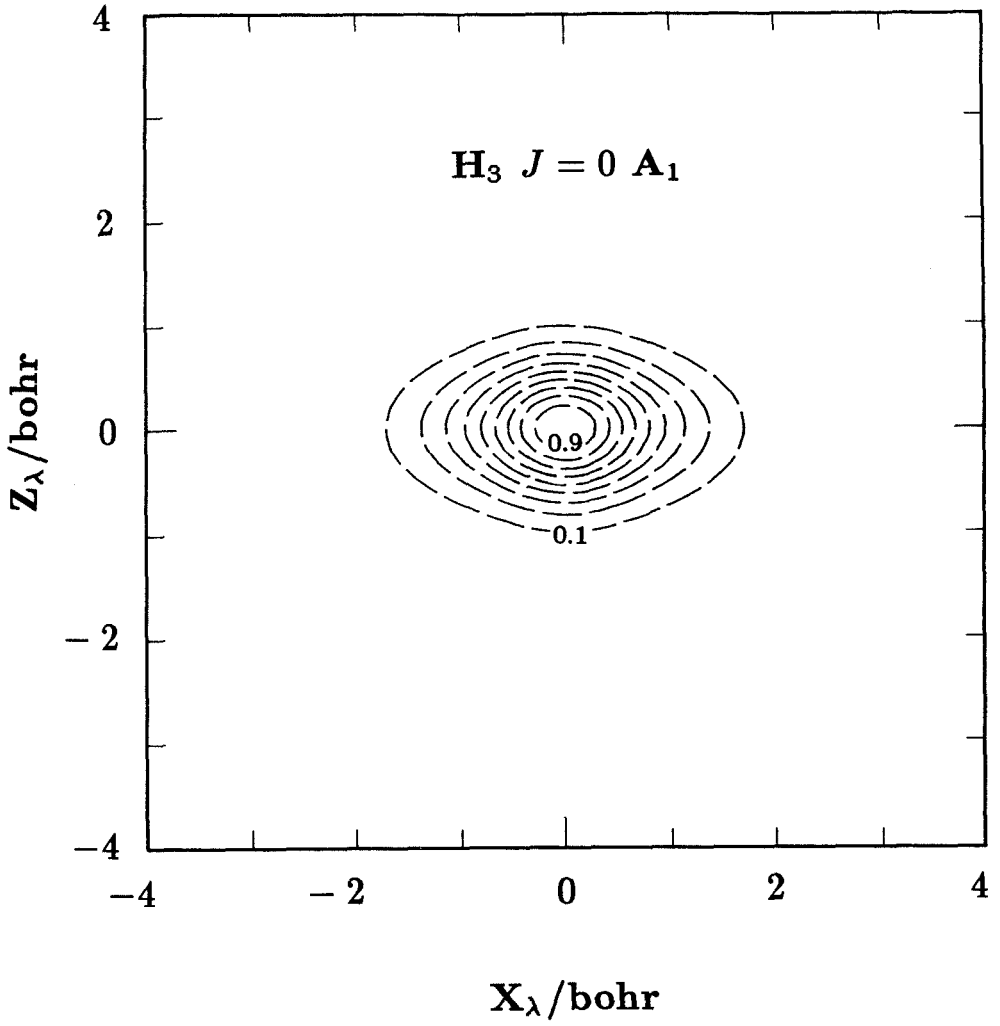

Fig. 10

Chapter 5

Calculation of the Ro-vibrational Bound States of H_3 in Its First Excited Electronic State Using the Hyperspherical Coordinate Propagation Method

5.1. Introduction

In this chapter, a propagation method in hyperspherical coordinates for obtaining the ro-vibrational bound states of triatomic molecules is presented and applied to the H_3 system in its first excited electronic state with the DMBE potential energy surface of Varandas and co-workers[1]. This method successfully incorporated not only the full nuclear permutation symmetry of H_3, but also the molecular Aharanov-Bohm effect described by Mead and Truhlar[2] (also called the Berry's geometric phase[3]) induced by the conical intersection between the potential energy surfaces of the ground and the first excited electronic states of H_3. The eigenenergies of those bound states (without inclusion of the geometric phase) are in good agreement with those obtained in the previous calculation described in chapter 4 by using the variational method of Tennyson and Sutcliffe[4,5]. The effect of the geometric phase is shown to be very important as it significantly changes the quantum numbers, eigenenergies and the wavefunctions of those bound ro-vibrational states.

The motivation for this method is two-fold. As discussed in chapter 4, it is not trivial to incorporate the full P_3 nuclear permutation symmetry of H_3 into the variational calculation of ro-vibrational eigenstates, even though it is highly desirable to do so. The reason is that the basis functions used efficiently in those variational methods[4-6] do not form irreducible representations of the P_3 nuclear permutation symmetry group. In order to produce such representation, the

internal coordinate system should treat the three identical nuclei in an equivalent manner. Hyperspherical coordinates, in one of several variations, have been recently used in quantum scattering calculations[7-19] and ro-vibrational bound state calculations of identical atom triatomic molecular systems[20-23], and permit easy inclusion of the full P_3 nuclear permutation symmetry.

In equilateral triangular geometries, the ground and the first excited electronic states of H_3 are degenerate with each other. When the nuclear geometric configuration deviates from the equilateral triangular shape, the degeneracy is lifted. As Longuet-Higgins, Herzberg and co-workers[24-27] have pointed out, the effect of the conical intersection causes the real-valued electronic wavefunctions of both electronic states to change signs as one follows an arbitrary but closed path in the internal nuclear configuration space around the line of conical intersection configuration. Since the total electronic and nuclear wavefunction has to be single valued, this implies a same sign change for the nuclear wave-function. In order to present a correct and consistent treatment of the electronic and nuclear wavefunctions, this sign change is absolutely necessary and must be included in the solution of the nuclear spatial wavefunction[2]. It will be shown in this chapter that in the hyperspherical coordinate system we have used, the effect of geometric phase (sign change) can be included easily.

More details can be found in chapter 4 about the background of the ro-vibrational states of H_3 on the DMBE surface of its first excited electronic state[1]. In section 5.2, the conical intersection between the ground and first excited electronic states of H_3 will be discussed as an example of the manifestation of the effect of the geometric phase. The form of the electronic wavefunctions with the usual choice of phase factors in the vicinity of the conical intersection is also presented. In section 5.3, a full three-dimensional coupled-channel propagation

method in hyperspherical coordinates is presented, including a description on how to construct electro-nuclear wavefunctions with P_3 symmetry embedded into them. Results and discussions of calculations with and without including the geometric phase effect are presented in section 5.4.

5.2. Conical Intersection

The Born-Oppenheimer separation of the electronic motion from the nuclear one is the most fundamental concept in the physics and chemistry of molecular systems (see chapter 2). The electro-nuclear wavefunction corresponding to the ith electronic state is written (in a mixed notation convenient for our purposes) as

$$\Psi(\mathbf{r};\ \mathbf{R}) = \psi(\mathbf{R}) \mid \phi_i(\mathbf{r};\ \mathbf{R})\rangle \tag{1}$$

where $\mathbf{r}$ and $\mathbf{R}$ denotes the electronic and nuclear coordinates respectively. $\mid \phi_i(\mathbf{r};\ \mathbf{R})\rangle$ is the ith member of the set of orthonormal eigen-vectors of the electronic Hamiltonian $\hat{H}_e(\mathbf{r};\ \mathbf{R})$, *i.e.*,

$$\hat{H}_e(\mathbf{r};\ \mathbf{R}) \mid \phi_i(\mathbf{r};\ \mathbf{R})\rangle = U_i(\mathbf{R}) \mid \phi_i(\mathbf{r};\ \mathbf{R})\rangle \tag{2}$$

and

$$\langle \phi_i(\mathbf{r};\ \mathbf{R}) \mid \phi_j(\mathbf{r};\ \mathbf{R})\rangle = \delta_{i,j} \tag{3}$$

with the inner product referring to the Hilbert space of the electronic degrees of freedom only.

To obtain the equation for the nuclear wave-function we retain all derivatives of the electronic wavefunction with respect to nuclear coordinates. But all coupling to other electronic states is neglected. Form Eq. (10) of chapter 2, we have

$$\{\hat{T}_N + U_i(\mathbf{R})\}\psi_i(\mathbf{R}) + F_{i,i}(\mathbf{R})\psi_i(\mathbf{R}) + G_{i,i}(\mathbf{R})\psi_i(\mathbf{R}) = E\psi_i(\mathbf{R}) \tag{4}$$

The definitions of $\hat{T}_N$, $U_i(\mathbf{R})$, $F_{i,i}(\mathbf{R})$ and $G_{i,i}(\mathbf{R})$ are available in Eqs. (2), (7), (10)-(12) of chapter 2.

Let us introduce a mass-scaled coordinates

$$\mathbf{R'}_A = (\frac{M_A}{M})^{\frac{1}{2}}\mathbf{R}_A \tag{5}$$

where the M_A is the mass of the A'th nucleus (as defined in chapter 2) and M is the mass arbitrarily chosen to be the effective mass of the system. In this coordinates, the total nuclear kinetic energy operator becomes

$$\hat{T}_N = -\frac{\hbar^2}{2M}\nabla^2_{\mathbf{R'}} \tag{6}$$

where $\mathbf{R'}$ is a $3N_n$-dimensional vector formed by all $\mathbf{R'}_A$ and $\nabla_{\mathbf{R'}}$ is a gradient operator in the $3N_n$-dimension nuclear coordinates. N_n is the number of nuclei in the molecule (same as defined in chapter 2). In this mass-scaled coordinates, Eq. (4) becomes

$$\{-\frac{\hbar^2}{2M}\nabla^2_{\mathbf{R'}} + U_i(\mathbf{R'}) - \frac{\hbar^2}{M}\mathbf{F}(\mathbf{R'})\cdot\nabla_{\mathbf{R'}} - \frac{\hbar^2}{2M}G(\mathbf{R'})\}\psi(\mathbf{R'}) = E\psi(\mathbf{R'}) \tag{7}$$

where

$$\mathbf{F}(\mathbf{R'}) = \langle\phi_i(\mathbf{R'}) \mid \nabla_{\mathbf{R'}} \mid \phi_i(\mathbf{R'})\rangle \tag{8}$$

$$G(\mathbf{R'}) = \langle\phi_i(\mathbf{R'}) \mid \nabla^2_{\mathbf{R'}} \mid \phi_i(\mathbf{R'})\rangle \tag{9}$$

The fact is that Eqs. (1) to (3) determine the electronic wavefunction $\mid \phi_i(\mathbf{r}, \mathbf{R'})\rangle$ only up to a phase factor $e^{if(\mathbf{R'})}$. It follows immediately from Eq. (3) that $\mathbf{F}(\mathbf{R'})$ is purely imaginary and must vanish if $\mid \phi_i(\mathbf{r}, \mathbf{R'})\rangle$ is chosen to be real (that is, the phase$f(\mathbf{R'}) = 0$ for all $\mathbf{R'}$). Even if $\mathbf{F}(\mathbf{R'})$ does not vanish, we can multiply the electronic wavefunction by a phase factor $e^{if(\mathbf{R'})}$ for which $i\nabla_{\mathbf{R'}}f(\mathbf{R'})$ equals $-\mathbf{F}(\mathbf{R'})$ in order to cancel out the $\mathbf{F}(\mathbf{R'})$ term.

If the new $\mathbf{F}(\mathbf{R}')$ is calculated in the newly defined electronic wave-function $e^{if(\mathbf{R}')} \mid \phi_i(\mathbf{r};\ \mathbf{R}')\rangle$, it vanishes. This operation corresponds to a local gauge transformation. In many calculations, it is generally assumed that the phase factor has been chosen in this way, so that the $\mathbf{F}(\mathbf{R}')$ term can be left out.

However, if $\mathbf{F}(\mathbf{R}')$ has non-zero curl[28], it can not be made to vanish everywhere by a phase factor with a single-valued function $f(\mathbf{R}')$ because $\nabla_{\mathbf{R}'} \times \nabla_{\mathbf{R}'} f(\mathbf{R}') \equiv 0$. The phase factor $f(\mathbf{R}')$ can still be determined along any path to make $\mathbf{F}(\mathbf{R}')$ vanish, but there may be a net change in the phase of $\mid \phi(\mathbf{r};\ \mathbf{R}')\rangle$ on traversing a closed path, which means that $\mid \phi(\mathbf{r};\ \mathbf{R}')\rangle$ is no longer a single valued function of the nuclear configuration $\mathbf{R}'$.

Let us choose the the electronic wavefunctions to be real and investigate their behavior near a conical intersection. We will follow the argument of Herzberg and Longuet-Higgins[25] who had shown that the electronic wavefunction changes signs when the nuclear configuration completes a closed path around the conical intersection[27,28].

Only two electronic states need to be considered in this analysis. Near the vicinity of the conical intersection, we chose two diabatic electronic functions $\mid \phi_1\rangle$ and $\mid \phi_2\rangle$ as the real valued basis functions. They are orthonormal to each other and will be assumed independent to the nuclear configuration. For such a limited basis set, the matrix elements of the electronic Hamiltonian $\hat{H}_e$ are expressed as

$$H_{11} = \langle \phi_1 \mid \hat{H}_e \mid \phi_1 \rangle \tag{10}$$

$$H_{22} = \langle \phi_2 \mid \hat{H}_e \mid \phi_2 \rangle \tag{11}$$

$$H_{12} = H_{21} = \langle \phi_1 \mid \hat{H}_e \mid \phi_2 \rangle. \tag{12}$$

It is possible to express each of the two electronic eigenfunctions in the form

$$| \Phi\rangle = c_1 | \phi_1\rangle + c_2 | \phi_2\rangle \tag{13}$$

The following secular equation must be satisfied

$$\begin{pmatrix} H_{11} - E & H_{12} \\ H_{21} & H_{22} - E \end{pmatrix} \begin{pmatrix} c_1 \\ c_2 \end{pmatrix} = 0, \tag{14}$$

where E is the electronic energy and all quantities are real.

In order for Eqs. (13) and (14) to have degenerate solutions (conical intersection), it is necessary to satisfy two independent conditions, namely,

$$H_{11} = H_{22} \tag{15}$$

$$H_{12}(= H_{21}) = 0 \tag{16}$$

and this requires at least two independent nuclear coordinates. In the case of the H_3 system, there are three internal coordinates that are enough for this purpose. Let us chose a local (x, y, z) coordinate system where the conical intersection happens at $x = y = 0$ with any fixed z. Because the eigen-energy difference between two eigen-states is linear with the deviation of nuclear configuration away from the degenerate one (*i.e.*, it is proportional to x and y), the secular equations may be cast in the following form without any loss of generality:

$$\begin{pmatrix} W + h_1 x - E & ly \\ ly & W + h_2 x - E \end{pmatrix} \begin{pmatrix} c_1 \\ c_2 \end{pmatrix} = 0. \tag{17}$$

The corresponding eigenvalues are

$$E_{\pm} = W + mx \pm \sqrt{(k^2 x^2 + l^2 y^2)} \tag{18}$$

with m and k defined as

$$m = \frac{1}{2}(h_1 + h_2) \tag{19}$$

$$k = \frac{1}{2}(h_1 - h_2). \tag{20}$$

It is easy to see that this is the equation of a double cone with the vertex at the origin, as the two potential energy surfaces would form around the conical intersection.

Let us define an angle θ by equations

$$kx = R\cos\theta \tag{21}$$

$$ly = R\sin\theta \tag{22}$$

$$R = \sqrt{(k^2x^2 + l^2y^2)} > 0 \tag{23}$$

The eigenvalues and eigenfunctions are then expressed as

$$E_{\pm} = W + R(\cos\theta \pm 1) \tag{24}$$

and

$$| \Phi^+(\theta, R, z)\rangle = \sin\frac{\theta}{2} | \phi_1\rangle + \cos\frac{\theta}{2} | \phi_2\rangle \tag{25}$$

$$| \Phi^-(\theta, R, z)\rangle = \cos\frac{\theta}{2} | \phi_1\rangle - \sin\frac{\theta}{2} | \phi_2\rangle. \tag{26}$$

Notice that the choice of phase factor in this case is precisely the conventional one, with the following relations satisfied by the eigen-functions

$$\langle\Phi^+ | \Phi^+\rangle = \langle\Phi^- | \Phi^-\rangle = 1 \tag{27}$$

$$\langle\Phi^+ | \Phi^-\rangle = 0 \tag{28}$$

$$\langle\Phi^+ | \frac{\partial}{\partial\theta} | \Phi^+\rangle = \langle\Phi^- | \frac{\partial}{\partial\theta} | \Phi^-\rangle = 0 \tag{29}$$

except now the electronic wavefunctions $| \Phi^+\rangle$ and $| \Phi^-\rangle$ will change signs as we move around the z axis of coordinates while keeping R and z constant and allowing θ to go from 0 to 2π.

Actually, this sign-change (or non-single value-ness) is a topological characteristic which holds not only for small R (near the vicinity of the conical

intersection point where our derivation is valid) but for any R value[25]. It has been proven to be a special case[29-32] of the Berry's geometric phase[3].

Since this phenomenon bears some similarity of the situation where an electron moves under the influence of a confined magnetic flux[33] (of one quanta), it has also been named the molecular Aharanov-Bohm effect (MAB) by Mead and Truhlar[2].

There are two ways to treat the electronic and nuclear wavefunctions that include the effect of the geometric phase (or MAB effect). The first one, as demonstrated, takes the conventional approach for the choice of phase factor. As the electronic wavefunctions are real under this approach, they have their signs changed after a complete path that encloses the conical intersection, and the nuclear wavefunctions are required to do the same in order to have a combined total electro-nuclear wavefunction which is single-valued. The second one uses another convention for the phase factor in order to obtain single valued electronic wave-functions[2,34]. This can be done by simply multiplying the real electronic wavefunction (which displays the sign change) by a function $e^{if(\mathbf{R}')}$ which also has a sign change after a complete path in the internal nuclear configuration space. The electronic wavefunctions are now complex and the $\mathbf{F}(\mathbf{R}')$ term in Eq. (8) will be important in the equation for the nuclear wavefunction (see Eq. (7)). Since the term with $\mathbf{F}(\mathbf{R}')$ is purely imaginary, the nuclear wavefunctions may also be complex.

5.3. Methodology

Let $A_\alpha, A_\beta, A_\gamma$ of masses $m_\alpha, m_\beta, m_\gamma$ be the three atoms of the triatomic system, and (λ, ν, κ) be any cyclic permutation of (α, β, γ). The interaction between the atoms does not depend on the position of the center of mass of the system nor on the orientation of the triangle with respect to the laboratory reference frame. The motion of the center of mass of the system is not of concern and can be removed easily. Following the same procedure as in chapter 4, after the removal of the motion of the center of mass, the Hamiltonian for the internal nuclear motion in the Jacobi coordinates is expressed as

$$\hat{H} = -\frac{\hbar^2}{2\mu_{\lambda,\nu\kappa} R'_\lambda} \frac{\partial^2}{\partial R'^2_\lambda} R'_\lambda - \frac{\hbar^2}{2\mu_{\nu\kappa} r'_\lambda} \frac{\partial^2}{\partial r'^2_\lambda} r'_\lambda + \frac{\mathrm{l}^2_\lambda}{2\mu_{\lambda,\nu\kappa} R'^2_\lambda} + \frac{\mathrm{j}^2_\lambda}{2\mu_{\nu\kappa} r'^2_\lambda} + V^\lambda(R'_\lambda, r'_\lambda, \gamma_\lambda) \tag{30}$$

where the internuclear vector for the diatom $A_\nu A_\kappa$ is $\mathbf{r}'_\lambda$ and $\mathbf{R}'_\lambda$ is the vector of A_λ with respect to the center of mass of the $A_\nu A_\kappa$ pair (these vectors are unprimed in chapter 4) γ_λ is the angle formed by those two vectors. $V^\lambda(R'_\lambda, r'_\lambda, \gamma_\lambda)$ is the electronically adiabatic potential energy function describing the effective interactions of the three particles The effective masses are defined by

$$\mu_{\nu\kappa} = \frac{m_\nu m_\kappa}{(m_\nu + m_\kappa)} \tag{31}$$

$$\mu_{\lambda,\nu\kappa} = \frac{m_\lambda (m_\nu + m_\kappa)}{(m_\lambda + m_\nu + m_\kappa)} \tag{32}$$

and l_λ and j_λ are angular momentum operators associated with vectors $\mathbf{R}'_\lambda$ and $\mathbf{r}'_\lambda$. The total rotational angular momentum operator of these three nuclei is

$$\mathbf{J} = \mathrm{l}_\lambda + \mathrm{j}_\lambda \tag{33}$$

We now introduce Delves' mass-scaled coordinates[35,36]) defined by

$$\mathbf{R}_\lambda = a_\lambda \mathbf{R}'_\lambda \tag{34}$$

$$\mathbf{r}_\lambda = a_\lambda^{-1} \mathbf{r}'_\lambda \tag{35}$$

$$a_\lambda = \left(\frac{\mu_{\lambda,\nu\kappa}}{\mu_{\nu\kappa}}\right)^{\frac{1}{4}} = \left(\frac{\mu_{\lambda,\nu\kappa}}{\mu}\right)^{\frac{1}{2}} \tag{36}$$

Now the nuclear Hamiltonian in the mass-scaled coordinates is

$$\hat{H} = \frac{-\hbar^2}{2\mu}(\nabla^2_{\mathbf{R}_\lambda} + \nabla^2_{\mathbf{r}_\lambda}) + V^\lambda(R_\lambda, r_\lambda, \gamma_\lambda) \tag{37}$$

where

$$\mu = \left(\frac{m_\lambda m_\nu m_\kappa}{m_\lambda + m_\nu + m_\kappa}\right)^{\frac{1}{2}} \tag{38}$$

The nuclear motion of the triatomic system can be thought of as that of a single particle with mass μ moving in a six-dimensional space $(\mathbf{R}_\lambda, \mathbf{r}_\lambda)$. R_λ, r_λ and γ_λ describe the shape of the triangle formed by the three nuclei. Three additional Euler angles are needed to describe the overall rotation of the triangle relative to a laboratory reference frame.

The hyperspherical method uses the hyper-radius

$$\rho = (R_\lambda^2 + r_\lambda^2)^{\frac{1}{2}} \tag{39}$$

to describe the global size of the triatomic system and a set of five angles ς to describe its shape and orientation in space[7-19]. It can be easily proven that ρ is invariant under any permutation of λ, ν, κ index for those three particles.

Before we go into the specific definitions for the five angles ς, let us consider the form of the electronic and nuclear wavefunctions and the way those equations are solved. In our treatment, we will neglect all spin-orbit and spin-spin interactions as in the usual treatment of light-atom molecular systems. In

the Born-Oppenheimer approximation, the electro-nuclear wavefunction can be written as a product of the electronic part ψ_e, which we choose to be real (following the usual convention for the phase factor of electronic wave-functions), and the nuclear part. The latter can be factored into a nuclear spin part and a spacial part $\psi^{JM\Pi\Gamma}$. J is the total nuclear rotational angular momentum quantum number, M its projection onto a laboratory-fixed axis, Π the parity with respect to the inversion of the nuclei through the system' center of mass and Γ the irreducible representation of the nuclear permutation group P_3 to which $\Psi^{JM\Pi\Gamma}$, the combined electro-nuclear wavefunction excluding the nuclear spin part, belongs:

$$\Psi^{JM\Pi\Gamma} = \psi^{JM\Pi\Gamma}(\rho,\varsigma) \mid \psi_e(\mathbf{q}_e;\rho,\varsigma)\rangle \tag{40}$$

$\mathbf{q}_e$ refers to the set of all (spatial and spin) electronic coordinates. $\psi^{JM\Pi\Gamma}$ is an eigenfunctions of the nuclear motion Hamiltonian :

$$\hat{H}_n = -\frac{\hbar^2}{2\mu}\rho^{-5}\frac{\partial}{\partial\rho}\rho^5\frac{\partial}{\partial\rho} + \frac{\hat{\Lambda}^2}{2\mu\rho^2} + V(\rho,\varsigma) \tag{41}$$

where μ is the three-body reduced mass defined in Eq. (38), $\hat{\Lambda}$ the grand canonical angular momentum whose explicit form depends on the choice of these five angular variables ς, and $V(\rho,\varsigma)$ the Born–Oppenheimer electronic potential energy function.

The nuclear function $\psi^{JM\Pi\Gamma}$ is expanded in a basis of local hyperspherical surface functions (LHSF) $\Phi_n^{JM\Pi\Gamma}$ evaluated at $\overline{\rho}$:

$$\psi^{JM\Pi\Gamma}(\rho,\varsigma) = \rho^{-\frac{5}{2}}\sum_n F_n^{J\Pi\Gamma}(\rho;\overline{\rho})\Phi_n^{JM\Pi\Gamma}(\varsigma;\overline{\rho}) \tag{42}$$

The LHSF are defined as the eigen-functions of the fixed hyperradius nuclear Hamiltonian:

$$[\frac{\hat{\Lambda}^2}{2\mu\overline{\rho}^2} + V(\overline{\rho},\varsigma)]\Phi_n^{JM\Pi\Gamma}(\varsigma;\overline{\rho}) = \epsilon_n^{J\Pi\Gamma}(\overline{\rho})\Phi_n^{JM\Pi\Gamma}(\varsigma;\overline{\rho}) \tag{43}$$

Since all angles have finite domains, the solutions of Eq. (43) will form a discrete orthonormal basis set in the five-angle ς space.

The coefficients $F_n^{J\Pi\Gamma}$ in Eq. (42) are solutions of a set of coupled-channel differential equations in ρ, which we solve using piece-wise diabatic bases[7-12,15]. The equations for $F_n^{J\Pi\Gamma}$ are obtained directly using Eq. (43) and the orthonormal properties of the LHSF. They are:

$$\frac{d^2}{d\rho^2}F_n^{J\Pi\Gamma}(\rho;\overline{\rho}) + \sum_{n'} U_{n,n'}^{J\Pi\Gamma}(\rho;\overline{\rho})F_{n'}^{J\Pi\Gamma}(\rho;\overline{\rho}) = 0 \tag{44}$$

where

$$U_{n,n'}^{J\Pi\Gamma}(\rho;\overline{\rho}) = \delta_{n,n'}\left(\frac{2\mu}{\hbar^2}\{E - (\overline{\rho}/\rho)^2\epsilon_n^{J\Pi\Gamma}(\overline{\rho})\} - \frac{15}{4\rho^2}\right) + \triangle V_{n,n'}^{J\Pi\Gamma}(\rho;\overline{\rho}) \tag{45}$$

with

$$\triangle V_{n.n'}^{J\Pi\Gamma}(\rho;\overline{\rho}) = \frac{2\mu}{\hbar^2}\langle\Phi_n^{J\Pi\Gamma}(\varsigma;\overline{\rho}) \mid (\overline{\rho}/\rho)^2 V(\overline{\rho},\varsigma) - V(\rho,\varsigma) \mid \Phi_{n'}^{J\Pi\Gamma}(\varsigma;\overline{\rho})\rangle \tag{46}$$

The integration in Eq. (46) is over the volume element of the five-angle ς.

It is easy to see that Eq. (44) can be viewed as an initial value problem. For this set of coupled-channel second-order ordinary differential equations, if the value and the first derivative of $F_n(\rho;\overline{\rho})$ is known at the initial ρ value, the solution of Eq. (44) can be obtained using step-by-step finite difference or equivalent propagation methods.

The LHSFs at a single $\overline{\rho}$ are not efficient enough for expanding the nuclear wave-function for all values of ρ. The strategy is to divide the full range of ρ into

many small segments and calculate one set of LHSFs at each of a family of $\overline{\rho}_i$ values, where $i = 1, 2, ...$ one per each segment. For each $\overline{\rho}_i$ value, the system of coupled equations can be integrated directly as an initial value problem. With the exception of the very first segment beginning at ρ_0, the initial conditions follow from continuity of the wave-function and its first derivative between segments. This information is carried in the overlap matrices which are calculated between two sets of LHSFs at adjoining values of hyperradius: $\overline{\rho}_i$ and $\overline{\rho}_{i+1}$. The overlap matrices are defined by:

$$O^{J\Pi\Gamma}_{n,n'}(\overline{\rho}_{i+1}, \overline{\rho}_i) = \langle \Phi^{J\Pi\Gamma}_n(\varsigma; \overline{\rho}_{i+1}) \mid \Phi^{J\Pi\Gamma}_{n'}(\varsigma; \overline{\rho}_i) \rangle \tag{47}$$

These overlap matrices provide a way to transform functions in one segment $F^{J\Pi\Gamma}_n(\rho; \overline{\rho}_i)$ into functions in the next segment $F^{J\Pi\Gamma}_n(\rho; \overline{\rho}_{i+1})$ following

$$F^{J\Pi\Gamma}_n(\rho; \overline{\rho}_{i+1}) = \sum_{n'} O^{J\Pi\Gamma}_{n,n'}(\overline{\rho}_{i+1}, \overline{\rho}_i) F^{J\Pi\Gamma}_{n'}(\rho; \overline{\rho}_i) \tag{48}$$

The first derivative with respect to ρ is transformed by the same Eq. (48) because the LSHF's are used as a diabatic basis set. $O^{J\Pi\Gamma}_{n,n'}(\overline{\rho}_{i+1}, \overline{\rho}_i)$ has a very obvious geometric analog with the transformation matrix which rotates a n-dimensional Cartesian coordinate system.

For assumed values of the ro-vibrational energies E, the solutions are propagated forward and backward from small and large ρ values where they have negligible amplitudes and with chosen values for the first derivatives. This method used is that of De Vogelaere[37]. The energy is scanned iteratively until the quantization condition that the forward and backward solutions match smoothly at an intermediate value of ρ is reached. It can be proven that this procedure for obtaining the eigenenergies does not depend on the choice of the first derivatives for the forward and backward propagation. It is exactly the same as the well

known numerical methods for solving eigenstate-eigenfunction problems of the one–dimensional quantum systems. The only complication is the fact that now we have multiple channels instead of the single channel of the one-dimensional case.

In the present study, we use the Whitten–Smith[16] definition of the five angular coordinates ς as modified by Johnson[17-19]. Three Euler angles $(\alpha\beta\gamma)$ specify the orientation of the body-fixed frame in space with respect to the laboratory reference frame. The axes of this frame lie along the principle axes of inertia: the Z axis is chosen to be parallel to $\mathbf{r}_\lambda \times \mathbf{R}_\lambda$ (or perpendicular to the plane of the triatomic molecule) and the X axis is associated with the smallest moment of inertia and is oriented such that $r_{\lambda X} \geq 0$. Two angles $(\theta, \varphi_\lambda)$ describe the shape of the molecular triangle and are defined by:

$$r_{\lambda X} = \rho\cos(\frac{\pi}{4} - \frac{\theta}{2})\sin(\frac{\varphi_\lambda}{2}) \tag{49a}$$

$$r_{\lambda Y} = -\rho\sin(\frac{\pi}{4} - \frac{\theta}{2})\cos(\frac{\varphi_\lambda}{2}) \tag{49b}$$

$$R_{\lambda X} = \rho\cos(\frac{\pi}{4} - \frac{\theta}{2})\cos(\frac{\varphi_\lambda}{2}) \tag{49c}$$

$$R_{\lambda Y} = \rho\sin(\frac{\pi}{4} - \frac{\theta}{2})\sin(\frac{\varphi_\lambda}{2}) \tag{49d}$$

The ranges for these angles are $0 \leq \theta \leq \frac{\pi}{2}$ and $0 \leq \varphi_\lambda \leq 2\pi$. Notice that θ is also invariant under any permutation of these three particles[17]. It is straightforward to verify that indeed the coordinate system defined by Eqs. (49a-49d) does have its X axis along the principle axis of smallest moment of inertia orientated along which $\mathbf{r}_\lambda$ has a positive projection on it. $\theta = 0$ corresponds to the symmetric top configuration (an equilateral triangle for three identical particles) in which the principal axes of inertia X and Y are undefined, which in turn makes φ_λ undefined too. $\theta = \frac{\pi}{2}$ corresponds to the collinear nuclear configuration where

the Z axis is not specifically defined as long as it is perpendicular to the X axis which in this case containing three atoms.

The grand canonical angular momentum in this set of angular variables is given explicitly by[16-19]:

$$\hat{\Lambda}^2 = -4\hbar^2\{\frac{1}{\sin 2\theta}\frac{\partial}{\partial\theta}\sin 2\theta\frac{\partial}{\partial\theta} + \frac{1}{\sin^2\theta}\frac{\partial^2}{\partial\varphi_\lambda^2}\} + \frac{4i\hbar\cos\theta}{\sin^2\theta}\hat{J}_Z\frac{\partial}{\partial\varphi_\lambda} + \frac{2[\hat{J}^2 - \hat{J}_Z^2]}{\cos^2\theta} + \frac{\hat{J}_Z^2}{\sin^2\theta} + \frac{\sin\theta}{\cos^2\theta}[\hat{J}_+^2 + \hat{J}_-^2] \quad (50)$$

where $\hat{J}_Z$ is the body-fixed Z component of the total rotational angular momentum $\hat{J}$, and $\hat{J}_\pm = \hat{J}_X \pm i\hat{J}_Y$. The $\hat{J}^2$, $\hat{J}_Z$, and $\hat{J}_\pm$ operators only act on the three Euler angles.

5.3.1 Basis set for the LSHF

Eq. (43) for the LHSF is solved variationally by expansion in a body-fixed basis $\chi_{n_\theta n_\varphi}^{JMK}(\varsigma)$ built with direct products of simple analytical functions[15] :

$$\chi_{n_\theta n_\varphi}^{JMK}(\varsigma) = e^{in_\varphi\varphi_\lambda} f_{n_\theta}(\theta) D_{MK}^J(\alpha\beta\gamma) \quad (51)$$

$D_{MK}^J(\alpha\beta\gamma)$ is the well known Wigner rotation function[38] and n_φ is an integer or half of an odd integer (both positive and negative) depending on whether the effect of conical intersection is included or not. $f_{n_\theta}(\theta)$ are simple trigonometric functions, such that the LHSF have correct behaviors near the singularities of the kinetic energy operator at $\theta = 0$ and $\frac{\pi}{2}$. In practice, the f_{n_θ} are chosen as

$$f_{n_\theta} = \begin{bmatrix}\cos(n_\theta\theta)\\ \sin(n_\theta\theta)\end{bmatrix} \quad (52)$$

with n_θ integer or half odd integer, in terms of which the hyperspherical harmonics[39-41] (whose θ dependence is usually written as a polynomial in $\cos(\theta)$) can be written (see Eq. (31) in Ref. 39, Eqs. (20–23) in Ref. 40 or Eq. (32) in

Ref. 41). Since the domain for θ is between 0 and $\frac{\pi}{2}$, $f_{n_\theta}(\theta)$ is a single–valued function even though n_θ can be half of an odd integer.

5.3.2 Symmetry considerations

We now focus our attention on the special case of three identical nuclei and describe how to build electro-nuclear wavefunctions $\Psi^{JM\Pi\Gamma}$ which are bases for the irreducible representations of the P_3 permutation group of the three identical nuclei. The operations of this group correspond to simple changes in φ_λ (which are related to the isomorphism between P_3 and C_{3v}) as indicated in Table 1. If $\epsilon^e_{\nu\kappa}(= \pm 1)$ is the symmetry of the electronic wavefunction with respect to the $\nu \leftrightarrow \kappa$ permutation, then the linear combinations defined by :

$$\chi^{JMK\epsilon^{en}_{\nu\kappa}}_{n_\theta|n_\varphi|} = \chi^{JMK}_{n_\theta|n_\varphi|} + \epsilon^{en}_{\nu\kappa}\epsilon^{e}_{\nu\kappa}(-1)^{J+K+2n_\varphi}\chi^{JM,-K}_{n_\theta,-|n_\varphi|} \tag{53}$$

give electro-nuclear wave-functions $\Psi^{JM\Pi\Gamma}$ (see Eq. (40)) with the $\epsilon^{en}_{\nu\kappa}(= \pm 1)$ symmetry with respect to the $\nu \leftrightarrow \kappa$ permutation.

If there is no conical intersection between electronic states, a non-degenerate electronic wavefunction $\mid \psi_e(\mathbf{q}_e;\rho,\varsigma)\rangle$ belongs to a one–dimensional representation of the nuclear permutation group (A_1 for $\epsilon^e_{\nu\kappa} = +1$, or A_2 for $\epsilon^e_{\nu\kappa} = -1$), and is also single-valued with respect to the nuclear geometry configuration. For this reason, the nuclear wavefunction also needs to be single–valued, which subsequently means that $\mid n_\varphi \mid$ has to be an integer (which leads naturally to $(-1)^{2n_\varphi} \equiv 1$). Table 2 indicates how the total angular momentum, the parity and the irreducible representation Γ of P_3 to which $\Psi^{JM\Pi\Gamma}$ belongs determines the set of quantum numbers n_φ.

Let us consider two special cases. When $J = M = K = 0$ and $\mid n_\varphi \mid = 3m$, basis functions defined in Eq. (53) will give $\sin(3m\varphi_\lambda)$ (an A_2-type function) or

$\cos(3m\varphi_\lambda)$ (an A_1-type function). When $J = M = K = 0$ and $\mid n_\varphi \mid = 3m \pm 1$, pairs of basis functions of the form

$$\begin{bmatrix} \sin(3m \pm 1)\varphi) \\ \cos(3m \pm 1)\varphi) \end{bmatrix}$$

(with m integer) can be easily proven to form an E representation of the P_3 permutation group.

If there is a conical intersection between two electronic states for equilateral triangular configurations of the nuclei and if the geometric phase is taken into account, in the vicinity of the conical intersection ($\theta = 0$) the φ_λ dependence of those two non-degenerate Born-Oppenheimer electronic wave-functions is given by (see Eqs. (25) and (26)):

$$\mid \psi_e^- \rangle \approx \cos\frac{\varphi_\lambda}{2} \mid \psi_e^{E_1} \rangle - \sin\frac{\varphi_\lambda}{2} \mid \psi_e^{E_2} \rangle \qquad (\epsilon_{\nu\kappa}^e = -1, \text{ lower energy}) \quad (54a)$$

or

$$\mid \psi_e^+ \rangle \approx \cos\frac{\varphi_\lambda}{2} \mid \psi_e^{E_2} \rangle + \sin\frac{\varphi_\lambda}{2} \mid \psi_e^{E_1} \rangle \qquad (\epsilon_{\nu\kappa}^e = +1, \text{ higher energy}) \quad (54b)$$

where $(\mid \psi_e^{E_1} \rangle, \mid \psi_e^{E_2} \rangle)$ are two degenerate ρ–dependent but φ_λ–independent states at $\theta = 0$ which form a basis for the E irreducible representation of P_3 ($\mid \psi_e^{E_1} \rangle$ being symmetric for the $\nu \leftrightarrow \kappa$ permutation and $\mid \psi^{E_2} \rangle$ anti-symmetric). Under the permutation operation of the P_3 permutation group, angle φ_λ transforms as described in Table 1. Although $(\mid \psi_e^{E_1} \rangle, \mid \psi_e^{E_2} \rangle)$ do not depend on φ_λ explicitly, the permutation operation does change the internal coordinate system in which $(\mid \psi_e^{E_1} \rangle, \mid \psi_e^{E_2} \rangle)$ are described (this is a passive view of symmetric operations). If we take the active view of those symmetric operations, then $(\mid \psi_e^{E_1} \rangle, \mid \psi_e^{E_2} \rangle)$ would behave like a pair of unit vectors $[\mathbf{e}_x, \mathbf{e}_y]$ under C_{3v}, except that the rotation angles are $-120°$ and $-240°$ instead of $120°$ and $240°$

as described in Table 1 for φ_λ. As mentioned before, $\mid \psi_e^- \rangle$ and $\mid \psi_e^+ \rangle$ are both singlet (non-degenerate) electronic states with their phase factors to be chosen in such a way as to make both of them real functions. Their behavior under operation of the P_3 nuclear permutation is listed in Table 1. It can be seen that although permutations of the nuclei can only change the sign of $\mid \psi_e^\pm \rangle$, these Born-Oppenheimer *electronic* wavefunctions do not belong to any one–dimensional irreducible representation of P_3 and are also discontinuous in the internal configuration space when crossing the plane of $\varphi_\lambda = 0$.

Continuous *electro-nuclear* wave-functions that do form irreducible representations of P_3 can be built if the new set of n_φ indicated in Table 2 is used for the *nuclear* wave-functions. Let us consider two special cases again in order to appreciate this point. When $J = M = K = 0$ and $n_{\varphi_\lambda} = 3m + \frac{3}{2}$, the basis function in Eq. (53) can be

$$\sin(3m + \frac{3}{2})\varphi_\lambda \tag{55a}$$

$$\cos(3m + \frac{3}{2})\varphi_\lambda \tag{55b}$$

with m integer. The transformations of both functions under P_3 are listed in Table 1. It is obvious that they are not one-dimensional irreducible representations of P_3. The following behavior

$$\sin(3m + \frac{3}{2})\varphi_\lambda \mid \psi_e^- \rangle \rightarrow A_2 \tag{56a}$$

$$\sin(3m + \frac{3}{2})\varphi_\lambda \mid \psi_e^+ \rangle \rightarrow A_1 \tag{56b}$$

$$\cos(3m + \frac{3}{2})\varphi_\lambda \mid \psi_e^- \rangle \rightarrow \text{not allowed} \tag{56c}$$

$$\cos(3m + \frac{3}{2})\varphi_\lambda \mid \psi_e^+ \rangle \rightarrow \text{not allowed} \tag{56d}$$

is however obeyed by the indicated products. Following the same argument, it can be proven that when $J = M = K = 0$ and $n_{\varphi_\lambda} = 3m \pm \frac{1}{2}$, pairs of functions like

$$\begin{bmatrix} \sin(3m \pm \frac{1}{2}) \mid \psi_e^+ \rangle \\ \cos(3m \pm \frac{1}{2}) \mid \psi_e^+ \rangle \end{bmatrix}$$

and

$$\begin{bmatrix} \sin(3m \pm \frac{1}{2}) \mid \psi_e^- \rangle \\ \cos(3m \pm \frac{1}{2}) \mid \psi_e^- \rangle \end{bmatrix}$$

form E irreducible representations of the P_3 permutation group.

5.4. Results and discussion

The potential energy surface for H_3 in its first excited electronic state used in this calculation is the upper sheet of the DMBE surfaces of Varandas *et al.*[1]. The same surface has been used in the variational calculation of ro-vibrational bound states of H_3 in chapter 4. Figs. 1–5 illustrate the main features of the electronic potential in the internal configuration space. It has a quasi-cylindrical symmetry (C_{3v} to be exact) around the Y_λ axis (defined in ref.42 and Eqs. (25)–(37) of chapter 3) which corresponds to the axis of the conical intersection and to the local minima on the fixed ρ spheres. It has an absolute minimum for $\rho = 2.6$ bohr, $\theta = 0$ corresponding to an energy of 2.72 eV with respect to the bottom of the ground electronic state H_2 well. In the vicinity of that minimum, the potential increases steeply and almost linearly as a function of θ, but more slowly as a function of ρ. This is demonstrated clearly in Figs. 2, 4 and 5. This feature of the potential energy surface suggests that the energy quanta for the vibration in the symmetric stretching mode is much smaller than that the energy quanta for the asymmetric modes.

The basis set functions for a fixed $\overline{\rho}$ value in the hyperspherical coordinates, coupled-channel propagation method are constructed by specifying n_θ, n_φ and the symmetry of the combined electro-nuclear wave-function to be obtained. About 20 n_θ values, and between 4 (A_1 or A_2 symmetry) and 8 (E symmetry) $|n_\varphi|$ values were used in the construction of the local hyperspherical surface functions (LHSF). Between 6 (A_1 or A_2 symmetry) and 12 (E symmetry) LHSF are used to construct the final nuclear wave-function. This means that the number of channels for the coupled-channel propagation method is 6 for wave-functions of A_1 and A_2 symmetry, and 12 for wave-functions of E-type symmetry.

The LHSF have been computed typically at 50 $\overline{\rho}$ values between 1.5 bohr and 6.5 bohr. At these limiting hyper-radii the nuclear wavefunctions for those low-lying bound ro-vibrational states are believed to be very close to zero because the potential energy is high. The convergence of the eigenenergies for the LHSF and those for the final ro-vibrational bound states is of the order of 10^{-4} eV. The compactness of the hyperspherical expansion comes from the quasi-cylindrical symmetry of the potential around the $\theta = 0$ line (small number of n_φ values) and from the steep increase of the potential as a function of θ (small number of LHSF).

5.4.1 Results without including the effect of the geometric phase

First we calculated the ro-vibrational bound states without including the geometric phase which can be compared directly to the results obtained by using the variational method of Tennyson and Sutcliffe (see chapter 4). Although in chapter 4 the variational method (TS) has been discussed already, we present here a brief overview in order to permit a comparison between the hyperspherical method and the TS method.

The TS method uses a body frame with its Z_λ axis in the direction of $\mathbf{R'}_\lambda$ and computes the bound states variationally by expansion on a product basis of two Morse–like functions (in R'_λ and r'_λ) for the radial part, and of associated Legendre functions for the γ_λ angular part. The basis functions for the three Euler angles are also the Wigner rotation matrix functions[38], the same as used in the hyperspherical method. There are six parameters in the radial basis functions, which need to be optimized before the calculation of the interested ro-vibrational bound states. The optimized Morse parameters which we chose are indicated in Table 3. Nearly 1400 such product functions have been used for each J, each inversion parity Π and each of the two symmetries for the

permutation of the two identical atoms ν and κ. This unusually large number of basis functions (only 880 such functions were used to get fully converged results on H_3^+ in Tennyson and Sutcliffe' study[43]) is required by the shape of the potential energy surface and the sudden change of its first derivative in the vicinity of the conical intersection axis.

Table 4 lists and compares the ro-vibrational energy levels of H_3 for the upper sheet of the DMBE potential energy surface obtained by the hyperspherical method and the TS variational method without inclusion of the geometric phase effect. The (ν_1, ν_2, l) are quantum numbers of symmetric mode, anti-symmetric mode and vibrational rotational quantum numbers used in the normal mode analysis[44]. In chapter 4, the (ν_{A_1}, ν_E, l) notation was used instead. The symmetry assignments and degeneracy of an eigen–level in the hyperspherical method are exact, while in the TS method, the symmetry assignments are difficult to make for closely spaced eigenstates (see chapter 4 for details). Table 4 also shows that the convergence of the energy levels is always better with the hyperspherical method than with the TS method. The quality of the TS calculation for $J = 1$ odd parity is not as good as the TS calculation for $J = 0$ since the global size of the basis has been kept constant instead of being doubled. For a given total angular momentum and parity, the quality of the TS results decreases as the energy increases, and in particular, states diffuse along ρ (corresponding to high v_1 values, see below) are poorly represented. This suggests that different sets of optimized parameters of the Morse–like functions should be used in the TS method for compact and diffuse states.

The hyperspherical method can be compared with the TS method from computational and formal points of view:

• The basis used in the TS method to expand the bound state wave-functions do not have the P_3 permutation symmetry, but only the P_2 symmetry of two identical nuclei. As a result, plots of the bound state wavefunctions show that, even for the $J = 0$ case where the energy convergence is better than 10^{-3} eV, the shape of the TS wave-functions do not exhibit the correct symmetry properties of a system of three identical particles, whereas they are embedded in the LHSF basis used in the hyperspherical method.

• It is obvious that the TS method does not permit easy inclusion of the geometric phase due to the conical intersection, whereas the hyperspherical method does.

• The hyperspherical method takes advantage of the fact that the potential energy surface has a quasi-cylindrical (C_{3v}, to be exact) symmetry and the large excitation quanta of the LHSF resulting from the the tight cone-shaped feature with a vertex on the Y_λ axis ($\theta = 0$). But the TS method does not have the flexibility needed to make use of such fact. Even worse, the performance of the TS method is greatly compromised by the sharp conical feature in the potential energy surface.

• The TS method is conceptually simple and much easier to use. Its Hamiltonian matrix elements are calculated very efficiently. One calculation gives all eigenenergies and eigefunctions of interest. For the hyperspherical propagation method, propagation with several trial energy values has to be performed iteratively before the eigenenergy of a single eigenstate is reached. The same procedure has to be repeated again for another eigenenergy.

• The hyperspherical method requires less memory: smaller basis sets can be used for the variational solution of the two–dimensional LHSF equation than for the three–dimensional variational solution of the bound states in the TS method.

However, the hyperspherical method required about two times more CPU time than the TS method, since in addition to computing the LHSF (which is done only once per J, parity and irreducible representation), the actual propagation has to be repeated many times. The total CPU time did not exceed 40 minutes on a SCS–40 for a typical run for $J = 0$, and A_1 plus E permutation symmetries. In addition, the hyperspherical method does not involve adjustable parameters that have to be optimized in the TS method.

From the above discussion, we conclude that it would be nice to combine the positive features of both methods. The TS method can be used in the first step of the calculation to obtain the approximate locations (upper bounds, of course) of the eigenstates. The approximate energies are then used as initial trial energies for these eigenstates in the second step, where the propagation in the hyperspherical coordinates are performed in order to refine the eigenenergies, and especially, the eigenfunctions.

5.4.2 Results with inclusion of the effect of the geometric phase

Fig. 6 and Table 5 demonstrate the important modifications of the bound rovibrational energies when the geometric phase is included in the hyperspherical calculation. These changes can be understood in a much easier way if one defines quantum numbers for the bound states of Tables 4 and 5 by modeling the nuclear wavefunction in the following way:

• We retain only a single term in the expansion of the bound states in the LHSF basis (Eqs. (44)). This Born–Oppenheimer–type approximation, also used to model reactive scattering resonances[45,46], is very accurate in the present case where the frequency associated with the hyper-radial mode is smaller than those of the fixed–ρ bending modes: the resulting bound state energies are shifted by less than 0.4 meV. This approximation suggests that we define the quantum

number v_1 associated with the hyperradial motion as the number of nodes of the hyperradial function $F_n^{J\Pi\Gamma}(\rho)$. This mode corresponds to the breathing normal mode in the limit of small amplitude vibrations, but in the present case, it can have large amplitudes with an excitation as large as v_1=5 (see Table 5).

• We assume that the fixed–ρ bending vibration has small amplitude, so that the wavefunction is concentrated near θ=0. This approximation is reasonable due to the steep increase of the potential as a function of θ. It suggests that we neglect the asymmetric top coupling elements in the kinetic energy (last term of Eq. (50)) and the φ_λ–dependence in the potential. The (non–symmetrized) LHSF can then be factored as :

$$\Phi_n^{JM\Pi} = e^{in_\varphi \varphi_\lambda} g_{v_2 l}(\theta;\rho) D^J_{MK}(\alpha,\beta,\gamma) \tag{57}$$

where $g_{v_2 l}$ is defined by :

$$\begin{aligned}[\frac{-2\hbar^2}{\mu\rho^2}(\frac{1}{\theta}\frac{\partial}{\partial\theta}\theta\frac{\partial}{\partial\theta} - \frac{l^2}{\theta^2}) + V(\rho,\theta)]g_{v_2 l}(\theta;\rho) = \\ [\epsilon^{JK}_{v_2 l}(\rho) - (\frac{J(J+1)-\frac{K^2}{2}}{\mu\rho^2} \pm \frac{lK}{\mu\rho^2})\hbar^2]g_{v_2 l}(\theta;\rho)\end{aligned} \tag{58}$$

Eq. (58) is the small θ limit of Eq. (44) (see also Eq. (50)). l quantizes the absolute value of the vibrational angular momentum in a new body frame, which is an Eckart frame associated with the equilibrium position of the nuclei in the equilateral triangular configuration[47], and is given by $l = |n_\varphi - \frac{K}{2}|$. v_2 is the bending vibrational quantum number and is defined by analogy with the two–dimensional harmonic oscillator such that the number of θ–nodes of $g_{v_2 l}$ is $\frac{1}{2}(v_2 - l)$ (see ref. 48). v_2 and l are both integers when the geometric phase is not considered and become half of odd integers when it is taken into account. If the potential were a harmonic function of θ, the bound state energies would increase

linearly with v_2 for each v_1 value. Although the potential is only an approximate linear function of θ, Tables 4 and 5 indicate that the dependence of the bound state energies on v_2 is not far from linear. Therefore, as shown on Fig. 6, each of the levels with the effect of the geometric phase included (v_2 half–odd–integer) is almost half way in energy between two consecutive ones without the effect of this phase included (v_2 integer).

Due to the Pauli principle and to the symmetries of the nuclear spin wavefunction with respect to interchange of the identical nuclei, the only allowed electro-nuclear wave-functions $\Psi^{JM\Pi\Gamma}$ should have A_2 or E nuclear permutation symmetries, and they correspond to quartet and doublet nuclear spins respectively. The number of such levels that satisfy the Pauli principle and their spin symmetries change significantly when the effect of the geometric phase is included.

5.4.3 Conclusions

We have described a new hyperspherical propagation method for the calculation of bound ro-vibrational states. This method is well adapted to systems of three identical particles, because it allows easy inclusion of the full permutation symmetries of the system and of the effect of conical intersections on the phase of the nuclear wave-function.

We have shown that, in the case of the bound rovibrational states in the first electronically excited state of H_3, the geometric phase results in bending modes having half–odd–integer quantum numbers and in important changes of the ro-vibrational state energies and of their symmetry properties[49]. Similarly important changes in the results of quantum scattering calculations for H_3 on its ground state potential energy surface also occurs[50,51].

5.5. References

1. A.J.C. Varandas, F.B. Brown, C.A. Mead, D.G. Truhlar and N.C. Blais, *J. Chem. Phys.* **86**, 6258 (1987).
2. C.A. Mead and D.G. Truhlar, *J. Chem. Phys.* **70**, 2284 (1979).
3. M.V. Berry, *Pro. R. Soc. Lond.*, **A 392**, 45 (1984).
4. J. Tennyson, *Comp. Phys. Comm.*, **42**, 257 (1986).
5. J. Tennyson, *Comp. Phys. Rep.*, **4**, 1 (1986).
6. S. Carter and N.C. Handy, *Comp. Phys. Rep.*, **5**, 115 (1986).
7. R.T. Ling and A. Kuppermann, in *Electronic and Atomic Collisions, Abstract of the 9th International Conference on the Physics of Electronic and Atomic Collisions*, Seattle, Washington, 24–30 July 1975, Vol. 1, eds. J.S. Risley, R. Geballe (Univ. Washington Press, Seattle, 1975) pp. 353-354.
8. A. Kuppermann and P.G. Hipes, *J. Chem. Phys.* **84**, 5962 (1986).
9. P.G. Hipes and A. Kuppermann, *Chem. Phys. Lett.* **133**, 1 (1987).
10. S.A. Cuccaro, P.G. Hipes and A. Kuppermann, *Chem. Phys. Lett.* **154**, 155 (1989).
11. S.A. Cuccaro, P.G. Hipes and A. Kuppermann, *Chem. Phys. Lett.* **157**, 440 (1989).
12. R.T. Pack and G.A. Parker, *J. Chem. Phys.* **87**, 3888 (1987).
13. J. Linderberg, S. Padkjaer, Y Öhrn, B. Vessal, *J. Chem. Phys.* **90**, 7035 (1988).
14. B. Lepetit, J.M. Launay and M. Le Dourneuf, *Chem. Phys.* **106**, 103 (1986).
15. J.M. Launay and M. Le Dourneuf, *Chem. Phys. Lett.* **163**, 178 (1989).
16. R.C. Whitten and F.T. Smith, *J. Math. Phys.*, **9**, 1103 (1968).
17. B.R. Johnson, *J. Chem. Phys.* **73**, 5051 (1980).
18. B.R. Johnson, *J. Chem. Phys.* **79**, 1906 (1983).

19. B.R. Johnson, *J. Chem. Phys.* **79**, 51916 (1983).

20. R. Wallace, *Chem. Phys.* **37**, 93 (1979).

21. J.G. Frey, *Chem. Phys. Lett.* **102**, 421 (1983).

22. J.G. Frey and B.J. Howard, *Chem. Phys.* **99**, 415 (1985).

23. R.M. Whitnell and J.C. Light, *J. Chem. Phys.* **90**, 1774 (1989).

24. H.C. Longuet–Higgins, U. Öpik, M.H.L. Pryce and R.A. Sack, *Proc. Roy. Soc.*, **A 244**, 1 (1958).

25. G. Herzberg and H.C. Longuet–Higgins, *Discuss. Faraday Soc.*, **35**, 77 (1963).

26. H.C. Longuet–Higgins, *Adv. in Spec.*, **2** 429 (1961).

27. H.C. Longuet–Higgins, *Proc. Roy. Soc. London*, **A 344**, 147 (1975).

28. C.A. Mead and D.G. Truhlar, *J. Chem. Phys.* **77**, 6090 (1982).

29. R.L. Whetten and E.R. Grant, *J. Chem. Phys.* **81**, 691 (1984).

30. R.L. Whetten, G.S. Reza, and E.R. Grant, *Ann. Rev. Phys. Chem.*, **36**, 277 (1985).

31. R.Y. Chiao and Y.S. Wu, *Phys. Rev. Lett.*, **57**, 933 (1986).

32. G. Delacrétaz, E.R. Grant, R.L. Whetten, L. Wöste and J.W. Zwanziger, *Phys. Rev. Lett.*, **24** 2598 (1986).

33. Y. Aharonov and D. Bohm, *Phys. Rev.*, **115** 485 (1959).

34. C.A. Mead, *Chem. Phys.* **49**, 23 (1980).

35. L.M. Delves, *Nucl. Phys.*, **9** 391 (1959).

36. L.M. Delves, *Nucl. Phys.*, **20** 275 (1960).

37. R. De Vogelaere, *J. Res. Natl. Bur. Std.*, **54**, 119 (1955).

38. A.S. Davydov, *Quantum Mechanics* 2nd ed. (Pergamon Press, Oxford, 1976) pp. 151–161.

39. W. Zickendraht, *Ann. Phys.*, **35**, 18 (1965).

40. H. Mayer, *J. Phys.*, **A 8**, 1562 (1975).

41. L. Wolniewicz, *J. Chem. Phys.* **90**, 371 (1989).

42. A. Kuppermann, *Chem. Phys. Lett.* **32**, 374 (1975).

43. J. Tennyson and B.T. Sutcliffe, *Mol. Phys.*, **51**, 887 (1984).

44. E. Bright Wilson, J.C. Decius and P.C. Cross, *Molecular Vibrations* (Dover, New York, 1980) pp. 17.

45. J.M. Launay and B. Lepetit, *Chem. Phys. Lett.* **144**, 346 (1988).

46. B. Lepetit and J.M. Launay, *Chem. Phys. Lett.* **151**, 287 (1988).

47. E. Bright Wilson, J.C. Decius and P.C. Cross, *Molecular Vibrations* (Dover, New York, 1980) ch. 11.

48. S. Flügge, *Practical Quantum Mechanics* (Springer, New York, 1974) Problem 42.

49. B. Lepetit, Z. Peng and A. Kuppermann, *Chem. Phys. Lett.* **166**, 572 (1990).

50. C.A. Mead, *J. Chem. Phys.* **72**, 3839 (1980).

51. B. Lepetit and A. Kuppermann, *Chem. Phys. Lett.* **166**, 581 (1990).

5.6. Tables

Table 1

Effect of permutations of the nuclei on the angle φ_λ.

Permutation	$P_{\lambda\nu\kappa}{}^a$	$P_{\nu\kappa\lambda}{}^b$	$P_{\kappa\lambda\nu}{}^c$	$P_{\nu\kappa}{}^d$	$P_{\lambda\nu}{}^d$	$P_{\lambda\kappa}{}^d$
Value of $\varphi_\lambda{}^e$	φ_λ	$\varphi_\lambda + \frac{2\pi}{3}$	$\varphi_\lambda + \frac{4\pi}{3}$	$2\pi - \varphi_\lambda$	$\frac{2\pi}{3} - \varphi_\lambda$	$\frac{4\pi}{3} - \varphi_\lambda$
$\sin(3m + \frac{3}{2})\varphi_\lambda$	1	-1	1	1	1	-1
$\cos(3m + \frac{3}{2})\varphi_\lambda$	1	-1	1	1	-1	1
$\lvert \psi_e^- \rangle$	1	-1	1	-1	-1	1
$\lvert \psi_e^+ \rangle$	1	-1	1	1	1	-1

a. $P_{\lambda\nu\kappa}$ is the identity permutation.

b. $P_{\nu\kappa\lambda}$ refers to the cyclic permutation $\lambda\nu\kappa \longrightarrow \nu\kappa\lambda$.

c. $P_{\kappa\lambda\nu}$ refers to the cyclic permutation $\lambda\nu\kappa \longrightarrow \kappa\lambda\nu$.

d. P_{ij} refers to the pairwise permutation of nuclei i and j.

e. The changes in φ_λ are true modulo 2π, since φ_λ must remain in the range $[0,2\pi]$.

Table 2

Choice of n_φ for each parity Π and irreducible representation Γ of the nuclear permutation group P_3.

Π	Γ [c]	n_φ [d]
Even[a]	A_1/A_2	$3m$
Odd[a]	E	$3m \pm 1$
Even[b]	A_1/A_2	$3m + \frac{3}{2}$
Odd[b]	E	$3m \pm \frac{1}{2}$

a. without consideration of the geometric phase due to the conical intersection.

b. with consideration of the geometric phase due to the conical intersection.

c. Γ is the irreducible representation of P_3 to which the combined electro-nuclear wave-function $\Psi^{JM\Pi\Gamma}$ belongs.

d. n_φ is a non–negative integer or half of an odd integer.

Table 3

Optimized parameters for the Morse-like functions in R'_λ and r'_λ.

Coordinate	$D_e(au)$ [a]	$\omega_e(au)$ [a]	$r_e(au)$ [a]
R'_λ	0.230 0.262	0.0130 0.0100	1.96 2.01
r'_λ	0.262 0.232	0.0122 0.0102	2.09 2.32

a. These parameters are defined in Eqs. (24) to (29) of chapter 4.

Table 4

Bound state energies

without inclusion of the geometric phase effect[a].

$v_1 v_2 l^b$	$J = 0^c$			$J = 1$ even parity^c			$J = 1$ odd parity^c		
0 0 0	3.7210	A_1	3.7218	3.7282	A_2	3.7294	3.7264	E	3.7276
1 0 0	3.9216	A_1	3.9223	3.9284	A_2	3.9297	3.9266	E	3.9281
2 0 0	4.1067	A_1	4.1073	4.1130	A_2	4.1145	4.1114	E	4.1131
3 0 0	4.2759	A_1	4.2766	4.2817	A_2	4.2839	4.2802	E	4.2831
4 0 0	4.4282	A_1	4.4301	4.4336	A_2	4.4386	4.4322	E	4.4398
5 0 0	4.5621	A_1	4.5734	4.5665	A_2	4.5803	4.5656	E	4.5894
0 1 1	4.2886	E	4.2886	4.2955	E	4.2956	4.2971	A_1	4.2975
							4.2969	A_2	4.2972
							4.2904	E	4.2908
1 1 1	4.4533	E	4.4533	4.4596	E	4.4598	4.4610	A_1	4.4618
							4.4608	A_2	4.4615
							4.4550	E	4.4557
2 1 1	4.5980	E	4.5983	4.6036	E	4.6048	4.6049	A_1	4.6083
							4.6047	A_2	4.6093
							4.5996	E	4.6028
3 1 1	4.7212	E		4.7261	E	4.7349	4.7272	A_1	4.7370
							4.7270	A_2	4.7355
							4.7225	E	
0 2 0	4.6806	A_1	4.6813	4.6871	A_2	4.6893	4.6842	E	4.6878

a. The energy is in eV and its origin corresponds to the bottom of the ground electronic state of the isolated H_2 molecule. The symmetry assignments are for the nuclear spacial wave-functions only.

b. Quantum numbers used to classify the states (see text).

c. The left column gives the hyperspherical method results and the right column the TS method results. The central column gives the irreducible representation of the permutation group of the nuclei to which the spatial part of the nuclear wavefunction belongs.

Table 5

Hyperspherical method bound state energies with the inclusion of the geometric phase effect[a,b].

$v_1 v_2 l$ [c]	$J = 0$	$J = 1$ even parity	$J = 1$ odd parity
$0\ \frac{1}{2}\ \frac{1}{2}$	4.0215 (E)	4.0286 (E)	4.0256 $(A_1)^d$ 4.0243 (A_2) 4.0284 (E)
$1\ \frac{1}{2}\ \frac{1}{2}$	4.2049 (E)	4.2114 (E)	4.2087 $(A_1)^d$ 4.2076 (A_2) 4.2113 (E)
$2\ \frac{1}{2}\ \frac{1}{2}$	4.3710 (E)	4.3769 (E)	4.3744 $(A_1)^d$ 4.3734 (A_2) 4.3768 (E)
$3\ \frac{1}{2}\ \frac{1}{2}$	4.5189 (E)	4.5243 (E)	4.5220 $(A_1)^d$ 4.5210 (A_2) 4.5241 (E)
$4\ \frac{1}{2}\ \frac{1}{2}$	4.6468 (E)	4.6517 (E)	4.6496 $(A_1)^d$ 4.6487 (A_2) 4.6515 (E)
$0\ \frac{3}{2}\ \frac{3}{2}$	4.5005 $(A_1)^d$ 4.5700 (A_2)	4.5071 (A_2) 4.5768 $(A_1)^d$	4.5050 (E) 4.5753 (E)
$1\ \frac{3}{2}\ \frac{3}{2}$	4.6425 $(A_1)^d$ 4.7177 (A_2)	4.6484 (A_2) 4.7237 $(A_1)^d$	4.6466 (E) 4.7223 (E)

a. The energy is in eV and its origin corresponds to the bottom of the ground electronic state of the isolated H_2 molecule.

b. The irreducible representations are the ones for the permutation group of the nuclei to which the combined electro-nuclear wave-function $\Psi^{JM\Pi\Gamma}$ belongs.

c. Quantum numbers used to classify the states (see text).

d. Levels with A_1 symmetry are included for completeness, but are forbidden by the Pauli principle.

5.7. Figures and captions

Fig. 1. Equipotential contours of the DMBE first electronically excited state potential energy surface in symmetrized hyperspherical coordinates[42] for Z_λ = 0 bohr. In the corresponding internal configuration space, the coordinates $(\rho, \theta, \varphi_\lambda)$ defined in the text correspond to spherical polar coordinates with respect to the Y_λ axis. This axis is also the one along which the excited DMBE potential conically intersects the lower one. The origin of energy is chosen to be that of the minimum of the $H_2(X\ ^1\Sigma_g^+)$ potential energy curve. The equipotentials are equally spaced by 0.25 eV in the range [3.0 eV, 5.0 eV]. The contours for 3.0 eV and 4.0 eV are specifically indicated. Along constant Y_λ lines, the surface shows the usual "vee"–shaped behavior characteristic of conical intersections. The approximate constancy of the X_λ–spacing between the equipotentials in this figure is a manifestation of this linear variation. Equipotentials on cuts along other planes containing the Y_λ axis, in the vicinity of this axis, are very similar to the ones displayed in this figure, i.e., the surface has a local nearly cylindrical symmetry around Y_λ.

Fig. 2. DMBE potential energy curve along the Y_λ axis (equilateral triangle geometry). Along this axis, $Y_\lambda = \rho$. The coordinates are the those defined in Fig. 1. The energy curve has its minimum at Y_λ = 2.6 bohr. The origin of energy is that of Fig. 1.

Fig. 3. Equipotential contours of the DMBE excited electronic potential energy surface for Y_λ = 2.6 bohr. See caption to Fig. 1 for other details. The equipotentials are equally spaced in energy by 0.5 eV in the range [3.0 eV,

6.0 eV], with the innermost one corresponding to 3.0 eV. It clearly displays the quasi-cylindrical symmetry around the Y_λ axis.

Fig. 4. DMBE potential energies for $Y_\lambda = 2.6$ bohr and $Z_\lambda = 0.0$ bohr in symmetrized hyperspherical coordinates[42]. E_1^{DMBE} is the DMBE potential energy for the ground state of H_3 and E_2^{DMBE} is that for the first excited state. The origin of energy is the one defined in the caption for Fig. 1. The conical intersection between E_1^{DMBE} and E_2^{DMBE} can be clearly seen at $X_\lambda = 0$.

Fig. 5. DMBE potential energies for $Y_\lambda = 2.6$ bohr and $Z_\lambda = 0.0$ bohr. See caption to Fig. 4 for other details.

Fig. 6. Ro-vibronic energy levels associated with the first electronically excited state of H_3. The full lines are the levels including the effect of the geometric phase while the dashed ones exclude that effect. The quantum numbers v_1, v_2 and l are defined in the text. The origin for the energy scale is the bottom of the isolated ground electronic H_2 potential energy curve. These levels are for the $J = 0$ states, but the $J = 1$ levels are nearly degenerate with them, the splitting being of the order of 10^{-2} eV. Their nuclear permutation symmetries depend on J and on the parity Π, as well as whether the geometric phase is or is not included (see Tables 4 and 5). There are two levels for each of the sets of quantum numbers $(v_1 = 0, v_2 = l = \frac{3}{2})$ and $(v_1 = 1, v_2 = l = \frac{3}{2})$, which would be degenerate if the potential were exactly cylindrically symmetric around the Y_λ axis (see text and Figs. 1 and 3).

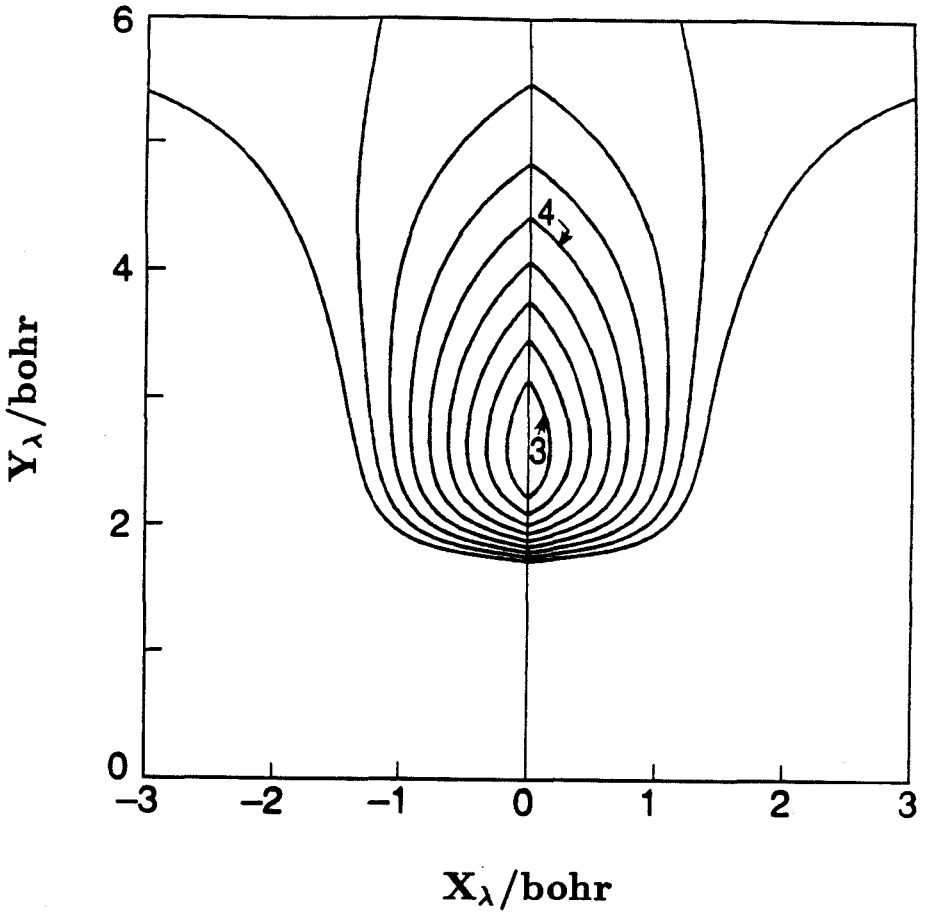

Fig. 1

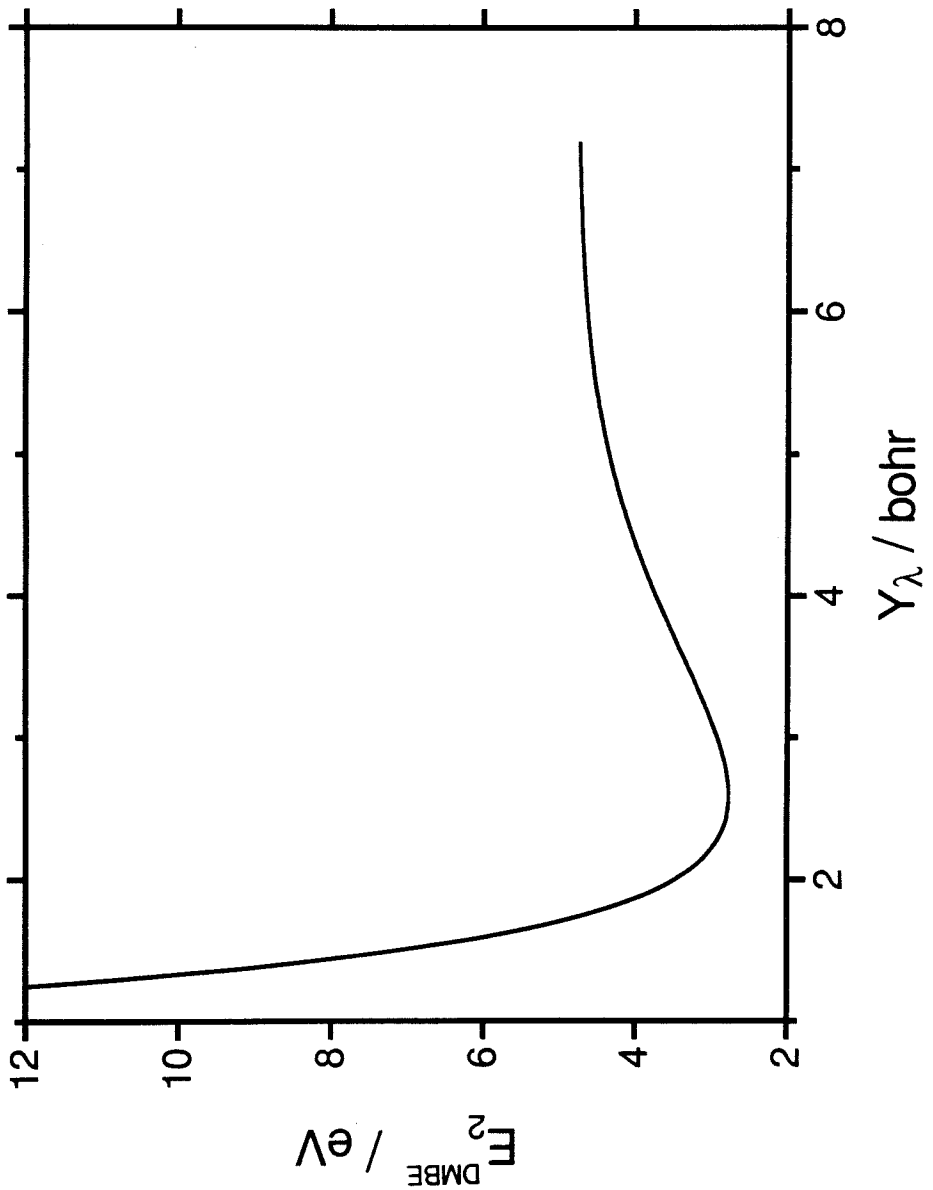

Fig. 2

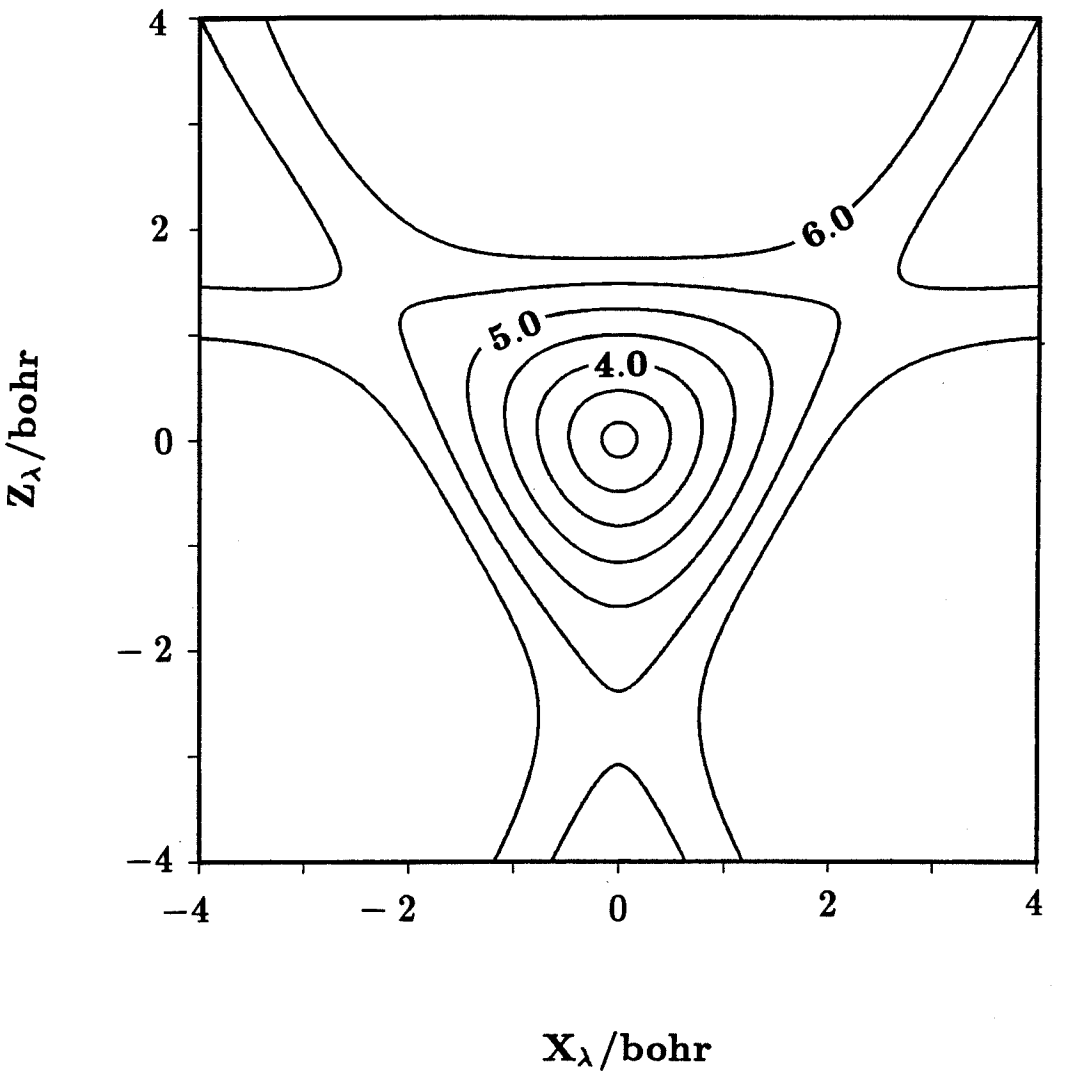

Fig. 3

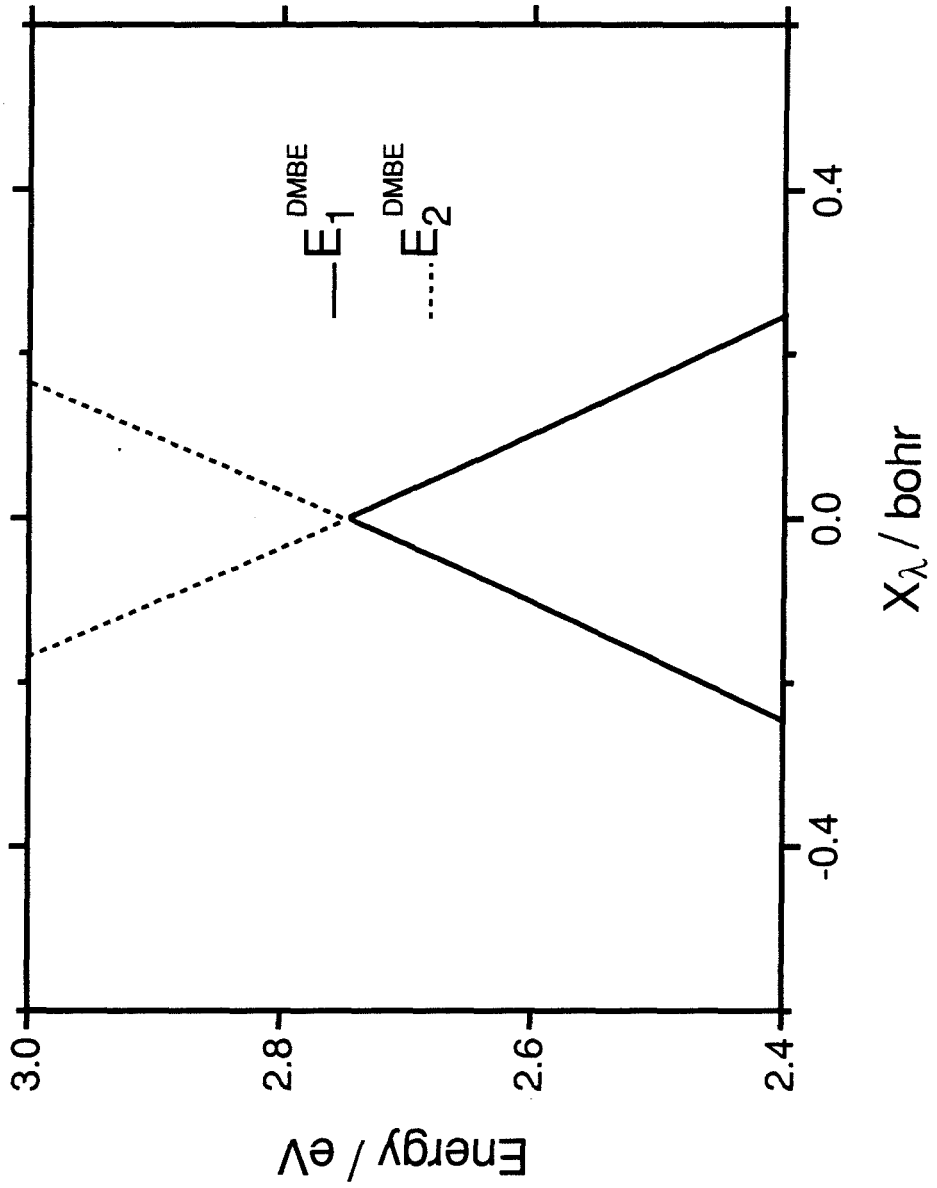

Fig. 4

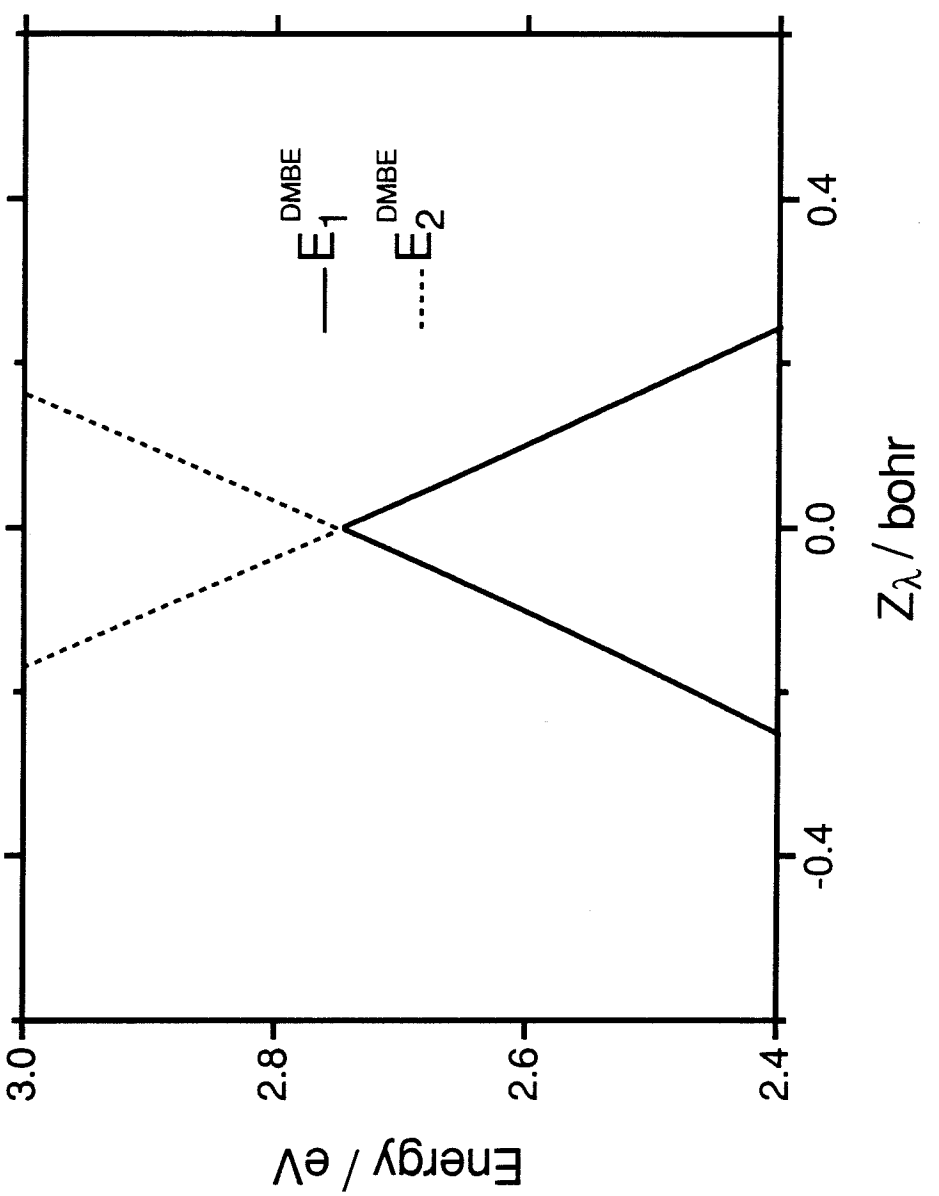

Fig. 5

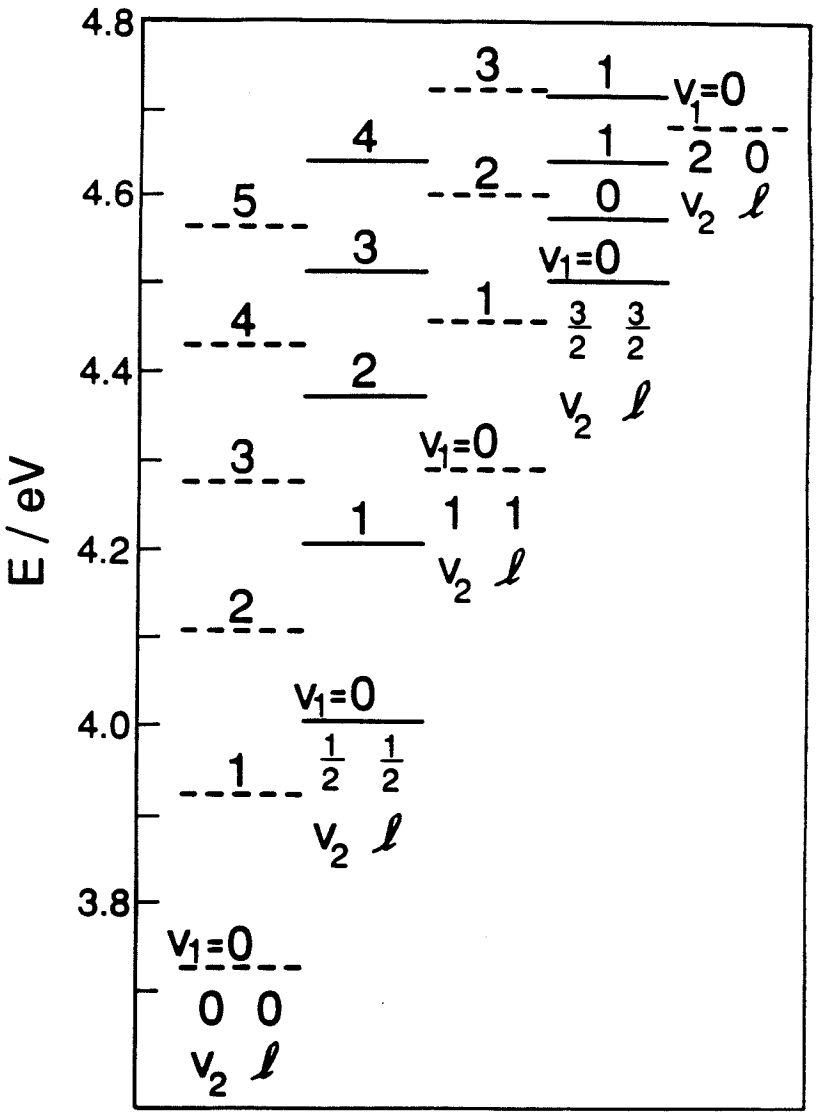
4.8
4.6
4.4
4.2
4.0
3.8
E / eV
3
1
v1=0
4
1
2 0
2
0
v2 ℓ
5
3
v1=0
1
3/2 3/2
4
2
v2 ℓ
v1=0
3
1 1
1
v2 ℓ
2
v1=0
1/2 1/2
1
v2 ℓ
v1=0
0 0
v2 ℓ

Fig. 6

Chapter 6

Ro-vibrational Bound States for the $2p_z\ ^2A_2''$ Electronic State of H_3

6.1. Introduction

In chapter 3, we have obtained a rotated Morse cubic-curve spline (RMCS) potential energy surface for H_3 in the $2p_z\ ^2A_2''$ electronic state from *ab initio* quantum calculations. In order to address the accuracy of this surface, as Carter and Handy pointed out[1], the best way is to obtain the ro-vibrational structure of the nuclear motion supported by this potential energy surface, and then compare it with experimental results of high-resolution spectroscopy. In this chapter, the calculation of the ro-vibrational bound states on the RMCS potential energy surface for the $2p_z\ ^2A_2''$ electronic state of H_3 is presented. The calculated ro-vibrational energy levels are compared with those obtained from experiment and several suggestions are presented for the improvement of the surface.

Since the potential energy surface of H_3 in its ground electronic state does not support bound ro-vibrational states of nuclear motion[2,3], the first observation of its Rydberg state emission spectra by Herzberg[4] inspired a lot of activity, both of an experimental[5-12] and theoretical[13-21] nature. Among the low-lying Rydberg electronic states, the $2p_z\ ^2A_2''$ state stands out as being long-lived. Gellene and Porter have estimated that its lifetime can be as long as 87 μseconds for those pure vibrational states[10]. Garvey and Kuppermann have observed meta-stable H_3 neutral species in their arc-discharge source with a lifetime longer than 40 μseconds[11], which they attribute to be rotationless H_3 in its $2p_z\ ^2A_2''$ electronic state. Because H_3 molecules in other states tend to

decay through radiation or predissociation channels (or both) in about 10^{-9} seconds or shorter[4-10,13], several μseconds after their generation the only H_3 molecules left would be the ones in this meta-stable rotationless $2p_z\ ^2A_2''$ state. Many experiments are based on this important fact which leads to observations of high excited Rydberg spectra having simple structures[22-31]. Dodhy *et al.* were able to prepare H_3 in a single initial state and observe the zero kelvin Rydberg spectra of H_3[26]. They also discovered that high n Rydberg states can be long-lived, too[26,27]. The lifetime of the radiation decay between $n = 3$ and $n = 2$ Rydberg states has been observed in experiments, and theoretically calculated values[28-29] are in good agreement with those results.

The experimental data on ro-vibrational structure of the H_3 Rydberg states are abundant. In the early experiments of the H_3 Rydberg spectra, the rotation constants in low-lying Rydberg electronic states were determined by Herzberg and co-workers through emission spectroscopy[7-10]. Those rotational constants are very close to those of the H_3^+ ion measured by Oka[32]. This clearly confirms the structure of the Rydberg states of H_3 as an H_3^+ ion core plus a Rydberg electron. Later, in high-resolution photo-excitation experiments, Helm and co-workers[22-25], and Keterlle and co-workers[30-31] were able to obtain the vibrational quanta for both the symmetric and asymmetric modes of H_3 in the $2p_z\ ^2A_2''$ electronic state. The results for the asymmetric vibration mode is 2602 cm^{-1} [22] or 2618.34 cm^{-1} [30]. The result for the symmetric vibration mode is 3255.4 cm^{-1} [25]. More information on Rydberg states of H_3 has been discussed in review articles by Herzberg[33], Gellene and Porter[34], and Watson[35]. From results obtained by himself and co-workers and by Herzberg and co-workers, Helm estimated that the long-lived rotationless ($N = 0$, $K = 0$) ground vibrational level of H_3 in its $2p_z\ ^2A_2''$ electronic state lies 898 cm^{-1} above the $J = 1$, $K = 0$

ground vibrational level of H_3 in its $2s\ ^2A_1'$ electronic state[23]. This leads to an estimate of the lifetime of the $2p_z\ ^2A_2''$ state even longer than those of previous theoretical treatments[11,13,20].

Without the full potential energy surface, the previous theoretical work on the H_3 Rydberg states was only able to obtain partial information about their ro-vibrational structures[13,17,20] After obtaining *ab inito* energy levels of H_3 at several equilateral triangular geometries, the symmetric vibrational quanta can be estimated. The equilibrium distance R_e of the equilateral triangular H_3 can be used to estimate the first rotation constant B_e $(= \hbar^2/2m_H R_e^2)$. Only after the full potential energy surface becomes available can the direct calculation of the ro-vibrational structure be made.

6.2. Method and numerical details

The variational method of Tennyson and Sutcliffe[36] was used in the studies of the ro-vibrational structure of the $2p_z\ ^2A_2''$ electronic state of H_3. An outline of this method has been given in chapter 4. More detail can be found in the original papers of Tennyson and Sutcliffe[36-38].

The potential energy surface of H_3 in its $2p_z\ ^2A_2''$ electronic state we used is the rotated-Morse-spline-fit (RMSF) surface obtained from our *ab initio* calculation of H_3 (see chapter 3). The origin of the potential energy is chosen to be that at the configuration of $2H(1s) + H(2p_z)$. This surface has features similar to the ground electronic state of the H_3^+ ion, with a deep smooth well at the equilateral triangular geometry with an inter-nuclear distance of 1.642 bohr (1.662 bohr for H_3^+[32]). The features of this surface are shown in Figs. 1 and 2. Because of the similarity of the shape of the potential energy surfaces of H_3 in the $2p_z\ ^2A_2''$ electronic state and of H_3^+ ion in its ground electronic state, the variational method of Tennyson and Sutcliffe is believed to be very effective as it has been used for the system of H_3^+ ion in its ground electronic state[37,38]. The $2p_z\ ^2A_2''$ electronic state forms an A_2 representation of the nuclear permutation symmetry, while the ground state of H_3^+ forms an A_1 representation. Since the total electro-nuclear wavefunction has to satisfy the Pauli principle, that is, to be of A_2-type, the ground ro-vibrational state of H_3 in the $2p_z\ ^2A_2''$ electronic state can be a state without any vibrational or rotational excitations (with the total nuclear spin $S = 3/2$), while this state is not allowed for the H_3^+ ion[37,38].

The basis functions we used have the P_2 nuclear permutation symmetry of AB_2-type molecules embedded into them, as discussed in chapter 4 or in the original papers of Tennyson[36]. Again, the calculations with even basis functions

can be separated from the calculations with odd basis functions. The resulting singlet states of even basis functions form A_1 representations of the nuclear permutation symmetry, while the singlet states of odd basis set functions form A_2 representations. If one state of even basis set functions and one state of odd ones are degenerate with each other, then they form a doublet E representation of the nuclear permutation group P_3.

There are two sets of ro-vibrational constants to be calculated, the harmonic vibration quanta (of the symmetric and asymmetric modes), and the rotation constants. Different calculations have been performed with different sets of Morse parameters for the basis sets optimized differently.

For obtaining the vibration frequencies, calculations have been performed with $J = 0$, aimed at obtaining many vibrational excitations. The Morse parameters were obtained by minimizing the 40th vibration state energy with even basis functions. For the case of calculating the rotation constants, several calculations with $J = 0$, 1, 2, 3 wee performed, aimed at obtaining the rotational excitations of the ground vibrational state. The Morse parameters for this case were obtained by minimizing the ground vibrational state energy for $J = 0$ (also with even basis functions). Then the rotation constants can be derived from the analysis of the rotational excitation energies to the rotationless ground vibrational state.

The basis functions were selected by the methods mentioned in chapter 4 using several selection parameters[36]. The size of the basis set ranges from 200 to 1700 depending on what kind of ro-vibrational levels are to be calculated and the value of the total rotational angular momentum J. The major part of the calculation were performed on the Cray X-MP machine in the JPL supercomputing center. The largest memory size needed was about 3.5 MWords.

The longest CPU time used for a ro-vibrational calculation was about 15 minutes, excluding optimization of the basis set.

6.3. Results and discussion

The Morse parameters used in the calculations were first optimized. The first set of optimized parameters was designed to cover many pure vibrational eigenstates with $J = 0$. We followed the same approach used in Tennyson and Sutcliffe's[37,38] work on the H_3^+ ion, which optimized the Morse parameters to minimize the eigenenergy of the 40th eigen-state using even j basis functions. The even j basis set used in our Morse parameter tuning has 448 functions, which is set of medium size. The second set of optimized parameters was designed to minimize the lowest vibrational state with a compact-size basis set. The basis set used in the Morse parameter tuning (with $J = 0$ again) has 200 even j basis functions. The resulting Morse parameters are needed in calculations with $J \geq 1$ to obtain the rotational constants of H_3 in the $2p_z\ ^2A_2''$ electronic state. The details of the Morse parameter optimization can be found in chapter 4 or directly from publications of Tennyson and Sutcliffe[36]. The results were given in Table 1 along with the selection parameters used in the tuning processes.

6.3.1 J=0 pure vibrational states

After the Morse parameters were optimized, the size of the basis set used in $J = 0$ calculations was increased systematically in order to test the convergence of the vibrational energies. The results are shown in Tables 2 and 3. The lower twenty states of even j basis functions are converged to about 1 cm^{-1}. The 40th state is converged to only about 10 cm^{-1}. Comparatively, the resulting eigenenergies with odd j basis functions converged quite well. The lower twenty states are converged to better than 0.5 cm^{-1}. Even the 30th state is converged to about 1 cm^{-1}. We are not sure of the reason for this difference.

Table 4 shows the excitation energies of the lowest twenty states with respect to the ground vibrational state of energy which occurs at -72190.7 cm^{-1} with respect to the H($2p$) + 2H($1s$) state, or 6.0015 eV with respect to the H($1s$) + $H_2(X\ ^1\Sigma_g^+)$ state. The near degeneracy of the even and odd j basis calculations also shows that the degree of convergence for those eigen-states is quite high. The symmetry assignments are straightforward: singlets from calculations of even j basis functions are of A_1-type, singlets from calculation of odd j basis functions are of A_2-type, and a pair of degenerate states, one for even j basis functions and one for odd ones, form an E-type representation of the P_3 nuclear permutation group. The assignments of vibrational quantum numbers using a normal mode analysis are almost the same as those in the study of the H_3^+ ions by Tennyson and Sutcliffe[37,38]. ν_{A_1} is the quantum for the symmetric vibration mode, ν_E is that for the asymmetric vibration mode and l the vibrational-rotational quantum number[39]. For the low-lying states, the assignments are easy and unambiguous. But for higher states, the large anharmonicity and the increasing coupling between normal modes prevented us from giving unambiguous normal mode quantum numbers to them. Because the $2p_z\ ^2A_2''$ electronic state is of A_2-type under the P_3 nuclear permutation symmetry, the A_1-type nuclear spatial functions have to be paired up with A_1-type nuclear spin functions ($S = 3/2$); the E-type nuclear spatial functions paired with E-type spin functions ($S = 1/2$). Since there are no A_2-type spin functions available for H_3, A_2-type ro-vibrational states are not allowed. That is, the statistical weights for A_1, E and A_2-type eigen-states in Table 4 are 4:2:0.

The first ro-vibrational excited state is an E state that corresponds to a single excitation of the asymmetric vibration mode of $H_3(2p_z\ ^2A_2'')$. The second excited state is an A_1 state, which is the lowest excitation in the symmetric

vibration mode of $H_3(2p_z\ ^2A_2'')$. They gave $\nu_E = 2533\ cm^{-1}$ and $\nu_{A_1} = 3227\ cm^{-1}$ for that electronic state. These two values are fairly close to those for the H_3^+ ion in its ground electronic state, for which $\nu_E = 2521.6\ cm^{-1}$ [32] and $\nu_{A_1} = 3178.28\ cm^{-1}$ [30]. As pointed out in section 6.1, the experimental results of those vibration quanta for H_3 are $\nu_E = 2602\ cm^{-1}$ [22], and $\nu_E = 2618.34\ cm^{-1}$ [30], and $\nu_{A_1} = 3255.4\ cm^{-1}$ [25]. Our calculated ν_E is off by 85 cm^{-1} and ν_{A_1} by 28 cm^{-1} from the experimental values. The agreement is only moderate. Since the method of Tennyson and Sutcliffe is a reliable one, especially for lower-lying ro-vibrational states, the source of error could only be the inaccuracy of the potential energy surface. The potential energy surface seems to be flatter around the bottom of its well than the accurate surface. This agrees with the discussion in chapter 3 about the problems associated with the rotated Morse cubic-curve spline (RMCS) fit procedure of representing our *ab initio* calculation. We conclude that the potential energy surface of H_3 in the $2p_z\ ^2A_2''$ electronic state although reasonable, still needs to be improved.

6.3.2 Rotational constants of H_3 in the $2p_z\ ^2A_2''$ electronic state.

In order to obtain the rotational constants of H_3 in the $2p_z\ ^2A_2''$ electronic state, we have calculated rotational excitations of the ground vibrational state. Since the size of the basis functions needed for $J \geq 1$ is proportional to $J(J+1)$, the second set of optimized Morse parameters, aimed at obtaining well-converged low-lying states with a basis set of moderate size, were used. The results of $J = 0, 1, 2, 3$ are shown in Table 5.

If the coupling between rotation and vibration is neglected, the degeneracy of the ground vibrational state would be of $(2J+1)$-fold. This point is demonstrated in Table 5 by those $2J+1$ closely spaced rotational eigenstates. Because of the

coupling between rotation and vibration, the degeneracy has been lifted. The E state degeneracy due to nuclear permutation symmetry is still being satisfied by the eigenstates with total rotation angular momentum $J \geq 1$. The rotational excitation energies with respect to the $J = 0$ ground vibrational state are listed in Table 6. The quantum number K is the projection of the total rotational angular momentum J along the axis perpendicular to the plane of the H_3 molecule, which is used as a conventional symmetric-top label[40]. Using the well known perturbation-type formulas[41]:

$$\begin{aligned} F(J,K) =& B_e J(J+1) - (B_e - C_e)K^2 - D_J J^2(J+1)^2 \\ & - D_{JK} J(J+1)K^2 - D_K K^4 + ..., \end{aligned} \tag{1}$$

we were able to fit the rotational levels using a least-square fitting method and obtain the rotational constants. The results of the five-parameter, fifteen-point fitting are listed in Table 7 along with the experimental values of Dabrowski and Herzberg[7] and those of Oka[32] for the H_3^+ ion in its ground electronic state. The equilibrium internuclear distance of H_3 is obtained by

$$E(J) = (\hbar^2/2I)J(J+1) = B_e J(J+1) \tag{2}$$

$$I = mR_e^2 \tag{3}$$

where m is the mass of the H atom.

The high degree of similarity between our present results and those of Oka for H_3^+, together with the similarity of the vibrational quanta ν_E and ν_{A_1} between the present calculations and that of Oka[32] and Ketterle *et al.*[30] for H_3^+, strongly implies that the potential energy surface of $2p_z\ ^2A_2''$ electronic state has a very similar feature to that of the H_3^+ ground state. This result enhances the picture

of the H_3 $2p_z$ $^2A_2''$ state as a H_3^+ ion core plus a $2p_z$ Rydberg electron, which has a very weak coupling with the motion of the H_3^+ ion core.

The agreement of our results with the experimental ones for $H_3(2p_z\ ^2A_2'')$ from the work by Dabrowski and Herzberg[7] is not as good, but still reasonable. This suggests that the good agreement of our results with the experimental H_3^+ values is somewhat fortuitous. The discrepancy between our calculated ν_{A_1}, ν_E and rotational constants and the corresponding experimental values suggests that the potential energy surface used in this calculation, namely the rotated Morse cubic spline (RMCS) fit to the *ab initio* $2p_z\ ^2A_2''$ surface needs to be improved. In addition, the experimental determination of those rotational constants can also be improved. In the work by Dabrowski and Herzberg[7], only three rotational constants were determined independently. C_e is assumed to be $(1/2)B_e$, which means that the H_3 molecule is taken to be a rigid equilateral triangle without any distortion caused by rotation. D_K is derived from the planarity relation[42] as

$$2D_J + 3D_{JK} + 4D_K = 0. \tag{4}$$

The results for the rotational constants of the H_3^+ ion of Oka[32] and of Tennyson and Sutcliffe[37,38] clearly show that for that species $C_e \neq (1/2)B_e$ which means that the distortion caused by rotation is important and should be taken into consideration. This observation points out a possible limitation in the experimental determination of the rotational constants of H_3 in the $2p_z\ ^2A_2''$ electronic state.

6.4. References

1. S. Carter and N.C. Handy, *Comp. Phys. Report*, **5**, 115-172 (1986).
2. D.G. Truhlar and C.J. Horowitz, *J. Chem. Phys.* **68**, 2457 (1978).
3. A.J.C. Varandas, F.B. Brown, C.A. Mead, D.G. Truhlar and N.C. Blais, *J. Chem. Phys.* **86**, 6258 (1987).
4. H. Herzberg, *J. Chem. Phys.* **70**, 4806 (1979).
5. M. Vogler, *Phys. Rev. A*, **19**, 1 (1979).
6. J.G.K, Watson, *Phys. Rev. A*, **22**, 2279 (1980).
7. I. Dabrowski and G. Herzberg, *Can. J. Phys.*, **58**, 1238 (1980).
8. G. Herzberg and J.G.K. Watson, *Can. J. Phys.*, **58**, 1250 (1980).
9. G. Herzberg, H. Lew, J.J. Sloan, and J.K.G. Watson, *Can. J. Phys.*, **59**, 428 (1981).
10. G. Herzberg, J.T. Hougen, and J.K.G. Watson, *Can. J. Phys.*, **60**, 1261 (1982).
11. G.I. Gellene and R.F. Porter, *J. Chem. Phys.* **79**, 5975 (1983).
12. J.F. Garvey and A. Kuppermann, *Chem. Phys. Lett.* **107**, 491 (1984).
13. H. King and K. Morokuma, *J. Chem. Phys.* **71**, 3213 (1979).
14. M. Jungen, *J. Chem. Phys.* **71**, 3540 (1979).
15. R.L. Martin, *J. Chem. Phys.* **71**, 3541 (1979).
16. K.C. Kulander and M.F. guest, *J. Phys.*, **B 12**, L501 (1979).
17. Ch. Nager and M. Jungen, *Chem. Phys.* **70**, 189 (1982).
18. S. Raynor and D.R. Herschbach, *J. Phys. Chem.*, **86**, 3592 (1982).
19. A.C. Roach and P.J. Kuntz, *J. Chem. Phys.* **84**, 822 (1986).
20. I.D. Petsalakis, G. Theodorakopoulos and J.S. Wright, *J. Chem. Phys.* **89**, 6850 (1988).

21. G.H.F. Diercksen, W. Duch and J. Karwowski, *Chem. Phys. Lett.* **168**, 69 (1990).

22. Hanspeter Helm, *Phy. Rev. Lett.*, **56**, 42 (1986).

23. Hanspeter Helm, *Phy. Rev. A*, **38**, 3425 (1988).

24. Hanspeter Helm, *Phy. Rev. Lett.*, **61**, 298 (1988).

25. H. Helm, L.J. Lembo, P.C. Cosby and D.L. Huestis, "Fundamentals of Laser Interactions,"edited by Ehlotzky, pp. 264-289 (Springer-Verlag, 1989).

26. A. Dodhy, W. Ketterle, H.P. Messmer and H. Walther, *Chem. Phys. Lett.* **151**, 133 (1988).

27. S.F. Selgren and G.I. Gellene, *Chem. Phys. Lett.* **146**, 485 (1988).

28. H. Figger, M.N. Dixit, R. Maier, W. Schrepp, H. Walther, I.R. Peterkin and J.G.K. Watson, *Phys. Rev. Lett.*, **52**, 906 (1984).

29. H. Figger, Y. Fukuda, W. Ketterle and H. Walther, *Can. J. Phys.*, **62**, 1274 (1984).

30. W. Ketterle, H.P. Messmer and H. Walther, *Europhys. Lett.*, **8**, 333 (1989).

31. Wolfgang Ketterle, *Chem. Phys. Lett.* **160**, 139 (1989).

32. T. Oka, *Phys. Rev. Lett.*, **45**. 531 (1980).

33. G. Herzberg, *Ann. Rev. Phys. Chem.*, **38**, 27 (1987).

34. G.I. Gellene and R.F. Porter, *Acc. Chem. Res.*, **23**, 141 (1990).

35. J.K.G. Watson, in press.

36. J. Tennyson, *Comm. Phys. Report*, **4**, 1 (1986).

37. J. Tennyson and B.T. Sutcliffe, *Mol. Phys.* **51**, 887 (1984).

38. J. Tennyson and B.T. Sutcliffe, *J. Chem. Soc., Faraday Trans. 2*, **82**, 1151 (1986).

39. E.B. Wilson, J.C. Decius and P.C. Cross, *Molecular Vibrations*, (Dover, New York, 1980) Chap. 11.

40. G. Herzberg, *Molecular Spectra and Molecular Structure II. Infrared and Raman Spectra of Polyatomic Molecules*, (Van Nostrans, 1945), Chap. 1.

41. Z.I. Slawsky and D.M. Dennison, *J. Chem. Phys.* **7**, 509 (1939).

42. J.M. Dowling, *J. Mol. Spectrosc.*, **6**, 550 (1961).

43. A. Kuppermann, *Chem. Phys. Lett.* **32**, 374 (1975).

44. W. Meyer and P. Botschwina, *J. Chem. Phys.* **84**, 891 (1986).

6.5. Tables

Table 1

Parameters for the Morse–like functions for H_3 in the $2p_z\ ^2A_2''$ state.

Coordinate	$D_e(a.u.)^a$	$\omega_e(a.u.)^a$	$r_e(a.u.)^a$
r	0.210	0.0110	2.23
R	0.110	0.0087	1.82

Coordinate	$D_e(a.u.)^b$	$\omega_e(a.u.)^b$	$r_e(a.u.)^b$
r	0.222	0.0110	2.00
R	0.232	0.0085	1.71

a. Parameters were optimized with respect to the 40th eigenstate of the even j basis calculation. Selection parameters were $N_{max} = 1$, $M_m = N_n = 7$, $L_j = 12$ and $N_{basis} = 448$. This set of parameters was used in the $J = 0$ calculation, aimed at obtaining as many converged eigenstates as possible.

b. Parameters were optimized with respect to the ground state of the even j basis calculation. Selection parameters were $N_{max} = 1$, $M_m = N_n = 4$, $L_j = 14$ and $N_{basis} = 200$. This set of parameters was used in the $J \geq 1$ calculations, aimed at providing a compact basis set for the lower states.

Table 2

Convergence test for H_3 in the $2p_z\ ^2A_2''$ state[a]

for $J = 0$ and j even

Lable of states[b]	Basis One[c]	Basis Two[d]	Basis Three[e]	Basis Four[f]
1	-0.721900	-0.721904	-0.721896	-0.721907
2	-0.696549	-0.696560	-0.696568	-0.696570
3	-0.689597	-0.689615	-0.689614	-0.689634
4	-0.675153	-0.675168	-0.675165	-0.675170
5	-0.671896	-0.671931	-0.671942	-0.671944
6	-0.665511	-0.665528	-0.665541	-0.665544
7	-0.658231	-0.658258	-0.658274	-0.658295
8	-0.652150	-0.652255	-0.652275	-0.652276
9	-0.658586	-0.648775	-0.648780	-0.648786
10	-0.644338	-0.644391	-0.644399	-0.644402
11	-0.642298	-0.642352	-0.642373	-0.642377
12	-0.635404	-0.635463	-0.635485	-0.635487
13	-0.631148	-0.631386	-0.631403	-0.631411
14	-0.629628	-0.630136	-0.630171	-0.630189
15	-0.627765	-0.627809	-0.627847	-0.627867
16	-0.624234	-0.624786	-0.634809	-0.624815
17	-0.621175	-0.621473	-0.621508	-0.621510
18	-0.620613	-0.620981	-0.620999	-0.621010
19	-0.614996	-0.615135	-0.615163	-0.615169
20	-0.613629	-0.613738	-0.613773	-0.613780
40	-0.577015	-0.577461	-0.577614	-0.577709

a. The numbers in this table are the vibrational energies in 10^5 cm^{-1}. The origin of energy is that of the H($2p_z$) + 2H($1s$) state. The energy of the bottom of the $2p_z\ ^2A_2''$ well is -0.770737×10^5 cm^{-1}.

b. The states are numbered in the order of increasing energy.

c. $N_{max} = 1$, $M_m = N_n = 7$, $L_j = 12$ and N_{basis}=448.

d. $N_{max} = 1$, $M_m = 7$, $N_n = 10$, $L_j = 18$ and N_{basis}=880.

e. $N_{max} = 1$, $M_m = N_n = 10$, $L_j = 18$ and N_{basis}=1184.

f. $N_{max} = 1$, $M_m = N_n = 11$, $L_j = 22$ and N_{basis}=1695.

Table 3

Convergence test for H_3 in the $2p_z\ ^2A_2''$ state[a] for $J = 0$ and j odd

Lable of state[b]	Basis One[c]	Basis Two[d]	Basis Three[e]	Basis Four[f]
1	-0.696571	-0.696574	-0.696577	-0.696575
2	-0.671934	-0.671945	-0.671951	-0.671950
3	-0.665538	-0.665542	-0.665548	-0.665548
4	-0.652267	-0.652275	-0.652279	-0.652279
5	-0.646755	-0.646785	-0.646798	-0.646798
6	-0.642337	-0.642371	-0.642383	-0.642382
7	-0.635468	-0.635477	-0.635492	-0.635493
8	-0.630076	-0.630196	-0.630207	-0.630206
9	-0.624758	-0.624799	-0.624821	-0.624820
10	-0.621394	-0.621498	-0.621513	-0.621513
11	-0.618403	-0.618477	-0.618504	-0.618505
12	-0.613668	-0.613767	-0.613788	-0.613789
13	-0.611207	-0.611350	-0.611356	-0.611355
14	-0.606337	-0.606370	-0.606400	-0.606399
15	-0.605687	-0.605930	-0.605961	-0.605962
16	-0.603375	-0.603732	-0.603764	-0.603764
17	-0.598882	-0.599085	-0.599124	-0.599125
18	-0.597045	-0.597385	-0.597431	-0.597432
19	-0.594060	-0.594234	-0.594256	-0.594256
20	-0.592599	-0.592960	-0.592980	-0.592981
30	-0.573086	-0.573545	-0.573646	-0.573655

a. The numbers in this table are the vibrational energies in 10^5 cm^{-1}. The origin of energy is that of the H($2p_z$) + 2H($1s$) state. The energy of the bottom of the $2p_z\ ^2A_2''$ well is -0.770737×10^5 cm^{-1}.

b. The states are numbered in the order of increasing energy.

c. $N_{max} = 1$, $M_m = N_n = 7$, $L_j = 13$ and N_{basis}=448.

d. $N_{max} = 1$, $M_m = 7$, $N_n = 10$, $L_j = 19$ and N_{basis}=880.

e. $N_{max} = 1$, $M_m = N_n = 10$, $L_j = 19$ and N_{basis}=1184.

f. $N_{max} = 1$, $M_m = N_n = 11$, $L_j = 21$ and N_{basis}=1555.

Table 4

Vibrational ($J = 0$) energies[a] of H_3 in the $2p_z\ ^2A_2''$ state

(ν_{A_1}, ν_E, l)	even j[b]	Symmetry	odd j[c]
0,0,0	0.0000	A_1	
0,1,1	2533.7	E	2533.2
1,0,0	3227.3	A_1	
0,2,0	4673.7	A_1	
0,2,2	4996.3	E	4995.7
1,1,1	5636.3	E	5635.9
2,0,0	6361.2	A_1	
0,3,1	6963.1	E	6962.8
0,3,3	7312.1	A_1	
0,3,3		A_2	7510.9[d]
1,2,0	7750.5	A_1	
1,2,2	7953.0	E	7952.5
2,1,1	8642.0	E	8641.4
	9049.6	A_1	
	9171.8	E	9170.1
	9404.0	A_1	
	9709.2	E	9708.7
	10039.7	E	10039.4
	10089.6	A_1	
	10673.8	A_1	
	10812.7	E	10811.8

a. In cm^{-1}. The origin of energy is the calculated ground $J = 0$ vibrational state.

b. Even j basis with $N_{max} = 1$, $M_m = N_N = 11$, $L_j = 22$ and $N_{basis} = 1695$.

c. Odd j basis with $N_{max} = 1$, $M_m = N_N = 11$, $L_j = 21$ and $N_{basis} = 1555$.

d. Although A_2 states are not allowed (see text), this energy is given for completion.

Table 5

Eigenstates and eigenenergies[a] of H_3 in the $2p_z\ ^2A_2''$ electronic state.

$J = 0$ with even parity

even j basis $N_{basis} = 392$	symmetry	
-0.721913	A_1	

$J = 1$ with odd parity

even j basis $N_{basis} = 735$	symmetry	odd j basis $N_{basis} = 784$
-0.721274	E	-0.721277

$J = 1$ with even parity

	symmetry	odd j basis $N_{basis} = 392$
	A_2	-0.721049

$J = 2$ with even parity

even j basis N_{basis} =1078	symmetry	odd j basis N_{basis} =1127
-0.720226	E	-0.720228
-0.719324	A_1	

$J = 2$ with odd parity

even j basis $N_{basis} = 686$	symmetry	odd j basis $N_{basis} = 735$
-0.719549	E	-0.719550

$J = 3$ with even parity

even j basis $N_{basis} = 980$	symmetry	odd j basis $N_{basis} = 1078$
-0.717648	E	-0.717650
	A_2	-0.716765

$J = 3$ with odd parity

even j basis N_{basis} =1372	symmetry	odd j basis N_{basis} =1470
-0.718770	E	-0.718773
-0.716982	E	-0.716986

a. in 10^5 cm^{-1}. The selection parameters were $N_{max} = 1$, $M_m = N_N = 6$, $L_j \leq 15$.

Table 6

Low-lying rotational energies[a]

of H_3 in the $2p_z\ ^2A_2''$ electronic state.

J	$\mid K \mid$	even j		odd j
0	0	0.00	A_1	
1	1	63.9	E	63.6
	0		A_2	86.3
2	2	168.7	E	168.5
	1	236.4	E	236.3
	0	258.9	A_1	
3	3	314.3	E	314.0
	2	426.5	E	426.3
	1	493.1	E	492.7
	0		A_2	514.8

a. in cm^{-1}. The origin of energy is that of the $J = 0$ state calculated to lie 6.0015 eV above the $H(1s) + H_2(X\ ^2\Sigma_g^+)$ state.

Table 7

Rotational constants of H_3 in the $2p_x\ ^2A_2''$ electronic state.

Rotational constant	This work	Experiment[a] (H_3)	Experiment[b] (H_3^+)
$B_e(cm^{-1})$	43.36	44.530	43.57
$C_e(cm^{-1})$	20.51	22.266	20.71
$D_J(cm^{-1})$	0.038	0.0539	0.05
$D_{JK}(cm^{-1})$	-0.074	-0.0909	-0.100
$D_K(cm^{-1})$	0.038	0.0412	0.04
R_e(bohr)	1.666[c] 1.642[d]	1.638	1.662[e] 1.65[f]

a. Dabrowski and Herzberg, see ref. 7.

b. Oka, see ref. 32 (ground electronic state of H_3^+).

c. Position of minimum of the E_4 potential energy surface calculated from the rotational constants.

d. Position of minimum of the E_4 RMCS potential energy surface.

e. Position of minimum of the ground state surface of H_3^+ calculated from the rotational constants.

f. Position of minimum of the ground state surface of H_3^+ from *ab initio* calculation (see ref. 44).

6.6. Figures and captions

Fig. 1. Potential energy curve of $H_3(2p_z\ ^2A_2'')$ for equilateral geometries. The surface is the RMCS fit to the *ab initio* calculation of E_4. R is the internuclear distance. The origin of energy is chosen to be that of the minimum of the $H_2(X\ ^1\Sigma_g^+)$ potential energy curve. The bottom of the present potential well is located at $R = 1.64$ bohr.

Fig. 2. Two-dimensional equipotential contour plots of the E_4 RMCS potential energy surface in hyperspherical coordinates[43] with $Y_\lambda = 2.16$ bohr. The contour energies are in the range [5.5 eV, 10.0 eV] with increments of 0.5 eV. The energy origin is the one defined in the caption for Fig. 1.

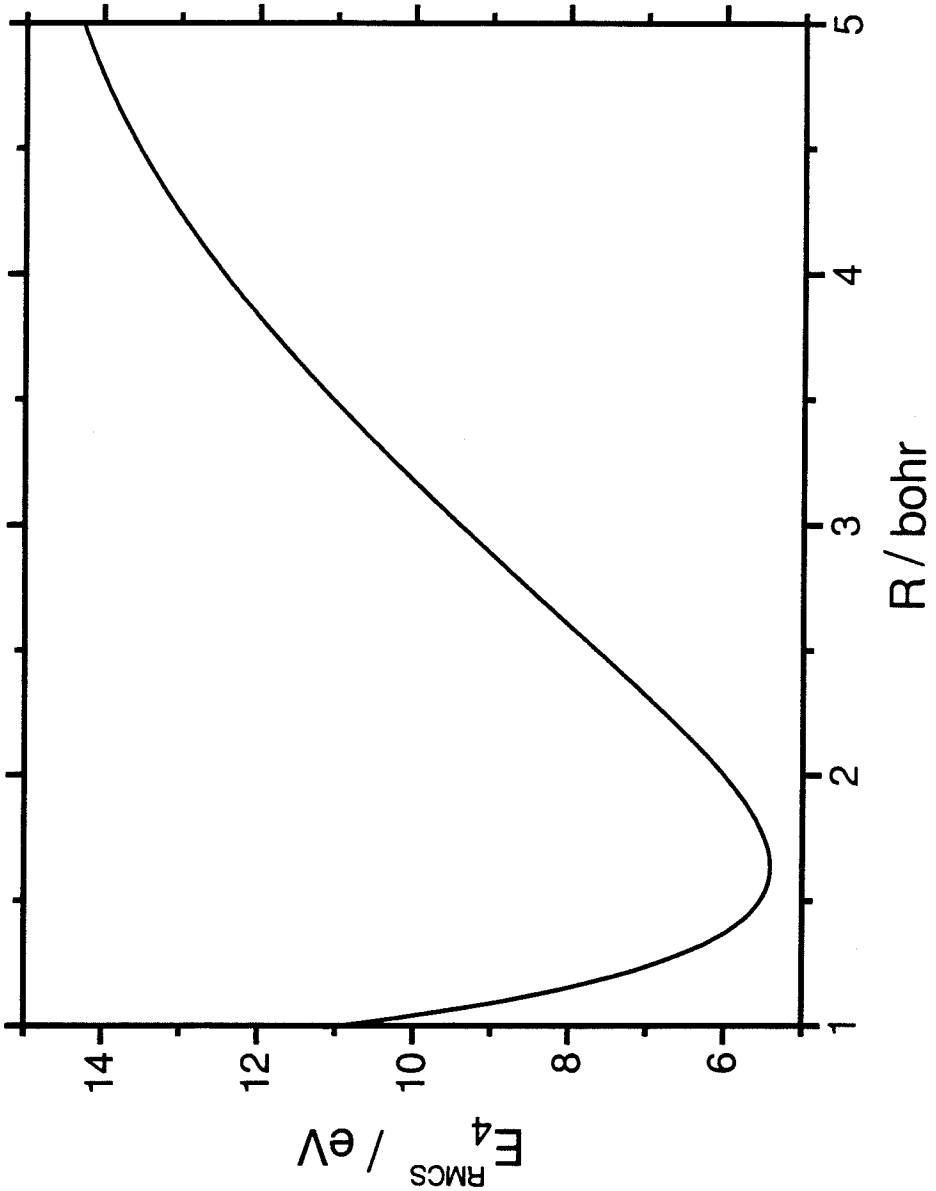

Fig. 1

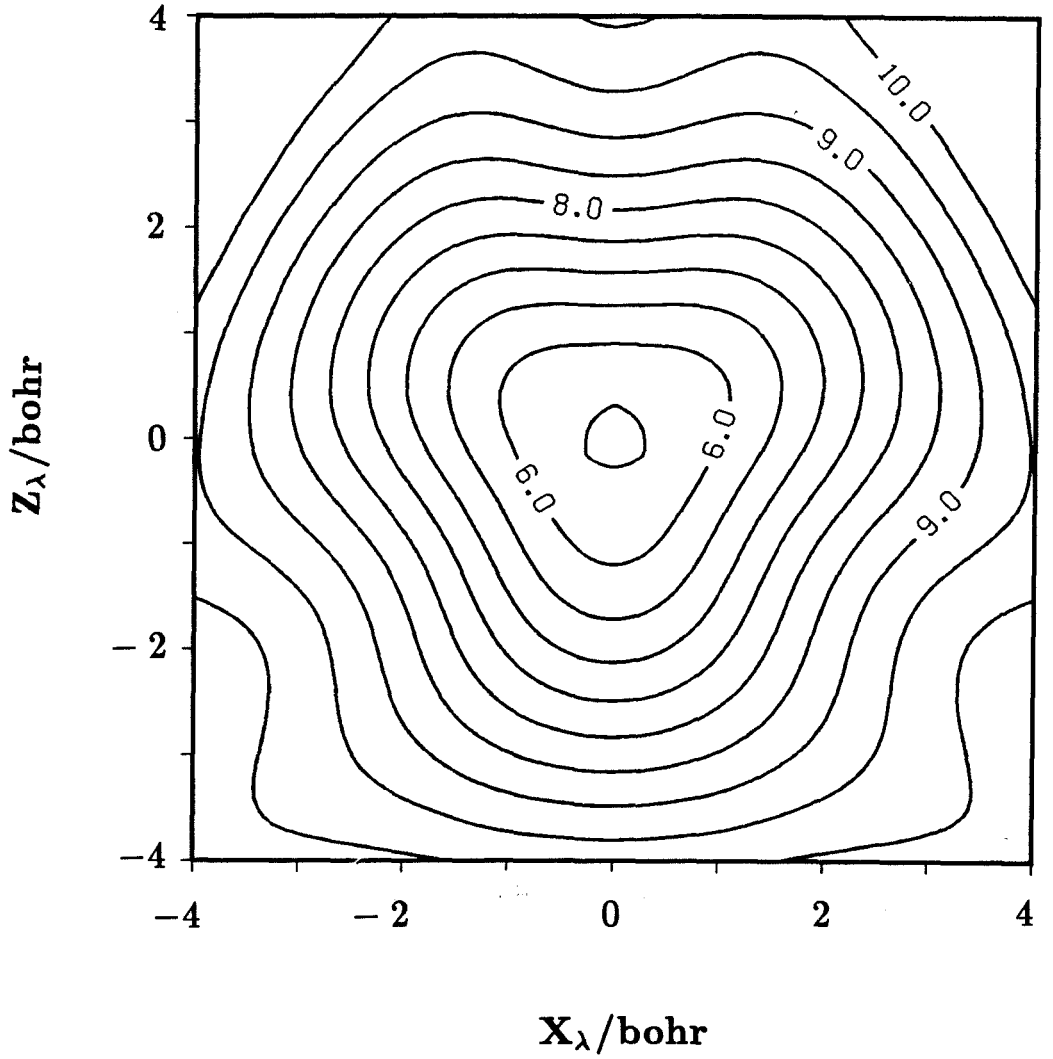

Fig. 2

Chapter 7

Summary

We have conducted an *ab initio* quantum study of first four electronic states of the H_3 system and of the nuclear motions in the second and fourth of these states. The calculated Rydberg spectra compare well with previous theoretical studies and known experimental results. Together, the *ab initio* potential functions for these four states display diverse behavior as functions of nuclear geometry. The results for the ground state and the third excited state have been fitted by the rotated Morse cubic spline (RMCS) method to give two 3-D full potential energy surfaces. They provide the most important step towards understanding the structure and dynamics of these states. The electric dipole transition moments between the lowest four electronic states have also been calculated. They are important for understanding the lifetimes of metastable states, their laser spectroscopy, and the transition state spectroscopy of the ground state of this important system.

The ro-vibrational eigenstates of H_3 on the upper sheet of the Double Many Body Expansion (DMBE) surfaces (in the absence of coupling to the ground state) have been calculated using a variational method and a new hyperspherical coordinate propagation method. The full P_3 nuclear permutation symmetry and the molecular Aharonov-Bohm (MAB) (or geometric phase) effect were included in the hyperspherical propagation method. The MAB effect has a profound influence on the bound ro-vibrational states of that state.

The ro-vibrational bound states of H_3 in the fourth ($2p_z\ ^2A_2''$) surface were also studied. The Rydberg nature of this electronic state leads to ro-vibrational nuclear motion similar to that of the H_3^+ ion. Comparison between the calculated

values of the ro-vibrational constants and the corresponding experimental results suggests that the $2p_z\ ^2A_2''$ RMCS surface still needs some improvement.

Appendix 1. Results of *ab inito* calculations for 560 nuclear geometry configurations

1A. Energies (in hartree) at $\gamma = 60°$ and $\theta = 0°$.

R_1 (bohr)	E_1	E_2	E_3	E_4
1.0	-1.622441	-1.247942	-1.247178	-1.247278
1.1	-1.648230	-1.273649	-1.272642	-1.273006
1.2	-1.663260	-1.288095	-1.288020	-1.288093
1.25	-1.667807	-1.292622	-1.292556	-1.292644
1.28	-1.669714	-1.294869	-1.294348	-1.294625
1.3	-1.670741	-1.295823	-1.295359	-1.295653
1.35	-1.672463	-1.297517	-1.297022	-1.297275
1.4	-1.673032	-1.297611	-1.297573	-1.297869
1.45	-1.672561	-1.297544	-1.297145	-1.297440
1.47	-1.672193	-1.302043	-1.296807	-1.297039
1.5	-1.671380	-1.309243	-1.296058	-1.296284
1.51	-1.671074	-1.311590	-1.295713	-1.295965
1.52	-1.670748	-1.313977	-1.295374	-1.295609
1.55	-1.669569	-1.320523	-1.294221	-1.294429
1.57	-1.668683	-1.324843	-1.293396	-1.293538
1.6	-1.667198	-1.331383	-1.277669	-1.278657
1.8	-1.653720	-1.367800	-1.277669	-1.278657
2.0	-1.636826	-1.396752	-1.263367	-1.261768
2.2	-1.618928	-1.419648	-1.255112	-1.243821

1B. Electric dipole transition moments (in a.u.) at $\gamma = 60°$ and $\theta = 0°$.

R_1 (bohr)	$T_{41}(z)$	$T_{42}(z)$	$T_{43}(z)$	$T_{31}(x)$	$T_{31}(y)$	$T_{32}(x)$	$T_{32}(y)$	$T_{21}(x)$	$T_{21}(y)$
1.0	.740	.269(+1)	.124					.330	-.345(-1)
1.1	.741	.273(+1)	-.179						
1.2	.739	.259(+1)	-.411					.347	.139
1.25	.740	.228(+1)	-.885	-.195	.674	-.108(+1)	.177(+1)	.390	.284
1.28	.740	.243(+1)	.179	-.487(-2)	.731	.102	.242(+1)	.436	-.355(-1)
1.3	.739	.243(+1)	.183	-.527(-2)	.730	.104	.242(+1)	.439	-.358(-1)
1.35	.739	.244(+1)	.187	-.610(-2)	.730	.103	.243(+1)	.435	-.360(-1)
1.4	.738	.233(+1)	.255(-1)					.411	.225
1.45	.738	.244(+1)	.200	-.828(-2)	.728	.104	.243(+1)	.435	-.370(-1)
1.47	.740	-.274(+1)	-.183	.117(-1)	-.726	-.209(-2)	.393(-2)	.365(-3)	-.153(-2)
1.5	.738	-.188(-2)	-.189	.135(-3)	-.725	-.221(-2)	.294(-2)	.163(-3)	-.107(-2)
1.51	.939	.170(-2)	.190	-.130(-3)	.725	-.209(-2)	.275(-2)	.101(-3)	-.983(-3)
1.52	.739	.207(-2)	.190	-.139(-1)	.724	.230(-2)	-.364(-2)	.204(-3)	-.154(-2)
1.55	.739	.161(-2)	.194	-.152(-1)	.723	.215(-2)	-.271(-2)	.253(-4)	.101(-2)
1.57	.739	.130(-2)	.196	-.163(-1)	.722	.208(-2)	-.235(-2)	.944(-4)	.839(-3)
1.6	.736	-.756(-3)	.226(+1)	.369	.288	.981(-3)	-.233(-2)	-.570(-4)	-.502(-3)
1.8	.733	-.479(-3)	.242(+1)	.455	-.273(-1)	-.957(-3)	.240(-2)	-.131(-3)	-.281(-3)
2.0	.733	-.639(-3)	.594					-.261(-3)	-.164(-3)
2.2	.750	-.442(-3)	.406						

2A. Energies (in hartree) at $\gamma = 60°$ and $\theta = 20°$.

R_1 (bohr)	E_1	E_2	E_3	E_4
1.0	-1.622463	-1.248392	-1.247862	-1.248146
1.1	-1.648204	-1.274322	-1.273621	-1.273972
1.2	-1.663356	-1.289569	-1.288836	-1.289150
1.3	-1.670804	-1.297243	-1.296282	-1.296730
1.4	-1.673356	-1.299922	-1.289626	-1.299077
1.45	-1.672646	-1.313609	-1.298147	-1.298755
1.5	-1.671486	-1.311240	-1.298338	-1.297650
1.6	-1.667264	-1.332724	-1.294676	-1.293525
1.7	-1.661236	-1.351681	-1.289250	-1.287598
1.8	-1.653843	-1.368786	-1.283350	-1.280403
1.9	-1.645638	-1.383886	-1.284057	-1.272310
2.0	-1.636950	-1.368786	-1.283857	-1.263874
2.2	-1.618953	-1.420340	-1.280852	-1.246024

2B. Electric dipole transition moments (in a.u.) at $\gamma = 60°$ and $\theta = 20°$.

R_1 (bohr)	$T_{41}(z)$	$T_{42}(z)$	$T_{43}(z)$	$T_{31}(x)$	$T_{31}(y)$	$T_{32}(x)$	$T_{32}(y)$	$T_{21}(x)$	$T_{21}(y)$
1.0	.726	.575	.242(+1)	.408	-.179	.735	.212(+1)	.122	.690
1.1	.724	.182	.248(+1)						
1.2	.721	.360	.245(+1)	.428	-.115				
1.3	.718	-.291	.245(+1)	.436	-.949(-1)	-.433	-.240(+1)	-.617(-1)	-.694
1.4	.713	.259	.246(+1)	.447	-.780(-1)	.372	.239(+1)	.397(-1)	.677
1.45	.714	.305						.599(-1)	.383
1.5	.712	-.743(-1)	-.408	-.892(-1)	-.659	-.767(-1)	.112	-.157(-1)	-.572(-1)
1.6	.702	-.359(-1)							
1.7	.699	-.223(-1)	-.242	-.152(-1)	-.626	-.726(-1)	.272(-1)	-.863(-2)	-.986(-2)
1.8	.686	-.173(-1)	.832					-.830(-2)	-.558(-2)
1.9	.686	-.135(-1)	-.199	-.303	-.208(-1)	.567	.255	-.672(-2)	.384(-2)
2.0	.659	-.123(-1)	.301					.531(-2)	-.322(-2)
2.2	.676	-.858(-2)	-.160						

3A. Energies (in hartree) at $\gamma = 60°$ and $\theta = 30°$.

R_1 (bohr)	E_1	E_2	E_3	E_4
1.0	-1.621341	-1.256359	-1.252731	-1.254373
1.1	-1.647110	-1.283716	-1.279251	-1.280801
1.2	-1.662215	-1.300431	-1.295103	-1.296600
1.3	-1.669804	-1.310194	-1.303432	-1.304930
1.4	-1.672016	-1.318034	-1.308156	-1.307942
1.5	-1.670483	-1.330138	-1.311643	-1.307219
1.6	-1.666332	-1.345748	-1.312611	-1.303966
1.7	-1.660351	-1.361788	-1.313890	-1.298835
1.8	-1.653050	-1.376574	-1.314843	-1.292694
1.9	-1.644871	-1.390268	-1.315061	-1.285705
2.0	-1.636103	-1.402770	-1.314117	-1.278404
2.6	-1.583814	-1.454498		-1.236755

3B. Electric dipole transition moments (in a.u.) at $\gamma = 60°$ and $\theta = 30°$.

R_1 (bohr)	T_{41}(z)	T_{42}(z)	T_{43}(z)	T_{31}(x)	T_{31}(y)	T_{32}(x)	T_{32}(y)	T_{21}(x)	T_{21}(y)
1.0	.657	.144	.262(+1)	-.490	.338(-1)				
1.1	.647	.112	.264(+1)						
1.2	.632	.113	.265(+1)	.449	-.580(-2)	-.131	-.252(+1)	.188(-2)	-.584
1.3	.620	-.330(-1)	.264(+1)						
1.4	.600	-.290	.221(+1)	.472	-.217	-.101(+1)	-.155(+1)	-.708(-1)	-.413
1.5	.589	-.275	.120(+1)	.350	-.364	-.146(+1)	-.258	-.135	-.184
1.6	.568	-.165	-.981	-.396	.283	.143(+1)	.140	-.103	-.972(-1)
1.7	.545	-.104	.833	.445	-.160	-.132(+1)	-.152	-.762(-1)	-.571(-1)
1.8	.519	.607(-1)						-.568(-1)	-.245(-1)
1.9	.492	-.525(-1)	.564	.475	-.500(-1)	-949	-.131	-.422(-1)	-.263(-1)
2.0	.447	-.396(-1)						-.328(-1)	-.141(-1)
2.6	-.164	-.599(-2)						-.549(-2)	-.307(-2)

4A. Energies (in hartree) at $\gamma = 60°$ and $\theta = 35°$.

R_1 (bohr)	E_1	E_2	E_3	E_4
1.0	-1.614957	-1.281981	-1.272456	-1.275587
1.1	-1.641214	-1.311598	-1.299749	-1.303051
1.2	-1.656725	-1.331558	-1.316788	-1.320090
1.3	-1.664653	-1.345216	-1.326295	-1.329490
1.4	-1.667211	-1.355503	-1.331773	-1.333536
1.5	-1.666128	-1.365303	-1.334055	-1.333675
1.6	-1.662399	-1.375270	-1.336481	-1.331217
1.7	-1.656561	-1.385976	-1.336992	-1.326946
1.8	-1.649633	-1.396523	-1.336599	-1.321108
1.9	-1.641621	-1.406937	-1.334674	-1.314569
2.0	-1.633278	-1.416761	-1.332444	-1.307131
2.2	-1.615678	-1.434771	-1.326260	-1.291824

4B. Electric dipole transition moments (in a.u.) at $\gamma = 60°$ and $\theta = 35°$.

R_1 (bohr)	$T_{41}(z)$	$T_{42}(z)$	$T_{43}(z)$	$T_{31}(x)$	$T_{31}(y)$	$T_{32}(x)$	$T_{32}(y)$	$T_{21}(x)$	$T_{21}(y)$
1.0	.536	.326	.283(+1)	.459	.159(-1)	-.164	-.260(+1)	.377(-1)	-.489
1.1	.519	.237	.290(+1)	.453	-.689(-2)	-.480	-.262(+1)	.136(-1)	-.454
1.2	.494	.221	.284(+1)	.502	-.169(-1)	-.304	-.244(+1)	.341(-1)	-.409
1.3	.473	.138	.284(+1)						
1.4	.449	.928(-1)	.277(+1)	.558	-.279(-1)	-.687	-.205(+1)	-.582(-1)	-.289
1.5	.425	.481(-2)	.227(+1)						
1.6	.401	-.260(-1)	.166(+1)					-.403(-1)	-.133
1.7	.373	.465(-1)	.132(+1)						
1.8	.346	.404(-1)	.110(+1)					.412(-1)	.509(-1)
1.9	.316	.344(-1)	.957						
2.0	.293	-.264(-1)	.861					-.281(-1)	-.155(-1)
2.2	.237	.157(-1)	.724					.133(-1)	.130(-2)

5A. Energies (in hartree) at $\gamma = 60°$ and $\theta = 40°$.

R_1 (bohr)	E_1	E_2	E_3	E_4
1.0	-1.578302	-1.361381	-1.346675	-1.346043
1.2	-1.627544	-1.414960	-1.389836	-1.390439
1.4	-1.644261	-1.439576	-1.400643	-1.402608
1.6	-1.644186	-1.451720	-1.394938	-1.398039
1.8	-1.635271	-1.459626	-1.380789	-1.384681
2.0	-1.621765	-1.466251	-1.362396	-1.366771
2.2	-1.606750	-1.472448	-1.342713	-1.346809
2.4	-1.591319	-1.478409	-1.328232	-1.326263
2.6	-1.576867	-1.483414	-1.319946	-1.305992
2.8	-1.563374	-1.487444	-1.311101	-1.386560
3.0	-1.551353	-1.490820	-1.302177	-1.268127

5B. Electric dipole transition moments (in a.u.) at $\gamma = 60°$ and $\theta = 40°$.

R_1 (bohr)	$T_{41}(z)$	$T_{42}(z)$	$T_{43}(z)$	$T_{31}(x)$	$T_{31}(y)$	$T_{32}(x)$	$T_{32}(y)$	$T_{21}(x)$	$T_{21}(y)$
1.0	.396	.616	.275(+1)	.654	-.192(-1)	-.568	-.215(+1)	.153	-.355
1.2	.344	.327	.283(+1)	.665	-.927(-1)	-.526	-.194(+1)	.155	-.184
1.4	.297	.327	.283(+1)	.665	-.927(-1)	-.526	-.194(+1)	.155	-.184
1.6	.254	.240	.285(+1)	.666	.115	.467	.169(+1)	.160	-.999(-2)
1.8	.449	.160	.287(+1)	.623	-.134	-.444	-.141(+1)	.155	-.296(-1)
2.0	.181	-.105	.287(+1)	.694	-.147	.408	.116(+1)	-.141	-.204(-1)
2.2	.149	-.661(-1)	.279(+1)	.775	-.152	.410	.891	-.122	-.456(-1)
2.4	.120	-.442(-1)	.124(+1)	-.831	.500(-1)	-.411	-.147	-.106	-.555(-1)
2.6	.937(-1)	-.305(-1)	-.715	-.816	-.225(-1)	-.383	.872(-1)	-.882(-1)	-.569(-1)
2.8	.711(-1)	.221(-1)	-.533	-.821	-.696(-1)	.353	-.186	.737(-1)	.526(-1)
3.0	.510(-1)	-.178(-1)	-.429	-.816	-.997(-1)	-.318	.242	-.599(-1)	-.457(-1)

6A. Energies (in hartree) at $\gamma = 60°$ and $\theta = 41°$.

R_1 (bohr)	E_1	E_2	E_3	E_4
1.1	-1.592047	-1.415816	-1.395930	-1.393409
1.2	-1.613330	-1.437790	-1.411724	-1.410256
1.3	-1.626362	-1.452619	-1.419424	-1.418943
1.4	-1.633562	-1.462663	-1.421590	-1.422094
1.6	-1.635987	-1.473665	-1.414808	-1.416775
1.8	-1.628792	-1.479461	-1.398888	-1.402382
2.0	-1.617101	-1.483539	-1.378994	-1.383352
2.2	-1.602965	-1.486453	-1.356707	-1.362065
2.4	-1.588679	-1.489406	-1.334404	-1.340208
2.6	-1.574481	-1.492086	-1.319142	-1.318567

6B. Electric dipole transition moments (in a.u.) at $\gamma = 60°$ and $\theta = 41°$.

R_1 (bohr)	$T_{41}(z)$	$T_{42}(z)$	$T_{43}(z)$	$T_{31}(x)$	$T_{31}(y)$	$T_{32}(x)$	$T_{32}(y)$	$T_{21}(x)$	$T_{21}(y)$
1.1	.350	.533	.273(+1)	.782	-.772(-1)	-.577	-.208(+1)	.189	-.299
1.2	.321	-.442	.275(+1)	.778	-.981(-1)	.555	.206(+1)	-.181	.254
1.3	.296	.372	-.277(+1)	-.770	.114	.535	.198(+1)	.180	-.208
1.4	.271	.324	-.278(+1)	-.759	.126	.514	.190(+1)	.184	-.166
1.6	.228	.239	-.281(+1)	-.740	.144	.473	.169(+1)	.191	-.857(-1)
1.8	.191	.163	.283(+1)	.726	-.156	-.424	-.144(+1)	.189	-.186(-1)
2.0	.159	-.119	.284(+1)	.710	-.164	.377	.122(+1)	-.182	-.319(-1)
2.2	.131	-.793(-1)	.284(+1)	.712	-.169	.342	.102(+1)	-.167	-.599(-1)
2.4	.100	-.508(-1)	.282(+1)	.765	-.163	.335	.810	.145	-.719(-1)
2.6	.830(-1)	-.358(-1)	.178(+1)	.915	-.539(-1)	.375	.245	-.123	-.738(-1)

7A. Energies (in hartree) at $\gamma = 60°$ and $\theta = 42°$.

R_1 (bohr)	E_1	E_2	E_3	E_4
1.2	-1.592639	-1.459573	-1.432895	-1.428896
1.3	-1.608733	-1.475637	-1.441280	-1.438291
1.4	-1.618374	-1.486194	-1.443363	-1.441709
1.6	-1.624640	-1.497521	-1.436014	-1.436391
1.8	-1.620392	-1.501792	-1.419338	-1.421214
2.0	-1.610509	-1.502946	-1.397270	-1.401158
2.2	-1.597839	-1.503386	-1.373742	-1.378706
2.4	-1.584455	-1.503453	-1.349353	-1.355431
2.6	-1.571115	-1.502920	-1.325875	-1.332421

7B. Electric dipole transition moments (in a.u.) at $\gamma = 60°$ and $\theta = 42°$.

R_1 (bohr)	$T_{41}(z)$	$T_{42}(z)$	$T_{43}(z)$	$T_{31}(x)$	$T_{31}(y)$	$T_{32}(x)$	$T_{32}(y)$	$T_{21}(x)$	$T_{21}(y)$
1.2	.295	-.423	.271(+1)	.966	-.150	.564	.199(+1)	-.217	.236
1.3	.267	-.349	.273(+1)	.936	-.166	.533	.194(+1)	-.209	.185
1.4	.241	.313	-.274(+1)	-.906	.175	.505	.186(+1)	.214	-.142
1.6	.197	-.220	.277(+1)	.862	-.187	.456	.167(+1)	-.215	.639
1.8	.162	.162	.280(+1)	.820	-.190	-.408	-.146(+1)	.219	-.908(-3)
2.0	.133	-.120	.281(+1)	.779	-.191	.365	.127(+1)	-.216	-.453(-1)
2.2	.109	-.828(-1)	.282(+1)	.745	-.189	.325	.108(+1)	-.204	-.759(-1)
2.4	.871(-1)	-.544(-1)	.284(+1)	.729	-.185	.296	.918	-.185	-.895(-1)
2.6	.702(-1)	-.395(-1)	.284(+1)	.747	-.174	.282	.758	-.162	-.918(-1)

8A. Energies (in hartree) at $\gamma = 60°$ and $\theta = 43°$.

R_1 (bohr)	E_1	E_2	E_3	E_4
1.0	-1.488283	-1.408634	-1.396697	-1.385589
1.2	-1.562401	-1.476317	-1.449294	-1.441662
1.4	-1.596525	-1.507874	-1.463159	-1.458815
1.6	-1.608609	-1.521198	-1.456915	-1.455231
1.8	-1.608405	-1.525586	-1.439948	-1.440482
2.0	-1.601571	-1.525231	-1.417277	-1.419800
2.2	-1.591074	-1.523185	-1.391950	-1.396323
2.4	-1.579169	-1.520208	-1.366426	-1.371903
2.6	-1.566859	-1.517006	-1.340836	-1.347478

8B. Electric dipole transition moments (in a.u.) at $\gamma = 60°$ and $\theta = 43°$.

R_1 (bohr)	$T_{41}(z)$	$T_{42}(z)$	$T_{43}(z)$	$T_{31}(x)$	$T_{31}(y)$	$T_{32}(x)$	$T_{32}(y)$	$T_{21}(x)$	$T_{21}(y)$
1.0	.370	.789	-.251(+1)	-.130(+1)	.177	.615	.176(+1)	.425	-.368
1.2	.270	-.372	.264(+1)	.126(+1)	-.245	.554	.194(+1)	-.245	.210
1.4	.206	.261	-.271(+1)	-.114(+1)	.245	.509	.182(+1)	.228	-.109
1.6	.155	.182	.273(+1)	.104(+1)	-.246	-.445	-.166(+1)	.226	-.338(-1)
1.8	.124	-.137	.276(+1)	.963	-.240	.389	.146(+1)	-.234	-.242(-1)
2.0	.100	-.102	-.278(+1)	-.891	.228	-.355	-.128(+1)	-.237	-.644(-1)
2.2	.820(-1)	-.722(-1)	.280(+1)	.828	-.217	.313	.110(+1)	-.232	-.924(-1)
2.4	.646(-1)	-.484(-1)	.282(+1)	.775	-.207	.285	.968	-.217	-.106
2.6	.524(-1)	-.378(-1)	.283(+1)	.735	-.197	.254	.836	-.196	-.108

9A. Energies (in hartree) at $\gamma = 60°$ and $\theta = 44°$.

R_1 (bohr)	E_1	E_2	E_3	E_4
1.0	-1.417761	-1.383715	-1.374341	-1.358108
1.2	-1.516840	-1.476638	-1.450055	-1.438424
1.4	-1.565265	-1.521901	-1.475444	-1.467901
1.6	-1.586406	-1.542155	-1.474488	-1.470366
1.8	-1.592057	-1.548929	-1.459523	-1.458300
2.0	-1.589118	-1.548893	-1.437233	-1.438398
2.2	-1.581544	-1.544892	-1.411348	-1.414588
2.4	-1.571644	-1.539636	-1.384722	-1.389198
2.6	-1.561087	-1.533678	-1.357419	-1.363612

9B. Electric dipole transition moments (in a.u.) at $\gamma = 60°$ and $\theta = 44°$.

R_1 (bohr)	$T_{41}(z)$	$T_{42}(z)$	$T_{43}(z)$	$T_{31}(x)$	$T_{31}(y)$	$T_{32}(x)$	$T_{32}(y)$	$T_{21}(x)$	$T_{21}(y)$
1.0	-.296	.735	.251(+1)	-.167(+1)	.338	-.604	-.181(+1)	-.504	.335
1.2	.198	-.269	.263(+1)	.159(+1)	-.379	.542	.198(+1)	-.233	.149
1.4	.142	-.166	.267(+1)	.145(+1)	-.358	.482	.179(+1)	-.208	.533(-1)
1.6	.108	-.110	.273(+1)	.128(+1)	-.320	.447	.123(+1)	-.212	-.121(-1)
1.8	.833(-1)	-.818(-1)	.272(+1)	.116(+1)	-.303	.394	.146(+1)	-.226	-.591(-1)
2.0	.557(-1)	-.626(-1)	.275(+1)	.105(+1)	-.280	.349	.129(+1)	-.239	-.916(-1)
2.2	.466(-1)	-.443(-1)	.277(+1)	.951	-.254	.308	.112(+1)	-.243	-.112
2.4	.364(-1)	-.312(-1)	.281(+1)	.865	-.237	.279	.987	-.236	-.123
2.6	.287(-1)	-.247(-1)	.282(+1)	.793	-.219	.250	.872	-.221	-.124

10A. Energies (in hartree) at $\gamma = 60°$ and $\theta = 45°$.

R_1 (bohr)	E_1	E_2	E_3	E_4
1.0	-1.286448	-1.286430	-1.280663	-1.258265
1.2	-1.441703	-1.441650	-1.415028	-1.398848
1.4	-1.518046	-1.518017	-1.468988	-1.458043
1.6	-1.554349	-1.554268	-1.482113	-1.475586
1.633	-1.557748	-1.557719	-1.481972	-1.475958
1.64	-1.558556	-1.558507	-1.481895	-1.475980
1.8	-1.569022	-1.568989	-1.474258	-1.471001
2.0	-1.571945	-1.571928	-1.455205	-1.454669
2.2	-1.568548	-1.568561	-1.430550	-1.432079
2.4	-1.561349	-1.561420	-1.403023	-1.406783
2.6	-1.552813	-1.552907	-1.375206	-1.380527
2.8	-1.544312	-1.544450	-1.347990	-1.354630
3.0	-1.536907	-1.536859	-1.322044	-1.329407

10B. Electric dipole transition moments (in a.u.) at $\gamma = 60°$ and $\theta = 45°$.

R_1 (bohr)	$T_{41}(z)$	$T_{42}(z)$	$T_{43}(z)$	$T_{31}(x)$	$T_{31}(y)$	$T_{32}(x)$	$T_{32}(y)$	$T_{21}(x)$	$T_{21}(y)$
1.0	-.432(-3)	-.194(-3)	.261(+1)	-.225(+1)	-.944(-1)	-.927(-1)	.226(+1)	.586(-1)	-.512(-2)
1.2	.541(-3)	.120(-3)	.263(+1)	.199	.204(+1)	.204(+1)	-.198	-.916(-1)	-.182
1.4	-.483(-3)	-.489(-3)	.265(+1)	-.161	-.183(+1)	-.184(+1)	.159	-.131	-.227(-1)
1.6	.809(-3)	.546(-3)	.268(+1)	.122(+1)	-.110(+1)	.109(+1)	.122(+1)	-.202(-1)	-.172
1.633	-.557(-3)	.922(-3)	.269(+1)	-.121(+1)	.106(+1)	.106(+1)	.121(+1)	.235(-1)	.179
1.64	-.830(-3)	.378(-3)	.269(+1)	-.138(+1)	.801	.803	.139(+1)	.909(-1)	.157
1.8	.647(-3)	-.538(-3)	.271(+1)	.362	.141(+1)	-.141(+1)	.361	.189	.103
2.0	.497(-3)	.723(-3)	.274(+1)	.372	.125(+1)	.125(+1)	-.371	-.207	-.135
2.2	-.140(-3)	.100(-2)	.275(+1)	.424	.107(+1)	.106(+1)	-.421	-.194	-.182
2.4	.904(-3)	-.556(-3)	.278(+1)	.474	.918	-.917	.472	.161	.225
2.6	.152(-2)	-.153(-3)	.280(+1)	.446	.812	-.814	.444	.148	-.226
2.8	.150(-2)	-.203(-3)	.281(+1)	.443	.702	.700	-.349	-.111	-.226
3.0	.710(-3)	-.758(-4)	.282(+1)	-.388	-.639	-.632	.385	-.104	-.196

11A. Energies (in hartree) at $\gamma = 90°$ and $\theta = 0°$.

R_1 (bohr)	E_1	E_2	E_3	E_4
1.0	-1.622473	-1.247703	-1.247111	-1.247289
1.2	-1.663262	-1.288335	-1.288025	-1.288119
1.3	-1.670771	-1.295871	-1.295509	-1.295634
1.4	-1.672935	-1.297882	-1.297754	-1.297874
1.45	-1.672515	-1.297313	-1.297036	-1.297441
1.5	-1.671378	-1.309228	-1.296111	-1.296269
1.55	-1.669557	-1.320744	-1.294262	-1.294449
1.6	-1.667157	-1.331182	-1.292143	-1.292097
1.7	-1.661084	-1.350785	-1.285666	-1.286008
1.8	-1.653745	-1.367762	-1.278433	-1.278651
2.0	-1.636828	-1.396678	-1.261583	-1.261791
2.1	-1.627821		-1.253421	-1.252827

11B. Electric dipole transition moments (in a.u.) at $\gamma = 90°$ and $\theta = 0°$.

R_1 (bohr)	$T_{41}(z)$	$T_{42}(z)$	$T_{43}(z)$	$T_{31}(x)$	$T_{31}(y)$	$T_{32}(x)$	$T_{32}(y)$	$T_{21}(x)$	$T_{21}(y)$
1.0	.741	-.255(+1)	-.185(-1)	.386(-1)	.734	-.121	-.256(+1)	-.395	.164(-1)
1.2	.740	.244(+1)	-.241(-1)	.478(-1)	.732				
1.3	.740	.244(+1)	-.299(-1)	.537(-1)	.731	.158	.244(+1)	.435	-.254(-1)
1.4	.739	.240(+1)	-.367(-1)	.577(-1)	.727	.162	.239(+1)	.452	-.281(-1)
1.45	.740	.360(-1)						.615(-1)	.726
1.5	.740	.153(-3)	-.392(-1)	.636(-1)	.724	.217(-2)	.155(-3)	-.779(-4)	-.684(-3)
1.55	.740	.958(-4)	-.422(-1)	.658(-1)	.722	.205(-2)	.895(-4)	-.357(-4)	-.443(-3)
1.6	.738	.542(-4)	.224(+1)	.471	-.345(-1)	.631(-4)	-.126(-2)	-.795(-5)	-.365(-3)
1.7	.738	.320(-4)	-.482(-1)	.733(-1)	.712	.190(-2)	.156(-4)	-.474(-5)	-.243(-3)
1.8	.736	-.486(-4)	.235(+1)	.469	-.405(-1)	-.113(-3)	.331(-3)	.508(-5)	.212(-3)
2.0	.732	-.424(-4)	-.344(-1)					.352(-4)	.180(-3)
2.1	.734		-.221						

12A. Energies (in hartree) at $\gamma = 90°$ and $\theta = 20°$.

R_1 (bohr)	E_1	E_2	E_3	E_4
1.0	-1.622500	-1.248407	-1.247918	-1.248045
1.1	-1.648282	-1.274240	-1.273685	-1.273867
1.2	-1.663317	-1.289458	-1.288781	-1.288983
1.3	-1.670765	-1.297152	-1.296395	-1.296583
1.4	-1.673022	-1.299635	-1.298615	-1.298822
1.5	-1.671468	-1.309515	-1.297918	-1.297315
1.6	-1.667207	-1.331466	-1.294033	-1.293150
1.7	-1.661214	-1.350912	-1.288143	-1.287138
1.8	-1.653855	-1.368058	-1.281043	-1.279825
1.9	-1.645679	-1.383352	-1.276389	-1.271668
2.0	-1.636951	-1.396906	-1.275709	-1.263032

12B. Electric dipole transition moments (in a.u.) at $\gamma = 90°$ and $\theta = 20°$.

R_1 (bohr)	$T_{41}(z)$	$T_{42}(z)$	$T_{43}(z)$	$T_{31}(x)$	$T_{31}(y)$	$T_{32}(x)$	$T_{32}(y)$	$T_{21}(x)$	$T_{21}(y)$
1.0	.728	.170	.247(+1)	.431	.151(-1)	.190(-2)	-.248(+1)	-.280(-1)	-.718
1.1	.727	.246	.246(+1)	.435	.335(-1)	.769(-1)	-.246(+1)	-.193(-1)	-.713
1.2	.725	.132	.246(+1)	.441	-.494(-2)	-.793(-1)	-.245(+1)	-.465(-1)	-.706
1.3	.723	-.117	.247(+1)	.439	-.133(-1)	.120	.247(+1)	.565(-1)	.706
1.4	.720	.998(-1)	.246(+1)	.444	-.247(-1)	-.161	-.244(+1)	-.661(-1)	-.690
1.5	.719	-.118(-1)	.100	-.731(-2)	.464	.538(-1)	.136(-1)	.522(-2)	.438(-1)
1.6	.714	.576(-2)	.715(-1)					-.101(-2)	-.109(-1)
1.7	.712	-.364(-2)	-.556(-1)	.945(-1)	.645	-.345(-1)	.125(-3)	-.176(-3)	.526(-2)
1.8	.703	-.349(-2)	.759(-1)					-.832(-3)	.334(-2)
1.9	.698	.314(-2)	-.519						
2.0	.685	-.251(-2)	-.260						

13A. Energies (in hartree) at $\gamma = 90°$ and $\theta = 30°$.

R_1 (bohr)	E_1	E_2	E_3	E_4
1.0	-1.621774	-1.254616	-1.251420	-1.252720
1.1	-1.647580	-1.281256	-1.277587	-1.278774
1.2	-1.662676	-1.297319	-1.292906	-1.294162
1.3	-1.670270	-1.306044	-1.300899	-1.301963
1.4	-1.672547	-1.310723	-1.303652	-1.304551
1.5	-1.671068	-1.319083	-1.303589	-1.303234
1.6	-1.666829	-1.336486	-1.304112	-1.299335
1.7	-1.660810	-1.354667	-1.306123	-1.293532
1.8	-1.653533	-1.370963	-1.306896	-1.286595
1.9	-1.645355	-1.385463	-1.306584	-1.278843
2.0	-1.636639	-1.398977	-1.305314	-1.270538
2.2	-1.618722	-1.421141	-1.299739	-1.253897

13B. Electric dipole transition moments (in a.u.) at $\gamma = 90°$ and $\theta = 30°$.

R_1 (bohr)	$T_{41}(z)$	$T_{42}(z)$	$T_{43}(z)$	$T_{31}(x)$	$T_{31}(y)$	$T_{32}(x)$	$T_{32}(y)$	$T_{21}(x)$	$T_{21}(y)$
1.0	.675	-.170(-1)	.261(+1)	.414	-.507(-1)	-.287	-.256(+1)	-.776(-1)	-.651
1.1	.670	-.181(-1)	.261(+1)	.419	-.565(-1)	-.327	-.254(+1)	-.843(-1)	-.635
1.2	.660	-.257(-1)	.261(+1)	.431	-.599(-1)	-.327	-.249(+1)	-.901(-1)	-.609
1.3	.654	-.259(-1)	.261(+1)	.441	-.608(-1)	.308	.248(+1)	.905(-1)	.588
1.4	.641	.872(-1)	.259(+1)	.463	-.465(-1)	-.210	-.229(+1)	-.757(-1)	-.517
1.5	.635	.122	.170(+1)	.408	.270	.424	-.103(+1)	-.832(-1)	-.267
1.6	.618	.636(-1)	.115(+1)					.136(-1)	-.963(-1)
1.7	.608	.357(-1)	.695	-.372	.167(-1)	-.496	.521	.144(-1)	-.494(-1)
1.8	.584	-.263(-1)	-.605					-.951(-1)	.297(-1)
1.9	.562	-.203(-1)	.528						
2.0	.533	-.173(-1)	-.485						
2.2									

14A. Energies (in hartree) at $\gamma = 90°$ and $\theta = 35°$.

R_1 (bohr)	E_1	E_2	E_3	E_4
1.0	-1.617504	-1.273575	-1.264579	-1.268146
1.1	-1.643821	-1.301748	-1.291366	-1.294582
1.2	-1.659311	-1.319674	-1.306880	-1.310344
1.3	-1.667219	-1.331108	-1.315472	-1.318471
1.4	-1.669783	-1.339010	-1.319509	-1.321315
1.5	-1.668543	-1.347003	-1.322917	-1.320191
1.6	-1.664643	-1.356680	-1.325394	-1.316695
1.7	-1.658861	-1.369059	-1.326487	-1.310975
1.8	-1.651689	-1.381609	-1.326245	-1.304309
2.0	-1.635209	-1.405613	-1.323008	-1.288520
2.2	-1.617683	-1.425864	-1.316627	-1.272041

14B. Electric dipole transition moments (in a.u.) at $\gamma = 90°$ and $\theta = 35°$.

R_1 (bohr)	$T_{41}(z)$	$T_{42}(z)$	$T_{43}(z)$	$T_{31}(x)$	$T_{31}(y)$	$T_{32}(x)$	$T_{32}(y)$	$T_{21}(x)$	$T_{21}(y)$
1.0	.573	-.223(-1)	.283(+1)	.426	-.664(-1)	-.324	-.268(+1)	-.881(-1)	-.521
1.1	.561	-.795(-1)	.281(+1)						
1.2	.544	-.165(-1)	.282(+1)	.462	-.832(-1)	-.338	-.251(+1)	-.992(-1)	-.444
1.3	.531	-.109(-1)	.278(+1)						
1.4	.511	-.269(-1)	.258(+1)	.543	-.771(-1)	.107	.204(+1)	.668(-1)	.327
1.5	.498	.744(-1)	.195(+1)	.557	-.326(-1)	.389	-.144(+1)	-.207(-1)	-.242
1.6	.473	.885(-1)	.134(+1)					-.119(-1)	-.154
1.7	.458	-.747(-1)	.102(+1)	.520	-.600(-1)	-.775	.690	-.217(-1)	.981(-1)
1.8	.429	-.540(-1)	-.850					-.228(-1)	-.628(-2)
2.0	.374	.338(-1)	-.695					.163(-1)	-.288(-1)
2.2	.309	-.217(-1)	-.621					-.113(-1)	.136(-1)

15A. Energies (in hartree) at $\gamma = 90°$ and $\theta = 40°$.

R_1 (bohr)	E_1	E_2	E_3	E_4
1.0	-1.591540	-1.341624	-1.326515	-1.327431
1.1	-1.621263	-1.368385	-1.351206	-1.353163
1.2	-1.639543	-1.389561	-1.366069	-1.367891
1.4	-1.655033	-1.409353	-1.373704	-1.376528
1.6	-1.653578	-1.418580	-1.365572	-1.369175
1.7	-1.649402	-1.421327	-1.358005	-1.362088
1.8	-1.643481	-1.426837	-1.351998	-1.353666
1.9	-1.636678	-1.431208	-1.345577	-1.344422
2.0	-1.629193	-1.436798	-1.342353	-1.334537
2.1	-1.621246	-1.442076	-1.338969	-1.324251
2.2	-1.613174	-1.447706	-1.334844	-1.313999

15B. Electric dipole transition moments (in a.u.) at $\gamma = 90°$ and $\theta = 40°$.

R_1 (bohr)	$T_{41}(z)$	$T_{42}(z)$	$T_{43}(z)$	$T_{31}(x)$	$T_{31}(y)$	$T_{32}(x)$	$T_{32}(y)$	$T_{21}(x)$	$T_{21}(y)$
1.0	.424	-.290	.284(+1)	.546	-.168	-.474	-.247(+1)	-.167	-.324
1.1	.401	-.332	.286(+1)						
1.2	.380	-.267	.288(+1)	.547	-.178	-.450	-.231(+1)	-.169	-.242
1.4	.340	.227	.289(+1)	.554	-.190	.437	.208(+1)	.162	.147
1.6	.303	-.160	-.290(+1)	-.582	.205	.346	.176(+1)	-.131	-.627(-1)
1.7	.284	-.143	.288(+1)						
1.8	.266	-.943(-1)	.274(+1)	-.690	.253	.733(-1)	.134(+1)	-.784(-1)	-.577(-2)
1.9	.247	.650(-1)	.199(+1)						
2.0	.228	.420(-1)	.106(+1)					.370(-1)	-.185(-1)
2.1	.208	.180(-1)	.106(+1)						
2.2	.191	.180(-1)	.886					.174(-1)	-.228(-1)

16A. Energies (in hartree) at $\gamma = 90°$ and $\theta = 41°$.

R_1 (bohr)	E_1	E_2	E_3	E_4
1.0	-1.578103	-1.360384	-1.347850	-1.347047
1.1	-1.609733	-1.389549	-1.371903	-1.372315
1.2	-1.629885	-1.408142	-1.385302	-1.386651
1.4	-1.647994	-1.427744	-1.391543	-1.394282
1.6	-1.648681	-1.437255	-1.381960	-1.385703
1.8	-1.640102	-1.442296	-1.364686	-1.368941
1.9	-1.633887	-1.445362	-1.355121	-1.358855
2.0	-1.626746	-1.448579	-1.347526	-1.348493
2.2	-1.611668	-1.456454	-1.339580	-1.326663
2.4	-1.595934	-1.464768	-1.330721	-1.304798

16B. Electric dipole transition moments (in a.u.) at $\gamma = 90°$ and $\theta = 41°$.

R_1 (bohr)	$T_{41}(z)$	$T_{42}(z)$	$T_{43}(z)$	$T_{31}(x)$	$T_{31}(y)$	$T_{32}(x)$	$T_{32}(y)$	$T_{21}(x)$	$T_{21}(y)$
1.0	.403	.498	.277(+1)						
1.1	.378	-.435	.279(+1)						
1.2	.353	-.396	.282(+1)	.605	-.228	-.500	-.228(+1)	-.219	-.198
1.4	.311	.339	.284(+1)	.594	-.233	.510	.207(+1)	.209	.107
1.6	.273	-.228	-.288(+1)	-.595	.239	.436	.172(+1)	-.178	-.230(-1)
1.8	.238	.155	-.290(+1)	-.627	.262	-.303	-.141(+1)	.132	-.317(-1)
1.9	.221	.114	-.283(+1)						
2.0	.203	.876(-1)	.240(+1)	.775	-.367	-.786(-1)	.985	.804(-1)	-.511(-1)
2.2	.170	.482(-1)	-.105(+1)					.480(-1)	-.505(-1)
2.4	.138	.238(-1)	-.771					.260(-1)	-.423(-1)

17A. Energies (in hartree) at $\gamma = 90°$ and $\theta = 42°$.

R_1 (bohr)	E_1	E_2	E_3	E_4
1.0	-1.558267	-1.385144	-1.370345	-1.366794
1.1	-1.593259	-1.414719	-1.394731	-1.392348
1.2	-1.616260	-1.433544	-1.407622	-1.406560
1.3	-1.630606	-1.445307	-1.412893	-1.412903
1.4	-1.638776	-1.452215	-1.412728	-1.413528
1.5	-1.642223	-1.455817	-1.408433	-1.410263
1.6	-1.642360	-1.457620	-1.401236	-1.403854
1.8	-1.635894	-1.459643	-1.382109	-1.385773
2.0	-1.624044	-1.462380	-1.360159	-1.363817
2.1	-1.617129	-1.464439	-1.349907	-1.352520
2.2	-1.610075	-1.466824	-1.344246	-1.340977
2.4	-1.595158	-1.472333	-1.335742	-1.317721

17B. Electric dipole transition moments (in a.u.) at $\gamma = 90°$ and $\theta = 42°$.

R_1 (bohr)	$T_{41}(z)$	$T_{42}(z)$	$T_{43}(z)$	$T_{31}(x)$	$T_{31}(y)$	$T_{32}(x)$	$T_{32}(y)$	$T_{21}(x)$	$T_{21}(y)$
1.0	.385	-.564	.272(+1)	.738	-.311	-.449	-.216(+1)	-.312	-.226
1.1	.354	-.498	-.274(+1)						
1.2	.327	.441	-.278(+1)	.698	-.298	.549	.206(+1)	.280	.133
1.3	.303	.405	-.278(+1)	-.676	.296	-.565	-.197(+1)	.272	.885(-1)
1.4	.282	.374	.279(+1)	.660	-.295	.565	.188(+1)	.265	.446(-1)
1.5	.261	.341	-.281(+1)	-.644	.294	-.556	-.177(+1)	.254	.417(-1)
1.6	.244	.303	-.283(+1)	-.634	.295	-.534	-.125(+1)	.239	-.329(-1)
1.8	.211	.220	-.286(+1)	-.628	.303	-.441	-.139(+1)	.196	-.827(-1)
2.0	.182	.143	.287(+1)	.677	-.346	.289	.113(+1)	.143	-.101
2.1	.162	.115	.249(+1)						
2.2	.146	.887(-1)	.146(+1)					.932(-1)	-.931(-1)
2.4	.118	.535(-1)	-.867					.606(-1)	-.740(-1)

18A. Energies (in hartree) at $\gamma = 90°$ and $\theta = 43°$.

R_1 (bohr)	E_1	E_2	E_3	E_4
1.0	-1.528559	-1.401973	-1.388667	-1.381565
1.2	-1.596587	-1.454220	-1.428682	-1.425080
1.3	-1.614783	-1.466773	-1.434483	-1.432224
1.4	-1.626119	-1.473767	-1.434293	-1.433293
1.5	-1.632266	-1.477069	-1.429783	-1.429917
1.6	-1.634508	-1.478136	-1.422479	-1.423500
1.8	-1.631207	-1.477589	-1.401907	-1.404715
2.0	-1.621659	-1.476850	-1.377578	-1.381675
2.2	-1.608793	-1.477797	-1.352935	-1.357011
2.4	-1.594890	-1.480747	-1.341350	-1.332312

18B. Electric dipole transition moments (in a.u.) at $\gamma = 90°$ and $\theta = 43°$.

R_1 (bohr)	$T_{41}(z)$	$T_{42}(z)$	$T_{43}(z)$	$T_{31}(x)$	$T_{31}(y)$	$T_{32}(x)$	$T_{32}(y)$	$T_{21}(x)$	$T_{21}(y)$
1.0	.366	-.856	.253(+1)	.900	-.481	-.398	-.178(+1)	-.505	-.981(-1)
1.2	.287	.568	-.268(+1)	-.824	.433	-.635	-.188(+1)	.380	.343(-1)
1.3	.260	.517	-.271(+1)	-.783	.416	-.672	-.182(+1)	.395	-.743(-1)
1.4	.236	.568	-.268(+1)	-.824	.433	-.635	-.188(+1)	.380	.343(-1)
1.5	.216	.428	-.275(+1)	-.715	.394	-.686	-.166(+1)	.327	-.794(-2)
1.6	.198	.386	-.277(+1)	-.689	.387	-.668	-.156(+1)	.313	-.112
1.8	.166	.295	-.281(+1)	-.653	.377	-.597	-.134(+1)	.271	-.154
2.0	.139	.216	-.284(+1)	-.640	.384	-.489	-.112(+1)	.271	-.163
2.2	.116	.144	.277(+1)	.738	-.479	.287	.907	.157	-.147
2.4	.938(-1)	.892(-1)	.110(+1)						

19A. Energies (in hartree) at $\gamma = 90°$ and $\theta = 44°$.

R_1 (bohr)	E_1	E_2	E_3	E_4
1.1	-1.531133	-1.438783	-1.421951	-1.413233
1.2	-1.567121	-1.464465	-1.441274	-1.434531
1.3	-1.592049	-1.480203	-1.450407	-1.445439
1.4	-1.608679	-1.489582	-1.452401	-1.449065
1.6	-1.624983	-1.495323	-1.442374	-1.441889
1.8	-1.626886	-1.493580	-1.421994	-1.423792
2.0	-1.620507	-1.489822	-1.396799	-1.400164
2.2	-1.609667	-1.487922	-1.370006	-1.374499
2.4	-1.596601	-1.487878	-1.346626	-1.348462

19B. Electric dipole transition moments (in a.u.) at $\gamma = 90°$ and $\theta = 44°$.

R_1 (bohr)	$T_{41}(z)$	$T_{42}(z)$	$T_{43}(z)$	$T_{31}(x)$	$T_{31}(y)$	$T_{32}(x)$	$T_{32}(y)$	$T_{21}(x)$	$T_{21}(y)$
1.1	.253	-.996	.246(+1)						
1.2	.213	.785	.256(+1)	.966	-.668	.771	.155(+1)	.524	-.169
1.3	.117	.668	.263(+1)	.896	-.631	.852	.158(+1)	.460	-.175
1.4	.154	.597	.267(+1)	.837	-.592	.887	.154(+1)	.424	-.192
1.6	.124	.483	-.272(+1)	-.743	.537	-.881	-.142(+1)	.378	-.226
1.8	.102	.376	-.277(+1)	-.676	.498	-.805	-.125(+1)	.338	-.226
2.0	.843(-1)	.288	-.280(+1)	-.635	.478	-.700	-.107(+1)	.292	-.244
2.2	.697(-1)	.207	.284(+1)	.633	-.487	.569	.894	.232	-.215
2.4	.567(-1)	.135	.198(+1)	.776	-.647	.152	.482	.172	-.174

20A. Energies (in hartree) at $\gamma = 90°$ and $\theta = 45°$.

R_1 (bohr)	E_1	E_2	E_3	E_4
1.0	-1.383615	-1.337607	-1.327236	-1.314789
1.1	-1.461247	-1.400643	-1.388370	-1.376527
1.2	-1.516313	-1.442643	-1.425661	-1.415553
1.3	-1.555459	-1.486864	-1.446795	-1.438792
1.4	-1.582777	-1.469982	-1.457049	-1.450954
1.6	-1.613407	-1.501118	-1.456355	-1.453872
1.8	-1.623765	-1.501486	-1.439820	-1.440288
2.0	-1.622287	-1.497336	-1.416216	-1.418412
2.2	-1.613913	-1.493215	-1.388795	-1.392739
2.4	-1.602219	-1.491530	-1.361100	-1.365951
2.6	-1.589137	-1.491261	-1.343220	-1.339370

20B. Electric dipole transition moments (in a.u.) at $\gamma = 90°$ and $\theta = 45°$.

R_1 (bohr)	$T_{41}(z)$	$T_{42}(z)$	$T_{43}(z)$	$T_{31}(x)$	$T_{31}(y)$	$T_{32}(x)$	$T_{32}(y)$	$T_{21}(x)$	$T_{21}(y)$
1.0	.170(-5)	.210(+1)	.158(+1)	-.703	.703	.546	.546	.107(+1)	-.107(+1)
1.1	.692(-6)	.156(+1)	.213(+1)						
1.2	-.121(-5)	.116(+1)	.237(+1)	-.928	.928	-.907	-.907	.585	-.585
1.3	-.139(-5)	.909	-.251(+1)	-.900	.900	-.112(+1)	-.112(+1)	.472	-.472
1.4	-.104(-5)	.753	-.258(+1)	-.850	.850	-.120(+1)	-.120(+1)	.413	-.413
1.6	-.255(-6)	.580	-.267(+1)	-.740	.740	-.120(+1)	-.120(+1)	.356	-.356
1.8	-.242(-6)	.463	-.272(+1)	-.658	.568	-.111(+1)	-.111(+1)	.345	-.345
2.0	-.902(-7)	.362	-.276(+1)	.601	-.601	-.980	-.980	-.322	.322
2.2	.109(-6)	.269	-.280(+1)	-.571	.571	-.833	-.833	.283	-.283
2.4	-.505(-7)	-.186	.283(+1)	-.601	.601	-.668	-.668	.206	-.206
2.6	-.291(-7)	-.120	.133(+1)					.168	-.169

21A. Energies (in hartree) at $\gamma = 120°$ and $\theta = 0°$.

R_1 (bohr)	E_1	E_2	E_3	E_4
1.0	-1.622465	-1.247946	-1.247132	-1.247256
1.1	-1.648171	-1.273626	-1.272880	-1.272977
1.2	-1.663304	-1.288462	-1.287827	-1.288079
1.3	-1.670788	-1.295976	-1.295299	-1.295563
1.4	-1.672945	-1.297961	-1.297536	-1.297815
1.5	-1.671365	-1.309189	-1.295973	-1.296187
1.6	-1.667181	-1.331353	-1.292474	-1.292014
1.8	-1.653736	-1.367692	-1.279054	-1.278498
1.9	-1.645512	-1.382954	-1.269930	-1.270332
2.0	-1.636821	-1.396607	-1.261619	-1.261697
2.2	-1.618876	-1.419595	-1.255290	-1.243671

21B. Electric dipole transition moments (in a.u.) at $\gamma = 120°$ and $\theta = 0°$.

R_1 (bohr)	$T_{41}(z)$	$T_{42}(z)$	$T_{43}(z)$	$T_{31}(x)$	$T_{31}(y)$	$T_{32}(x)$	$T_{32}(y)$	$T_{21}(x)$	$T_{21}(y)$
1.0	.741	.279(+1)	.317(-1)	-.802(-1)	-.730	-.279	-.279(+1)	.280	-.218(-1)
1.1	.741	.276(+1)	-.818(-1)						
1.2	.740	.274(+1)	-.141					.303	-.449(-2)
1.3	.740	.275(+1)	-.225						
1.4	.740	.272(+1)	-.560					.301	.101
1.5	.742	.871(-3)	.419(-1)	-.130	-.719	-.170(-2)	-.140(-2)	-.203(-3)	-.563(-3)
1.6	.739	.347(-3)	.263(+1)	.289	-.215	-.665(-3)	-.594(-3)	.300(-3)	-.167(-3)
1.8	.738	.163(-3)	.773					.390(-4)	-.153(-3)
1.9	.739	-.497(-4)	.325(-1)	.261	.659	-.133(-2)	-.662(-3)	-.518(-4)	.806(-4)
2.0	.735	.599(-4)	.268	-.289	-.587	-.136(-2)	-.134(-2)	.184(-4)	-.139(-4)
2.2	.755	.786(-4)	.139(-2)	.728	-.120(+1)	.147(-1)	-.145(-1)	.196(-4)	-.852(-4)

32A. Energies (in hartree) at $\gamma = 150°$ and $\theta = 20°$.

R_1 (bohr)	E_1	E_2	E_3	E_4
1.0	-1.622452	-1.247753	-1.247340	-1.247195
1.1	-1.648216	-1.273447	-1.273132	-1.272908
1.2	-1.663287	-1.288484	-1.288138	-1.288003
1.3	-1.670770	-1.296153	-1.295778	-1.295496
1.4	-1.672874	-1.298179	-1.297771	-1.297734
1.5	-1.671450	-1.309245	-1.296129	-1.296140
1.6	-1.667182	-1.331342	-1.292051	-1.291945
1.7	-1.661186	-1.350599	-1.285568	-1.285820
1.8	-1.653743	-1.367848	-1.278318	-1.278453
2.0	-1.636765	-1.396697	-1.261356	-1.261554
2.2	-1.618786	-1.419560	-1.242694	-1.243539

32B. Electric dipole transition moments (in a.u.) at $\gamma = 150°$ and $\theta = 20°$.

R_1 (bohr)	$T_{41}(z)$	$T_{42}(z)$	$T_{43}(z)$	$T_{31}(x)$	$T_{31}(y)$	$T_{32}(x)$	$T_{32}(y)$	$T_{21}(x)$	$T_{21}(y)$
1.0	.742	.282(+1)	.229					.254	-.104(-1)
1.1	.742	.280(+1)	-.184						
1.2	.741	.285(+1)	.715(-1)					.234	.338(-1)
1.3	.741	.288(+1)	-.295(-1)						
1.4	.740	.291(+1)	.165					.163	.800(-2)
1.5	.749	.110(-2)	.314	.858(-1)	-.731	-.112(-2)	-.128(-2)	.182(-3)	-.441(-3)
1.6	.739	.505(-3)	.284(+1)	.653(-1)	.229	-.140(-2)	-.672(-4)	.384(-4)	-.102(-3)
1.7	.739	.475(-3)	.177(+1)					.165(-3)	-.226(-3)
1.8	.738	.254(-3)	.233(+1)	-.201	.423	.205(-1)	-.952(-3)	.241(-3)	-.810(-4)
2.0	.737	.256(-3-)	.115(+1)					.293(-3)	-.537(-4)
2.2	.737	.372(-3)	.212(+1)						

23A. Energies (in hartree) at $\gamma = 120°$ and $\theta = 30°$.

R_1 (bohr)	E_1	E_2	E_3	E_4
1.0	-1.622002	-1.251948	-1.250013	-1.251001
1.1	-1.647886	-1.278065	-1.275784	-1.276776
1.2	-1.662918	-1.293355	-1.290847	-1.291970
1.3	-1.670549	-1.301465	-1.298603	-1.299450
1.4	-1.672803	-1.305628	-1.300420	-1.301885
1.5	-1.671199	-1.322071	-1.302112	-1.300389
1.6	-1.667050	-1.340337	-1.299203	-1.296259
1.7	-1.661051	-1.357601	-1.296001	-1.290280
1.8	-1.653719	-1.373034	-1.295531	-1.283093
2.0	-1.636813	-1.400784	-1.294373	-1.266692
2.2	-1.618930	-1.421965	-1.289869	-1.249609

23B. Electric dipole transition moments (in a.u.) at $\gamma = 120°$ and $\theta = 30°$.

R_1 (bohr)	$T_{41}(z)$	$T_{42}(z)$	$T_{43}(z)$	$T_{31}(x)$	$T_{31}(y)$	$T_{32}(x)$	$T_{32}(y)$	$T_{21}(x)$	$T_{21}(y)$
1.0	.687	-.166	.256(+1)	.411	-.907(-1)	-.414	-.254(+1)	-.113	-.662
1.1	.685	.116	.255(+1)						
1.2	.677	-.159	.255(+1)	.426	-.106				
1.3	.676	.425(-1)	.254(+1)						
1.4	.664	-.605	.216(+1)	.484	.226				
1.5	.660	-.217	.720	.327	.506	-.671	.551(-1)	-.785(-1)	.112
1.6	.648	-.123	.795					-.628(-1)	.600(-1)
1.7	.639	-.819(-1)	.835	.513	.153	-.117(+1)	.378	-.454(-1)	.396(-1)
1.8	.623	-.618(-1)	-.621					-.364(-1)	.284(-1)
2.0	.582	-.414(-1)						-.221(-1)	.168(-1)
2.2	.508	-.292(-1)	-.453						

24A. Energies (in hartree) at $\gamma = 120°$ and $\theta = 35°$.

R_1 (bohr)	E_1	E_2	E_3	E_4
1.0	-1.619018	-1.265038	-1.259437	-1.262103
1.1	-1.645285	-1.291891	-1.285384	-1.288015
1.2	-1.660679	-1.308434	-1.301017	-1.303198
1.3	-1.668565	-1.319053	-1.310192	-1.310845
1.4	-1.671099	-1.330136	-1.315893	-1.313312
1.5	-1.669876	-1.344870	-1.318530	-1.311898
1.6	-1.665853	-1.359186	-1.317558	-1.308006
1.7	-1.660003	-1.373093	-1.315737	-1.302126
1.8	-1.652856	-1.385700	-1.314015	-1.295145
2.0	-1.636043	-1.408674	-1.310514	-1.279232
2.2	-1.618316	-1.427969	-1.305284	-1.262605

24B. Electric dipole transition moments (in a.u.) at $\gamma = 120°$ and $\theta = 35°$.

R_1 (bohr)	$T_{41}(z)$	$T_{42}(z)$	$T_{43}(z)$	$T_{31}(x)$	$T_{31}(y)$	$T_{32}(x)$	$T_{32}(y)$	$T_{21}(x)$	$T_{21}(y)$
1.0	.596		.272(+1)	.424	-.130				
1.1	.587	.342	.271(+1)						
1.2	.575	.207	-.269(+1)	-.477	.121	-.452	-.247(+1)	.162	.487
1.3	.563	.114	.242(+1)						
1.4	.548	-.419	-.155(+1)					-.118	.261
1.5	.538	-.291	-.116(+1)	-.493	-.240	.132(+1)	-.363	-.155	.162
1.6	.514	-.213						-.131	.115
1.7	.502	-.151	-.973	-.598	-.500(-1)	.142(+1)	-.411	.126(-1)	.799(-2)
1.8	.475	-.117	.861					-.941(-1)	.679(-1)
2.0	.418	-.765(-1)	-.708					-.597(-1)	.435(-1)
2.2	.348	-.573(-1)	-.639					-.389(-1)	.280(-1)

35A. Energies (in hartree) at $\gamma = 150°$ and $\theta = 40°$.

R_1 (bohr)	E_1	E_2	E_3	E_4
1.0	-1.603835	-1.303067	-1.298178	-1.299651
1.1	-1.632864	-1.328545	-1.322661	-1.324353
1.2	-1.650727	-1.344147	-1.336873	-1.338417
1.3	-1.660624	-1.354214	-1.344321	-1.345063
1.4	-1.664853	-1.368975	-1.348702	-1.346505
1.5	-1.664930	-1.385764	-1.348863	-1.344177
1.6	-1.662155	-1.400042	-1.346503	-1.339544
1.7	-1.657131	-1.412197	-1.341649	-1.333069
1.8	-1.650724	-1.422572	-1.336810	-1.325375
1.9	-1.643172	-1.431313	-1.331001	-1.316789
2.0	-1.635227	-1.438944	-1.325989	-1.307824
2.2	-1.618048	-1.451438	-1.316336	-1.289373

35B. Electric dipole transition moments (in a.u.) at $\gamma = 150°$ and $\theta = 40°$.

R_1 (bohr)	$T_{41}(z)$	$T_{42}(z)$	$T_{43}(z)$	$T_{31}(x)$	$T_{31}(y)$	$T_{32}(x)$	$T_{32}(y)$	$T_{21}(x)$	$T_{21}(y)$
1.0	.425	.186(+1)	.215(+1)	.374	-.318	.136	.269	.437	.248
1.1	.408	.164(+1)	.217(+1)						
1.2	.391	.164(+1)	.230(+1)	.446	-.282	.144	.715	.422	.225
1.3	.374	.104(+1)	.261(+1)						
1.4	.357	.170	-.246(+1)	-.771	.243(-2)	.910	-.913	-.121	.130
1.5	.342	-.174(-1)	.230(+1)	.796	.514(-2)	-.952	.507	-.208	.130
1.6	.321	-.751(-1)	.191(+1)	.792	.372(-1)	-.937	.338	-.231	.892(-1)
1.7	.304	-.596(-1)	.205(+1)						
1.8	.238	-.805(-1)	.170(+1)	.937	-.439	.102(+1)	.246	-.217	.724(-1)
1.9	.266	-.616(-1)	.173(+1)						
2.0	.243	-.718(-1)	.146(+1)	.111(+1)	-.150	-.114(+1)	.229	-.183	.593(-1)
2.2	.202	-.602(-1)	.120(+1)	.126(+1)	-.248	-.118(+1)	.209	-.145	.464(-1)

26A. Energies (in hartree) at $\gamma = 120°$ and $\theta = 41°$.

R_1 (bohr)	E_1	E_2	E_3	E_4
1.0	-1.589492	-1.338027	-1.326620	-1.327683
1.2	-1.640457	-1.380659	-1.363330	-1.365625
1.3	-1.651964	-1.391008	-1.369670	-1.371833
1.4	-1.657604	-1.397202	-1.369875	-1.372590
1.5	-1.658879	-1.402899	-1.366946	-1.369658
1.6	-1.656933	-1.409515	-1.363618	-1.364150
1.7	-1.652908	-1.417464	-1.361253	-1.356622
1.8	-1.647181	-1.425829	-1.358304	-1.348046
2.0	-1.632725	-1.441533	-1.348123	-1.328704
2.2	-1.616358	-1.454045	-1.336254	-1.308113

26B. Electric dipole transition moments (in a.u.) at $\gamma = 120°$ and $\theta = 41°$.

R_1 (bohr)	$T_{41}(z)$	$T_{42}(z)$	$T_{43}(z)$	$T_{31}(x)$	$T_{31}(y)$	$T_{32}(x)$	$T_{32}(y)$	$T_{21}(x)$	$T_{21}(y)$
1.0	.391	.116(+1)	.256(+1)						
1.2	.350	.100(+1)	.267(+1)	.509	-.259	.142	.171(+1)	.385	.170
1.3	.332	.876	.272(+1)	.529	-.253	.182	.176(+1)	.366	.142
1.4	.312	.720	.277(+1)	.566	-.247	.120	.174(+1)	.322	.112
1.5	.293	.500	.282(+1)						
1.6	.278	.329	.261(+1)	.799	-.235	-.313	.141(+1)	.133	.749(-1)
1.7	.263	.203	-.199(+1)	-.860	.223	.634	-.972	.398(-1)	.690(-1)
1.8	.243	.875(-1)	.154(+1)					-.159(-1)	.676(-1)
2.0	.207	.193(-1)	.122(+1)					-.618(-1)	-.600(-1)
2.2	.173	-.464(-1)	.101(+1)					-.665(-1)	.515(-1)

27A. Energies (in hartree) at $\gamma = 120°$ and $\theta = 42°$.

R_1 (bohr)	E_1	E_2	E_3	E_4
1.0	-1.574167	-1.357616	-1.346503	-1.345485
1.2	-1.630923	-1.400301	-1.382594	-1.383408
1.3	-1.644578	-1.409632	-1.387627	-1.389217
1.4	-1.652030	-1.415015	-1.387575	-1.389664
1.5	-1.654727	-1.418542	-1.384029	-1.386375
1.6	-1.665998	-1.422259	-1.377492	-1.380253
1.7	-1.650853	-1.427405	-1.371177	-1.372296
1.8	-1.645949	-1.434103	-1.367812	-1.363070
2.0	-1.632527	-1.448402	-1.357841	-1.342396
2.2	-1.616715	-1.460288	-1.344881	-1.320627

27B. Electric dipole transition moments (in a.u.) at $\gamma = 120°$ and $\theta = 42°$.

R_1 (bohr)	$T_{41}(z)$	$T_{42}(z)$	$T_{43}(z)$	$T_{31}(x)$	$T_{31}(y)$	$T_{32}(x)$	$T_{32}(y)$	$T_{21}(x)$	$T_{21}(y)$
1.0	.357	.149(+1)	.235(+1)	.512	-.326	-.777(-1)	.985	.540	.129
1.2	.307	.111(+1)	-.255(+1)	-.542	.290	-.216	-.151(+1)	.468	.917(-1)
1.3	.287	.105(+1)	.261(+1)	.546	-.281	.179	.150(+1)	.458	.642(-1)
1.4	.267	.894	.266(+1)	.558	-.274	.267	.156(+1)	.421	.410(-1)
1.5	.249	.726	.270(+1)						
1.6	.234	.533	.280(+1)	.676	-.287	.104	.144(+1)	.278	.144(-1)
1.7	.219	.379	.264(+1)	.847	-.300	-.153	.127(+1)	.174	.179(-1)
1.8	.202	.223						.829(-1)	.274(-1)
2.0	.173	.860(-1)	.131(+1)					-.180(-1)	.414(-1)
2.2	.144	.365(-1)	.111(+1)					-.505(-1)	.438(-1)

28A. Energies (in hartree) at $\gamma = 120°$ and $\theta = 43°$.

R_1 (bohr)	E_1	E_2	E_3	E_4
1.0	-1.550337	-1.374534	-1.362901	-1.359848
1.1	-1.590216	-1.402065	-1.388083	-1.385811
1.2	-1.616756	-1.417478	-1.400200	-1.400334
1.3	-1.634220	-1.428106	-1.407128	-1.406673
1.4	-1.644450	-1.432640	-1.406552	-1.407374
1.5	-1.649278	-1.434517	-1.402369	-1.403910
1.6	-1.650665	-1.435811	-1.395375	-1.397711
1.8	-1.645067	-1.442066	-1.377916	-1.479707
2.0	-1.633226	-1.453894	-1.376266	-1.357910
2.2	-1.618415	-1.465391	-1.354617	-1.334842

28B. Electric dipole transition moments (in a.u.) at $\gamma = 120°$ and $\theta = 43°$.

R_1 (bohr)	$T_{41}(z)$	$T_{42}(z)$	$T_{43}(z)$	$T_{31}(x)$	$T_{31}(y)$	$T_{32}(x)$	$T_{32}(y)$	$T_{21}(x)$	$T_{21}(y)$
1.0	.306	.185(+1)	.200(+1)	-.494	.360	.271	-.731(-1)	.739	-.430(-1)
1.1	.276	.161(+1)	.222(+1)						
1.2	.250	.153(+1)	.230(+1)	.546	-.332	.132(-1)	.784	.633	-.461(-1)
1.3	.229	.123(+1)	-.246(+1)						
1.4	.210	.106(+1)	.253(+1)	.583	-.331	.290	.131(+1)	.529	-.597(-1)
1.5	.196	.955	.261(+1)						
1.6	.180	.748	.265(+1)	.616	-.309	.289	.132(+1)	.423	-.749(-1)
1.8	.155	.419	-.276(+1)	-.841	.363	-.798(-1)	-.116(+1)	.225	-.420(-1)
2.0	.132	.183	.159(+1)					.605(-1)	.110(-2)
2.2	.112	.876(-1)	.121(+1)					-.150(-1)	.250(-1)

29A. Energies (in hartree) at $\gamma = 120°$ and $\theta = 44°$.

R_1 (bohr)	E_1	E_2	E_3	E_4
1.1	-1.558448	-1.408844	-1.394734	-1.390954
1.2	-1.593654	-1.429306	-1.412795	-1.409983
1.3	-1.617634	-1.440913	-1.421383	-1.419370
1.4	-1.632951	-1.446677	-1.423217	-1.422152
1.6	-1.646464	-1.448293	-1.413555	-1.414566
1.8	-1.645249	-1.448631	-1.394558	-1.397038
1.9	-1.641277	-1.451601	-1.383523	-1.386242
2.0	-1.635844	-1.456198	-1.376105	-1.374753
2.4	-1.606646	-1.476362	-1.350112	-1.326540

29B. Electric dipole transition moments (in a.u.) at $\gamma = 120°$ and $\theta = 44°$.

R_1 (bohr)	$T_{41}(z)$	$T_{42}(z)$	$T_{43}(z)$	$T_{31}(x)$	$T_{31}(y)$	$T_{32}(x)$	$T_{32}(y)$	$T_{21}(x)$	$T_{21}(y)$
1.1	.184	.190(+1)	.191(+1)						
1.2	.160	.166(+1)	.215(+1)	.589	-.360	.137(-1)	.389	.743	-.221
1.3	.142	.148(+1)	.228(+1)						
1.4	.129	.130(+1)	.240(+1)	.601	-.340	.312	.953	.621	-.199
1.6	.107	.100(+1)	.255(+1)	.603	-.328	.423	.115(+1)	.534	-.192
1.8	.898(-1)	.638	.269(+1)	.672	-.353	.362	.109(+1)	.385	-.150
1.9	.842(-1)	.480	.280(+1)	.802	-.404	.311	.103(+1)	.277	-.109
2.0	.709(-1)	.326	-.225(+1)	-.961	.476	-.115	-.779	.179	-.704(-1)
2.4	.518(-1)	.813(-1)	.112(+1)						

30A. Energies (in hartree) at $\gamma = 120°$ and $\theta = 45°$.

R_1 (bohr)	E_1	E_2	E_3	E_4
1.0	-1.415697	-1.324580	-1.309275	-1.304294
1.1	-1.492397	-1.378857	-1.364738	-1.359671
1.2	-1.546707	-1.413234	-1.398861	-1.394372
1.4	-1.610930	-1.446633	-1.427396	-1.424990
1.6	-1.638751	-1.454114	-1.426506	-1.426177
1.8	-1.645768	-1.452227	-1.410932	-1.412556
1.9	-1.644471	-1.452186	-1.400662	-1.402631
2.0	-1.640819	-1.454210	-1.389127	-1.391669
2.2	-1.629508	-1.463306	-1.373018	-1.367525

30B. Electric dipole transition moments (in a.u.) at $\gamma = 120°$ and $\theta = 45°$.

R_1 (bohr)	$T_{41}(z)$	$T_{42}(z)$	$T_{43}(z)$	$T_{31}(x)$	$T_{31}(y)$	$T_{32}(x)$	$T_{32}(y)$	$T_{21}(x)$	$T_{21}(y)$
1.0	-.584(-6)	.242(+1)	.110(+1)	.425	-.245	-.927	-.161(+1)	-.123(+1)	-.710
1.1	.424(-6)	.225(+1)	.143(+1)						
1.2	.961(-6)	.204(+1)	.172(+1)	-.560	.323	.321	.566	.887	-.512
1.4	.195(-6)	.157(+1)	.220(+1)	.639	-.369	.267	.463	.690	-.398
1.6	-.132(-6)	.122(+1)	.242(+1)	.631	-.364	.525	.910	.585	-.338
1.8	.149(-6)	.901	.257(+1)	.628	-.363	.601	.104(+1)	.493	-.284
1.9	.126(-6)	.706	.262(+1)						
2.0	-.176(-6)	.544	.276(+1)	.725	-.418	.541	.936	.317	-.183
2.2	-.794(-9)	.261	.177(+1)						

31A. Energies (in hartree) at $\gamma = 150°$ and $\theta = 0°$.

R_1 (bohr)	E_1	E_2	E_3	E_4
1.0	-1.622452	-1.247753	-1.247340	-1.247195
1.1	-1.648216	-1.273447	-1.273132	-1.272908
1.2	-1.663287	-1.288484	-1.288138	-1.288003
1.3	-1.670770	-1.296153	-1.295778	-1.295496
1.4	-1.672874	-1.298179	-1.297771	-1.297734
1.5	-1.671450	-1.309245	-1.296129	-1.296140
1.6	-1.667182	-1.331342	-1.292051	-1.291945
1.7	-1.661186	-1.350599	-1.285568	-1.285820
1.8	-1.653743	-1.367848	-1.278318	-1.278453
2.0	-1.636765	-1.396697	-1.261356	-1.261554
2.2	-1.618786	-1.419560	-1.242694	-1.243539

31B. Electric dipole transition moments (in a.u.) at $\gamma = 150°$ and $\theta = 0°$.

R_1 (bohr)	$T_{41}(z)$	$T_{42}(z)$	$T_{43}(z)$	$T_{31}(x)$	$T_{31}(y)$	$T_{32}(x)$	$T_{32}(y)$	$T_{21}(x)$	$T_{21}(y)$
1.0	.742	.282(+1)	.229					.254	-.104(-1)
1.1	.742	.280(+1)	-.184						
1.2	.741	.285(+1)	.715(-1)					.234	.338(-1)
1.3	.741	.288(+1)	-.295(-1)						
1.4	.740	.291(+1)	.165					.163	.800(-2)
1.5	.749	.110(-2)	.314	.858(-1)	-.731	-.112(-2)	-.128(-2)	.182(-3)	-.441(-3)
1.6	.739	.505(-3)	.284(+1)	.653(-1)	.229	-.140(-2)	-.672(-4)	.384(-4)	-.102(-3)
1.7	.739	.475(-3)	.177(+1)					.165(-3)	-.226(-3)
1.8	.738	.254(-3)	.233(+1)	-.201	.423	.205(-1)	-.952(-3)	.241(-3)	-.810(-4)
2.0	.737	.256(-3-)	.115(+1)					.293(-3)	-.537(-4)
2.2	.737	.372(-3)	.212(+1)						

32A. Energies (in hartree) at $\gamma = 150°$ and $\theta = 20°$.

R_1 (bohr)	E_1	E_2	E_3	E_4
1.0	-1.622414	-1.247243	-1.247081	-1.247458
1.1	-1.648230	-1.272914	-1.272623	-1.273199
1.2	-1.663302	-1.287988	-1.287620	-1.288224
1.3	-1.670817	-1.295532	-1.295122	-1.295700
1.4	-1.673018	-1.297649	-1.297291	-1.297926
1.5	-1.671431	-1.296262	-1.295631	-1.296390
1.6	-1.667232	-1.332627	-1.292101	-1.292126
1.7	-1.661204	-1.351758	-1.286303	-1.285977
1.8	-1.653735	-1.368628	-1.278531	-1.278667
1.9	-1.645701	-1.383526	-1.271051	-1.270447
2.0	-1.636897	-1.397145	-1.265526	-1.261806
2.2	-1.618827	-1.420063	-1.263457	-1.243733

32B. Electric dipole transition moments (in a.u.) at $\gamma = 150°$ and $\theta = 20°$.

R_1 (bohr)	$T_{41}(z)$	$T_{42}(z)$	$T_{43}(z)$	$T_{31}(x)$	$T_{31}(y)$	$T_{32}(x)$	$T_{32}(y)$	$T_{21}(x)$	$T_{21}(y)$
1.0	.733	.536	.246(+1)						
1.1	.732	.297	.248(+1)						
1.2	.731	.261	.245(+1)	.438	.406(-1)				
1.3	.730	.535	.243(+1)						
1.4	.729	.818(-1)	.249(+1)	.435	-.129(-1)				
1.5	.727	.250	.246(+1)						
1.6	.724	-.267(-1)	.499	.501	.687(-1)	-.259(-1)	.609(-2)	-.133(-1)	.390(-2)
1.7	.723	-.160(-1)	.147	-.159	-.688	.212(-1)	.151(-1)	-.891(-2)	.355(-2)
1.8	.718	.965(-2)	.150(-1)					.724(-2)	-.219(-2)
1.9	.717	.100(-1)	-.134					.509(-2)	-.180(-2)
2.0	.711	.711(-2)	-.241					.464(-2)	-.142(-2)
2.2	.720	-.480(-2)	-.510(-1)					-.296(-2)	.102(-2)

33A. Energies (in hartree) at $\gamma = 150°$ and $\theta = 30°$.

R_1 (bohr)	E_1	E_2	E_3	E_4
1.0	-1.622152	-1.249608	-1.248643	-1.249691
1.1	-1.647990	-1.275442	-1.274066	-1.275403
1.2	-1.663088	-1.290683	-1.289228	-1.290420
1.3	-1.670670	-1.298485	-1.296946	-1.297891
1.4	-1.672915	-1.300449	-1.298483	-1.300138
1.5	-1.671339	-1.326075	-1.299147	-1.298580
1.6	-1.667197	-1.343538	-1.295193	-1.294426
1.7	-1.661197	-1.360071	-1.290696	-1.288376
1.8	-1.653773	-1.375041	-1.287718	-1.281092
1.9	-1.645627	-1.388832	-1.287734	-1.273064
2.0	-1.636924	-1.401102	-1.287227	-1.264610
2.2	-1.618985	-1.422596	-1.284052	-1.247528

33B. Electric dipole transition moments (in a.u.) at $\gamma = 150°$ and $\theta = 30°$.

R_1 (bohr)	$T_{41}(z)$	$T_{42}(z)$	$T_{43}(z)$	$T_{31}(x)$	$T_{31}(y)$	$T_{32}(x)$	$T_{32}(y)$	$T_{21}(x)$	$T_{21}(y)$
1.0	.694	-.119(+1)	.224(+1)	.356	-.351				
1.1	.691	-.112(+1)	.226(+1)						
1.2	.687	-.114(+1)	.224(+1)	.377	-.349				
1.3	.683	-.971	.231(+1)						
1.4	.676	.133(+1)	.203(+1)	.346	-.393				
1.5	.670	-.209	-.896						
1.6	.661	-.133	.192(+1)	.605	.256	-.373	.540(-1)	-.769(-1)	.311(-1)
1.7	.654	-.888(-1)	.121(+1)						
1.8	.642	-.697(-1)	.805	.700	-.824(-2)	-.154(+1)	.262	-.529(-1)	.174(-1)
1.9	.628	-.573(-1)	-.553						
2.0	.605	-.492(-1)	-.431	-.686	.144	.129(+1)	-.246	-.318(-1)	.106(-1)
2.2	.534	-.372(-1)	-.404	-.738	.221	.101(+1)	-.206	-.202(-1)	.695(-1)

34A. Energies (in hartree) at $\gamma = 150°$ and $\theta = 35°$.

R_1 (bohr)	E_1	E_2	E_3	E_4
1.0	-1.619869	-1.259062	-1.255995	-1.258222
1.1	-1.645992	-1.284960	-1.282071	-1.283950
1.2	-1.661456	-1.300492	-1.298026	-1.298939
1.3	-1.669235	-1.313985	-1.307984	-1.306461
1.4	-1.671737	-1.333271	-1.310669	-1.308825
1.5	-1.670412	-1.349845	-1.310154	-1.307288
1.6	-1.666318	-1.364872	-1.307779	-1.303319
1.7	-1.660346	-1.377822	-1.304577	-1.297302
1.8	-1.653127	-1.390017	-1.302376	-1.290360
1.9	-1.645750	-1.401181	-1.301273	-1.282522
2.0	-1.636523	-1.411501	-1.300136	-1.274444
2.2	-1.618688	-1.429296	-1.296687	-1.258112

34B. Electric dipole transition moments (in a.u.) at $\gamma = 150°$ and $\theta = 35°$.

R_1 (bohr)	$T_{41}(z)$	$T_{42}(z)$	$T_{43}(z)$	$T_{31}(x)$	$T_{31}(y)$	$T_{32}(x)$	$T_{32}(y)$	$T_{21}(x)$	$T_{21}(y)$
1.0	.609	.120(+1)	.242(+1)	.379	-.302	.101(+1)	.152(+1)	.264	.511
1.1	.599	-.108(+1)	.248(+1)						
1.2	.590	-.886	.244(+1)	.476	-.219	-.795	-.192(+1)	-.244	-.507
1.3	.580	-.785	-.151(+1)						
1.4	.568	-.398	-.146(+1)	-.467	-.374	.711	.903(-1)	-.243	.981(-1)
1.5	.555	-.284	-.143(+1)						
1.6	.537	-.214	.143(+1)	.632	.253			-.182	.619(-1)
1.7	.528	-.163	.133(+1)	.753	.146	-.131(+1)	.145	-.156	.517(-1)
1.8	.497	-.135	-.111(+1)	-.848	-.192(-1)			-.130	.431(-1)
1.9	.471	-.112	.919						
2.0	.442	-.979(-1)	.805	.903	-.142			-.893(-1)	.296(-1)
2.2	.364	-.714(-1)	.676	.931	-.222			-.584(-1)	.198(-1)

35A. Energies (in hartree) at $\gamma = 150°$ and $\theta = 40°$.

R_1 (bohr)	E_1	E_2	E_3	E_4
1.0	-1.603835	-1.303067	-1.298178	-1.299651
1.1	-1.632864	-1.328545	-1.322661	-1.324353
1.2	-1.650727	-1.344147	-1.336873	-1.338417
1.3	-1.660624	-1.354214	-1.344321	-1.345063
1.4	-1.664853	-1.368975	-1.348702	-1.346505
1.5	-1.664930	-1.385764	-1.348863	-1.344177
1.6	-1.662155	-1.400042	-1.346503	-1.339544
1.7	-1.657131	-1.412197	-1.341649	-1.333069
1.8	-1.650724	-1.422572	-1.336810	-1.325375
1.9	-1.643172	-1.431313	-1.331001	-1.316789
2.0	-1.635227	-1.438944	-1.325989	-1.307824
2.2	-1.618048	-1.451438	-1.316336	-1.289373

35B. Electric dipole transition moments (in a.u.) at $\gamma = 150°$ and $\theta = 40°$.

R_1 (bohr)	$T_{41}(z)$	$T_{42}(z)$	$T_{43}(z)$	$T_{31}(x)$	$T_{31}(y)$	$T_{32}(x)$	$T_{32}(y)$	$T_{21}(x)$	$T_{21}(y)$
1.0	.425	.186(+1)	.215(+1)	.374	-.318	.136	.269	.437	.248
1.1	.408	.164(+1)	.217(+1)						
1.2	.391	.164(+1)	.230(+1)	.446	-.282	.144	.715	.422	.225
1.3	.374	.104(+1)	.261(+1)						
1.4	.357	.170	-.246(+1)	-.771	.243(-2)	.910	-.913	-.121	.130
1.5	.342	-.174(-1)	.230(+1)	.796	.514(-2)	-.952	.507	-.208	.130
1.6	.321	-.751(-1)	.191(+1)	.792	.372(-1)	-.937	.338	-.231	.892(-1)
1.7	.304	-.596(-1)	.205(+1)						
1.8	.238	-.805(-1)	.170(+1)	.937	-.439	.102(+1)	.246	-.217	.724(-1)
1.9	.266	-.616(-1)	.173(+1)						
2.0	.243	-.718(-1)	.146(+1)	.111(+1)	-.150	-.114(+1)	.229	-.183	.593(-1)
2.2	.202	-.602(-1)	.120(+1)	.126(+1)	-.248	-.118(+1)	.209	-.145	.464(-1)

36A. Energies (in hartree) at $\gamma = 150°$ and $\theta = 41°$.

R_1 (bohr)	E_1	E_2	E_3	E_4
1.0	-1.595191	-1.320298	-1.314255	-1.314918
1.1	-1.626046	-1.344987	-1.338291	-1.339105
1.2	-1.645481	-1.360419	-1.351581	-1.352821
1.3	-1.656528	-1.368950	-1.357718	-1.359089
1.4	-1.661824	-1.377715	-1.359162	-1.360243
1.5	-1.662693	-1.391888	-1.360873	-1.357518
1.6	-1.660523	-1.406447	-1.358936	-1.352425
1.7	-1.656031	-1.419096	-1.353344	-1.345289
1.8	-1.650102	-1.429478	-1.347856	-1.339198
1.9	-1.642812	-1.438485	-1.340980	-1.327850
2.0	-1.635081	-1.446076	-1.335046	-1.318717
2.2	-1.618270	-1.458014	-1.323456	-1.298455

36B. Electric dipole transition moments (in a.u.) at $\gamma = 150°$ and $\theta = 41°$.

R_1 (bohr)	$T_{41}(z)$	$T_{42}(z)$	$T_{43}(z)$	$T_{31}(x)$	$T_{31}(y)$	$T_{32}(x)$	$T_{32}(y)$	$T_{21}(x)$	$T_{21}(y)$
1.0	.383	.215(+1)	.182(+1)						
1.1									
1.2	.345	.176(+1)	.214(+1)	.422	-.283	-.233(-1)	.265	.512	.154
1.3	.329	.159(+1)	.227(+1)	.492	-.263	-.844(-1)	.574	.445	.147
1.4	.310	.757	.266(+1)	.789	-.146	-.442	.139(+1)	.146	.139
1.5	.296	.263	.246(+1)						
1.6	.277	.675(-1)	.203(+1)	.841	-.711(-1)	-.811	.503	-.180	.893(-1)
1.7	.264	.268(-1)	.219(+1)						
1.8	.242	-.232(-1)	.184(+1)	.964	-.241(-1)	-.872	.297	-.215	.740(-1)
1.9									
2.0	.208	-.374(-1)	.161(+1)	.114(+1)	-.163	-.957	.235	-.197	.632(-1)
2.2	.188	-.519(-1)	.134(+1)	.131(+1)	-.261	-.102(+1)	.199	-.164	.526(-1)

37A. Energies (in hartree) at $\gamma = 150°$ and $\theta = 42°$.

R_1 (bohr)	E_1	E_2	E_3	E_4
1.0	-1.582089	-1.338566	-1.330939	-1.331025
1.2	-1.637830	-1.377847	-1.368108	-1.368656
1.3	-1.650861	-1.385719	-1.373971	-1.374874
1.4	-1.657763	-1.390880	-1.374464	-1.375699
1.5	-1.659930	-1.398150	-1.371933	-1.372674
1.6	-1.658741	-1.410839	-1.371431	-1.367080
1.7	-1.655141	-1.423890	-1.366046	-1.359657
1.8	-1.649764	-1.435000	-1.360354	-1.350829
2.0	-1.635521	-1.452300	-1.345894	-1.331311
2.2	-1.619199	-1.464307	-1.331898	-1.310775

37B. Electric dipole transition moments (in a.u.) at $\gamma = 150°$ and $\theta = 42°$.

R_1 (bohr)	$T_{41}(z)$	$T_{42}(z)$	$T_{43}(z)$	$T_{31}(x)$	$T_{31}(y)$	$T_{32}(x)$	$T_{32}(y)$	$T_{21}(x)$	$T_{21}(y)$
1.0	.337	.236(+1)	.144(+1)	.274	-.323			.672	.601(-1)
1.2	.297	.201(+1)	.182(+1)	.375	-.279	-.217	-.488	.637	.647(-1)
1.3	.279	.190(+1)	.194(+1)	.418	-.263	-.174	-.224	.593	.642(-1)
1.4	.259	.145(+1)	.223(+1)	.528	-.245	-.171	.416	.472	.643(-1)
1.5	.245	.812	-.262(+1)						
1.6	.229	.323	.226(+1)	.917	-.827	-.616	.787	-.436(-1)	.725(-1)
1.7	.216	.170	.231(+1)						
1.8	.200	.670(-1)	.194(+1)	.993	-.110	-.683	.371	-.182	.703(-1)
2.0	.171	.746(-2)	.173(+1)						
2.2	.144	-.165(-1)	.148(+1)	.133(+1)	-.268	-.814	.190	-.182	.567(-1)

38A. Energies (in hartree) at $\gamma = 150°$ and $\theta = 43°$.

R_1 (bohr)	E_1	E_2	E_3	E_4
1.0	-1.560822	-1.354596	-1.344365	-1.343897
1.2	-1.626207	-1.395280	-1.384144	-1.384188
1.3	-1.642539	-1.402703	-1.390394	-1.390673
1.4	-1.652254	-1.406193	-1.391267	-1.391788
1.5	-1.656552	-1.408352	-1.388312	-1.388741
1.6	-1.657129	-1.414124	-1.382440	-1.383068
1.7	-1.654758	-1.425161	-1.378965	-1.375378
1.8	-1.650481	-1.436901	-1.373347	-1.366274
2.0	-1.637464	-1.455933	-1.357996	-1.345738
2.2	-1.621550	-1.468908	-1.341778	-1.324095

38B. Electric dipole transition moments (in a.u.) at $\gamma = 150°$ and $\theta = 43°$.

R_1 (bohr)	$T_{41}(z)$	$T_{42}(z)$	$T_{43}(z)$	$T_{31}(x)$	$T_{31}(y)$	$T_{32}(x)$	$T_{32}(y)$	$T_{21}(x)$	$T_{21}(y)$
1.0	.276	.251(+1)	-.109(+1)	-.252	.289	.434	.195(+1)	.830	-.462(-1)
1.2	.232	.223(+1)	.152(+1)	.335	-.251	-.351	-.113(+1)	.766	-.301(-1)
1.3	.216	.213(+1)	.167(+1)	.375	-.238	-.238	-.879	.728	-.266(-1)
1.4	.198	.183(+1)	.189(+1)	.441	-.229	-.211	-.305	.668	-.220(-1)
1.5	.187	.153(+1)	.210(+1)						
1.6	.172	.865	-.264(+1)	-.844	.217	.228	-.843	.252	.175(-1)
1.7	.162	.446	.245(+1)						
1.8	.148	.215	.213(+1)	.101(+1)	-.158	-.443	.515	-.103	.532(-1)
2.0	.127	.683(-1)	.188(+1)	.114(+1)	-.206	.246	.794(-1)	-.184	.603(-1)
2.2	.107	.183(-1)	.163(+1)	.131(+1)	-.276	-.552	.183	-.191	.581(-1)

39A. Energies (in hartree) at $\gamma = 150°$ and $\theta = 44°$.

R_1 (bohr)	E_1	E_2	E_3	E_4
1.0	-1.521113	-1.356993	-1.343064	-1.341960
1.1	-1.571026	-1.387786	-1.374866	-1.373860
1.2	-1.605491	-1.406205	-1.393520	-1.392637
1.3	-1.628558	-1.415520	-1.402706	-1.402157
1.4	-1.643215	-1.419572	-1.405167	-1.405196
1.5	-1.651412	-1.419880	-1.403239	-1.403484
1.6	-1.654881	-1.420180	-1.398004	-1.398565
1.7	-1.654804	-1.423809	-1.390696	-1.391217
1.8	-1.652116	-1.433254	-1.384542	-1.382334
1.9	-1.647447	-1.444279	-1.378459	-1.372114
2.0	-1.641385	-1.454297	-1.370952	-1.361464
2.2	-1.626461	-1.469580	-1.353604	-1.338870

39B. Electric dipole transition moments (in a.u.) at $\gamma = 150°$ and $\theta = 44°$.

R_1 (bohr)	$T_{41}(z)$	$T_{42}(z)$	$T_{43}(z)$	$T_{31}(x)$	$T_{31}(y)$	$T_{32}(x)$	$T_{32}(y)$	$T_{21}(x)$	$T_{21}(y)$
1.0	.180	.257(+1)	.862					.101(+1)	-.169
1.1	.157	.251(+1)	.104(+1)						
1.2	.140	.240(+1)	.120(+1)	.291	-.188	-.434	-.170(+1)	.903	-.145
1.3	.127	.231(+1)	-.143(+1)						
1.4	.116	.214(+1)		.388	-.179			.793	-.123
1.5	.108	.196(+1)	.176(+1)						
1.6	.993(-1)	.156(+1)	.199(+1)	.519	-.187	-.134	-.912(-1)	.608	-.917(-1)
1.7	.925(-1)	.102(+1)	-.246(+1)						
1.8	.851(-1)	.520	.242(+1)	.102(+1)	-.221	-.954(-1)	.774	.869(-1)	.375(-2)
1.9	.806(-1)	.303	.233(+1)						
2.0	.715(-1)	.166	.198(+1)	.110(+1)	-.238	-.206	.345	-.130	.446(-1)
2.2	.605(-1)	.652(-1)	.177(+1)	.126(+1)	-.293	-.257	.184	-.186	.541(-1)

40A. Energies (in hartree) at $\gamma = 150°$ and $\theta = 45°$.

R_1 (bohr)	E_1	E_2	E_3	E_4
1.0	-1.430252	-1.308355	-1.290660	-1.289632
1.1	-1.506566	-1.360002	-1.344250	-1.343280
1.2	-1.560367	-1.392268	-1.377973	-1.377037
1.3	-1.597939	-1.411371	-1.397890	-1.396958
1.4	-1.623289	-1.421444	-1.407738	-1.407224
1.5	-1.639695	-1.425146	-1.410677	-1.410552
1.6	-1.649215	-1.425269	-1.408690	-1.409160
1.8	-1.654183	-1.425590	-1.395917	-1.396714
1.9	-1.652050	-1.433264	-1.388053	-1.387465
2.0	-1.647526	-1.443999	-1.382505	-1.377206
2.2	-1.634472	-1.463215	-1.365844	-1.354677

40B. Electric dipole transition moments (in a.u.) at $\gamma = 150°$ and $\theta = 45°$.

R_1 (bohr)	$T_{41}(z)$	$T_{42}(z)$	$T_{43}(z)$	$T_{31}(x)$	$T_{31}(y)$	$T_{32}(x)$	$T_{32}(y)$	$T_{21}(x)$	$T_{21}(y)$
1.0	.546(-6)	.260(+1)	-.587					.122(+1)	-.328
1.1	.108(-6)	.257(+1)	.707						
1.2	.138(-6)	.252(+1)	.896					.102(+1)	-.273
1.3	.314(-6)	.246(+1)	.108(+1)						
1.4	.120(-5)	.233(+1)	.130(+1)	.346	-.927(-1)	-.407	-.152(+1)	.891	-.239
1.5	.469(-6)	.222(+1)	.150(+1)						
1.6	-.106(-6)	.199(+1)	.169(+1)	.440	-.118	-.201	-.748	.779	-.209
1.8	.118(-6)	.122(+1)	.215(+1)	.619	-.116	.331	.124	.470	-.126
1.9	.326(-6)	.673	.265(+1)						
2.0	.546(-6)	.358	.220(+1)	.105(+1)	-.281	.139	.518	-.351(-2)	.939(-3)
2.2	.715(-6)	.132	.191(+1)	.117(+1)	-.312	.557(-1)	.208	-.152	.407(-1)

41A. Energies (in hartree) at $\gamma = 180°$ and $\theta = 0°$.

R_1 (bohr)	E_1	E_2	E_3	E_4
1.0	-1.622411	-1.247049	-1.246984	-1.247192
1.1	-1.648203	-1.273168	-1.272737	-1.272967
1.2	-1.663273	-1.287824	-1.287778	-1.288010
1.3	-1.670766	-1.295267	-1.295108	-1.295499
1.4	-1.673020	-1.297438	-1.297381	-1.297734
1.5	-1.671435	-1.309302	-1.295808	-1.296085
1.6	-1.667258	-1.331377	-1.291770	-1.291910
1.7	-1.661156	-1.350706	-1.285466	-1.285818
1.8	-1.653795	-1.367858	-1.278349	-1.278448
1.9	-1.645634	-1.383097	-1.270268	-1.270237
2.0	-1.636842	-1.496687	-1.261682	-1.261512
2.1	-1.627985	-1.408843	-1.254054	-1.252511

41B. Electric dipole transition moments (in a.u.) at $\gamma = 180°$ and $\theta = 0°$.

R_1 (bohr)	$T_{41}(z)$	$T_{42}(z)$	$T_{43}(z)$	$T_{31}(x)$	$T_{31}(y)$	$T_{32}(x)$	$T_{32}(y)$	$T_{21}(x)$	$T_{21}(y)$
1.0	.743	.246(+1)	-.436(-6)					.368	.212
1.1	.743	-.245(+1)	.872(-6)						
1.2	.742	.255(+1)	-.469(-1)					.343	.198
1.3	.741	.756(-8)	.942	.507	.507	-.658	.658	-.519	.519
1.4	.741	-.152(+1)	-.186(-6)						
1.5	.747	.152(-2)	-.104(-7)	-.523	.523	-.112(-2)	.112(-2)	.166(-3)	.166(-3)
1.6	.740	.702(-3)	.131(+1)					.964(-7)	.321(-7)
1.7	.751	.388(-3)						.160(-3)	.160(-3)
1.8	.751	.282(-3)	-.208	.570	.570	.204(-2)	.204(-2)	.120(-3)	.120(-3)
1.9	.749	.190(-3)	-.284	.593	.593	.217(-1)	.217(-1)	.819(-4)	.819(-4)
2.0	.748	.158(-3)	-.310	.680	.680	.300(-2)	.300(-2)	.665(-4)	.665(-4)
2.1	.756	.935(-4)	.128(-2)	-.995	-.995	-.261(-1)	-.261(-1)	.137(-3)	.137(-3)

42A. Energies (in hartree) at $\gamma = 180°$ and $\theta = 20°$.

R_1 (bohr)	E_1	E_2	E_3	E_4
1.0	-1.622484	-1.247226	-1.247179	-1.247340
1.1	-1.648285	-1.272968	-1.272866	-1.273088
1.2	-1.663381	-1.287925	-1.287810	-1.288121
1.3	-1.670850	-1.295365	-1.295220	-1.295534
1.4	-1.673099	-1.297513	-1.297292	-1.297775
1.6	-1.667241	-1.332765	-1.291677	-1.291939
1.8	-1.653756	-1.368619	-1.278718	-1.278475
1.9	-1.645614	-1.383761	-1.270854	-1.270273
2.0	-1.636931	-1.397152	-1.265599	-1.261571
2.2	-1.618955	-1.419813	-1.263082	-1.243563

42B. Electric dipole transition moments (in a.u.) at $\gamma = 180°$ and $\theta = 20°$.

R_1 (bohr)	$T_{41}(z)$	$T_{42}(z)$	$T_{43}(z)$	$T_{31}(x)$	$T_{31}(y)$	$T_{32}(x)$	$T_{32}(y)$	$T_{21}(x)$	$T_{21}(y)$
1.0	.733	.243(+1)	-.161(-6)					.382	.221
1.1	.732	.145(-5)	.239(+1)						
1.2	.731	.199(-5)	.233(+1)	.418	.241				
1.3	.730	.604(-7)	.235(+1)						
1.4	.729	-.359(-6)	.226(+1)	.446	.258				
1.6	.726	-.312(-1)	.189(+1)						
1.8	.720	.141(-1)	.136(+1)					.567(-2)	.328(-2)
1.9	.715	-.108(-1)	.870						
2.0	.713	.920(-2)	-.220					.363(-2)	.209(-2)
2.2	.731	-.526(-2)	-.302(-1)					-.211(-2)	-.122(-2)

43A. Energies (in hartree) at $\gamma = 180°$ and $\theta = 30°$.

R_1 (bohr)	E_1	E_2	E_3	E_4
1.0	-1.622215	-1.249050	-1.248375	-1.249137
1.1	-1.648051	-1.274747	-1.274048	-1.274896
1.2	-1.663130	-1.289719	-1.289144	-1.289858
1.3	-1.670682	-1.297079	-1.296706	-1.297329
1.4	-1.672936	-1.307898	-1.299294	-1.299535
1.6	-1.667232	-1.344696	-1.293762	-1.293797
1.7	-1.661096	-1.360643	-1.288691	-1.287780
1.8	-1.655812	-1.375557	-1.284917	-1.280476
2.0	-1.636958	-1.401503	-1.284918	-1.263932
2.2	-1.618974	-1.422840	-1.282193	-1.246803

43B. Electric dipole transition moments (in a.u.) at $\gamma = 180°$ and $\theta = 30°$.

R_1 (bohr)	$T_{41}(z)$	$T_{42}(z)$	$T_{43}(z)$	$T_{31}(x)$	$T_{31}(y)$	$T_{32}(x)$	$T_{32}(y)$	$T_{21}(x)$	$T_{21}(y)$
1.0	.698	-.276(-4)	.249(+1)	.392	.226				
1.1	.694	.386(-3)	.247(+1)						
1.2	.689	.117(-5)	.246(+1)	.424	.245				
1.3	.686	.148(-6)	.245(+1)						
1.4	.682	-.416	-.769(-7)	-.475	.475	.295	-.294	-.103	-.103
1.6	.666	-.144	.220(+1)	.574	.331	-.406	-.235	-.746(-1)	-.431(-1)
1.7	.659	-.100	.189(+1)						
1.8	.644	-.769(-1)	.100(+1)					-.476(-1)	-.275(-1)
2.0	.612	-.533(-1)	-.438					-.306(-1)	-.177(-1)
2.2	.543	-.413(-1)	-.377					-.199(-1)	-.115(-1)

44A. Energies (in hartree) at $\gamma = 180°$ and $\theta = 35°$.

R_1 (bohr)	E_1	E_2	E_3	E_4
1.0	-1.620043	-1.256737	-1.253399	-1.256882
1.1	-1.646230	-1.282308	-1.281103	-1.282492
1.2	-1.661582	-1.297222	-1.296713	-1.297480
1.3	-1.669484	-1.314899	-1.304887	-1.305003
1.4	-1.671932	-1.335097	-1.306991	-1.307219
1.5	-1.670578	-1.351868	-1.305435	-1.305864
1.6	-1.666545	-1.366790	-1.302802	-1.301731
1.7	-1.660586	-1.379426	-1.299181	-1.295926
1.8	-1.653300	-1.391317	-1.296831	-1.289094
1.9	-1.645267	-1.402010	-1.296182	-1.289119
2.0	-1.636600	-1.412197	-1.295823	-1.273090
2.2	-1.618778	-1.430010	-1.293655	-1.257033

44B. Electric dipole transition moments (in a.u.) at $\gamma = 180°$ and $\theta = 35°$.

R_1 (bohr)	$T_{41}(z)$	$T_{42}(z)$	$T_{43}(z)$	$T_{31}(x)$	$T_{31}(y)$	$T_{32}(x)$	$T_{32}(y)$	$T_{21}(x)$	$T_{21}(y)$
1.0	.613	-.250(-6)	.252(+1)	.432	.249				
1.1	.604	-.137(-4)	.264(+1)						
1.2	.595	.811(-5)	.250(+1)	.474	.274				
1.3	.585	-.790	-.217(-1)						
1.4	.572	-.404	.102(-4)					-.212	-.122
1.5	.561	-.286	.144(-3)						
1.6	.542	-.215	.227(+1)	.683	.394	-.812	-.469	-.164	-.948(-1)
1.7	.523	-.173	.195(+1)						
1.8	.503	-.135	.151(+1)	.879	.508	-.144(+1)	-.831	-.122	-.705(-1)
1.9	.515	-.125	.104(+1)						
2.0	.448	-.100	-.899					-.865(-1)	-.500(-1)
2.2	.369	-.747(-1)	-.646	-.926	-.534	.125(+1)	.723	-.579(-1)	-.334(-1)

45A. Energies (in hartree) at $\gamma = 180°$ and $\theta = 40°$.

R_1 (bohr)	E_1	E_2	E_3	E_4
1.0	-1.605101	-1.296708	-1.295441	-1.295795
1.1	-1.634040	-1.320998	-1.320060	-1.320445
1.2	-1.651859	-1.335553	-1.334308	-1.334514
1.3	-1.661655	-1.341974	-1.341019	-1.341324
1.4	-1.665773	-1.369098	-1.344433	-1.342881
1.5	-1.665772	-1.387639	-1.343075	-1.340872
1.6	-1.662792	-1.402282	-1.339437	-1.336197
1.8	-1.651202	-1.424868	-1.329026	-1.322190
1.9	-1.643796	-1.433334	-1.323437	-1.313946
2.0	-1.635545	-1.440588	-1.318439	-1.305029
2.1	-1.626998	-1.447061	-1.314175	-1.296020
2.2	-1.618413	-1.452706	-1.310417	-1.286991

45B. Electric dipole transition moments (in a.u.) at $\gamma = 180°$ and $\theta = 40°$.

R_1 (bohr)	$T_{41}(z)$	$T_{42}(z)$	$T_{43}(z)$	$T_{31}(x)$	$T_{31}(y)$	$T_{32}(x)$	$T_{32}(y)$	$T_{21}(x)$	$T_{21}(y)$
1.0	.424	.281(+1)	-.562(-4)					.514	.297
1.1	.408	.280(+1)	.225(-5)						
1.2	.391	.276(+1)	-.184(-5)					.546	.315
1.3	.373	.276(+1)	-.167(-4)						
1.4	.358	-.940(-1)	.274(+1)	.652	.377	-.772	-.446	-.244	-.141
1.5	.339	-.115	.269(+1)						
1.6	.323	-.112	.259(+1)	.763	.440	-.802	-.463	-.251	-.149
1.8	.283	-.984(-1)	.230(+1)	.936	.541	-.941	-.543	-.223	-.129
1.9	.261	-.912(-1)	.210(+1)						
2.0	.244	-.823(-1)	.189(+1)	.113(+1)	.652	-.108(+1)	-.623	-.185	-.107
2.1	.224	-.715(-1)	.156(+1)						
2.2	.197	-.752(-1)	.139(+1)					-.147	-.846(-1)

46A. Energies (in hartree) at $\gamma = 180°$ and $\theta = 41°$.

R_1 (bohr)	E_1	E_2	E_3	E_4
1.0	-1.596986	-1.313556	-1.309994	-1.310355
1.1	-1.627705	-1.337582	-1.334249	-1.334641
1.2	-1.646950	-1.351739	-1.348060	-1.348359
1.3	-1.657950	-1.359107	-1.354793	-1.354717
1.4	-1.663007	-1.373223	-1.357525	-1.356078
1.5	-1.663759	-1.392612	-1.356568	-1.353565
1.6	-1.661557	-1.408643	-1.352383	-1.348611
1.8	-1.650791	-1.432086	-1.340183	-1.333759
2.0	-1.635695	-1.448099	-1.327525	-1.315697
2.2	-1.618680	-1.459275	-1.316395	-1.296363

46B. Electric dipole transition moments (in a.u.) at $\gamma = 180°$ and $\theta = 41°$.

R_1 (bohr)	$T_{41}(z)$	$T_{42}(z)$	$T_{43}(z)$	$T_{31}(x)$	$T_{31}(y)$	$T_{32}(x)$	$T_{32}(y)$	$T_{21}(x)$	$T_{21}(y)$
1.0	.381	.277(+1)	.452(-5)					.565	.326
1.1	-.363	.279(+1)	-.514(-5)						
1.2	.343	.273(+1)						.579	.334
1.3	-.326	.244(+1)	.695(-6)						
1.4	.309	.395	-.273(+1)	-.731	-.422	.802	.463	-.102	-.591(-1)
1.5	.291	.697(-1)	.272(+1)						
1.6	.276	-.168(-1)	.266(+1)	.795	.459	-.732	-.423	-.236	-.136
1.8	.241	-.532(-1)	.244(+1)	.942	.544	-.809	-.467	-.232	-.134
2.0	.207	-.524(-1)	.208(+1)	.113(+1)	.655	-.916	-.529	-.204	-.118
2.2	.172	-.557(-1)	.159(+1)						

47A. Energies (in hartree) at $\gamma = 180°$ and $\theta = 42°$.

R_1 (bohr)	E_1	E_2	E_3	E_4
1.0	-1.584578	-1.332253	-1.325303	-1.325850
1.1	-1.618318	-1.356014	-1.349753	-1.350133
1.2	-1.639963	-1.369583	-1.363508	-1.363775
1.3	-1.652824	-1.376330	-1.369881	-1.369986
1.4	-1.659407	-1.380871	-1.370634	-1.370913
1.6	-1.660222	-1.411736	-1.366451	-1.362818
1.7	-1.656468	-1.425931	-1.360268	-1.355559
1.8	-1.650873	-1.437466	-1.352857	-1.347103
2.1	-1.636481	-1.454559	-1.338105	-1.328102
2.1	-1.628257	-1.460880	-1.330985	-1.318094
2.2	-1.619727	-1.465916	-1.324556	-1.307330

47B. Electric dipole transition moments (in a.u.) at $\gamma = 180°$ and $\theta = 42°$.

R_1 (bohr)	$T_{41}(z)$	$T_{42}(z)$	$T_{43}(z)$	$T_{31}(x)$	$T_{31}(y)$	$T_{32}(x)$	$T_{32}(y)$	$T_{21}(x)$	$T_{21}(y)$
1.0	.331	.273(+1)	.308(-5)					.641	.370
1.1	-.310	.271(+1)	-.196(+1)						
1.2	.291	.269(+1)	-.496(-5)					.643	.371
1.3	-.273	.261(+1)	-.254(-5)						
1.4	.258	.195(+1)	.195(-5)	-.125	.216			.413	.239
1.6	.226	.175	.270(+1)	.837	.483	-.651	-.376	-.172	-.992(-1)
1.7	-.211	.640(-1)	.265(+1)						
1.8	.196	.170(-1)	.255(+1)	.950	.549	-.642	-.371	-.228	-.132
2.0	.168	-.198(-1)	.227(+1)	.113(+1)	.650	-.705	-.407	-.220	-.127
2.1	.154	-.271(-2)	.209(+1)						
2.2	.148	-.406(-1)	.184(+1)						

48A. Energies (in hartree) at $\gamma = 180°$ and $\theta = 43°$.

R_1 (bohr)	E_1	E_2	E_3	E_4
1.0	-1.564117	-1.348271	-1.337518	-1.338086
1.1	-1.603170	-1.373090	-1.363273	-1.363807
1.2	-1.628992	-1.386949	-1.377986	-1.378457
1.3	-1.645266	-1.393829	-1.384804	-1.385262
1.4	-1.654485	-1.395822	-1.385982	-1.386431
1.5	-1.658537	-1.398549	-1.383289	-1.383719
1.6	-1.658842	-1.410358	-1.380045	-1.378179
1.7	-1.656273	-1.425664	-1.374680	-1.370737
1.8	-1.651732	-1.438825	-1.367404	-1.361893
2.0	-1.638414	-1.458318	-1.350689	-1.341953
2.2	-1.622337	-1.470867	-1.334332	-1.320749

48B. Electric dipole transition moments (in a.u.) at $\gamma = 180°$ and $\theta = 43°$.

R_1 (bohr)	$T_{41}(z)$	$T_{42}(z)$	$T_{43}(z)$	$T_{31}(x)$	$T_{31}(y)$	$T_{32}(x)$	$T_{32}(y)$	$T_{21}(x)$	$T_{21}(y)$
1.0	.270	.272(+1)	-.330(-5)	-.133	.230			.746	.430
1.1	-.245	.272(+1)	.286(-5)					.717	.414
1.2	.226	.270(+1)	-.186(-4)	-.111	.192			.671	.414
1.3	-.209	.263(+1)	.187(-5)						
1.4	.194	.251(+1)	.543(-5)	-.946(-1)	.164			.671	.387
1.5	.182	.183(+1)	.882(-6)						
1.6	.170	.670	.267(+1)	.867	.501	-.504	-.291	.364(-1)	.210(-1)
1.7	-.159	.272	.268(+1)						
1.8	.148	.134	.264(+1)	.964	.556	-.478	-.276	-.188	-.109
2.0	.126	.331(-1)	.243(+1)	.111(+1)	.643	-.498	-.287	-.223	-.129
2.2	.109	-.195(-2)	.211(+1)	.131(+1)	.755	-.542	-.313	-.213	-.123

49A. Energies (in hartree) at $\gamma = 180°$ and $\theta = 44°$.

R_1 (bohr)	E_1	E_2	E_3	E_4
1.0	-1.524978	-1.350087	-1.335289	-1.335647
1.2	-1.609048	-1.398038	-1.385911	-1.386400
1.3	-1.631853	-1.407005	-1.395488	-1.396027
1.4	-1.646024	-1.410246	-1.398947	-1.399337
1.5	-1.654058	-1.409569	-1.397501	-1.397930
1.6	-1.657174	-1.409844	-1.392903	-1.393244
1.7	-1.656868	-1.418789	-1.386637	-1.386191
1.8	-1.653851	-1.433015	-1.381661	-1.377527
2.0	-1.642730	-1.456477	-1.364032	-1.357209
2.2	-1.627519	-1.471743	-1.346121	-1.335228

49B. Electric dipole transition moments (in a.u.) at $\gamma = 180°$ and $\theta = 44°$.

R_1 (bohr)	$T_{41}(z)$	$T_{42}(z)$	$T_{43}(z)$	$T_{31}(x)$	$T_{31}(y)$	$T_{32}(x)$	$T_{32}(y)$	$T_{21}(x)$	$T_{21}(y)$
1.0	.172	.267(+1)	-.425(-5)					.901	.520
1.2	.136	.270(+1)	.179(-5)	-.667(-1)	.116			.816	.471
1.3	-.123	.268(+1)	.632(-5)						
1.4	.113	.260(+1)	-.111(-5)					.781	.451
1.5	-.103	.251(+1)	-.128(-5)						
1.6	.962(-1)	.197(+1)	-.552(-7)					.553	.319
1.7	-.892(-1)	.863	.262(+1)						
1.8	.832(-1)	.377	.268(+1)	.960	.554			-.716(-1)	-.413(-1)
2.0	.710(-1)	.112	.256(+1)	.107(+1)	.618	-.251	-.145	-.202	-.117
2.2	.612(-1)	.339(-1)	.232(+1)	.124(+1)	.718	-.270	-.156	-.224	-.129

50A. Energies (in hartree) at $\gamma = 180°$ and $\theta = 45°$.

R_1 (bohr)	E_1	E_2	E_3	E_4
1.0	-1.434609	-1.301948	-1.283374	-1.283540
1.1	-1.510762	-1.353007	-1.336663	-1.336849
1.2	-1.564466	-1.384957	-1.370293	-1.370514
1.3	-1.601646	-1.403383	-1.390318	-1.390462
1.4	-1.626915	-1.412905	-1.400325	-1.400933
1.5	-1.643011	-1.416094	-1.403978	-1.404503
1.6	-1.652252	-1.415210	-1.402812	-1.403312
1.63	-1.653734	-1.415034	-1.401517	-1.402225
1.65	-1.654444	-1.414504	-1.400590	-1.401300
1.67	-1.655162	-1.414108	-1.399519	-1.400290
1.7	-1.656114	-1.413906	-1.398229	-1.398664
1.73	-1.656952	-1.413952	-1.396053	-1.396637
1.75	-1.656479	-1.414190	-1.395340	-1.395903
1.78	-1.656513	-1.416482	-1.392451	-1.393023
1.8	-1.656594	-1.418199	-1.391131	-1.391509
1.9	-1.653957	-1.431787	-1.385831	-1.382534
2.0	-1.649371	-1.445225	-1.377716	-1.372591
2.2	-1.636000	-1.465544	-1.358956	-1.350585

50B. Electric dipole transition moments (in a.u.) at $\gamma = 180°$ and $\theta = 45°$.

R_1 (bohr)	$T_{41}(z)$	$T_{42}(z)$	$T_{43}(z)$	$T_{31}(x)$	$T_{31}(y)$	$T_{32}(x)$	$T_{32}(y)$	$T_{21}(x)$	$T_{21}(y)$
1.0	-.130(-5)	.268(+1)	.656(-5)					.107(+1)	.615
1.1	.227(-5)	.269(+1)	.505(-5)						
1.2	.853(-6)	.268(+1)	.361(-5)					.919	.531
1.3	.675(-6)	.269(+1)	.464(-5)						
1.4	.278(-5)	.268(+1)	.160(-4)					.834	.481
1.5	.517(-6)	.265(+1)	.175(-5)						
1.6	.202(-5)	.257(+1)	.548(-5)					.781	.451
1.63	-.143(-5)	.247(+1)	.157(-6)						
1.65	-.227(-6)	.243(+1)	.300(-5)						
1.67	.357(-5)	.237(+1)	-.134(-5)						
1.7	.151(-5)	.222(+1)	.199(-5)						
1.73	-.402(-2)	.200(+1)	-.139(-5)						
1.75	-.611(-2)	.189(+1)	-.623(-1)						
1.78	.120(-5)	.146(+1)	-.708(-5)						
1.8	.558(-6)	.124(+1)	.142(-6)					.307	.177
1.9	.195(-6)	.515	.268(+1)						
2.0	.137(-5)	.260	.266(+1)	.101(+1)	.586	-.215(-7)	-.498(-7)	-.126	-.730(-1)
2.2	.111(-6)	.879(-1)	.249(+1)	.115(+1)	.666	-.428(-7)	.258(-7)	-.211	-.122

Appendix 2. Reprint and preprint of publications

1. B. Lepetit, Z. Peng and A. Kuppermann, "Calculation of bound rovibrational states on the first electronically excited state of the H_3 system", *Chem. Phys. Lett.*, **166**, pp. 572-580 (1990).

2. Z. Peng, A. Kuppermann and J.S. Wright, "Excited electronic potential energy surfaces and transition moments for the H_3 system", *Chem. Phys. Lett.*, in press.

Volume 166, number 5,6 CHEMICAL PHYSICS LETTERS 9 March 1990

CALCULATION OF BOUND ROVIBRATIONAL STATES ON THE FIRST ELECTRONICALLY EXCITED STATE OF THE H_3 SYSTEM

B. LEPETIT [1], Z. PENG [2] and A. KUPPERMANN

Arthur Amos Noyes Laboratory of Chemical Physics, Division of Chemistry and Chemical Engineering [3], California Institute of Technology, Pasadena, CA 91125, USA

Received 25 October 1989; in final form 4 December 1989

The bound rovibrational states of the upper manifold of the two lowest electronic states of H_3 have been calculated using variational and hyperspherical coordinate propagation methods, neglecting in both the coupling between those electronic states. Inclusion of the effect of the geometric phase induced by the conical intersection between those manifolds (sometimes referred to as the molecular Aharonov–Bohm effect) is shown to change significantly the number, the energies and the wavefunctions of those bound rovibrational states. Quantum numbers are defined which permit a physical understanding of these changes.

1. Introduction

The Rydberg spectrum of the H_3 system has been extensively studied by Herzberg and coworkers [1]. Of particular interest is the experimental discovery of a long-lived metastable state [1–3]. On the theoretical side, investigations have been restricted to the calculation of electronic energies for a few nuclear geometries [4–7], but the complete electronic potential energy surfaces, necessary to investigate the rovibrational structures of the spectrum and to compute accurately the lifetimes of the excited states, are available only for the ground and the first electronically excited states (DMBE potential [8]). In the equilateral triangular nuclear configuration, these two electronic states are degenerate and their electronic wavefunctions belong to the $^2E'$ representation of the D_{3h} group. Displacement away from the equilateral triangular geometry lifts this degeneracy and generates a conical intersection between two Jahn–Teller sheets [9]. Whereas the lower sheet is responsible for $H+H_2$ reactive scattering below about 3 eV [10–17], the upper one supports rovibrational quasi-bound states, which can predissociate by rovibronic coupling to the ground electronic state [18,19].

In this Letter, we assume that the upper Jahn–Teller sheet is decoupled from the lower one and therefore supports bound rovibrational states. We compare two methods of computing these states on the DMBE excited potential energy surface. One is the variational method of Tennyson and Sutcliffe [20,21] (referred to as TS method in this paper). The other, described in section 2, is a hyperspherical propagation method which uses modified Whitten–Smith coordinates [22,23] and derives from reactive scattering theory [10–13,24]. It generalizes earlier molecular bound state calculations limited to $J=0$ [25,26]. We show in section 3 that the hyperspherical method is very appropriate to the H_3 system because:

– It allows easy inclusion of the full permutation symmetries of the three identical nuclei, whereas the TS method only allows inclusion of the permutation symmetries of two identical atoms.

– It permits inclusion of the effect of the conical intersection on the phase of the nuclear wavefunction [27–29]. This effect results from the sign change of the electronic wavefunction as one follows a closed path in the

[1] Permanent address: UPR 261 du CNRS, Observatoire de Paris, 92195 Meudon, France.

[2] Work performed in partial fulfillment of the requirements for the Ph.D. Degree in Physics at the California Institute of Technology.

[3] Contribution No. 8052.

Volume 166, number 5,6 CHEMICAL PHYSICS LETTERS 9 March 1990

nuclear configuration space around the line along which the two $^2E'$ electronic states conically intersect. It corresponds to a particular case of Berry's geometric phase [30] which has been experimentally observed in the Na_3 system [31]. Since the total electronuclear wavefunction is continuous and single valued, there has to be a compensating sign change in the nuclear part of the wavefunction, which can be included easily in the hyperspherical method. The effect of the conical intersection on the phase of the nuclear wavefunction is sometimes referred to as the molecular Aharonov–Bohm effect [28,29,32], but we will use the simpler name "geometric phase" in the following.

2. Hyperspherical method

Let A_α, A_β, A_γ be the atoms of the system, and (λ, ν, κ) be any cyclic permutation of (α, β, γ). r_λ is the mass-scaled [33] internuclear vector for the diatom $A_\nu A_\kappa$ and $\boldsymbol{R}_\lambda$ the mass-scaled vector of A_λ with respect to the center of mass of $A_\nu A_\kappa$. The hyperspherical method uses the hyperradius $\rho = (R_\lambda^2 + r_\lambda^2)^{1/2}$ to describe the global size of the triatomic system and a set of five angles ζ to describe its shape and orientation in space [10–13,22,23,33,34]. In this paper, we will neglect all spin–orbit and spin–spin interactions. In the Born–Oppenheimer approximation, the electronuclear wavefunction can be written as a product of the electronic part ψ_e, which we choose to be real, and the nuclear part. The latter can be factored into a nuclear spin part and a spacial part $\psi^{JM\Pi\Gamma}$. J is the total nuclear angular momentum quantum number, M its projection onto a laboratory-fixed axis, Π the parity with respect to the inversion of nuclear coordinates and Γ the irreducible representation of the nuclear permutation group (P_3) to which $\Psi^{JM\Pi\Gamma}$, the electronuclear wavefunction excluding the nuclear spin part, belongs:

$$\Psi^{JM\Pi\Gamma} = \psi^{JM\Pi\Gamma}(\rho, \zeta)\, \psi_e(\boldsymbol{q}_e; \rho, \zeta)\,. \tag{1}$$

$\boldsymbol{q}_e$ refers to the set of all, spacial and spin, electronic coordinates. $\psi^{JM\Pi\Gamma}$ is an eigenfunction of the nuclear motion Hamiltonian:

$$H = -\frac{\hbar^2}{2\mu}\rho^{-5}\frac{\partial}{\partial\rho}\rho^5\frac{\partial}{\partial\rho} + \frac{\hat{\Lambda}^2}{2\mu\rho^2} + V(\rho, \zeta)\,, \tag{2}$$

where μ is the three-body reduced mass, $\hat{\Lambda}$ the grand canonical angular momentum and V the Born–Oppenheimer electronic potential energy function. The nuclear function $\psi^{JM\Pi\Gamma}$ is expanded in a basis of local hyperspherical surface functions (LHSF) $\Phi_n^{JM\Pi\Gamma}$:

$$\psi^{JM\Pi\Gamma}(\rho, \zeta) = \frac{1}{\rho^{5/2}}\sum_n F_n^{J\Pi\Gamma}(\rho)\, \Phi_n^{JM\Pi\Gamma}(\zeta; \rho)\,. \tag{3a}$$

The LHSF are defined as the eigenfunctions of the fixed hyperradius nuclear Hamiltonian:

$$\left(\frac{\hat{\Lambda}^2}{2\mu\rho^2} + V(\rho, \zeta)\right)\Phi_n^{JM\Pi\Gamma}(\zeta; \rho) = \epsilon_n^{J\Pi\Gamma}(\rho)\; \Phi_n^{JM\Pi\Gamma}(\zeta; \rho)\,. \tag{3b}$$

The coefficients $F_n^{J\Pi\Gamma}$ in eq. (3a) are solutions of a set of coupled differential equations in ρ, which we solve using piece-wise diabatic bases [10,34]. For assumed values of the rovibrational energies, the solutions are propagated forward and backward from small and large ρ values where they have negligible amplitudes. The energy is scanned iteratively until the quantization condition that the forward and backward solutions match smoothly at an intermediate value of ρ is reached.

In the present study, we use the Whitten–Smith [22] definition of the five angular coordinates ζ as modified by Johnson [23]. Three Euler angles $(\alpha\beta\gamma)$ specify the orientation of the body frame in space. The axes of this frame lie along the principle axes of inertia: the Z axis is parallel to $\boldsymbol{r}_\lambda \times \boldsymbol{R}_\lambda$ and the X axis is associated to

Volume 166, number 5,6 CHEMICAL PHYSICS LETTERS 9 March 1990

the smallest moment of inertia and is oriented such that $r_{\lambda X} \geq 0$. Two angles $(\theta, \varphi_\lambda)$ describe the shape of the molecular triangle and are defined by

$$r_{\lambda X} = \rho \cos(\pi/4 - \theta/2) \sin(\varphi_\lambda/2) , \tag{4a}$$

$$r_{\lambda Y} = -\rho \sin(\pi/4 - \theta/2) \cos(\varphi_\lambda/2) , \tag{4b}$$

$$R_{\lambda X} = \rho \cos(\pi/4 - \theta/2) \cos(\varphi_\lambda/2) , \tag{4c}$$

$$R_{\lambda Y} = \rho \sin(\pi/4 - \theta/2) \sin(\varphi_\lambda/2) . \tag{4d}$$

The ranges for these angles are $0 \leqslant \theta \leqslant \pi/2$ and $0 \leqslant \varphi_\lambda \leqslant 2\pi$. $\theta = 0$ corresponds to the symmetric top configuration (an equilateral triangle for three identical particles) in which the principal axes of inertia X and Y are undefined.

The grand canonical angular momentum is given explicitly by [22,23]

$$\hat{\Lambda}^2 = -4\hbar^2 \left(\frac{1}{\sin 2\theta} \frac{\partial}{\partial \theta} \sin 2\theta \frac{\partial}{\partial \theta} + \frac{1}{\sin^2\theta} \frac{\partial^2}{\partial \varphi_\lambda^2} \right) + \frac{4i\hbar \cos\theta}{\sin^2\theta} \hat{J}_Z \frac{\partial}{\partial \varphi_\lambda} + \frac{2(\hat{J}^2 - \hat{J}_Z^2)}{\cos^2\theta} + \frac{\hat{J}_Z^2}{\sin^2\theta} + \frac{\sin\theta}{\cos^2\theta} (\hat{J}_+^2 + \hat{J}_-^2) , \tag{5}$$

where $\hat{J}_Z$ is the body-fixed Z component of the total angular momentum $\hat{J}$, and $\hat{J}_\pm = \hat{J}_X \pm i\hat{J}_Y$.

Eq. (3b) is solved variationally by expansion in a body-fixed basis $\chi^{JMK}_{n_\theta n_\varphi}$ built with products of simple analytical functions [13]:

$$\chi^{JMK}_{n_\theta n_\varphi} = \exp(i n_\varphi \varphi_\lambda) f_{n_\theta}(\theta) D^J_{MK}(\alpha\beta\gamma) , \tag{6}$$

D^J_{MK} is a Wigner rotation matrix [35] and n_φ is integer or half of an odd integer. $f_{n_\theta}(\theta)$ are simple trigonometric functions, such that the LHSF have correct behaviors near the singularities of the kinetic energy operator $\theta = 0$ and $\pi/2$. In practice, the f_{n_θ} can be chosen as the functions $\cos(n_\theta\theta)$ or $\sin(n_\theta\theta)$, with n_θ integer or half odd integer, in terms of which the hyperspherical harmonics (whose θ dependence is usually written as a polynomial in $\cos\theta$) can be written (eq. (31) in ref. [36], eqs. (20)–(23) in ref. [37] or eq. (32) in ref. [38]).

We now focus attention on the special case of three identical nuclei and we describe how to build electronuclear wavefunctions $\Psi^{JM\Pi\Gamma}$ which are bases for the irreducible representations of the permutation group of the nuclei (P_3). The operations of this group correspond to simple changes in φ_λ (which are related to the isomorphism between P_3 and C_{3v}) as indicated in table 1. If $\epsilon^e_{\nu\kappa}$ ($= \pm 1$) is the symmetry of the electronic wavefunction with respect to the $\nu \leftrightarrow \kappa$ permutation, then the linear combinations defined by

$$\chi^{JMK\epsilon^{en}_{\nu\kappa}}_{n_\theta |n_\varphi|} = \chi^{JMK}_{n_\theta |n_\varphi|} + \epsilon^{en}_{\nu\kappa} \epsilon^e_{\nu\kappa} (-1)^{J+K+2n_\varphi} \chi^{JM,-K}_{n_\theta, -|n_\varphi|} , \tag{7}$$

give electronuclear wavefunctions $\Psi^{JM\Pi\Gamma}$ (eq. (1)) with the $\epsilon^{en}_{\nu\kappa}$ ($= \pm 1$) symmetry with respect to the $\nu \leftrightarrow \kappa$ permutation.

If there is no conical intersection between electronic states, the electronic wavefunction $\psi_e(q_e; \rho, \zeta)$ belongs to a one-dimensional representation of the nuclear permutation group (A_1 for $\epsilon^e_{\nu\kappa} = +1$, or A_2 for $\epsilon^e_{\nu\kappa} = -1$). Table 2 indicates how the total angular momentum, the parity and the irreducible representation Γ of P_3 to which $\Psi^{JM\Pi\Gamma}$ belongs determines the set of quantum numbers n_φ.

Table 1
Effect of permutations of the nuclei on the angle φ_λ

Permutation	$P_{\lambda\nu\kappa}$ [a]	$P_{\nu\kappa\lambda}$ [b]	$P_{\nu\kappa\lambda}$ [c]	$P_{\nu\kappa}$ [d]	$P_{\lambda\nu}$ [d]	$P_{\lambda\kappa}$ [d]
value of φ_λ [e]	φ_λ	$\varphi_\lambda + 2\pi/3$	$\varphi_\lambda + 4\pi/3$	$2\pi - \varphi_\lambda$	$2\pi/3 - \varphi_\lambda$	$4\pi/3 - \varphi_\lambda$

[a] $P_{\lambda\nu\kappa}$ is the identity permutation. [b] $P_{\nu\kappa\lambda}$ refers to the cyclic permutation $\lambda\nu\kappa \rightarrow \nu\kappa\lambda$. [c] $P_{\kappa\lambda\nu}$ refers to the cyclic permutation $\lambda\nu\kappa \rightarrow \kappa\lambda\nu$.
[d] P_{ij} refers to the pairwise permutation of nuclei i and j.
[e] The changes in φ_λ are true modulo 2π, since φ_λ must remain in the range $[0, 2\pi]$.

Table 2
Choice of n_φ for each parity Π and irreducible representation Γ of the nuclear permutation group P_3

Π	Γ [c]	n_φ
even, without phase [a]	A_1/A_2	$3m$ [d]
odd, with phase [b]	E	$3m\pm1$ [d]
even, with phase [b]	A_1/A_2	$3m+\frac{3}{2}$ [d]
odd, without phase [a]	E	$3m\pm\frac{1}{2}$ [d]

[a] Without consideration of the geometric phase due to the conical intersection.
[b] With consideration of the geometric phase due to the conical intersection.
[c] Γ is the irreducible representation of P_3 to which $\Psi^{JM\Pi\Gamma}$ (see text and eq. (1)) belongs.
[d] m is a non-negative integer.

If there is a conical intersection between electronic states for equilateral triangular configurations of the nuclei and if the geometric phase is taken into account, one can show [27–29] that in the vicinity of the conical intersection ($\theta=0$), the φ_λ dependence of the Born–Oppenheimer electronic wavefunction is given by

$$\psi_e \approx \cos(\varphi_\lambda/2)\,\psi_e^{E_1} - \sin(\varphi_\lambda/2)\,\psi_e^{E_2} \quad (\epsilon^e_{\nu\kappa}=-1)\,, \tag{8a}$$

or

$$\psi_e \approx \cos(\varphi_\lambda/2)\,\psi_e^{E_2} + \sin(\varphi_\lambda/2)\,\psi_e^{E_1} \quad (\epsilon^e_{\nu\kappa}=+1)\,, \tag{8b}$$

where $(\psi_e^{E_1}, \psi_e^{E_2})$ are two degenerate ρ-dependent but φ_λ-independent states at $\theta=0$ which form a basis for the E irreducible representation of P_3 ($\psi_e^{E_1}$ being symmetric for the $\nu\leftrightarrow\kappa$ permutation and ψ^{E_2} antisymmetric). Although permutations of the nuclei can only change the sign of ψ_e, these Born–Oppenheimer *electronic* wavefunctions do not belong to a one-dimensional irreducible representation of P_3 and are discontinuous in the internal configuration space [39] in the plane $\varphi_\lambda=0$. However, continuous *electronuclear* wavefunctions which belong to irreducible representations of P_3 can be built if the new set of n_φ indicated in table 2 is used for the *nuclear* wavefunctions.

3. Results

Fig. 1 illustrates the main features of the electronic potential in the internal configuration space defined in

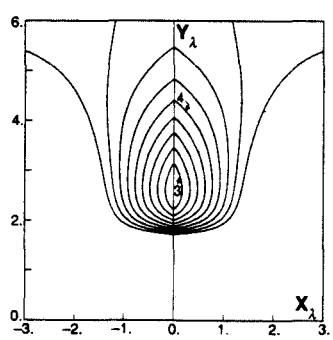

Fig. 1. Plot of the DMBE excited electronic potential V in the internal configuration space defined in ref. [39] along the plane $\varphi_\lambda=\pi/2, 3\pi/2$ (i.e. $Z_\lambda=0$). In this space, the coordinates $(\rho, \theta, \varphi_\lambda)$ defined in the text correspond to spherical polar coordinates with respect to the Y_λ axis of the figure. This axis is also the one along which the excited DMBE potential conically intersects the lower one. The equipotentials are equally spaced by 0.25 eV in the range [3, 5 eV]. The contours for $V=3$ and 4 eV are specifically indicated. The distances on the X_λ and Y_λ axes are in bohr. Along constant Y_λ lines, V shows the usual "V"-shaped behaviour characteristic of conical intersections. The approximate constancy of the X_λ spacing between the equipotentials in this figure is a manifestation of this linear dependence. Equipotentials on cuts along other planes containing the Y_λ axis look, in the vicinity of this axis, very similar to the ones displayed in this figure, i.e. V has a local nearly cylindrical symmetry around Y_λ.

ref. [39]. It has a quasi-cylindrical symmetry around the Y_λ axis of that figure ($\theta=0$) which corresponds to the axis of the conical intersection and to the local minima on the fixed ρ spheres. It has an absolute minimum for $\rho=2.6$ bohr, $\theta=0$ corresponding to an energy of 2.72 eV with respect to the bottom of the ground electronic state H_2 well. In the vicinity of that minimum, the potential increases steeply and almost linearly as a function of θ, but more slowly as a function of ρ.

Table 3 compares the rovibrational energy levels for this potential obtained by the hyperspherical method and the TS variational method without consideration of the geometric phase.

The hyperspherical method uses 20 n_θ values, between 4 (A_1 and A_2 symmetry) and 8 (E symmetry) $|n_\varphi|$ values (eqs. (6) and (7)), between 6 (A_1 or A_2 symmetry) and 12 (E symmetry) LHSF (eq. (3)). The LHSF have been computed at typically 50 ρ values between 1.5 and 6.5 bohr. The convergence of the LHSF and rovibrational energies is of the order of 10^{-4} eV. The compactness of the hyperspherical expansion comes from the quasi-cylindrical symmetry of the potential around the $\theta=0$ line (small number of n_φ values) and from the steep increase of the potential as a function of θ (small number of LHSF).

The TS method uses a body frame with its Z axis in the direction of $\boldsymbol{R}_\lambda$ and computes the bound states variationally by expansion on a product basis of two Morse-like functions (in R_λ and r_λ) for the radial part and of associated Legendre functions for the angular part. The optimized parameters of the Morse potential which we chose are indicated in table 4. Nearly 1400 such product functions have been used for each J, each inversion parity Π and each of the two symmetries for the permutation of the two identical atoms ν and κ. This unusually large number of basis functions (only 880 such functions were used to get fully converged results on H_3^+ in ref. [40]) is required by the shape of the potential and the sudden change of its derivative in the vicinity of the conical intersection axis. Table 3 shows that the convergence of the energy levels is always worse with the TS method than with the hyperspherical method. The quality of the TS calculation for $J=1$ odd parity is not

Table 3
Bound state energies without consideration of the geometric phase [a]

v_1v_2l [b]	$J=0$ [c]			$J=1$ even parity [c]			$J=1$ odd parity [c]		
0 0 0	3.7210	A_1	3.7218	3.7283	A_2	3.7294	3.7264	E	3.7276
1 0 0	3.9216	A_1	3.9223	3.9284	A_2	3.9297	3.9266	E	3.9281
2 0 0	4.1067	A_1	4.1073	4.1130	A_2	4.1145	4.1114	E	4.1131
3 0 0	4.2759	A_1	4.2766	4.2817	A_2	4.2849	4.2802	E	4.2831
4 0 0	4.4282	A_1	4.4301	4.4336	A_2	4.4386	4.4322	E	4.4398
5 0 0	4.5621	A_1	4.5734	4.5665	A_2	4.5803	4.5656	E	4.5894
0 1 1	4.2886	E	4.2886	4.2955	E	4.2956	4.2971	A_1	4.2975
							4.2969	A_2	4.2972
							4.2904	E	4.2908
1 1 1	4.4533	E	4.4533	4.4596	E	4.4598	4.4610	A_1	4.4618
							4.4608	A_2	4.4615
							4.4550	E	4.4557
2 1 1	4.5980	E	4.5983	4.6036	E	4.6048	4.6049	A_1	4.6083
							4.6047	A_2	4.6093
							4.5996	E	4.6028
3 1 1	4.7212	E		4.7261	E	4.7349	4.7272	A_1	4.7370
							4.7270	A_2	4.7355
							4.7225	E	
0 2 0	4.6806	A_1	4.6813	4.6871	A_2	4.6893	4.6842	E	4.6878

[a] The energy is in eV and its origin corresponds to the bottom of the ground electronic state of the isolated H_2 molecule.

[b] Quantum numbers used to classify the states (see text).

[c] The left column gives the hyperspherical method results and the right column the TS method results. The central column gives the irreducible representation of the permutation group of the nuclei to which the spacial part of the nuclear wavefunction belongs.

Volume 166, number 5,6 CHEMICAL PHYSICS LETTERS 9 March 1990

Table 4
Optimized parameters of the Morse-like functions in R_λ and r_λ

	D_e (au) [a]	ω_e (au) [a]	r_e (au) [a]
$J=0$	0.230 [b]	0.0130 [b]	1.96 [b]
$J=1$	0.262 [b]	0.0100 [b]	2.01 [b]
$J=0$	0.262 [c]	0.0122 [c]	2.09 [c]
$J=1$	0.232 [c]	0.0102 [c]	2.32 [c]

[a] These parameters are defined in eqs. (19) and (20) of ref. [20].
[b] Parameters for the Morse-like functions in R_λ.
[c] Parameters for the Morse-like functions in r_λ.

as good as the TS calculation for $J=0$ since the global size of the basis has been kept constant instead of being doubled. For a given total angular momentum and parity, the quality of the TS results decreases as the energy increases, and in particular, states diffuse along ρ (corresponding to high v_1 values, see below) are poorly represented. This suggests that different sets of optimized parameters of the Morse-like functions should be used for compact and diffuse states.

The hyperspherical method can be compared with the TS method from computational and formal points of view:

- The hyperspherical method requires less memory: smaller basis sets can be used for the variational solution of the two-dimensional LHSF equation (see eq. (3b)) than for the three-dimensional variational solution of the bound states in the TS method. However, the hyperspherical method required about two times more CPU time than the TS method, since the computation of the LHSF has to be repeated many times, but did not exceed 40 min of total CPU time on an SCS-40 for a typical run $J=0$, A_1 plus E permutation symmetries. In addition, the hyperspherical method does not involve adjustable parameters which have to be optimized in the TS method.

- The bases used in the TS method to expand the bound state wavefunctions do not have the P_3 permutation symmetry, but only the P_2 symmetry of two identical nuclei. As a result, plots of the bound state wavefunctions show that, even in the $J=0$ case where the energy convergence is better than 10^{-3} eV, the shape of the TS wavefunctions do not exhibit the correct symmetry properties of a system of three identical particles, whereas they are imbedded in the LHSF basis used in the hyperspherical method. Moreover, the TS method does not

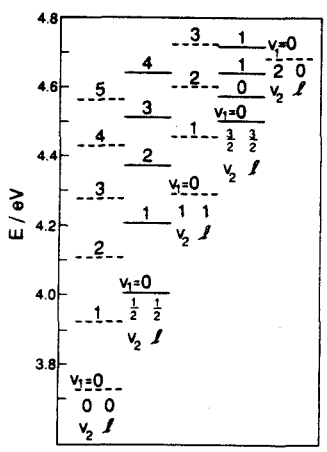

Fig. 2. Rovibronic energy levels associated to the first electronically excited state of H_3. The full lines are the levels including the effect of the geometric phase while the dashed ones exclude that effect. The quantum numbers v_1, v_2 and l are defined in the text. The origin for the energy scale is the bottom of the isolated ground electronic H_2 potential energy curve. These levels are for the $J=0$ states, but the $J=1$ levels are nearly degenerate with them, the splitting being of the order of 10^{-2} eV. Their nuclear permutation symmetries depend on J and on the parity Π, as well as whether the geometric phase is or is not included (see tables 3 and 5). There are two levels for each of the sets of quantum numbers ($v_1=0$, $v_2=l=\frac{1}{2}$) and ($v_1=1$, $v_2=l=\frac{1}{2}$), which would be degenerate if the potential were exactly cylindrically symmetric around the Y_λ axis (see text and fig. 1).

Volume 166, number 5,6 CHEMICAL PHYSICS LETTERS 9 March 1990

Table 5
Hyperspherical method energy levels including the effect of the geometric phase [a,b]

$v_1 v_2 l$ [c]	$J=0$	$J=1$ even parity	$J=1$ odd parity
$0\,\frac{1}{2}\,\frac{1}{2}$	4.0215 (E)	4.0286 (E)	4.0256 (A_1) [d]
			4.0243 (A_2)
			4.0284 (E)
$1\,\frac{1}{2}\,\frac{1}{2}$	4.2049 (E)	4.2114 (E)	4.2087 (A_1) [d]
			4.2076 (A_2)
			4.2113 (E)
$2\,\frac{1}{2}\,\frac{1}{2}$	4.3710 (E)	4.3769 (E)	4.3744 (A_1) [d]
			4.3734 (A_2)
			4.3768 (E)
$3\,\frac{1}{2}\,\frac{1}{2}$	4.5189 (E)	4.5243 (E)	4.5220 (A_1) [d]
			4.5210 (A_2)
			4.5241 (E)
$4\,\frac{1}{2}\,\frac{1}{2}$	4.6468 (E)	4.6517 (E)	4.6496 (A_1) [d]
			4.6487 (A_2)
			4.6515 (E)
$0\,\frac{3}{2}\,\frac{3}{2}$	4.5005 (A_1) [d]	4.5071 (A_2)	4.5050 (E)
	4.5700 (A_2)	4.5768 (A_1) [d]	4.5733 (E)
$1\,\frac{3}{2}\,\frac{3}{2}$	4.6425 (A_1) [d]	4.6484 (A_2)	4.6466 (E)
	4.7177 (A_2)	4.7237 (A_1) [d]	4.7223 (E)

[a] The energy is in eV and its origin corresponds to the bottom of the ground electronic state of the isolated H_2 molecule.
[b] The irreducible representations are the ones for the permutation group of the nuclei to which $\Psi^{JM\Pi\Gamma}$ belongs.
[c] Quantum numbers used to classify the states (see text).
[d] Levels with A_1 symmetry are included for completeness, but are forbidden by the Pauli principle.

permit inclusion of the geometric phase due to the conical intersection whereas the hyperspherical method does.

Fig. 2 and table 5 show the important modifications of the bound rovibrational energies when the geometric phase is included in the hyperspherical calculation. These changes can be understood if one defines quantum numbers to the bound states of tables 3 and 5 by modeling the nuclear wavefunction in the following way [#1]:

- We retain a single term in the expansion of the bound states in the LHSF basis (eq. (3a)). This Born–Oppenheimer-type approximation, also used to model reactive scattering resonances [24], is very accurate in the present case where the frequency associated to the hyperspherical mode is smaller than those of the fixed-ρ bending modes: the resulting bound state energies are shifted by less than 0.4 meV. This approximation suggests that we define the quantum number v_1 associated with the hyperradial motion as the number of nodes of the hyperradial function $F_n^{J\Pi\Gamma}(\rho)$ (eq. (3a)). This mode corresponds to the breathing normal mode in the limit of small amplitude vibrations, but in the present case, it can have large amplitudes with an excitation as large as $v_1=5$ (table 3).

- We assume that the fixed-ρ bending vibration has small amplitude, so that the wavefunction is concentrated near $\theta=0$. This approximation is reasonable due to the steep increase of the potential as a function of θ. It suggests that we neglect the asymmetric top coupling elements in the kinetic energy (last term of eq. (5)) and the φ_λ dependence in the potential. The (non-symmetrized) LHSF can then be factored as

$$\Phi_n^{JM\Pi} = \exp(i n_\varphi \varphi_\lambda)\, g_{v_2 l}(\theta;\rho)\, D^J_{MK}(\alpha,\beta,\gamma)\,, \tag{9a}$$

where $g_{v_2 l}$ is defined by

[#1] The actual energy values given in tables 3 and 5 are calculated accurately; this model is used only to assign quantum numbers to these levels.

$$\left[-\frac{2\hbar^2}{\mu\rho^2}\left(\frac{1}{\theta}\frac{\partial}{\partial\theta}\theta\frac{\partial}{\partial\theta}-\frac{l^2}{\theta^2}\right)+V(\rho,\theta)\right]g_{v_2l}(\theta;\rho)=\left[\epsilon^{JK}_{v_2l}(\rho)-\left(\frac{J(J+1)-\frac{1}{2}K^2}{\mu\rho^2}\pm\frac{lK}{\mu\rho^2}\right)\hbar^2\right]g_{v_2l}(\theta;\rho)\,. \qquad (9b)$$

Eq. (9b) is the small-θ limit of eq. (3b) (see also eq. (5)). l quantizes the absolute value of the vibrational angular momentum in a new body frame, which is an Eckart frame associated to the equilibrium position of the nuclei in the equilateral triangular configuration [41], and is given by $l=|n_\varphi-\frac{1}{2}K|$. v_2 is the bending vibrational quantum number and is defined by analogy with the two-dimensional harmonic oscillator such that the number of θ nodes of g_{v_2l} is $\frac{1}{2}(v_2-l)$ [42]. v_2 and l are both integers when the geometric phase is not considered and become both half odd integers when it is taken into account. If the potential were a harmonic function of θ, the bound state energies would increase linearly with v_2 for each v_1 value. Although the potential is an approximate linear function of θ, tables 3 and 5 indicate that the dependence of the bound state energies on v_2 is not far from linear. Therefore, as shown in fig. 2, each of the levels with the geometric phase (v_2 half odd integer) is almost half way in energy between two consecutive ones without this phase (v_2 integer).

The quantum numbers v_2 and l defined above are closely related to the ones (n and j) defined in ref. [31] for the analysis of the geometric phase in the $2\,^2E'$ Na_3 excited state. However, due to important differences in the shapes of the electronic potentials (minimum for equilateral triangular configurations in the present excited H_3 state, but for distorted configurations [9] in the Na_3 potential used in ref. [31]), the dependence of the bound state energies on these quantum numbers is different in the two systems.

Due to the Pauli principle and to the symmetries of the nuclear spin wavefunction with respect to interchange of the identical nuclei, the only allowed electronuclear wavefunctions $\Psi^{JM\Pi\Gamma}$ (eq. (1)) have A_2 or E nuclear permutation symmetries, and they correspond to quartet and doublet nuclear spins respectively. The number of such levels which satisfy the Pauli principle and their spin symmetries change significantly when the effect of the geometric phase is included.

4. Conclusions

We have described a new hyperspherical propagation method for the calculation of bound rovibrational states. This method is well adapted to systems of three identical particles, because it allows easy inclusion of the full permutation symmetries of the system and of the effect of conical intersections on the phase of the nuclear wavefunction.

We have shown that, in the case of the bound rovibrational states in the first electronically excited state of H_3, the geometric phase results in bending modes having half odd integer quantum numbers and in important changes of the rovibrational state energies and of their symmetry properties. In the following paper [43], we study the influence of the geometric phase on the chemical reaction which occurs in the ground electronic state of H_3.

Acknowledgement

This work has been supported in part by Air Force Astronautics Laboratory contract F04611-86-K-0067 and by DOE grant DE-AS03-83ER. Most of the calculations were performed on the CRAY-XMP/48 and SCS-40 computers at the NSF San Diego Supercomputing Center. BL thanks the "Centre National de la Recherche Scientifique" for financial support and J.M. Launay for useful discussions on the hyperspherical method.

References

[1] G. Herzberg, J. Chem. Phys. 70 (1979) 4806;
I. Dabrowski and G. Herzberg, Can. J. Phys. 58 (1980) 1238;

G. Herzberg and J.K.G. Watson, Can. J. Phys. 58 (1980) 1250;
G. Herzberg, H. Lew, J.J. Sloan and J.K.G. Watson, Can. J. Phys. 59 (1981) 428;
G. Herzberg, J.J. Sloan and J.K.G. Watson, Can. J. Phys. 60 (1982) 1261.
[2] H. Helm, Phys. Rev. Letters 56 (1986) 42.
[3] J. Garvey and A. Kuppermann, Chem. Phys. Letters 107 (1984) 491.
[4] H. King and K. Morokuma, J. Chem. Phys. 71 (1979) 3213.
[5] M. Jungen, J. Chem. Phys. 71 (1979) 3540.
[6] R. Martin, J. Chem. Phys. 71 (1979) 3541.
[7] I.D. Petsalakis, G. Theodorakopoulos and J.S. Wright, J. Chem. Phys. 89 (1988) 6850.
[8] A.J.C. Varandas, F.B. Brown, C.A. Mead, D.G. Truhlar and N.C. Blais, J. Chem. Phys. 86 (1987) 6258.
[9] H.A. Jahn and E. Teller, Proc. Roy. Soc. A 161 (1937) 220.
[10] G.C. Schatz and A. Kuppermann, J. Chem. Phys. 65 (1976) 4668;
R.T. Ling and A. Kuppermann, in: Electronic and Atomic Collisions, Abstract of the 9th International Conference on the Physics of Electronic and Atomic Collisions, Seattle, Washington, 24–30 July 1975, Vol. 1, eds. J.S. Risley and R. Geballe (Univ. Washington Press, Seattle, 1975) pp. 353, 354;
A. Kuppermann and P.G. Hipes, J. Chem. Phys. 84 (1986) 5962;
P.G. Hipes and A. Kuppermann, Chem. Phys. Letters 133 (1987) 1;
S.A. Cuccaro, P.G. Hipes and A. Kuppermann, Chem. Phys. Letters 154 (1989) 155; 157 (1989) 440.
[11] R.T Pack and G.A. Parker, J. Chem. Phys. 87 (1987) 3888.
[12] J. Linderberg, S. Padkjær, Y. Öhrn and B. Vessal, J. Chem. Phys. 90 (1989) 6254.
[13] J.M. Launay and M. Le Dourneuf, Chem. Phys. Letters 163 (1989) 178.
[14] J.Z.H. Zhang and W.H. Miller, Chem. Phys. Letters 153 (1988) 465; 159 (1989) 130.
[15] A.B. Elkowitz and R.E. Wyatt, J. Chem. Phys. 62 (1975) 2504; 63 (1975) 702;
D.E. Manopoulos and R.E. Wyatt, Chem. Phys. Letters 159 (1989) 123.
[16] R.B. Walker, E.B. Stechel and J.C. Light, J. Chem. Phys. 69 (1978) 2922;
F. Webster and J.C. Light, J. Chem. Phys. 90 (1989) 300.
[17] M. Mladenovic, M. Zhao, D.G. Truhlar, D.W. Schwenke, Y. Sun and D.J. Kouri, J. Phys. Chem. 92 (1988) 7035; Chem. Phys. Letters 146 (1988) 358.
[18] M. Vogler, Phys. Rev. A 19 (1979) 1.
[19] J.K.G. Watson, Phys. Rev. A 22 (1980) 2279.
[20] J. Tennyson, Computer Phys. Commun. 42 (1986) 257.
[21] J. Tennyson, Computer Phys. Rept. 4 (1986) 1.
[22] R.C. Whitten and F.T. Smith, J. Math. Phys. 9 (1968) 1103.
[23] B.R. Johnson, J. Chem. Phys. 73 (1980) 5051; 79 (1983) 1906, 1916.
[24] J.M. Launay and B. Lepetit, Chem. Phys. Letters 144 (1988) 346;
B. Lepetit and J.M. Launay, Chem. Phys. Letters 151 (1988) 287.
[25] R. Wallace, Chem. Phys. 37 (1979) 93.
[26] J.G. Frey, Chem. Phys. Letters 102 (1983) 421;
J.G. Frey and B.J. Howard, Chem. Phys. 99 (1985) 415.
[27] H.C. Longuet-Higgins, U. Öpik, M.H.L. Pryce and R.A. Sack, Proc. Roy. Soc. A 244 (1958) 1;
G. Herzberg and H.C. Longuet-Higgins, Discussions Faraday Soc. 35 (1963) 77;
H.C. Longuet-Higgins, Advan. Spectry. 2 (1961) 429.
[28] C.A. Mead and D.G. Truhlar, J. Chem. Phys. 70 (1979) 2284.
[29] C.A. Mead, Chem. Phys. 49 (1980) 23.
[30] M.V. Berry, Proc. Roy. Soc. A 392 (1984) 45.
[31] G. Delacrétaz, E.R. Grant, R.L. Whetten, L. Wöste and J.W. Zwanziger, Phys. Rev. Letters 56 (1986) 2598.
[32] Y. Aharonov and D. Bohm, Phys. Rev. 115 (1959) 485.
[33] L.M. Delves, Nucl. Phys. 9 (1959) 391; 20 (1960) 275.
[34] B. Lepetit, J.M. Launay and M. Le Dourneuf, Chem. Phys. 106 (1986) 103.
[35] A.S. Davydov, Quantum mechanics, 2nd Ed. (Pergamon Press, Oxford, 1976) pp. 151–161.
[36] W. Zickendraht, Ann. Phys. 35 (1965) 18.
[37] H. Mayer, J. Phys. A 8 (1975) 1562.
[38] L. Wolniewicz, J. Chem. Phys. 90 (1989) 371.
[39] A. Kuppermann, Chem. Phys. Letters 32 (1975) 374.
[40] J. Tennyson and B.T. Sutcliffe, Mol. Phys. 51 (1984) 887.
[41] E.B. Wilson, J.C. Decius and P.C. Cross, Molecular vibrations (Dover, New York, 1980) ch. 11.
[42] S. Flügge, Practical quantum mechanics (Springer, Berlin, 1974) problem 42.
[43] B. Lepetit and A. Kuppermann, Chem. Phys. Letters 166 (1990) 581.

EXCITED ELECTRONIC POTENTIAL ENERGY SURFACES AND TRANSITION MOMENTS FOR THE H_3 SYSTEM

Z. Peng [1] and Aron Kuppermann

Arthur Amos Noyes Laboratory of Chemical Physics
Division of Chemistry and Chemical Engineering [2]
California Institute of Technology
Pasadena, CA 91125, USA

and

James S. Wright

Ottawa-Carleton Chemistry Institute
Carleton University, Ottawa, Canada K1S5B6

(Received August 1990)

ABSTRACT

Four electronic states of H_3 have been studied using a multi-reference configuration interaction method and a basis set of 75 AOs. The calculations were carried out at a fixed bond angle of 60°. The four states include the ground state and the Rydberg $2s$ and $2p_z$-states, as well as the state which in the equilateral triangular geometry is related to the ground state by a conical intersection. Electric dipole transition moments were calculated between all of these states at every geometry. The potential energies obtained for the various states show that the atomic and diatomic asymptotes are accurately described, and that the barriers, wells and energy differences also show good agreement compared to literature values, where available. The ground state and $2p_z$ Rydberg state potential energy surfaces were fitted over the whole geometric configuration space spanned using a rotated Morse curve-cubic spline approach, and show smooth contour maps appropriate for studies in excited-state reaction dynamics.

---

[1] Work performed in partial fulfillment of the requirements for the Ph.D. Degree in Physics at the California Institute of Technology.

[2] Contribution number 8183.

1. Introduction

Classical and quantum-dynamical studies of atom-molecule reactions require reliable potential surfaces as a starting point. Some good global surfaces have been obtained, particularly for the H + H_2 reaction. The potential energy data of Liu [1] and Siegbahn and Liu [2] (hereafter LS) were fitted by Truhlar and Horowitz [3] to give the LSTH surface, which incorporated some scaling to correct the *ab initio* calculation to accurate diatomic limits, and for several years provided a standard of accuracy for the field. The more recent double many-body expansion (DMBE) surface of Varandas *et al.* [4], although having a larger rms error than the LSTH one, may be more accurate at higher energies.

For excited states, even for H + H_2, the number of available *ab initio* calculations is sparse, although they are of considerable current interest. Important early work in this direction includes the theoretical study of Rydberg spectra of H_3 by King and Morokuma [5], Jungen [6], Martin [7], Kulander and Guest [8], Nager and Jungen [9], and Raynor and Herschbach [10], and the series on transition state spectroscopy by Polanyi and co-workers [11-13]. A thorough study of excited electronic potential energy surfaces of H_3 was done by Roach and Kuntz [14] using the semiempirical DIM method. Some recent work on H_3 was done by Petsalakis, Theodorakopoulos and one of the present authors [15] (hereafter PTW) and also by Diercksen *et al.* [16]. Reviews on the Rydberg spectra of H_3 have been given by Herzberg [17], Watson [18], and Gellene and Porter [19].

Another area of interest in H_3 excited states is the study of ro-vibrational bound states which they may support. In particular, in the absence of electronically non-adiabatic couplings to the ground state, the upper sheet of the DMBE surface [4] supports such bound states [20], which also demonstrates the importance of the effect of the conical intersection [20-24]. Ideally, to study dynamics involving multiple electronic surfaces one requires not only the potential energy data but also the electronic transition moments and non-adiabatic coupling matrix elements between surfaces. Although such coupling elements between the upper and lower sheets of the DMBE surface are available [4,25], they have not been calculated so far for other H_3 surfaces.

In this Letter we report an *ab initio* study of four electronic states of H_3 at a fixed bond angle of 60°. It is desirable at the start of such a study to meet several criteria for the accuracy of the various surfaces. For this purpose we compare atomic and diatomic limits for ground and excited states to known values, and triatomic features to LS and LSTH for the ground state of H_3. Excited-state features are compared to the study of Rydberg spectra by PTW [15] and to that of Diercksen *et al.* [16]. The functional representation of the potential energy data for the four surfaces is discussed, and the extension of the calculation to a global set of geometries is indicated. Finally, contour maps of the ground-

state surface and the Rydberg surface for which the $2p_z$ orbital is populated are shown.

2. Method of Calculation

Choice of an appropriate basis set was determined by the necessity of obtaining the following:

(i) accurate atomic excitation energies for $1s \rightarrow 2s$ and $1s \rightarrow 2p$ transitions, (ii) accurate values for the H_2 energy in its ground electronic state $X\ ^1\Sigma_g^+$ and excited state $b\ ^3\Sigma_u^+$, (iii) a ground-state surface for H_3 of accuracy comparable to that of the LSTH surface, and (iv) reasonably good agreement with the known Rydberg spectrum of H_3 and the previous calculations of PTW [15] and with Diercksen *et al.*[16].

After some experimentation, the basis sets used by LS [2] for the ground state of H_3 and by Talbi and Saxon [26] for the Rydberg spectrum of H_3^+ were adapted for the present purpose. The valence $(9s/4s)$ basis was taken from LS, and has an outer exponent of 0.06618. Three more Rydberg $s-$functions were added, with an approximately even-tempered ratio of 2.4, giving exponents 0.02758, 0.01149 and 0.00420. The polarization/Rydberg $p-$basis was taken from Talbi and Saxon [26], with exponents 1.6, 0.4, 0.09 and 0.025. Finally, the 6-component $d-$function with exponent 1.0 was taken from LS. The full basis set, denoted $(12s4p1d/7s4p1d)$ has therefore 25 contracted AOs, of which three $s-$functions and two $p-$functions are essentially Rydberg in nature.

In order to allow for proper dissociation, it was found necessary to place the full AO set on each nuclear center, for a total basis set size of 75 AOs. This diffuse overlapping basis could lead to linear dependence problems [26]. To minimize the chance of this occurring, we used the HONDO routine [27] for evaluating the necessary integrals. The high accuracy of that routine led to no linear dependence when this basis set was used.

The molecule was placed in the xy plane, and all calculations were carried out using the point group C_s. In C_s the symmetry type a' is symmetric with respect to the xy plane whereas a'' is antisymmetric. The SCF-MOs were constructed using the occupation $(1a')^2(1a'')^1$. The configuration-interaction energy was calculated using the MRD-CI method of Buenker and co-workers [28-30]. All 75 MOs were kept for the CI step. The CI space of A' symmetry was constructed using 45-49 reference configurations, depending on the geometry. The selection threshold used was 2 μhartree, and the lowest three eigenvalues were obtained. This resulted in the generation of 50,000 to 60,000 configuration functions out of which 5,000 to 6,000 were selected for the final CI calculation. For the lowest eigenvalue A'' calculations, 19-32 reference configurations were employed. Use of a threshold of 0.5 μhartree resulted in 800-3,000 selected configurations out of 20,000 to 40,000 generated. Extrapolation of the energy to zero threshold in the usual way gave the

MRD-CI energy, which provided the data for generating the potential energy surfaces.

There are four states of interest, which we label E_1, E_2, E_3 and E_4, where the first three are the states of A' symmetry and E_4 is the A'' one. Using the symmetry notation appropriate for the equilateral triangular (D_{3h}) geometry, E_1 corresponds to the ground state $^2E'$ ($1a'^2 1e'$), E_2 to the state degenerate with the ground one, E_3 to the $^2A_1'$ ($1a'^2 2s$) state and E_4 to the $^2A_2''$ ($1a'^2 2p_z$) state. Although E_1 and E_2 are degenerate in D_{3h} geometry, the degeneracy is lifted as the triangle is distorted, and this is what generates the conical intersection between E_1 and E_2. Electric dipole transition moments between all electronic states were calculated for each geometrical configuration.

Selection of the geometries at which the *ab initio* calculations were done was guided by the rotated Morse curve–cubic spline (RMCS) potential energy fitting method [31-33]. We label the two internuclear distances as R_1 and R_2 and the bond angle between them as γ. In this paper we restrict our attention to the surfaces at $\gamma = 60°$, so that the previous RMCS-CI treatment of the H_3 ground state surface at $\gamma = 180°$ provides a good reference for the treatment [34]. Briefly, the "swing angle" θ is defined as the angle by which the Morse curves are rotated with respect to the swing point located at (10 bohr, 10 bohr) in R_1 and R_2 Cartesian coordinates. In this system $\theta = 0°$ corresponds to the ray at $R_2 =$ 10 bohr, R_1 is variable and $\theta = 45$ corresponds to the symmetric $R_1 = R_2$ configuration. θ-rays were chosen at 0°, 20°, 30°, 35°, 40°, 41°, 42°, 43°, 44° and 45°. Data points were taken at increments of 0.2 bohr in R_1. Typically 7-9 data points were calculated per ray (giving E_1, E_2, E_3, E_4 and the electric dipole transition moments for each point), with more points added when necessary. A similar treatment was used by Mayne *et al.* [13], who interpolated DIM data using a rotated Morse curve approach.

Data points at each θ-ray were then fitted using a 5-parameter generalized Morse function (GMF5) [35], containing the variables D_e (well depth relative to the swing point), l_e (distance in bohr from the minimum of GMF5 to the swing point), β_0 (curvature parameter in bohr^{-1}), λ_1 (linear correction to β_0 in bohr^{-1}), and λ_2 (quadratic correction to β_0 in bohr^{-2}). The data were reflected about $\theta = 45°$ to generate data at 19 θ-rays and the five Morse parameters were then interconnected using natural cubic splines. This provided a set of five θ-dependent parameters ($D_e(\theta)$, etc.), which maps out the (R_1, R_2) space for $\gamma = 60°$. Finally, the spline fits were examined for smoothness and any nonphysical oscillations were removed.

3. Results and Discussion

Results for atomic and molecular hydrogen are given in Table 1. With the basis set of $(12s4p1d/7s4p1d)$, the $1s \rightarrow 2s$ transition energy is very accurate (10.2045 eV, which is within 0.0001 eV of the exact value), whereas the $1s \rightarrow 2p$ transition energy is less accurate (10.2118 eV, an error of 0.0074 eV) due to the smaller Rydberg $p-$basis, but still reasonable.

The energy of ground-state H_2 is close to that of Liu [1] and better than that of LS [2]. The computed D_e at 1.40 bohr is 4.7255 eV whereas the exact value is 4.7477 eV [36], an error of 0.02 eV. The excited state $b\ ^3\Sigma_u^+$, which has configuration $\sigma_g\sigma_u$, is calculated to lie 10.605 eV above the ground state, compared to the 10.623 eV value of Kolos and Wolniewicz [36], so this important valence-shell transition is also accurate to within 0.02 eV.

Table 2 shows the MRD-CI energy of the four electronic states of H_3, for equilateral triangular, linear equidistant and linear asymmetric geometries. In the appropriate point group the dominant configurations are the following:

D_{3h}: E_1: $1a_1'^2\ 1e'$, E_2: $1a_1'^2\ 1e'$, E_3: $1a_1'^2\ 2p_x$, E_4: $1a_1'^2\ 2p_z$;

$D_{\infty h}$: E_1: $1\sigma_g^2\ 1\sigma_u$, E_2: $1\sigma_g^2\ 2s$, E_3: mixed, E_4: $1\sigma_g^2\ 2p_z$;

$C_{\infty v}$: E_1: $1\sigma^2\ 2\sigma$, E_2: $1\sigma^2\ 2s$, E_3: mixed, E_4: $1\sigma^2\ 2p_z$.

In fact, assigning single dominant configurations to E_2 and E_3 in $D_{\infty h}$ and $C_{\infty v}$ symmetry is oversimplified, since an avoided crossing was found for $D_{\infty h}$ near $R_1 = 1.85$ bohr and for $C_{\infty v}$ near $R_1 = 1.4$ bohr (see also ref. 14).

The lowest-energy conical intersection for the E_1 surface occurs at $R_1 = R_2 = R_3 = 1.973$ bohr, and at an energy of -1.572084 hartree (GMF5 fit), and the E_1 H + H_2 energy in $C_{\infty v}$ ($\gamma = 180°$ and $R_2 = 10$ bohr) occurs at $R_1 = 1.403$ bohr, and at an energy of -1.673019 hartree (GMF5 fit). This gives a lowest conical intersection energy with respect to separated H + H_2 of 0.100935 hartree or 2.747 eV. For comparison, the corresponding energy for the LSTH surface [3] is 2.756 eV and occurs at $R_1 = R_2 = R_3 = 1.981$ bohr. For the DMBE surface [4] the corresponding values are 2.748 eV and 1.973 bohr. As a result, the lowest conical intersection energy and the corresponding geometry are in good agreement with accurate published values, especially the DMBE ones.

The $E_1 \rightarrow E_2$ transition energy in $D_{\infty h}$, corresponding to $\sigma_u \rightarrow 2s$, can be obtained from the analytically-continued DMBE function [4], giving 5.728 eV, and from the DIM calculation of Roach and Kuntz [14], who obtained 6.292 eV at $R_1 = 2.0$ bohr. The present data from Table 2 show a value of 5.555 eV. At $R_1 = 1.76$ bohr the three calculations are in better agreement, giving 6.379 eV (DMBE), 6.466 eV (ref. 14) and our value of 6.529 eV.

The $E_1 \rightarrow E_4$ transition energy in D_{3h}, corresponding to $e' \rightarrow 2p_z$, has been computed by Diercksen *et al.* [16] as well as by PTW [15]. Using $R_1 = 1.633$ bohr and CI spaces of 15290, 22570 and 47060, Diercksen *et al.* obtained transition energies of 2.17, 2.21 and 2.11 eV, respectively. Our data at $R_1 = 1.633$ bohr give 2.23 eV and PTW obtained 2.24 eV. From the experimental spectrum [17-18] we estimate that the vertical transition at $R_1 = 1.633$ bohr should occur at about 2.15 eV, so that our present E_4 energy appears to be too high by about 0.08 eV. Possibly another more diffuse $p-$function in the basis set would help to correct this error. However, in general our criteria for accurate multiple surface energetics have been met.

The squares T_{ij}^2 of the electric dipole transition moments between states E_i and E_j (ij = 21, 31, 32, 43) for D_{3h} geometries are given in Table 3. Allowed transitions in D_{3h} occur for $e' \rightarrow 2s$ (T_{31} and T_{32}) and $2s \rightarrow 2p_z$ (T_{43}). It can be seen that the $E_1 \rightarrow E_2$ electric dipole moment between two degenerate states is not zero since the calculation is carried out in C_s symmetry and the description of the two states is not quite equivalent (see also Table 2, where the C_s energies are not perfectly degenerate), but this moment is nevertheless very small. T_{43}^2 increases with R_1, as expected (since it should become 9.00 a.u.^{2} in the limit of $R_1 \rightarrow \infty$). And its value of 7.24 compares well with the PTW one of 7.23 at 1.64 bohr. If the same method of estimation is used as in PTW [15], both results from PTW and the present work lead to the same lifetime of about 70 μs for the $2p_z \rightarrow 2s$ electric dipole radiation process. In Table 3, T_{31}^2 and T_{32}^2 are almost identical. They would be exactly identical if D_{3h} symmetry instead of C_s symmetry has been used in the wavefunction calculations. Their sum at 1.64 bohr is 5.12 a.u.^{2} while PTW obtained 4.89 a.u.^{2}. One reason for the difference is that present calculation employed a larger basis set than that of PTW. Another is that in the current treatment we located Rydberg AOs on each nucleus, whereas PTW used a single set located at the center of the triangle.

Using the RMCS method, energies of states E_1 and E_4 were fitted to provide continuous surfaces at $\gamma = 60°$. Figures 1 and 2 show the contour maps of surfaces of E_1 and E_4 respectively. In creating these maps the parameters D_e, l_e and β_0 required no smoothing, whereas the curvature correction terms λ_1 and λ_2, which are small and have larger standard errors, required smoothing to remove nonphysical spline oscillations. The resulting surfaces are smooth and continuous, showing the barrier (cusp) on E_1 along $R_1 = R_2$ ($\theta = 45°$) and the well in E_4 centered at $\theta = 45°$. These surfaces are ideally suited to studies of reaction dynamics which include transitions between surfaces, and can be easily scaled to improve asymptotic, barrier, and potential well properties [33].

The RMCS method is not appropriate for fitting the E_2 surface because of its repulsive nature [37]. Furthermore, the presence of avoided crossings both in E_2 and E_3

requires more elaborate potential energy fitting methods [38]. For these reasons we have not yet fitted them. Also, the best functional representation of the electric dipole transition moment between surfaces has not yet been established. However, the potential energy and transition moment data have now been completed for the additional bond angles 90°, 120°, 150° and 180°, so that the mapping of a global surface for all bond angles is possible. These surfaces and fitting techniques will be reported in a subsequent publication.

Acknowledgments

We acknowledge and thank the US Air Force Astronautics Laboratory (contract F04611-86-0016-67), the Department of Energy (grant DE-AS03-83ER), and NSERC (Canada) for financial support. We also thank the NAS program of the NASA-Ames Research Center and the NSF-San Diego Supercomputer Center for use of their CRAY Y-MP systems, and the Jet Propulsion Laboratory for use of their CRAY X-MP computer, on which most of the calculations were done. Special thanks are due to Prof. R.J. Buenker for supplying us with the CRAY version of the MRD-CI code used in these calculations. Z. Peng thanks Dr. Pablo Bruna for assistance.

References

1. B. Liu, *J. Chem. Phys.* **58**, 1925 (1973).
2. P. Siegbahn and B. Liu, *J. Chem. Phys.* **68**, 2457 (1978).
3. D.G. Truhlar and C.J. Horowitz, *J. Chem. Phys.* **68**, 2466 (1978); **71**, 1514(E) (1979).
4. A.J.C. Varandas, F.B. Brown, C.A. Mead, D.G. Truhlar and N.C. Blais, *J. Chem. Phys.* **86**, 6258 (1987).
5. H.F. King and K. Morokuma, *J. Chem. Phys.* **71**, 3213 (1979).
6. M. Jungen, *J. Chem. Phys.* **71**, 3540 (1979).
7. R.L. Martin, *J. Chem. Phys.* **71**, 3541 (1979).
8. K.C. Kulander and M.F. Guest, *J. Phys.* **B 12**, L501 (1979)
9. Ch. Nager and M. Jungen, *Chem. Phys.* **70**, 189 (1982).
10. S. Raynor and D.R. Herschbach, *J. Phys. Chem.* **86**, 3592 (1982).
11. H.J. Foth, H.R. Mayne, R.A. Poirier, J.C. Polanyi and H.H. Teller, *Laser Chem.* **2**, 229 (1983).
12. H.R. Mayne, R.A. Poirier and J.C. Polanyi, *J. Chem. Phys.* **80**, 4025 (1984).
13. H.R. Mayne, J.C. Polanyi, N. Sathyamurthy and S. Raynor, *J. Chem. Phys.* **88**, 4064 (1984).
14. A.C. Roach and P.J. Kuntz, *J. Chem. Phys.* **84**, 822 (1986).
15. I. Petsalakis, J. Theodorakopoulos and J.S. Wright, *J. Chem. Phys.* **89**, 6850 (1988).
16. G.H.F. Diercksen, W. Duch and J. Karwowski, *Chem. Phys. Lett.* **168**, 69 (1990).
17. G. Herzberg, *Ann. Rev. Phys. Chem.* **38**, 27 (1987).
18. J.K.G. Watson, in press.
19. G.I. Gellene and R.F. Porter, in press.
20. B. Lepetit, Z. Peng and A. Kuppermann, *Chem. Phys. Lett.* **166**, 572 (1990).
21. C. Alden Mead and D.G. Truhlar, *J. Chem. Phys.* **70**, 2284 (1979).
22. C. Alden Mead, *J. Chem. Phys.* **72**, 3839 (1980).
23. C. Alden Mead, *Chem. Phys.*, **49**, 23 (1980).
24. B. Lepetit and A. Kuppermann, *Chem. Phys. Lett.* **166**, 581 (1990).
25. N.C. Blais, D.G. Truhlar and C. Alden Mead, *J. Chem. Phys.* **89**, 6204 (1988).
26. D. Talbi and R.P. Saxon, *J. Chem. Phys.* **89**, 2235 (1988).
27. The program HONDO can be obtained from the Quantum Chemistry Program Exchange.
28. R.J. Buenker, in: Molecular Physics and Quantum Chemistry into the '80', ed. P.G. Burton (University of Wollongong, Wollongong, 1980)
29. R.J. Buenker, in: Studies in Physical and Theoretical Chemistry, Vol. 21 (Current Aspect of Quantum Chemistry 1981), ed. R. Carbo (Elsevier Scientific, Amsterdam,

1982), p. 17.

30. R.J. Buenker and R.A. Phillips, *J. Mol. Struct.* THEOCHEM **123** 291 (1985).
31. J.M. Bowman and A. Kuppermann, *Chem. Phys. Lett.* **34**, 523 (1975).
32. J.N.L. Conner, W. Jakubetz and J. Manz, *Mol. Phys.* **29**, 347 (1975).
33. J.S. Wright and S.K. Gray, *J. Chem. Phys.* **69**, 67 (1978).
34. J.S. Wright and E. Kruus, *J. Chem. Phys.* **85**, 7251 (1986).
35. P.J. Kuntz and A.C. Roach, *J. Chem. Soc. Faraday Trans.* 2, **68** 259 (1972).
36. W. Kolos and L. Wolniewiez, *J. Chem. Phys.* **43**, 2429 (1965).
37. Sukarma Thareja and N. Sathyamurthy, *J. Chem. Soc., Faraday Trans. 2* **81**, 717 (1985)
38. S. Chapman, M. Dupuis and S. Green, *Chem. Phys.* **78**, 93 (1983).

Table 1

Selected results for the CI energy for H and H_2 using the $(12s4p1d/7s4p1d)$ basis set[a].

Species	Internuclear distance[b] (bohr)	Energy[c] (hartree)	Reference
H($1s$)		-0.499998	This work
H($1s$)		-0.500000	exact
H($2s$)		-0.124992	This work
H($2s$)		-0.125000	exact
H($2p$)		-0.124723	This work
H($2p$)		-0.125000	exact
H_2 ($X\ ^1\Sigma_g^+$)	1.40	-1.173652	This work
		-1.173704	[1]
		-1.1733	[2]
		-1.174474	[36]
H_2 ($b\ ^3\Sigma_u^+$)	1.40	-0.783904	This work
		-0.784150	[36]

a) Atomic energies are SCF orbital energies; molecular energies are full single and double excitation CI.

b) For the H_2 molecule calculations.

c) With respect to the configuration of separated electrons and protons.

Table 2

MRD-CI energies of four electronic states of H_3 at selected geometries[a].

Symmetry of nuclear geometry[a]	Internuclear distances (bohr)			Energy[b] (hartree)			
	R_1	R_2	R_3	E_1	E_2	E_3	E_4
D_{3h}	1.2	1.2	1.2	-1.441703	-1.441650	-1.415028	-1.398848
($\gamma = 60°$)	1.4	1.4	1.4	-1.518046	-1.518017	-1.468988	-1.458043
	1.6	1.6	1.6	-1.554349	-1.554268	-1.482113	-1.475586
	1.633	1.633	1.633	-1.557748	-1.557717	-1.481972	-1.475958
	1.64	1.64	1.64	-1.558556	-1.558507	-1.481895	-1.475980
	1.8	1.8	1.8	-1.569022	-1.568989	-1.474258	-1.471001
	2.0	2.0	2.0	-1.571945	-1.571928	-1.455205	-1.454669
	2.2	2.2	2.2	-1.568548	-1.568561	-1.430550	-1.432079
	2.4	2.4	2.4	-1.561349	-1.561420	-1.403023	-1.406783
$D_{\infty h}$	1.2	1.2	2.4	-1.564466	-1.384957	-1.370293	-1.370514
($\gamma = 180°$)	1.4	1.4	2.8	-1.626915	-1.412905	-1.400325	-1.400933
	1.6	1.6	3.2	-1.652252	-1.415210	-1.402812	-1.403312
	1.8	1.8	3.6	-1.656594	-1.418199	-1.391131	-1.391509
	2.0	2.0	4.0	-1.649371	-1.445225	-1.377716	-1.372591
$C_{\infty v}$	1.2	10.0	11.2	-1.663273	-1.287824	-1.287778	-1.288010
($\gamma = 180°$)	1.4	10.0	11.4	-1.673020	-1.297438	-1.297355	-1.297734
	1.6	10.0	11.6	-1.667258	-1.331377	-1.291776	-1.291910
	1.8	10.0	11.8	-1.653795	-1.367858	-1.278349	-1.278448
	2.0	10.0	12.0	-1.636842	-1.396687	-1.261682	-1.261512

a) All calculations were carried out in C_s symmetry. E_1, E_2 and E_3 are the lowest three energies of A' symmetry and E_4 is the lowest one of A'' symmetry.

b) With respect to the configuration of separated electrons and protons.

Table 3

Square of the electric dipole transition moment $T_{ij}^2 = \langle \Psi_i \mid \mu \mid \Psi_j \rangle^2$ (in a.u.^{2}) for H_3 in the equilateral triangular geometry.

R_1 (bohr)	T_{21}^2	T_{31}^2	T_{32}^2	T_{43}^2
1.2	0.009	4.20	4.20	6.92
1.4	0.018	3.38	3.42	7.02
1.6	0.030	2.70	2.68	7.18
1.633	0.032	2.59	2.60	7.22
1.64	0.033	2.54	2.58	7.24
1.8	0.047	2.12	2.12	7.34
2.0	0.061	1.70	1.70	7.51
2.2	0.071	1.32	1.30	7.56
2.4	0.077	1.07	1.05	7.73

Captions for Figures

Figure 1: Contour map of the ground-state potential energy surface (E_1 and $\gamma = 60°$) for H_3, showing the rays and points for which *ab initio* data were generated. The rays shown correspond to 45° (diagonal), 44°, 43°, 42°, 41°, 40°, 35°, and 30°. Contour energies vary from −4.0 (inner contour) to −1.0 eV relative to $3H(1s)$, in increments of 0.5 eV.

Figure 2: Contour map of the excited state potential energy surface (E_4 and $\gamma = 60°$) for H_3. Rays and points have the same meaning as in Figure 1. Contour energies vary from −9.0 (inner contour) to −3.0 eV relative to $2H(1s) + H(2p)$, in increments of 1.0 eV.

Figure 1

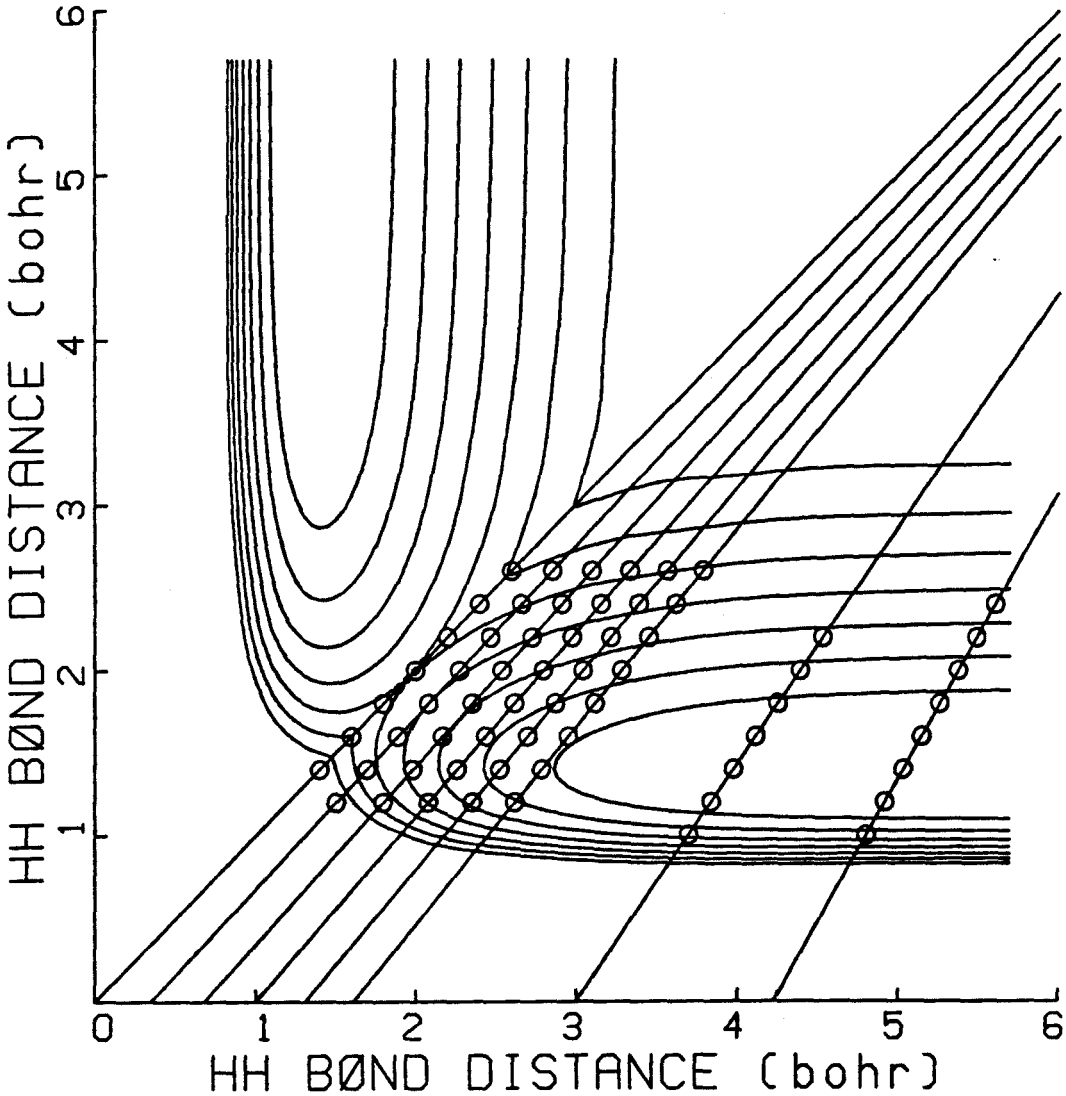

Figure 2